ELECTROMYOGRAPHY (EMG) TECHNIQUES FOR THE ASSESSMENT AND REHABILITATION OF MOTOR IMPAIRMENT FOLLOWING STROKE

EDITED BY: Cliff S. Klein, Sheng Li, Xiaogang Hu and Xiaoyan Li
PUBLISHED IN: Frontiers in Neurology

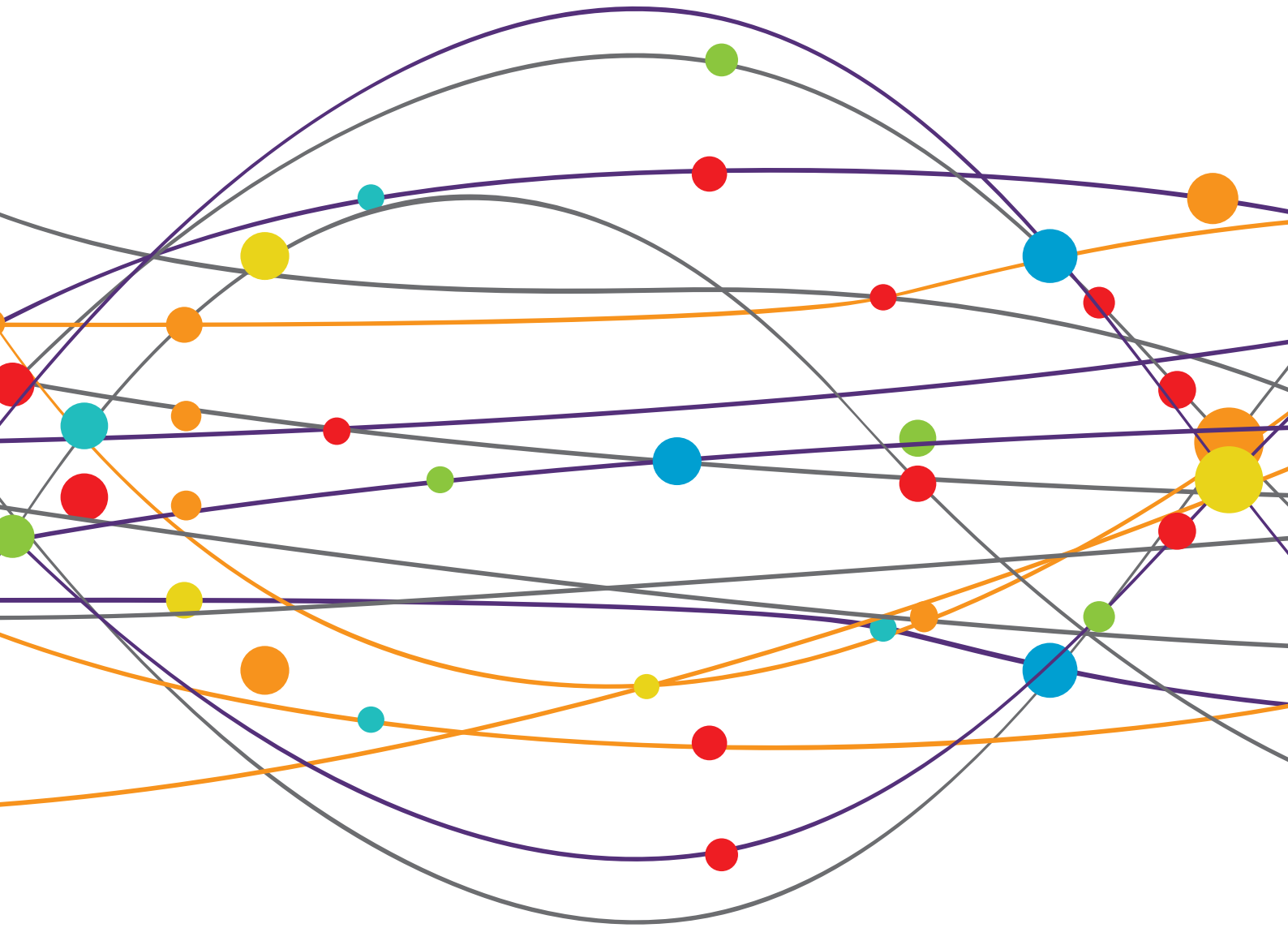

frontiers Research Topics

frontiers

ISSN 1664-8714
ISBN 978-2-88945-853-0
DOI 10.3389/978-2-88945-853-0

About Frontiers

Frontiers is more than just an open-access publisher of scholarly articles: it is a pioneering approach to the world of academia, radically improving the way scholarly research is managed. The grand vision of Frontiers is a world where all people have an equal opportunity to seek, share and generate knowledge. Frontiers provides immediate and permanent online open access to all its publications, but this alone is not enough to realize our grand goals.

Frontiers Journal Series

The Frontiers Journal Series is a multi-tier and interdisciplinary set of open-access, online journals, promising a paradigm shift from the current review, selection and dissemination processes in academic publishing. All Frontiers journals are driven by researchers for researchers; therefore, they constitute a service to the scholarly community. At the same time, the Frontiers Journal Series operates on a revolutionary invention, the tiered publishing system, initially addressing specific communities of scholars, and gradually climbing up to broader public understanding, thus serving the interests of the lay society, too.

Dedication to Quality

Each Frontiers article is a landmark of the highest quality, thanks to genuinely collaborative interactions between authors and review editors, who include some of the world's best academicians. Research must be certified by peers before entering a stream of knowledge that may eventually reach the public - and shape society; therefore, Frontiers only applies the most rigorous and unbiased reviews.
Frontiers revolutionizes research publishing by freely delivering the most outstanding research, evaluated with no bias from both the academic and social point of view. By applying the most advanced information technologies, Frontiers is catapulting scholarly publishing into a new generation.

What are Frontiers Research Topics?

Frontiers Research Topics are very popular trademarks of the Frontiers Journals Series: they are collections of at least ten articles, all centered on a particular subject. With their unique mix of varied contributions from Original Research to Review Articles, Frontiers Research Topics unify the most influential researchers, the latest key findings and historical advances in a hot research area! Find out more on how to host your own Frontiers Research Topic or contribute to one as an author by contacting the Frontiers Editorial Office: researchtopics@frontiersin.org

ELECTROMYOGRAPHY (EMG) TECHNIQUES FOR THE ASSESSMENT AND REHABILITATION OF MOTOR IMPAIRMENT FOLLOWING STROKE

Topic Editors:
Cliff S. Klein, Guangdong Work Injury Rehabilitation Center, China
Sheng Li, University of Texas Health Science Center at Houston, and TIRR Memorial Hermann Research Center, United States
Xiaogang Hu, University of North Carolina at Chapel Hill and North Carolina State University, United States
Xiaoyan Li, University of Texas Health Science Center at Houston, and TIRR Memorial Hermann Research Center, United States

Citation: Klein, C. S., Li, S., Hu, X., Li, X., eds. (2019). Electromyography (EMG) Techniques for the Assessment and Rehabilitation of Motor Impairment Following Stroke. Lausanne: Frontiers Media. doi: 10.3389/978-2-88945-853-0

Table of Contents

frontiers in Neurology

EDITORIAL
published: 18 December 2018
doi: 10.3389/fneur.2018.01122

Editorial: Electromyography (EMG) Techniques for the Assessment and Rehabilitation of Motor Impairment Following Stroke

Cliff S. Klein[1]*, *Sheng Li*[2]*, *Xiaogang Hu*[3]* and *Xiaoyan Li*[2]*

[1] Guangdong Work Injury Rehabilitation Center, Guangzhou, China, [2] University of Texas Health Science Center at Houston, and TIRR Memorial Hermann Research Center, Houston, TX, United States, [3] Joint Department of Biomedical Engineering, University of North Carolina at Chapel Hill and North Carolina State University, Raleigh, NC, United States

Keywords: electromyography, MUSC, motor, rehabilitation, stroke

Editorial on the Research Topic

Electromyography (EMG) Techniques for the Assessment and Rehabilitation of Motor Impairment Following Stroke

OPEN ACCESS

Edited and reviewed by:
Jean-Claude Baron,
University of Cambridge,
United Kingdom

***Correspondence:**
Cliff S. Klein
c-klein@northwestern.edu
Sheng Li
Sheng.Li@uth.tmc.edu
Xiaogang Hu
xhu13@ncsu.edu
Xiaoyan Li
xiaoyan.li@uth.tmc.edu

Specialty section:
This article was submitted to Stroke, a section of the journal Frontiers in Neurology

Received: *30 November 2018*
Accepted: *06 December 2018*
Published: *18 December 2018*

Citation:
Klein CS, Li S, Hu X and Li X (2018) Editorial: Electromyography (EMG) Techniques for the Assessment and Rehabilitation of Motor Impairment Following Stroke. Front. Neurol. 9:1122. doi: 10.3389/fneur.2018.01122

The nineteen papers of the research topic Electromyography (EMG) Techniques for the Assessment and Rehabilitation of Motor Impairment Following Stroke highlight a variety of ways that EMG may be used to better understand and treat stroke-induced brain damage. Seven papers addressed the impact of weekly training on EMG properties and function post-stroke, and one paper examined the effect of a robotic exoskeleton on gait during a single training session (**Exercise/therapy interventions**). Six of the seven training studies were concerned with upper limb function (one of which also assessed corticomuscular coupling), and one examined the effect of foot drop stimulator training. The six upper limb studies used a variety of training modalities including Wii-based upper limb therapy (two papers from one group), EMG-driven robotic devices with or without neuromuscular electrical stimulation (NMES) (three papers), and traditional physical/occupational therapy (one paper).

Another seven papers were focused on using EMG to examine motor impairment after stroke (**Mechanisms of motor impairment).** These included one study that addressed coupling between the index finger and thumb, whereas another addressed upper limb synergies during reaching. One paper examined EMG co-contraction during gait, and one addressed gait EMG during obstacle crossing. One group examined reticulospinal pathways during elbow flexor activity using startling acoustic stimulation. Another studied masticatory muscle activity following brainstem stroke. Finally, one group addressed coupling between the electroencephalogram (EEG) and EMG signals during upper limb movements.

Four studies used novel EMG processing techniques to study motor control and impairment post-stroke **(Novel EMG processing techniques).** These included new approaches to intramuscular EMG decomposition, coherence of motor unit firing patterns from surface EMG, clustering index analysis of surface EMG, and pattern recognition from high density surface EMG.

EXERCISE/THERAPY INTERVENTIONS

A number of studies examined the effects of an exercise/therapy program, or a single exercise session, on EMG and motor function. Some also addressed the associated cortical plasticity.

Upper Limb

Many addressed the effect of exercise/therapy on upper limb muscle activation properties. Hesam-Shariati et al. examined changes in upper limb EMG activity resulting from the standardized 14-day Wii-based Movement Therapy program (i.e., Wii-tennis, golf, baseball) in chronic stroke survivors. They found that training lead to different patterns of EMG changes that were related to the level of motor deficit. In their companion paper Hesam-Shariati et al. they quantified muscle synergies *during* therapy (Wii baseball swing) based on EMG activity of the affected arm muscles using a non-negative matrix factorization algorithm. They were able to identify differences in the number of muscle synergies used by patients as a function of the level of motor deficit.

Device-assisted interventions offer a way to study and train patients with more severe limb impairment. In a case study, Lu et al. used forearm EMG signals to detect a stroke survivor's motion intent, and then used the EMG to drive a hand exoskeleton to assist with finger motion in real time. After 10-weeks of robot-assisted hand therapy, the patient showed improved grip strength and hand function. The results demonstrate the feasibility of robot-assisted training driven by myoelectric pattern recognition in chronic stroke survivors.

After a stroke, it is critically important to start rehabilitation early to take advantage of the highly plastic period of the neural system. In a pilot randomized control trial, Qian et al. evaluated the effects of 1 month (20 sessions) of EMG-driven NMES combined with robotic assistance, targeting the elbow, wrist, and fingers of subacute stroke survivors. EMG parameters, including the co-contraction index and the activation level of targeted muscles were used to monitor the muscle coordination patterns. They found that the NMES combined with robotic training could achieve higher motor outcomes at the distal joints and more effective reduction in muscle tone than traditional therapy.

Some investigators also addressed training-related cortical plasticity and corticomuscular coupling. Wilkins et al. found EMG-driven NMES task-specific arm/hand training (7 weeks) improved hand opening and functional use in chronic stroke survivors with moderate to severe motor impairments. Functional improvement was paralleled with functional reorganization in the ipsilesional primary sensorimotor cortex. The neural plastic reorganization after functional improvement was also seen with strengthened corticomuscular coupling. In a case study of a subacute stroke subject, Zheng et al. evaluated corticomuscular coupling between EEG and EMG (biceps) signals during elbow flexion before and after 1 month of regular physical and occupational therapy. Corticomuscular coherence was increased in the affected limb with functional improvement, but not in the non-affected limb. These results exemplify that stroke survivors with severe motor impairments may still have the potential to improve hand function if appropriate interventions are used to induce neural plasticity.

Lower Limb

Pilkar et al. used different EMG-based indices to quantify the effects of a foot drop stimulator on muscle activation during gait over a 6 month period of community walking. A wavelet-based time-frequency analysis approach was used to quantify activation changes of multiple ankle muscles in chronic stroke survivors. The findings suggest alterations in motor unit recruitment strategies after foot drop stimulator use. The outcomes establish the efficacy of a foot drop stimulator as a rehabilitation intervention that may promote motor recovery in addition to reducing foot drop.

Quantitative and continuous monitoring of muscle activation is necessary to adjust training protocols in a timely manner. Androwis et al. used novel EMG analysis (Burst Duration Similarity Index) to quantify the intensity and timing of muscle activation during a single session of robotic gait therapy in acute stroke survivors. The authors showed that a robotic exoskeleton can reduce the soleus and rectus femoris muscle activity in the affected limb during stance phase, and can also improve the timing of muscle activation in the affected limb.

Mechanisms of Motor Impairment

Surface EMG together with other signals recorded peripherally or centrally provides a means to assess mechanisms of motor impairment. Jones and Kamper studied the coupling of the index finger and thumb during close-open pinching motions in chronic stroke survivors. A Cable-Actuated Finger Exoskeleton was used to perturb joints of the index finger during pinching motions, while finger/thumb muscle surface EMG and finger kinematics were recorded. They found that involuntary finger-thumb coupling was present during the dynamic pinching task, with perturbation of the index finger impacting thumb activity. This finding reveals a potential mechanism to improve hand mobility following stroke. Li et al. analyzed motor synergies during arm reaching based on surface EMG recordings from multiple muscles and correlated with reaching kinematics. They were able to detect task-specific deficits in reaching movements after stroke

Ma et al. studied lower limb muscle activity during obstacle crossing using surface EMG in chronic stroke survivors. EMG activity of the leading limb during the swing phase was larger in all muscles in the stroke compared to the control group, and TA activity increased with obstacle height in both groups. Co-contraction between agonist-antagonist muscle pairs was larger in the stroke group in the leading/ trailing limb during certain phases. The authors suggested that the greater muscle activation during obstacle crossing following stroke may have a negative impact on balance.

It remains unclear whether co-contraction of agonist-antagonist muscles is excessive and impacts gait significantly following stroke. In chronic stroke survivors, Banks et al. quantified surface EMG co-contraction of agonist-antagonist muscle pairs in three ways (no normalization, normalized to the maximal EMG of the gait cycle, normalized to the M-wave) and determined their association with gait impairment during treadmill walking. Co-contraction during the terminal stance phase was not different between healthy controls and the stroke subjects, regardless of the normalization method. Normalization also did not impact the ability to resolve group differences. Furthermore, the correlation between stance phase

co-contraction and walking speed was modest. Pathological co-contraction may not be a primary factor contributing to impaired gait in most stroke survivors. The authors suggest other approaches that account for timing and amplitude components of the EMG (i.e., muscle synergy analysis) may better capture the relevant deficits.

The coupling strength between the EEG and EMG signals during motion is instructive in assessing motor function. Gao et al. studied subacute stroke patients completing tasks such as hand gripping and elbow bending. Stroke subjects demonstrated greater strength in the bi-directional corticomuscular coupling between the EEG and EMG signals. Such changes suggest a compensational strategy after the brain lesion.

It is difficult to assess activities of brainstem nuclei *in vivo* even with the most advanced neuroimaging techniques. Startling acoustic stimulation is known to stimulate the reticulospinal pathways, thus allowing the opportunity to assess the role of brainstem motor system indirectly. Li et al. analyzed changes in EMG and force in response to startling acoustic stimulation during isometric elbow flexion in stroke survivors and healthy controls. They reported that the sound-induced force and EMG increase in stroke survivors was not significantly different from those in healthy controls. As such, there results suggest that the reticulospinal projections do not increase their contributions to muscle strength in stroke. Jian et al. analyzed surface EMG signals of bilateral masticatory muscles in stroke survivors after brainstem stroke using multiple EMG parameters. In addition to expected differences between muscles and sides, they did not observe the head position effect on muscle activation on both sides. These are valuable information as the results could advance the understanding whether head positions alter chewing and swallowing activities in stroke survivors.

Novel EMG Processing Techniques

Examining motor unit discharge and recruitment patterns post-stroke can disclose valuable information pertaining to impaired spinal versus supraspinal motor control. EMG decomposition into constituent motor unit action potential (MUAP) trains, however, is challenging with severe superposition of multiple MUAPs. Ren et al. developed a new intramuscular EMG decomposition technique to improve the accuracy of EMG decomposition with interference patterns. The technique was implemented by using six stages of analysis including feature extraction, clustering, refinement of the classification, and splitting of the superimposed MUAPs. A high accuracy of MUAP detection was reported in 8 subacute stroke survivors (88%) and 20 healthy control participants (94%).

Dai et al. quantified the different types of connectivity in the spinal networks and changes in their relative contributions after a stroke. By comparing the coherence of motor unit firing pattern across different isometric contractions, they identified significant changes in coherence in three frequency bands: delta (1–4 Hz), alpha (8–12 Hz), and beta (15–30 Hz) in the paretic hand muscles. These changes reflect increased common synaptic inputs in the subcortical pathway and provide evidence on different origins of impaired muscle activation in stroke.

To further differentiate neurogenic and myopathic changes in the muscle, Tang et al. applied clustering index analysis to examine surface EMG in the distal and proximal muscles of the upper limb from 12 stroke survivors. They observed abnormally high or low clustering index values in the paretic muscles compared to healthy controls. This finding may indicate that both neurogenic and myopathic changes may occur in paretic muscles.

Selection of appropriate features from surface EMG is essential for development of highly effective pattern recognition algorithms in the EMG-controlled devices. Wang et al. developed a novel pattern recognition technique for precise discrimination of 20 hand/upper limb functional movements in stroke survivors. Specifically, they applied wavelet packet to extract the neural control features and used the Fisher's class separability index and the sequential feedforward selection analyses to select appropriate channels in high density surface EMG. Such implementation can facilitate use of surface EMG control in stroke rehabilitation.

AUTHOR CONTRIBUTIONS

All authors made an equal contribution to the work, and approved it for publication.

Conflict of Interest Statement: The authors declare that the research was conducted in the absence of any commercial or financial relationships that could be construed as a potential conflict of interest.

frontiers in Neurology

ORIGINAL RESEARCH
published: 07 August 2018
doi: 10.3389/fneur.2018.00630

Electromyography Assessment During Gait in a Robotic Exoskeleton for Acute Stroke

Ghaith J. Androwis[1,2], *Rakesh Pilkar*[1,3], *Arvind Ramanujam*[1] and *Karen J. Nolan*[1,2,3]*

[1] Human Performance and Engineering Research, Kessler Foundation, West Orange, NJ, United States, [2] Children's Specialized Hospital, Mountainside, NJ, United States, [3] Department of Physical Medicine and Rehabilitation, Rutgers–New Jersey Medical School, Newark, NJ, United States

Background: Robotic exoskeleton (RE) based gait training involves repetitive task-oriented movements and weight shifts to promote functional recovery. To effectively understand the neuromuscular alterations occurring due to hemiplegia as well as due to the utilization of RE in acute stroke, there is a need for electromyography (EMG) techniques that not only quantify the intensity of muscle activations but also quantify and compare activation timings in different gait training environments.

Purpose: To examine the applicability of a novel EMG analysis technique, Burst Duration Similarity Index (BDSI) during a single session of inpatient gait training in RE and during traditional overground gait training for individuals with acute stroke.

Methods: Surface EMG was collected bilaterally with and without the RE device for five participants with acute stroke during the normalized gait cycle to measure lower limb muscle activations. EMG outcomes included integrated EMG (iEMG) calculated from the root-mean-square profiles, and a novel measure, BDSI derived from activation timing comparisons.

Results: EMG data demonstrated volitional although varied levels of muscle activations on the affected and unaffected limbs, during gait with and without the RE. During the stance phase mean iEMG of the soleus ($p = 0.019$) and rectus femoris (RF) ($p = 0.017$) on the affected side significantly decreased with RE, as compared to without the RE. The differences in mean BDSI scores on the affected side with RE were significantly higher than without RE for the vastus lateralis (VL) ($p = 0.010$) and RF ($p = 0.019$).

Conclusions: A traditional amplitude analysis (iEMG) and a novel timing analysis (BDSI) techniques were presented to assess the neuromuscular adaptations resulting in lower extremities muscles during RE assisted hemiplegic gait post acute stroke. The RE gait training environment allowed participants with hemiplegia post acute stroke to preserve their volitional neuromuscular activations during gait iEMG and BDSI analyses showed that the neuromuscular changes occurring in the RE environment were characterized by correctly timed amplitude and temporal adaptations. As a result of these adaptations, VL and RF on the affected side closely matched the activation patterns of healthy gait. Preliminary EMG data suggests that the RE provides an effective gait training environment for in acute stroke rehabilitation.

Keywords: electromyography, rehabilitation, stroke, hemiplegic gait, robotic exoskeleton

OPEN ACCESS

Edited by:
Xiaogang Hu,
University of North Carolina at Chapel Hill, United States

Reviewed by:
Xiaoyan Li,
McGovern Medical School, University of Texas, United States
Mu Qiao,
Louisiana Tech University, United States
Aviroop Dutt-Mazumder,
University of Michigan, United States

***Correspondence:**
Karen J. Nolan
knolan@kesslerfoundation.org

Specialty section:
This article was submitted to Stroke, a section of the journal Frontiers in Neurology

Received: *03 October 2017*
Accepted: *12 July 2018*
Published: *07 August 2018*

Citation:
Androwis GJ, Pilkar R, Ramanujam A and Nolan KJ (2018) Electromyography Assessment During Gait in a Robotic Exoskeleton for Acute Stroke. Front. Neurol. 9:630. doi: 10.3389/fneur.2018.00630

INTRODUCTION

Recovery of function post stroke is based on neural adaptation, and progressive task specific repetitive training based on the principles of neuroplasticity (1, 2). While major advances have been made in early intervention for the treatment of patients post stroke, the majority of survivors have residual mobility challenges and hemiplegia (3, 4). Hemiplegia typically manifests in pronounced asymmetrical deficits and is one of the most common disabling impairments resulting from stroke (5). Asymmetrical gait can be associated with muscle weakness, leading to inefficient ambulation, balance control challenges and risk of musculoskeletal injury to the non-paretic limb (6, 7). Task-oriented, high-repetition movements can improve muscular strength, motor control and movement coordination in patients post stroke (2). The task-specific training pertains to the training driven to achieve a functional task such as walking rather than focusing on minimizing an impairment (8, 9). In acute phase, traditional gait rehabilitation administered by a physical therapist is strenuous, inconsistent (in terms of movements generated) and less intense (in terms of number of steps). Integrating robotic exoskeleton (RE) technology into standard of care programs during the critical acute phase when the injured nervous system is highly plastic could maximize repetitive practice (9, 10), improve functional outcome measurements and provide quality gait training (10, 11). Programmable RE technology can also be used to advance progression during treatment and under the guidance of a physical therapist can emulate some features of manual assistance in a consistent and reproducible manner (2). The RE based training involves repetitive task-oriented (gait) movements and weight shifts to promote functional recovery. RE gait training may lead to changes in muscle activation as it provides task-specific movements to the lower limbs, increased step dosing and may provide a more symmetrical gait pattern (12).

An additional challenge in acute stroke is that many patients have a difficult time producing volitional movements that can be practiced repeatedly especially during the acute stage. In order to recover from physiological and functional lower extremity deficits, the task-related activities should include contributions from appropriate muscle groups during practice of these movements (13). Using an RE during gait rehabilitation in the acute phase may allow volitional muscle activation and improved phasic coordination (activation timing) during walking. However, the accuracy of these muscle contributions should be tracked. Surface electromyography (EMG) is one of the most effective, non-invasive tools which provides easy access to underlying neuromuscular processes that cause muscles to generate force, produce movement and achieve any functional task (14). During gait, EMG data reveals characteristic patterns of activation associated with each involved muscle in terms of onset timings, burst durations and levels of activations (15). These characteristic patterns significantly differ between healthy and pathological gait and this information can be used to assess the levels of improvement in muscle function, motor control, and neuromuscular adaptations post rehabilitation interventions. Bilateral EMG recordings of lower extremities can be further utilized to compare changes on the paretic side with respect to non-paretic side to assess inter-limb synchronization post RE intervention in individuals with stroke related hemiplegia.

To effectively understand the alterations occurring due to the RE, there is a need for EMG techniques that not only quantify the intensity of muscle activations but also quantify and compare activation timings for a single muscle during different gait training environments (e.g., overground or RE assisted). Although EMG amplitude is one of the most common variables reported in the literature (14, 16, 17), it does not distinctively provide temporal information (on–off timings). Particularly, in a cyclic activity such as gait, it is not only important for lower extremity muscles to produce activations but also activate them at the accurate time, especially for individuals with neurological disability such as acute stroke (16). In the post-stroke gait rehabilitation setting, the need to assess temporal information is even more apparent as muscle activation timing may be altered due to, (1) hemiplegia secondary to stroke and (2) the presence of a RE. The temporal features extracted from EMG data can allow the assessment of accuracy of participant's volitional contributions during training but also assess the modifications that the RE guided gait training may have. Several techniques have been used to extract the temporal information of muscle activations; however, their applicability in the domain of RE based gait training in acute stroke is limited.

The purpose of this investigation was to examine the applicability of a novel EMG analysis technique, Burst Duration Similarity Index (BDSI) during a single session of inpatient gait training in a RE and during traditional over ground gait training for individuals with acute stroke. EMG outcomes included standard measures of integrated EMG (iEMG) calculated from the root-mean-square (RMS) profiles, and a novel measure, BDSI (18) which quantifies the similarity between the two muscle activations by measuring co-excitation (common active regions) and co-inhibition (common inactive regions) during gait. Using iEMG and BDSI EMG analyses techniques, we hypothesized that the RE gait training environment will preserve the volitional neuromuscular activations in acute stroke. Volitional neuromuscular activations represent the residual post stroke muscle function during walking in the lower limbs. Our secondary hypothesis is that the RE gait training environment will change the activation timing of lower extremity muscles, measured by applying the BDSI technique, to match established normative healthy gait muscle activation timing patterns (15).

METHODOLOGY

Participants

Eligible participants were admitted to an acute inpatient rehabilitation facility, diagnosed with stroke (<6 months), between the age 18 and 82 years and had to physically fit into the RE device (height between 1.5 and 1.8 m; weight <99.7 kg). Five participants with acute stroke and unilateral hemiparesis (Age

51 ± 17 years; Height 1.7 ± 0.1 m; Weight 81.6 ± 3.6 kg; Time since injury 34.8 ± 34 days; Length of stay in acute inpatient rehabilitation 36 ± 24.6 days; Admission Motor Functional Independence Measure (FIM) 26 ± 4; three males, two females; two with right hemiplegia) were recruited for RE gait training during inpatient rehabilitation in conjunction with traditional therapy, **Table 1**. Participants had unilateral hemiplegia and lower extremity motor strength scores for all participants affected and unaffected side are presented in **Table 2**. All participants had: (1) no history of injury or pathology (unrelated to their stroke) within the last 90 days; (2) lower limb joint range of motion (ROM) within normal functional limits for ambulation; (3) no lower limb joint contracture or spasticity that limits ROM during ambulation; (4) sufficient strength of the contralateral limb to use an assistive device for ambulation; (5) upper body strength to balance with a walker or cane; (6) no skin issues that would prevent wearing the device; (7) stable blood pressure, with no diagnosis of persistent orthostatic hypotension, uncontrolled hypertension, or coronary artery disease. Participants were excluded if they had joint contractures of the hip, knee, or ankle that would prohibit the fitting of the RE, or concomitant medical conditions that would prevent inpatient gait training. Individuals were able to ambulate for 10 m with physical therapist assistance with and without the RE. All procedures performed in this investigation were approved by the Human Subjects Review Board and informed consent was obtained prior to participation in the study.

Robotic Exoskeleton (RE) Device

Robotic gait training was provided to participants during stroke rehabilitation at an inpatient rehabilitation hospital through a commercially available FDA approved robotic exoskeleton (EksoGT, Ekso Bionics, Inc. Richmond, CA, USA). The RE is intended for overground gait rehabilitation under the guidance of a licensed physical therapist. The device provides motor assistance to patients by driving their angular joints of the lower extremity through a repetitive predefined trajectory to complete the gait pattern. The device is attached to the user with backpack style shoulder harnessing, a torso brace, affixed to the legs with upper thigh straps and shin guards on the shank, and a secure foot binding (**Figure 1**). The RE includes two powered joints (hip and knee) which provide bilateral angular motion and a passively sprung ankle joint with adjustable stiffness that provides resistance in the sagittal plane (dorsiflexion and plantarflexion). ROM provided at the ankle is from −10 to 20° dorsiflexion. The actuated ROM at the hip is −20 to 135° and the actuated range for the knee is 0 to 120°. Additional ROM is provided to assist with functions such as standing and sitting. The physical therapist can adjust the walking pattern (i.e., step speed and length) to facilitate progression and variable assistance to each

TABLE 1 | Study participants' demographic information.

Participant	Type of assistive device		Gender	Age (years)	Height (m)	Weight (kg)	Affected side	Motor FIM		Length of stay (LOS) (days)	Time since injury (days)
	With RE	Without RE						Admission	Discharge		
P1	RW	RW	M	73	1.70	80.6	Right	25	60	10	14
P2	QC	QC	F	30	1.63	87.8	Left	31	50	28	33
P3	QC, DW	NBQC	M	38	1.75	79.2	Left	20	57	49	94
P4	QC	QC	F	56	1.60	78.8	Left	27	42	13	19
P5	NBQC	NBQC	M	58	1.75	81.9	Right	27	66	11	14

Type of Assistive Device: QC, quad cane; NBQC, narrow base quad cane; DW, dorsiflexion wrap; RW, rolling walker.
Motor Functional Independence Measure (FIM), Admission—The FIM Motor score measured at the time of admission to inpatient rehabilitation.
Motor Functional Independence Measure (FIM), Discharge—The FIM Motor score measured at the time of discharge from inpatient rehabilitation.
Length of Stay—Calculated as the time in days from admission to an acute inpatient rehabilitation facility to the date of gait testing.
Time Since Injury—Calculated from the date of the participants stroke (date of injury) to the date of gait testing.

TABLE 2 | Study participants' lower extremity strength scores.

Joint movement	Affected side					Unaffected side				
	P1	P2	P3	P4	P5	P1	P2	P3	P4	P5
Hip flexion	3+	1	3–	1	2–	4	5	5	5	5
Hip extension	3	1	3+	1	3	4	5	5	5	5
Hip abduction	3	0	2–	1	2+	4	5	5	5	5
Knee extension	5	2+	3+	2+	3	4	5	5	5	5
Dorsiflexion	3+	0	0	0	0	5	5	5	5	5
Plantarflexion	5	0	1	0	0	5	5	5	5	5

P, participant; Strength measurements performed by treating physical therapist (maximum score was 5).

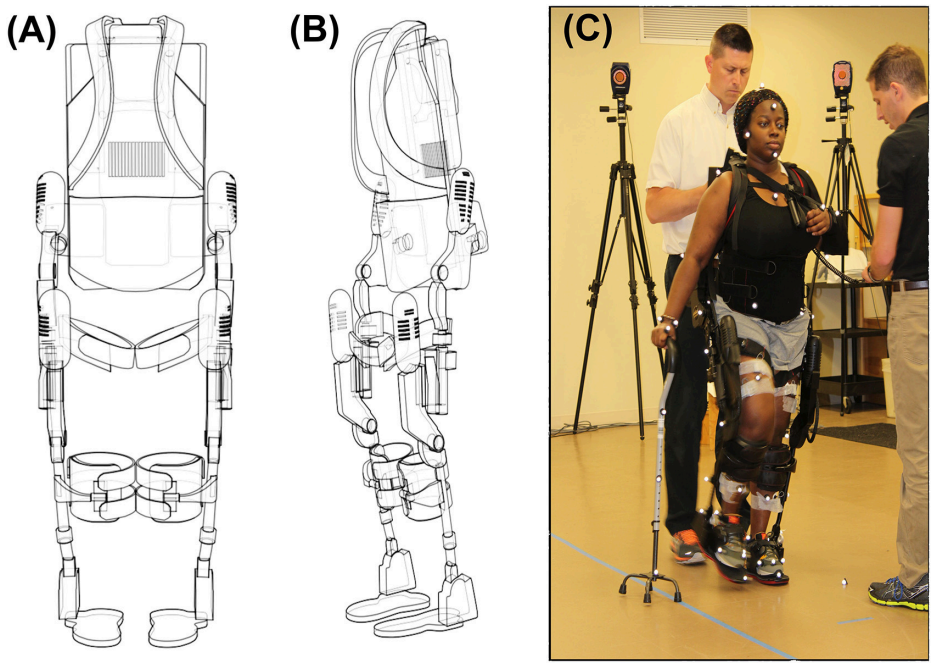

FIGURE 1 | (A) Frontal view of the EksoGT, **(B)** Oblique view of EksoGT, **(C)** One representative participant in the commercially available RE device (EksoGT, Ekso Bionics, Inc. Richmond, CA, USA) during gait analysis and EMG data collection. (Media consent provided by the participant for publication).

leg. The control technique of the robot depends on participants shifting their center of mass (COM) laterally and forward onto the leading limb, while offloading the trailing limb during toe-off in preparation for the next step (RE step mode: ProStep+). The RE can be used in conjunction with assistive devices (cane, walker, hemiwalker, etc.).

Experimental Procedures

During a single session of inpatient gait training participants diagnosed with stroke performed walking trials on level ground at a self-selected pace under two conditions: (1) walking overground with an assistive device (similar to their traditional inpatient gait training environment) and (2) walking in the RE device with an assistive device. **Table 1** identifies the type of assistive device used for each participant for ambulation with and without RE. Retroreflective markers were placed on anatomical landmarks and on the RE for all walking trials. EMG data were collected from six lower extremity muscles: tibialis anterior (TA); gastrocnemius (GA); soleus (SOL); rectus femoris (RF); vastus lateralis (VL); and biceps femoris (BF). During all walking trials, participants were allowed to stop and rest if necessary and research staff provided non-contact guarding for safety. The total duration of the experimental session was ∼2 h. Kinematic data were collected at 60 Hz (Motion Analysis, Inc., Santa Rose, CA, USA), and time synched with wireless EMG data collected at 2,520 Hz (Noraxon, Inc., Scottsdale, AZ, USA). During initial post processing in Cortex software (Motion Analysis, Inc., Santa Rose, CA, USA) heel strike and toe-off gait cycle events were identified for all walking trials with and without RE. Heel strike and toe-off were determined based on the event of heel contact with the ground (or first foot contact in pathological gait) and the event of toe lift off of the ground (or the last foot contact with the floor in pathological gait) respectively. These temporal events were used for all subsequent EMG analyses to identify and normalize the affected and unaffected gait cycles as well as to identify and normalize the stance and swing phases of gait. An average of 11 gait cycles (minimum of 8 and a maximum of 14) were used for analysis of the with RE condition and an average of six gait cycles (minimum of 5 and a maximum of 6) were used for the without RE condition for each subject. EMG and temporal events were exported for further custom analysis in MATLAB (MATLAB R2014B, The MathWorks Inc., Natick, MA).

Data Processing and Outcome Measures

EMG data were band pass filtered (zero-lag, 4th order Butterworth; cut-off frequencies of 20 and 300 Hz) and notch filtered at 60 Hz. Filtered data were full wave rectified and root mean squared (RMS) with a 70 ms time window to smooth the data. For standardization, EMG data were normalized to 100% of a gait cycle based on the temporal events (heel strikes and toe-offs) extracted from the kinematic data. Each gait cycle (heel strike to heel strike) was subdivided into stance (heel strike to toe off) and swing (toe off to subsequent heel strike) phases. The stance and swing phases of the gait cycle were each normalized to 100% for standardization and to allow comparisons between and within subjects.

EMG outcomes included: (1) Amplitude analysis: integrated EMG (iEMG) and (2) Timing Analysis: Burst Duration Similarity Index (BDSI).

Integrated EMG (iEMG)

iEMG is defined as the area under the curve of the rectified EMG signal. It is a parameter routinely utilized to compare EMG activation and is considered a measure of voluntary muscle drive. An increase in iEMG may be caused by an increase in firing frequency and the recruitment of additional motor units (19). In the current investigation, EMG data were segmented based on temporal events to indicate stance and swing phases. The iEMG during the normalized stance (0–100%) and normalized swing (0–100%) phases of gait were computed using a trapezoidal numerical integration in MATLAB as described in Equation 1 (20). Changes in iEMG were calculated for all collected muscles with and without RE. The calculated values of iEMG were averaged across participants and means and standard deviations were used for analysis.

$$\int_a^b f(x)\,dx \approx \frac{b-a}{2N}\sum_{n=1}^{N}\left(f(x_n) + f(x_{n+1})\right) \quad (1)$$

N equals the length of the signal. In the integration process the term $\frac{b-a}{2N}$ is a representation of spacing between each point.

Burst Duration Similarity Index (BDSI)

BDSI compares muscle activations (EMG "on") as well as inhibitions (EMG "off") and quantifies the match between the two EMG signals (18). For BDSI calculations, band pass filtered EMG data were normalized to 0–100% of gait cycles. For each participant, EMGs collected during all gait cycles for all walks were ensemble-average to get a single EMG representation for each muscle for each condition (with/without RE). Each EMG profile was processed using Teager Kaiser Energy Operator (TKEO). TKEO uses a sliding window approach to calculate the instantaneous energy changes with respect to neighboring samples. As a result, it amplifies the energy of the action potential spikes and differentiates between the relaxed and contracted muscle (21, 22). The baseline noise level for TKEO output was calculated and a threshold of eight standard deviations (SD) above the calculated baseline noise was determined. An EMG signal with amplitude above the calculated threshold for 10% of gait cycle was considered "ON" while amplitudes below the threshold for 10% was defined as the "OFF" period. Duration of 10% gait cycle was selected based on our previously reported data (18). Once the ON-OFF timings were determined for EMGs collected from each muscle during each walking condition, the BDSI between the two EMG signals, s_1 and s_2, of length N was determined in the following two steps,

(i) Create timing vectors as,

On-timing: a binary vector of length N with 1 indicating simultaneous activation of s_1 and s_2 and 0 otherwise.
Off-timing: a binary vector of length N with 1 indicating simultaneous inactivation of s_1 and s_2 and 0 otherwise.

(ii) The BDSI, as a function of two EMG signals, $f(s_1,\ s_2)$, is calculated as,

$$BDSI = f(s_1,\ s_2) = \frac{sum\left(On - timing\right) + sum(Off - timing)}{N} \times 100 \quad (2)$$

BDSI were calculated by comparing EMGs collected from each muscle with and without RE as well as comparing to normative healthy adult gait activation. On-timing and off-timing vectors for healthy adult gait were generated from well-established normative data (15). Adult gait muscle activation timing information (in percent) presented in Perry et al. (15) was utilized as a healthy reference for the on-off durations during a normalized gait (100% gait cycle), and used in binary form (0–OFF, 1–ON) for comparison with the collected data (with and without RE) to compute BDSI scores.

Figure 2 demonstrates the EMG onset detection for a left RF muscle of one representative participant with and without the RE. Solid blue lines represent ON–OFF time points during a normalized gait (0–100% gait cycle) determined using TKEO processed 8 SD threshold method. Healthy gait is represented by solid red lines. Co-excitation (solid green) represents regions during a normalized gait when RF activation matched with the same for healthy gait. Co-inhibition represents the regions where both EMGs under comparison were inactive. Equation (2) was used to quantify the similarity based on co-excitation and co-inhibition in terms of BDSI.

Statistical Analysis

Paired sample t-tests were performed to determine if there were significant differences in mean iEMG and BDSI scores in two conditions: (1) walking overground with an assistive device (similar to their traditional inpatient gait training environment) and (2) walking in the RE device with an assistive device. Secondary analyses investigated if the RE gait training environment altered the activation timing of lower extremity muscles to match healthy muscle activation timing patterns. Paired sample t-tests were used to determine if there were significant differences between the affected and unaffected side while walking overground and in the RE.

RESULTS

Electromyography Amplitude Analysis of Lower Extremity Muscles

Mean EMG data demonstrate volitional although varied levels of muscle activations on the affected (**Figure 3A**) and unaffected limbs (**Figure 3B**), during gait with and without RE. These muscle activiations are characterized by variations in both amplitude and timing. In addition, the activations do not consistently correlate with the activation timing of healthy gait.

Bilateral Mean iEMG Changes With the RE

During the stance phase mean iEMG of SOL [with RE: 5.9 ± 3.9; without RE: 23.0 ± 11.8, $t_{(4)} = -3.79$, $p = 0.019$; effect size = 2.18, power = 94.61%] and RF [with RE 3.6 ± 1.8, without RE 9.8 ± 4.4, $t_{(4)} = -3.92$, $p = 0.017$; effect size = 2.34, power =

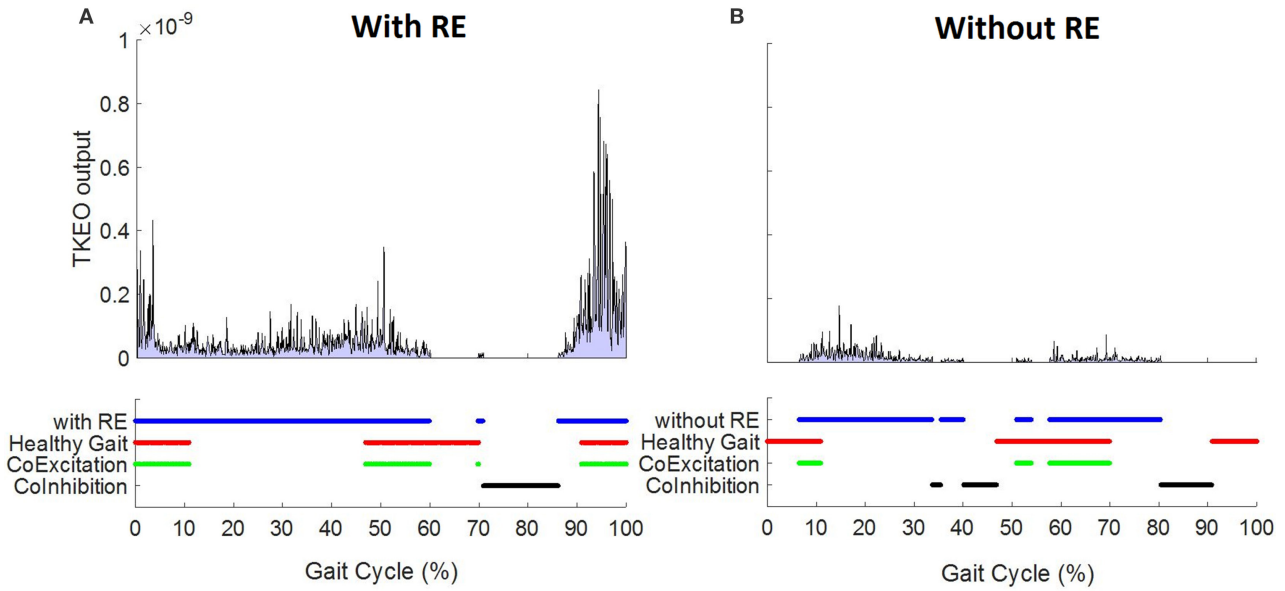

FIGURE 2 | Left RF EMG onset detection using TKEO – 8 standard deviation threshold method for a 58 year old representative participant **(A)** with and **(B)** without RE.

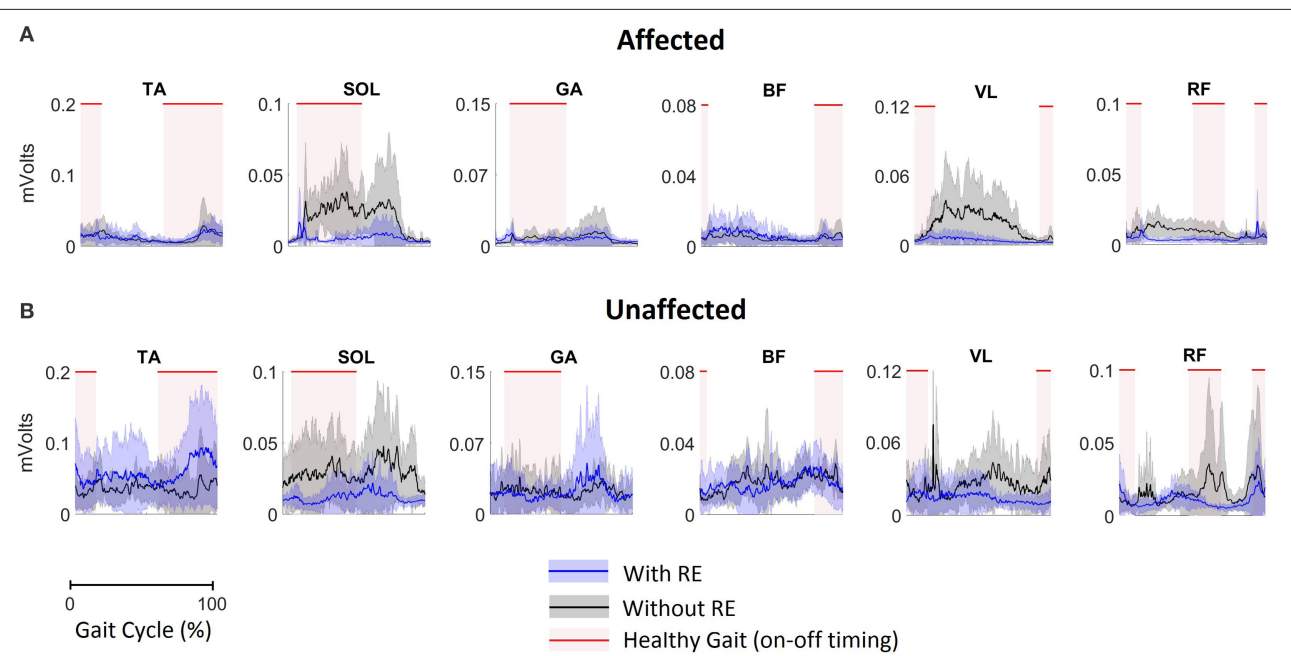

FIGURE 3 | EMG activation of **(A)** the affected limb and **(B)** the unaffected limb for all participants ($n = 5$) during gait with and without RE. Shaded rectangular areas with red horizontal lines indicate when a muscle is active based on normative healthy adult gait, Perry et al. (15).

96.78%] on the affected side significantly decreased with RE, as compared to without the RE (**Figure 4A**), however, no significant differences were found for the other muscles on the affected side with the RE, as compared to without the RE (**Figure 4A**). During the swing phase, no significant differences were found for any muscles on the affected side with the RE, as compared to without RE (**Figure 4B**). There was an increase in iEMG of the TA during the swing phase on the affected side with the RE, but this change was not significant ($p = 0.127$).

During the stance phase mean iEMG of SOL [with RE: 12.5 $\pm$ 10.5; without RE: 29.4 $\pm$ 15.0, $t_{(4)} = -3.91$, $p = 0.017$] on the unaffected side significantly decreased with the RE, as compared to without the RE (**Figure 4C**). An increase in iEMG was observed for the TA during the stance phase of the unaffected

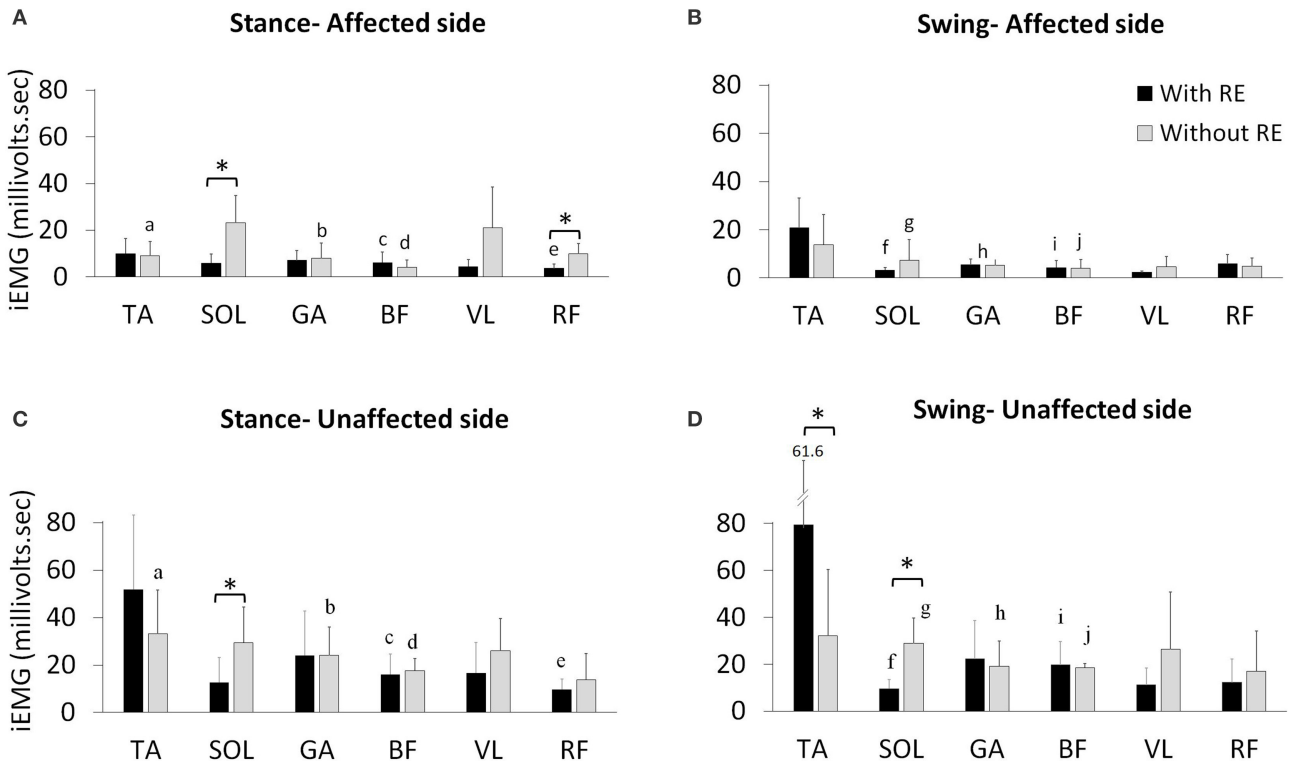

FIGURE 4 | Mean iEMG of the TA, SOL, GA, BF, VL, and RF with and without the RE during the affected **(A)** stance and **(B)** swing phase of gait and the unaffected **(C)** stance and **(D)** swing phase of gait. *Within limb significant differences during stance and swing across gait training environments ($p \leq 0.05$). [a–j]The inter-limb comparisons during the stance and swing phases within the same gait training environment (with or without RE). a. TA affected vs. unaffected without RE during stance ($p \leq 0.05$), b. GA affected vs. unaffected without RE during stance ($p \leq 0.05$), c. BF affected vs. unaffected with RE during stance ($p \leq 0.05$), d. BF affected vs. unaffected without RE during stance ($p \leq 0.05$), e. RF affected vs. unaffected with RE during stance ($p \leq 0.05$), f. SOL affected vs. unaffected with RE during swing ($p \leq 0.05$), g. SOL affected vs. unaffected without RE during swing ($p \leq 0.05$), h. GA affected vs. unaffected without RE during swing ($p \leq 0.05$), i. BF affected vs. unaffected with RE during swing ($p \leq 0.05$), j. BF affected vs. unaffected without RE during swing ($p \leq 0.05$).

side with the RE, as compared to without the RE, but this change was not significant ($p = 0.145$). During the stance phase, no other significant differences were found for the other muscles on the unaffected side with the RE, as compared to without RE. During the swing phase on the unaffected side mean iEMG of the TA [with RE: 79.4 ± 61.6; without RE: 32.0 ± 28.2, $t_{(4)} = -3.00$, $p = 0.039$] significantly increased while the SOL [with RE: 9.5 ± 3.8, without RE: 28.9 ± 10.8, $t_{(4)} = -5.77$, $p = 0.004$; effect size = 2.78, power = 99.39%] significantly decreased with the RE, as compared to without the RE (**Figure 4D**). During the swing phase no significant differences were found for the other muscles on the unaffected side with the RE, as compared to without RE.

Inter-limb iEMG Comparisons Without the RE

During the stance phase mean iEMG of TA [affected side 9.0 ± 6.2, unaffected side 33.1 ± 18.5, $t_{(4)} = -3.84$, $p = 0.018$], GA [affected side 7.9 ± 6.4, unaffected side 24.0 ± 11.8, $t_{(4)} = -2.79$, $p = 0.049$] and BF [affected side 4.1 ± 3.0, unaffected side 17.5 ± 5.2, $t_{(4)} = -9.95$, $p < 0.001$] significantly decreased without the RE on the affected side (**Figures 4A,C**). During the stance phase without the RE, no significant differences were found for the other muscles (**Figures 4A,C**). During the swing phase, mean iEMG of SOL [affected side 7.3 ± 8.4; unaffected side 28.9 ± 10.8, $t_{(4)} = -3.74$, $p = 0.020$], GA [affected side 5.1 ± 5.9, unaffected side 19.2 ± 10.6, $t_{(4)} = -2.81$, $p = 0.048$], and BF [affected side 4.1 ± 3.6, unaffected side 18.5 ± 1.7, $t_{(4)} = -14.28$, $p = 0.002$] significantly decreased without the RE on the affected side (**Figures 4B,D**). During the swing phase without RE, no significant differences were found for the other muscles on the affected as compared to the unaffected side (**Figures 4B,D**).

Inter-limb iEMG Comparisons With the RE

During the stance phase, mean iEMG of BF [affected side 6.1 ± 4.5; unaffected side 16.0 ± 8.4, $t_{(4)} = -4.62$, $p = 0.009$] and RF [affected side 3.6 ± 1.8, unaffected side 9.6 ± 4.4, $t_{(4)} = -3.03$, $p = 0.038$] significantly decreased with RE on the affected side (**Figures 4A,C**). During the swing phase with RE, no significant differences were found for the other muscles on the affected as compared to the unaffected side (**Figures 4A,C**). During the swing phase, mean iEMG of SOL [affected side 3.2 ± 1.2; unaffected side 9.5 ± 3.8, $t_{(4)} = -3.50$, $p = 0.024$] and BF [affected side 4.2 ± 3.0, unaffected side

19.8 ± 9.8, $t_{(4)} = -3.20$, $p = 0.032$] significantly decreased with RE on the affected side (**Figures 4B,D**). During the swing phase with RE, no significant differences were found for the other muscles on the affected as compared to the unaffected side (**Figures 4B,D**).

In summary, the EMG amplitude analysis presented in terms of iEMG shows that the RE preserves the volitional muscle activation during walking. Moreover, while iEMG for TA is amplified, iEMG for SOL and RF is reduced during RE-assisted walking. To comprehensively understand these alterations, muscle activation timings were analyzed using BDSI.

Burst Duration Similarity Index (BDSI)

BDSI scores were calculated for each muscle collected during normalized gait with and without RE and were averaged over all participants. **Figure 5A** shows the mean BDSI scores calculated by comparing muscle activation timings on the affected side with and without RE and **Figure 5B** shows the mean BDSI calculated by comparing muscle activation timings on the unaffected side. Higher BDSI scores (closer to 1) indicate the similarity in muscle activation timings with and without RE. In contrast, lower BDSI scores (closer to 0) in **Figures 5A,B** suggest the dissimilarity in muscle activation timings with and without the RE suggesting the alteration in the muscle activation during the RE assisted walking trials.

The RF muscle on the affected side showed the lowest BDSI score (0.42 ± 0.15) indicating the most dissimilarity in activation of RF muscle between with and without RE conditions (**Figure 5A**). The BF muscle was shown to produce the most similar muscle activations bilaterally (affected side: 0.73 ± 0.19, unaffected side: 0.7 ± 0.17) during both conditions (**Figures 5A,B**). **Figure 5C** shows the mean BDSI scores calculated by comparing muscle activation timings on the affected side to healthy gait muscle activations timings (15) during walking, with and without the RE. Higher BDSI values (closer to 1) suggest a closer match to healthy gait muscle activation timing (**Figures 5C,D**). The mean BDSI scores were higher for the TA (with RE: 0.53 ± 0.27; without RE: 0.42 ± 0.17), VL (with RE: 0.59 ± 0.22; without RE: 0.26 ± 0.16), and RF (with RE: 0.6 ± 0.02; without RE: 0.44 ± 0.09) on the affected side with the RE as compared to without the RE (**Figure 5C**). The mean BDSI scores on the affected side with the RE were significantly higher than without the RE for the VL [$t_{(4)} = 4.6$, $p = 0.010$; effect size = 2.06, power = 92.35%] and RF [$t_{(4)} = 3.79$, $p = 0.019$; effect size = 1.78, power = 83.91%]. These results suggest that utilization of the RE during walking significantly resulted in the temporal adaptations of VL and RF to more closely match healthy muscle activation patterns during gait. The posterior lower extremity muscles, SOL (with RE: 0.61 ± 0.24; without RE: 0.64 ± 0.08), GA (with RE: 0.57 ± 0.07; without RE: 0.66 ± 0.1) and BF (with RE: 0.50 ± 0.29; without RE: 0.64 ± 0.1) on the affected side showed a better match to the healthy muscle activation patterns without the RE when compared to with the RE, though no significant differences were found possibly due to the variability among the participants. On the unaffected side, the mean BDSI scores were higher for the SOL (with RE: 0.64 ± 0.1; without RE: 0.44 ± 0.14), GA (with RE: 0.5 ± 0.14; without RE: 0.46 ± 0.08), VL (with RE: 0.37 ± 0.08; without RE: 0.31 ± 0.2) and RF (with RE: 0.52 ± 0.1; without RE: 0.48 ± 0.11) with the RE when compared to walking without the RE, however, these differences were not significant for GA ($p = 0.671$), VL ($p = 0.495$), RF ($p = 0.551$), and near-significant for SOL ($p = 0.054$).

DISCUSSION

This investigation presented a traditional feature (iEMG) and a novel temporal feature (BDSI) of EMG data collected during RE-assisted walking in acute stroke. RE-assisted walking is a collective work of instrumentation power and varied levels of effort from a participant. Assessing these different levels of effort in terms of electrophysiological responses (via EMG) is essential for understanding the role of a user as well as the RE during gait training. In the acute phase post-stroke when the brain is highly plastic, these individual roles and the interaction between the user and the RE are essential in developing and evaluating the advanced training paradigms for gait rehabilitation. Further, the features extracted from the EMG data such as iEMG and BDSI allow the assessment of these individual roles and interactions during RE-assisted gait training. These features also help to understand if the neuromuscular adaptations occurring due to the RE are in accordance with the normative muscle activation patterns.

Significance of iEMG and BDSI Techniques

In this investigation, iEMG is presented as the amplitude measure and changes in iEMG may indicate variations in the levels of effort for a single muscle (15). iEMG, unlike root-mean-squared (RMS) or mean amplitudes, represents the neural drive to the muscle over a specified time. When iEMG is presented over an unspecified time interval it would simply represent the average over that unspecified time. In a cyclic activity such as gait, EMG profiles show characteristic patterns during different phases of gait. Therefore, utilization of iEMG for EMG quantification during gait phases may be more appropriate as these phases occur during a certain time duration in a gait cycle. Along with the amplitude parameter, we present a novel timing parameter, BDSI (18) to assess the temporal changes in muscle activation during gait, with and without the RE. Previous research has demonstrated the applicability of the BDSI algorithm to show a training effect on the TA muscle during hemiplegic gait post foot drop stimulator utilization (18).

TKEO (21, 22) based EMG processing was performed to improve the accuracy of onset detection and resultant BDSI scores on five additional lower extremity muscles (SOL, GA, BF, VL, and RF) including the TA. Although our onset detection component relies on a traditional approach of threshold detection (23), our BDSI calculation provides a novel way to compare EMG onset timings across many conditions. Since the BDSI calculation is performed on binary sequences (0: no activation, 1: activation), it not only allows for intra-limb (with and without RE), and inter-limb (affected vs.

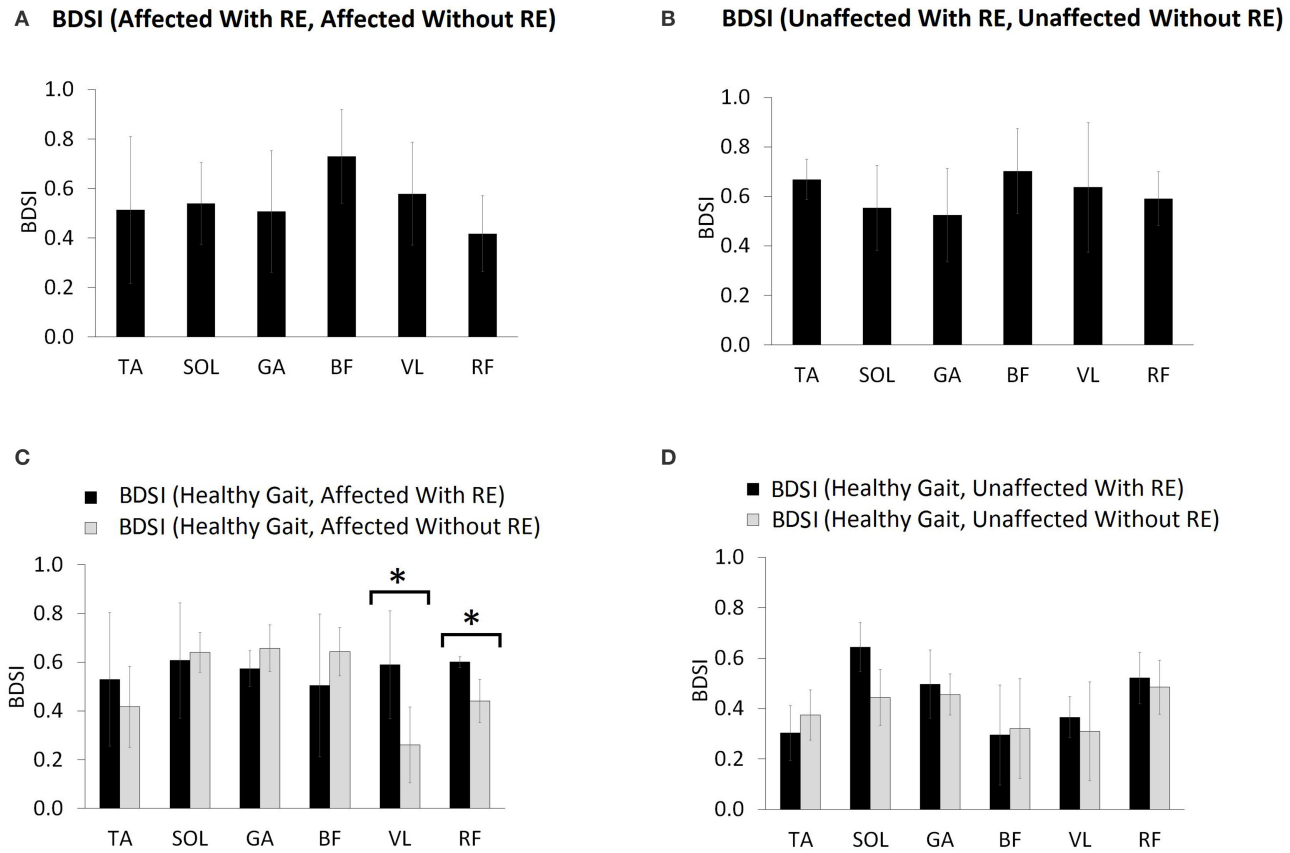

FIGURE 5 | Mean BDSI calculated using Equation (2), by comparing **(A)** affected side with and without RE, **(B)** unaffected side with and without RE, **(C)** affected side compared to normative healthy gait muscle activation timing (15), with and without RE and **(D)** unaffected side compared to healthy gait with and without RE. The titles (for **A,B**) and the legends (for **C**,**D**) show the exact arguments used in the Equation (1) for computing BDSI. *$p \leq 0.05$.

unaffected) comparisons but also provides the opportunity to compare to muscle activation timing patterns during healthy gait (15).

Neuromechanical Responses in RE Environment

Amplitude Adaptations Using iEMG

We hypothesized that the RE gait training environment will preserve the volitional neuromuscular activations in acute stroke. iEMG analyses showed that muscle activation levels during RE gait training environment were maintained, reduced, as well as, enhanced, and there was no single common pattern associated with all tested muscles. This may suggest that the RE did not completely override the volitional muscle activations and the residual neuromuscular function post stroke was preserved and participants were actively engaged during the gait training. Although the inter-limb differences in EMG patterns post hemiplegia have been widely reported in the literature (24), they are not well established for acute stroke in a RE gait training environment.

In the current investigation we began to evaluate the effect of the RE on inter-limb activation. The iEMG analyses showed that for individuals post stroke in the RE environment the TA (during stance) and the GA (during stance and swing) muscles were no longer significantly different between the affected and unaffected side. This change could be due to the variability (shown by higher standard deviations) among the subjects (**Figure 4**) and may not be due to the reduced inter-limb differences in iEMG values for both muscles. There were increased TA activations bilaterally with the RE which may be due to several reasons: (1) the RE may promote the TA activation by providing a controlled trajectory and stable support during swing, allowing the muscle to activate in a stable environment; (2) TA may try to perform the ankle dorsiflexion against the foot strap during the swing phase, resulting in increased activation. There were significant reductions in iEMG values for SOL (stance), RF (stance) on the affected side with RE. This response seemed to be consistent for 4 out of 5 participants (shown as amplitude adaptations in **Figure 6A** for P2, P3, P4, and P5). During the stance phase with the RE, the significant decrease in the activation of SOL was observed potentially due to the quasi-static position of the sprung ankle joint at ∼90°. It has also been reported that SOL muscle activation decreases when an external device is utilized such as an ankle foot orthotic (AFO) (25). In the presence

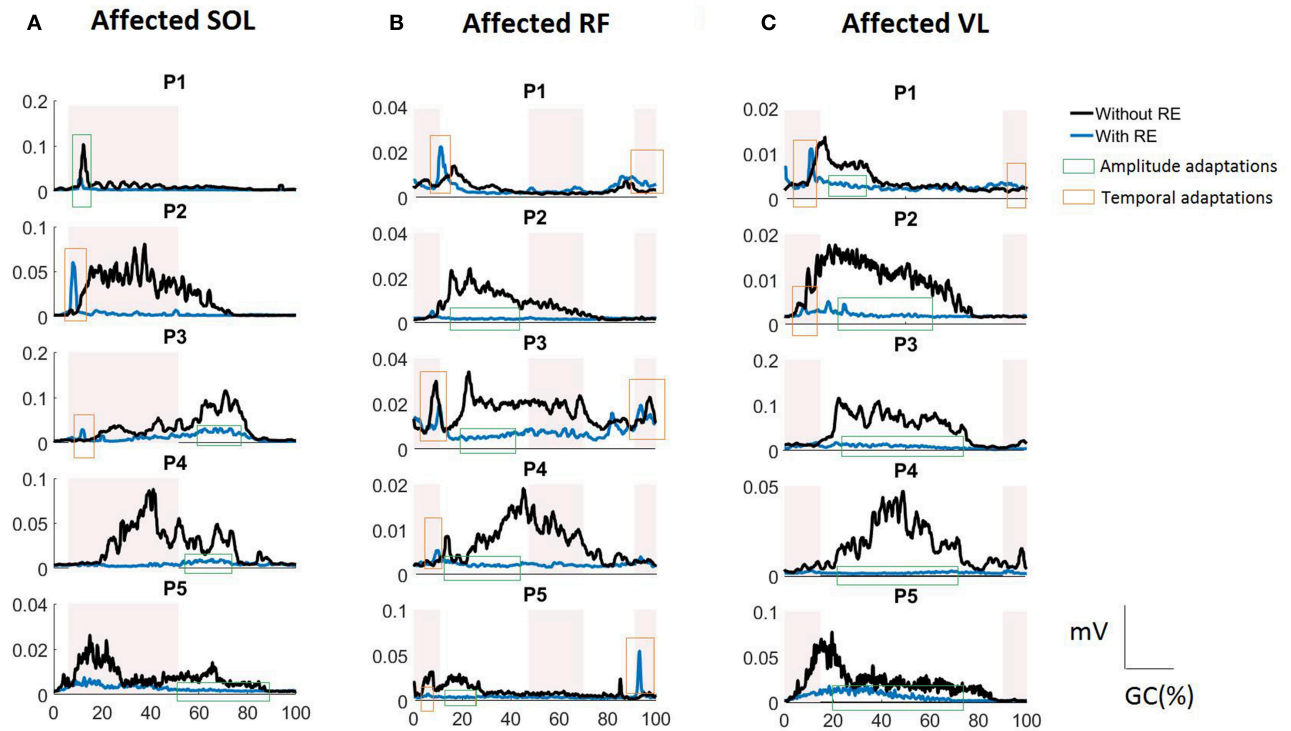

FIGURE 6 | RMS EMG profiles for **(A)** SOL, **(B)** RF, and **(C)** VL of the affected side in the RE gait training environment for each study participant (P1 to P5). The shaded rectangular areas represent the periods of healthy muscle activations. Amplitude adaptations (shown as a green rectangle) represent the events where excessive muscle activation was reduced in the RE environment. Temporal adaptations (shown as a red rectangle) represent the events where the muscle activation was correctly time-shifted to the correct phase of the gait cycle in the RE environment.

of RE, the need to plantar flex against the ground for joint stabilization is reduced due to the weight bearing provided by RE, thus resulting in reduction of SOL activation, bilaterally. During the stance phase with the RE, the significant decrease in RF activation may be related to the reduction in "excessive" hip flexion at initial contact due to controlled trajectory guidance provided by RE. This was particularly apparent in affected RF profiles of participants P2, P3, and P4 (**Figure 6B**) where RF activations were reduced during 12–46% of a GC and 71–90% of a GC. Similar amplitude adaptations were observed for affected VL in the RE environment for all the participants, suggesting the consistency of these amplitude adaptation across the group.

Overall, iEMG analyses show the presence of active neuromuscular participation which may be essential for optimizing the rehabilitation outcomes during highly plastic acute phase post stroke. Ensuring that these adaptations are in accordance with the healthy muscle activation patterns is essential for effective gait training.

Temporal Adaptations Using BDSI

Our novel feature, BDSI allowed for this assessment with hypothesis that the RE gait training environment will alter the activation timings of lower extremity muscles to match the normative healthy gait muscle activation patterns. BDSI analysis showed that, in terms of activation timings, RF and VL on the affected side were significantly altered to match the normative muscle activation patterns in the RE training environment. EMG profiles showed that RF and VL, the muscles predominantly used for knee flexion/extension during walking had sustained contractions without the RE (**Figures 6B,C**) potentially due to the disrupted loading mechanisms on the affected side. While the amplitudes were higher for the RF and VL in the traditional gait training environment, BDSI analysis showed that these activations were characterized by inaccurate timings, compared to healthy gait (15). This was particularly apparent for P2, P3, and P4 as shown in **Figures 6B,C** (see the amplitude adaptations notations). In the RE environment the VL and RF had reduced activations (shown in **Figures 6B,C**) during the "off" periods (compared to healthy gait cycle) but preserved volitional activation during the "on" periods (shown as temporal adaptations in **Figures 6B,C**), closely matching the overall healthy activation timings during gait as evidenced by the significantly higher BDSI scores as a group (**Figure 5C**). These modifications could be due to the "powered" assistance provided during the loading response and knee extension during terminal swing or due to the possibility that the RE is programmed to follow a pre-determined trajectory that may not facilitate full knee extension and flexion. As surface EMGs were used in this investigation, RF may have recorded the crosstalk from vastii during loading responses (15). Hence, it may be difficult to identify the exact

alterations occurring in RF muscle activation as a result of hemiplegia post stroke or due to the presence of RE. Apart from providing quantifiable comparisons for muscle activation timings with healthy muscle activation timings, BDSI feature also allowed for intra-limb comparisons with different gait training environments.

Inter-subject Variability

Although there were several improvements seen in terms of iEMG (bilateral VL, unaffected TA during stance) and BDSI (affected TA and SOL, GA, VL, RF on the unaffected side), these changes were not significant. This may be due to the variability in the data among the participants. In acute stroke, factors such as time since stroke and severity of the stroke can contribute to varied levels of residual function as well as responses to the RE intervention. All participants were currently admitted and participating in gait training at the same inpatient rehabilitation facility, and the motor FIM for all participants at admission was comparable (range from 20 to 31 points) indicating a similar level of motor impairment at admission. The 13 FIM motor items range from 13–91 points and rates an individual's ability to perform motor activities of daily living independently (26). All participants improved their FIM motor score from admission to discharge with an average improvement of 29 ± 11 points, the minimal clinically important difference (MCID) for the motor FIM is 17 points. While all participants had similar motor FIM scores at admission they were at different stages in their rehabilitation and recovery and time post stroke varied from 14 to 94 days and their length of stay at the time of gait testing varied from 10 to 49 days. Four participants were admitted to inpatient rehabilitation within 3–6 days post stroke, while one participant was not admitted until 45 days post stroke and this participant had the lowest motor FIM score at admission. All participants were able to successfully use the RE device with the assistance of a physical therapist as well as participate in inpatient gait rehabilitation. It is important to note that each participant progressed at an independent rate and may have been at a different timepoints in their recovery which will also have an impact on the EMG activation patterns during dynamic movements.

Limitations and Future Considerations

This investigation presented an EMG technique and was not intended to comprehensively compare the efficacy of RE to traditional gait training and therefore only a single session was evaluated. Although we were able to demonstrate changes in activation of lower extremity muscles with the use of RE in acute stroke, our interpretations of the RE as a rehabilitation intervention is limited by the small sample size. Additionally, there may be variability due to the different levels of assistance provided by RE and physical therapists. Future work will include the kinematic indices which could be utilized to further understand the neuromuscular adaptations resulting due to RE in a larger sample.

CONCLUSION

The EMG amplitude and timing analysis were presented to assess the neuromuscular adaptations resulting in lower extremities muscles during RE assisted hemiplegic gait post acute stroke. The RE assisted gait training environment allowed participants with hemiplegia post acute stroke to preserve their volitional neuromuscular activations during gait. The RE promoted activations of the VL and RF on the affected side to more closely match the activation patterns of healthy gait. The purpose of this investigation was to present an EMG technique and not to comprehensively evaluate the efficacy of RE over traditional standard of care. Instead, we demonstrated that patients were actively contracting and participated in both environments, therefore both environments represent potentially beneficial modalities in gait rehabilitation. Accurate understanding of the electrophysiological responses in individuals with stroke while walking is essential to develop and measure advanced training paradigms for gait rehabilitation. Preliminary EMG data suggests that the RE provides an effective gait training environment for acute stroke rehabilitation. Further, the combination of iEMG and BDSI techniques provides a comprehensive set of assessments to measure changes in muscle activation levels, excitation and inhibition during walking, with and without RE conditions in individuals with hemiplegia post acute stroke.

ETHICS STATEMENT

This study was carried out in accordance with the recommendations of Kessler Foundation Institutional Review Board with written informed consent from all subjects. All subjects gave written informed consent in accordance with the Declaration of Helsinki. The protocol was approved by the Kessler Foundation Institutional Review Board.

AUTHOR CONTRIBUTIONS

KJN: contributed to the conception and design of the investigation; KJN, RP and AR: contributed towards data acquisition; AR: initial post-processing of the motion analysis data; RP and GA: performed the EMG analysis; All authors contributed to the interpretation of the data, manuscript writing and revision.

ACKNOWLEDGMENTS

This research was funded by Kessler Foundation (West Orange NJ, USA). The authors would like to thank Kessler Institute for Rehabilitation (West Orange and Saddle Brook, NJ, USA) for their assistance in this investigation.

REFERENCES

1. Krebs HI, Volpe B, Hogan N. A working model of stroke recovery from rehabilitation robotics practitioners. *J Neuroeng Rehabil.* (2009) 6:6. doi: 10.1186/1743-0003-6-6
2. Esquenazi A, Maler IC, Schuler TA, Beer SM, Borggraefe I, Campen K, et al. Clinical application of robotics and technology in the restoration of walking. In: Reinkensmeyer D, Dietz V, editors. *Neurorehabilitation Technology*. Cham: Springer (2016). p. 223–48.
3. Mozaffarian D, Benjamin EJ, Go AS, Arnett DK, Blaha MJ, Cushman M, et al. Heart disease and stroke statistics—2015 update: a report from the American Heart Association. *Circulation* (2015) 131:e29–322. doi: 10.1161/CIR.0000000000000152
4. Byl NN, Abrams GM, Pitsch E, Fedulow I, Kim H, Simkins M, et al. Chronic stroke survivors achieve comparable outcomes following virtual task specific repetitive training guided by a wearable robotic orthosis (UL-EXO7) and actual task specific repetitive training guided by a physical therapist. *J Hand Ther.* (2013) 26:343–52; quiz 352. doi: 10.1016/j.jht.2013.06.001
5. Morone G, Fusco A, Di Capua P, Coiro P, Pratesi L. Walking training with foot drop stimulator controlled by a tilt sensor to improve walking outcomes: a randomized controlled pilot study in patients with stroke in subacute phase. *Stroke Res Treat.* (2012) 2012:523564. doi: 10.1155/2012/523564
6. Patterson KK, Gage WH, Brooks D, Black SE, McIlroy WE. Evaluation of gait symmetry after stroke: a comparison of current methods and recommendations for standardization. *Gait Posture* (2010) 31:241–6. doi: 10.1016/j.gaitpost.2009.10.014
7. Patterson KK, Parafianowicz I, Danells CJ, Closson V, Verrier MC, Staines WR, et al. Gait asymmetry in community-ambulating stroke survivors. *Arch Phys Med Rehabil.* (2008) 89:304–10. doi: 10.1016/j.apmr.2007.08.142
8. Dobkin BH. Training and exercise to drive poststroke recovery. *Nat Rev Neurol.* (2008) 4:76. doi: 10.1038/ncpneuro0709
9. Dobkin BH. Strategies for stroke rehabilitation. *Lancet Neurol.* (2004) 3:528–36. doi: 10.1016/S1474-4422(04)00851-8
10. Hornby TG, Campbell DD, Kahn JH, Demott T, Moore JL, Roth HR. Enhanced gait-related improvements after therapist-versus robotic-assisted locomotor training in subjects with chronic stroke: a randomized controlled study. *Stroke* (2008) 39:1786–92. doi: 10.1161/STROKEAHA.107.504779
11. Russo A, Perret MA, Endersby K, Kesten AG, King MA, Chervin K, et al. Utilization of a robotic exoskeleton to provide increased mass practice for gait training and its impact on discharge destination for individuals with acute stroke. *Stroke* (2016) 47:ATP149.
12. Androwis GJ, Nolan KJ. Evaluation of a robotic exoskeleton for gait training in acute stroke: A case study. In: González-Vargas J, Ibáñez J, Contreras-Vidal JL, van der Kooij H, Pons JL, editors. *Wearable Robotics: Challenges and Trends, Biosystems and Biorobotics*. Vol. 16 (Cham: Springer) (2017). p. 9–13. doi: 10.1007/978-3-319-46532-6
13. Daly JJ, Ruff RL. Construction of efficacious gait and upper limb functional interventions based on brain plasticity evidence and model-based measures for stroke patients. *Sci World J.* (2007) 7:2031–45. doi: 10.1100/tsw.2007.299
14. De Luca CJ. The use of surface electromyography in biomechanics. *J Appl Biomech.* (1997) 13:135–63. doi: 10.1123/jab.13.2.135
15. Perry J, Burnfield JM. *Gait Analysis: Normal and Pathological Function.* 2nd ed. Thorofare, NJ: Slack Inc. (2010).
16. Hibbs A, Thompson K, French D, Hodgson D, Spears I. Peak and average rectified EMG measures: which method of data reduction should be used for assessing core training exercises? *J Electromyogr Kinesiol.* (2011) 21:102–11. doi: 10.1016/j.jelekin.2010.06.001
17. Ekstrom RA, Soderberg GL, Donatelli RA. Normalization procedures using maximum voluntary isometric contractions for the serratus anterior and trapezius muscles during surface EMG analysis. *J Electromyogr Kinesiol.* (2005) 15:418–28. doi: 10.1016/j.jelekin.2004.09.006
18. Pilkar R, Yarossi M, Nolan KJ. EMG of the tibialis anterior demonstrates a training effect after utilization of a foot drop stimulator. *Neurorehabilitation* (2014) 35:299–305. doi: 10.3233/NRE-141126
19. Merletti R, Parker PA. *Electromyography: Physiology, Engineering, and Non-Invasive Applications.* Vol. 11. Hoboken, NJ: IEEE Press, John Wiley & Sons, Inc. (2004). doi: 10.1002/0471678384
20. International Society of Electrophysiological Kinesiology. *Ad Hoc Committee Units, Terms and Standards in the Reporting of EMG Research*, (Goteborg) (1980).
21. Li X, Zhou P, Aruin A. Teager–Kaiser energy operation of surface EMG improves muscle activity onset detection. *Ann Biomed Eng.* (2007) 35:1532–8. doi: 10.1007/s10439-007-9320-z
22. Solnik S, Rider P, Steinweg K, DeVita P, Hortobagyi T. Teager–Kaiser energy operator signal conditioning improves EMG onset detection. *Eur J Appl Physiol.* (2010) 110:489–98. doi: 10.1007/s00421-010-1521-8
23. Hodges PW, Bui BH. A comparison of computer-based methods for the determination of onset of muscle contraction using electromyography. *Electroencephalogr Clin Neurophysiol.* (1996) 101:511–9. doi: 10.1016/S0921-884X(96)95190-5
24. Woolley SM. Characteristics of gait in hemiplegia. *Top Stroke Rehabil.* (2001) 7:1–18. doi: 10.1310/JB16-V04F-JAL5-H1UV
25. Arch ES, Stanhope SJ, Higginson JS. Passive-dynamic ankle-foot orthosis replicates soleus but not gastrocnemius muscle function during stance in gait: insights for orthosis prescription. *Prosthet Orthot Int.* (2016) 40:606–16. doi: 10.1177/0309364615592693
26. Imada Y, Tokunaga M, Fukunaga K, Sannomiya K, Inoue R, Hamasaki H, et al. Relationship between cognitive FIM score and motor FIM gain in patients with stroke in a Kaifukuki rehabilitation ward. *Jpn J Compr Rehabil Sci.* (2014) 5:12–8. doi: 10.11336/jjcrs.5.12

Conflict of Interest Statement: The authors declare that the research was conducted in the absence of any commercial or financial relationships that could be construed as a potential conflict of interest.

frontiers in Neurology

ORIGINAL RESEARCH
published: 01 March 2018
doi: 10.3389/fneur.2018.00084

Involuntary Neuromuscular Coupling between the Thumb and Finger of Stroke Survivors during Dynamic Movement

Christopher L. Jones[1] and Derek G. Kamper[2]*

[1] HD LifeSciences, Stoneham, MA, United States, [2] UNC/NC State Joint Department of Biomedical Engineering, Rehabilitation Engineering Core, Raleigh, NC, United States

Finger–thumb coordination is crucial to manual dexterity but remains incompletely understood, particularly following neurological injury such as stroke. While being controlled independently, the index finger and thumb especially must work in concert to perform a variety of tasks requiring lateral or palmar pinch. The impact of stroke on this functionally critical sensorimotor control during dynamic tasks has been largely unexplored. In this study, we explored finger–thumb coupling during close–open pinching motions in stroke survivors with chronic hemiparesis. Two types of perturbations were applied randomly to the index with a novel Cable-Actuated Finger Exoskeleton: a sudden joint acceleration stretching muscle groups of the index finger and a sudden increase in impedance in selected index finger joint(s). Electromyographic signals for specific thumb and index finger muscles, thumb tip trajectory, and index finger joint angles were recorded during each trial. Joint angle perturbations invoked reflex responses in the flexor digitorum superficialis (FDS), first dorsal interossei (FDI), and extensor digitorum communis muscles of the index finger and heteronymous reflex responses in flexor pollicis brevis of the thumb ($p < 0.017$). Phase of movement played a role as a faster peak reflex response was observed in FDI during opening than during closing ($p < 0.002$) and direction of perturbations resulted in shorter reflex times for FDS and FDI ($p < 0.012$) for extension perturbations. Surprisingly, when index finger joint impedance was suddenly increased, thumb tip movement was substantially increased, from 2 to 10 cm ($p < 0.001$). A greater effect was seen during the opening phase ($p < 0.044$). Thus, involuntary finger–thumb coupling was present during dynamic movement, with perturbation of the index finger impacting thumb activity. The degree of coupling modulated with the phase of motion. These findings reveal a potential mechanism for direct intervention to improve poststroke hand mobility and provide insight on prospective neurologically oriented therapies.

Keywords: exoskeleton, motor control, coupling, reflex, hand, robot, rehabilitation

OPEN ACCESS

Edited by:
Xiaogang Hu, University of North Carolina at Chapel Hill, United States

Reviewed by:
Sheng Li, University of Texas Health Science Center at Houston, United States
Jun Yao, Northwestern University, United States
Jongsang Son, Shirley Ryan AbilityLab, United States

****Correspondence:***
Christopher L. Jones
christopherljones@gmail.com

Specialty section:
This article was submitted to Stroke, a section of the journal Frontiers in Neurology

Received: *29 June 2017*
Accepted: *06 February 2018*
Published: *01 March 2018*

Citation:
Jones CL and Kamper DG (2018) Involuntary Neuromuscular Coupling between the Thumb and Finger of Stroke Survivors during Dynamic Movement. Front. Neurol. 9:84. doi: 10.3389/fneur.2018.00084

INTRODUCTION

The dexterity of the digits of the hand is one of the hallmarks of human motor control and a central factor in the evolution of our species. The highly individuated movement enables complex and dynamic interaction with the environment, such as for manipulating tools and objects. Motion (1) and force (2) independence are especially great in the index finger and thumb, the two most functionally important digits.

Yet, coordination between these digits is critical for proper execution of a number of important tasks. During object manipulation through pinch, for example, the thumb and index fingertip forces must create equal and oppositely directed forces to prevent slip of the object. Alteration in the force created by one digit, such as might arise due to perturbations or changing conditions such as sweat, requires immediate compensation by the other digit.

The finger and thumb have multiple degrees-of-freedom (DOF) available which can be exploited to match the other digit's movement; this redundancy, however, contributes substantially to variability in movement (3). By introducing coupling between these DOF, variability in motor output can be reduced (4), thereby improving performance of the digits in a coordinated task. Accordingly, research has shown evidence for neural coupling between neuromuscular units for different digits in the human hand. For example, EMG–EMG coherence was observed between pairs of finger and thumb muscles during a pinching task (5) and during a three-digit grasping paradigm (6).

In stroke survivors, unfortunately, coordination between finger and thumb may be disrupted. For example, we have observed strong coupling between thumb and finger flexors when stretch is applied to the nominally passive finger flexors (7). We have also seen this aberrational finger flexor-thumb flexor coupling during voluntary isometric task performance (7).

Study of finger–thumb coupling during dynamic tasks, however, has been limited. While perturbation techniques are often used to study motor control in the arm (8), this methodology is more challenging in the hand due to the many DOF present within a relatively small volume. Cole and Abbs examined response to an extension perturbation of the thumb in neurologically intact individuals (9, 10), but thumb motion was limited to a single joint and perturbations were applied to only one thumb joint. Schettino et al. recently examined perturbation of the index finger during a reach-to-grasp task, but kinetic perturbations only were applied and muscle activation patterns were not addressed (11).

Even fewer such studies have been performed with stroke survivors. Thus, for this study, we examined thumb-finger coupling during a natural dynamic movement in stroke survivors. Using a novel actuated finger exoskeleton, we introduced precise perturbations to the index finger during a voluntary palmar pinch-open task. First, we investigated possible reflex coupling at the spinal level by applying rapid rotation of the metacarpophalangeal (MCP) joint to evoke a stretch reflex in the finger muscles. We hypothesized that this would elicit heteronymous reflexes in the unperturbed thumb motoneurons with a similar delay. We further hypothesized that this coupling would be stronger when perturbations were applied during the closing phase of a pinch movement than when applied during digit opening. Next, we examined possible hierarchical control during the pinching task by perturbing the index finger trajectory. We hypothesized that perturbations which altered the index finger trajectory would lead to corresponding alterations in the pathway of the thumb to reduce task error. Furthermore, we expected the effect on thumb movement to be greater when the index finger was perturbed during the closing phase of pinch when coupling of movement was most critical.

MATERIALS AND METHODS

The Cable-Actuated Finger Exoskeleton (CAFE) (12, 13) was employed to perturb joints of the index finger. This rigid exoskeleton structure has joints that are aligned with the flexion/extension axis of each of the three index finger joints: metacarpophalangeal (MCP), proximal interphalangeal (PIP), and distal interphalangeal (DIP). The structure runs along the radial side of the finger and couples to the finger through bars contacting the dorsal and palmar sides of each finger segment. Rotation of the exoskeleton joint, thus, produces equivalent rotation of the anatomical joint. Cables running from electric servomotors located proximal to the wrist connect to gears located at each joint (**Figure 1**). Winding of the cable about a spool connected to the motor thereby produces joint rotation. One motor produces flexion and another produces extension at each joint, for a total of six motors. The cables run through a series of pulleys before terminating at the appropriate joint. By placing the gearing directly at the joint, the relative influence of cable force at a joint other than the targeted joint is reduced. Further compensation is achieved through the controller. Precise, independent control of each joint of the index finger can be achieved over a wide range of velocities and torques.

Participants

A convenience sample of eight adult individuals with chronic hemiparesis resulting from a single stroke incurred at least 6 months prior, with a mean (±SD) age of 63 (±9) years, participated in the study. Subjects were selected based on having moderate hand impairment as characterized by a rating of

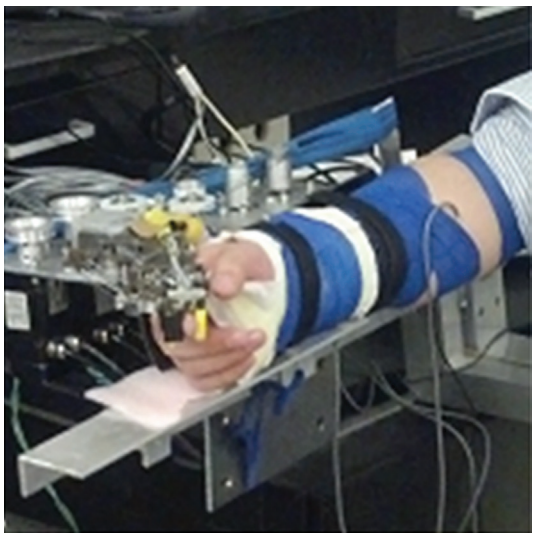

FIGURE 1 | Finger connected to Cable-Actuated Finger Exoskeleton device for performing the experiments. Motors are located off the splinted hand and wrist such that they can be supported by an external structure, the TA-WREX (21, 22).

Stage of Hand 4 or 5 on the Chedoke-McMaster Stroke Assessment (14). Subjects at these levels typically exhibit substantial gross finger extension, but have difficulty producing individuated finger movements. A significant spastic reflex in the finger flexors has been detected in stroke survivors with this level of impairment (15). The group consisted of two females and six males. All participants were right-hand dominant. This investigation was conducted at the Rehabilitation Institute of Chicago and all participants provided written consent in accordance with processes approved by the Northwestern University Institutional Review Board.

Protocol

Each subject participated in two sessions. During the initial session, we captured the kinematics of the subject's natural pinching motion while the wrist was held in a fixed, neutral posture. Beginning with the finger and thumb positioned in an open-handed posture by the device, subjects were asked to create a palmar pinching motion with the index finger and thumb (closing phase). Once the thumb and index finger made approximate contact, the subject was instructed to immediately begin to open the digits to return them to the original posture (opening phase). Precise contact position and movement duration was subject-specific to allow completion of movement and a naturally paced trajectory, although participants were required to complete the full close–open motion within 2 s for a minimum frequency of 0.5 Hz. All movements were initiated with audible cues to first prepare to move and then to initiate movement. The kinematics of the index finger during the movement were recorded using an external camera system (Optotrak, 3020, 3010, Northern Digital, Inc., Waterloo, ON, Canada) employing infrared markers at each of the finger joints (MCP, PIP, DIP) and fingertip. Marker locations were sampled at a rate of 100 Hz. We subsequently used these data to compute the joint angles that served as the desired motion trajectories in the second session.

During the second session, subjects participated in two sets of experimental conditions, each consisting of a within-subject repeated measures experimental design to examine finger–thumb interactions during voluntary movement. Digit kinematics and muscle activity were measured for both sets of experimental conditions. Thumb tip location was captured with the Optotrak camera system, while index finger joint angles were recorded by the CAFE at 1 kHz. Activation of specified finger and thumb muscles, selected for their participation in finger–thumb pinch (16–20) and accessibility for electrode placement, were recorded with EMG electrodes. Surface electrodes (Delsys, Inc., Boston, MA, USA) were placed over flexor digitorum superficialis (FDS), extensor digitorum communis (EDC), and first dorsal interossei (FDI) of the index finger and over flexor pollicis brevis (FPB) and abductor pollicis brevis (APB) of the thumb. EMG signals were sampled at 1 kHz. Data collection is synchronized at time of collection between the Optotrak and EMG DAQ simultaneously *via* a shared electrical signal.

With the subject seated comfortably, we coupled their index finger to the CAFE device. We then splinted the subject's wrist and forearm to a platform of an external device (TA-WREX) (21, 22) to support the weight of the arm and the exoskeleton motors and fix wrist flexion/extension and abduction/adduction.

Joint Angular Perturbation

To examine index finger–thumb reflexive coupling during goal-directed palmar pinching, we instructed subjects to create the same pinching motion as they did during the first session. In this session, however, the CAFE moved according to the joint angle trajectories recorded during the prior session. Subjects performed isokinetic movements with the index finger and were instructed to push against the device in the direction of motion during movement, resulting in an average muscle force generation of roughly 10% of maximum voluntary contraction (MVC) throughout both the closing and opening phases. This baseline muscle activation increases the probability of generating a reflex in response to applied muscle stretch (23). To determine the MVC, a series of three alternating flexion and extension contractions are performed prior to trials, the peak EMG values of which are compared to the peak EMG envelope following reflex response; the greatest of which are taken as the MVC value for the respective muscle.

During random trials, position-controlled angular perturbations of approximately 40° at 600°/s were applied to the MCP joint of the index finger to elicit a stretch reflex in certain index finger muscles. These perturbations were applied roughly halfway through either the opening or closing movement phase (±10° variation), in either the flexion (stretching MCP extensors) or extension (stretching MCP flexors) direction (**Figure 2A**). Ten trials were performed for each phase-direction perturbation condition (closing-extension, closing-flexion, opening-extension, and opening-flexion), along with 20 no-perturbation control trials, for a total of 60 trials. A series of at least 10 control trials were presented before any perturbation was introduced to allow the participant to become familiarized with the system. Additionally, we exposed subjects to the movement of the device to test the fit and the accuracy of the movement profile, as well as to build comfort with the system, prior to the beginning of the first control trials.

Joint Impedance Perturbation

In the second set of trials, we used the CAFE to disrupt the movement of the finger during natural palmar pinching motions. Subjects created the same close–open pinching movement as in the previous experiment. However, in this experiment, the exoskeleton minimizes contact force between itself and the user, thus reducing the muscle activation required to move and not also preventing the exoskeleton from assisting in the movement.

During certain trials, the CAFE applied an impedance perturbation to the MCP or PIP + DIP (perturbed together) joints of the index finger. The impedance perturbation consisted of an abrupt transition to a very stiff joint, essentially locking movement of the joint(s) of the device for 750 ms (**Figure 2B**). In this manner, we could alter the index finger trajectory without displacing the joints (which could evoke a stretch reflex). Perturbations were applied approximately halfway through each phase of movement (±10° variation). Thus, there were

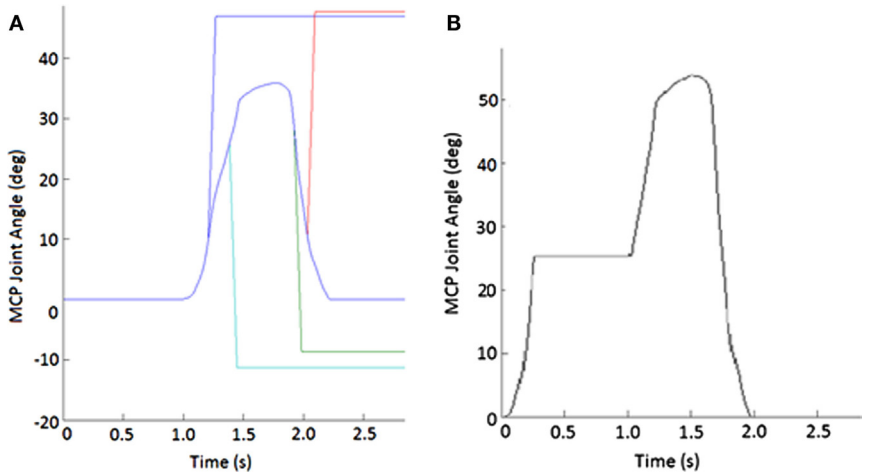

FIGURE 2 | Example of perturbations. **(A)** Displacement applied to metacarpophalangeal (MCP) joint to create stretch of finger muscles. Blue line shows unperturbed subject-specific trajectory while the other lines show flexion (increasing angle) or extension (decreasing joint angle) or extension imposed during either the closing or opening phase of movement. **(B)** Impedance of MCP joint suddenly increased for 750 ms during the closing phase of the pinching task.

four phase-joint perturbation combinations: MCP perturbation during closing (closing-MCP), IP perturbation during closing (closing-IP), MCP perturbation during opening (opening-MCP), and IP perturbation during opening (opening-IP). Each subject performed 10 trials of each perturbation condition with 20 no-perturbation control trials, presented in random order, for a total of 60 trials. A series of at least 10 control trials was presented before any perturbation was introduced, and rest was provided as needed.

Data Analysis

EMG signals were analyzed to quantify the reflex response for the experiment involving rapid muscle stretch. Thumb motion data from the Optotrack were the primary outcome measure for the experiment involving the sudden change in exoskeleton joint impedance.

Stretch Reflex

To find the shorter-latency reflex responses to the perturbations, we examined the EMG envelope during the 150-ms window following the onset of perturbation. This time span captures the reflexive, but not voluntary muscle activation in response to perturbation. EMG of each muscle was rectified and then low-pass filtered forwards and backwards through a fifth-order Butterworth filter with a cutoff frequency of 40 Hz to create the EMG envelope. This envelope was then normalized by the maximum envelope value across all trials and the initial MVCs for the corresponding muscle and subject.

From these absolute measures, perturbed and unperturbed EMG, we created two outcome measures: A-EMG, the absolute value of each normalized EMG signal and D-EMG, the difference between the EMG during the perturbed trial and the unperturbed trials. In order to examine whether the stretch produced reflex activity, we compared peak A-EMG with and without perturbation for each muscle by employing multiple analysis of covariance (MANCOVA). Due to violations in assumptions of normality, we used the non-parametric Mann–Whitney *U* test to look at the impact of movement phase (closing/opening) and stretch direction (extension/flexion) on D-EMG. We examined the impact of phase and direction on time to peak reflex EMG response using MANCOVA. Individual *post hoc* ANOVA are performed to quantify individual effects where appropriate.

Impedance Perturbation

For the impedance perturbation experiment, we examined thumb tip kinematics, recorded with the Optotrak system. We first examined the aperture during the movement and then focused on the time window covering the period from the start of index finger perturbation until the time at which the unperturbed phase ended. Specifically, we computed the normal distance between fingertip and thumb tip Optotrak markers, computing the total aperture during movement.

We then isolated the thumb movement from the exoskeleton-controlled finger movement by computing the Euclidian norm of the thumb tip position, zeroed at the angle and the time of perturbation (positive indicates closing and negative indicates opening). We then compared the thumb trajectory for each individual trial to the average trajectory of the unperturbed trials for the same subject by computing the root mean squared error (RMSE) between the two. We employed ANOVA to examine the effects of condition (perturbed/unperturbed), movement phase (closing/opening), and joint (MCP/IP) on RMSE.

RESULTS

Subjects performed pinching movements in the CAFE as instructed for both the reflex and impedance experiments. All subjects completed both sets of experiments.

Stretch Perturbation

While subjects made active, volitional pinching movements, stretch perturbations produced strong reflex activity. Post-perturbation

peak EMG was greater than the time-matched EMG for unperturbed trials for every muscle ($p < 0.017$) with the exception of APB. A-EMG (absolute magnitude) following perturbation was typically greater than in the unperturbed case by 10–15% of MVC. Thus, stretch of a given set of finger muscles produced reflex responses in all observed index finger muscles, as well as in the thumb flexor FPB (**Figure 3**). However, no such reflex response was observed in APB (**Figure 3**).

The delay between the initiation of the perturbation and the time to peak reflex EMG (TR) was significantly dependent upon both movement phase (closing or opening) and perturbation direction (flexion or extension), but the size of the reflex response (D-EMG) did not vary significantly with either. Moving the MCP into extension (thereby lengthening the finger flexor muscles), resulted in a shorter time to peak reflex for both FDS and FDI ($p < 0.012$). Furthermore, TR for FDI was also significantly affected by phase of the movement ($p < 0.002$) such that the delay was shorter during the opening portion of the movement than during the closing portion. The mean delay for FDS and FPB was very similar for a stretch perturbation of FDS during closing, but the FPB peak response was delayed by 25 ms, on average, with respect to the FDS peak reflex response during opening (**Figure 4**).

Impedance Perturbation

Surprisingly, for each type of impedance perturbation (MCP/IP, closing/opening), the aperture remained relatively unchanged (**Figure 5**). This is evident during the onset of each perturbation where the finger is delayed, indicating the thumb movement is accelerated in the absence of finger movement.

Thus, rather than stopping or slowing to match the checked movement of specific index finger joints, thumb movement increased beyond previous levels (**Figure 6**). ANOVA results revealed that the RMSE in thumb trajectory from the mean unperturbed trajectory was significantly impacted by the perturbation ($p < 0.001$), with greater RMSE during perturbed trials (**Figure 7A**).

The increased thumb movement occurred in the intended direction of movement. Hence, during closing, thumb flexion after index finger perturbation became greater, more closely matching what would be expected in unimpaired individuals performing this movement, particularly at the thumb MCP

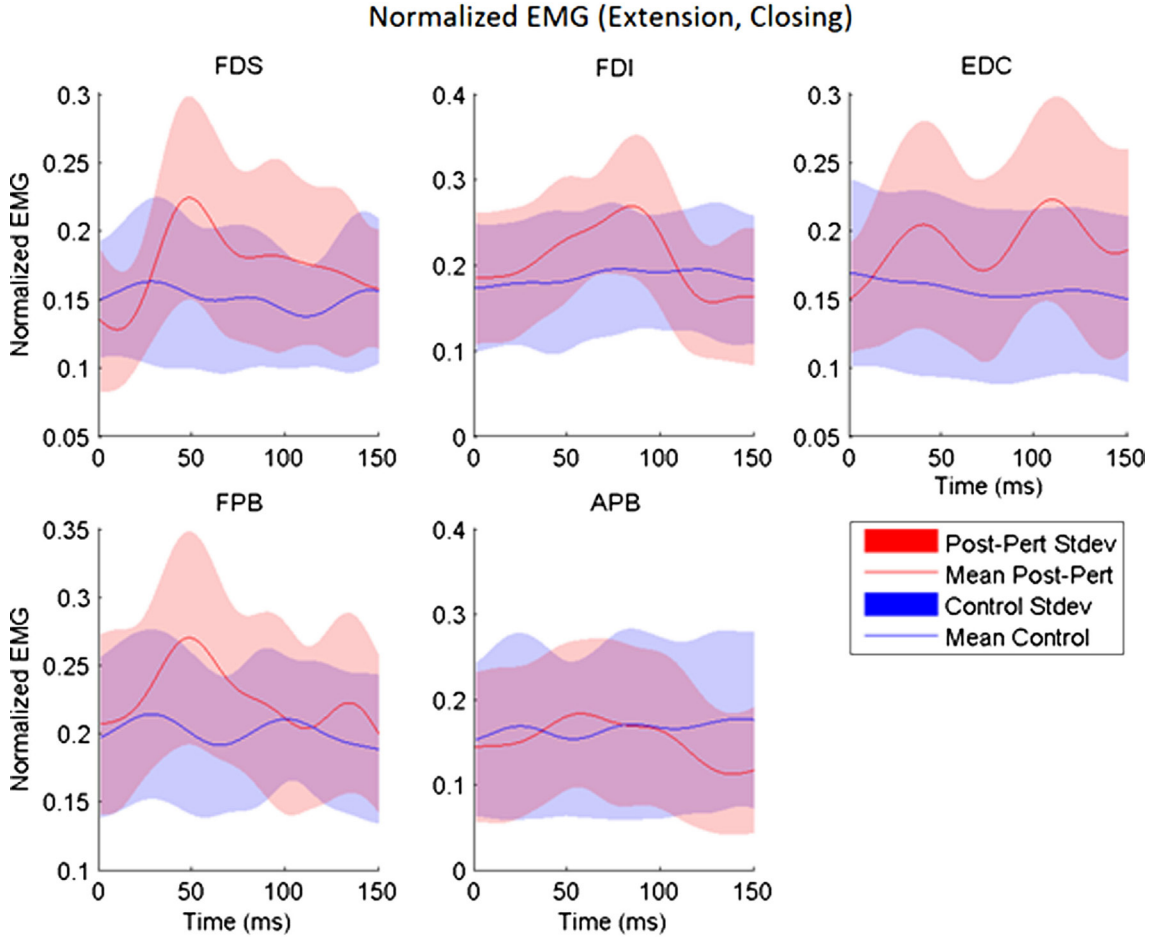

FIGURE 3 | Across-subjects mean EMG envelopes for each muscle following extension perturbation during the closing phase. Unperturbed (blue) and perturbed (red) conditions are shown with their across-subjects mean values (line) and associated SDs (shaded).

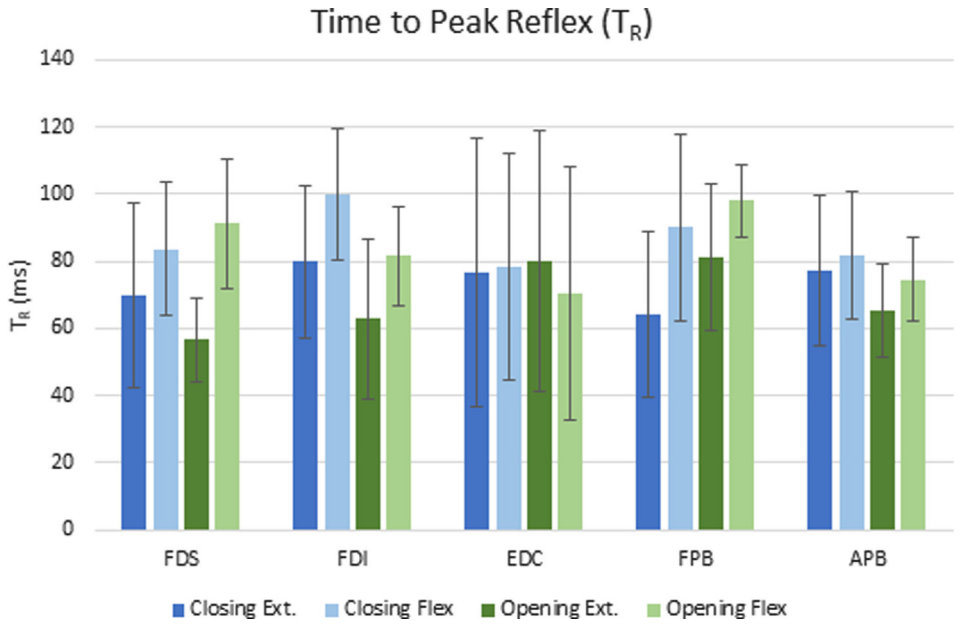

FIGURE 4 | Mean elapsed time (ms) to peak reflex response (TR) for each condition across subjects. Error bars indicate ±1 SD.

joint. Even more startling, a large increase in thumb extension was observed for perturbations applied to the index finger during the opening phase. Thus, RMSE was significantly affected by phase of movement ($p < 0.044$), with greater RMSE during opening (**Figure 7B**). While greater mean thumb displacements were observed for perturbation of the MCP joint during closing and the IP joints during opening, there was no significant effect of the joint(s) perturbed (finger MCP or IP) on thumb movement.

DISCUSSION

Using a novel finger exoskeleton, we were able to assess involuntary coupling present between the thumb and index finger during a dynamic movement in stroke survivors. Kinematic and EMG data revealed strong, perturbation-dependent interactions between index finger and thumb muscles in the stroke survivors.

Reflex Response

Imposed stretch perturbations of the index finger muscles during the dynamic task evoked significant reflex EMG activity in all of the measured index finger muscles. In nominally passive stroke survivors (those who are not actively utilizing muscles), we have observed that a similar rapid stretch of the finger flexors, such as FDS, likewise produces a significant stretch reflex in the stretched muscles (24). This study shows that this behavior is also evident during voluntary movement in stroke survivors, as has been described for the elbow (25, 26). The observed reflex behavior in shortening muscles, such as EDC during an extension perturbation, is reminiscent of the occasional reflex response observed in EDC during stretch of the spastic flexors in passive stroke survivors (24). It should be noted that the delay to the peak EDC reflex during extension was longer than that for FDS, thereby suggesting a longer reflex loop.

Stretch of EDC during the flexion perturbation also resulted in reflex generation. This contrasts to the case in passive stroke survivors, within whom stretch of finger extensors such as EDC generally fails to produce any reflex response (15). The EDC stretch produced a reflex response present in the finger flexors as well. Reflex activity in the non-stretched muscles may arise from loss of reciprocal inhibition or even a transition to reciprocal excitation following the stroke (27, 28).

In support of our hypothesis, we also observed reflex coupling between certain finger and thumb muscles. Thus, stretch of finger muscles produced reflex responses in a non-stretched thumb muscle, FPB. We previously observed this phenomenon in passive stroke survivors (29), but this is the first time we have been able to verify that these coupled reflexes can be evoked during voluntary movement. Intriguingly, significant reflex behavior was not induced in all thumb muscles, but rather in FPB and not in APB. Thus, it appears that coupling may be greater between thumb and finger flexors, as we observed in the passive condition (29). It should be noted that rapid stretch of thumb muscles in passive stroke survivors failed to elicit a spastic stretch reflex (30). Limited APB reflex may also be attributed to a reduction in heterogeneous extrinsic–intrinsic connections (7). FDS, FDI, and FPB reflex timing follow the same temporal pattern of reflex activation with peak EMG occurring 19–25 ms earlier for extension perturbations, as compared with flexion perturbations. It should be noted that thumb movement was controlled voluntarily throughout the task and so may have varied. As one head of FDI originates on the thumb metacarpal, thumb movement may have influenced FDI length and thus excitability, resulting in increased

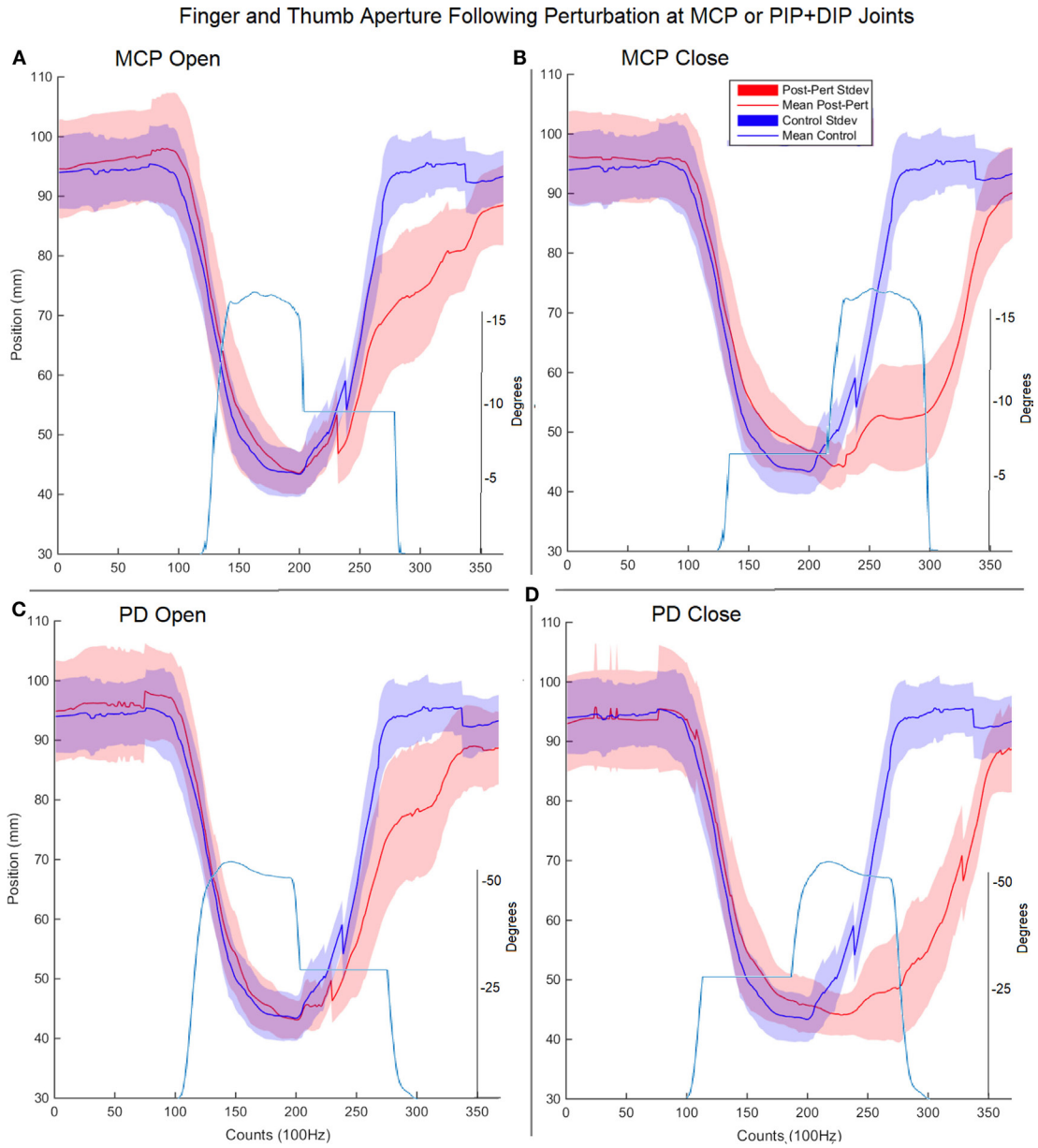

FIGURE 5 | Finger and thumb aperture during perturbed (red) and unperturbed (blue) trials following perturbations. Each perturbation condition is shown, **(A)** metacarpophalangeal (MCP) perturbation during opening, **(B)** MCP perturbation during closing, **(C)** proximal interphalangeal (PIP)/distal interphalangeal (DIP) joint during opening, **(D)** PIP/DIP during closing. Examples of joint angle trajectories with perturbations are provided for reference; note, flat region indicates joint-locked perturbation.

variability between trials and differing strategies between subjects.

The magnitude of the heteronymous reflex activity observed in the thumb muscles due to stretch of the index finger muscles did not vary significantly with movement phase. However, while the time to peak reflex response was very similar for FDS and FPB during closing, it was much longer for FPB during opening, when less coordination was required between the thumb and index finger. Thus, modulation of the finger–thumb coupling may occur with movement phase, although it may be partially impaired in stroke survivors. Indeed, the interaction of phase and direction was non-significant for every muscle. This absence of an effect may suggest the loss of capacity for modulating index finger and thumb neurological coupling specific to the motor control task. This is consistent with previous findings of unmodulated hyperreflexia across static postures of the wrist (31) where, despite changing posture of the wrist, reflex gains remained unmodulated, as well as a general deficit in modulation of EMG patterns in the finger and thumb (32, 33). By contrast, phase-dependent reflex modulation has been reported in a previous study examining cyclical arm movements (cycling) in neurologically intact individuals (34).

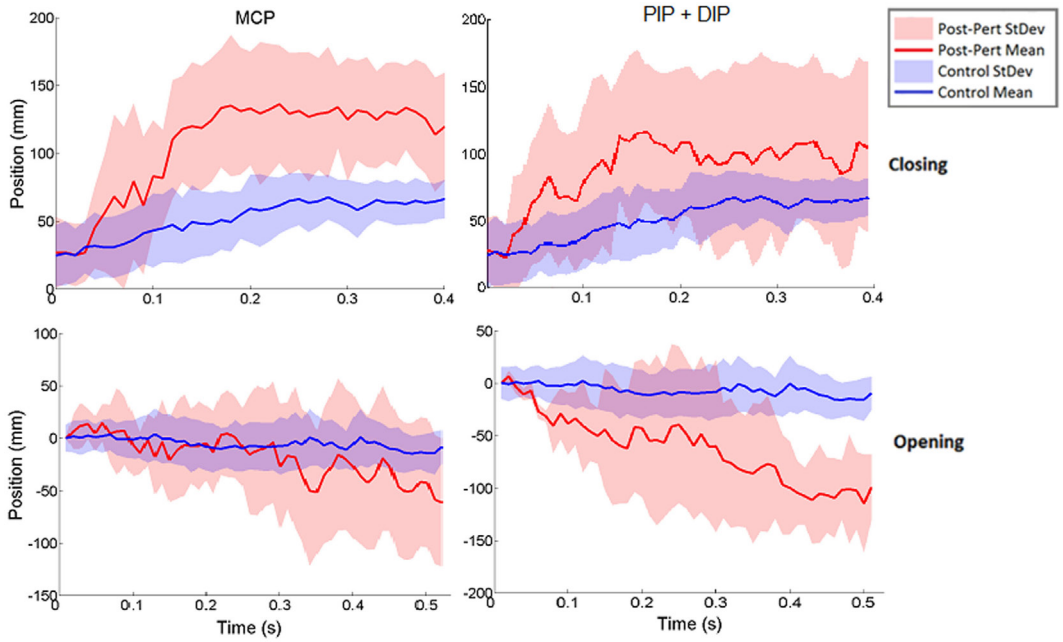

FIGURE 6 | Norm of 3D thumb tip displacement vector following metacarpophalangeal (MCP) (left column) or IP (right column) joint-locked perturbation during closing (top) or opening (bottom). Movement is shown for the period of time from initiation of perturbation to end of movement phase for the unperturbed trials. Mean perturbed (red line) and unperturbed (blue line) trajectories are shown with associated SDs (shaded regions). *Y*-axis zeroed to the angle of perturbation such that negative angles are in closing and positive angles are in opening directions.

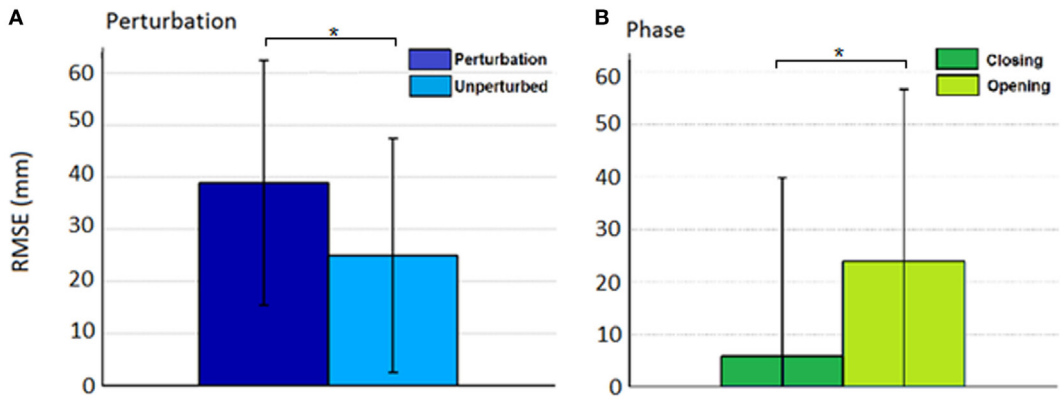

FIGURE 7 | Root mean squared error (RMSE) for the effect of **(A)** condition (perturbed/unperturbed) and **(B)** phase (closing/opening).

Impedance Perturbation

The response of thumb tip motion to imposed disruption of index finger movement was especially intriguing. Contrary to our hypothesis, impeding finger movement led to increased thumb movement. The thumb is observed to maintain the anticipated aperture, indicating an accelerated trajectory. This movement is beyond what was achieved without any perturbations, flexing further during closing and extending further during opening following perturbation. During the closing phase perturbed trials, thumb motion showed acceleration just prior to reaching the unperturbed point of contact, thereby suggesting that the thumb was indeed responding to an imposed deficit in the index finger by moving further than normal to meet the finger. This movement may have been encouraged by stabilizing the index finger *via* increased joint impedance. Alternatively, greater thumb movement may have arisen as the result of increased somatosensory feedback arising from perturbation contact forces in the index finger.

The most striking result was the increase in thumb extension during the opening phase for the perturbed trials. Stroke survivors typically have difficulty in creating active thumb extension (34). This was evident in our stroke survivors who typically generated less than 2 cm of thumb extension during the unperturbed trials. When the index finger impedance was

suddenly increased, however, mean thumb extension increased to over 10 cm, an amount roughly equivalent to what would be expected in neurologically intact subjects. The mechanisms behind this improvement are unclear. One possibility is that the perturbation leads to increased involuntary activation of all digit extensor muscles.

Coupling

The presence of a coupled response between the index finger and thumb affirms previous findings during coordinated rapid grasping tasks in neurologically intact individuals (9, 10, 35) and indicates a preservation of coupling following stroke. Thumb kinematic responses to index finger perturbation align with previously demonstrated influence over thumb kinematics during healthy grasp (36). This outcome supports the notion of preservation of components of motor control following stroke, including coupling between digits (37, 38). The presence of phase changes indicates there is some preservation of modulation of index finger–thumb coupling, in contrast to findings following reflex-inducing perturbations. The modulation effects are present across larger temporal scales (0.5–0.75 s).

The remarkable improvement of thumb movement in response to impedance of index finger movement may arise as the result of excitatory or inhibitory coupling between index finger and thumb muscles. During the opening phase, impedance to finger movement could give rise to increased activation of finger extensor muscles which, in the presence of coupling to the thumb, could create reciprocal excitation of thumb extensors and/or reciprocal inhibition of thumb flexors; both of these would result in improved movement of the thumb. However, due to the use of surface electrodes, extensor EMG data were not available for the thumb in this study; efforts should be made to include thumb extensor EMG in future investigations.

One such route of coupling may follow the reticulospinal pathway, which has been demonstrated to integrate somatosensory feedback into motor control (39). Inhibition through such a pathway may improve movements in the presence of large somatosensory stimuli. In this way, somatosensory stimulation of the index finger may provide a pathway for intervention following stroke to promote thumb movement. Similar targeted haptic feedback has been shown to improve motor control in the arm (40–42).

Potential Limitations

These experiments only examined reflexes during part of the movement: midway through the closing and opening phases of movement. Further experiments examining reflex modulation across the range of postures during the movement would better inform the extent of modulation and contributions of reflex activity to motor control during pinch.

Sample size was limited. Part of the goal of this study was to ensure feasibility of use of the CAFE with stroke survivors. Further exploration of the observed increase in thumb extension resulting from index finger perturbation in more subjects is warranted. Future work in conjunction with a thumb exoskeleton or other enhanced thumb kinematic measures will enable increased insight into thumb muscle behavior.

Additionally, reflex modulation may have been impacted by contact with the exoskeleton. Somatosensory cutaneous afferents have been shown to contribute to neuromodulation at the spinal cord (43). Contact with the exoskeleton was designed to be constant throughout the flexion or extension phase as subjects were instructed to maintain a specific voluntary activation level. Coupling of interaction between finger and thumb extensor muscles could not be examined as thumb extensor activity was not monitored.

CONCLUSION

While the index finger and thumb are capable of highly individuated movements, they also exhibit substantial coupling in tasks requiring finger–thumb coordination. These results suggest that coupling is highly evident in stroke survivors and appears to maintain behavior appropriate to task despite the underlying hand impairment.

In particular, the thumb clearly experienced a coupled response during the dynamic pinching task following index finger perturbation. Intriguingly, sudden arrest of index finger extension led to a profound increase in active thumb extension, far beyond what was generated without the perturbation. Further research is needed to validate and explore this finding, but the potential significance for rehabilitation is great.

ETHICS STATEMENT

This investigation was conducted at the Rehabilitation Institute of Chicago (RIC) and all participants provided written consent in accordance with processes approved by the Northwestern University Institutional Review Board.

AUTHOR CONTRIBUTIONS

This work was conceived, conducted, analyzed, and authored by CJ and DK.

ACKNOWLEDGMENTS

We thank Mr. Tom Worsnopp, Dr. Michael Peshkin, Dr. Ed Colgate, Dr. Nilanjan Sarkar, and Dr. Furui Wang for their assistance in development of the CAFE. This work was included in part in the Ph.D. dissertation of Dr. Christopher L. Jones (44).

FUNDING

This work was supported by grants from the American Heart Association (13PRE14610017) and the Eunice Kennedy Shriver National Institute of Child Health and Human Development within NIH (1R21HD055478-01).

REFERENCES

1. Schieber MH, Santello M. Hand function: peripheral and central constraints on performance. *J Appl Physiol* (2004) 96(6):2293–300. doi:10.1152/japplphysiol.01063.2003
2. Gao F, Latash ML, Zatsiorsky VM. Internal forces during object manipulation. *Exp Brain Res* (2005) 165(1):69–83. doi:10.1007/s00221-005-2282-1
3. Santello M, Flanders M, Soechting JF. Patterns of hand motion during grasping and the influence of sensory guidance. *J Neurosci* (2002) 22(4):1426–35.
4. Santello M. Kinematic synergies for the control of hand shape. *Arch Ital Biol* (2002) 140(3):221–8.
5. Kilner JM, Alonso-Alonso M, Fisher R, Lemon RN. Modulation of synchrony between single motor units during precision grip tasks in humans. *J Physiol* (2002) 541(Pt 3):937–48. doi:10.1113/jphysiol.2001.013305
6. Poston B, Enoka JA, Enoka RM. Endpoint accuracy for a small and a large hand muscle in young and old adults during rapid, goal-directed isometric contractions. *Exp Brain Res* (2008) 187(3):373–85. doi:10.1007/s00221-008-1309-9
7. Kamper DG, Fischer HC, Conrad MO, Towles JD, Rymer WZ, Triandafilou KM. Finger-thumb coupling contributes to exaggerated thumb flexion in stroke survivors. *J Neurophysiol* (2014) 111(12):2665–74. doi:10.1152/jn.00413.2013
8. Lacquaniti F, Borghese NA, Carrozzo M. Transient reversal of the stretch reflex in human arm muscles. *J Neurophysiol* (1991) 66(3):939–54. doi:10.1152/jn.1991.66.3.939
9. Cole KJ, Abbs JH. Kinematic and electromyographic responses to perturbation of a rapid grasp. *J Neurophysiol* (1987) 57(5):1498–510. doi:10.1152/jn.1987.57.5.1498
10. Cole KJ, Gracco VL, Abbs JH. Autogenic and nonautogenic sensorimotor actions in the control of multiarticulate hand movements. *Exp Brain Res* (1984) 56(3):582–5. doi:10.1007/BF00238001
11. Schettino LF, Adamovich SV, Tunik E. Coordination of pincer grasp and transport after mechanical perturbation of the index finger. *J Neurophysiol* (2017) 117(6):2292–7. doi:10.1152/jn.00642.2016
12. Jones CL, Wang F, Osswald C, Kang X, Sarkar N, Kamper DG, et al. Control and kinematic performance analysis of an actuated finger exoskeleton for hand rehabilitation following stroke. *IEEE/RAS-EMBS BioRob*. Tokyo, Japan (2010). p. 282–7.
13. Jones CL, Wang F, Morrison R, Sarkar N, Kamper DG. Design and development of the cable actuated finger exoskeleton for hand rehabilitation following stroke. *IEEE Trans Mechatron* (2014) 19(1):131–40. doi:10.1109/TMECH.2012.2224359
14. Gowland C, VanHullenaar S, Torresin W, Moreland J, Vanspall B, Barrecca S, et al. *Chedoke-McMaster Stroke Assessment: Development, Validation and Administration Manual*. Hamilton, Canada: Chedoke-McMaster Hospitals and McMaster University (1995).
15. Kamper DG, Fischer HC, Cruz EG, Rymer WZ. Weakness is the primary contributor to finger impairment in chronic stroke. *Arch Phys Med Rehabil* (2006) 87(9):1262–9. doi:10.1016/j.apmr.2006.05.013
16. Maier MA, Hepp-Reymond MC. EMG activation patterns during force production in precision grip. II. Muscular synergies in the spatial and temporal domain. *Exp Brain Res* (1995) 103(1):123–36. doi:10.1007/BF00241970
17. Maier MA, Hepp-Reymond MC. EMG activation patterns during force production in precision grip. I. Contribution of 15 finger muscles to isometric force. *Exp Brain Res* (1995) 103(1):108–22. doi:10.1007/BF00241969
18. Danion F, Gallea C. The relation between force magnitude, force steadiness, and muscle co-contraction in the thumb during precision grip. *Neurosci Lett* (2004) 368(2):176–80. doi:10.1016/j.neulet.2004.07.006
19. Goetz TJ, Costa JA, Slobogean G, Patel S, Mulpuri K, Travlos A. Contribution of flexor pollicis longus to pinch strength: an in vivo study. *J Hand Surg Am* (2012) 37(11):2304–9. doi:10.1016/j.jhsa.2012.07.027
20. Gagne M, Schneider C. Dynamic changes in corticospinal control of precision grip during wrist movements. *Brain Res* (2007) 1164:32–43. doi:10.1016/j.brainres.2007.06.014
21. Iwamuro BT, Cruz EG, Connelly LL, Fischer HC, Kamper DG. Effect of a gravity-compensating orthosis on reaching after stroke: evaluation of the Therapy Assistant WREX. *Arch Phys Med Rehabil* (2008) 89(11):2121–8. doi:10.1016/j.apmr.2008.04.022
22. Housman SJ, Scott KM, Reinkensmeyer DJ. A randomized controlled trial of gravity-supported, computer-enhanced arm exercise for individuals with severe hemiparesis. *Neurorehabil Neural Repair* (2009) 23(5):505–14. doi:10.1177/1545968308331148
23. Crago PE, Houk JC, Hasan Z. Regulatory actions of human stretch reflex. *J Neurophysiol* (1976) 39(5):925–35. doi:10.1152/jn.1976.39.5.925
24. Kamper DG, Rymer WZ. Quantitative features of the stretch response of extrinsic finger muscles in hemiparetic stroke. *Muscle Nerve* (2000) 23(6):954–61. doi:10.1002/(SICI)1097-4598(200006)23:6<954::AID-MUS17>3.0.CO;2-0
25. Mizrahi EM, Angel RW. Impairment of voluntary movement by spasticity. *Ann Neurol* (1979) 5(6):594–5. doi:10.1002/ana.410050620
26. Knutsson E, Martensson A, Gransberg L. Influences of muscle stretch reflexes on voluntary, velocity-controlled movements in spastic paraparesis. *Brain* (1997) 120(Pt 9):1621–33. doi:10.1093/brain/120.9.1621
27. Nielsen JB, Petersen NT, Crone C, Sinkjaer T. Stretch reflex regulation in healthy subjects and patients with spasticity. *Neuromodulation* (2005) 8(1):49–57. doi:10.1111/j.1094-7159.2005.05220.x
28. Crone C, Petersen NT, Gimenéz-Roldán S, Lungholt B, Nyborg K, Nielsen JB. Reduced reciprocal inhibition is seen only in spastic limbs in patients with neurolathyrism. *Exp Brain Res* (2007) 181(1):193–7. doi:10.1007/s00221-007-0993-1
29. Triandafilou KM, Fischer HC, Towles JD, Kamper DG, Rymer WZ. Diminished capacity to modulate motor activation patterns according to task contributes to thumb deficits following stroke. *J Neurophysiol* (2011) 106(4):1644–51. doi:10.1152/jn.00936.2010
30. Towles JD, Kamper DG, Rymer WZ. Lack of hypertonia in thumb muscles after stroke. *J Neurophysiol* (2010) 104(4):2139–46. doi:10.1152/jn.00423.2009
31. Meskers CG, Schouten AC, de Groot JH, de Vlugt E, van Hilten BJ, van der Helm FC, et al. Muscle weakness and lack of reflex gain adaptation predominate during post-stroke posture control of the wrist. *J Neuroeng Rehabil* (2009) 6:29. doi:10.1186/1743-0003-6-29
32. Lee SW, Triandafilou K, Lock BA, Kamper DG. Impairment in task-specific modulation of muscle coordination correlates with the severity of hand impairment following stroke. *PLoS One* (2013) 8(7):e68745. doi:10.1371/journal.pone.0068745
33. Zehr EP, Carroll TJ, Chua R, Collins DF, Frigon A, Haridas C, et al. Possible contributions of CPG activity to the control of rhythmic human arm movement. *Can J Physiol Pharmacol* (2004) 82(8–9):556–68. doi:10.1139/y04-056
34. Lang CE, Macdonald JR, Reisman DS, Boyd L, Jacobson Kimberley T, Schindler-Ivens SM, et al. Observation of amounts of movement practice provided during stroke rehabilitation. *Arch Phys Med Rehabil* (2009) 90(10):1692–8. doi:10.1016/j.apmr.2009.04.005
35. Cole KJ, Abbs JH. Coordination of three-joint digit movements for rapid finger-thumb grasp. *J Neurophysiol* (1986) 55(6):1407–23. doi:10.1152/jn.1986.55.6.1407
36. Yokogawa R, Hara K. Manipulabilities of the index finger and thumb in three tip-pinch postures. *J Biomech Eng* (2004) 126(2):212–9. doi:10.1115/1.1691444
37. Santello M, Flanders M, Soechting JF. Postural hand synergies for tool use. *J Neurosci* (1998) 18(23):10105–15.
38. Mason CR, Gomez JE, Ebner TJ. Hand synergies during reach-to-grasp. *J Neurophysiol* (2001) 86(6):2896–910. doi:10.1152/jn.2001.86.6.2896
39. Nguyen HB, Lee SW, Harris-Love ML, Lum PS. Neural coupling between homologous muscles during bimanual tasks: effects of visual and somatosensory feedback. *J Neurophysiol* (2017) 117(2):655–64. doi:10.1152/jn.00269.2016
40. Gomez-Rodriguez M, Peters J, Hill J, Schölkopf B, Gharabaghi A, Grosse-Wentrup M. Closing the sensorimotor loop: haptic feedback facilitates decoding of motor imagery. *J Neural Eng* (2011) 8(3):036005. doi:10.1088/1741-2560/8/3/036005
41. Squeri V, Masia L, Taverna L, Morasso P. Improving the ROM of wrist movements in stroke patients by means of a haptic wrist robot. *Conf Proc IEEE Eng Med Biol Soc* (2011) 2011:2077–80. doi:10.1109/IEMBS.2011.6090385

42. Squeri V, Casadio M, Vergaro E, Giannoni P, Morasso P, Sanguineti V. Bilateral robot therapy based on haptics and reinforcement learning: feasibility study of a new concept for treatment of patients after stroke. *J Rehabil Med* (2009) 41(12):961–5. doi:10.2340/16501977-0400
43. Kofler M, Fuhr P, Leis AA, Glocker FX, Kronenberg MF, Wissel J, et al. Modulation of upper extremity motor evoked potentials by cutaneous afferents in humans. *Clin Neurophysiol* (2001) 112(6):1053–63. doi:10.1016/S1388-2457(01)00540-5
44. Jones CL. *Cable Actuated Finger Exoskeleton Development and Examination of Index Finger and Thumb Coupling [Ph.D. Dissertation]*. Chicago, IL: Illinois Institute of Technology (2014).

Conflict of Interest Statement: The authors declare that the research was conducted in the absence of any commercial or financial relationships that could be construed as a potential conflict of interest.

frontiers in Neurology

ORIGINAL RESEARCH
published: 23 January 2018
doi: 10.3389/fneur.2018.00002

Intramuscular EMG Decomposition Basing on Motor Unit Action Potentials Detection and Superposition Resolution

*Xiaomei Ren[1], Chuan Zhang[2,3], Xuhong Li[4], Gang Yang[1], Thomas Potter[2] and Yingchun Zhang[2,3]**

[1] School of Electrical Engineering and Information, Sichuan University, Chengdu, China, [2] Department of Biomedical Engineering, University of Houston, Houston, TX, United States, [3] Guangdong Provincial Work Injury Rehabilitation Hospital, Guangzhou, China, [4] The Third Xiangya Hospital, Central South University, Changsha, China

A novel electromyography (EMG) signal decomposition framework is presented for the thorough and precise analysis of intramuscular EMG signals. This framework first detects all of the active motor unit action potentials (MUAPs) and assigns single MUAP segments to their corresponding motor units. MUAP waveforms that are found to be superimposed are then resolved into their constituent single MUAPs using a peel-off approach and similarly assigned. The method is composed of six stages of analytical procedures: preprocessing, segmentation, alignment and feature extraction, clustering and refinement, supervised classification, and superimposed waveform resolution. The performance of the proposed decomposition framework was evaluated using both synthetic EMG signals and real recordings obtained from healthy and stroke participants. The overall detection rate of MUAPs was 100% for both synthetic and real signals. The average accuracy for synthetic EMG signals was 87.23%. Average assignment accuracies of 88.63 and 94.45% were achieved for the real EMG signals obtained from healthy and stroke participants, respectively. Results demonstrated the ability of the developed framework to decompose intramuscular EMG signals with improved accuracy and efficiency, which we believe will greatly benefit the clinical utility of EMG for the diagnosis and rehabilitation of motor impairments in stroke patients.

Keywords: EMG decomposition, segments detection, minimum spanning tree, superposition waveform resolution, pseudo-correlation measure

OPEN ACCESS

Edited by:
Xiaoyan Li,
University of Texas, United States

Reviewed by:
Hongbo Xie,
Queensland University of Technology, Australia
Xiaogang Hu,
University of North Carolina at Chapel Hill, United States
Chang-Hwan Im,
Hanyang University, South Korea

****Correspondence:***
Yingchun Zhang
yzhang94@uh.edu

Specialty section:
This article was submitted to Stroke, a section of the journal Frontiers in Neurology

Received: *29 September 2017*
Accepted: *03 January 2018*
Published: *23 January 2018*

Citation:
Ren X, Zhang C, Li X, Yang G, Potter T and Zhang Y (2018) Intramuscular EMG Decomposition Basing on Motor Unit Action Potentials Detection and Superposition Resolution. Front. Neurol. 9:2. doi: 10.3389/fneur.2018.00002

INTRODUCTION

Electromyography (EMG) signals carry information regarding the motor unit action potential trains (MUAPTs) generated by the motor units (MUs) that are recruited during muscle contraction. Each MUAPT is made of a series of intermittent discharges that take the form of spatially dispersed individual motor unit action potentials (MUAPs). Intramuscular EMG is commonly acquired by means of indwelling needles or fine wire sensors that provide direct and targeted contact with the musculatures. Clinically, intramuscular EMG is used as a routine method for the electrophysiological examination of neuromuscular symptoms.

EMG decomposition reverses the process of signal generation by separating the de-noised EMG signal into its constituent MUAPTs. This process is accomplished by identifying MUAP waveforms

generated by the MUs adjacent to the detection surface and assigning these MUAPs to their corresponding MUAPTs. Characteristic properties of a decomposed MUAP, such as wave shape and firing pattern (1), can provide critical details regarding the health of the nervous system—details that are essential for the clinical diagnosis of neuropathies and myopathies (2–6), and the investigation of the neuromuscular control loop (7). Unfortunately, EMG decomposition is often a difficult and challenging task due to both external interferences, such as poor signal-to-noise ratio (SNR), movement artifacts, shifts in needle position, and so on, and interior challenges, such as waveform variations, intermittent MU firing, and the superposition of multiple MUAPs. EMG decomposition, therefore, requires a complex of advanced signal processing techniques. In the past few decades, many researchers have sought to develop advanced EMG decomposition techniques (8–15). The resultant decomposition methods can be grouped into three categories based on the extent of human interaction: manual, semi-automatic, and automatic (16). Following the manual method, MUAP analysis is performed directly by users who visually inspect and identify the distinctive MUAP patterns (17). This method is time-consuming in practice, highly experience-dependent, and incapable of resolving superimposed waveforms (18, 19). Hence, the development of automatic MUAP extraction methods is imperative to improve the work efficiency and clinical applicability of EMG decomposition. Despite the unremitting effort devoted to the optimization of automatic intramuscular EMG decompositions (5, 16, 20–23), there is still an unmet need for more accurate, complete, and reliable EMG decomposition techniques.

In this paper, we propose a novel intramuscular EMG decomposition framework by advancing the completeness and accuracy of MUAP decomposition. This framework is realized through six stages of analytical procedures: (1) EMG signal de-noising, (2) MUAP segmentation and extraction, (3) MUAPs alignment, feature extraction, and similarity measurement, (4) MUAP clustering and cluster refinement, (5) supervised classification, and (6) superimposed waveform resolution. Following this framework, we have attempted to improve the decomposition performance in four ways. First, we utilized a modified segment extraction scheme that is capable of detecting complete MUAP sets by incorporating amplitude threshold detection and resting segment recognition techniques. Second, single and overlapped MUAP waveforms were identified based on a phasic detection scheme, where phase templates were chosen based on the neurological condition of the tested muscle. The single MUAP segments of each MU underwent a clustering process that markedly reduced the buffer size and processing time required for this task. Third, all recognized single MUAP segments were aligned by centering their main peaks (regardless of polarity). Finally, we resolved superimposed waveforms using a peel-off approach based on measurements of pseudo-correlation (PsC). The performance of the proposed decomposition framework was evaluated using both synthetic EMG signals and real recordings obtained from healthy and stroke participants. Results demonstrated the favorable performance of the developed framework in decomposing intramuscular EMG signals with improved accuracy and efficiency.

MATERIALS AND METHODS

Subjects

Twenty healthy subjects (20–35 years of age, 16 males and 4 females) participated in our data collection. No subject reported any history of neuromuscular diseases. Eight subacute hemiparetic stroke subjects (46–74 years of age, 6 males and 2 females, within 1 month of the ictal event) were recruited from the Third Xiangya Hospital of Central South University in China. The research protocol was approved by the local research ethics committee. All subjects were informed about the purpose and details of the experiment prior to the data collection.

Data Acquisition

All EMG signals were recorded from the biceps brachii muscle. Subjects were seated in a chair with either the right forearm (for healthy subjects) or the affected forearm (for the stoke patients) supported by a horizontal table. Subjects were then asked to maintain elbow flexion at a 90° angle with their palms facing upward. A conventional needle electrode (9013s0032, Natus Neurology, USA) was inserted into the muscle belly at a depth of approximately 1 cm. Each subject was then asked to perform 10-s constant-force isometric contractions by resisting a load with pre-trained force. Each subject performed three contractions at both mild (3–4 MUs detected) and moderate (6–8 MUs detected) force levels. A 3-min break was provided following each contraction to avoid muscle fatigue. Signal quality and force level were monitored on a real-time display screen with audio feedback. All clinical procedures were performed by an experienced physician (Xuhong Li). The frequency band of the standard EMG instrument was set to 2 Hz–10 kHz. All signals were sampled at 48 kHz and stored for off-line decomposition using an EMG workstation (Dantec Keypoint Focus, Natus Neurology, USA).

Generation of Synthetic EMG Signals

Synthetic EMG signals are valuable for evaluating decomposition results as, unlike real recordings, the exact firing patterns and waveform templates of the synthetic MUs are known. The use of synthetic EMG signals thereby represents the only way to assess the sensitivity of decomposition algorithms to different parameters. In this study, 5-s segments of EMG signals (sampled at 30 kHz) were generated based on a model proposed by Farina et al. (24), where each segment consisted of one or more channels of synthetic intramuscular EMG recordings. The model was built using a library of real MUAP pools to better approximate biological signals. This library included 40 MUAP waveforms artificially extracted from real EMG signals. Each waveform was expanded by associated Hermite expansion functions in a 16-dimensional space. The firing pattern was generated based on both regular and random firing. The regular firing component of this pattern was created using a mean inter-pulse interval within a stationary-renewal point process, while the embodied random-firing component were determined by uniform random variables (i.e., the positions of the random firing, which were determined by uniform random variables, were used to denote the pattern of the random firing). The synthetic EMG signals were

then corrupted by adding random white noise with a variable SNR and background noise. The random noise was simulated as band-pass filtered Gaussian white noise with a zero mean and normally distributed random sequences. The frequency band of the band pass filter was 100 Hz–10 kHz. The background noise was the residual signal obtained by subtracting all recognized active MUAP segments from the original EMG signal. Thirty sets of synthetic EMG signals were generated to evaluate the performance of the proposed decomposition framework.

De-Noising through Wavelet Filtering and Threshold Estimation

Signal preprocessing followed the methods described in our previous publications (25, 26). Briefly, a wavelet filter was first applied to remove random interference by identifying the wavelets whose frequency range lay outside the 30 Hz–8 kHz window and setting their coefficients to zero. A hard-threshold estimation method was subsequently implemented to eliminate background noise. After performing threshold estimation, the de-noised EMG signals could be reconstructed by an inverse discrete wavelet transform (WT) using modified wavelet coefficients. Additional single-channel-independent component analysis method and digital notch filtration were applied to further remove the residual power-line interference when necessary (25, 26).

Segmentation and Isolated/Overlapped MUAP Segments Separation

All active MUAP segments were first identified using a modified segmentation scheme. A detection window of 1.25 ms was shifted through the entire EMG signal. A resting segment was recognized if the absolute values of the signal within the window were continuously lower than the pre-set amplitude threshold. Whenever two or more successive resting epochs were detected, the signals spanning between these epochs were extracted as the active segments, in which the signal exceeded this pre-set amplitude threshold. The boundaries of identified active epochs were then spatially expanded by at least 0.2 ms to ensure that the whole MUAP waveform was preserved. This amplitude threshold level was defined as k multiplied by the estimated noise power, σ_n^2. The noise power of the inactive segments was estimated automatically according to Eqs 1 and 2, based on original EMG signal. The value of k was selected by the investigator according to the force level, with a range of 5–8.

$$\sigma_i^2 = \frac{1}{L_R} \sum_{k=i}^{i+L_R-1} s_{\mathrm{EMG}}^2[k], \tag{1}$$

where L_R is the length of a window and the $s_{\mathrm{EMG}}[k]$ is the discrete EMG signal. σ_n^2 is calculated as the minimum value of σ_i^2 according to Eq. 2

$$\sigma_n^2 = \min \sigma_i^2. \tag{2}$$

Extracted MUAP-containing segments can be either isolated or overlapped. Isolated MUAPs that discharge multiple times can be easily recognized and labeled using clustering methods. Conversely, overlapped MUAP waveforms are created by the partial or full superposition of two or more single MUAPs discharging simultaneously, making the constituent waveforms much more difficult to parse. According to Thornton and Michell (27), MUAPs from a healthy musculature may contain up to four phases while an increase in MUAP phases may be indicative of the MU remodeling period that occurs after pathological denervation. In this study, the subject-specific recognition of isolated/overlapped MUAPs was carried out by assigning a tetraphasic (4-phase) template to the EMG signals from healthy participants and a hexaphasic (6-phase) template to the signals from stroke participants. The phasic properties of the MUAPs are affected by many variables, so it may be improper to assign phasic parameters a fixed value. Thus, the extraction results were evaluated and phasic thresholds were fine-tuned if some of the isolated MUAPs were incorrectly assigned to the overlapped sets. In our experiment, we applied a pentaphasic (5-phase) template for 6 of the 20 healthy data sets and octophasic (8-phase) template for 3 of the 8 stroke data sets. Superimposed waveforms always possess longer durations so, during alignment, segments were zero padded to match the duration of the longest event (22, 28). A very large buffer size would be required if all active segments were to be aligned. To save buffer size and computing time, segment grouping was performed in advance and only the isolated MUAPs were inputted for alignment and clustering. Overlapped MUAPs were not processed until the superimposed waveforms are resolved (see Resolving Superimposed Waveforms Using the Peel-Off Approach Based on Pseudo-Correlation).

Extracted active segments with only one phase or a MUAP duration shorter than 1.5 ms were regarded as invalid and excluded from the detected MUAP set. Finally, the remaining single MUAP segments were retained as a valid set for the following alignment. The beginning points of these active segments, representing the onsets of the MU firing instances, were assembled into a separate one-dimensional array.

MUAP Waveforms Alignment and Feature Extraction

At this stage, all of the detected MUAP waveforms were aligned with their main peaks (either positive or negative) at the spatial center and shorter waveforms were zero padded so that all segments were of equal length. This alignment scheme can enhance the sensitivity in discerning and grouping MUAPs into their MU origins.

Wavelet-domain features have been shown to improve stability when analyzing EMG signals that are contaminated by high frequency background noise or baseline drift (1, 16). As a result, we implemented WT at the sixth level using the aligned MUAP segment data. The wavelet coefficients from the third through sixth levels of aligned MUAP segments were chosen as the feature space. For WT, we used a compactly supported biorthogonal wavelet base, namely the Daubechies compactly supported wavelet with five vanishing moments, or db5.

After feature extraction, the distance matrix was calculated based on the variance of the error normalized by the sum of the RMS values for the paired segments (20). This is denoted as

$$d(s_1, s_2) = \frac{E(e^2(n)) - E^2(e(n))}{\sqrt{E(s_1^2(n))} + \sqrt{E(s_2^2(n))}}, \tag{3}$$

where $s_1(n)$ and $s_2(n)$ are the two active segments to be compared and $e(n)$ is their error signal. The distance measure defined by Eq. 3 was used as a similarity measure for clustering.

Clustering and Refinement Using the Minimum Spanning Tree (MST) Method

The MUAP set was partitioned into its constituent MUAPTs based on the similarity measure presented above. To do this, we utilized a single-linkage hierarchical clustering algorithm that permits a simple graph-theoretical interpretation, namely the MST method. The MST method, considered best suited for EMG clustering (1), is able to cluster the MUAPs with low variation from one occurrence to the next and does not depend on the presentation order of the samples. We generally set the number of cluster equal to 8–12 depending on the size of the detected single MUAP segments.

A subsequent cluster refining procedure was performed to verify if any potential class should be deleted or subdivided. Clusters with at least three templates were chosen as potential MUAP classes, while those with less than three templates were regarded as invalid MU clusters and excluded. All MUAP segments belonging to these deleted clusters were moved to an unclassified set for subsequent supervised classification. At times, two different MU clusters can be incorrectly assigned to the same cluster due to similarities in their characteristic waveforms. In these cases, the mis-clustered MUs should also be subdivided based on the MST method. MUAPT templates were then calculated as the mean waveforms of each MUAP cluster. After clustering, we obtained the initial sets of MU clusters and the unassigned MUAPs were set aside to be classified in the next step.

Supervised Classification Based on the Minimum Distance Classifier

At this stage, we used the supervised minimum distance classifier, which is based on measurements of Euclidean distance, to classify the MUAP waveforms in the unassigned candidate set. The classification program was based on the wavelet coefficient features and valid clustering results. During classification, the threshold was set to the lowest mean value obtained from the inter-class distances. Signal instability and electrode movement can cause MUAP shapes to vary from discharge to discharge. Therefore, a weighted averaging technique reported by Zennaro et al. (7) was utilized to adapt the MUAP class template.

Resolving Superimposed Waveforms Using the Peel-Off Approach Based on Pseudo-Correlation

During muscle contraction, a portion of the entire MU pool is recruited and the intermittent firing pattern of each recruited MU can be extracted as its MUAPT. Multiple MUs that discharge simultaneously or within a very short interval will results in the superposition of MUAP waveforms. Resolving these waveforms is the process of identifying the overlapped MUAP segments and splitting them into their constituent single MUAPs. In our study, a peel-off approach based on PsC was adopted to resolve the superimposed waveforms after the isolated MUAP segments had been successfully classified.

According to Florestal et al. (5), PsC outperforms standard techniques such as cross-correlation-based matched filters and the normalized Euclidean distance. In addition, the PsC between superimposed segments and MU template waveforms can be calculated directly without alignment. Therefore, it is feasible to use PsC as the similarity measure between the superposed segments and MU template waveforms. The PsC between a superimposed segment and a MU template waveform at point k, PsC_k, is defined (5, 29) as

$$PsC_k = \frac{\sum_{j=1}^{m}(x_j y_{k+j} - |x_j - y_{k+j}| \max\{|x_j|, |y_{k+j}|\})}{\sum_{j=1}^{m}(\max\{|x_j|, |y_{k+j}|\})^2}, k = 1, 2, \cdots, n, \quad (4)$$

where x_j is clustered MU template waveform, y_j the superimposed segment, and m and n are the size of x and y, respectively.

The waveform that has the greatest PsC at the point k was regarded as the optimal match and was first subtracted from the superimposed segment aligned at point k. The matched MUAP waveform and its firing time k were then, respectively, assigned to the corresponding MU cluster and associated firing time array. Then the MUAP waveform that had the second greatest PsC was similarly subtracted and assigned. The resolving process continued repeating until segment subtraction resulted in a negative PsC value or an increase in the residual signal energy. In our work, the number of the iterations was experientially set to 3, which was the maximal MUAP number included in the superposed waveform.

Performance Indices

The following three measures related to the MUAP waveform detection and the EMG decomposition process were used to evaluate the performance of the EMG decomposition system.

Detection Ratio

The detection ratio (DR%) was used to measure the rate of the successful detection of active MUAP segments. The DR% is defined as

$$\mathrm{DR\%} = \frac{\mathrm{NM}_{\mathrm{detected}}}{\mathrm{NM}_{\mathrm{total}}} \times 100\%,$$

where $\mathrm{NM}_{\mathrm{total}}$ is the total number of MUAP segments—either the size of recruited library of MUs (for synthetic signals) or the number of MUs manually obtained by a neurophysiologist (for real signals)—and $\mathrm{NM}_{\mathrm{detected}}$ is the number of MUAP segments detected.

The Assignment Ratio

The assignment ratio (AR%) measures the rate of MUAP assignment using the proposed EMG decomposition framework. It is defined as

$$\mathrm{AR\%} = 1 - \frac{\mathrm{NM}_{\mathrm{unassigned}}}{\mathrm{NM}_{\mathrm{detected}}} \times 100\%,$$

where $\mathrm{NM}_{\mathrm{unassigned}}$ is the number of MUAP segments not assigned by the EMG decomposition framework and $\mathrm{NM}_{\mathrm{detected}}$ the total number of MUAP segments detected.

The Correct Classification Rate

The correct classification rate (CCR%) assesses the performance of the whole EMG decomposition system. It is defined as the ratio of $NM_{correct}$ (the number of correctly decomposed MUAPs) to $NM_{detected}$ (the total number of MUAPs detected):

$$CCR\% = \frac{NM_{correct}}{NM_{detected}} \times 100\%.$$

RESULTS

In our study, the DR% of the MUAP detection program for all real and generated EMG recordings reached 100% by using the novel MUAP segment detection scheme.

The complete decomposition of the superimposed waveforms resulted in a marked improvement in the assignment ratio. In this paper, the average assignment ratios (AR%s) of our decomposition system were 99.79% for the synthetic signals, and 98.66 and 91.52% for real recordings from healthy and stroke participants, respectively (listed in **Table 1**).

TABLE 1 | Decomposition results from synthetic and real EMG signals.

EMG data	Synthetic EMG	Real EMG (healthy)	Real EMG (stroke)
DR%	100	100	100
AR%	99.79	98.66	91.52
CCR%	87.23	88.63	94.45

DR%, detection ratio; AR%, assignment ratio; CCR%, correct classification rate.

Figures 1A,B show representative examples of real de-noised EMG signals and the correspondingly assigned MUAP signals, respectively. After decomposition, the classified MUAPs were subtracted from the original EMG signal in order to obtain the residual signal, which is shown in **Figure 1C**. A total of 216 active MUAP segments were detected with an AR% of 99.54% for the signals shown in **Figure 1**. Only one MUAP segment in this case (marked by the bold arrow in **Figure 1D**) could not be assigned by the proposed framework.

Figure 2 illustrates representative decomposition results based on the synthetic EMG signal, together with the firing patterns and the six identified MUAP template waveforms. **Figure 2A** shows the MUAP template waveforms decomposed from the signal shown in **Figure 2B**. **Figure 2B** depicts the de-noised synthetic EMG signal. **Figure 2C** demonstrates the corresponding MU firing patterns for each MU class identified by the decomposition framework.

Figure 3 then provides one example of the decomposition results from a stroke patient. **Figure 3A** shows the MUAP template waveforms for the three MUAPTs identified from the de-noised signal (shown in **Figure 3B**). **Figure 3C** shows the

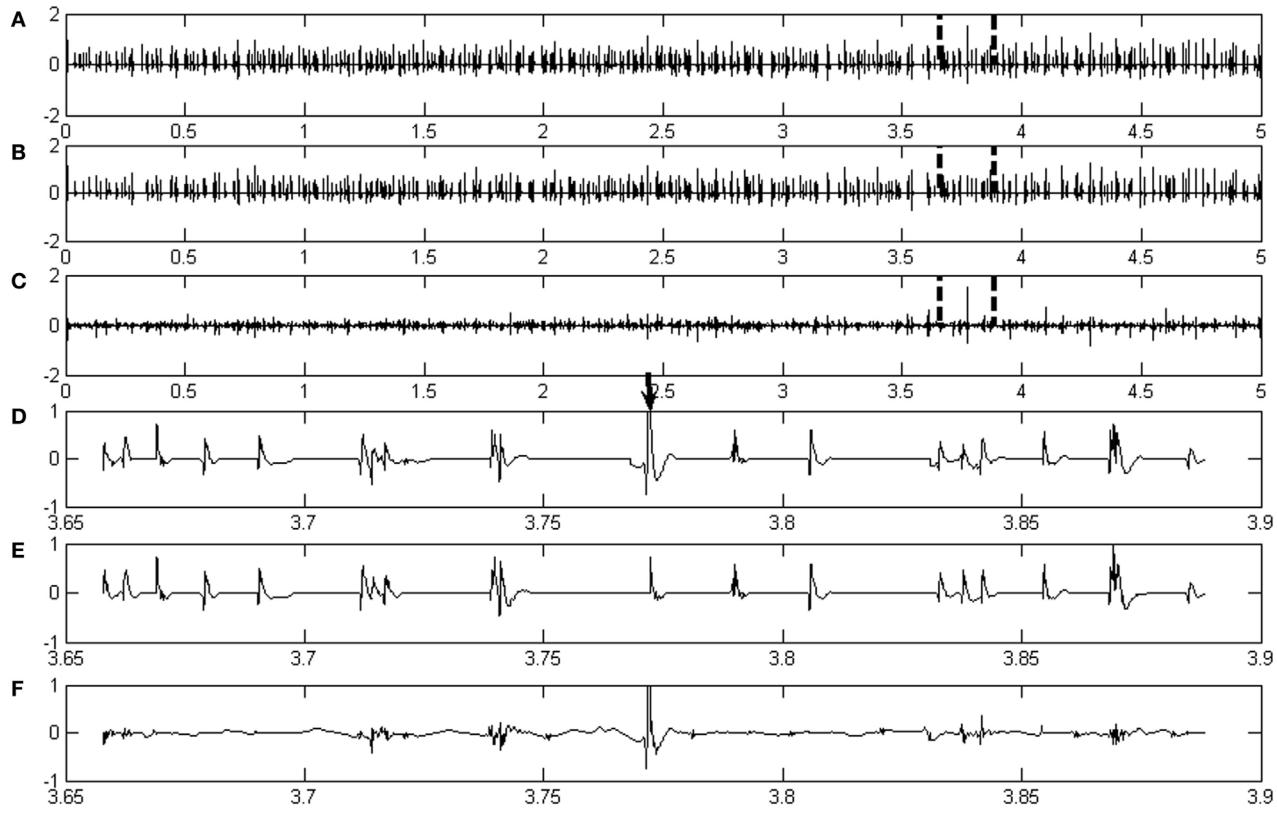

FIGURE 1 | **(A–C)** are, respectively, the real EMG signals from a healthy subject, the assigned motor unit action potential (MUAP) signals, and the residual signal by subtracting the assigned MUAP signals from the original signal. **(D–F)** are, respectively, the details of a section of signals denoted in panels **(A–C)**.

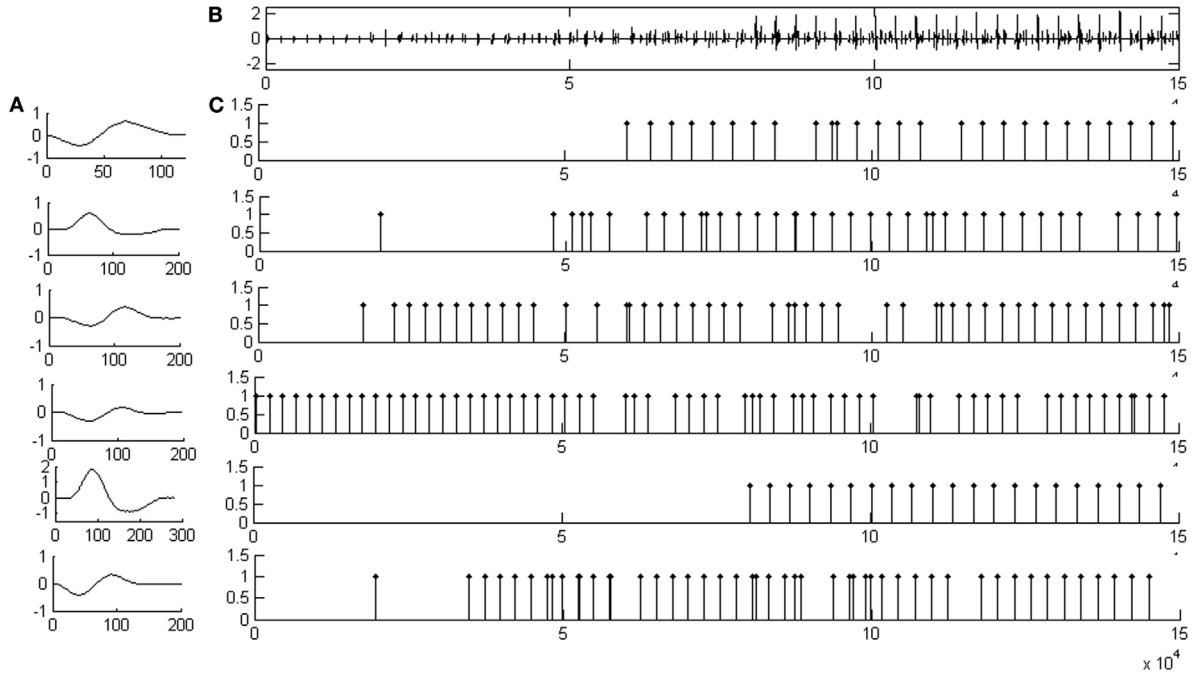

FIGURE 2 | An example of decomposition result based on a synthetic EMG signal. **(A)** The motor unit action potential template waveforms of all motor unit action potential train decomposed from the signal shown in **(B)**. **(B)** The de-noised signal based on a synthetic EMG signal. **(C)** The resulting motor unit (MU) firing patterns for each MU classes identified by the whole decomposition system.

corresponding MU firing patterns for each MU class identified by the decomposition framework.

Table 1 illustrates the decomposition results based on the synthetic and real EMG signals. The decomposition results from the synthetic signals were compared to the known information of the EMG model. The results of the real EMG signals were compared to manual decomposition analysis (assumed gold-standard), performed by an experienced neurophysiologist.

According to **Table 1**, the CCR% was 87.23% for synthetic EMG signals, and 88.63 and 94.45% for real recordings from healthy subjects and stroke patients, respectively.

Accurate clustering results are critical to the decomposition performance. In our study, we performed a cluster refining step to improve the accuracy of results. Cluster refinement in this case included deleting invalid clusters and subdividing one incorrectly identified cluster into two or more clusters. **Figure 4A** demonstrates a MU cluster after preliminary clustering, where two clusters were found incorrectly grouped due to similarities in their waveforms. Further clustering refinement was performed based on methods described in Section "Clustering and Refinement Using the Minimum Spanning Tree (MST) Method," where an MST method was adopted to further subdivide the erroneous cluster into two separate MU clusters, shown as in **Figure 4B**. Following this method, the erroneous cluster was successfully subdivided into two separate MU clusters.

The whole analysis process was conducted using a custom MATLAB script and performed on 2.5 GHz Intel i7 desktop computer. The average processing time for decomposing a 10-s-long EMG data was approximately 15–20 min.

DISCUSSION

EMG decomposition has been widely employed to provide information of alterations in motor unit characteristics in stroke patients (30). Achieving the complete and accurate motor unit firing pattern is vital for the understanding of pathological alterations in patients, as well as for clinical diagnosis and management. Therefore, the goal of this EMG decomposition framework is to identify complete MUAP segments in the EMG signal and classify them accurately into their constituent MUAPTs. Both the template waveforms and firing rates of the MUAPTs are largely dependent on the configuration of the needle electrode, the relative position of electrode to the muscle fibers, the level of contraction, and the pathological condition of the muscle. In this study, we developed an EMG signal decomposition framework based on a novel MUAP segmentation method and the resolution of superimposed MUAP waveforms. Results showed strong decomposition performance with high values for DR%, AR%, and CCR%. It should be noted that the CCR%s obtained for the stroke subject EMG signals were higher than those found in the other two conditions (signals from simulated and healthy subjects), signifying a potential clinical application for this method in the assessment of neurogenic disorders. This is probably due to a well-studied denervation process that occurs in post-stroke patients (30). Compromised MU recruitment in these cases often leads to sparser MU firing patterns and consequently higher identification accuracy.

A high DR% value is critical, as the successful extraction of MUAPs greatly impacts subsequent decomposition procedures

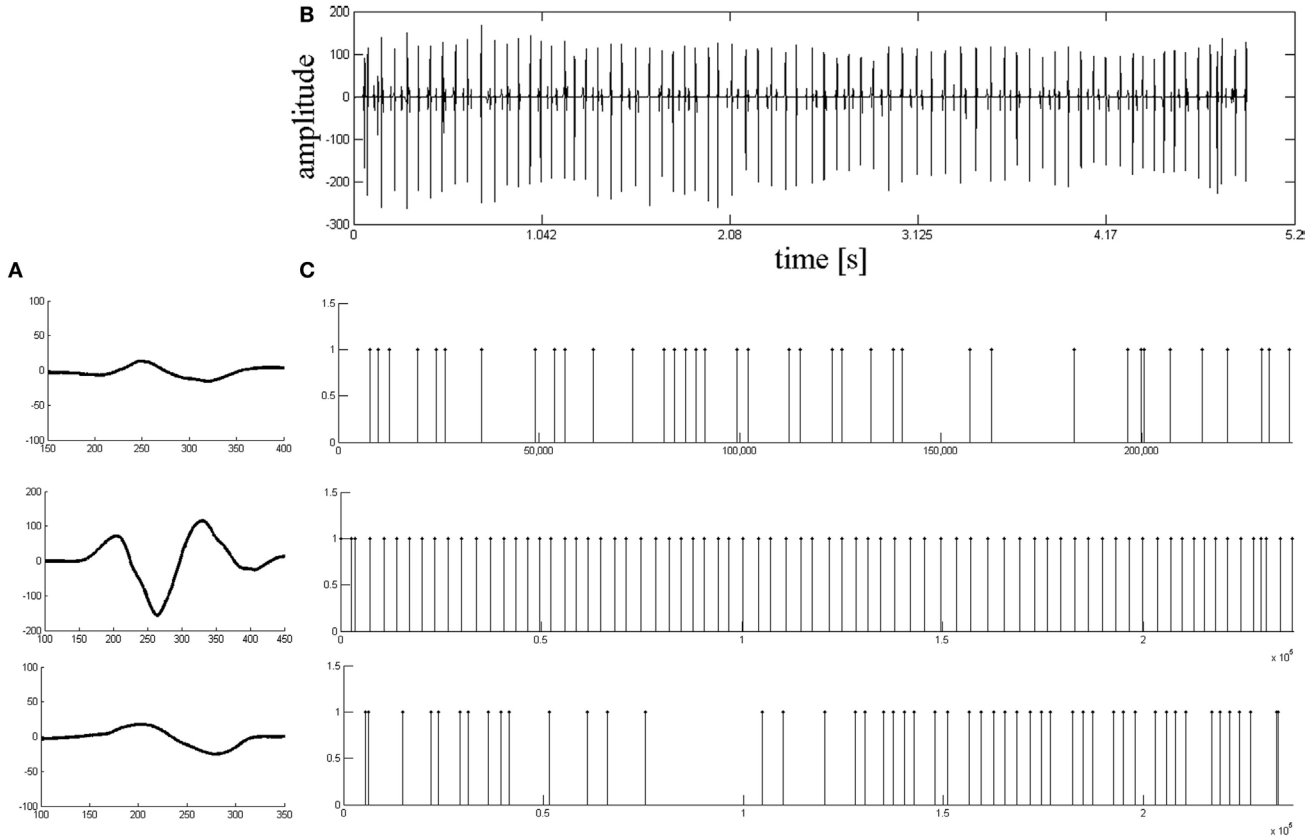

FIGURE 3 | The results of decomposition based on the real EMG signals from a stroke subject. **(A)** Motor unit action potential template waveforms of all motor unit action potential train decomposed from the signal shown in **(B)**. **(B)** The de-noised signal based on the stroke EMG signal. **(C)** The relative motor unit (MU) firing patterns for each MU classes identified by the whole decomposition system.

and, consequently, the AR% and CCR%. All active MUAP segments and resting segments comprise the whole EMG signal. Due to signal disparities, direct identification of MUAP segments is more difficult than the identification of the resting epochs. Thus, we utilized a wavelet hard-threshold estimation technique to attenuate instrumental and background noises, then applied a novel segmentation scheme based on resting segment detection. All active MUAP segments were further detached by subtracting rest segments from the original signal. The employment of a modified segmentation scheme greatly enhanced the performance, achieving a DR% value of 100% and demonstrating the complete detection of all active MUAP segments. Conventional segmentation methods often fail to identify some active MUAPs, even when using different rigid detection thresholds, because of the abnormal waveform complexity (26). Therefore, this complete detection of MUAPs—reaching a DR% of 100%—is unlikely to be achieved using conventional approaches.

Motor unit action potential segments detected in the aforementioned manner can be either isolated MUAP segments or superimposed MUAP waveforms. Then isolated/overlapped MUAP segments were separated based on either tetra- or hexaphasic waveform recognition methods. Segments with more than four MUAP phases for healthy subjects or six phases for stroke subjects were generally recognized to contain superposed MUAPs and separated for further analysis to resolve the superposition. Thus, by grouping segments based on their isolated MUAP characteristics in the first instance, the efficiency of the decomposition system was improved greatly. The implemented main peak alignment method further served to improve the methodical distinguishability of MUAPs originating from different MU clusters, resulting in more accurate and efficient results.

In our study, the MUAP waveforms were clustered using a single-linkage hierarchical clustering algorithm. This technique is suitable for the clustering of MUAPs with slow variation and does not depend on the presentation order of the samples. However, the results of clustering are very sensitive to the value of the discriminatory threshold. Clustering results were, therefore, verified through visual inspection. Invalid clusters were excluded or subdivided again using the MST algorithm to ensure that all final clusters are valid. In addition, the fuzzy *k*-means algorithm is based on the minimization of a global cost function, which is related to its classification ability. It is our ongoing effort to further integrate these two clustering algorithms and, in doing so, achieve optimal clustering results.

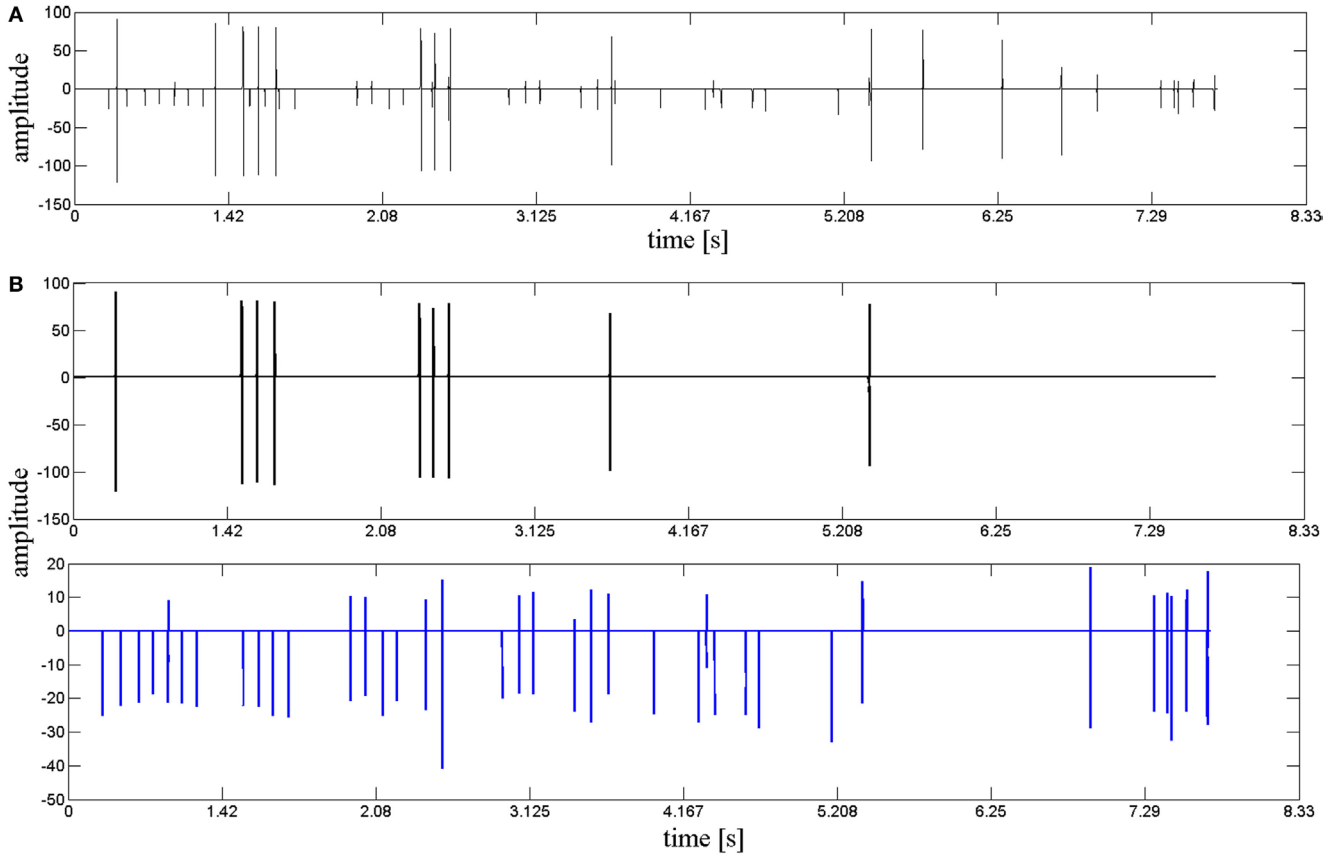

FIGURE 4 | The result of the cluster refinement. **(A)** A motor unit (MU) firing incorrectly clustered after original clustering. **(B)** Two correct MU firings (displayed, respectively, in black and blue) subdivided by cluster refinement.

To obtain a thorough EMG decomposition, superimposed waveforms need to be resolved into their constituent MUAPs. This stage is the most time-consuming and critical procedure in the whole EMG decomposition framework. As it is essential to obtain a high-level AR% and complete information, the consistent achievement of AR%s over 90% by the new framework represents a marked improvement over the 67% classification rate achieved by our previous methods (25). Two typical types of superposed waveform resolution approaches have been commonly employed: peel-off and modeling (31). In this study, we resolved superimposed waveforms using the peel-off approach based on a pseudo-correlation method that improves resolution efficiency. Despite its apparent efficacy, it should be noted that the peel-off method is incapable of identifying MUAP waveforms that superimpose in a destructive manner (1). Waveform resolution based on modeling can yield a more accurate separation but is also more time-consuming. Therefore, identifying a method that improves the efficiency and accuracy of superimposed waveform decomposition remains a focus for further exploration.

In summary, an effective EMG decomposition framework was developed. First, we utilized a novel MUAP segment extraction method to detect all active MUAP segments. This procedure was based on amplitude threshold detection and resting segment recognition. We then grouped the MUAP segments into single and overlapped waveforms using tetraphasic or hexaphasic detection schemes to save buffer size and improve computational efficiency. Third, all recognized single MUAP segments were aligned with the main peak at the center for the effective assessment of waveform similarities. Finally, we resolved superimposed waveforms using a peel-off approach based on a measure of PsC. By incorporating multiple analytical approaches, this developed EMG decomposition framework achieves accurate and complete results without hampering computational speed, which we believe will greatly benefit clinical EMG utilities.

ETHICS STATEMENT

The study protocol was approved by the West China ethics committee of Sichuan University and the Institutional Review Board of Third Xiangya Hospital, Central South University.

AUTHOR CONTRIBUTIONS

XR led the development of the proposed decomposition algorithm, participated in healthy subject experiment, data acquisition and analysis, and paper writing. CZ participated in stroke patient

experiment, data acquisition, and paper writing; XL participated in stroke patient recruitment, data acquisition, and analysis; and GY participated in algorithm development, data acquisition, and data analysis. TP participated in data analysis and the article polish. YZ participated in study design, algorithm development, data acquisition and analysis, and paper writing.

FUNDING

This work was supported in part by the National Natural Science Foundation, Guangdong Provincial Work Injury Rehabilitation Hospital, University of Houston and Third Xiangya Hospital at Central South University.

REFERENCES

1. Stashuk D. EMG signal decomposition: how can it be accomplished and used? *J Electromyogr Kinesiol* (2001) 11(3):151–73. doi:10.1016/s1050-6411(00)00050-x
2. Pattichis CS, Schizas CN, Middleton LT. Neural network models in EMG diagnosis. *IEEE Trans Biomed Eng* (1995) 42(5):486–96. doi:10.1109/10.376153
3. Stålberg E, Falck B, Sonoo M, Stålberg S, Åström M. Multi-MUP EMG analysis—a two year experience in daily clinical work. *Electroencephalogr Clin Neurophysiol* (1995) 97(3):145–54. doi:10.1016/0924-980x(95)00007-8
4. McGill KC, Lateva ZC, Marateb HR. EMGLAB: an interactive EMG decomposition program. *J Neurosci Methods* (2005) 149(2):121–33. doi:10.1016/j.jneumeth.2005.05.015
5. Florestal JR, Mathieu PA, Malanda A. Automated decomposition of intramuscular electromyographic signals. *IEEE Trans Biomed Eng* (2006) 53(5):832–9. doi:10.1109/tbme.2005.863893
6. Nawab SH, Wotiz RP, De Luca CJ. Decomposition of indwelling EMG signals. *J Appl Physiol* (2008) 105(2):700–10. doi:10.1152/japplphysiol.00170.2007
7. Zennaro D, Wellig P, Koch VM, Moschytz GS, Laubli T. A software package for the decomposition of long-term multichannel EMG signals using wavelet coefficients. *IEEE Trans Biomed Eng* (2003) 50(1):58–69. doi:10.1109/tbme.2002.807321
8. LeFever RS, De Luca CJ. A procedure for decomposing the myoelectric signal into its constituent action potentials—part I: technique, theory, and implementation. *IEEE Trans Biomed Eng* (1982) 29(3):149–57. doi:10.1109/tbme.1982.324881
9. McGill KC, Cummins KL, Dorfman LJ. Automatic decomposition of the clinical electromyogram. *IEEE Trans Biomed Eng* (1985) 32(7):470–7. doi:10.1016/0013-4694(83)92253-8
10. Stashuk D, De Bruin H. Automatic decomposition of selective needle-detected myoelectric signals. *IEEE Trans Biomed Eng* (1988) 35(1):1–10. doi:10.1109/10.1330
11. Hassoun MH, Wang C, Spitzer A. NNERVE: neural network extraction of repetitive vectors for electromyography. I. Algorithm. *IEEE Trans Biomed Eng* (1994) 41(11):1039–52. doi:10.1109/10.335842
12. Christodoulou CI, Pattichis CS. Unsupervised pattern recognition for the classification of EMG signals. *IEEE Trans Biomed Eng* (1999) 46(2):169–78. doi:10.1109/10.740879
13. Rasheed S, Stashuk D, Kamel M. A software package for interactive motor unit potential classification using fuzzy k-NN classifier. *Comput Methods Programs Biomed* (2008) 89(1):56–71. doi:10.1016/j.cmpb.2007.10.006
14. Florestal J, Mathieu P, McGill K. Automatic decomposition of multichannel intramuscular EMG signals. *J Electromyogr Kinesiol* (2009) 19(1):1–9. doi:10.1016/j.jelekin.2007.04.001
15. Nawab SH, Chang S-S, De Luca CJ. High-yield decomposition of surface EMG signals. *Neurophysiol Clin* (2010) 121(10):1602–15. doi:10.1016/j.clinph.2009.11.092
16. Parsaei H, Stashuk DW, Rasheed S, Farkas C, Hamilton-Wright A. Intramuscular EMG signal decomposition. *Crit Rev Biomed Eng* (2010) 38(5):435–65. doi:10.1615/critrevbiomedeng.v38.i5.20
17. Kouchaki S, Boostani R, Parsaei H. A new feature selection method for classification of EMG signals. *2012 16th CSI International Symposium on Artificial Intelligence and Signal Processing (AISP)*. Shiraz, Fars, Iran: IEEE (2012). p. 585–90.
18. Katsis CD, Exarchos TP, Papaloukas C, Goletsis Y, Fotiadis DI, Sarmas I. A two-stage method for MUAP classification based on EMG decomposition. *Comput Biol Med* (2007) 37(9):1232–40. doi:10.1016/j.compbiomed.2006.11.010
19. Malanda A, Navallas J, Rodriguez-Falces J, Rodriguez-Carreño I, Gila L. Averaging methods for extracting representative waveforms from motor unit action potential trains. *J Electromyogr Kinesiol* (2015) 25(4):581–95. doi:10.1016/j.jelekin.2015.04.007
20. Nikolic M, Sorensen JA, Dahl K, Krarup C. Detailed analysis of motor unit activity. *Proceedings of the 19th Annual International Conference of the IEEE Engineering in Medicine and Biology Society, 1997*. Chicago, IL, USA: IEEE (1997). p. 1257–60.
21. Andrade AO, Nasuto SJ, Kyberd P. Extraction of motor unit action potentials from electromyographic signals through generative topographic mapping. *J Franklin Inst* (2007) 344(3):154–79. doi:10.1016/j.jfranklin.2006.10.006
22. Erim Z, Lin W. Decomposition of intramuscular EMG signals using a heuristic fuzzy expert system. *IEEE Trans Biomed Eng* (2008) 55(9):2180–9. doi:10.1109/tbme.2008.923915
23. Nikolic M, Krarup C. EMGTools, an adaptive and versatile tool for detailed EMG analysis. *IEEE Trans Biomed Eng* (2011) 58(10):2707–18. doi:10.1109/tbme.2010.2064773
24. Farina D, Crosetti A, Merletti R. A model for the generation of synthetic intramuscular EMG signals to test decomposition algorithms. *IEEE Trans Biomed Eng* (2001) 48(1):66–77. doi:10.1109/10.900250
25. Ren X, Hu X, Wang Z, Yan Z. MUAP extraction and classification based on wavelet transform and ICA for EMG decomposition. *Med Biol Eng Comput* (2006) 44(5):371. doi:10.1007/s11517-006-0051-3
26. Ren X, Yan Z, Wang Z, Hu X. Noise reduction based on ICA decomposition and wavelet transform for the extraction of motor unit action potentials. *J Neurosci Methods* (2006) 158(2):313–22. doi:10.1016/j.jneumeth.2006.06.005
27. Thornton RC, Michell AW. Techniques and applications of EMG: measuring motor units from structure to function. *J Neurol* (2012) 259(3):585–94. doi:10.1007/s00415-011-6350-0
28. Mebarkia K, Bekka REh, Reffad A, Disselhorst-Klug C. Fuzzy MUAP recognition in HSR-EMG detection basing on morphological features. *J Electromyogr Kinesiol* (2014) 24(4):473–87. doi:10.1016/j.jelekin.2014.04.006
29. Karimimehr S, Marateb HR, Muceli S, Mansourian M, Mañanas MA, Farina D. A real-time method for decoding the neural drive to muscles using single-channel intra-muscular EMG recordings. *Int J Neural Syst* (2017) 27(6):1750025. doi:10.1142/s0129065717500253
30. Hu X, Suresh AK, Rymer WZ, Suresh NL. Assessing altered motor unit recruitment patterns in paretic muscles of stroke survivors using surface electromyography. *J Neural Eng* (2015) 12(6):066001. doi:10.1088/1741-2560/12/6/066001
31. Etawil H, Stashuk D. Resolving superimposed motor unit action potentials. *Med Biol Eng Comput* (1996) 34(1):33–40. doi:10.1007/bf02637020

Conflict of Interest Statement: The authors declare that the research was conducted in the absence of any commercial or financial relationships that could be construed as a potential conflict of interest.

frontiers in Neurology

ORIGINAL RESEARCH
published: 15 January 2018
doi: 10.3389/fneur.2017.00731

Surface Electromyographic Examination of Poststroke Neuromuscular Changes in Proximal and Distal Muscles Using Clustering Index Analysis

Weidi Tang[1], Xu Zhang[1], Xiao Tang[1], Shuai Cao[1], Xiaoping Gao[2] and Xiang Chen[1]*

[1] *Department of Electronic Science and Technology, University of Science and Technology of China, Hefei, China,*
[2] *Department of Rehabilitation Medicine, First Affiliated Hospital of Anhui Medical University, Hefei, China*

Whether stroke-induced paretic muscle changes vary across different distal and proximal muscles remains unclear. The objective of this study was to compare paretic muscle changes between a relatively proximal muscle (the biceps brachii muscle) and two distal muscles (the first dorsal interosseous muscle and the abductor pollicis brevis muscle) following hemisphere stroke using clustering index (CI) analysis of surface electromyograms (EMGs). For each muscle, surface EMG signals were recorded from the paretic and contralateral sides of 12 stroke subjects versus the dominant side of eight control subjects during isometric muscle contractions to measure the consequence of graded levels of contraction (from a mild level to the maximal voluntary contraction). Across all examined muscles, it was found that partial paretic muscles had abnormally higher or lower CI values than those of the healthy control muscles, which exhibited a significantly larger variance in the CI *via* a series of homogeneity of variance tests ($p < 0.05$). This finding indicated that both neurogenic and myopathic changes were likely to take place in paretic muscles. When examining two distal muscles of individual stroke subjects, relatively consistent CI abnormalities (toward neuropathy or myopathy) were observed. By contrast, consistency in CI abnormalities were not found when comparing proximal and distal muscles, indicating differences in motor unit alternation between the proximal and distal muscles on the paretic sides of stroke survivors. Furthermore, CI abnormalities were also observed for all three muscles on the contralateral side. Our findings help elucidate the pathological mechanisms underlying stroke sequels, which might prove useful in developing improved stroke rehabilitation protocols.

Keywords: muscle weakness, clustering index, surface electromyography, neuromuscular changes, stroke rehabilitation

OPEN ACCESS

Edited by:
Xiaogang Hu,
University of North Carolina at Chapel Hill, United States

Reviewed by:
Rong Song,
Sun Yat-sen University, China
Jun Yao,
Northwestern University, United States

****Correspondence:***
Xu Zhang
xuzhang90@ustc.edu.cn

Specialty section:
This article was submitted to Stroke, a section of the journal Frontiers in Neurology

Received: *07 September 2017*
Accepted: *18 December 2017*
Published: *15 January 2018*

Citation:
Tang W, Zhang X, Tang X, Cao S, Gao X and Chen X (2018) Surface Electromyographic Examination of Poststroke Neuromuscular Changes in Proximal and Distal Muscles Using Clustering Index Analysis. Front. Neurol. 8:731. doi: 10.3389/fneur.2017.00731

INTRODUCTION

Muscle weakness is the most common clinical symptom of many neuromuscular diseases (such as stroke and spinal cord injury) and it greatly impacts the day-to-day quality of life for patients and their caregivers (1, 2). Stroke studies have reported that weakness related to voluntary muscle contraction is a primary cause of impairments, including spastic hypertonia and abnormal movement

coordination (3). This contributes to impaired motor control (4). Therefore, it is of great importance to understand the specific pathological mechanisms underlying muscle weakness after a stroke, which is a prerequisite for designing effective stroke rehabilitation protocols.

The interruption of the corticospinal tract and muscle atrophy are commonly accepted as two potential contributors to the muscle weakness of stroke survivors (5, 6). How a cerebral lesion affects motor unit (MU) survival and function, however, still remains ambiguous. Since the MU offers a structure–function framework for understanding the neuromuscular system, investigations into MU alternations provide valuable insights into the neuropathology of stroke-induced muscle weakness. Many muscle biopsy studies have reported various contradictory findings. For example, little difference was found between the paretic side and contralateral side of stroke survivors even within populations of stroke subjects and control subjects (7, 8). However, some other muscle biopsy studies showed atrophy of type II fibers, small angular fibers, grouped atrophy, and fiber-type grouping (9, 10), which all indicated degeneration of MUs. The same results were observed in electrophysiological studies. Some studies have found spontaneous fibrillation potentials and positive sharp waves in paretic muscles (6, 9, 11). Furthermore, reduced compound muscle action potentials and MU number estimates were also reported (12–14). Nevertheless, other electrophysiological studies did not report consistent findings (15–17). These studies were associated with either invasive procedures or laborious electrical stimulations. In contrast, surface electromyogram (EMG) is an alternative approach for examining MU alternations in a noninvasive manner. Surface EMG studies in stroke patients have been previously performed through an EMG-force relation (18–20), peak amplitude distribution (21), and power spectral analysis (22). These studies have reported mixed observations, suggesting that there are a variety of complex neural and muscular changes collectively contributing to muscle weakness following a stroke (23–25).

However, different choices with respect to the muscles examined might be another explanation for the previously mixed observations. Muscles in various body parts often show different changes poststroke. For example, in an experiment involving simultaneous flexion of proximal and distal paretic muscles of stroke survivors, which included the deltoids, biceps, and wrist/finger flexors, the wrist/finger flexors had the lowest coefficient of variation (26). Furthermore, the finger flexor was also reported to have a higher motor unit action potential (MUAP) median frequency and larger range of MUAP RMS amplitude than biceps brachii (BB) muscles following stroke (27). One possible hypothesis to explain this is that the pathological MU alternation may take place in different muscles to different degrees and this might vary from proximal to distal positions. Therefore, it is necessary to explore whether there are differences in the MU alternation between proximal and distal muscles on the paretic sides of stroke survivors.

This study presented a novel study of the proximal and distal muscles of stroke subjects using the clustering index (CI) method. The CI method, originally proposed by Uesugi et al. (28), is applied on surface EMG signals to quantitatively assess the clustering degrees for the signals. The clustering or density degree of surface EMG signal, as characterized by the value of CI, can be a useful indicator of neuromuscular changes. It was found that highly clustered EMG interference patterns can be a sign of neurogenic changes, while flat and dense EMG interference patterns might indicate myopathic changes (28–30). Thus, the CI method has strong diagnostic power in differentiating neurogenic and myopathic changes (28). Taking advantage of such a powerful tool, we aimed to discriminate neurogenic and/or myopathic changes taking place in the paretic muscles of stroke survivors and we compared these changes among the proximal and distal muscles examined. Similarities or differences between the proximal and distal muscles after a stroke, if discernable by a CI analysis, might help to understand the specific pathological mechanisms underlying muscle weakness. This would contribute to the development of a more accurate rehabilitation protocol targeting different muscles.

MATERIALS AND METHODS

Subjects

Twelve stroke subjects (S1–S12, age: 63 ± 12 years, mean ± SD, range: 46–82 years) and eight age-matched healthy control subjects (C1–C8, age: 58 ± 10 years, range:48–75 years) were recruited for this study, which was approved by the Medical Ethics Review Committee at the First Affiliated Hospital of Anhui Medical University (FAHAMU, Hefei, Anhui Province, China). Study inclusion criteria included: (1) experience of first stroke with an initial onset >14 days; (2) medically stable with clearance to participate; (3) experience of hemiparesis with mild to severe muscle weakness on the paretic side; (4) ability to fully or partially perform voluntary contraction of the three examined muscles on the paretic side, including the BB muscle, the first dorsal interosseous (FDI) muscle, and the abductor pollicis brevis (APB) muscle; (5) no history of severe muscle spasticity for the three examined muscles based upon a modified Ashworth scale not exceeding 1 for any muscle; and (6) no history of concurrent neurological disorders or other symptoms (such as neuropathy or radiculopathy). All stroke subjects were recruited from the inpatient department of rehabilitation medicine in the FAHAMU. Clinical assessments performed prior to each patient's participation included both an assessment of motor recovery after a stroke based on the Brunnstrom stage and the upper-extremity component of the Fugl-Meyer test. Detailed information pertaining to the stroke subjects is presented in **Table 1**. Written consent was obtained from all subjects before the initiation of experiments.

Experiments

Ag/AgCl disc surface electrodes (Junkang, Shanghai, China) with a recording diameter of 10 mm were used for recording surface EMG signals. The surface EMG data were collected from the biceps, FDI muscle, and APB muscle on both sides of all stroke subjects and on the dominant side of all control subjects. After the skin was prepared with medical alcohol, a pair of electrodes was firmly attached to each targeted muscle and oriented in the direction of the muscle fibers with an inter-electrode distance

(center-to-center distance) of about 20 mm to produce a single-differential channel of surface EMG signals. A round electrode was placed on an arm fossa cubitalison on the same side as a reference. **Figure 1** illustrates the electrode placement on the right arm as an example.

TABLE 1 | Demographic information for each stroke subject.

ID #	Age in a range (years)	Duration (days)	Paretic side	B stage	F-M	MAS
S1	75–80	27	L	3	33	0
S2	71–75	89	L	2	15	0
S3	51–55	153	L	5	45	0
S4	81–85	34	L	5	55	0
S5	45–50	30	L	4	43	0
S6	55–60	71	L	4	21	0
S7	71–75	31	L	4	39	0
S8	55–60	47	R	3	38	0
S9	51–55	51	R	3	42	0
S10	61–65	28	L	2	29	0
S11	81–85	24	R	5	37	0
S12	45–50	45	L	4	34	0

B stage, Brunnstrom stage; F-M, upper-extremity Fugl-Meyer assessment; MAS, Modified Ashworth Scale.

During the experiment, subjects were seated in a comfortable chair with their tested arm bent approximately 90° and placed on a height-adjustable table. The stroke patients were also allowed to lie in an examination bed with their tested arm held still and placed against the inside of the body. The recordings were performed on each side of the subject in random order.

For each subject, the experiment was carried out in multiple trials. In each trial, the subjects were asked to perform a specific task according to the main function of the muscle being examined. We designed specific tasks to examine the APB, FDI, and BB muscles, including adducting the thumb, abducting the index finger, and elbow flexion, respectively. In a single trial, each task was performed as isometric muscle contractions with different contraction levels ranging from a mild to submaximal to, ultimately, maximal voluntary contractions (MVC). The contraction strengths roughly corresponded to 10, 30, 50, 70, and 90% of the full MVC. The contraction strengths were subjectively determined by each subject. In this regard, the MVC presented here was not accurately measured, but instead roughly estimated as the maximal level that each subject was encouraged to reach. At the same time, a resistance force was provided by the experimenter to help generate an isometric contraction. The corresponding resistance force was almost equal to the force provided by each subject.

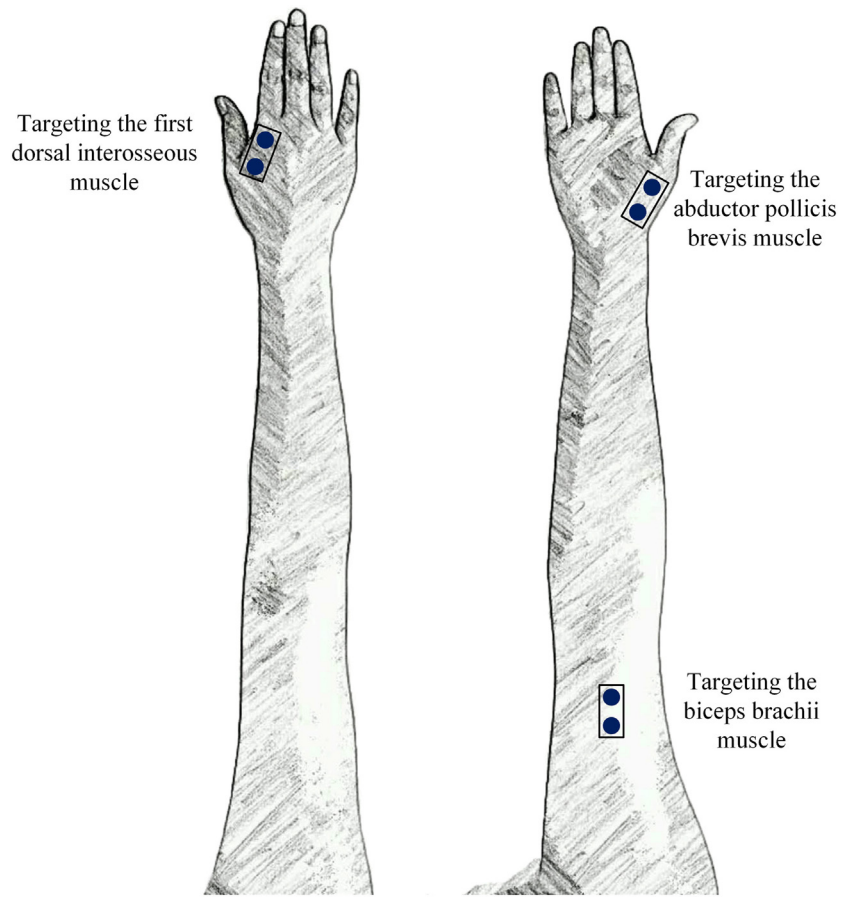

FIGURE 1 | The placement of three surface electromyogram (EMG) sensors that targeted three muscles in each arm.

In order to examine the APB muscle, a resistance force on the tested thumb was generated. As for the FDI muscle, a resistance force was applied on the index finger. When the BB muscle was examined, the subjects were instructed to perform elbow flexion with their elbow flexed at 90°, while a resistance force was applied on the inner side of the forearm. We encouraged the subjects to remain as stable as possible for at least 3 s during each type of contraction in order to ensure that the interference EMG patterns recorded for each trial exhibited a sequence of graded contraction levels. For each task, multiple (almost 3) trials were performed in order to obtain a sufficient amount of data. Sufficient rest was allowed between consecutive trials to avoid mental and muscular fatigue.

Surface EMG data were recorded using a custom-made data acquisition system supporting up to 128 EMG channels. Each recorded EMG channel was amplified by a two-stage amplifier with a total gain of 60 dB, which was band-pass filtered at 20–500 Hz and subsequently converted into digitalized data with a 16-bit A/D converter. The sampling rate for each channel was set to 1,000 Hz. All recorded data were transferred to a laptop computer *via* a USB cable for off-line analysis in Matlab (The Mathworks, MA, USA) using customized programs.

Data Analysis

Each surface EMG channel was preprocessed using a zero-lag fourth-order Butterworth band-pass filter at 20–500 Hz to eliminate low-frequency motion artifacts and high-frequency interference. If necessary, a set of second-order notch filters at the 50-Hz power line interference and its harmonics were also applied.

Since we collected data from three different muscles, the following data analyses were performed on individual muscles. Specifically, for each muscle, data segmentation was done after preprocessing. According to the experimental protocol, the recorded surface EMG data in each trial generated graded interference patterns. Thus, a series of non-overlapping epochs with a 1-s duration were segmented from the recorded data, using a straightforward scheme based on the signal amplitude thresholding (31). These epochs were selected from stable isometric muscle contractions. Those epochs with varying contraction strengths were discarded. We obtained approximately 10 epochs from each trial, including epochs at different force strengths. Finally, for each muscle, we obtained approximately 30 epochs from different force strengths. The following CI analysis was performed on these epochs from each muscle.

In order to calculate CI values, the signal for each epoch was divided into a series of non-overlapping consecutive windows of the same length. We set the window length as 15 ms, which was considered to include approximately one individual MUAP in this study (28–30). We assumed that there were k windows derived in an epoch, and the area of each window was A_i. The differential sequences for the area values between every consecutive window (DA_i), every second window (DB_i), and every third window (DC_i) were defined as follows:

$$DA_i = A_{i+1} - A_i, \qquad \text{for } i = 1,2,\ldots,k-1, \tag{1}$$

$$DB_i = A_{i+2} - A_i, \qquad \text{for } i = 1,2,\ldots,k-2, \tag{2}$$

$$DC_i = A_{i+3} - A_i, \qquad \text{for } i = 1,2,\ldots,k-3. \tag{3}$$

Consequently, we can calculate CI according to the following equation:

$$CI = \left(\sum_{i=1}^{k-1} DA_i^2 + \sum_{i=1}^{k-2} DB_i^2 + \sum_{i=1}^{k-3} DC_i^2 \right) / 6 \times \sum_{i=1}^{k} A_i^2. \tag{4}$$

The CI values ranged from 0 to 1, while the higher values were derived from signals with higher area clustering degrees, which appeared isolated in large action potential spikes (30).

Since the CI value is affected by muscle contraction strength, its effect needed to be taken into consideration prior to the establishment of diagnostic criteria. A linear relationship was reported between the CI value and the signal area (representing the muscle contraction strength calculated by $\text{Area} = \sum_{i=1}^{k} A_i$) of the epochs from all healthy control subjects using a double-logarithmic scale, and it was recommended by the proposer of the CI method. We found this was also the case for our data and the processed the data in the same way. Therefore, each analysis epoch was expressed as a point in the CI-area plot with the value of log (Area) and log (CI). For each muscle examined, the points derived from all the analysis epochs were scattered to form a data cloud in a CI-area plot. More details can be found in **Figure 2** and the Section "Results."

Quantification of the normal data reference was the prerequisite for identifying muscle abnormalities using the CI method. To define the normal range in the CI-area plot, we performed a linear regression analysis on epochs ($1 \leq \text{Area} \leq 100$ μV·s) collected from the corresponding control muscles for both log (CI) and log (Area). Subsequently, for each epoch, the deviation of CI on the logarithmic scale from the linear regression line was calculated. These deviation values were averaged over all the epochs from each examined muscle, and a mean residual (R_m) was obtained. The R_m was then used to assess the presence of abnormalities for each muscle.

Afterward, the mean μ_R and SD σ_R of the R_m values for all corresponding muscles of all controls were calculated. On this basis, a Z-score for the R_m, which was calculated by $(R_m - \mu_R)/\sigma_R$, was defined for a tested muscle in a given subject. According to the original literature regarding the CI method (28, 30), Z-scores were used as the final representative indicator for the diagnostic assessment. We defined a muscle with a Z-score outside ±2.5 as abnormal. Assuming that the normal data obey a Gaussian/normal distribution, probability for a Z-score outside ±2.5 (with a deviation of 2.5 times SD from the mean) is less than 1.25%. With such a low probability, a Z-score outside this range was defined to be abnormal. Further, muscle with a Z-score higher than +2.5 was diagnosed as neurogenic, while a Z-score lower than −2.5 indicated a myopathic change.

Statistical Analysis

We first performed a series of homogeneity of variance tests (F-tests) on Z-scores derived from any two of the three groups (the paretic, the contralateral, and the control) for each of the three examined muscles/positions. Then, a series of Student's

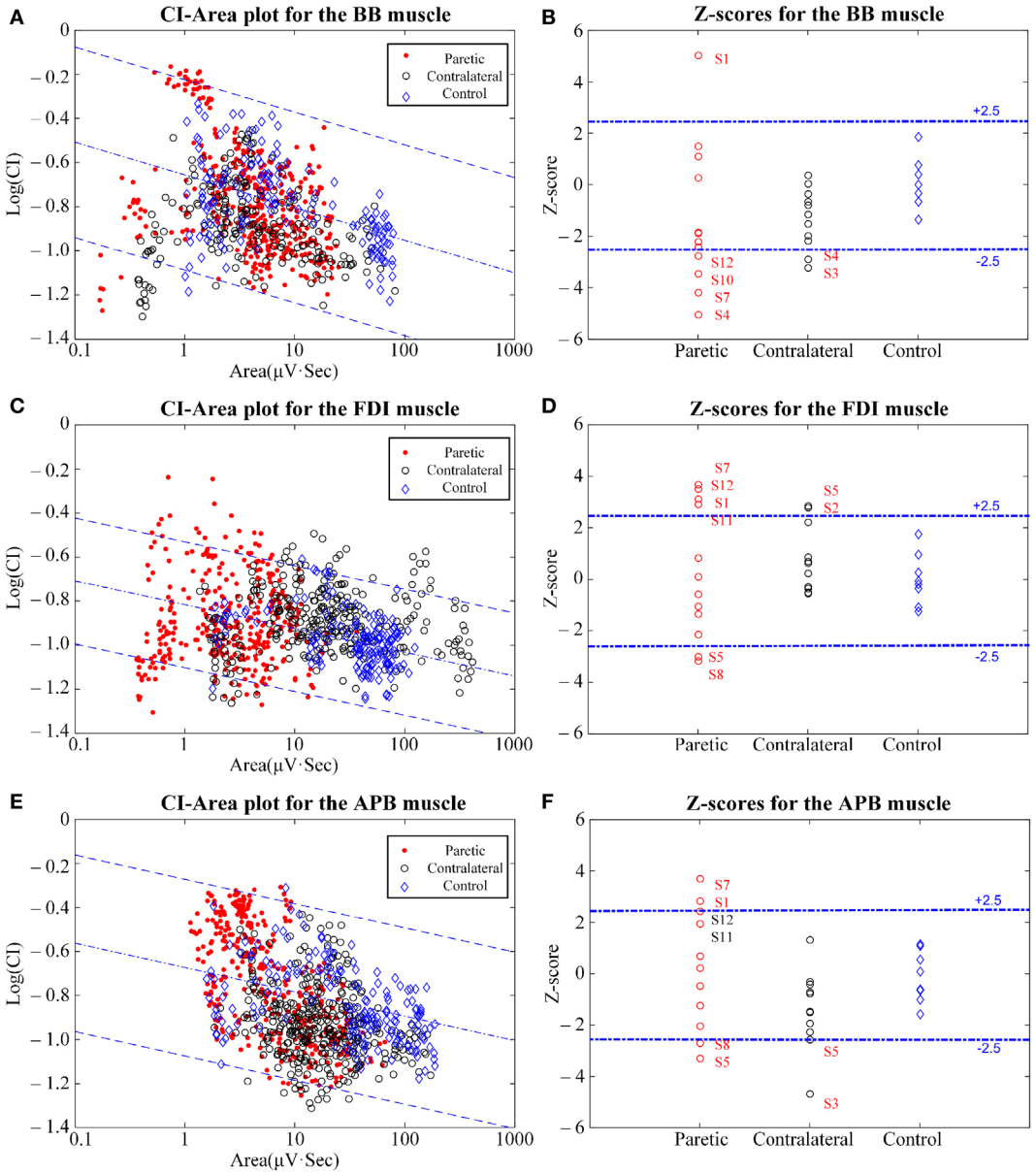

FIGURE 2 | The clustering index (CI)-area plot [**(A,C,E)** left panel] and the resultant *Z*-scores [**(B,D,F)** right panel] using CI analysis of the biceps brachii (BB) muscle **(A,B)**, the first dorsal interosseous (FDI) muscle **(C,D)**, and the abductor pollicis brevis (APB) muscle **(E,F)**. In the CI-area plots, the red dots represent the paretic muscles, the black circles represent the contralateral muscles, and the blue rhombuses represent the control muscles. In the subplots for the *Z*-scores, the muscles with *Z*-scores outside the normal range and some approximating to the normal range are marked with their subject IDs.

t-tests were performed to compare the *Z*-scores derived from both the paretic muscle group and the control muscle group for each of three examined muscles/positions. Moreover, a two-way repeated-measure analysis of variance (ANOVA) was applied to the *Z*-scores with both sides (two observation levels: contralateral and paretic) and muscles/positions (three observation levels: BB, FDI, and APB) considered as within-subject factors. When necessary, *post hoc* pairwise multiple comparisons with a Bonferroni correction were used. The level of statistical significance was set to $p < 0.05$ for all analyses. All statistical analyses were completed using SPSS software (ver. 16.0, SPSS Inc., Chicago, IL, USA).

RESULTS

Figure 2 shows the results of the CI-area plot and the *Z*-scores for the signals of all three muscles examined on the contralateral and the paretic sides of all stroke subjects and on the dominant sides of all control subjects. In the CI-area plots, we observed that all the control data were distributed over the normal area (spanning within ±2.5 times the SE of the linear regression), while some epochs from the paretic and contralateral muscles were scattered outside the normal range. In particular, a portion of the epochs from the paretic muscles were found to be distributed beyond or

below the normal range. Furthermore, epochs from the paretic muscles were always distributed at a narrower horizontal range when compared with those from the contralateral muscles and the control muscles.

Of all the control subjects, the *Z*-scores derived from the BB muscle (0.00 ± 1.00, mean ± SD), the FDI muscle (0.00 ± 1.00), and the APB muscle (-0.13 ± 0.99) scored within the predefined normal range from −2.5 to +2.5. In contrast, on the paretic side of all stroke subjects, the *Z*-scores were reported to be -1.33 ± 2.83 for paretic BB muscles, 0.23 ± 2.54 for paretic FDI muscles, and 0.068 ± 2.28 for paretic APB muscles. Some subjects displayed *Z*-scores outside the normal range. This was true for each of the three paretic muscles examined. On the contralateral side of all stroke subjects, the *Z*-scores were -1.30 ± 1.11 for the contralateral BB muscle, -1.41 ± 1.46 for the contralateral APB muscle, and 0.67 ± 1.28 for the contralateral FDI muscle.

The homogeneity of variance test revealed that paretic muscles had significant larger variances in *Z*-scores than the control muscles ($p < 0.05$) for each of the three muscles examined. In contrast, both the contralateral muscles and the control muscles exhibited homogeneity of variance for the *Z*-scores, and no significant differences were observed between them for any of the three examined muscles ($p > 0.05$). The Student's *t*-tests revealed no significant differences in *Z*-scores between the paretic muscles and the control muscles ($p > 0.05$). In addition, the two-way repeated-measure ANOVA only yielded an overall significant effect of muscle/position ($F = 6.04$, $p = 0.008$), while the side-related effect ($F = 0.299$, $p = 0.595$) and the interaction ($F = 2.071$, $p = 0.15$) between both factors were found to be insignificant. The FDI muscle was found to yield higher *Z*-scores than any of the other two muscles, and statistical significance was obtained by *post hoc* pairwise comparisons ($p = 0.006$ for FDI versus BB muscle; $p = 0.008$ for FDI versus APB muscle). No statistical significance was found between the BB muscle and the FDI muscle ($p = 0.329$).

In particular, on the paretic side, one BB muscle from the subject S1, four FDI muscles from S1, S7, S11, and S12, and two APB muscles from S1 and S7, all had *Z*-scores greater than +2.5. These were diagnosed as being neurogenic changes. At the same time, four BB muscles from S4, S7, S10, and S12, two FDI muscles, and two APB muscles both from S5 and S8 all had *Z*-scores below −2.5. For these cases, myopathic abnormalities were reported. The paretic muscles that are not mentioned above had *Z*-scores within the normal range. Moreover, on the contralateral sides, two BB muscles from S4 and S3, in addition to two APB muscles from S5 and S3, had *Z*-scores below −2.5. Meanwhile, two FDI muscles from S2 and S5 had *Z*-scores above +2.5. The other remaining contralateral muscles were all reported to be normal.

DISCUSSION

In this study, we examined the FDI muscle, APB muscle, and BB muscle on both sides of all stroke subjects, in addition to the dominant sides of all control subjects using the CI method. The CI method was employed because of its reported diagnostic power in discriminating neuromuscular changes. Each paretic muscle examined showed diverse CI alternations when compared with the corresponding control muscle. Moreover, abnormalities in the two distal muscles (the FDI muscle and the APB muscle) have been obviously consistent, while this has not been the case for the proximal muscle (the biceps) when compared to distal muscles at the individual level. Regardless, abnormalities have also been reported on the contralateral side using the CI analysis.

Another reason for applying the CI method was its simple and convenient protocol as a result of manipulating and examining surface EMGs. Aside from its noninvasive aspects, the protocol does not involve accurate measurements of muscle force with a load cell, which is regarded to be tedious and time consuming (19–22). Although previous studies reported that accurate force measurements were crucial for providing substantial information (4) during routine clinical EMG examination, clinical electrophysiologists offer appropriate resistance to the tested muscle to estimate its level of activation (28–30). The use of this approach allows this study to have potentially wide applications in clinical practice.

This study confirms the previous report that CI analysis of surface EMG signals is capable of revealing complex neuromuscular changes occurring in paretic muscles following a stroke (29). For each examined muscle, some stroke subjects showed abnormally high *Z*-scores on the paretic side, indicating neuropathic changes. The abnormal increase in CI values in paretic muscles may be attributed to MU loss, reorganization of the MU architecture [including fiber-type grouping (10, 14)], and muscle fiber reinnervation (21, 23, 24, 32, 33), impairment of MU control properties [such as compression of MU recruitment threshold (18, 21, 34)], an increase in MUAP synchronization (35–37), and a reduction in MU firing rates (37–39). All of these factors are very likely to occur after a stroke as reported by previous studies. For some paretic muscles, we observed an abnormal decrease in CI leading to *Z*-scores that were lower than the predefined normal range, indicating myopathic changes. A CI decrease means that a flatter and denser surface EMG was very likely due to muscle fiber atrophy (9, 40, 41) and a selective degeneration of the large and superficial MUs (41–43). Both phenomena have been reported in stroke studies. For the other paretic muscles, their *Z*-scores fell within the normal range. However, their experience of substantial muscle weakness needs to be carefully considered. Two primary reasons may relate to the "normal" CI examination. One reason is a combination or canceling effect of both neurogenic and myopathic processes. The other is a deficit of the descending central drive. In the event of upper motor neuron lesions, the lower motor neurons and the muscles themselves might still function more or less normally without significant degeneration (25). Therefore, the paretic muscles that do not display EMG abnormalities still suffer from substantial muscle weakness.

It is worth noting that in the original CI method, CI decreases are mainly attributed to myopathic changes. The differential loss of relatively larger MUs is regarded as leading to the CI decreases in this study, but it is only a factor indicating neurogenic changes. This limits the traditional distinction between neurogenic and myopathic changes using the CI method. Therefore, it is necessary

to supplement and even revise the way CI results are interpreted in order to draw diagnostic conclusions given the findings from this stroke study. Furthermore, we find that muscle fiber atrophy and the differential loss of larger MUs are both factors potentially contributing to the CI decrease. In the early phases since stroke onset (which is true for a majority of stroke subjects in this study), however, there is limited chance for the former factor to occur (9, 40). Therefore, the differential loss of larger MUs is regarded as the primary reason for the abnormal CI decrease observed in our study.

Across three different muscles on the paretic side, the two distal muscles showed almost consistent results, whereas the corresponding proximal muscle had obviously inconsistent CI scores for the same stroke subjects. This is a really interesting finding that needs to be further explained. The anatomical innervation structure would be one reason. It is well known that the FDI and APB muscles are dominated by the ulnar nerve and the median nerve, respectively, and both originate from the C8 andT1 spinal cord segments. In contrast, the BB muscle is dominated by the musculocutaneous nerve derived from the C5, C6, and C7 spinal cord segments. The difference in spinal cord segments and nerve root levels may contribute to diverse paretic muscle changes across both distal and proximal muscles at the individual subject level. This implies that the pathological changes as a result of the hemisphere brain damage have significant structural characteristics.

Different muscular structures and their original characteristics may be another reason. For example, the tissues (such as the fat or skin) between the electrode and the targeted muscle are considered to be a volume conductor likely to filter out high-frequency components of surface EMG signals. This effect of the volume conductor is always enhanced by the proximal BB muscles because of its thicker tissue composition compared to the other two distal muscles. Therefore, the ability for the CI-based surface EMG to discern some neurogenic changes (such as muscle fiber reinnervation and MU architecture reorganization) might be compromised because they likely result in reinnervated, enlarged MUs that specifically contribute to high-frequency EMG activities. As mentioned above, these neurogenic processes should lead to a CI increase. When various processes occur involving both concurrent CI increases and decreases, the reduced impact of the processes leading to a CI increase may collectively decrease CI values. This could account for the overall CI decrease in BB muscle when compared with the other two distal muscles.

Additionally, both of the distal muscles are regarded as dominantly carrying small MUs composed of slow-twitch, low-force muscle fibers, which are suitable for fine motor control. In contrast, the BB muscle consists of a greater portion of larger MUs with faster muscle fibers that generate larger forces. It has been discussed above that the selective loss of larger and superficial MUs is potentially taking place in paretic muscles, leading to a decrease in the CI. Therefore, the BB muscle is hypothesized to lose its larger MUs because of the impact of a stroke, whereas this factor may not be evident for smaller and more distal muscles. This hypothesis is partially supported by our experimental data. Part B of **Figure 2** show that 4 out of the 12 paretic BB muscles that had abnormally decreased CI and *Z*-scores, many more than that number (2) of distal paretic FDI and APB muscles reported CI abnormalities with *Z*-scores below −2.5. Thus, a greater proportion of larger MUs in the proximal BB muscle likely degenerate following a stroke compared to small distal muscles like the FDI and APB.

It is surprising that the CI-revealed neuromuscular abnormalities appeared in some muscles on the contralateral side of stroke subjects regardless of the muscle position. This finding is inconsistent with our current understanding that the contralateral muscles are considered to be neurologically intact. The muscle abnormalities on the contralateral side might be attributed to impaired interactions in the partially damaged brain (44, 45). Furthermore, motor control in muscle that is compensatory on the contralateral side after hemiparesis is another reason (46). For example, changes in control strategies in the motor neuron pool may lead to altered MU recruitment strategies and firing properties. This finding suggests the necessity of delivering a treatment to the contralateral muscles during stroke rehabilitation.

The main limitation of this study was the limited choice of either proximal or distal muscles. Future investigations will be continuously performed with more muscles in order to draw stronger conclusions. Moreover, although CI measurements can provide a valuable assessment of paretic muscles, more delicate analyses are required to further discriminate the underlying complex factors contributing to the observed CI patterns (47). Modeling (18, 48) might be an effective approach to detect the CI marker's sensitivity with respect to individual factors, which will help to obtain a more accurate interpretation of abnormal CI findings. All of these efforts will help us better understand muscle pathologies that arise after a stroke, which is the prerequisite for designing and developing effective stroke rehabilitation protocols.

ETHICS STATEMENT

This study was approved by the Medical Ethic Review Committee at the First Affiliated Hospital of Anhui Medical University (FAHAMU, Hefei, Anhui Province, China). The written consent was obtained from all subjects before experiments.

AUTHOR CONTRIBUTIONS

WT analyzed the data, interpreted the results, and wrote the first draft of the manuscript. XZ designed the study, including data collection, analysis, interpretation, and a substantial revision of the manuscript. XT and SC participated in data collection and interpretation. XG and XC participated in data analysis, interpretation, and manuscript revision. All authors approved the final version of the manuscript.

FUNDING

This work was supported in part by the National Natural Science Foundation of China under Grants 61771444 and 61401421.

REFERENCES

1. Pellatt GC. Neurogenic continence. Part 1: pathophysiology and quality of life. *Br J Nurs* (2008) 17(13):836–41. doi:10.12968/bjon.2008.17.13.30534
2. Zhang X, Zhou P. High-density myoelectric pattern recognition toward improved stroke rehabilitation. *IEEE Trans Biomed Eng* (2012) 59(6):1649–57. doi:10.1109/TBME.2012.2191551
3. Kamper DG, Fischer HC, Cruz EG, Rymer WZ. Weakness is the primary contributor to finger impairment in chronic stroke. *Arch Phys Med Rehabil* (2006) 87(9):1262–9. doi:10.1016/j.apmr.2006.05.013
4. Chang SH, Zhou P, Rymer WZ, Li S. Spasticity, weakness, force variability, and sustained spontaneous motor unit discharges of resting spastic–paretic biceps brachii muscles in chronic stroke. *Muscle Nerve* (2013) 48(1):85–92. doi:10.1002/mus.23699
5. Chokroverty S, Medina J. Electrophysiological study of hemiplegia: motor nerve conduction velocity, brachial plexus latency, and electromyography. *Arch Neurol* (1978) 35(6):360–3. doi:10.1001/archneur.1978.00500300034005
6. Brown WF, Snow R. Denervation in hemiplegic muscles. *Stroke* (1990) 21(12):1700–4. doi:10.1161/01.STR.21.12.1700
7. Qiu Y, Wada Y, Otomo E, Tsukagoshi H. Morphometric study of cervical anterior horn cells and pyramidal tracts in medulla oblongata and the spinal cord in patients with cerebrovascular diseases. *J Neurol Sci* (1991) 102(2):137–43. doi:10.1016/0022-510X(91)90061-B
8. Terao SI, Li M, Hashizume Y, Osano Y, Mitsuma T, Sobue G. Upper motor neuron lesions in stroke patients do not induce anterograde transneuronal degeneration in spinal anterior horn cells. *Stroke* (1997) 28(12):2553–6. doi:10.1161/01.STR.28.12.2553
9. Dattola R, Girlanda P, Vita G, Santoro M, Roberto ML, Toscano A, et al. Muscle rearrangement in patients with hemiparesis after stroke: an electrophysiological and morphological study. *Eur Neurol* (1993) 33(2):109–14. doi:10.1159/000116915
10. Segura RP, Sahgal V. Hemiplegic atrophy: electrophysiological and morphological studies. *Muscle Nerve* (1981) 4(3):246–8. doi:10.1002/mus.880040312
11. Spaans F, Wilts G. Denervation due to lesions of the central nervous system: an EMG study in cases of cerebral contusion and cerebrovascular accidents. *J Neurol Sci* (1982) 57(2):291–305. doi:10.1016/0022-510X(82)90036-3
12. Li X, Wang YC, Suresh NL, Rymer WZ, Zhou P. Motor unit number reductions in paretic muscles of stroke survivors. *IEEE Trans Inf Technol Biomed* (2011) 15(4):505–12. doi:10.1109/TITB.2011.2140379
13. Hara Y, Masakado Y, Chino N. The physiological functional loss of single thenar motor units in the stroke patients: when does it occur? Does it progress? *Neurophysiol Clin* (2004) 115(1):97–103. doi:10.1016/j.clinph.2003.08.002
14. McComas AJ, Fawcett PRW, Campbell MJ, Sica REP. Electrophysiological estimation of the number of motor units within a human muscle. *J Neurol Neurosurg Psychiatry* (1971) 34(2):121–31. doi:10.1136/jnnp.34.2.121
15. Alpert S, Idarraga S, Orbegozo J, Rosenthal AM. Absence of electromyographic evidence of lower motor neuron involvement in hemiplegic patients. *Arch Phys Med Rehabil* (1971) 52(4):179.
16. Kouzi I, Trachani E, Anagnostou E, Rapidi CA, Ellul J, Sakellaropoulos GC, et al. Motor unit number estimation and quantitative needle electromyography in stroke patients. *J Electromyogr Kinesiol* (2014) 24(6):910–6. doi:10.1016/j.jelekin.2014.09.006
17. Alpert S, Jarrett S, Lerner IM, Rosenthal AM. Electromyographic findings in early hemiplegia. *Arch Phys Med Rehabil* (1973) 54(10):464.
18. Zhou P, Suresh NL, Rymer WZ. Model based sensitivity analysis of EMG–force relation with respect to motor unit properties: applications to muscle paresis in stroke. *Ann Biomed Eng* (2007) 35(9):1521–31. doi:10.1007/s10439-007-9329-3
19. Zhou P, Li X, Zev Rymer W. EMG-force relations during isometric contractions of the first dorsal interosseous muscle after stroke. *Top Stroke Rehabil* (2013) 20(6):537–43. doi:10.1310/tsr2006-537
20. Tang A, Rymer WZ. Abnormal force – EMG relations in paretic limbs of hemiparetic human subjects. *J Neurol Neurosurg Psychiatry* (1981) 44(8):690–8. doi:10.1136/jnnp.44.8.690
21. Li X, Suresh A, Zhou P, Rymer WZ. Alterations in the peak amplitude distribution of the surface electromyogram poststroke. *IEEE Trans Biomed Eng* (2013) 60(3):845–52. doi:10.1109/TBME.2012.2205249
22. Yao B, Zhang X, Li S, Li X, Chen X, Klein CS, et al. Analysis of linear electrode array EMG for assessment of hemiparetic biceps brachii muscles. *Front Hum Neurosci* (2015) 9:569. doi:10.3389/fnhum.2015.00569
23. Li Y, Chen X, Zhang X, Zhou P. Several practical issues toward implementing myoelectric pattern recognition for stroke rehabilitation. *Med Eng Phys* (2014) 36(6):754–60. doi:10.1016/j.medengphy.2014.01.005
24. Li X, Shin H, Zhou P, Niu X, Liu J, Rymer WZ. Power spectral analysis of surface electromyography (EMG) at matched contraction levels of the first dorsal interosseous muscle in stroke survivors. *Neurophysiol Clin* (2014) 125(5):988–94. doi:10.1016/j.clinph.2013.09.044
25. Zhang X, Wei Z, Ren X, Gao X, Chen X, Zhou P. Complex neuromuscular changes post-stroke revealed by clustering index analysis of surface electromyogram. *IEEE Trans Neural Syst Rehabil Eng* (2017) 25(11):2105–12. doi:10.1109/TNSRE.2017.2707582
26. Miller LC, Thompson CK, Negro F, Heckman CJ, Farina D, Dewald JP. High-density surface EMG decomposition allows for recording of motor unit discharge from proximal and distal flexion synergy muscles simultaneously in individuals with stroke. *2014 36th Annual International Conference of the IEEE Engineering in Medicine and Biology Society (EMBC)*. Chicago, IL: IEEE (2014). p. 5340–4.
27. McPherson LM, Negro F, Thompson CK, Sanchez L, Heckman CJ, Dewald J, et al. Properties of the motor unit action potential shape in proximal and distal muscles of the upper limb in healthy and post-stroke individuals. *2016 IEEE 38th Annual International Conference of the Engineering in Medicine and Biology Society (EMBC)*. Orlando, FL: IEEE (2016). p. 335–9.
28. Uesugi H, Sonoo M, Stålberg E, Matsumoto K, Higashihara M, Murashima H, et al. "Clustering Index method": a new technique for differentiation between neurogenic and myopathic changes using surface EMG. *Neurophysiol Clin* (2011) 122(5):1032–41. doi:10.1016/j.clinph.2010.08.012
29. Zhang X, Barkhaus PE, Rymer WZ, Zhou P. Machine learning for supporting diagnosis of amyotrophic lateral sclerosis using surface electromyogram. *IEEE Trans Neural Syst Rehabil Eng* (2014) 22(1):96–103. doi:10.1109/TNSRE.2013.2274658
30. Higashihara M, Sonoo M, Yamamoto T, Nagashima Y, Uesugi H, Terao Y, et al. Evaluation of spinal and bulbar muscular atrophy by the clustering index method. *Muscle Nerve* (2011) 44(4):539–46. doi:10.1002/mus.22119
31. Zhang X, Chen X, Li Y, Lantz V, Wang K, Yang J. A framework for hand gesture recognition based on accelerometer and EMG sensors. *IEEE Trans Syst Man Cybern A Syst Hum* (2011) 41(6):1064–76. doi:10.1109/TSMCA.2011.2116004
32. Lukács M. Electrophysiological signs of changes in motor units after ischaemic stroke. *Neurophysiol Clin* (2005) 116(7):1566–70. doi:10.1016/j.clinph.2005.04.005
33. Lukács M, Vécsei L, Beniczky S. Changes in muscle fiber density following a stroke. *Neurophysiol Clin* (2009) 120(8):1539–42. doi:10.1016/j.clinph.2009.06.001
34. Hu X, Suresh AK, Rymer WZ, Suresh NL. Assessing altered motor unit recruitment patterns in paretic muscles of stroke survivors using surface electromyography. *J Neural Eng* (2015) 12(6):066001. doi:10.1088/1741-2560/12/6/066001
35. Hausmanowa-Petrusewicz I, Kopec J. EMG parameters changes in the effort pattern at various loads in diseased muscle. *Electromyogr Clin Neurophysiol* (1982) 23(3):213–28.
36. Datta AK, Farmer SF, Stephens JA. Central nervous pathways underlying synchronization of human motor unit firing studied during voluntary contractions. *J Physiol* (1991) 432:401. doi:10.1113/jphysiol.1991.sp018391
37. Gemperline JJ, Allen S, Walk D, Rymer WZ. Characteristics of motor unit discharge in subjects with hemiparesis. *Muscle Nerve* (1995) 18(10):1101–14. doi:10.1002/mus.880181006
38. Hu XL, Tong KY, Hung LK. Firing properties of motor units during fatigue in subjects after stroke. *J Electromyogr Kinesiol* (2006) 16(5):469–76. doi:10.1016/j.jelekin.2005.09.005
39. Li X, Holobar A, Gazzoni M, Merletti R, Rymer WZ, Zhou P. Examination of poststroke alteration in motor unit firing behavior using high-density surface EMG decomposition. *IEEE Trans Biomed Eng* (2015) 62(5):1242–52. doi:10.1109/TBME.2014.2368514
40. Chokroverty S, Reyes MG, Rubino FA, Barron KD. Hemiplegic amyotrophy: muscle and motor point biopsy study. *Arch Neurol* (1976) 33(2):104–10. doi:10.1001/archneur.1976.00500020032006

41. Kallenberg LA, Hermens HJ. Motor unit properties of biceps brachii in chronic stroke patients assessed with high-density surface EMG. *Muscle Nerve* (2009) 39(2):177–85. doi:10.1002/mus.21090
42. Knight CA, Kamen G. Superficial motor units are larger than deeper motor units in human vastus lateralis muscle. *Muscle Nerve* (2005) 31(4):475–80. doi:10.1002/mus.20265
43. Lukacs M, Vécsei L, Beniczky S. Large motor units are selectively affected following a stroke. *Neurophysiol Clin* (2008) 119(11):2555–8. doi:10.1016/j.clinph.2008.08.005
44. Yarosh CA, Hoffman DS, Strick PL. Deficits in movements of the wrist ipsilateral to a stroke in hemiparetic subjects. *J Neurophysiol* (2004) 92(6):3276–85. doi:10.1152/jn.00549.2004
45. Harris ML, Polkey MI, Bath PM, Moxham J. Quadriceps muscle weakness following acute hemiplegic stroke. *Clin Rehabil* (2001) 15(3):274–81. doi:10.1191/026921501669958740
46. Levin MF, Hui-Chan C. Ankle spasticity is inversely correlated with antagonist voluntary contraction in hemiparetic subjects. *Electromyogr Clin Neurophysiol* (1994) 34(7):415–25.
47. Chen X, Wang ZJ, McKeown M. Joint blind source separation for neurophysiological data analysis: multiset and multimodal methods. *IEEE Signal Process Mag* (2016) 33(3):86–107. doi:10.1109/MSP.2016.2521870
48. Hu X, Rymer WZ, Suresh NL. Motor unit firing rate patterns during voluntary muscle force generation: a simulation study. *J Neural Eng* (2014) 11(2):026015. doi:10.1088/1741-2560/11/2/026015

Conflict of Interest Statement: The authors declare that this research was conducted in the absence of any commercial or financial relationships that could be construed as a potential conflict of interest.

frontiers in Neurology

CASE REPORT
published: 10 January 2018
doi: 10.3389/fneur.2017.00728

Using Corticomuscular Coherence to Reflect Function Recovery of Paretic Upper Limb after Stroke: A Case Study

*Yang Zheng[1], Yu Peng[2,3], Guanghua Xu[1], Long Li[2] and Jue Wang[2]**

[1] State Key Laboratory for Manufacturing Systems Engineering, School of Mechanical Engineering, Xi'an Jiaotong University, Xi'an, China, [2] The Key Laboratory of Biomedical Information Engineering of Ministry of Education, School of Life Science and Technology, Institute of Biomedical Engineering, Xi'an Jiaotong University, Xi'an, China, [3] The Department of Rehabilitation Medicine, First Affiliated Hospital of Xi'an Jiaotong University, Xi'an, China

Purpose: Motor deficits after stroke are supposed to arise from the reduced neural drive from the brain to muscles. This study aimed to demonstrate the feasibility of reflecting the motor function improvement after stroke with the measurement of corticomuscular coherence (CMC) in an individual subject.

Method: A stroke patient was recruited to participate in an experiment before and after the function recovery of his paretic upper limb, respectively. An elbow flexion task with a constant muscle contraction level was involved in the experiment. Electromyography and electroencephalography signals were recorded simultaneously to estimate the CMC. The non-parameter statistical analysis was used to test the significance of CMC differences between the first and second times of experiments.

Result: The strongest corticomuscular coupling emerged at the motor cortex contralateral to the contracting muscles for both the affected and unaffected limbs. The strength of the corticomuscular coupling between activities from the paretic limb muscles and the contralateral motor cortex for the second time of experiment increased significantly compared with that for the first time. However, the CMC of the unaffected limb had no significant changes between two times of experiments.

Conclusion: The results demonstrated that the increased corticomuscular coupling strength resulted from the motor function restoration of the paretic limb. The measure of CMC can reflect the recovery of motor function after stroke by quantifying interactions between activities from the motor cortex and controlled muscles.

Keywords: stroke, electromyography, electroencephalography, corticomuscular coherence, motor impairment

OPEN ACCESS

Edited by:
Sheng Li,
University of Texas Health Science Center at Houston, United States

Reviewed by:
Xu Zhang,
University of Science and Technology of China, China
Dong Feng Huang,
Sun Yat-sen University, China

****Correspondence:***
Jue Wang
juewangxjtu1@gmail.com

Specialty section:
This article was submitted to Stroke, a section of the journal Frontiers in Neurology

Received: *27 September 2017*
Accepted: *18 December 2017*
Published: *10 January 2018*

Citation:
Zheng Y, Peng Y, Xu G, Li L and Wang J (2018) Using Corticomuscular Coherence to Reflect Function Recovery of Paretic Upper Limb after Stroke: A Case Study. Front. Neurol. 8:728. doi: 10.3389/fneur.2017.00728

INTRODUCTION

Stroke is one of the major diseases that cause long-term motor deficits of adults (1). However, our poor understanding of the mechanisms underlying motor impairments after stroke limits greatly the development of effective intervention and evaluation methods. In general, motor impairments after stroke are deemed to arise from changes in both neural and muscle properties. Poststroke changes in

the neural system have been studied from different points of view such as the decreased excitability of the affected cortex (2, 3) and the increased inhibitory effect from the unaffected hemisphere on the affected hemisphere (4). Spasm and flaccid paresis of muscles are believed to result from the loss of control input from the brain at different phases after stroke. Even though stroke survivors have been demonstrated to have significant descending information flow in the affected side during the chronic period (5), there is evidence that poststroke impairments reflect the reduced central neural drive to muscles. Mima et al. and Fang et al. found that the functional coupling between cortical commands and consequent muscle activities of stroke subjects were weaker than that of healthy controls (6, 7). The conduction time from the central cortical rhythm to peripheral oscillations in the affected side was significantly prolonged compared with that of the unaffected side after stroke (8).

It is believed that stroke interrupts the motor-related neural network and then reduces the neural drive to the muscles. The coherent activities between the motor cortex and the muscles are believed to reflect the synchronized discharge of corticospinal cells (9). It can be estimated by analyzing the frequency domain coherence (10) between electromyography (EMG) and electroencephalography (EEG) signals termed as corticomuscular coherence (CMC). Although previous studies have demonstrated that the CMC strength of poststroke subjects was weaker than that of healthy controls, it is still not clear whether the corticomuscular coupling will enhance along with the motor function recovery to directly reflect the motor function state of paretic limbs after stroke. In the current study, a poststroke patient was recruited to participate in two times of experiments involving an elbow flexion task. The time interval between two times of experiments was determined to guarantee that the patient had obtained an obvious motor function recovery of the affected upper extremity. CMC from two times of experiments was estimated and compared to verify whether motor function recovery can be reflected by the change of corticomuscular coupling strength.

BACKGROUNDS

Experiment and Subject

An elbow flexion task was designed for the stroke patient because only poor rehabilitation outcomes can be generally obtained for hand. The force applied by the elbow flexion was monitored by a strain gage and fed back to the patient visually to help him finish the task with moderate and constant muscle contractions (11), because coherence analyses (12, 13) have demonstrated that the coupling is most pronounced in the beta-band range during steady muscle contractions and the beta-band CMC is assumed to be associated with strategies for controlling submaximal muscle forces (12, 14, 15). The designed motion task and the visual feedback information on screen are illustrated in **Figures 1A,B**, respectively. A trial was initiated when a circle and a target ring showed on screen and was over when they disappeared. Each trial lasted 11 s and there was a 2-s long interval between adjacent trials. Each run contained 20 trials and each side of upper limbs performed two runs, respectively. The subject practiced before data recording until the target force could be reached within the first 2 s of each trial.

The Net Amps 300 system together with a polygraph input box (Electrical Geodesics Inc.) was selected to amplify the EEG and EMG signals. An elastic cap that has 128 electrodes was used to detect EEG activities, and EMG signals were recorded from the biceps brachii using two adhesive surface electrodes with a 2-cm interelectrode distance. The reference electrode for EEG recording was located at the "Cz" position. The ground electrode, common for EEG and EMG signals, was positioned on the midline of the scalp at the level of the prefrontal cortex. EEG and EMG signals were sampled at 1,000 Hz together with event markers to synchronize with force signals. Force data were recorded simultaneously from the strain gage at a sampling rate of 200 Hz. All signals were saved on a hard disk for off-line analyses.

The subject suffered from his first cerebral hemorrhage at the right basal ganglia and had paralysis of his left upper extremity.

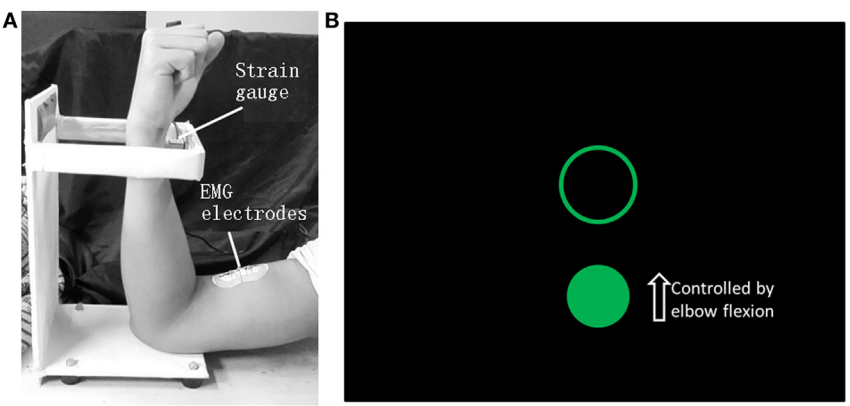

FIGURE 1 | The motion task of elbow flexion **(A)** and the visual feedback information on screen **(B)**. When the biceps brachii contracts, the wrist will press the strain gage and the force level can be detected. The circle can be shifted vertically by applying force to the strain gage and the position of the ring is fixed. The subject was requested to move the circle into the ring as soon as possible when a trial started and maintain the force until the end of a trial when the circle and the ring both disappeared. The force needed to shift the circle into the ring was 3 N.

His age was 35. No cognition impairment was reported. Two times of experiments were performed with an interval of 1 month. The first time was carried out 6 weeks after the stroke onset. During the period, the subject was in hospital and received regular rehabilitation trainings including physical therapy and occupational therapy. The Fugl-Meyer (upper limb section) score was 15 points for the first time of experiment and a Fugl-Meyer score of 38 points was obtained for the second time. The subject participated in the experiment with the approval of the local ethics committee and the informed consent in accordance with the Declaration of Helsinki. The written informed consent was obtained from the subject for the publication of this case report.

Data Analyses

The same CMC estimation method was used as in our previous study (11). Original EEG and EMG signals were first filtered using a two-pass finite impulse response filter with a pass band from 3 to 45 Hz. Artifacts caused by eye blinks, cardiac activities, and power-line interferences were eliminated with the independent component analysis method (16, 17). Then, EEG and EMG signals within the muscle contraction period of each trial were segmented to 1 s long segments with no overlap. EEG signals from all electrodes within each segment were transformed into the reference-free current source density (CSD) distribution using the scalp surface Laplacian (18–20). The CMC spectrum for each EEG electrode was determined by calculating the coherence between the corresponding CSD signal and the unrectified EMG signal with the multitaper method (21).

A non-parameter statistic method (22) was used to compare the difference of the CMC between the first and second times of experiments. This method can solve the unequal estimation bias problem and the multiple comparison problem in the statistical analysis of frequency domain coherence differences under two different conditions (22). The original CMC difference $C_1(f) - C_2(f)$ was transformed to the z-spectrum CMC difference,

$$Z(f) = \frac{\left(\tanh^{-1}\left(C_1(f)\right) - n_1\right) - \left(\tanh^{-1}\left(C_2(f)\right) - n_2\right)}{\sqrt{n_1 + n_2}},$$

where $n_1 = 1/d_1 - 2$, $n_2 = 1/d_2 - 2$, $C_1(f)$ and $C_2(f)$ are the CMC spectrum of condition 1 and 2, respectively. d_1 and d_2 are the number of degrees of freedom for coherence estimation (22). The procedure to estimate the p-value included several steps. Data segments from both conditions were first merged into a single set and then randomly selected to construct new data sets for both conditions. The result of this procedure was called a random partition and the corresponding $Z(f)$ was estimated. A test statistic that was based on the clustering of adjacent frequencies (22) was extracted from $Z(f)$ to avoid the multiple comparison problem. The procedures above were repeated for a large number of times (5,000 times), and a histogram of the test statistics from all random partitions was constructed. From the test statistic calculated with the actually observed data and the histogram constructed with all random partitions, the proportion of the random partitions that resulted in a larger test statistic than the observed one, i.e., the Monte Carlo p value, was calculated.

Results

The topographies of beta-band (15–30) CMC from the first and second times of experiments are illustrated in **Figures 2** and **3**, respectively. **Figures 2A** and **3A** illustrate the CMC topographies between activities from the cortex and the right biceps brachii. **Figures 2B** and **3B** show the results with the left biceps brachii as the peripheral reference. A consistent result was that the strongest CMC emerged at the contralateral motor area to the contracting muscles. Meanwhile, there were minor differences about the electrode locations where the strongest CMC showed up between the first and second times of experiments. They might result from the small shift of wearing positions of the electrode cap. Further statistical analyses were based on the CMC spectrum obtained at the electrodes where the strongest beta-band corticomuscular coupling emerged.

The non-parameter statistical analysis was performed to verify whether there were significant differences of the beta-band CMC between the first and second times of experiments. The CMC spectrum between activities from the left biceps brachii (affected side) and the contralateral motor cortex is illustrated in **Figure 4A**. For the first time of experiment, the spectrum peaks

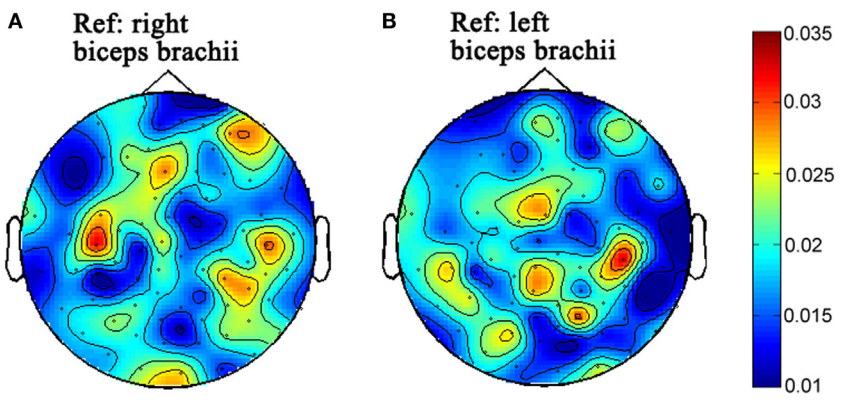

FIGURE 2 | The topographies of beta-band (15–30 Hz) corticomuscular coherence with the peripheral reference of right biceps brachii **(A)** and left biceps brachii **(B)**, respectively for the first time of experiment.

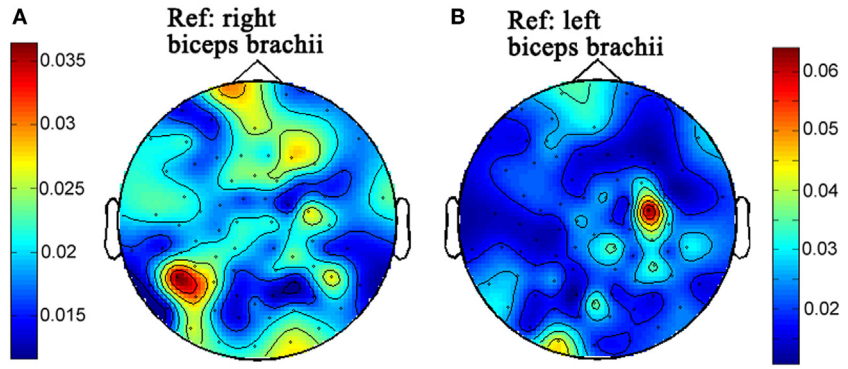

FIGURE 3 | The topographies of beta-band (15–30 Hz) corticomuscular coherence with the peripheral reference of right biceps brachii **(A)** and left biceps brachii **(B)**, respectively for the second time of experiment.

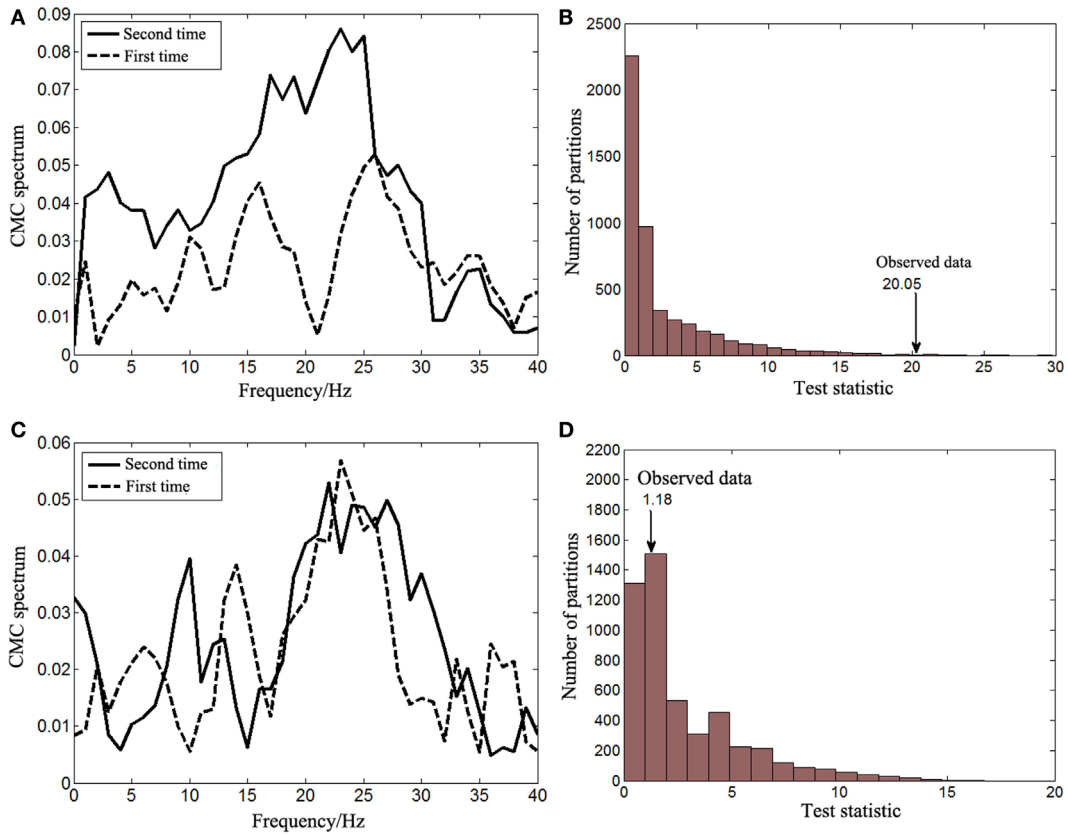

FIGURE 4 | The corticomuscular coherence (CMC) spectrum between activities from the right motor cortex and the left biceps brachii **(A)** and the results of the corresponding statistical analysis for the beta-band CMC differences between two times of experiments **(B)**. The CMC spectrum between activities from the left motor cortex and the right biceps brachii **(C)** and the results of the corresponding statistical analysis for the beta-band CMC differences between two times of experiments **(D)**.

within the beta band were located at 16 and 26 Hz, respectively and there was a sharp decrease at 21 Hz. For the second time of experiment, the spectrum peaks were similarly located within the beta band at around 18 and 23 Hz. The beta-band CMC magnitude of the second time was apparently larger than that of the first time. The null hypothesis was that the beta-band CMC of the second time was not larger than that of the first time when muscles of the affected side contracted. The distribution of test statistics from 5,000 random partitions is shown in **Figure 4B**. The test statistic of the observed data was 20.05 and the resulting Monte Carlo p-value was 0.005. Thus, the null hypothesis was rejected and the beta-band CMC of the second time was

significantly larger than that of the first time when muscles of the affected side contracted.

The significance of the beta-band CMC difference between the first and second times of experiments when the right biceps brachii (unaffected side) contracted was also tested with the non-parameter statistical analysis. The CMC spectrum of both times of experiments is illustrated in **Figure 4C**. There was no obvious difference of the CMC spectrum within the beta band. The peaks were both located at approximately 24 Hz and their amplitudes were similar. The null hypothesis was, therefore, set to be that there was no significant difference of the beta-band CMC between the first and second times of experiments when muscles of the unaffected side contracted. The distribution of test statistics from 5,000 random partitions is shown in **Figure 4D**, and the test statistic of the observed data was 1.18 with a Monte Carlo *p*-value of 0.7306. The null hypothesis cannot be rejected and, therefore, it was correct.

DISCUSSIONS

Poststroke motor deficits arise essentially from the damages to the descending spinal tracks. The damage makes the brain lose control of limb muscles. CMC is believed to be a direct measure of interactions between physiological oscillatory activities from the brain and the controlled muscles. Therefore, the corticomuscular coupling strength might be weakened by stroke theoretically. However, it is not known whether stroke survivors can regain the normal strength level of corticomuscular coupling after motor function recovery. The most significant result of the current study was that the corticomuscular coupling strength between activities from the paretic limb muscles and the contralateral motor cortex increased along with the recovery of the patient's paretic limb. However, the CMC of the unaffected limb had no significant changes, which demonstrated that the familiarization with the task could not contribute to the increase of the corticomuscular coupling strength in the current study. Therefore, the increased coupling strength of the affected limb would only result from the motor function recovery of the paretic upper limb. This means that the measure of CMC can reflect the change of abilities for the brain to control muscular activities after stroke. Further studies will recruit more stroke subjects and focus on the sensitivity of the CMC as a measure to quantify the motor function state of paretic limbs.

The corticomuscular coupling is weakened for poststroke patients compared with healthy controls (6, 7). The results in the current study further demonstrated that the recovery of motor function was related to the enhanced corticomuscular coupling. In addition, previous studies showed that improved fine movement control was related to higher CMC (13, 23) and motor learning was associated with increased CMC and better performance (23). Thus, it may be speculated that increasing the corticomuscular coupling strength of the paretic limb for stroke patients is both the goal and the way for regaining motor function. Many factors have been identified to influence the corticomuscular coupling strength and some of them have the potential to be utilized in limb rehabilitation interventions (11). Above all, the results of the current study remind us that exploring the influence of rehabilitation interventions on corticomuscular coupling may provide another way to verify their validity from a new point.

In the current study, the CMC showed significant beta-band differences. This was inconsistent with Fang's study in which CMC differences between stroke patients and healthy controls mainly occurred in the gamma band (6). This might be caused by the fact that different motion tasks were used. The elbow flexion task in the current study involved isometric muscle contractions with static output force while the reaching task in Fang's study was more related to isometric muscle contractions with dynamic output force. Omlor et al. (24) demonstrated that corticomuscular coupling occurred within the beta band under the condition of isometric muscle contractions with static output force; whereas the most significant CMC shifted to the gamma band with isometric muscle contractions with dynamic output force. The difference of coherent frequency bands might reflect different ways for the brain to control muscle contractions under different conditions.

The CMC spectrum in **Figure 4** showed that the peak magnitude of beta-band CMC of the affected side was larger than that of the unaffected side after recovery. This is consistent with the results from Mima's study in which stroke survivors at their chronic phase were recruited (7). The study demonstrated that the corticomuscular coupling of unaffected side was significantly stronger than that of affected side during power grip and wrist extension. However, the corticomuscular coupling of unaffected side was slightly weaker during elbow flexion compared with that of affected side even though it is counterintuitive. The exact underlying mechanism is not known but might be associated with the contribution of the descending direct corticospinal pathway to the proximal and distal muscles after stroke (25). Further studies will be needed to verify its universality and fully understand the neural mechanism.

The limitation of the current study was that we cannot tell whether the increased corticomuscular coupling strength resulted from spontaneous recovery or motor rehabilitation training. Since the patient was at his subacute stage of stroke, spontaneous recovery could happen. Meanwhile, he received physical and occupational therapy that also might result in his recovery. Therefore, it cannot be verified through our study whether the spontaneous recovery or the rehabilitation training alone, or both contributed to the increased corticomuscular coupling. This will be explored in our further studies.

CONCLUDING REMARKS

This study demonstrated that the corticomuscular coupling strength for the paretic limb increased along with its function recovery while the coupling strength for the unaffected limb did not change through a case study. We concluded that interrupted corticomuscular interactions account for the motor deficits and CMC, as a measure of coherent activities between motor cortex and controlled muscles, can reflect the function recovery of paretic limbs after stroke.

ETHICS STATEMENT

This study was carried out in accordance with the recommendations of the Biomedical Research Ethics Committee of School of Life Science and Technology in Xi'an Jiaotong University with written informed consent from the subject. The subject gave written informed consent in accordance with the Declaration of Helsinki. The protocol was approved by the Biomedical Research Ethics Committee of School of Life Science and Technology in Xi'an Jiaotong University.

AUTHOR CONTRIBUTIONS

Drafted manuscript and contributed to acquisition, analysis, and interpretation: YZ. Critically revised the manuscript for important intellectual content and gave final approval and agreement to be accountable for all aspects of the work: YZ, YP, GX, LL, and JW. Contributed to conception or design: YZ, YP, and LL. Contributed to conception and interpretation: GX and JW. Contributed to acquisition and interpretation: YP and LL.

FUNDING

This work was supported by the project funded by China Postdoctoral Science Foundation (Grant No. 2017M620445), the Integration Project of Major Research Plan of the Natural Science Foundation of China (Grant No. 91420301), the Project of the Natural Science Foundation of China (Grant No. 51475360), and the Suzhou Science and Technology Planning Project (Grant No. SYS201510).

REFERENCES

1. Sanders DH, Sanderson M, Hayes S, Kilrane M, Greig CA, Brazzelli MG, et al. Physical fitness training for stroke patients. *Stroke* (2016) 35(9):CD003316. doi:10.1002/14651858.CD003316.pub6
2. Traversa R, Cicinelli P, Pasqualetti P, Filippi M, Rossini PM. Follow-up of interhemispheric differences of motor evoked potentials from the 'affected' and 'unaffected' hemispheres in human stroke. *Brain Res* (1998) 803(1–2):1–8. doi:10.1016/S0006-8993(98)00505-8
3. Turton A, Wroe S, Trepte N, Fraser C, Lemon RN. Contralateral and ipsilateral EMG responses to transcranial magnetic stimulation during recovery of arm and hand function after stroke. *Electroencephalogr Clin Neurophysiol* (1996) 101(4):316–28. doi:10.1016/0924-980X(96)95560-5
4. Hummel FC, Cohen LG. Non-invasive brain stimulation: a new strategy to improve neurorehabilitation after stroke? *Lancet Neurol* (2006) 5(8):708–12. doi:10.1016/S1474-4422(06)70525-7
5. Meng F, Tong K-y, Chan S-t, Wong W-w, Lui K-h, Tang K-w, et al. Study on connectivity between coherent central rhythm and electromyographic activities. *J Neural Eng* (2008) 5(3):324. doi:10.1088/1741-2560/5/3/005
6. Fang Y, Daly JJ, Sun J, Hvorat K, Fredrickson E, Pundik S, et al. Functional corticomuscular connection during reaching is weakened following stroke. *Clin Neurophysiol* (2009) 120(5):994–1002. doi:10.1016/j.clinph.2009.02.173
7. Mima T, Toma K, Koshy B, Hallett M. Coherence between cortical and muscular activities after subcortical stroke. *Stroke* (2001) 32(11):2597–601. doi:10.1161/hs1101.098764
8. Meng F, Tong K-Y, Chan S-T, Wong W-W, Lui K-H, Tang K-W, et al. Cerebral plasticity after subcortical stroke as revealed by cortico-muscular coherence. *IEEE Trans Neural Syst Rehabil Eng* (2009) 17(3):234–43. doi:10.1109/TNSRE.2008.2006209
9. Baker SN, Olivier E, Lemon RN. Coherent oscillations in monkey motor cortex and hand muscle EMG show task-dependent modulation. *J Physiol* (1997) 501(Pt 1):225–41. doi:10.1111/j.1469-7793.1997.225bo.x
10. Rosenberg JR, Amjad AM, Breeze P, Brillinger DR, Halliday DM. The Fourier approach to the identification of functional coupling between neuronal spike trains. *Prog Biophys Mol Biol* (1989) 53(1):1–31. doi:10.1016/0079-6107(89)90004-7
11. Yang Z, Lin G, Gang W, Wang Y, Zi Y, Wang X, et al. The influence of unilateral contraction of hand muscles on the contralateral corticomuscular coherence during bimanual motor tasks. *Neuropsychologia* (2016) 85:199–207. doi:10.1016/j.neuropsychologia.2016.03.028
12. Kilner JM, Baker SN, Salenius S, Hari R, Lemon RN. Human cortical muscle coherence is directly related to specific motor parameters. *J Neurosci* (2000) 20(23):8838–45.
13. Kristeva R, Patino L, Omlor W. Beta-range cortical motor spectral power and corticomuscular coherence as a mechanism for effective corticospinal interaction during steady-state motor output. *Neuroimage* (2007) 36(3):785–92. doi:10.1016/j.neuroimage.2007.03.025
14. Conway BA, Halliday DM, Farmer SF, Shahani U, Maas P, Weir AI, et al. Synchronization between motor cortex and spinal motoneuronal pool during the performance of a maintained motor task in man. *J Physiol* (1995) 489 (Pt 3):917–24. doi:10.1113/jphysiol.1995.sp021104
15. Halliday DM, Conway BA, Farmer SF, Rosenberg JR. Using electroencephalography to study functional coupling between cortical activity and electromyograms during voluntary contractions in humans. *Neurosci Lett* (1998) 241(1):5–8. doi:10.1016/S0304-3940(97)00964-6
16. Jung TP, Makeig S, Westerfield M, Townsend J, Courchesne E, Sejnowski TJ. Removal of eye activity artifacts from visual event-related potentials in normal and clinical subjects. *Clin Neurophysiol* (2000) 111(10):1745–58. doi:10.1016/S1388-2457(00)00386-2
17. Jung TP, Makeig S, Humphries C, Lee TW, McKeown MJ, Iragui V, et al. Removing electroencephalographic artifacts by blind source separation. *Psychophysiology* (2000) 37(2):163–78. doi:10.1111/1469-8986.3720163
18. Graziadio S, Basu A, Tomasevic L, Zappasodi F, Tecchio F, Eyre JA. Developmental tuning and decay in senescence of oscillations linking the corticospinal system. *J Neurosci* (2010) 30(10):3663–74. doi:10.1523/JNEUROSCI.5621-09.2010
19. Boonstra TW, van-Wijk BCM, Praamstra P, Daffertshofer A. Corticomuscular and bilateral EMG coherence reflect distinct aspects of neural synchronization. *Neurosci Lett* (2009) 463(1):17–21. doi:10.1016/j.neulet.2009.07.043
20. Andrykiewicz A, Patino L, Naranjo JR, Witte M, Hepp-Reymond MC, Kristeva R. Corticomuscular synchronization with small and large dynamic force output. *BMC Neurosci* (2007) 8:101. doi:10.1186/1471-2202-8-101
21. Percival DB, Walden AT. *Spectral Analysis for Physical Applications*. Cambridge: Cambridge University Press (1993).
22. Maris E, Schoffelen JM, Fries P. Nonparametric statistical testing of coherence differences. *J Neurosci Methods* (2007) 163(1):161–75. doi:10.1016/j.jneumeth.2007.02.011
23. Mendez-Balbuena I, Huethe F, Schulte-Mönting J, Leonhart R, Manjarrez E, Kristeva R. Corticomuscular coherence reflects interindividual differences in the state of the corticomuscular network during low-level static and dynamic forces. *Cereb Cortex* (2012) 22(3):628–38. doi:10.1093/cercor/bhr147
24. Omlor W, Patino L, Heppreymond MC, Kristeva R. Gamma-range corticomuscular coherence during dynamic force output. *Neuroimage* (2007) 34(3):1191–8. doi:10.1016/j.neuroimage.2006.10.018
25. Turton A, Lemon R. The contribution of fast corticospinal input to the voluntary activation of proximal muscles in normal subjects and in stroke patients. *Exp Brain Res* (1999) 129(4):559–72. doi:10.1007/s002210050926

Conflict of Interest Statement: The authors declare that the research was conducted in the absence of any commercial or financial relationships that could be construed as a potential conflict of interest.

frontiers in Neurology

ORIGINAL RESEARCH
published: 04 January 2018
doi: 10.3389/fneur.2017.00716

Electroencephalogram–Electromyography Coupling Analysis in Stroke Based on Symbolic Transfer Entropy

*Yunyuan Gao[1], Leilei Ren[1], Rihui Li[2,3] and Yingchun Zhang[1,2,3]**

[1] College of Automation, Intelligent Control & Robotics Institute, Hangzhou Dianzi University, Hangzhou, China, [2] Department of Biomedical Engineering, University of Houston, Houston, TX, United States, [3] Guangdong Provincial Work-Injury Rehabilitation Hospital, Guangzhou, China

The coupling strength between electroencephalogram (EEG) and electromyography (EMG) signals during motion control reflects the interaction between the cerebral motor cortex and muscles. Therefore, neuromuscular coupling characterization is instructive in assessing motor function. In this study, to overcome the limitation of losing the characteristics of signals in conventional time series symbolization methods, a variable scale symbolic transfer entropy (VS-STE) analysis approach was proposed for corticomuscular coupling evaluation. Post-stroke patients (n = 5) and healthy volunteers (n = 7) were recruited and participated in various tasks (left and right hand gripping, elbow bending). The proposed VS-STE was employed to evaluate the corticomuscular coupling strength between the EEG signal measured from the motor cortex and EMG signal measured from the upper limb in both the time-domain and frequency-domain. Results showed a greater strength of the bi-directional (EEG-to-EMG and EMG-to-EEG) VS-STE in post-stroke patients compared to healthy controls. In addition, the strongest EEG–EMG coupling strength was observed in the beta frequency band (15–35 Hz) during the upper limb movement. The predefined coupling strength of EMG-to-EEG in the affected side of the patient was larger than that of EEG-to-EMG. In conclusion, the results suggested that the corticomuscular coupling is bi-directional, and the proposed VS-STE can be used to quantitatively characterize the non-linear synchronization characteristics and information interaction between the primary motor cortex and muscles.

Keywords: corticomuscular coupling, symbolic transfer entropy, stroke, electroencephalogram, electromyography

OPEN ACCESS

Edited by:
Xiaogang Hu, University of North Carolina at Chapel Hill, United States

Reviewed by:
Chang-Hwan Im, Hanyang University, South Korea
Zhen Yuan, University of Macau, China

****Correspondence:***
Yingchun Zhang
yzhang94@uh.edu

Specialty section:
This article was submitted to Stroke, a section of the journal Frontiers in Neurology

Received: *02 October 2017*
Accepted: *12 December 2017*
Published: *04 January 2018*

Citation:
Gao Y, Ren L, Li R and Zhang Y (2018) Electroencephalogram–Electromyography Coupling Analysis in Stroke Based on Symbolic Transfer Entropy. Front. Neurol. 8:716. doi: 10.3389/fneur.2017.00716

INTRODUCTION

Electroencephalogram (EEG) is a non-invasive brain imaging technique that uses scalp electrodes to measure the voltage fluctuations induced by the mass electrical activity of neurons (1). Electromyography (EMG) technique is usually used to record the electrical activity produced by skeletal muscles (2). In the process of movement, the central nervous system associated with relevant brain regions and the peripheral nerve system associated with specific muscles is automatically synchronized in addition to the synergistic effect between different brain regions (1, 2). As such, the synchronization strength reflects the interaction between the primary motor cortex and the muscles and provides theoretical basis for the rehabilitation of stroke and dyskinesia patients (3).

Since Conway et al. (4) first reported a correlation between EEG and EMG in the process of exercise in 1995, dynamic interactions between brain activities and muscle motion feedbacks have been

widely investigated. It was found that the coherence of EEG–EMG signals is closely related to the motion tasks (5). For instance, the oscillation in the beta band is associated with mild-to-moderate isometric contraction, and the oscillation in the low range of the gamma band is related to strategies for controlling stronger muscle force production and dynamic movements (6). Various coherence analysis techniques, including cortical–muscular functional coupling (7, 8), Granger causality analysis (9, 10), transfer entropy (TE) analysis (11, 12), and symbolic transfer entropy (STE) analysis (13) have been developed and applied to EEG and EMG signal coupling analysis. Among these, the STE technique is an effective method to analyze the relationship between neural and muscular activity coupling. In general, the STE yields characteristics not depending on the established model and non-linear quantitative analysis (14). It can be used to estimate the functional coupling strength and information transfer direction between cortices and muscles and to reveal movement control and response mechanisms during movements (15). For instance, the STE has been used to analyze the non-linear functional connection between EEG single and surface EMG signals of hand muscles (16), which demonstrated that the functional corticomuscular coupling is significant in the beta band in the static force output for healthy subjects.

However, the STE also holds ineligible challenges in practice. For example, the number of symbols applied in the time sequence in traditional STE is fixed, which is therefore not flexible and dynamic characteristics of signals are easily lost. In addition, the STE has only been applied to health subjects so far, has not been tested in stroke patient population yet (16–18).

To bridge this gap, a variable scale symbolic transfer entropy (VS-STE) analysis approach was developed in this study to better investigate the corticomuscular coupling in both post-stroke patients and healthy volunteers. In particular, the corticomuscular coupling strength was assessed based on the EEG signals measured from the motor cortex and EMG signals obtained from upper limb in both time-domain and frequency-domain. The EEG–EMG coupling strength of subjects were also quantitatively evaluated in terms of significant area, which provided evidence to apply corticomuscular coupling in the rehabilitative evaluation of motor function disorders.

MATERIALS AND METHODS

Experimental Design

Participants

Twelve male subjects, including a control group ($n = 7$, age: 25.7 ± 1.11 years, all right handed) and a patient group ($n = 5$, age: 47.8 ± 2.28 years) were recruited in this study. The details of the subjects are summarized in **Table 1**, where S1, S2, and S3 are patients with mild stroke, S4 and S5 are patients with severe stroke, and S6–S12 are healthy volunteers. The study protocol was approved by the Institutional Review Board of Guangdong Provincial Work Injury Rehabilitation Hospital. Prior to the experiment, all the subjects were informed of the details of the experiments and signed the informed consent form.

TABLE 1 | Demographic information the subjects.

Subject #	Age	Used hand	Status	Condition
S1	45	Left	Suffering from stroke for 2 months	Small amount of bleeding in right intracranial brain, left foot cannot walk flexibly
S2	47	Right	Suffering from stroke for 1 month	Right brain intracranial hemorrhage, limbs can only complete the basic actions
S3	49	Right	Suffering from stroke for 1 month	Right brain intracranial hemorrhage, limbs can complete basic movements
S4	51	Right	Suffering from stroke for 2 months	Right brain intracranial hemorrhage, upper limbs can only complete simple actions
S5	47	Right	Suffering from stroke for 1 month	Right brain intracranial hemorrhage, upper limbs can only complete simple actions
S6	27	Right	Healthy	No
S7	26	Right	Healthy	No
S8	24	Right	Healthy	No
S9	25	Right	Healthy	No
S10	27	Right	Healthy	No
S11	26	Right	Healthy	No
S12	25	Right	Healthy	No

Experimental Paradigm

To stabilize force outputs, a spring grip meter (EH101, Lynx Mall, China) was used in hand gripping tasks at 5 kg, 10 kg force levels, and elbow flexion task. The complete paradigm is illustrated in the **Figure 1**. All motor tasks for each subject started with a resting condition for 20 s, then subjects were asked to perform specific motor execution task for 5 s according to the instruction of a screen placed 1-m in front of their eyes, and then relaxed for 20 s. Each motor task contained five repeats, and all subjects performed each motor task using their left and right hand, respectively. After each motor task was completed, the subjects rested for 20 min before switched to next motor task to prevent muscle fatigue. Finally, the whole experiment ended up with 30 trials (2 hands $\times$ 3 tasks $\times$ 5 repeats) for each subject. As subjects S4 and S5 are severe stroke survivors, gripping tasks were only performed in the subject S4 at 5 and 10 kg force levels in both hands, and the 5 kg force level in both hands, and at 10 kg force level in the right hand in the subject S5. All other subjects successfully completed all experiments.

Data Collection

An EEG acquisition system (Brain Products GmbH, Germany) was utilized to collect 32-channel EEG signals from the whole head and 12-channel EMG signals from both sides of upper limbs (**Figure 2A**). EEG electrodes were placed on the scalp according to the international 10–20 standard system (FP1, FP2, F7, F8, F4, F3, FZ, FC5, FC1, FC2, FC6, T7, C3, CZ, C4, T8, CP5, CP1, CP2, CP6, TP9, P7, P3, PZ, P4, P8, TP10, PO9, O1, OZ, O2, PO10), and the binaural mastoid was used as reference electrodes. EMG signals were recorded from upper limb muscles including the flexor digitorum superficialis (FDS), brachioradialis muscle, radial wrist flexor, ulnar wrist flexor, musculus biceps brachii (MBB), and triceps (**Figure 2B**). The skin surface was carefully prepared and cleaned by alcohol before the electrodes were attached. The sampling frequency of EEG and EMG signals was set to 1,000 Hz.

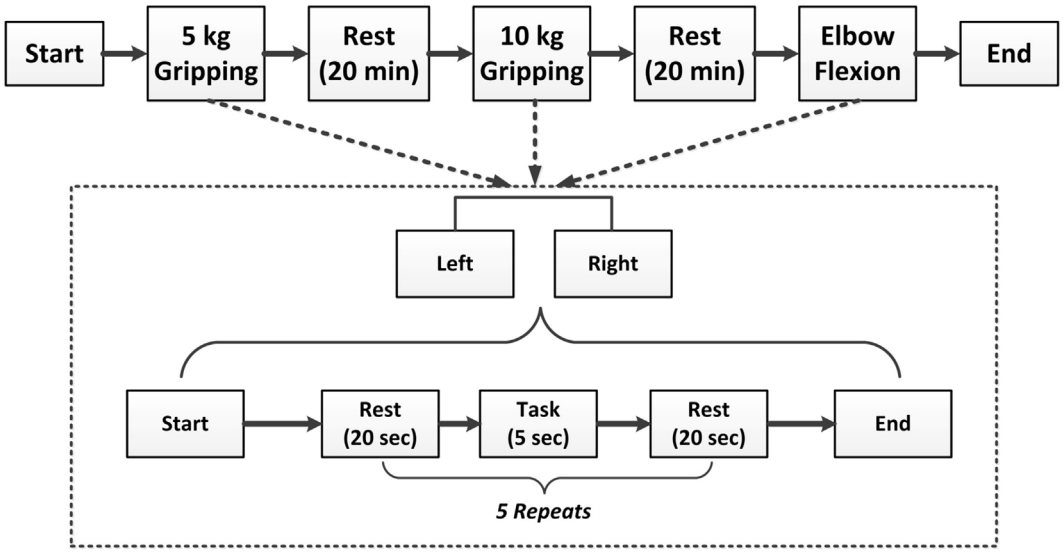

FIGURE 1 | Illustration of the experimental paradigm.

EEG and EMG Signal Preprocessing

To study the coupling relationships between the EEG and the EMG signals associated with various motor tasks, the EEG signals of C3, C4, CP5, and CP6 channels, which covered the premotor cortex and the somatosensory cortex of the brain, and the EMG signals of the FDS and biceps muscle were selected for further analysis.

As the EEG and EMG signals are vulnerable and susceptible to noise such as powerline interference and baseline drift, such artifacts were subsequently removed by the EEG recording amplifiers and analysis software during data collection. The independent component analysis was employed to remove electrooculogram artifact, and the wavelet decomposition was employed to remove motion artifact (19) and improve the quality of EEG and EMG signals for further analysis.

Variable-Scale Transfer Entropy Analysis

Time-Domain Analysis of EEG–EMG Signals

Symbolic transfer entropy analysis technique is an effective method to analyze the relationship between neural and muscular activity coupling. Symbolization (16–18), a technique processing coarse graining of the physiological signal before the calculation of TE, can capture large-scale dynamic characteristics of the signal and therefore reduce the effects of noise. For STE, the accuracy of symbolization affects the accuracy of the TE calculation and the dynamic coupling performance of the system. In particular, for traditional STE, fixed number of symbols is applied to symbolize the time sequence in advance. If the symbol sets is too large, data partitioning becomes smaller, which increases the computation cost and aggravates the noise. On the other hand, if the symbol set is too small, the data partition becomes thick, and the dynamic characteristics of signals are easily lost. To address the above shortcomings, a variable scale parameter symbolization method was proposed in this paper. The procedures of this proposed method is described as follow:

(1) Given a time series signal, the mean, maximum, and minimum values of the time series are first computed;

(2) A variable symbolic scale is set and denoted as piece, which segments the time series into pieces + 1 copies. The larger value of piece results in smaller segmentations and therefore more details of the signal can be retained;

(3) Then symbolize the time series. The segmentation fell into the smallest interval is assigned with the symbol $-\frac{\text{pieces}}{2}$, followed by $-\frac{\text{pieces}}{2}+0.5$, and so on. The largest symbol is $\frac{\text{pieces}}{2}$.

The specific function form is as shown in Eq. 1:

$$S(i)=\begin{cases} -\frac{\text{pieces}}{2} & \min(x)\le x(i)<\min(x)+\text{delta} \\ -\frac{\text{pieces}}{2}+0.5 & \min(x)+\text{delta}\le x(i)<\min(x)+2*\text{delta} \\ \quad . & \\ \quad . & \\ 0 \quad \min(x) & +(\text{pieces}-1)*\text{delta}\le x(i)<\min(x) \\ & +\text{pieces}*\text{delta}, \\ \quad . & \\ \quad . & \\ \frac{\text{pieces}}{2}-0.5 & \max(x)-2*\text{delta}\le x(i)<\max(x)-\text{delta} \\ \frac{\text{pieces}}{2} & \max(x)-\text{delta}\le x(i)\le\max(x) \end{cases} \tag{1}$$

where i represents the length of the time series, $S(i)$ represents the symbolized sequence, $\min(x)$ and $\max(x)$ represent the minimum and maximum values of the time series, delta represents the value of increasement per interval, which is $\frac{\max(x)-\min(x)}{\text{pieces}+1}$.

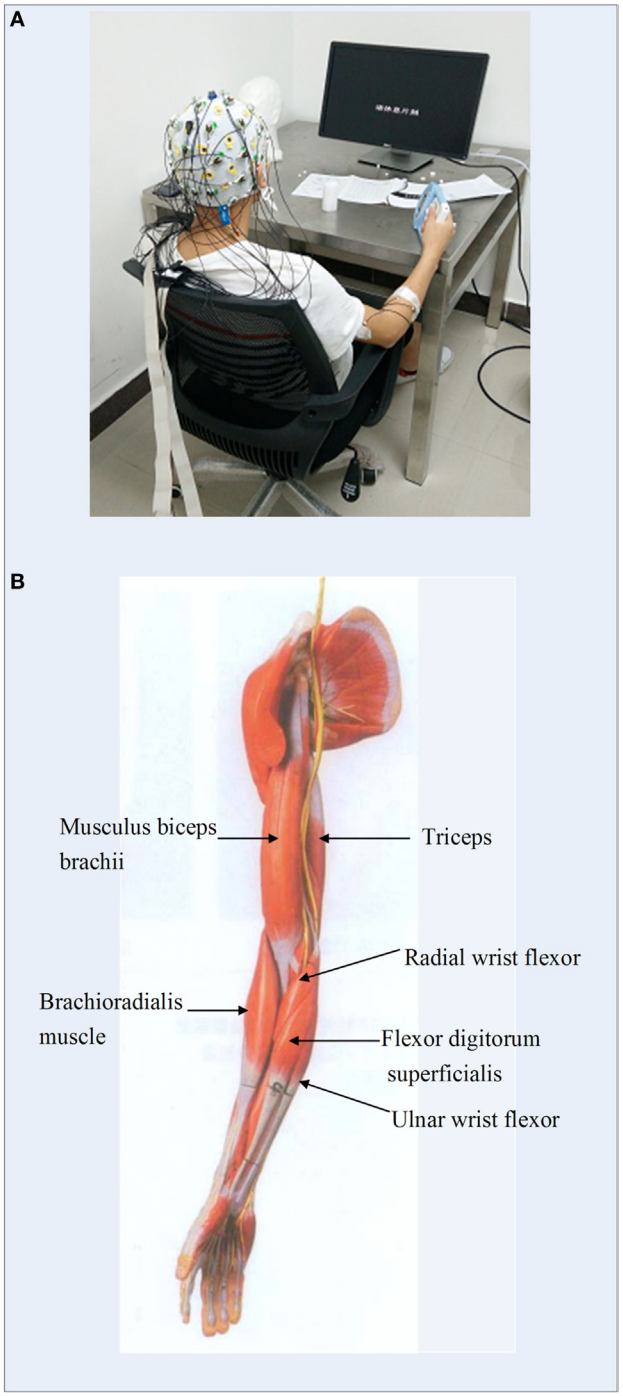

FIGURE 2 | **(A)** Experimental environment of the electroencephalogram and electromyography (EMG) data measurement; **(B)** illustration of the locations of EMG electrodes on upper limb.

TE is an indicator of the directional delivery of time series information, for instance, $TE_{X\to Y}$ denotes the amount of information transferred from X to Y.

If given time series $X = \{x_1, x_2, \ldots, x_T\}$ and $Y = \{y_1, y_2, \ldots, y_T\}$, where T is the length of the time series, x_1, y_1 are the first observation, and x_2, y_2 are the second observation of time series, respectively. The TE of Y to X is defined as $TE_{Y\to X}$ shown in Eq. 2, and the TE of X to Y is defined as $TE_{X\to Y}$ shown Eq. 3 (20–22):

$$TE_{Y\to X} = \sum_{x_{n+\tau},x_n,y_n} p(x_{n+\tau},x_n,y_n)\log_2\left(\frac{p(x_{n+\tau},x_n,y_n)p(x_n)}{p(x_n,y_n)p(x_{n+\tau},x_n)}\right), \quad (2)$$

$$TE_{X\to Y} = \sum_{x_{n+\tau},x_n,y_n} p(y_{n+\tau},x_n,y_n)\log_2\left(\frac{p(y_{n+\tau},x_n,y_n)p(y_n)}{p(x_n,y_n)p(y_{n+\tau},y_n)}\right), \quad (3)$$

where n is the discrete time index, τ is the predicted time, and $p(\cdot)$ represents the probability distribution.

Combining the variable scale parameter symbolization method and TE, a VS-STE approach was proposed in this paper to analyze the relationship between cerebral cortex and muscle electrical coupling and to explore the corticomuscular coupling. Generally, VS-STE is a method based on probability distribution and Shannon entropy to detect the asymmetry between time series, so as to obtain the causality between time series. In particular, the TE of EEG–EMG reflects the amount of information exchange between the cerebral cortex and motor neurons. Therefore, the TE of EEG to EMG represents the amount of information that the cerebral cortex transmits to the control muscle, and TE of EMG to EEG represents the amount of information that muscle cells feed back to the cerebral cortex.

Frequency-Domain Analysis of EEG–EMG Signals TE

After the pretreatment of Section "EEG and EMG Signal Preprocessing," two sets of EEG and EMG time series signals were marked as $X = \{x_1, x_2, \ldots, x_M\}$ and $Y = \{y_1, y_2, \ldots, y_M\}$, respectively. Then, the EEG and EMG signals, which ranged from 1 to 50 Hz, were filtered into 49 sub-band signals with a frequency interval of 1 Hz using a finite impulse response filter. Based on the definition of TE in Eqs 2 and 3, the TE of each sub-band of the EEG and EMG signals was expressed as $TE_{X\to Y}(f)$ and $TE_{Y\to X}(f)$, where f represents the sub-band frequency. In general, the greater the entropy, the larger the amount of information was transferred in this band.

Definition of Coupling Strength

To quantify the brain's ability to control the arm and the arm's response to the brain control command, a parameter named significant area was employed in this study to quantitatively describe the coupling strengths (CS) of EEG and EMG signals in different directions (16). Based on significant area, the CS from EEG to EMG is defined as $CS_{X\to Y}$, which shows the ability of the cerebral cortex to control the motor muscle, and $CS_{Y\to X}$, which indicates the response of the motor muscle to the control command, as shown in Eqs 4 and 5, respectively:

$$CS_{X\to Y} = \sum_f \Delta f \cdot TE_{X\to Y}(f), \quad (4)$$

$$CS_{Y\to X} = \sum_f \Delta f \cdot TE_{Y\to X}(f), \quad (5)$$

where Δf represents the sub-band resolution, $TE_{X\to Y}(f)$ and $TE_{Y\to X}(f)$ represent the TE at the frequency f in different directions.

RESULTS

Theoretically the premotor area in the cerebral cortex is primarily activated when the subject performed motor task on the contralateral limb. The primary motor area (M1) is activated when the body maintains a movement, while the primary somatosensory area (S1) is activated when the sensation of the limb is received (10). Therefore, EEG signals from C3/C4 channel located in the primary motor zone, CP5/CP6 channel in the primary somatic sensory area, and EMG signals from the FDS, the bicipital muscle (MBB) channel were selected to study the TE in the article. For each 5-s motor task, the selected data length was $N = 5{,}000$.

Determination of the Information Delay

There were certain delays in the flow of information in both directions between EEG and EMG (23). In particular, STE is believed to reach the peak between $\tau = 20$ and 30 ms. Therefore, in this case, the STE of EEG-to-EMG and EMG-to-EEG were computed across all subjects by shifting the delay τ from 0 to 50 ms on the EEG signal of the C3 channel and the EMG signal of right hand's FDS. Specifically, the delay of each individual subject was determined according to the optimal value of the STE (16). The STE of the subject S1 is shown in **Figure 3** as an example, which shows that the delay of subject S1 is 31 ms from EEG to EMG and 27 ms from EMG to EEG. The summary of all subjects is shown in **Table 2**. It can be observed that delays of the descending (EEG to EMG) and ascending (EMG to EEG) pathways are different for individual subject, but generally concentrated around 20–30 ms, which is consistent with the results of a previous study (24).

Scale Parameter Selection of VS-STE

As we introduced earlier, the scale parameter represents the degree of symbolization of the time series signal. If the number of symbols applied in the time sequence in STE is fixed beforehand, it is not flexible for further processing and the dynamic characteristics of the signals are easily lost. In this study, for each hand gripping task, EEG signals of C3/C4 channels and EMG signal of the FDS were first selected, then VS-STE method was used to analyze the coupling strength between EEG and EMG with respect to different scale parameters. For all subjects, the mean and SD of STE underwent 5 kg gripping, 10 kg gripping, and elbow flexion tasks in both hands after symbolization, are shown in **Figure 4**, respectively.

As shown in **Figure 4**, as the scale parameter *piece* increased, higher STE can be obtained from the symbolized time series, which indicated the loss of dynamic information

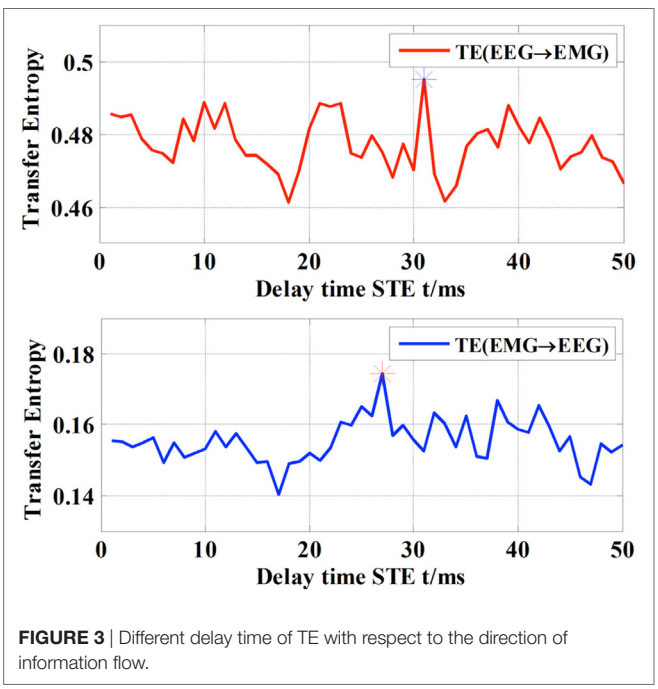

FIGURE 3 | Different delay time of TE with respect to the direction of information flow.

TABLE 2 | Delay time of all the subjects (ms).

	S1	S2	S3	S4	S5	S6	S7	S8	S9	S10	S11	S12
τ(EEG → EMG)/ms	31	27	25	29	31	21	25	23	26	19	24	27
τ(EMG → EEG)/ms	27	23	21	26	28	26	28	27	22	27	27	23

EEG, electromyography; EMG, electroencephalogram.

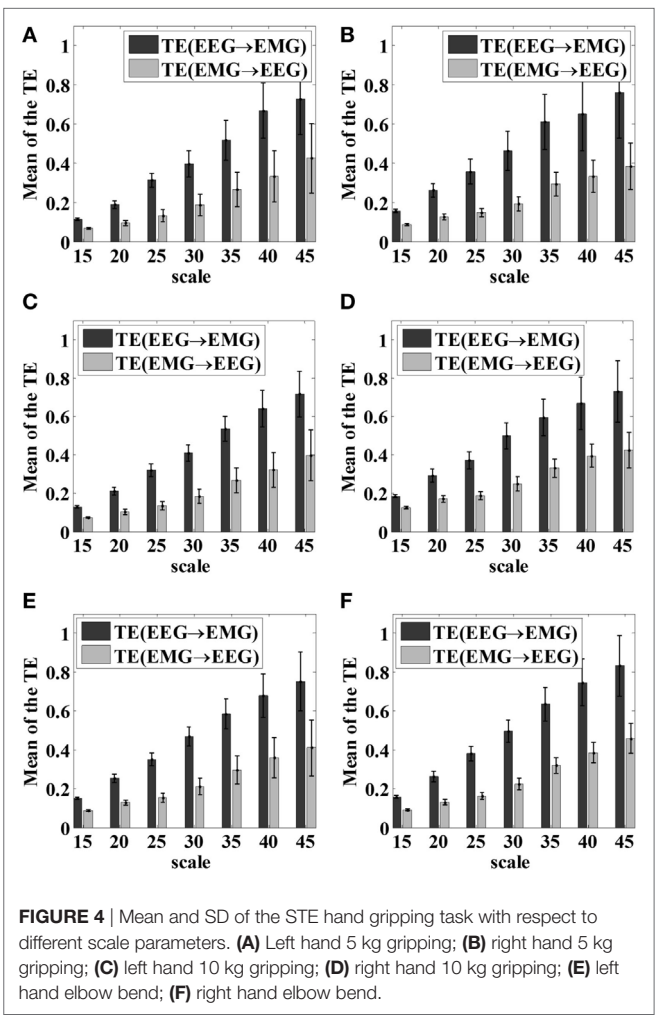

FIGURE 4 | Mean and SD of the STE hand gripping task with respect to different scale parameters. **(A)** Left hand 5 kg gripping; **(B)** right hand 5 kg gripping; **(C)** left hand 10 kg gripping; **(D)** right hand 10 kg gripping; **(E)** left hand elbow bend; **(F)** right hand elbow bend.

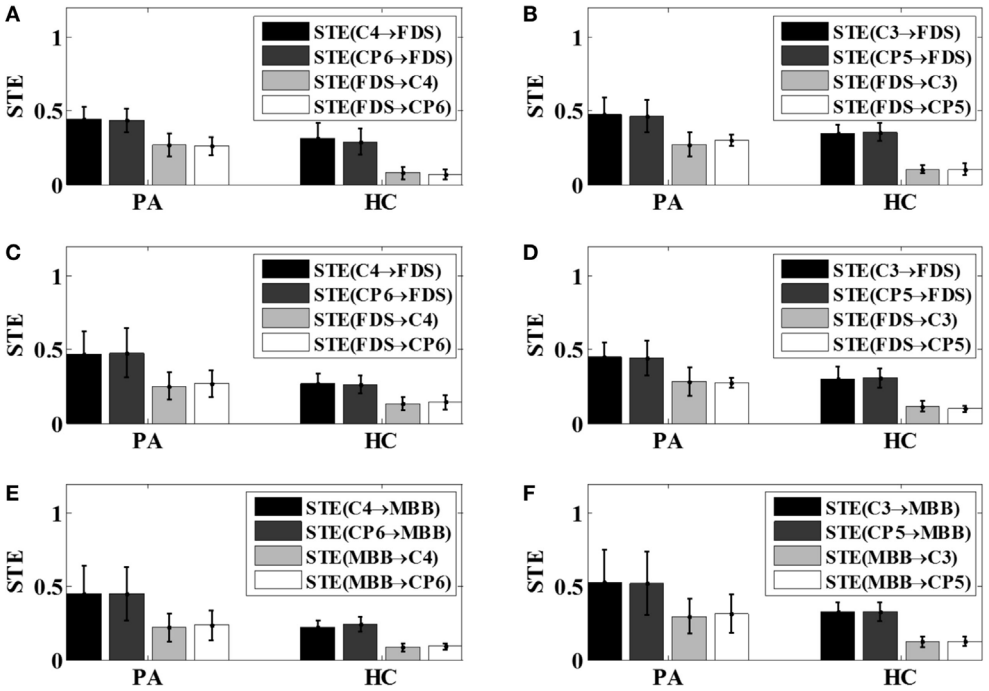

FIGURE 5 | The bi-directional STEs between electroencephalogram and electromyography with respect to different tasks. **(A)** Left hand 5 kg gripping; **(B)** right hand 5 kg gripping; **(C)** left hand 10 kg gripping; **(D)** right hand 10 kg gripping; **(E)** left hand elbow flexion; **(F)** right hand elbow flexion. PA, patients; HC, healthy controls; STE, symbolic transfer entropy.

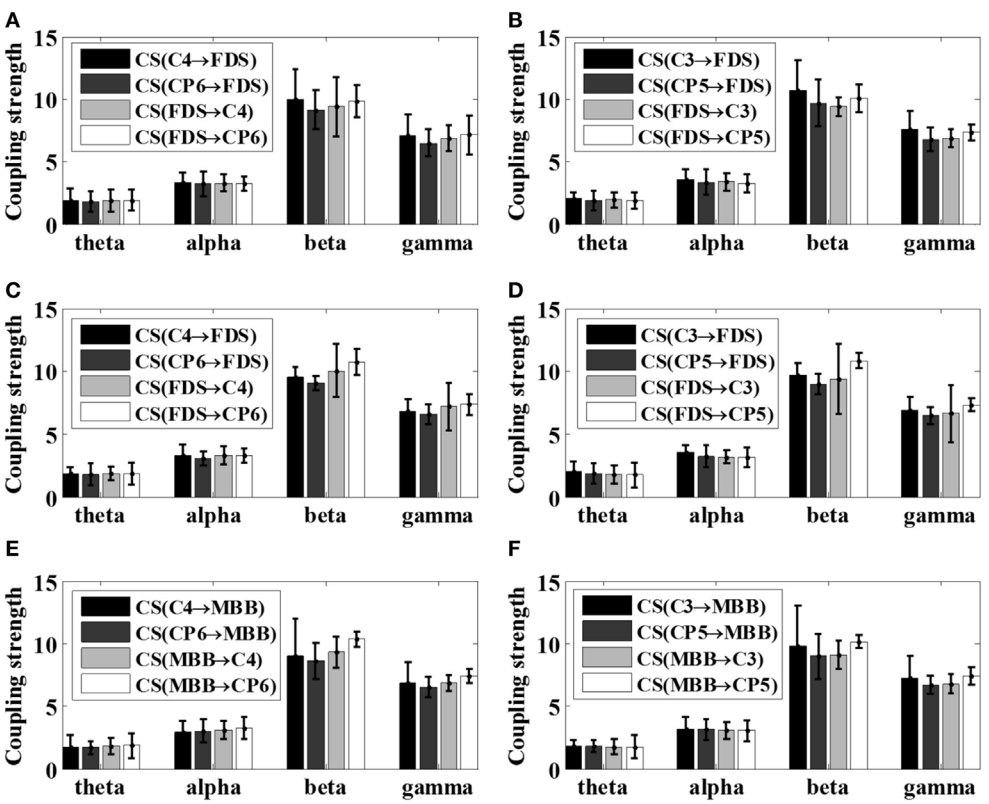

FIGURE 6 | Summarized coupling strength (CS) of patient group (S1–S5) with respect to various motor tasks. **(A)** Left 5 kg; **(B)** right 5 kg; **(C)** left 10 kg; **(D)** right 10 kg; **(E)** left elbow flexion; **(F)** right elbow flexion.

was alleviated. However, it was also observed that the SD increased as the scale parameter increased, resulting in higher fluctuation of the STE. Therefore, it is necessary to comprehensively consider the mean and SD of STE to choose the scale parameter.

To select the appropriate scale parameters for symbolization, the objective function G was defined in Eq. 6 as follow in this article:

$$\begin{cases} G = a * M - b * S \\ a + b = 1 \end{cases}, \quad (6)$$

where M and S denote the normalized mean and SD values of STE with respect to different scales, a and b are constants. Here, a and b are set to 0.5. The optimal scale parameter was then determined when the objective function reached its peak.

In this article, the scale parameter was set as 25 based on the Eq. 6, with which the time series was symbolized, then further coupling analysis of EEG–EMG signals was carried out.

Analysis of Time-Domain STE in Subjects

The bi-directional STE between EEG and EMG signals was computed using the pre-selected scale parameter for all motor tasks across all 12 subjects. The average bi-directional STEs between EEG and EMG signals of each group under different motor tasks were shown in **Figure 5**.

From **Figure 5**, it can be observed that for all motor tasks the mean value of STE from the EEG to EMG signals was greater than that from the EMG to EEG signals in the patient group as well as the control group. It can also be noticed that the mean value of the STE between the EEG and EMG signals in the patients tended to be higher than that of the healthy subjects, as demonstrated in **Figure 5**.

Analysis of Frequency-Domain STE in Subjects

Because different EEG rhythms may be involved in different ways during movement, the oscillatory responses of different frequency bands may be different with respect to various movements. Therefore, the STE between EEG and EMG signals were analyzed in multi-frequency bands for all subjects in this article. As reported in the previous study (16), significant area was employed to evaluate the coupling strength (CS) between EEG signals and EMG signals of specific frequency bands, including theta band (4–8 Hz, θ), alpha band (8–14 Hz, α), beta band (15–35 Hz, β), and gamma frequency band (35 Hz or more, γ). The results of the frequency-domain analysis for all the patients after stroke (S1–S5) and all healthy subjects were shown in **Figures 6** and **7**, respectively. The mean and SD of the coupling strength across all subjects were computed and summarized in **Table 3**.

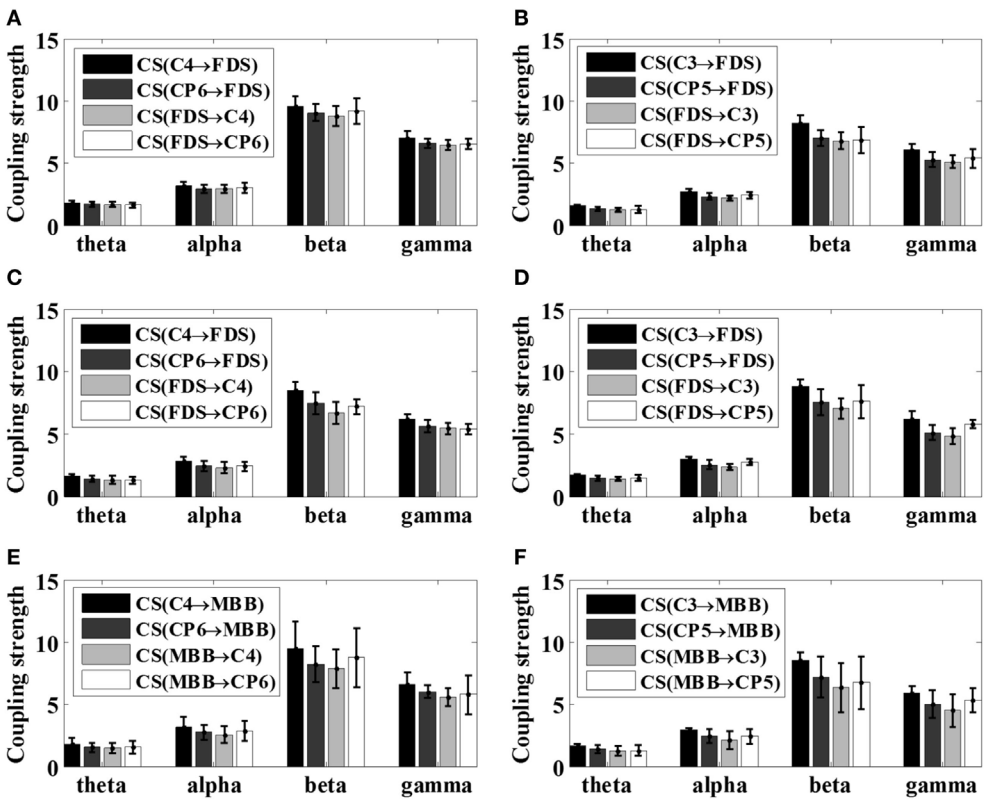

FIGURE 7 | Mean coupling strength (CS) of healthy subjects (S6–S12) with respect to various motor tasks. **(A)** Left 5 kg; **(B)** right 5 kg; **(C)** left 10 kg; **(D)** right 10 kg; **(E)** left elbow flexion; **(F)** right elbow flexion.

TABLE 3 | Comparison (mean ± SD) of the coupling strength across all subjects.

Tasks	Fre.	Group	Left hand		Right hand		Overall
			EEG > EMG	EMG > EEG	EEG > EMG	EMG > EEG	
5 kg	θ	PA	1.86 ± 0.43	1.89 ± 0.39	1.97 ± 0.48	1.90 ± 0.15	1.91 ± 0.05
		HC	1.74 ± 0.18	1.63 ± 0.20	1.42 ± 0.14	1.25 ± 0.19	1.51 ± 0.21
	α	PA	3.26 ± 0.75	3.28 ± 0.67	3.45 ± 0.79	3.31 ± 0.23	3.33 ± 0.09
		HC	3.05 ± 0.31	2.95 ± 0.36	2.48 ± 0.25	2.29 ± 0.24	2.69 ± 0.36
	β	PA	9.55 ± 1.39	9.60 ± 1.22	10.18 ± 1.58	9.74 ± 1.13	9.76 ± 0.29
		HC	9.31 ± 0.73	8.99 ± 0.93	7.63 ± 0.65	6.81 ± 0.87	8.19 ± 1.17
	γ	PA	6.79 ± 1.64	7.01 ± 1.54	7.16 ± 1.45	7.08 ± 0.83	7.01 ± 0.16
		HC	6.82 ± 0.44	6.49 ± 0.37	5.64 ± 0.55	5.26 ± 0.62	6.05 ± 0.72
10 kg	θ	PA	1.83 ± 0.52	1.87 ± 0.27	1.93 ± 0.39	1.79 ± 0.43	1.86 ± 0.06
		HC	1.50 ± 0.20	1.29 ± 0.29	1.58 ± 0.12	1.41 ± 0.20	1.45 ± 0.12
	α	PA	3.20 ± 0.85	3.30 ± 0.46	3.36 ± 0.58	3.16 ± 0.79	3.26 ± 0.09
		HC	2.62 ± 0.35	2.34 ± 0.38	2.76 ± 0.22	2.54 ± 0.24	2.57 ± 0.17
	β	PA	9.29 ± 0.51	10.39 ± 1.91	9.31 ± 1.06	10.10 ± 2.05	9.78 ± 0.56
		HC	7.95 ± 0.78	6.94 ± 0.74	8.18 ± 0.78	7.31 ± 1.07	7.59 ± 0.63
	γ	PA	6.72 ± 0.47	7.28 ± 1.31	6.71 ± 1.02	6.97 ± 1.71	6.92 ± 0.27
		HC	5.91 ± 0.42	5.39 ± 0.39	5.64 ± 0.63	5.30 ± 0.49	5.56 ± 0.44
Elbow bend	θ	PA	1.70 ± 0.60	1.82 ± 0.38	1.79 ± 0.62	1.75 ± 0.33	1.76 ± 0.05
		HC	1.68 ± 0.39	1.49 ± 0.47	1.53 ± 0.21	1.24 ± 0.42	1.48 ± 0.17
	α	PA	2.99 ± 0.58	3.17 ± 0.68	3.15 ± 1.07	3.06 ± 0.62	3.09 ± 0.08
		HC	2.97 ± 0.70	2.71 ± 0.76	2.67 ± 0.37	2.26 ± 0.65	2.65 ± 0.30
	β	PA	8.82 ± 2.44	9.83 ± 1.09	9.40 ± 1.97	9.64 ± 0.95	9.42 ± 0.44
		HC	8.87 ± 1.76	8.31 ± 1.98	7.87 ± 1.14	6.55 ± 2.04	7.90 ± 0.87
	γ	PA	6.67 ± 1.19	7.15 ± 0.79	6.69 ± 1.03	7.11 ± 0.76	6.98 ± 0.22
		HC	6.31 ± 0.74	5.67 ± 1.12	5.46 ± 0.86	4.92 ± 1.13	5.59 ± 0.43

PA, patients; HC, healthy controls; EEG, electromyography; EMG, electroencephalogram.

It is noticeable from **Figures 6** and **7** that the coupling strength of EEG-to-EMG and EMG-to-EEG in the beta and gamma bands of all subjects were larger than theta and alpha bands during the execution of three motor tasks. In particular, for patients group, the mean value of the coupling strength in beta frequency band all exceeded 9.42 (9.65 ± 0.20), while the controls group showed similar results in beta frequency band 7.59 (7.89 ± 0.29). In addition, as shown in **Figures 6** and **7** and **Table 3**, the results also demonstrated that in the beta band, the coupling strength from EEG to EMG was slightly higher than that from EMG to EEG band in control group, while for post-stroke patients the coupling strength from EEG to EMG appeared to be lower than that from EMG to EEG except 5 kg hand gripping in the right hand.

To better compare the difference of corticomuscular coupling strength between stroke patients and healthy subjects, according to the results in **Table 3**, the strength differences between the ascending neural pathway (EMG-to-EEG) and descending neural pathway (EEG-to-EMG) with respect to different motor tasks were evaluated by two sample *t* test using SPSS software (V22.0, IBM Corp., Armonk, NY, USA) within the β band. Results suggested that there is a significant difference ($p < 0.05$) in the coupling strength between patient group and control group, except for the 5 kg gripping task in right hand ($p = 0.3272 > 0.05$). As subject S4 and S5 were unable to complete the elbow flexion task due to severe stroke, the statistical test was not performed for elbow flexion task since the available samples in patient group was too small.

DISCUSSION AND CONCLUSION

In this study, the corticomuscular coupling strength of both post-stroke patients ($n = 5$) and healthy volunteers ($n = 7$) were assessed under various motor tasks using the proposed VS-STE analysis method.

In time-domain, the VS-STE between EEG signals selected from the primary motor area and the somatosensory sensory area of the brain, and EMG signals was analyzed with respect to different motor tasks in all the five post-stroke patients and seven healthy controls. The results revealed that the STE from EEG to EMG signals was increased in patients after stroke during movements compared to healthy controls (**Figure 5**), which indicated that the amount of information transferred from the motor cortex to the muscles tended to increase in the post-stroke patients to complete the same movement. The reason may lie in the fact that more cerebral cortex areas, such as sensory motor cortex, auxiliary exercise area, pre-exercise area, and ipsilateral posterior parietal cortex area, were needed to be activated for the post-stroke patients to complete and maintain stable movements (23). In addition, the STEs from EMG to EEG in all motor tasks were also increased in patient group compared to those of control group, which may be caused by control disorder resulted from the damage of the motor function area and thereby prevent them activating the motoneuron and motor cortex exactly (25). The neural mechanism behind the appearance of abnormal coordination patterns during post-stroke recovery are largely unknown, but they are possibly related to a loss in cortical control and an

increased usage of undamaged, indirect descending motor pathways *via* the brainstem (26).

In the frequency domain, the results showed in **Figures 6** and **7** and **Table 3** demonstrated that the corticomuscular coupling between the EEG and EMG signals was mainly reflected in the β bands and γ bands, indicating that the β and γ bands dominantly control the movement of the upper limb during exercise, which is consistent with the literature (27). One explanation lies in that the coupling of EEG and EMG occurs mainly in the beta band during the static force output, and then shifts to the high gamma band during the dynamic force output (11, 19). In addition, while the coupling strength from EEG to EMG in the beta band was slightly higher than that from EMG to EEG among healthy controls, post-stroke patients revealed lower coupling strength from EEG to EMG compared to the coupling strength from EMG to EEG except 5 kg hand gripping in the right hand. Studies have shown that the corticomuscular coupling in the beta band reflects the relative stable control state of the motor cortex, and the increased coupling strength from EMG to EEG in patients may indicate that intracranial hemorrhage may cause the neurons of the primary motor area unable to control steady movement, resulting an increase in the amount of information fed back to motor cortex to mobilize more neurons to work (27, 28). The above hypothesis is supported by the statistical analysis result of our proposed metric, which is the strength difference between the ascending neural pathway and descending neural pathway. Such result also demonstrated the capacity of the proposed VS-STE in evaluating the interaction between the cerebral cortex and the muscles. For the exception of 5 kg hand gripping in the right hand, which is regularly used and practiced in daily life, this may be attributed to the better recover progress in right hand among the patients during rehabilitation after the stroke (29).

One limitation of this preliminary study is that the results obtained by the proposed method cannot be effectively validated due to the small sample size of the subjects. However, we believed the current findings in this preliminary study do provide evidence and new insights to apply corticomuscular coupling assessment in the rehabilitative evaluation of motor function impairment after stroke. More subjects will be recruited in the future to further validate the proposed VS-STE analysis method.

ETHICS STATEMENT

The study protocol was approved by the Institutional Review Board of Guangdong Provincial Work Injury Rehabilitation Hospital. Prior to the experiment, all the subjects were informed of the details of the experiments and signed the informed consent form.

AUTHOR CONTRIBUTIONS

YG contributed to the study design, data analysis, and paper writing; LR contributed to data analysis and paper writing; RL contributed to the study design, result interpretation, and paper writing; YZ contributed to the study design, experimental design, result interpretation, and paper writing.

FUNDING

This study is supported in part by the Natural Science Foundation of Zhejiang Province (Grant No. LY18F030009), the Natural Nature Science Foundation of China (Grant No. 61372023, 61671197), Research Innovation Foundation of Hangzhou Dianzi University (Grant No. CXJJ2017051), the University of Houston and Guangdong Provincial Work Injury Rehabilitation Hospital.

REFERENCES

1. Bartsch R, Kantelhardt JW, Penzel T, Havlin S. Experimental evidence for phase synchronization transitions in the human cardiorespiratory system. *Phys Rev Lett* (2007) 98:054102. doi:10.1103/PhysRevLett.98.054102
2. Kim SY, Lim W. Emergence of ultrafast sparsely synchronized rhythms and their responses to external stimuli in an inhomogeneous small-world complex neuronal network. *Neural Netw* (2017) 93:57–75. doi:10.1016/j.neunet.2017.04.002
3. Liang TJ, Long YB. Modified constraint-induced movement therapy on lower extremity dyskinesia of stroke patients. *Chin J Rehabil* (2011) 26(5):339–41. doi:10.3870/zgkf.2011.05.006
4. Conway BA, Halliday DM, Shahani U, Maas P, Weir AI, Rosenberg JR, et al. Common frequency components identified from correlations between magnetic recordings of cortical activity and the electromyogram in man. *J Physiol* (1995) 483:35–69.
5. Chiang J, Wang ZJ, Mckeown MJ. A multiblock PLS model of cortico-cortical and corticomuscular interactions in Parkinson's disease. *Neuroimage* (2012) 63(3):1498–509. doi:10.1016/j.neuroimage.2012.08.023
6. Omlor W, Patino L, Hepp-Reymond MC, Kristeva R. Gamma-range corticomuscular coherence during dynamic force output. *Neuroimage* (2007) 34(3):1191–8. doi:10.1016/j.neuroimage.2006.10.018
7. Poortvliet PC, Tucker KJ, Finnigan S, Scott D, Sowman P, Hodges PW. Cortical activity differs between position- and force-control knee extension tasks. *Exp Brain Res* (2015) 233(12):3447–57. doi:10.1007/s00221-015-4404-8
8. Cremoux S, Tallet J, Dal Maso F, Berton E, Amarantini D. Impaired corticomuscular coherence during isometric elbow flexion contractions in human with cervical spinal cord injury. *Eur J Neurosci* (2017) 46(4):1991–2000. doi:10.1111/ejn.13641
9. Hu S, Wang H, Zhang J, Kong W, Cao Y. Causality from Cz to C3/C4 or between C3 and C4 revealed by granger causality and new causality during motor imagery[C]. *International Joint Conference on Neural Networks*. Beijing: IEEE (2014). p. 3178–85.
10. Tomasevic L, Zito G, Pasqualetti P, Filippi M, Landi D, Ghazaryan A, et al. Cortico-muscular coherence as an index of fatigue in multiple sclerosis. *Mult Scler* (2013) 19(3):334–43. doi:10.1177/1352458512452921
11. Ping X, Yang FM, Li XX, Yong Y, Chen XL, Zhang LT. Functional coupling analyses of electroencephalogram and electromyogram based on variational mode decompositiontransfer entropy. *Acta Phys Sin* (2016) 65(11):118701. doi:10.7498/aps.65.118701
12. Vicente R, Wibral M, Lindner M, Pipa G. Transfer entropy – a model-free measure of effective connectivity for the neurosciences. *J Comput Neurosci* (2011) 30(1):45–67. doi:10.1007/s10827-010-0262-3
13. Yao W, Wang J. Multi-scale permutation transfer entropy analysis of EEG. *Phys A Stat Mech Appl* (2017) 484(15):276–81. doi:10.1016/j.physa.2017.04.181
14. Wang Y, Hou FZ, Dai JF, Liu XF, Li J, Wang J. Analysis on relative transfer of entropy based on improved epileptic EEG. *Acta Phys Sin* (2014) 63(21):218701. doi:10.7498/aps.63.218701
15. Sha W, Jin L, Zhang ML, Wang J. Coupling analysis of electrocardiogram and electroencephalogram based on improved symbolic transfer entropy. *Acta Phys Sin* (2013) 62(23):238701. doi:10.7498/aps.62.238701
16. Ping X, Yang FM, Chen XL, Du YH, Wu XG. Functional coupling analyses of electroencephalogram and electromyogram based on multiscale

transfer entropy. *Acta Physica Sinica* (2015) 64(24):248702. doi:10.7498/aps.64.248702
17. Shen W, Wang J. Time irreversibility analysis of ECG based on symbolic relative entropy. *Acta Phys Sin* (2011) 60(11):2509–15. doi:10.7498/aps.60.118702
18. Zhang M, Chao C, Qian-Li M, Zong-Liang G, Jun W. Coupling analysis of multivariate bioelectricity signal based symbolic partial mutual information. *Acta Phys Sin* (2013) 62(6):068704. doi:10.7498/aps.62.068704
19. Ping X, Yang FM, Chen XL, Du YH, Wu XG. EEG-EMG synchronization analysis based on gabor wavelet transform-granger causality. *Chin J Biomed Eng* (2017) 36(1):28–38. doi:10.3969/j.issn.0258-8021.2017.01.004
20. Shao S, Guo C, Luk W, Weston S. Accelerating transfer entropy computation[C]. *International Conference on Field-Programmable Technology*. Shanghai: IEEE (2014).
21. Vicente R, Wibral M, Lindner M, Pipa G. Transfer entropy—a model-free measure of effective connectivity for the neurosciences. *J Comput Neurosci* (2011) 30(1):45–67. doi:10.1007/s10827-010-0262-3
22. Wang J, Yu ZF. Symbolic transfer entropy-based premature signal analysis. *Chin Phys B* (2012) 21(1):18702–5. doi:10.1088/1674-1056/21/1/018702
23. Jiao Y, Zhang XD, Lan L, Yang FM, Xia SM, Weng XC. Comparison of the brain activation pattern in passive single finger exercise between a normal testee and a stroke patient. *Chin J Clin Rehabil* (2005) 9(12):14–6. doi:10.3321/j.issn:1673~8225.2005.12.001
24. Witham CL, Riddle CN, Baker MR, Baker SN. Contributions of descending and ascending pathways to corticomuscular coherence in humans. *J Physiol* (2011) 589(Pt 15):3789–800. doi:10.1113/jphysiol.2011.211045
25. Takashi O, Masahiko M, Junichi U. Functional recovery in upper limb function in stroke survivors by using brain-computer interface a single case A-B-A-B design[C]. *35th Annual International Conference of the IEEE EMBS*. Osaka (2013). p. 265–8.
26. Chen A, Yao J, Dewald J. A novel experimental setup combining EEG and robotics to investigate brain activity driving controlled reaching movements in chronic stroke survivors[C]. *IEEE 10th International Conference on Rehabilitation Robotics*. Noordwijk (2007). p. 876–82.
27. Fermaglich J. Electric fields of the brain: the neurophysics of EEG. *JAMA* (1982) 247(13):1879. doi:10.1001/jama.1982.03320380071046
28. Siemionow V, Yue GH, Ranganathan VK, Liu JZ, Sahgal V. Relationship between motor activity-related cortical potential and voluntary muscle activation. *Exp Brain Res* (2000) 133(3):303–11. doi:10.1007/s002210000382
29. Miao P, Wang C, Li P, Wei S, Deng C, Zheng D, et al. Altered gray matter volume, cerebral blood flow and functional connectivity in chronic stroke patients. *Neurosci Lett* (2017) 662:331–8. doi:10.1016/j.neulet.2017.05.066

Conflict of Interest Statement: The authors declare that the research was conducted in the absence of any commercial or financial relationships that could be construed as a potential conflict of interest.

frontiers in Neurology

ORIGINAL RESEARCH
published: 22 December 2017
doi: 10.3389/fneur.2017.00699

Electromyography Exposes Heterogeneity in Muscle Co-Contraction following Stroke

*Caitlin L. Banks[1,2], Helen J. Huang[3], Virginia L. Little[1] and Carolynn Patten[1,2,4]**

[1] Neural Control of Movement Lab, Malcom Randall VA Medical Center, Gainesville, FL, United States, [2] Rehabilitation Science Doctoral Program, University of Florida, Gainesville, FL, United States, [3] Department of Mechanical and Aerospace Engineering, University of Central Florida, Orlando, FL, United States, [4] Department of Physical Therapy, University of Florida, Gainesville, FL, United States

Walking after stroke is often described as requiring excessive muscle co-contraction, yet, evidence that co-contraction is a ubiquitous motor control strategy for this population remains inconclusive. Co-contraction, the simultaneous activation of agonist and antagonist muscles, can be assessed with electromyography (EMG) but is often described qualitatively. Here, our goal is to determine if co-contraction is associated with gait impairments following stroke. Fifteen individuals with chronic stroke and nine healthy controls walked on an instrumented treadmill at self-selected speed. Surface EMGs were collected from the medial gastrocnemius (MG), soleus (SOL), and tibialis anterior (TA) of each leg. EMG envelope amplitudes were assessed in three ways: (1) no normalization, (2) normalization to the maximum value across the gait cycle, or (3) normalization to maximal M-wave. Three co-contraction indices were calculated across each agonist/antagonist muscle pair (MG/TA and SOL/TA) to assess the effect of using various metrics to quantify co-contraction. Two factor ANOVAs were used to compare effects of group and normalization for each metric. Co-contraction during the terminal stance (TSt) phase of gait is not different between healthy controls and the paretic leg of individuals post-stroke, regardless of the metric used to quantify co-contraction. Interestingly, co-contraction was similar between M-max and non-normalized EMG; however, normalization does not impact the ability to resolve group differences. While a modest correlation is revealed between the amount of TSt co-contraction and walking speed, the relationship is not sufficiently strong to motivate further exploration of a causal link between co-contraction and walking function after stroke. Co-contraction does not appear to be a common strategy employed by individuals after stroke. We recommend exploration of alternative EMG analysis approaches in an effort to learn more about the causal mechanisms of gait impairment following stroke.

Keywords: stroke, co-contraction, electromyography, walking, methodology, motor disorders

OPEN ACCESS

Edited by:
Sheng Li,
University of Texas Health Science Center at Houston, United States

Reviewed by:
Xiaogang Hu,
University of North Carolina at Chapel Hill, United States
Erwin Van Wegen,
VU University Medical Center, Netherlands

****Correspondence:***
Carolynn Patten
patten@phhp.ufl.edu

Specialty section:
This article was submitted to Stroke, a section of the journal Frontiers in Neurology

Received: *01 July 2017*
Accepted: *05 December 2017*
Published: *22 December 2017*

Citation:
Banks CL, Huang HJ, Little VL and Patten C (2017) Electromyography Exposes Heterogeneity in Muscle Co-Contraction following Stroke. Front. Neurol. 8:699. doi: 10.3389/fneur.2017.00699

INTRODUCTION

After a stroke, most individuals experience lifelong walking impairments, including forward propulsion deficits, which contribute to metabolically inefficient gait (1–4). Abnormal muscle activation patterns, especially excessive co-contraction, are commonly argued to be a major contributing factor to these walking impairments (5–7). Co-contraction refers to simultaneous activity in agonist and

antagonist muscles across the same joint (6, 8). This phenomenon is sometimes called agonist/antagonist co-activation or simply co-activation. However, co-activation can also refer to simultaneous activity in synergist muscles. Here, we will use the term co-contraction and address the relationship between agonist and antagonist muscle co-activity.

Co-contraction is a normal motor control strategy observed in healthy individuals during functional motor tasks. Its presence varies in response to environmental and task demands on different time scales. For example, when encountering uncertainty, such as challenges to posture and balance, increased co-contraction can be observed as an early response to the novel environment (9). Evidence suggests that co-contraction facilitates rapid torque development (10), compensates for non-linearities in muscle properties and torque scaling (11), and counteracts agonist torques and off-axis torques (12, 13). Thus, co-contraction affords a robust mechanism to rapidly counteract perturbations. Co-contraction is also often present when motor tasks are novel or require limb stabilization for performance accuracy. Over a longer time scale (e.g., minutes, hours or days), co-contraction decreases progressively. Indeed, an asymptote in co-contraction often serves as a hallmark of motor learning and adaptation (14, 15). Important to its role as a normal motor control strategy, co-contraction is actively modulated during movements such as walking, occurring more prominently at predictable points in the gait cycle to stabilize joints and enable efficient walking (8).

In contrast to this normal pattern of co-contraction, chronic presence of excessive or invariant co-contraction should reflect pathology (16). Disturbed voluntary muscle activation following stroke is thought to involve excessive co-contraction, which may stem from diffuse descending motor drive or exaggerated stretch reflexes generated in the antagonist muscle by movement (i.e., antagonist restraint) (17, 18). Clinical perspectives have emphasized the presence of excessive and invariant co-contraction in neuropathologic conditions, fueling an expectation that it is ubiquitously present (16, 19–21). However, the literature to date remains inconclusive regarding either its presence or causal role in motor dysfunction (10, 19–21). Furthermore, it is thought that co-contraction contributes to slow, inefficient walking after stroke (5, 6, 22, 23). Importantly, if excessive co-contraction is present during walking after stroke, it should be quantifiable and associated with robust measures of gait impairment, particularly, generation of plantarflexor power.

While objective, quantifiable methods exist for analyzing co-contraction in healthy individuals, the literature provides no "best" method to account for co-contraction as a feature of pathologic muscle activation patterns (24). We surveyed the existent literature and selected two popular metrics. The first, developed by Falconer and Winter, is a metric based on normal gait patterns from ten healthy adults (8). This method computes a ratio of antagonist to agonist electromyography (EMG) activity within each phase of the gait cycle. Another common method quantifies the "wasted contraction" (WC) shared between an agonist and antagonist muscle by denoting the smaller of the two traces as the WC and the remaining EMG activity as the "effective contraction," which generates movement. This approach was developed by researchers studying upper limb motor adaptation and computational motor control (25). To our knowledge, the WC measure has not been applied to evaluate co-contraction during walking. Both metrics evaluate muscle activation patterns in a manner that does not account for the biomechanical role of each muscle within the task. That is, the larger magnitude EMG signal is assumed to arise from the agonist and the smaller signal from the antagonist. However, this assumption does not always hold, especially after stroke. Impaired EMG amplitude and phasing following stroke may, therefore, require a metric that is sensitive to these changes in muscle roles throughout the gait cycle. EMG normalization also varies considerably when quantifying co-contraction, which may further influence data interpretation and outcomes.

The goal of the present study is to assess the relationship between ankle co-contraction and gait impairment following stroke. Given the challenges involved with detecting co-contraction in a pathologic population, we will investigate the effect of various methods for quantifying co-contraction. Here, we introduce a modified version of the Falconer and Winter metric in which the agonist and antagonist muscle roles are prescribed within each phase of the gait cycle. We will investigate the effects of co-contraction metric and EMG normalization in order to comprehensively assess the presence and magnitude of pathologic co-contraction. Our results will allow us to determine whether, and how, the metric impacts the ability to detect pathologic co-contraction patterns after stroke, while accounting for inconsistencies in the literature that may underlie detection of this phenomenon.

MATERIALS AND METHODS

Subjects

This is a subgroup analysis from a larger study. We included 15 individuals post-stroke and 9 healthy controls. Demographic data are presented in **Table 1**. Overall, participants were included if they were: greater than 18 years of age, able to walk independently for a distance of at least 15 m with or without an assistive device,

TABLE 1 | Demographics.

	Control	Stroke
Demographics		
n	9	15
Sex (m/f)	5/4	14/1
Age (years)	60 ± 9.33	65.87 ± 9.76
Self-selected walking speed (m/s)	1.40 ± 0.2[a]	0.93 ± 0.3[a]
Chronicity (years)		5.52 ± 3.73
Affected side (r/l)		8/7
Clinical characteristics		
Routine ankle foot orthosis (AFO) use (*n*)		4
LE Fugl-Meyer Motor Score (/34)		30 (16, 34)
Dynamic Gait Index (/24)		21 (10, 24)
Short Physical Performance Battery (/12)		11 (7, 12)

Demographic and clinical data are presented mean ± SD and median (range), respectively. Of the four individuals who routinely use an ankle-foot orthosis, three typically use a custom-molded AFO and one uses a prefabricated Aircast®.
[a]Indicates a significant difference between groups, $p < 0.05$.

and medically stable. Participants post-stroke were included following clinical presentation of a single, unilateral stroke—confirmed by neuroimaging—at least 6 months prior to enrollment. Individuals with brainstem or cerebellar involvement, bilateral involvement, major neurologic or neurodegenerative conditions other than stroke, orthopedic or cardiovascular conditions that precluded walking on a treadmill, or pregnancy were excluded.

Testing occurred at the Brain Rehabilitation Research Center in the Malcom Randall VA Medical Center in Gainesville, FL, USA.

Instrumentation and Protocol

Participants walked on an instrumented split-belt treadmill (Bertec, Columbus, OH, USA, sampling frequency 2,000 Hz) at their self-selected speed. No handrail support was provided and participants wore a modified mountain climbing harness for fall arrest (Robertson Harness, Henderson, NV, USA); no substantial body weight support was provided. Four participants regularly used a custom-molded ankle foot orthosis ($n = 3$) or ankle brace ($n = 1$) on the paretic leg. Two of these participants wore an Aircast® AirSport™ (DJO Global, Vista, CA, USA) for mediolateral support during testing, while all other participants were tested without ankle support. Reflective markers were placed over anatomical landmarks using a modified Helen Hayes marker set (26). Coordinates of the anterior superior iliac spines were located using a digitizing pointer (C-Motion, Inc., Germantown, MD, USA). Locations of the medial and lateral malleoli were digitized for AirCast® wearers due to interference with skin contact. Marker data were recorded by 12 infrared cameras (Vicon MX, Vicon Motion Systems Ltd., Oxford, UK) at 200 Hz.

Surface EMG was recorded using active preamplifiers (MA-420, Motion Lab Systems, Baton Rouge, LA, USA; input impedance >100,000,000 Ω, CMRR >100 dB at 65 Hz, noise <1.2 μV RMS, signal bandwidth 10–2,000 Hz) attached to gel surface electrodes (Cleartrace 2, Conmed, Utica, NY, USA). Skin was abraded and cleaned with alcohol, then electrodes were placed on the muscle belly of the medial gastrocnemius (MG), soleus (SOL), and tibialis anterior (TA) of each leg according to the SENIAM guidelines (27). To assure maximal resolution, amplifier gains were adjusted minimally by visual inspection during isolated ankle movements prior to data collection. EMG data were recorded in Signal (Version 6.0, Cambridge Electronic Design, Cambridge, England) at 2,000 Hz.

Maximal M-waves (M-max) were elicited through stimulation with a Digitimer stimulator (DS-7A or DS-7AH for high-current stimulation, Hertfordshire, UK) using either a hand-held bipolar stimulator probe (CareFusion, Middleton, WI, USA) or a custom monopolar ball electrode. M-max was elicited in the paretic or test leg MG/SOL or TA by supramaximal stimulation of the tibial nerve or common peroneal nerve, respectively (28). M-max amplitudes were averaged across 4–7 consecutive stimulations. One control subject was excluded from M-max analysis because data were overwritten.

Participants were instructed to walk with their arms relaxed at their sides. Data were collected in 1-min walking blocks, with seated or standing rest breaks taken as needed.

Data Analysis

EMG Processing

EMG data were band-pass filtered to remove noise (fourth order Butterworth, cutoff frequency 10–450 Hz), rectified, low-pass filtered (fourth order Butterworth), time-normalized to a 1,001-point gait cycle, and signal averaged (60 cycles), to establish a linear envelope. The ideal low-pass filter frequency was determined by each individual's mean stride time (cutoff frequency 5/stride time Hz; control 4.6 ± 0.3 Hz, stroke 3.9 ± 0.5 Hz), as recommended by Shiavi et al. (29). The linear envelopes were then amplitude-normalized in each of three ways: (1) no normalization (non), (2) to the maximum value across the gait cycle (max), or (3) to M-max. Data were processed using custom MATLAB scripts (The MathWorks r2015a, Natick, MA, USA).

Quantification of Co-Contraction

The gait cycle was divided into seven bins using gait events extracted from ground reaction force and heel marker data. The events defined bins following the standard established by the Rancho Los Amigos Medical Center Pathokinesiology Lab: loading response (LR), mid-stance (MSt), terminal stance (TSt), pre-swing (PSw), initial swing (ISw), mid-swing (MSw), and terminal swing (TSw) (30). The three swing bins each represent one-third of the swing phase.

We used three metrics to quantify co-contraction. The first metric, which we will denote as $CI_{traditional}$, was first described by Falconer and Winter (8). This metric represents a ratio of agonist/antagonist overlap to total muscle activation. The total antagonist activity within each bin, I_{ant}, is calculated as the area under the curve created by the smaller EMG envelope as indicated by the shaded region in the top row of plots in **Figure 1**. The total activity, I_{tot}, is the sum of the agonist and antagonist EMG areas within a given pair of muscles (i.e., MG/TA or SOL/TA). The co-contraction index can then be quantified as:

$$CI_{traditional} = \frac{2I_{ant}}{I_{tot}} * 100. \quad (1)$$

A CI value of 100% represents total co-contraction, while a value of 0% represents pure agonist activation. This measure has been widely cited and applied in the literature (31–35). We calculated two co-contraction indices for each phase of the gait cycle, one with the MG/TA pairing, and one with the SOL/TA pairing.

The second metric, CI_{fixed}, is analogous to the traditional Falconer and Winter metric, except the agonist/antagonist muscle relationship was fixed to the biomechanical function of these muscles within each of the seven bins of the gait cycle, as demonstrated by typical EMG patterns of healthy individuals (**Figure 1**, middle plots). During LR, ISw, MSw, and TSw, the TA should be the agonist muscle, while the MG should be the antagonist:

$$CI_{fixed} = \frac{2I_{MG}}{I_{tot}} * 100. \quad (2)$$

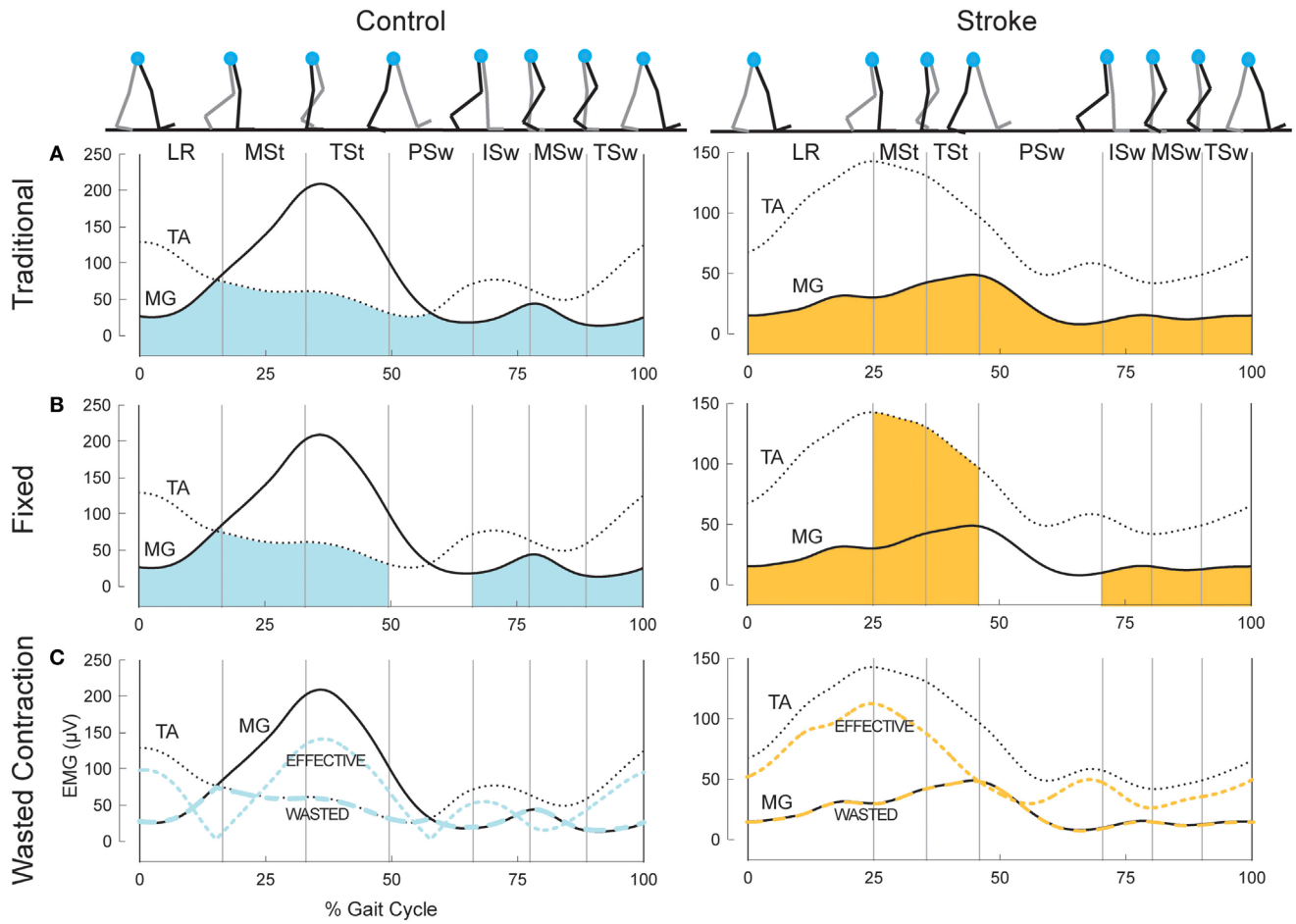

FIGURE 1 | Example co-contraction metrics. **(A)** Eight gait events dividing the gait cycle into seven phases: loading response (LR), mid-stance (MSt), terminal stance (TSt), pre-swing (PSw), initial swing (ISw), mid-swing (MSw), and terminal swing (TSw). Illustrated immediately below, is example EMG in the medial gastrocnemius (MG, solid) and tibialis anterior (TA, dotted) for a healthy control (left) and an individual post-stroke (right). The shaded area reflects the area under the lower trace at any point, used as the antagonist in the traditional co-contraction index calculations. **(B)** Illustration using the same example EMG as above, however the shaded area reflects the area under the muscle that should be the antagonist within each phase. PSw is not shaded because the antagonist muscle typically switches between MG and TA in this phase. **(C)** The resulting wasted contraction for the same subjects, the lower of the two traces (wide dashes), and the effective contraction, which is calculated as the higher trace minus the lower trace (narrow dashes). The wasted contraction index is the mean of the wasted contraction, expressed as a percentage of the maximum effective contraction.

During MSt and TSt, the MG should be the agonist and the TA the antagonist muscle:

$$CI_{fixed} = \frac{2I_{TA}}{I_{tot}} * 100. \quad (3)$$

In health, the ankle muscles switch agonist/antagonist roles in PSw; thus, we were unable to calculate a co-contraction index during PSw using this method. CI_{fixed} for the SOL/TA pairing was calculated in the same manner as Eqs 2 and 3 above; however, the SOL was used as the antagonist muscle during LR and the swing phases.

The final metric, illustrated in the bottom plots of **Figure 1**, was developed by Thoroughman and Shadmehr to represent the amount of "wasted contraction" that occurs due to co-contraction (25). Similar to $CI_{traditional}$, the smaller of the two EMG envelopes is designated to represent the contraction that is wasted by simultaneous activity in opposing muscles. This amount can be subtracted from the EMG envelope of the larger signal to determine "effective contraction," or the amount of agonist activation that effectively performed the movement. The wasted and effective contraction traces can be divided by the maximum effective contraction, resulting in units expressed as the percentage of maximum effective contraction. This step was necessary to compare the effects of EMG normalization since the units of wasted and effective contractions are the same as the units of the EMG traces from which they are based (e.g., microvolts). The mean wasted and effective contractions were calculated for each gait phase.

Quantification of Motor Impairment

Clinical and Functional Assessments

We used two functional assessments of motor impairment: the lower extremity Fugl-Meyer Assessment of Motor Performance

(LE FMA) and walking speeds (36). Self-selected and fastest comfortable walking speeds (SSWS and FCWS, respectively) were captured using 3–5 passes on a 16-foot GaitRite pressure-sensitive walkway (Platinum Plus System, Version 3.9, Havertown, PA, USA). SSWS involved walking at a casual, comfortable pace. Fastest comfortable speed was assessed as the fastest speed the participant could safely attain when walking, "as if you are crossing the street and the walk signal changed to a red hand." All clinical and functional assessments were performed by a licensed physical therapist (VLL).

Ankle Power

We used ankle power to quantify a key biomechanical aspect of walking function. Power was calculated using inverse dynamics by the following formula:

$$\mathbf{P} = \mathbf{M} \cdot \boldsymbol{\omega}, \tag{4}$$

where P is the rate of work done by the ankle muscles (i.e., power), M is the joint moment, and ω is the angular velocity (37, 38). An example ankle power curve is shown in **Figure 2**. The second peak of the ankle power curve, or A2, is prominent in late stance for both normal and pathologic gait (37, 39). A2 is often diminished with aging and in individuals post-stroke (39, 40). Although A2 scales with walking speed, the deficit in these individuals is present even when compared to speed-matched controls (41, 42). Because the plantarflexors are the primary mediators of A2 and A2 and accounts for both joint motion and muscular output through torque generation (43), this outcome is highly sensitive and relevant to functional changes after stroke.

Statistics

Data were tested for normality using a Shapiro–Wilk W test. In the cases where the assumption of normality was not met (all cases except SOL/TA $CI_{traditional}$), data were transformed using a base 10 logarithmic transformation. In the final case, raw data were analyzed. Separate two-factor ANOVAs assessed the effects of group (control or stroke) and normalization (maximum value, M-max, or no normalization) on each of the three co-contraction indices and muscle pairs (MG/TA, SOL/TA). Tukey's Honestly Significant Difference was performed *post hoc* when significant effects were detected. To account for multiple comparisons, significance was established using a Bonferroni corrected value of $p < 0.0083$. Spearman's correlations assessed the relationship between co-contraction and walking function. The Bonferroni corrected significance level for correlation analyses was $p < 0.0125$. Statistical testing was performed in JMP Pro 11 (SAS Institute, Inc., Cary, NC, USA).

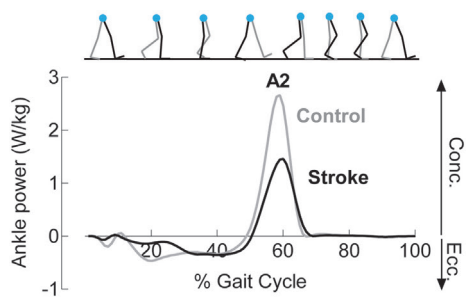

FIGURE 2 | Reduced concentric ankle plantarflexor power is noted following stroke. Example ankle power curves, derived from inverse dynamics, for a healthy control (gray) and an individual following stroke (black) demonstrate diminished peak concentric plantarflexor power (A2) late in the stance phase of gait.

RESULTS

Visual assessment of EMG patterns during walking revealed consistent patterns in healthy controls, accompanied by vast heterogeneity in the stroke group. Differences between healthy and stroke subjects are most relevant in TSt, where peak plantarflexor EMG tends to occur. TSt is also the gait phase when plantarflexor EMG contributes to A2—the most robust measure of gait function employed in this study. Moving forward, all results will be presented during TSt unless specified otherwise. Group co-contraction responses during TSt can be visualized by metric in **Figure 3** for the paretic leg and **Figure 4** for the non-paretic leg. Because the core findings are largely similar between legs and we are primarily interested in paretic leg function, we performed statistics only on the paretic leg.

The metric adjusted for the muscles' biomechanical roles, CI_{fixed}, showed no significant main effect of Group or Group × Normalization interaction. In the SOL/TA muscle pairing, there was a significant main effect of normalization method ($p = 0.0032$, **Figure 3**). *Post hoc* testing revealed that M-max normalization produced greater CI_{fixed} than maximum value normalization ($p = 0.0024$). The MG/TA pairing revealed no significant main effects.

$CI_{traditional}$ resulted in values similar to CI_{fixed} during TSt, and the statistical findings are largely the same. Both muscle pairings revealed no significant main effects of Group or Group × Normalization interactions. The SOL/TA pairing revealed a significant main effect of Normalization ($p = 0.0051$). *Post hoc* testing revealed that M-max normalization was again greater than maximum value normalization ($p = 0.0035$). The MG/TA pairing revealed no significant main effects.

The WC, when expressed as a percentage of the effective contraction, has the potential to create outliers when the two EMG traces are similar in magnitude. In the case of maximum value normalization, one subject's EMG produced an extreme value for both the MG/TA and SOL/TA muscle pairings, corresponding to z-scores of 6.3 and 7.0, respectively. Since no data transformation could normalize the dataset with outliers of that magnitude, we adjusted each of the outliers to a z-score of 3. This step allowed for adequate statistical comparison within the remaining dataset. Both the MG/TA and SOL/TA muscle pairings revealed only a significant main effect of Normalization ($p = 0.0008$ and $p = 0.0005$, respectively). *Post hoc* testing for the MG/TA pairing revealed that maximum value normalization produced greater WC values than both M-max ($p = 0.0044$) and WC derived from non-normalized EMG ($p = 0.0018$). In the SOL/TA muscle pairing, WC was greater with maximum value normalization than M-max normalization ($p = 0.0004$). Because the adjusted outlier would have created

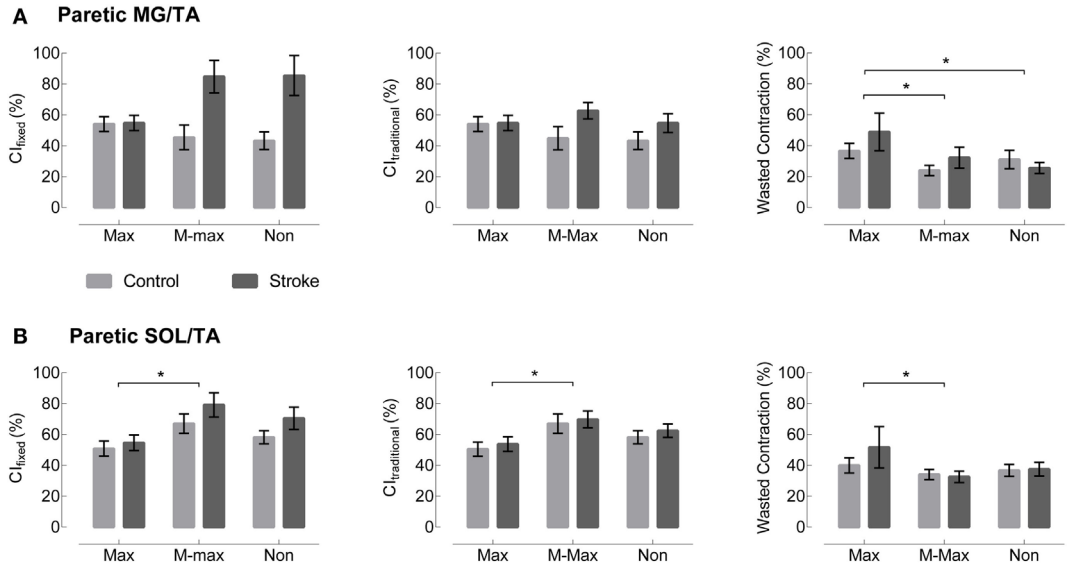

FIGURE 3 | Paretic leg co-contraction following stroke is not different from healthy controls. **(A)** Co-contraction of the medial gastrocnemius and tibialis anterior (MG/TA) in terminal stance is shown by three EMG normalization methods: maximum value (Max), maximal M-wave (M-max), and non-normalized (Non). Plots moving left to right represent three different co-contraction indices: a co-contraction ratio with fixed muscle roles derived from referencing healthy EMG (CI_{fixed}, left), a traditional index for co-contraction during normal walking ($CI_{traditional}$, center), and an index of the "wasted contraction" produced by antagonist activation countering agonist activation (right). There are no group differences between stroke (gray) and control (black) in any of the three comparisons. **(B)** Co-contraction of the soleus and tibialis anterior (SOL/TA) in terminal stance. Again, there were no significant differences between control and stroke. *Indicates significance with a Bonferroni-corrected $p < 0.0083$.

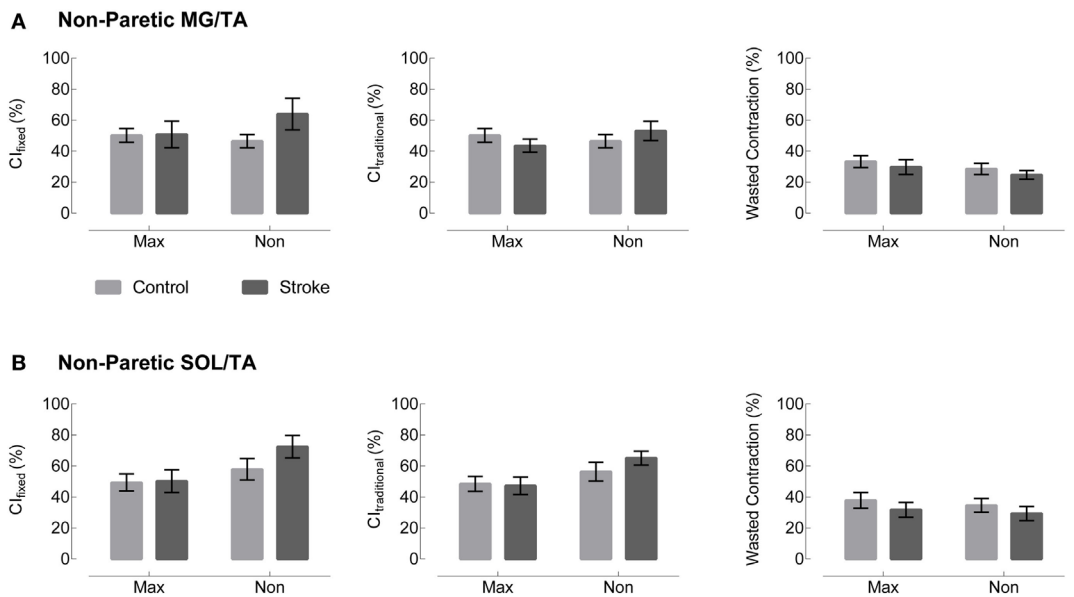

FIGURE 4 | Non-paretic leg co-contraction appears unchanged across group, metric, and normalization method. Plots moving left to right represent three different co-contraction indices: a co-contraction ratio with fixed muscle roles derived from referencing healthy EMG (CI_{fixed}, left), a traditional index for co-contraction during normal walking ($CI_{traditional}$, center), and an index of the "wasted contraction" produced by antagonist activation countering agonist activation (right). Co-contraction in terminal stance appears unchanged between control (gray) and stroke (black) in both **(A)** the medial gastrocnemius and tibialis anterior (MG/TA) and **(B)** the soleus and tibialis anterior (SOL/TA).

an even higher mean value for maximum value-normalized WC, these significant findings are consistent with the original direction of the adjusted outlier. When calculating WC, we observed an interesting phenomenon. Two subjects with visually different EMG patterns revealed comparable WC values in TSt (**Figure 5**). Aside from the maximum value normalization condition, the WC

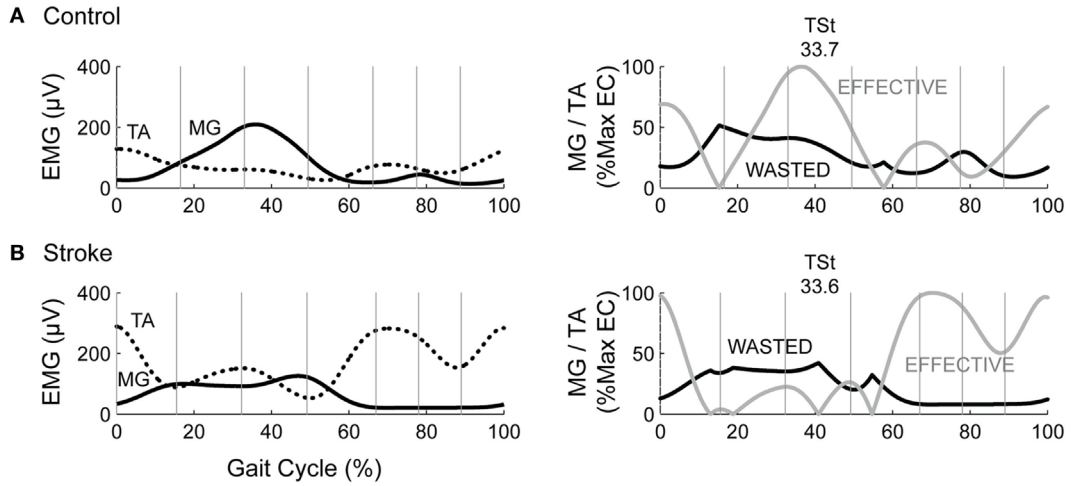

FIGURE 5 | Two subjects show vastly different EMG with same wasted contraction (WC) value in terminal stance. The left column depicts example EMG for the medial gastrocnemius (MG) and tibialis anterior (TA) muscles in **(A)** a healthy control and **(B)**. an individual post-stroke. The right column depicts the resultant wasted and effective contraction, with WC in TSt denoted above each plot.

values tended to have low variability, despite obvious visual differences present in the original EMG. This circumstance creates a problem for interpreting the WC results, which we will revisit in the Section in the discussion.

Non-normalized CI_{fixed} values are moderately correlated with functional metrics across groups. We observed similar results across all co-contraction indices. Because non-normalized data are most straightforward to interpret, we chose this metric to perform correlations with functional measures. Therefore, CI_{fixed} serves as representative of the patterns present across metrics. Four comparisons were made between CI_{fixed} and LE FMA, SSWS, FCWS, and A2 (**Figure 6**). CI_{fixed} was not significantly correlated with either LE FMA (Spearman's $\rho = -0.6079$, $p = 0.0162$) or A2, our most sensitive assessment of walking function ($\rho = -0.4557$, $p = 0.0252$). CI_{fixed} was significantly correlated with both SSWS ($\rho = -0.6438$, $p = 0.0007$) and FCWS ($\rho = -0.6026$, $p = 0.0018$).

DISCUSSION

Despite our systematic analysis of co-contraction during gait, we are unable to conclude that co-contraction is ubiquitously present post-stroke. As illustrated in **Figure 7**, this sample of individuals post-stroke revealed vast heterogeneity in EMG patterns, and no distinct pattern of co-contraction emerged. Furthermore, regardless of the metric used to assess co-contraction, our results fail to indicate clear differences between stroke and healthy controls. Although results reported here are limited to the TSt phase of gait, this finding is consistent across all gait phases. Nearly four decades of literature discuss pathological co-contraction after stroke, arguing for its presence as either study motivation or data interpretation, yet failing to show convincing evidence through results. Taken together with results of the current analysis, this lack of evidence leads us to reconsider the assumption that pathological co-contraction is a primary factor contributing to impaired gait post-stroke. The following discussion enumerates the details leading to this conclusion.

Early studies assessing EMG during gait post-stroke carefully described the authors' observations while presenting mostly qualitative evaluations and proposing future avenues of research. Knutsson and Richards are often credited for the suggestion that co-contraction could be a strategy employed in post-stroke gait, but they carefully acknowledged that the heterogeneity present within their sample limited their ability to draw distinct conclusions (22). Another group classified whole-leg muscle activation patterns, classifying less than half of their sample in the chronic phase of recovery as expressing excessive co-contraction (5). There is heterogeneity in virtually all motor outcomes measured following stroke, and that heterogeneity impacts the ability to assess treatment efficacy (44). Equally important, no strong evidence has emerged in favor of co-contraction as either the predominant strategy or one of a few common strategies employed by these individuals. Moreover, the evidence provides no indication that mitigating co-contraction is a productive treatment target. Working under the assumption that co-contraction indices provide useful information, therefore, limits our ability to appropriately quantify motor impairment within this population.

Heterogeneity of responses among individuals post-stroke leads many groups to seek a single metric, or a simple collection of metrics, which can parse these individual differences. Here, we employed a two-factor approach by combining EMG metrics with measures of motor or gait impairment. Although our data reveal some significant correlations, these are not sufficiently strong to support an argument for a causal link between co-contraction and impaired biomechanical function. Lower extremity coordination during gait requires much more than the ankle muscles; however, the vital importance of the ankle plantarflexors affords an ideal test-bed for assessing the relevance of lower extremity co-contraction post-stroke. Yet, no clear patterns emerged. It is worth noting that four of the individuals within this sample

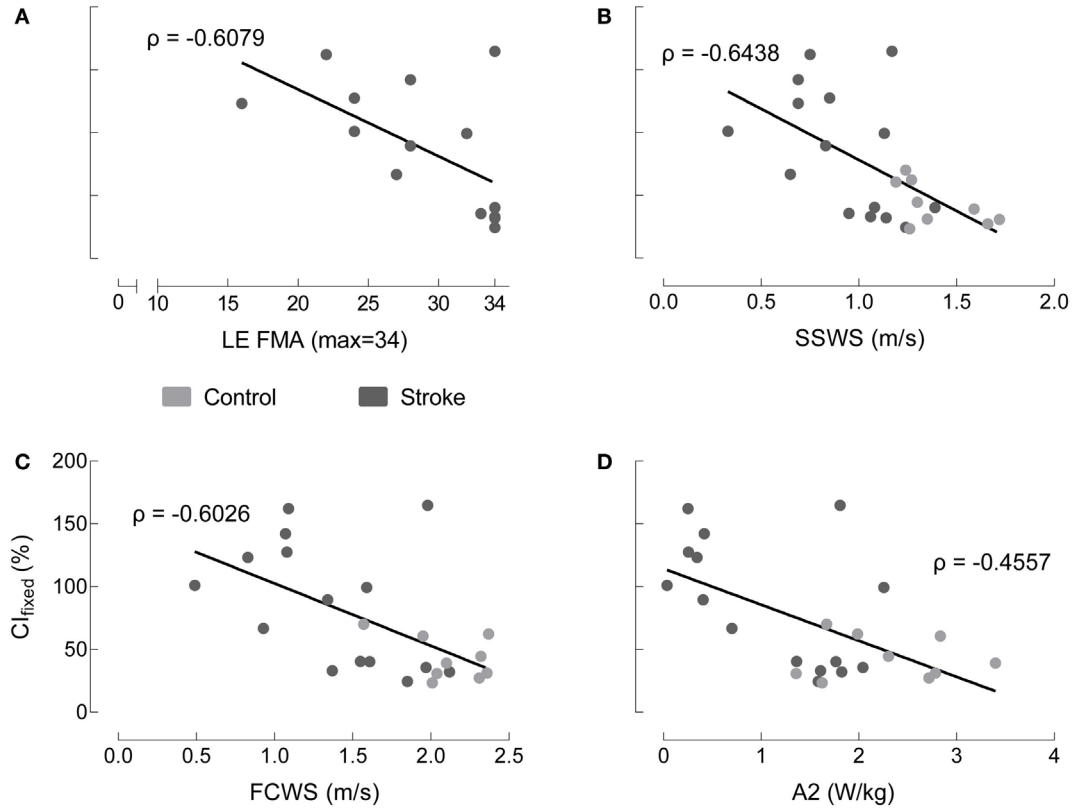

FIGURE 6 | Co-contraction index in terminal stance correlates to some, but not all, indices of motor function. Medial gastrocnemius/tibialis anterior CI_fixed in terminal stance with non-normalized EMG varies as a function of: **(A)** lower extremity Fugl-Meyer (LE FMA), **(B)** self-selected walking speed (SSWS), **(C)** fastest comfortable walking speed (FCWS), and **(D)** peak concentric ankle plantarflexor power (A2) for healthy controls (gray), individuals post-stroke (black). The only correlations reaching statistical significance occur with SSWS and FCWS.

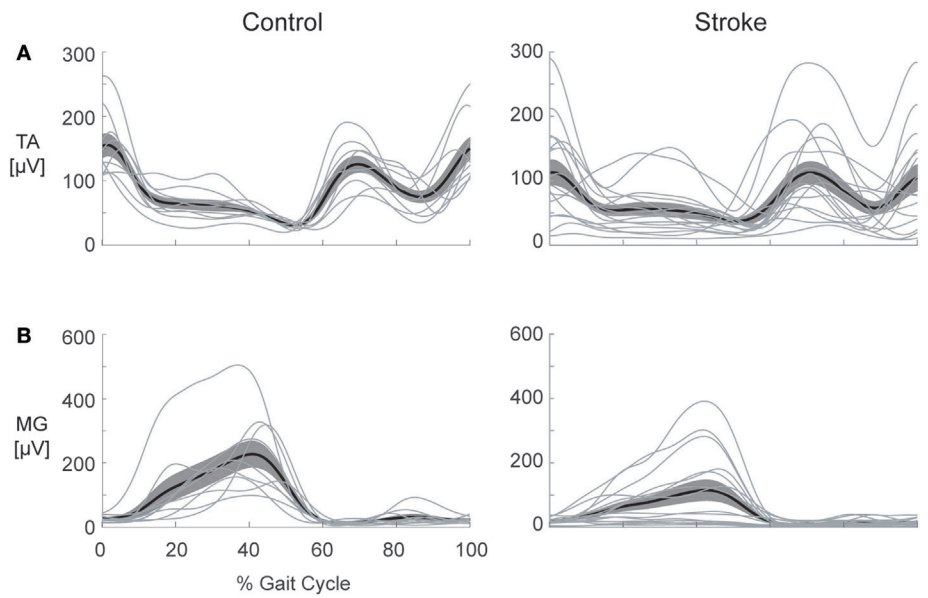

FIGURE 7 | Heterogeneity in electromyography (EMG) activation is present following stroke. Healthy control (left) and stroke (right) EMG envelopes are illustrated for the: **(A)** tibialis anterior (TA) and **(B)** medial gastrocnemius (MG). The heavy line depicts the ensemble average for each group and the cloud illustrates the SEM with individual subject responses overlaid (thin lines). Considerable variation in activation patterns of each muscle is apparent within the stroke group, illustrating the difficulty inherent in selecting a single metric to capture all of the possible deviations from the pattern of healthy controls.

regularly wore some form of ankle brace. The extent to which bracing impacted the EMG patterns differentially from the stroke itself is not known. We compared these participants against those who did not wear a brace and found no apparent differences. We acknowledge this is a limitation within our sample that may be worth exploring in the future. It is also important to note that EMG assesses the final common pathway (45), and these peripheral signals cannot be used to draw specific conclusions about central nervous system function. Although we expect surface EMG signals to provide information about motor coordination, co-contraction may not be sufficiently robust to explain central nervous system dysfunction.

Changing the co-contraction metric offered variable results. Contrary to our initial expectations, fixing the biomechanical roles of the muscles was only marginally more informative than the existing CI, which was not designed to account for abnormal muscle activation patterns. Importantly, the group-level results were the same; neither metric revealed differences between healthy individuals and individuals post-stroke. On the group level, even the WC metric performed similarly to the two co-contraction indices. However, thorough evaluation of the relationship of the individual numeric values to the EMG profiles provides insight that the WC metric does not perform well during gait. From production of extreme outliers to equivalent numeric values in obviously different EMG patterns (**Figure 5**), we can conclusively state that the WC metric is not useful for assessment of co-contraction in multi-segmental lower extremity tasks.

Normalization also provided varying results, creating a need for careful consideration of normalization procedures before, during, and after EMG assessment. Perhaps the most interesting result from the normalization analysis is the congruency of the M-max and non-normalized EMG co-contraction indices. Choosing not to normalize EMG can be advantageous because it avoids data transformation beyond recognition. Our findings support arguments presented by Lamontagne regarding EMG metrics in stroke (6). While EMG normalization is not strictly necessary in this context because calculating a ratio from normalized data effectively normalizes the data twice, most studies in the literature employ some type of normalization prior to calculating a co-contraction index (46–48). In our sample, maximum value normalization suggested a different picture of relative muscle activation than either M-max normalization or no normalization.

Co-contraction does not appear to be a universal characteristic of impaired gait post-stroke. We do not mean to suggest that excessive co-contraction does not occur in some individuals; however, the pattern does not occur sufficiently often enough to be considered a prominent compensatory strategy following stroke. Ours is not the first study to find a lack of strong evidence for the presence of excessive co-contraction following stroke. In both the upper and lower extremities, the current evidence suggests that reaching and walking deficits, respectively, are more likely to result from agonist activation impairment than co-contraction (49, 50). It is possible that co-contraction represents too narrow of a concept to represent and characterize neuromotor pathology post-stroke. Accordingly, it may be time to reconsider how we frame the problem. Aberrant EMG is descriptively characterized by timing and amplitude deficits, and the ability to organize responses to the biomechanical constraints of the task and environment (51). In this broader context, approaches other than a co-contraction metric may better capture the relevant deficits. Some recent efforts that have yet to be robustly evaluated in stroke include: Ricamato and Hidler's EMG metric that incorporates both timing and amplitude components (52); muscle synergy analysis (53, 54); and EMG-driven biomechanical modeling that effectively accounts for subject-specific neuromuscular constraints on dynamic outcomes (55). Our intent is not to prescribe any one of these methods to adequately quantify neurophysiologic impairments with EMG. Rather, we would argue that these and other alternatives be explored in an effort to learn more about the causal mechanisms of gait impairment following stroke.

Beyond an exercise in signal processing and EMG data analysis, our results provide an opportunity for discussion regarding the neural implications of co-contraction following stroke. Heterogeneity among individuals also presents a challenge for understanding behavior after stroke, especially in terms of muscle activation patterns. Our data illustrate that, even when assessed with a variety of metrics, co-contraction does not emerge as the strong indicator of neuromotor pathology the literature has conditioned us to expect. Instead, we must look to other EMG quantification methods that can provide greater insights regarding causal mechanisms of gait impairment.

ETHICS STATEMENT

All procedures were approved by the University of Florida Health Science Center Institutional Review Board (IRB-01) and all participants gave written informed consent prior to enrollment. Testing was conducted in accordance with the Declaration of Helsinki.

AUTHOR CONTRIBUTIONS

CB, HH, and CP conceived and designed experiments. CB and HH contributed analysis tools, prepared figures, and analyzed data. CB and VL performed experiments. CB, HH, VL, and CP interpreted results, revised manuscript, approved final version of manuscript, and agreed to be accountable for all aspects of the work. CB drafted manuscript.

ACKNOWLEDGMENTS

We thank the members of the Neural Control of Movement lab for their support, especially Dr. Eric Walker, Spencer Gilleon, and Theresa McGuirk for data collection and processing.

FUNDING

This research was supported by the Department of Veterans Affairs, Rehabilitation Research & Development Service [Project #O1435-P (CP) and Research Career Scientist Award #N9274-S (CP)]. CB received support from a University of Florida Graduate School Fellowship. The funders had no role in study design, data collection and analysis, decision to publish, or preparation of the manuscript.

REFERENCES

1. Pollock A, Baer G, Campbell P, Choo PL, Forster A, Morris J, et al. Physical rehabilitation approaches for the recovery of function and mobility following stroke. *Cochrane Database Syst Rev* (2014) 4:CD001920. doi:10.1002/14651858.CD001920.pub3
2. Dickstein R. Rehabilitation of gait speed after stroke: a critical review of intervention approaches. *Neurorehabil Neural Repair* (2008) 22(6):649–60. doi:10.1177/1545968308220060201
3. Burpee JL, Lewek MD. Biomechanical gait characteristics of naturally occurring unsuccessful foot clearance during swing in individuals with chronic stroke. *Clin Biomech (Bristol, Avon)* (2015) 30(10):1102–7. doi:10.1016/j.clinbiomech.2015.08.018
4. Chen G, Patten C, Kothari DH, Zajac FE. Gait differences between individuals with post-stroke hemiparesis and non-disabled controls at matched speeds. *Gait Posture* (2005) 22(1):51–6. doi:10.1016/j.gaitpost.2004.06.009
5. Shiavi R, Bugle HJ, Limbird T. Electromyographic gait assessment, Part 2: preliminary assessment of hemiparetic synergy patterns. *J Rehabil Res Dev* (1987) 24(2):24–30.
6. Lamontagne A, Richards CL, Malouin F. Coactivation during gait as an adaptive behavior after stroke. *J Electromyogr Kinesiol* (2000) 10:407–15. doi:10.1016/S1050-6411(00)00028-6
7. Den Otter AR, Geurts ACH, Mulder T, Duysens J. Abnormalities in the temporal patterning of lower extremity muscle activity in hemiparetic gait. *Gait Posture* (2007) 25:342–52. doi:10.1016/j.gaitpost.2006.04.007
8. Falconer K, Winter DA. Quantitative assessment of co-contraction at the ankle joint in walking. *Electromyogr Clin Neurophysiol* (1985) 25(2–3):135–49.
9. Flanders M, Cordo PJ. Quantification of peripherally induced reciprocal activation during voluntary muscle contraction. *Electroencephalogr Clin Neurophysiol* (1987) 67(5):389–94. doi:10.1016/0013-4694(87)90001-0
10. Corcos DM, Gottlieb GL, Penn RD, Myklebust B, Agarwal GC. Movement deficits caused by hyperexcitable stretch reflexes in spastic humans. *Brain* (1986) 109(Pt 5):1043–58. doi:10.1093/brain/109.5.1043
11. Gordon J, Ghez C. EMG patterns in antagonist muscles during isometric contraction in man: relations to response dynamics. *Exp Brain Res* (1984) 55(1):167–71. doi:10.1007/BF00240511
12. van Zuylen EJ, Gielen CC, Denier van der Gon JJ. Coordination and inhomogeneous activation of human arm muscles during isometric torques. *J Neurophysiol* (1988) 60(5):1523–48.
13. Corcos DM, Agarwal GC, Flaherty BP, Gottlieb GL. Organizing principles for single-joint movements. IV. Implications for isometric contractions. *J Neurophysiol* (1990) 64(3):1033–42.
14. Busse ME, Wiles CM, van Deursen WM. Muscle co-activation in neurological conditions. *Phys Ther Rev* (2005) 10(4):247–53. doi:10.1179/108331905X78915
15. Darainy M, Ostry DJ. Muscle cocontraction following dynamics learning. *Exp Brain Res* (2008) 190(2):153–63. doi:10.1007/s00221-008-1457-y
16. Twitchell TE. The restoration of motor function following hemiplegia in man. *Brain* (1951) 74(4):443–80. doi:10.1093/brain/74.4.443
17. Knutsson E, Martensson A, Gransberg L. Influences of muscle stretch reflexes on voluntary, velocity-controlled movements in spastic paraparesis. *Brain* (1997) 120(Pt 9):1621–33. doi:10.1093/brain/120.9.1621
18. Nathan PW. Factors affecting spasticity. *Int Rehabil Med* (1980) 2(1):27–30. doi:10.3109/09638288009163951
19. Sahrmann SA, Norton BJ. The relationship of voluntary movement to spasticity in the upper motor neuron syndrome. *Ann Neurol* (1977) 2(6):460–5. doi:10.1002/ana.410020604
20. Mizrahi EM, Angel RW. Impairment of voluntary movement by spasticity. *Ann Neurol* (1979) 5(6):594–5. doi:10.1002/ana.410050620
21. Dietz V, Berger W. Normal and impaired regulation of muscle stiffness in gait: a new hypothesis about muscle hypertonia. *Exp Neurol* (1983) 79(3):680–7. doi:10.1016/0014-4886(83)90032-8
22. Knutsson E, Richards C. Different types of disturbed motor control in gait of hemiparetic patients. *Brain* (1979) 102(2):405–30. doi:10.1093/brain/102.2.405
23. Detrembleur C, Dierick F, Stoquart G, Chantraine F, Lejeune T. Energy cost, mechanical work, and efficiency of hemiparetic walking. *Gait Posture* (2003) 18(2):47–55. doi:10.1016/S0966-6362(02)00193-5
24. Rosa MC, Marques A, Demain S, Metcalf CD, Rodrigues J. Methodologies to assess muscle co-contraction during gait in people with neurological impairment – a systematic literature review. *J Electromyogr Kinesiol* (2014) 24(2):179–91. doi:10.1016/j.jelekin.2013.11.003
25. Thoroughman KA, Shadmehr R. Electromyographic correlates of learning an internal model of reaching movements. *J Neurosci* (1999) 19(19):8573–88.
26. Kadaba MP, Ramakrishnan HK, Wootten ME. Measurement of lower extremity kinematics during level walking. *J Orthop Res* (1990) 8(3):383–92. doi:10.1002/jor.1100080310
27. Hermens HJ, Freriks B, Disselhorst-Klug C, Rau G. Development of recommendations for SEMG sensors and sensor placement procedures. *J Electromyogr Kinesiol* (2000) 10(5):361–74. doi:10.1016/S1050-6411(00)00027-4
28. Geertsen SS, Lundbye-Jensen J, Nielsen JB. Increased central facilitation of antagonist reciprocal inhibition at the onset of dorsiflexion following explosive strength training. *J Appl Physiol (1985)* (2008) 105(3):915–22. doi:10.1152/japplphysiol.01155.2007
29. Shiavi R, Frigo C, Pedotti A. Electromyographic signals during gait: criteria for envelope filtering and number of strides. *Med Biol Eng Comput* (1998) 36(2):171–8. doi:10.1007/BF02510739
30. Rancho Los Amigos Medical Center, Pathokinesiology Service, Rancho Los Amigos Medical Center Physical Therapy Dept. *Observational Gait Analysis*. Downey, CA: Los Amigos Research and Education Institute, Rancho Los Amigos National Rehabilitation Center (2001).
31. Amarantini D, Martin L. A method to combine numerical optimization and EMG data for the estimation of joint moments under dynamic conditions. *J Biomech* (2004) 37(9):1393–404. doi:10.1016/j.jbiomech.2003.12.020
32. Centomo H, Amarantini D, Martin L, Prince F. Muscle adaptation patterns of children with a trans-tibial amputation during walking. *Clin Biomech (Bristol, Avon)* (2007) 22(4):457–63. doi:10.1016/j.clinbiomech.2006.11.005
33. Rao G, Amarantini D, Berton E. Influence of additional load on the moments of the agonist and antagonist muscle groups at the knee joint during closed chain exercise. *J Electromyogr Kinesiol* (2009) 19(3):459–66. doi:10.1016/j.jelekin.2007.12.001
34. Sarcher A, Raison M, Ballaz L, Lemay M, Leboeuf F, Trudel K, et al. Impact of muscle activation on ranges of motion during active elbow movement in children with spastic hemiplegic cerebral palsy. *Clin Biomech (Bristol, Avon)* (2015) 30(1):86–94. doi:10.1016/j.clinbiomech.2014.10.009
35. Ranavolo A, Mari S, Conte C, Serrao M, Silvetti A, Iavicoli S, et al. A new muscle co-activation index for biomechanical load evaluation in work activities. *Ergonomics* (2015) 58(6):966–79. doi:10.1080/00140139.2014.991764
36. Fugl-Meyer AR, Jääskö L, Leyman I, Olsson S, Steglind S. The post-stroke hemiplegic patient. 1. A method for evaluation of physical performance. *Scand J Rehabil Med* (1975) 7(1):13–31.
37. Robertson DG, Winter DA. Mechanical energy generation, absorption and transfer amongst segments during walking. *J Biomech* (1980) 13(10):845–54. doi:10.1016/0021-9290(80)90172-4
38. Winter DA. Moments of force and mechanical power in jogging. *J Biomech* (1983) 16(1):91–7. doi:10.1016/0021-9290(83)90050-7
39. Olney SJ, Griffin MP, Monga TN, McBride ID. Work and power in gait of stroke patients. *Arch Phys Med Rehabil* (1991) 72(5):309–14.
40. Prince F, Corriveau H, Hebert R, Winter DA. Gait in the elderly. *Gait Posture* (1997) 5(2):128–35. doi:10.1016/S0966-6362(97)01118-1
41. Cofre LE, Lythgo N, Morgan D, Galea MP. Aging modifies joint power and work when gait speeds are matched. *Gait Posture* (2011) 33(3):484–9. doi:10.1016/j.gaitpost.2010.12.030
42. Jonkers I, Delp S, Patten C. Capacity to increase walking speed is limited by impaired hip and ankle power generation in lower functioning persons post-stroke. *Gait Posture* (2009) 29:129–37. doi:10.1016/j.gaitpost.2008.07.010
43. Meinders M, Gitter A, Czerniecki JM. The role of ankle plantar flexor muscle work during walking. *Scand J Rehabil Med* (1998) 30(1):39–46. doi:10.1080/003655098444309
44. Duncan PW, Sullivan KJ, Behrman AL, Azen SP, Wu SS, Nadeau SE, et al. Body-weight-supported treadmill rehabilitation after stroke. *N Engl J Med* (2011) 364(21):2026–36. doi:10.1056/NEJMoa1010790
45. Enoka RM, Duchateau J. Inappropriate interpretation of surface EMG signals and muscle fiber characteristics impedes understanding of the control of neuromuscular function. *J Appl Physiol (1985)* (2015) 119(12):1516–8. doi:10.1152/japplphysiol.00280.2015

46. Eken MM, Dallmeijer AJ, Doorenbosch CA, Dekkers H, Becher JG, Houdijk H. Coactivation during dynamometry testing in adolescents with spastic cerebral palsy. *Phys Ther* (2016) 96(9):1438–47. doi:10.2522/ptj.20140448
47. Chow JW, Yablon SA, Stokic DS. Coactivation of ankle muscles during stance phase of gait in patients with lower limb hypertonia after acquired brain injury. *Clin Neurophysiol* (2012) 123(8):1599–605. doi:10.1016/j.clinph.2012.01.006
48. Knarr BA, Zeni JA Jr, Higginson JS. Comparison of electromyography and joint moment as indicators of co-contraction. *J Electromyogr Kinesiol* (2012) 22(4):607–11. doi:10.1016/j.jelekin.2012.02.001
49. Wagner JM, Dromerick AW, Sahrmann SA, Lang CE. Upper extremity muscle activation during recovery of reaching in subjects with post-stroke hemiparesis. *Clin Neurophysiol* (2007) 118(1):164–76. doi:10.1016/j.clinph.2006.09.022
50. Clark DJ, Condliffe EG, Patten C. Activation impairment alters muscle torque-velocity in the knee extensors of persons with post-stroke hemiparesis. *Clin Neurophysiol* (2006) 117(10):2328–37. doi:10.1016/j.clinph.2006.07.131
51. Lamontagne A, Stephenson JL, Fung J. Physiological evaluation of gait disturbances post stroke. *Clin Neurophysiol* (2007) 118(4):717–29. doi:10.1016/j.clinph.2006.12.013
52. Ricamato AL, Hidler JM. Quantification of the dynamic properties of EMG patterns during gait. *J Electromyogr Kinesiol* (2005) 15(4):384–92. doi:10.1016/j.jelekin.2004.10.003
53. Clark DJ, Ting LH, Zajac FE, Neptune RR, Kautz SA. Merging of healthy motor modules predicts reduced locomotor performance and muscle coordination complexity post-stroke. *J Neurophysiol* (2010) 103:844–57. doi:10.1152/jn.00825.2009
54. Banks CL, Pai MM, McGuirk TE, Fregly BJ, Patten C. Methodological choices in muscle synergy analysis impact differentiation of physiological characteristics following stroke. *Front Comput Neurosci* (2017) 11:78. doi:10.3389/fncom.2017.00078
55. Meyer AJ, Patten C, Fregly BJ. Lower extremity EMG-driven modeling of walking with automated adjustment of musculoskeletal geometry. *PLoS One* (2017) 12(7):e0179698. doi:10.1371/journal.pone.0179698

Conflict of Interest Statement: The authors declare that the research was conducted in the absence of any commercial or financial relationships that could be construed as a potential conflict of interest.

frontiers in Neurology

ORIGINAL RESEARCH
published: 27 November 2017
doi: 10.3389/fneur.2017.00627

The Reticulospinal Pathway Does Not Increase Its Contribution to the Strength of Contralesional Muscles in Stroke Survivors as Compared to Ipsilesional Side or Healthy Controls

Sheng Li[1,2], Minal Bhadane[1,2], Fan Gao[3] and Ping Zhou[1,2]*

[1] Department of Physical Medicine and Rehabilitation, McGoven Medical School, University of Texas Health Science Center at Houston, Houston, TX, United States, [2] TIRR Memorial Hermann Research Center, TIRR Memorial Hermann Hospital, Houston, TX, United States, [3] The University of Texas Southwestern Medical Center, Dallas, TX, United States

OPEN ACCESS

Edited by:
Pavel Lindberg,
Centre for Psychiatry and Neuroscience (INSERM), France

Reviewed by:
Marc A. Maier,
Paris Diderot University, France
Mattias Hedlund,
Umeå University, Sweden

***Correspondence:**
Sheng Li
sheng.li@uth.tmc.edu

Specialty section:
This article was submitted to Stroke, a section of the journal Frontiers in Neurology

Received: 07 June 2017
Accepted: 09 November 2017
Published: 27 November 2017

Citation:
Li S, Bhadane M, Gao F and Zhou P (2017) The Reticulospinal Pathway Does Not Increase Its Contribution to the Strength of Contralesional Muscles in Stroke Survivors as Compared to Ipsilesional Side or Healthy Controls. Front. Neurol. 8:627. doi: 10.3389/fneur.2017.00627

Objective: Startling acoustic stimulation (SAS), via activation of reticulospinal (RS) pathways, has shown to increase muscle strength in healthy subjects. We hypothesized that, given RS hyperexcitability in stroke survivors, SAS could increase muscle strength in stroke survivors. The objective was to quantify the effect of SAS on maximal and sub-maximal voluntary elbow flexion on the contralesional (impaired) side in stroke survivors as compared to ipsilesional (non-impaired) side and healthy controls.

Design: Thirteen hemiparetic stroke survivors and 12 healthy subjects volunteered for this investigation. Acoustic stimulation was given at rest, during ballistic maximal and sustained sub-maximal isometric elbow contractions using low (80 dB) and high intensity sound (105 dB). The effect of acoustic stimuli was evaluated from EMG and force recordings.

Results: Prevalence of acoustic startle reflex with shorter latency in the impaired biceps was greater as compared to the response in the non-impaired side of stroke subjects and in healthy subjects. Delivery of SAS resulted in earlier initiation of elbow flexion and greater peak torque in healthy subjects and in stroke subjects with spastic hemiplegia during maximal voluntary elbow flexion tasks. During sub-maximal elbow flexion tasks, SAS-induced force responses were slightly greater on the impaired side than the non-impaired side. However, no statistically significant difference was found in SAS-induced responses between impaired and non-impaired sides at maximal and sub-maximal elbow flexion tasks.

Conclusion: The findings suggest RS hyperexcitability in stroke survivors with spastic hemiplegia. The results of similar SAS-induced responses between healthy and stroke subjects indicate that RS projections via acoustic stimulation are not likely to contribute to muscle strength for stroke survivors to a significant extent.

Keywords: spasticity, reticulospinal, stroke, acoustic stimulation, strength, muscle

INTRODUCTION

Weakness for voluntary contraction is a common sequela of a hemispheric stroke. Among other clinical symptoms, weakness is a primary contributor to the overall impairment (1) and specifically toward impaired motor control (2). Damage of ipsilesional motor cortex and its descending corticospinal (CS) pathway to spinal motoneurons after stroke is presumably a primary contributor to weakness. Muscle weakness can also be attributed to altered intracortical inhibition (3, 4). A number of motor rehabilitation interventions have been used for motor recovery, such as constraint-induced movement therapy (5, 6), robotic training (7–9), and body weight-supported treadmill training (10, 11). A previous longitudinal MRI study (12) has provided evidence that recovery of locomotor function after such repetitive motor training in post-stroke hemiplegia is accompanied by increased activation in the ipsilesional motor cortex and evolution from contralesional activation to ipsilesional activation.

Both CS and reticulospinal (RS) projections contribute to the motor output. Originated from the brainstem reticular system, the RS projections can influence the CS motor output from the motor cortex. The RS system can be stimulated by acoustic stimuli via a relatively simple reflex circuit, i.e., acoustic startle reflex (ASR). The reflex circuit in humans consists of the cochlear nucleus, the caudal pontine reticular nuclei, the motoneurons of the brainstem, and the spinal motoneurons activated via the medial RS pathway (13–15). After several trials of startling acoustic stimulation (SAS), ASR responses habituate, while ensuing SAS stimulates RS projections non-reflexively (16, 17). Ensuing SAS has been shown to reduce reaction time and facilitate motor initiation in healthy subjects (18–20) and after stroke (21). It can also augment the magnitude of voluntary muscle contraction in healthy subjects and Parkinson's patients (19, 22). Furthermore, the RS projections have been shown to compensate for damage of CS pathways for motor recovery after stroke in animal models (23–28).

The role of RS system in post-stroke motor recovery in humans is still unclear. RS hyperexcitability occurs as a result of unmasking and disinhibition effect from damage to the motor cortex and its descending CS projections in patients with spastic hemiplegia (29, 30). RS hyperexcitability contributes mainly to development of spasticity, but not to motor recovery after stroke (31, 32). However, there are reports suggesting a possible role of RS in motor recovery in stroke survivors. Integration of acoustic stimuli in the forms of rhythmic cueing or music therapy into training programs, possibly via non-reflexive stimulation of RS pathways, improves initiation and pacing of voluntary movement in stroke survivors (33–36). The results of motor improvement after such training could be attributed to repetitive training and/or acoustic stimulation. However, the role of acoustic stimulation in motor improvement can not be delineated. Furthermore, Aluru et al. (37) found that that auditory rhythmic cueing improved motor performance in stroke subjects with severe spastic paresis of wrist flexors but not in those subjects with minimal impairment or spastic co-contractions. The authors argued that auditory cueing and stimulation have different effects at different stages of post-stroke recovery via recruiting distinct neural substrates.

The purpose of the present study was to first examine whether startling acoustic stimulation (SAS) could induce greater augmentation in maximum voluntary contraction (MVC) in stroke subjects with spastic hemiplegia, since RS hyperexcitability was reported at this stage of recovery (29, 30). In clinical practice, most motor training interventions use repetitive exercises at sub-maximal levels. Therefore, we also aimed to examine whether SAS-induced force increment was greater in the spastic-paretic (impaired) side than the non-impaired side in stroke subjects at sub-maximum voluntary contraction. Accordingly, a cohort of stroke subjects with chronic spastic hemiplegia and healthy subjects received unexpected SAS in the beginning of experiments to examine the occurrence frequency of ASR at rest. Subjects then received SAS during MVC and sub-maximal elbow flexion tasks in a random order to quantify and compare the SAS-induced responses.

MATERIALS AND METHODS

Subjects

Twelve healthy subjects (age: 25–44 years; weight: 125–205 lb; five males and seven females; and three left handed and nine right handed) volunteered for this investigation. No subject had any known history or symptoms of neuromuscular or skeletal disorders. Thirteen hemiparetic stroke survivors (age: 48–92 years; eight males and five females; eight right and five left hemiplegia; and averaged 77 months after stroke) were recruited in the experiment. **Table 1** displays characteristics of the stroke subjects. Inclusion criteria were as follows: (1) ≥1 year post-stroke; (2) unilateral, single stroke (no restriction on type (ischemic or hemorrhagic) with unilateral spasticity; (3) mild-to-moderate spasticity [3 or less according to modified Ashworth scale (MAS)], note that some subjects did not have spasticity in elbow flexors but had spasticity in hand and finger flexors (not shown in the table); and (4) able to voluntarily contract impaired biceps. Exclusion criteria included patients who had (1) visual deficit and/or neglect; (2) hearing or cognitive impairment; (3) unstable medical conditions; (4) presence of contracture that would limit full elbow range of motion on the impaired side; and (5) unable to understand or follow study instructions. Written consent was obtained from all subjects for their participation in the study. This study was approved by the Committee for the Protection of Human Subjects at the University of Texas Health Science Center at Houston and TIRR Memorial Hermann Hospital.

Experimental Setting

Both stroke and healthy subjects used the same experimental setup. The subjects were seated on a height adjustable chair. Conventional single differential surface electrodes (Delsys 2.1, Boston, MA, USA) were used for EMG recordings. After skin preparation, bipolar surface electromyogram (sEMG) electrodes were placed over muscle belly of biceps brachii of both dominant and non-dominant sides, according to the SENIAM

TABLE 1 | Characteristics of stroke subjects (M: male, F: female, MAS: modified Ashworth scale; ip: impaired side; nip: non-impaired; ASR: acoustic startle reflex).

ID	Gender	Age (years)	Stroke onset (months)	Affected side	MAS of elbow flexor	MVC_ip (Nm)	MVC_nip (Nm)	ASR freq (impaired) (%)	ASR freq (non-impaired (%)	ASR freq (control %)
1	M	77	52	RIGHT	1	33	37.5	0	0	
2	F	58	81	RIGHT	1+	12	38	100	33	
3	F	59	81	LEFT	1	8.2	23	100	100	
4	M	60	25	LEFT	0	10	18	0	33	
5	F	61	109	LEFT	1	3.5	32	67	0	
6	M	48	67	LEFT	0	60	85	100	100	
7	M	75	14	LEFT	1	6.4	9	33	33	
8	M	92	109	RIGHT	1	17	20	100	67	
9	M	55	157	RIGHT	1+	7	40	100	0	
10	M	63	109	RIGHT	0	34	38	100	0	
11	M	68	64	RIGHT	1+	14	50	100	0	
12	F	66	88	RIGHT	1+	22	34	0	0	
13	F	62	46	RIGHT	2	18	37	0	0	
Average		64.9	77.1			19.6	35.5	61.5	28.2	14.1

Note: Subjects 7 & 9 were not pub.

recommendations (38). The electrode was secured using self-adhesive tape to ensure contact. The reference electrode of sEMG was attached to the lateral condyle of the humerus of the test arm. After placement of electrodes, the arm to be tested was firmly secured on a customized apparatus (**Figure 1**). The elbow joint was set to approximately 90° of flexion. The shoulder was positioned at approximately 45° of abduction and 30° of flexion. The forearm was firmly secured using four vertical plates at the proximal and distal forearm. Subjects were explicitly instructed to naturally relax their wrist and fingers, i.e., not to make a fist, or flex fingers and wrist, or to extend wrist and fingers. The center of the elbow joint was aligned with the axis of rotation of the shaft to prevent translation and rotation of the arm. The other arm of the subject was comfortably rested in an appropriately symmetrical position.

A single beep sound was generated by the computer using a 16-bit sound card (Creative Sound Blaster 16 SB1040EF) and Yamaha powered speaker (Model HS 50 M). Two levels of sound stimulus: "low" around 80 dB (for baseline response) and "high" around 105 dB (commonly used in the literature to elicit ASR) were used in this experiment. The intensity of the acoustic tone was measured and confirmed using a sound level meter (model 407730; Extech Instruments) at a distance of 30 cm from the speaker (approximately the distance to both ears of the subject).

Experimental Tasks

The experiments consisted of the following three tasks: (1) ASR rest tasks, (2) Ballistic maximum voluntary contraction (MVC) tasks, and (3) sub-maximal elbow flexion tasks. All subjects performed ASR rest tasks first, and the order of remaining two tasks was randomized to avoid the effect of order. Healthy subjects performed on their dominant side, and stroke subjects repeated movement tasks on both sides in a random order. Thirteen stroke subjects were enrolled in the study. All of them performed the resting startle task. One stroke subject could not finish the movement tasks and one more was omitted due to motor apraxia. Only 11 of them executed ballistic tasks.

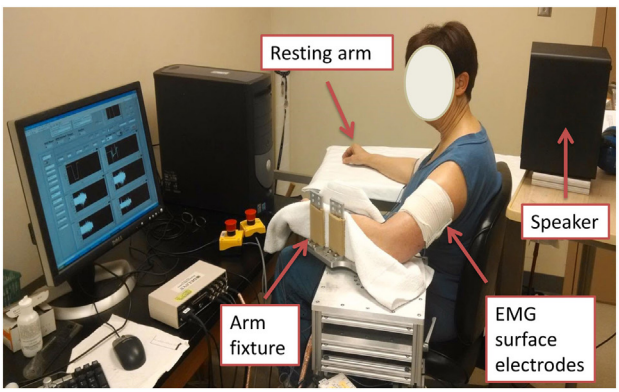

FIGURE 1 | Experimental settings.

ASR Rest Task

Subjects were asked to relax and sound was delivered randomly between the 8th and 10th second of a 15-s trial. At first, one low sound and then three high sounds were delivered with 2-min intervals. The same order was followed for all subjects to standardize the protocol. Subjects were explicitly asked to react naturally to the sound and continue to stay relaxed as much as possible until the end of the trial. ASR responses are usually habituated after three trials, while the ensuing high sound (SAS) continues to stimulate RS tracts without causing reflex responses in healthy subjects (16, 17, 39). Only EMG signals were recorded during this task.

Ballistic MVC Task

Subjects performed ballistic isometric elbow contractions in response to two levels of sound stimulus at a random order. They were instructed before each trial to flex elbow joint as fast and as strong as they can, after hearing the sound and hold it for 2–3 s, i.e., a reaction time task with elbow flexion MVC. They were also instructed to focus on one object (e.g., staring at the computer screen) and be consistent throughout all trials.

The sound was delivered randomly between the 4th and 8th second of a trial. Healthy subjects performed 10 trials on the dominant side, while to avoid fatigue stroke subjects performed six trials on each side. Subjects were allowed to rest between trials to minimize possible muscle fatigue. The same procedure was repeated on the other arm for stroke subjects. Before testing, subjects were required to practice the task 3–5 times before testing to familiarize themselves with the task and equipment. Similar to test trials, SAS was delivered during practice trials. The intervals between practice trials were about 30 s. As such, it was expected that practice trials were able to minimize the systematic bias, because the number of test trials was different between healthy and stroke subjects.

Sub-maximal Contraction Task

Subjects performed a series of isometric elbow flexion at sub-maximal levels. As in our recent study (40), elbow flexion MVC was first determined for each arm. The higher value of two MVC trials was estimated as the MVC value. Visual targets were established and displayed on the computer screen in a random order. Healthy subjects performed 3, 6, 10, 20, 30, and 40% of MVC on the dominant side. Stroke subjects performed 5, 10, 20, 30, and 40% of MVC on each side to minimize possible fatigue effect. The order of levels was randomized and balanced among subjects. Subjects were verbally cued for the beginning of a 20-s trial. Subjects then initiated elbow flexion against the vertical plates in a self-paced manner to achieve the visual target. Subjects were instructed to naturally curve the wrist and fingers during elbow flexion tasks. They were verbally encouraged to match the visual target as accurately as possible during all the trials. After the force was stabilized at the target level, high sound stimulus of 105 dB was given randomly between 6 and 8 s of the trial. Approximately 3–5 practice trials were allowed for all subjects to familiarize themselves with the task requirement. All sub-maximal isometric contractions were performed three times by healthy subjects and twice by stroke subjects to avoid fatigue. Between trials, subjects were allowed to have enough rest to minimize possible muscle fatigue.

Data Processing and Analysis

Torque was measured with a torque sensor (Model TRS 500; Transducers Techniques, CA, USA). The output of the surface EMG electrodes was connected to an EMG amplifier (Bagnoli 8; Delsys Inc., Boston) to a PC computer with a BNC-2090A connector block and a data acquisition board (National Instruments, Austin, TX, USA). Custom LabVIEW software (National Instruments) was used. All raw sEMG and torque signals were band-pass filtered at 20–450 Hz and were digitized at 1,000 sample/s. Data were saved for offline analysis using a customized MATLAB (MathWorks, MA, USA) program. Before further processing, mean of raw EMG signal of a trial was subtracted from the EMG data to nullify any data shift. EMG signal was then rectified and filtered (Butterworth, fourth order, low cutoff 10 Hz) for finding envelop of muscle activity. Baseline activity (100 ms at the beginning of trial) was subtracted from a complete trial to nullify any data shift. Data analysis was performed by MB who performed the experiments.

ASR Rest Task

As described in Li et al. (30), responses to acoustic startle were quantified by (1) onset latency: time interval between the stimulus and the onset of EMG burst and (2) burst amplitude: peak amplitude of filtered EMG signals within 500 ms after the stimulus. As in previous studies (41, 42), the startle response onset was defined as time when it took the baseline EMG to increase by 2 SDs. The onset was confirmed by visual inspection and marked on the raw EMG signals from biceps muscles. Burst amplitude was computed by subtracting the baseline value (200 ms before stimulation) from mean of 10 ms data centered on the peak EMG value. Response frequency was calculated as percent of trials with ASR responses as a group (**Table 2**).

Ballistic Movement Task

Reaction onset after the sound stimulation was marked by visual inspection of EMG response. Reaction time was calculated from the difference between sound stimulation and onset of biceps EMG signals. Trials with significantly late start or incomplete movement were considered as outliers and were discarded from analysis. Mean reaction time of all selected trials was calculated for each sound level. Torque data for each trial was arranged to start at reaction onset mark. A final torque profile was created by taking average of onset matched torque profiles from these trials. Peak torque was extracted from the average torque profile for each subject. Rate of force development was calculated by finding time required to reach 70% of MVC (19, 22).

Sub-maximal Contraction Task

Both EMG and torque responses to sound stimulation during sub-maximal contraction were quantified. The EMG response was quantified by subtracting baseline value (average over 200 ms before stimulation) from mean of 10 ms data centered on the peak EMG value. The torque response to sound stimulation was quantified by subtracting baseline value (average over 200 ms before stimulation) from the peak torque value. Average of all trials for each contraction level was calculated. The final torque response was normalized by MVC to avoid data variation as a result of anthropometry spread between subjects. Similarly, the EMG response was normalized by the corresponding EMG value obtained from the MVC task.

Statistical Analysis

Given large variations, descriptive statistical analyses including response frequency and paired *t*-tests were used to evaluate startle responses. For ballistic tasks, paired *t*-tests were performed to compare reaction time and peak torque between two sound levels for healthy subjects. Two-way repeated measures ANOVA was performed with the factors SIDE (x2, impaired/non-impaired side) and SOUND (x2 levels of sound stimulus) for reaction time, peak torque, and rate of force development analysis in stroke subjects. Paired and independent *t*-tests were performed to compare the percent peak torque change. To compare the torque and EMG responses in sub-maximal tasks across all the subjects, one-way repeated measures ANOVA for controls and two-way repeated measures ANOVA for stroke survivors were performed with the factors SIDE and LEVEL (x5/

TABLE 2 | Stroke subject acoustic startle reflex parameters: (1) onset latency (OL): time interval between the onset of stimulus and onset of EMG burst and (2) burst amplitude (BA): peak amplitude of rectified EMG.

Subj ID		Impaired side				Non-impaired side			
		T1	T2	T3	Response freq (%)	T1	T2	T3	Response freq (%)
1	OL	–	–	–	0.00	–	–	–	0
	BA	–	–	–		–	–	–	
2	OL	170	166	168	100	206	–	–	33
	BA	0.004	0.003	0.002		0.002	–	–	
3	OL	135	108	133	100	135	137	142	100
	BA	0.012	0.026	0.017		0.044	0.043	0.004	
4	OL	–	–	–	0	–	–	123	33
	BA	–	–	–		–	–	0.00	
5	OL	133	174	–	67	–	–	–	0
	BA	0.003	0.001	–		–	–	–	
6	OL	109	111	94	100	102	94	90	100
	BA	0.049	0.013	0.012		0.020	0.010	0.009	
7	OL	154	–	–	33	154	–	–	33
	BA	0.001	–	–		0.002	–	–	
8	OL	84	102	84	100	115	–	90	67
	BA	0.189	0.094	0.094		0.002	–	0.003	
9	OL	94	88	75	100	–	–	–	0
	BA	0.016	0.050	0.027		–	–	–	
10	OL	92	102	94	100	–	–	–	0
	BA	0.022	0.002	0.035		–	–	–	
11	OL	109	96	108	100	–	–	–	0
	BA	0.074	0.018	0.031		–	–	–	
12	OL	–	–	–	0	–	–	–	0
	BA	–	–	–		–	–	–	
13	OL	–	–	–	0	–	–	–	0
	BA	–	–	–		–	–	–	
Avg response freq (%)		69	62	54	62	38	15	31	28

Freq: frequency. T1, T2, and T3 stand for trials 1, 2, and 3, respectively.

x6 voluntary contraction levels). Means and standard deviations are presented in the text, while means and SEs are presented in the figures. $p < 0.05$ was chosen to indicate statistically significant differences.

RESULTS

ASR Rest Task

Averaged response frequency of acoustic startle response was 62% on the impaired side, 28% on the non-impaired side, and 14% for healthy subjects (**Tables 1** and **2**). Averaged EMG onset latency was 126 ± 30.1 ms on the impaired side, 142 ± 34.6 ms on the non-impaired side, and 137 ± 33.2 ms in the healthy subjects. The results were consistent with previous studies showing that stroke survivors were startled more frequently with shorter latency on the impaired side (30).

Ballistic Movement Task

As shown in representative trials (**Figure 2**), high sound led to an early initiation of contraction and a greater peak torque in both healthy and stroke subjects. In healthy subjects, high sound stimulation significantly reduced reaction time ($p = 0.001$) and increased peak torque ($p = 0.013$) compared with low sound. The same pattern of results was observed in stroke subjects. There were main effects of SOUND on reaction time ($F(1, 10) = 24.88$, $p = 0.0005$) and on peak torque ($F(1, 10) = 8.50$, $p = 0.0153$) for both impaired and non-impaired sides (**Figure 3**). The percent increment – the difference between peak torque induced by low sound and high sound and then normalized to the peak torque with low sound was not significantly different between the impaired side (15.8 ± 3.1%) and the non-impaired side (8.0 ± 3.9%). The percent increment in healthy subjects (6.0 ± 2.9%) was not statistically different from those in impaired and non-impaired sides of stroke subjects. There was no significant effect on the rate of force development between impaired and non-impaired sides of stroke subjects ($F(1, 10) = 3.8563$, $p = 0.07795$).

Sub-maximum Voluntary Contraction Task

As most of the functional movements do not require maximal strength, we also evaluated the effect of loud sounds within sub-maximal contraction range. We found that while maintaining sub-maximal isometric elbow flexion, a loud sound could trigger a response in both healthy and stroke subjects (**Figure 4**). The torque response ranged between 0.3 and 1.5% MVC in the

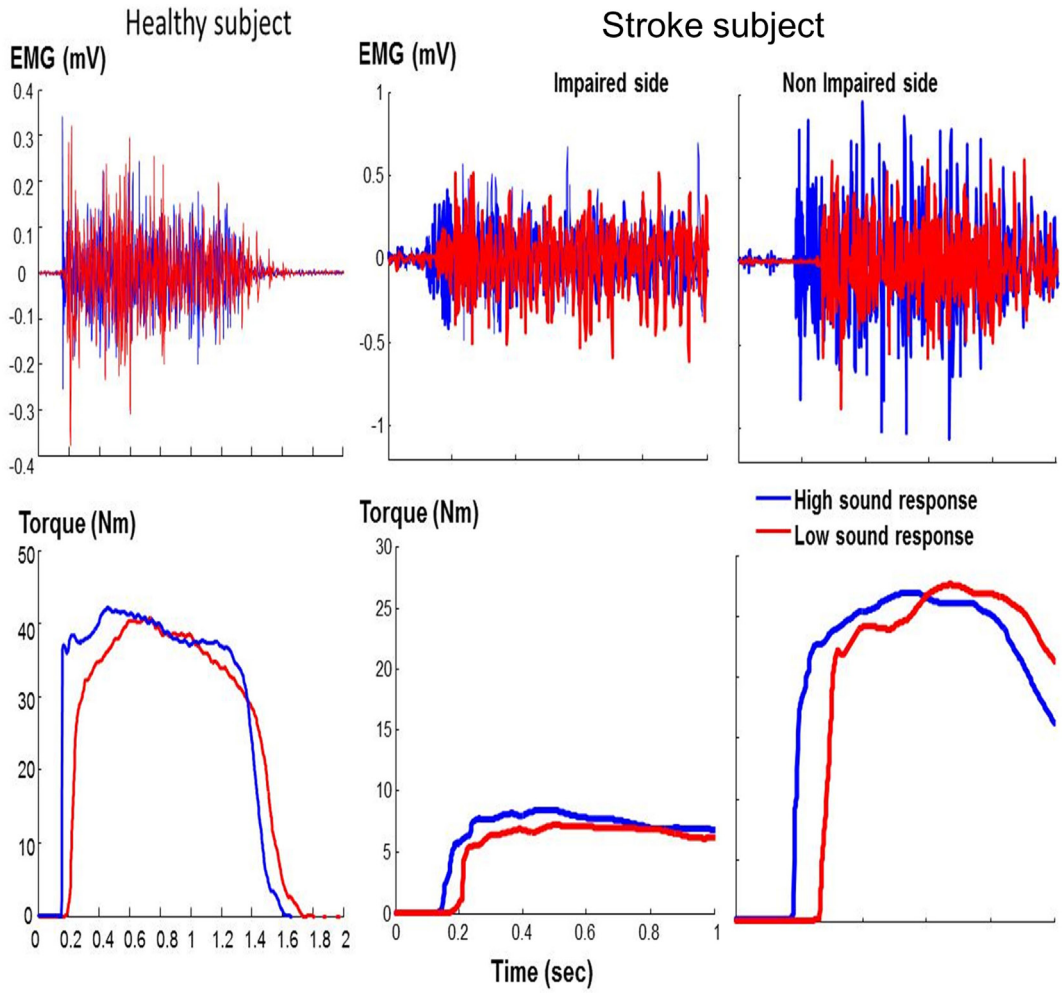

FIGURE 2 | Representative trials: healthy subject and stroke subject during maximum voluntary contraction elbow flexion tasks in response to startling acoustic stimulation. Note that the *x*-axis and *y*-axis values are the same for the stroke subject.

healthy subjects (**Figure 5A**). A similar range of triggered torque response (0.4–1.3% MVC) was observed on the non-impaired side of stroke subjects. In contrast, the triggered torque response was approximately 3–4 times greater on the impaired side of the stroke subjects (1.7–4.7% MVC), but with large variations (**Figure 5B**). There was a significant level dependence in torque response in healthy subjects ($F(5,55) = 4.45$, $p = 0.045$), but non-significant for EMG response ($F(5,55) = 4.45$, $p = 0.52$). Furthermore, a significant level dependence was observed in both torque ($F(4, 40) = 4.4382$, $p < 0.005$) and EMG response ($F(4, 40) = 15.348$, $p < 0.001$) for stroke subjects. However, no difference in normalized torque and EMG responses between impaired and non-impaired sides was found. This non-significant difference in torque response may be a consequence of normalization to MVC. We re-analyzed the SAS-induced torque responses by normalizing to the corresponding target value, i.e., percent torque increase per Nm. The same pattern of results (no statistical difference in torque response between impaired and non-impaired sides) was found. However, there was a trend toward significance ($p = 0.08$).

DISCUSSION

In the present study, we quantified responses to startling acoustic stimulation (SAS) from biceps brachii muscles in both healthy subjects and stroke subjects with chronic spastic hemiplegia at rest, during ballistic MVC elbow flexion and sub-maximal voluntary elbow flexion. Our results confirmed previous findings that (1) greater prevalence of ASR with shorter latency in the impaired biceps as compared to the response in the non-impaired side of stroke subjects and in healthy subjects and (2) delivery of SAS resulted in earlier initiation of elbow flexion and greater peak torque in healthy subjects. The novel findings included (1) SAS-induced reduction in reaction time and increased peak torque were also observed in stroke subjects with spastic hemiplegia during maximal voluntary elbow flexion tasks; (2) SAS-induced force responses in sub-maximal voluntary elbow flexion were similar in both healthy and stroke subjects; and (3) no statistically significant difference was found in SAS-induced responses between impaired and non-impaired sides at maximal and sub-maximal elbow flexion tasks.

Our findings of greater prevalence of ASR with shorter latency in the impaired biceps in stroke subjects with spastic hemiplegia were consistent with previous findings (29, 30). In a previous study (30), ASR occurred in 58.3% of all trials in the spastic biceps, while only 10% in the contralateral side of stroke subjects. In this study, we observed ASR responses in 61.5% of all trials in the impaired side, 28.2% in the non-impaired side of stroke subjects, and 14% in healthy subjects. These similar results support the idea of RS hyperexcitability in the impaired side of stroke survivors with spastic hemiplegia (29–32, 43).

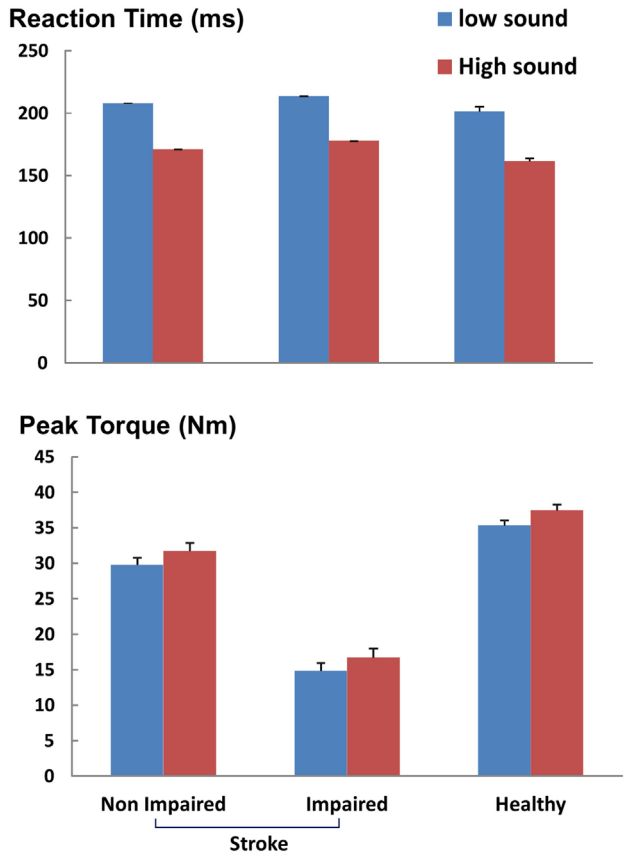

FIGURE 3 | Reaction time and peak torque during ballistic tasks. ms: milliseconds, Nm: newton-meter. Mean and SEs are shown.

After several trials of SAS, ASR responses habituate, while ensuing SAS stimulates RS projections non-reflexively (16, 17). In the subsequent MVC and sub-maximal elbow flexion tasks of our study, SAS stimulated RS projections non-reflexively. In MVC reaction time tasks, repetitive SAS induced earlier initiation, augmented peak force response with no difference in the rate of force development in both impaired and nonimpaired side of stroke subjects. These findings are consistent with those observed in healthy subjects and subjects with Parkinson's disease (18–20, 44). We further observed that SAS-induced force increment during sustained elbow flexion in sub-maximal tasks in both healthy and stroke subjects. These findings extended the effect of SAS to sub-maximal levels. These findings suggest that RS stimulation via SAS could contribute and increase force output during both MVC and sub-maximal elbow flexion tasks. Given RS hyperexcitability in the impaired side of stroke subjects, the finding of statistically non-significant SAS-induced force responses between impaired and non-impaired sides of stroke subjects and healthy subjects is not trivial.

Collectively, our findings suggest that RS hyperexcitability in stroke subjects with spastic hemiplegia is not likely to contribute to development of voluntary strength in these stroke survivors to a significant extent. RS hyperexcitability represents a phenomenon of maladaptive plasticity after stroke (31, 32, 43). For those stroke involving damage to motor cortex and its descending CS projections, cortico-reticular tracts ending in lateral reticular network are usually damaged due to their anatomically proximity

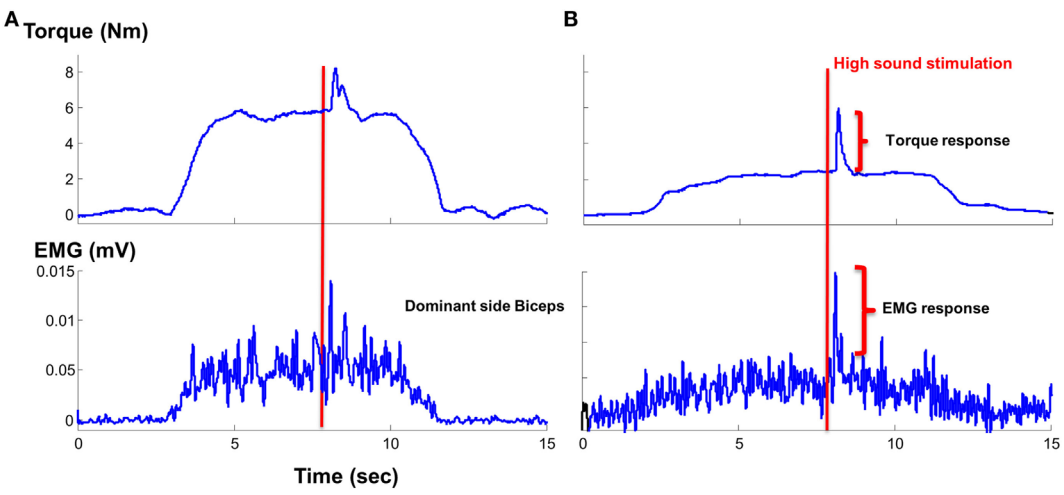

FIGURE 4 | Representative trials: **(A)** healthy subject and **(B)** stroke subject during sustained sub-maximal elbow flexion tasks in response to startling acoustic stimulation.

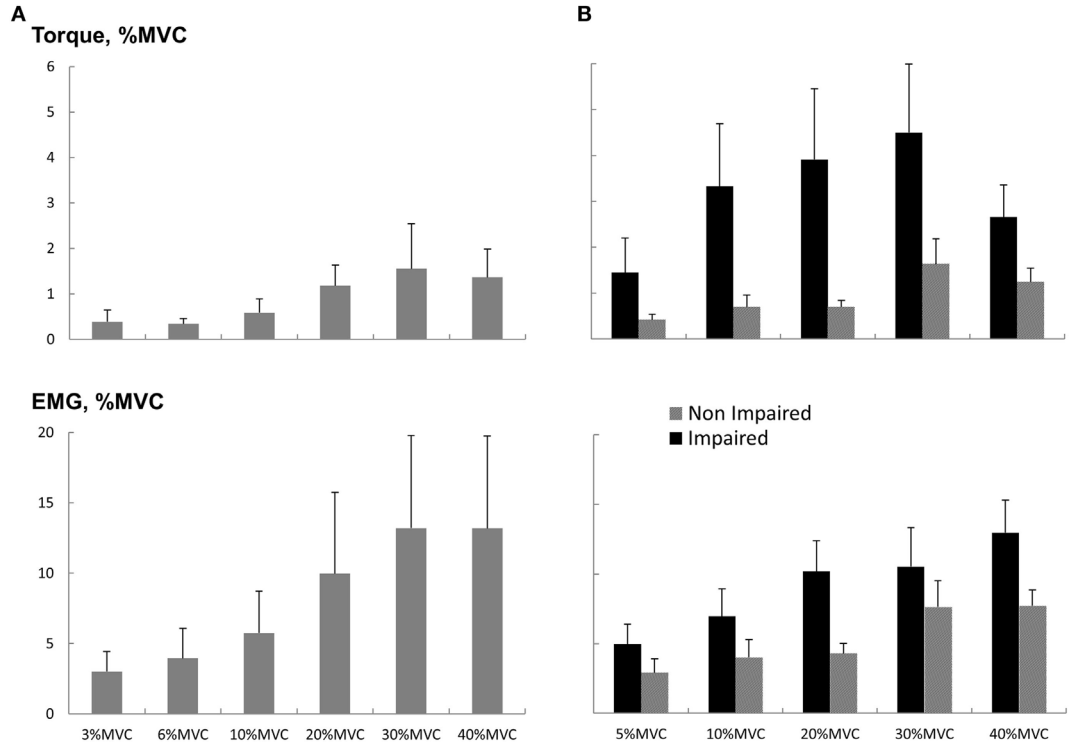

FIGURE 5 | Torque and EMG response to startling acoustic stimulation during sustained sub-maximal elbow flexion. **(A)** Healthy subjects and **(B)** stroke subjects. Magnitudes were normalized to the MVC values. Means and SEs are shown. Note that the *y*-axis values for **(A,B)** are the same.

with CS tracts. Subsequently, function of lateral RS projections diminishes. As a result of lack of unopposed activation, medial RS hyperexcitability and its excitatory descending input to spinal reflex circuits develops. Such maladaptive RS hyperexcitability is viewed as a primary mechanism mediating post-stroke spasticity (31, 32, 43). In the course of complete motor recovery through flaccid, spastic, and recovered stages, RS hyperexcitability is only observed in the spastic stage, but normal in the flaccid or recovered stages (30). Such findings suggest that motor recovery in a late recovered stage does not rely on RS projections. As mentioned in Section "Introduction," recovery in locomotor function is accompanied with increased ipsilesional cortical activation after repetitive motor training in stroke (12). This observation demonstrates the important role of ipsilesional motor cortex in motor recovery. Improvement in motor performance after motor rehabilitation program integrating with auditory cueing or pacing is likely to be mediated by repetitive exercise (33–36). It has been shown that intensive therapy improves motor function, but has no effect on spasticity (45). As mentioned in Section "Introduction" (37), motor training with auditory rhythmic cueing and stimulation improved motor performance in stroke subjects with severe spastic paresis of wrist flexors but not in those subjects with minimal motor impairment or spastic co-contractions. The results of different responses suggest that the outcome of motor training depends on the primary impairment. For example, if weakness is the primary impairment in subjects with severe spastic paresis, motor performance improves after increase in strength from motor training. However, no change is motor performance is expected if the primary impairment is spasticity (spastic co-contraction) or minimum weakness.

There are a number of limitations in this study. The sample sizes of healthy and stroke subjects were small. However, there were a robust pattern of findings as mentioned above (significant effects of SAS but not between two sides of stroke subjects or healthy subjects). Due to heterogeneity of stroke data, we viewed the results rather positively. Due to the experimental settings, we only recruited stroke subjects with the ability to perform voluntary elbow flexion. Stroke survivors with more severe impairment or spasticity (MAS $\geq$ 3) were not included. The results may not represent the features of all stroke survivors. Healthy subjects were not age matched and gender matched to stroke survivors. These factors may account for the large variations in results and may affect the results. Nevertheless, our results were in general consistent with previous findings. Future study will need to take into account these factors.

CONCLUSION

In summary, we quantified and compared responses to startling acoustic stimulation (SAS) from biceps muscles in both healthy subjects and stroke subjects with chronic spastic hemiplegia at rest, during ballistic MVC elbow flexion and sub-maximal voluntary elbow flexion. Our findings of greater ASR responses in the impaired side are consistent with previous findings of RS hyperexcitability in chronic stroke with spastic hemiplegia. Our

results also showed similar results of SAS-induced effects in the impaired side as compared to the non-impaired side of stroke subjects and healthy subjects. Collectively, these results suggest that RS projections via acoustic stimulation are not likely to contribute to development of voluntary strength in these stroke survivors to a significant extent.

ETHICS STATEMENT

This study was approved by the Committee for the Protection of Human Subjects at the University of Texas Health Science Center at Houston and TIRR Memorial Hermann Hospital.

AUTHOR CONTRIBUTIONS

SL, MB, FG, and PZ: experimental design. MB and FG: data collection. SL, MB, FG, and PZ: study concept and design, analysis and interpretation, and critical revision of the manuscript for important intellectual content. MB and FG: acquisition of data. SL: study supervision.

FUNDING

This study was supported in part by NIH grant R01NS060774, 1R21HD090453, and 1R21HD087128.

REFERENCES

1. Kamper DG, Fischer HC, Cruz EG, Rymer WZ. Weakness is the primary contributor to finger impairment in chronic stroke. *Arch Phys Med Rehabil* (2006) 87:1262–9. doi:10.1016/j.apmr.2006.05.013
2. Chang SH, Francisco GE, Zhou P, Rymer WZ, Li S. Spasticity, weakness, force variability, and sustained spontaneous motor unit discharges of resting spastic-paretic biceps brachii muscles in chronic stroke. *Muscle Nerve* (2013) 48:85–92. doi:10.1002/mus.23699
3. Manganotti P, Acler M, Zanette GP, Smania N, Fiaschi A. Motor cortical disinhibition during early and late recovery after stroke. *Neurorehabil Neural Repair* (2008) 22:396–403. doi:10.1177/1545968307313505
4. Hummel FC, Steven B, Hoppe J, Heise K, Thomalla G, Cohen LG, et al. Deficient intracortical inhibition (SICI) during movement preparation after chronic stroke. *Neurology* (2009) 72:1766–72. doi:10.1212/WNL.0b013e3181a609c5
5. Miltner WH, Bauder H, Sommer M, Dettmers C, Taub E. Effects of constraint-induced movement therapy on patients with chronic motor deficits after stroke: a replication. *Stroke* (1999) 30:586–92. doi:10.1161/01.STR.30.3.586
6. Wolf SL, Winstein CJ, Miller JP, Taub E, Uswatte G, Morris D, et al. Effect of constraint-induced movement therapy on upper extremity function 3 to 9 months after stroke: the EXCITE randomized clinical trial. *JAMA* (2006) 296:2095–104. doi:10.1001/jama.296.17.2095
7. Krebs HI, Hogan N, Aisen ML, Volpe BT. Robot-aided neurorehabilitation. *IEEE Trans Rehabil Eng* (1998) 6:75–87. doi:10.1109/86.662623
8. Volpe BT, Krebs HI, Hogan N, Edelsteinn L, Diels CM, Aisen ML. Robot training enhanced motor outcome in patients with stroke maintained over 3 years. *Neurology* (1999) 53:1874–6. doi:10.1212/WNL.53.8.1874
9. Krebs HI, Mernoff S, Fasoli SE, Hughes R, Stein J, Hogan N. A comparison of functional and impairment-based robotic training in severe to moderate chronic stroke: a pilot study. *NeuroRehabilitation* (2008) 23:81–7.
10. Hesse S, Werner C, Bardeleben A, Barbeau H. Body weight-supported treadmill training after stroke. *Curr Atheroscler Rep* (2001) 3:287–94. doi:10.1007/s11883-001-0021-z
11. Hoyer E, Jahnsen R, Stanghelle JK, Strand LI. Body weight supported treadmill training versus traditional training in patients dependent on walking assistance after stroke: a randomized controlled trial. *Disabil Rehabil* (2012) 34:210–9. doi:10.3109/09638288.2011.593681
12. Kim YH, You SH, Kwon YH, Hallett M, Kim JH, Jang SH. Longitudinal fMRI study for locomotor recovery in patients with stroke. *Neurology* (2006) 67:330–3. doi:10.1212/01.wnl.0000225178.85833.0d
13. Davis M, Gendelman DS, Tischler MD, Gendelman PM. A primary acoustic startle circuit: lesion and stimulation studies. *J Neurosci* (1982) 2:791.
14. Lee Y, Lopez DE, Meloni EG, Davis M. A primary acoustic startle pathway: obligatory role of cochlear root neurons and the nucleus reticularis pontis caudalis. *J Neurosci* (1996) 16:3775–89.
15. Koch M. The neurobiology of startle. *Prog Neurobiol* (1999) 59:107–28. doi:10.1016/S0301-0082(98)00098-7
16. Kuhn AA, Sharott A, Trottenberg T, Kupsch A, Brown P. Motor cortex inhibition induced by acoustic stimulation. *Exp Brain Res* (2004) 158:120–4. doi:10.1007/s00221-004-1883-4
17. Chen YT, Li S, Zhou P, Li S. Different effects of startling acoustic stimuli (SAS) on TMS-induced responses at rest and during sustained voluntary contraction. *Front Hum Neurosci* (2016) 10:396. doi:10.3389/fnhum.2016.00396
18. Valls-Sole J, Rothwell JC, Goulart F, Cossu G, Munoz E. Patterned ballistic movements triggered by a startle in healthy humans. *J Physiol* (1999) 516 (Pt 3):931–8. doi:10.1111/j.1469-7793.1999.0931u.x
19. Anzak A, Tan H, Pogosyan A, Brown P. Doing better than your best: loud auditory stimulation yields improvements in maximal voluntary force. *Exp Brain Res* (2011) 208:237–43. doi:10.1007/s00221-010-2474-1
20. Fernandez-Del-Olmo M, Rio-Rodriguez D, Iglesias-Soler E, Acero RM. Startle auditory stimuli enhance the performance of fast dynamic contractions. *PLoS One* (2014) 9:e87805. doi:10.1371/journal.pone.0087805
21. Honeycutt CF, Kharouta M, Perreault EJ. Evidence for reticulospinal contributions to coordinated finger movements in humans. *J Neurophysiol* (2013) 110:1476–83. doi:10.1152/jn.00866.2012
22. Anzak A, Tan H, Pogosyan A, Djamshidian A, Ling H, Lees A, et al. Improvements in rate of development and magnitude of force with intense auditory stimuli in patients with Parkinson's disease. *Eur J Neurosci* (2011) 34:124–32. doi:10.1111/j.1460-9568.2011.07735.x
23. Nathan PW, Smith MC. Long descending tracts in man. I. Review of present knowledge. *Brain* (1955) 78:248–303. doi:10.1093/brain/78.2.248
24. Lemon RN. Descending pathways in motor control. *Annu Rev Neurosci* (2008) 31:195–218. doi:10.1146/annurev.neuro.31.060407.125547
25. Sakai ST, Davidson AG, Buford JA. Reticulospinal neurons in the pontomedullary reticular formation of the monkey (*Macaca fascicularis*). *Neuroscience* (2009) 163:1158–70. doi:10.1016/j.neuroscience.2009.07.036
26. Riddle CN, Baker SN. Convergence of pyramidal and medial brain stem descending pathways onto macaque cervical spinal interneurons. *J Neurophysiol* (2010) 103:2821–32. doi:10.1152/jn.00491.2009
27. Ortiz-Rosario A, Berrios-Torres I, Adeli H, Buford JA. Combined corticospinal and reticulospinal effects on upper limb muscles. *Neurosci Lett* (2014) 561:30–4. doi:10.1016/j.neulet.2013.12.043
28. Herbert WJ, Powell K, Buford JA. Evidence for a role of the reticulospinal system in recovery of skilled reaching after cortical stroke: initial results from a model of ischemic cortical injury. *Exp Brain Res* (2015) 233:3231–51. doi:10.1007/s00221-015-4390-x
29. Jankelowitz SK, Colebatch JG. The acoustic startle reflex in ischemic stroke. *Neurology* (2004) 62:114–6. doi:10.1212/01.WNL.0000101711.48946.35
30. Li S, Chang SH, Francisco GE, Verduzco-Gutierrez M. Acoustic startle reflex in patients with chronic stroke at different stages of motor recvoery: a pilot study. *Top Stroke Rehabil* (2014) 21:358–70. doi:10.1310/tsr2104-358
31. Li S, Francisco G. New insights into the pathophysiology of post-stroke spasticity. *Front Hum Neurosci* (2015) 9:192. doi:10.3389/fnhum.2015.00192
32. Li S. Spasticity, motor recovery, and neural plasticity after stroke. *Front Neurol* (2017) 8:120. doi:10.3389/fneur.2017.00120
33. Whitall J, Waller SM, Silver KHC, Macko RF. Repetitive bilateral arm training with rhythmic auditory cueing improves motor function in chronic hemiparetic stroke. *Stroke* (2000) 31:2390–5. doi:10.1161/01.STR.31.10.2390
34. Schneider S, Schönle PW, Altenmüller E, Münte TF. Using musical instruments to improve motor skill recovery following a stroke. *J Neurol* (2007) 254:1339–46. doi:10.1007/s00415-006-0523-2

35. Jun EM, Roh YH, Kim MJ. The effect of music-movement therapy on physical and psychological states of stroke patients. *J Clin Nurs* (2013) 22:22–31. doi:10.1111/j.1365-2702.2012.04243.x
36. Pollock A, Farmer SE, Brady MC, Langhorne P, Mead GE, Mehrholz J, et al. Interventions for improving upper limb function after stroke. *Cochrane Database Syst Rev* (2014) 11:CD010820. doi:10.1002/14651858.CD010820.pub2
37. Aluru V, Lu Y, Leung A, Verghese J, Raghavan P. Effect of auditory constraints on motor learning depends on stage of recovery post stroke. *Front Neurol* (2014) 5:106. doi:10.3389/fneur.2014.00106
38. Hermens HJ, Freriks B, Merletti R, Stegeman D, Blok J, Rau G, et al. *SENIAM 8: European Recommendations for Surface Electromyography*. The Netherlands: Roessingh Research and Development Enschede (2000).
39. Fisher RJ, Sharott A, Kuhn AA, Brown P. Effects of combined cortical and acoustic stimuli on muscle activity. *Exp Brain Res* (2004) 157:1–9. doi:10.1007/s00221-003-1809-6
40. Bhadane M, Liu J, Rymer WZ, Zhou P, Li S. Re-evaluation of EMG-torque relation in chronic stroke using linear electrode array EMG recordings. *Sci Rep* (2016) 6:28957. doi:10.1038/srep28957
41. Li S, Stevens J, Rymer W. Interactions between imagined movement and the initiation of voluntary movement: a TMS study. *Clin Neurophysiol* (2009) 120:1154–60. doi:10.1016/j.clinph.2008.12.045
42. Li S, Rymer WZ. Voluntary breathing influences corticospinal excitability of nonrespiratory finger muscles. *J Neurophysiol* (2011) 105:512–21. doi:10.1152/jn.00946.2010
43. Trompetto C, Marinelli L, Mori L, Pelosin E, Curra A, Molfetta L, et al. Pathophysiology of spasticity: implications for neurorehabilitation. *Biomed Res Int* (2014) 2014:354906. doi:10.1155/2014/354906
44. Honeycutt CF, Perreault EJ. Planning of ballistic movement following stroke: insights from the startle reflex. *PLoS One* (2012) 7:e43097. doi:10.1371/journal.pone.0043097
45. Zondervan DK, Augsburger R, Bodenhoefer B, Friedman N, Reinkensmeyer DJ, Cramer SC. Machine-based, self-guided home therapy for individuals with severe arm impairment after stroke: a randomized controlled trial. *Neurorehabil Neural Repair* (2015) 29:395–406. doi:10.1177/1545968314550368

Conflict of Interest Statement: The authors declare that the research was conducted in the absence of any commercial or financial relationships that could be construed as a potential conflict of interest.

The reviewer MM and handling Editor declared their shared affiliation.

frontiers in Neurology

CLINICAL TRIAL
published: 04 September 2017
doi: 10.3389/fneur.2017.00447

Early Stroke Rehabilitation of the Upper Limb Assisted with an Electromyography-Driven Neuromuscular Electrical Stimulation-Robotic Arm

Qiuyang Qian[1], Xiaoling Hu[1], Qian Lai[1], Stephanie C. Ng[2], Yongping Zheng[1] and Waisang Poon[2]*

[1] *Interdisciplinary Division of Biomedical Engineering, The Hong Kong Polytechnic University, Hong Kong, Hong Kong,* [2] *Department of Surgery, Prince of Wales Hospital, The Chinese University of Hong Kong, Hong Kong, Hong Kong*

Background: Effective poststroke motor rehabilitation depends on repeated limb practice with voluntary efforts. An electromyography (EMG)-driven neuromuscular electrical stimulation (NMES)-robot arm was designed for the multi-joint physical training on the elbow, the wrist, and the fingers.

Objectives: To investigate the training effects of the device-assisted approach on subacute stroke patients and to compare the effects with those achieved by the traditional physical treatments.

Method: This study was a pilot randomized controlled trial with a 3-month follow-up. Subacute stroke participants were randomly assigned into two groups, and then received 20-session upper limb training with the EMG-driven NMES-robotic arm (NMES-robot group, $n = 14$) or the time-matched traditional therapy (the control, $n = 10$). For the evaluation of the training effects, clinical assessments including Fugl-Meyer Assessment (FMA), Modified Ashworth Score (MAS), Action Research Arm Test (ARAT), and Function Independence Measurement (FIM) were conducted before, after the rehabilitation training, and 3 months later. Session-by-session EMG parameters in the NMES-robot group, including normalized co-contraction Indexes (CI) and EMG activation level of target muscles, were used to monitor the progress in muscular coordination patterns.

Results: Significant improvements were obtained in FMA (full score and shoulder/elbow), ARAT, and FIM [$P < 0.001$, effect sizes (EFs) > 0.279] for both groups. Significant improvement in FMA wrist/hand was only observed in the NMES-robot group ($P < 0.001$, EFs $= 0.435$) after the treatments. Significant reduction in MAS wrist was observed in the NMES-robot group after the training ($P < 0.05$, EFs $= 0.145$) and the effects were maintained for 3 months. MAS scores in the control group were elevated following training ($P < 0.05$, EFs > 0.24), and remained at an elevated level when assessed 3 months later. The EMG parameters indicated a release of muscle co-contraction in the muscle pairs of biceps brachii and flexor carpi radialis and biceps brachii and triceps brachii, as well as a reduction of muscle activation level in the wrist flexor in the NMES-robot group.

OPEN ACCESS

Edited by:
Cliff Klein,
Guangdong Provincial Work Injury Rehabilitation Center, China

Reviewed by:
Jill Whitall,
University of Maryland, Baltimore, United States
Richard G. Carson,
Trinity College, Ireland

****Correspondence:***
Xiaoling Hu
xiaoling.hu@polyu.edu.hk

Specialty section:
This article was submitted to Stroke, a section of the journal Frontiers in Neurology

Received: *20 March 2017*
Accepted: *14 August 2017*
Published: *04 September 2017*

Citation:
Qian Q, Hu X, Lai Q, Ng SC, Zheng Y and Poon W (2017) Early Stroke Rehabilitation of the Upper Limb Assisted with an Electromyography-Driven Neuromuscular Electrical Stimulation-Robotic Arm. Front. Neurol. 8:447. doi: 10.3389/fneur.2017.00447

Conclusion: The NMES-robot-assisted training was effective for early stroke upper limb rehabilitation and promoted independence in the daily living comparable to the traditional physical therapy. It could achieve higher motor outcomes at the distal joints and more effective release in muscle tones than the traditional therapy.

Clinical Trial Registration: ClinicalTrials.gov, identifier NCT02117089; date of registration: April 10, 2014.

Keywords: stroke, upper limb, robot, neuromuscular electrical stimulation, electromyography

INTRODUCTION

Stroke is one of the leading causes of permanent disability in adults (1). Approximately 80% stroke survivors regain their walking independence (2). However, less than 25% survivors could achieve some limited recovery on the upper limb function, and only around 5% of them could obtain complete functional recovery 6 months later after the onset (2, 3). Dysfunctions in the upper limb are a combination of muscle weakness, spasticity, and discoordination among different muscle groups (4, 5). Significant spontaneous motor recovery usually occurs within the first several weeks to 6 months after stroke, i.e., in the subacute period (6). Physical rehabilitation in this early period can optimize the spontaneous neural plasticity and motor responsiveness, and result in maximized motor outcomes (7, 8). In comparison with the rehabilitation treatment administrated in the chronic period (i.e., 6 months later after the onset), motor functions resorted in the subacute period are more likely to be generalized into functional activities in the daily life (9, 10). One of the major reasons is that the persons with subacute stroke have not been used to adopt the unaffected limb only for daily tasks as commonly observed in the chronic. The traditional rehabilitation treatments in early stage after stroke are usually conducted manually by human therapists, which are time consuming and labor demanding (5). It is challenging to the current medical and health-care system to provide adequate or intensive rehabilitation treatments to persons with subacute stroke, due to the lack of professional manpower in the physical therapy industry even in developed countries (11) and the expanding of stroke populations worldwide (3).

Effective motor restoration after stroke depends on repeated and intensive practice of the paralyzed limbs with voluntary efforts (7, 12, 13). Repetitive practice with high-intensity has been proven to speed up the process of motor restorations (6, 13). The involvement of voluntary effort from the residual neuromuscular pathways has been convinced to carry out better performance with higher efficiency when compared with the continuous passive motion trainings (14, 15). Coordinated upper limb practices among different joints, especially the involvement of the distal joints (e.g., the wrist and fingers) have also been found more effective to translate the motor improvements into meaningful limb functions than single joint practice (16). However, due to the overall muscle weakness in early stage after stroke and a delayed motor return at the distal joints in comparison with the proximal, it is always a difficulty for human therapists to instruct and support the coordinated upper limb motions with the proximal (i.e., the shoulder and the elbow) and distal joints (i.e., the wrist and the fingers) together in the clinical practice (17). New techniques are needed to assist in the manually conducted upper limb coordinating rehabilitation.

Rehabilitation robots can assist human therapists to conduct the intensive and repeated physical training with different numbers and sizes of electrical motors. Various robots have been designed for poststroke upper limb rehabilitation (18–21). Among them, the robots with the involvement of voluntary efforts from the residual neuromuscular pathways demonstrated better rehabilitation effects than those with passive limb motions, i.e., the limb motions are entirely dominated by the machine (18). It has been found that physical trainings with passive motions only contributed to the temporary release of muscle spasticity. However, voluntary practice could improve the motor functions of the limb with longer sustainability (18, 22). Neuromuscular electrical stimulation (NMES) is a technique that can generate limb movements by applying electrical current on the paretic muscles (23). Poststroke rehabilitation assisted with NMES has been found to effectively prevent muscle atrophy and improve muscle strength (23, 24), and the stimulation also evokes sensory feedback to the brain during muscle contraction to facilitate motor relearning (25). NMES can improve limb functions by limiting "learned disuse" that stroke survivors are gradually accustomed to managing their daily activities without using certain muscles, which has been considered as a significant barrier to maximize the recovery (26). However, NMES alone is hard to achieve desired accuracy in kinematics, such as speed and trajectories, as in the robot-assisted training (27).

In our previous works, we designed a series of voluntary intention-driven rehabilitation robotics for physical training at the elbow, the wrist, and fingers (22, 28–31). Residual electromyography (EMG) from the paretic muscles was used to control the robots to provide assistive torques to the limb for desired motions (31, 32). Later, we integrated NMES into the EMG-driven robot as an intact system for wrist rehabilitation. It has been found that the combined assistance with both robot and NMES could reduce the excessive muscular activities at the elbow and improve the muscle activation levels related to the wrist in chronic stroke, which was absent in the pure robot-assisted training (31). Pure robot-assisted upper limb training also showed no superiority on motor improvements on chronic stroke in comparison with the traditional treatments in a reported randomized controlled trial (33). More recently, combined treatment with robot and NMES for the wrist by other research group also demonstrated more promising rehabilitation effectiveness in the upper limb motor recovery than pure robot training (34). However, most of the

proposed devices are for single joint treatment, and the related trials were conducted on chronic stroke. We hypothesized that poststroke multi-joint coordinated training with both NMES and robot in the subacute stroke period could improve the muscular coordination in the whole upper limb and translate the motor improvements into daily functions. In this work, we developed an EMG-driven NMES-robotic arm for multi-joint coordinated training on the elbow, wrist, and fingers. The feasibility of the EMG-driven NMES-robotic arm assisted upper limb training on subacute stroke, and the training effectiveness were investigated through a pilot randomized controlled trial in comparison with the traditional upper limb physical rehabilitation.

METHODOLOGY

The EMG-Driven NMES-Robot System

The integrated EMG-driven NMES-robot training system (**Figure 1**) can assist a stroke survivor to perform the sequencing motions, i.e., (1) elbow extension, (2) synchronized wrist extension and hand open, (3) wrist flexion, and (4) elbow flexion, which simulates the coordination of the joints in arm reaching, hand grasping, and withdrawing motions in daily activities. The starting position of the motion cycle was set as elbow joint extended at 180° and the wrist extended at 45°, respectively. The range of motion (ROM) for the elbow joint in the system was set from 30° flexed to 180° extended; and the ROM for the wrist joint was from 60° flexed to 45° extended. The ROMs for the elbow and wrist joints had been tested on their feasibilities when applied to stroke participants in our previous works (27, 28, 31). The paretic arm of a participant could be fixed in a solid exoskeleton orthosis through a bracing system. The movement of the mechanical exoskeleton for the elbow and the wrist parts are controlled by two independent servo motors (MX 106, ROBOTIS, with a maximal stall torque of 8.4 Nm) (27) (**Figure 1A**). When using the system in this work, the paretic upper limb of a participant mounted with the system was lifted up to a horizontal level with a hanging system (**Figure 1B**). It was understood that stroke survivors in early stage (e.g., subacute period) usually experienced more muscular weakness rather than spasticity as in the chronic period, and most stroke survivors at this period could not even lift up their paretic limbs with voluntary effort, which was mainly due to the muscle atrophy at the shoulder. The hanging system was necessary for a subacute stroke participant to perform the upper limb tasks with the system in the study.

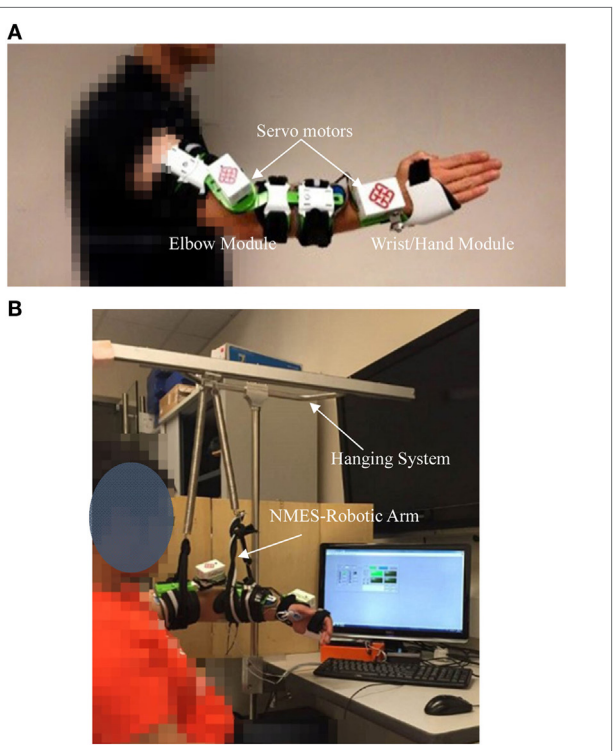

FIGURE 1 | The experimental and training setup of the electromyography-driven neuromuscular electrical stimulation (NMES)-robot system: **(A)** the mechanical exoskeleton module of the system consisted of the wrist part and the elbow part; **(B)** the training setup in a session assisted with the NMES-robot training system, the visual feedback interface, and the hanging system.

Four-channel NMES was applied on the muscles of biceps brachii (BIC) during elbow flexion, triceps brachii (TRI) during elbow extension, flexor carpi radialis (FCR) for wrist flexion, and the last channel on both the extensor carpi ulnaris (ECU) and extensor digitorum (ED) for wrist extension and the associated hand open (i.e., finger extension). The muscles of the ECU and ED are close to each other anatomically with narrow muscle bellies on the dorsal side of the forearm, and can be recruited together by just one-channel surface NMES (35). They were treated as a muscle union (ECU-ED) for both NMES and EMG detection in this work. The function of the motors and NMES were under the control of the EMG detected from the BIC, TRI, FCR, and ECU-ED muscles. The configuration for the EMG and NMES electrodes on a target muscle is shown in **Figure 2**, which also has been adopted in our previous NMES-robot system for wrist rehabilitation (32). For the ECU-ED muscle union, the EMG and NMES electrodes were located on the common area of the muscle bellies of the two. There was no NMES or robotic support to the hand close motion, since most of the stroke survivors experienced difficulties in hand open rather than hand close (5, 36), and NMES on finger flexors also may accelerate the development of the muscle tones in the fingers (5).

Assistance from both the robot and NMES modules was under the control of EMG signals from the target muscles and helped the participant to conduct the phasic and sequential limb tasks, i.e., (1) elbow extension, (2) wrist extension and hand open, (3) wrist flexion, and (4) elbow flexion. EMG-triggered control was adopted in this work, i.e., in each motion phase, once the EMG activation level of a driving muscle exceeded a preset threshold [three times of the SD above the EMG baseline in the rest, by following the standard detection of the onset of voluntary EMG in a contracting muscle (37)], the related joint motor would move with a constant velocity of 10°/s (either flexion or extension within the ROMs), and it was a joint angular velocity acceptable for stroke survivors in our previous works (31, 32). Meanwhile, constant NMES would also be turned on by the voluntary EMG level which surpassed the triggering threshold and be delivered

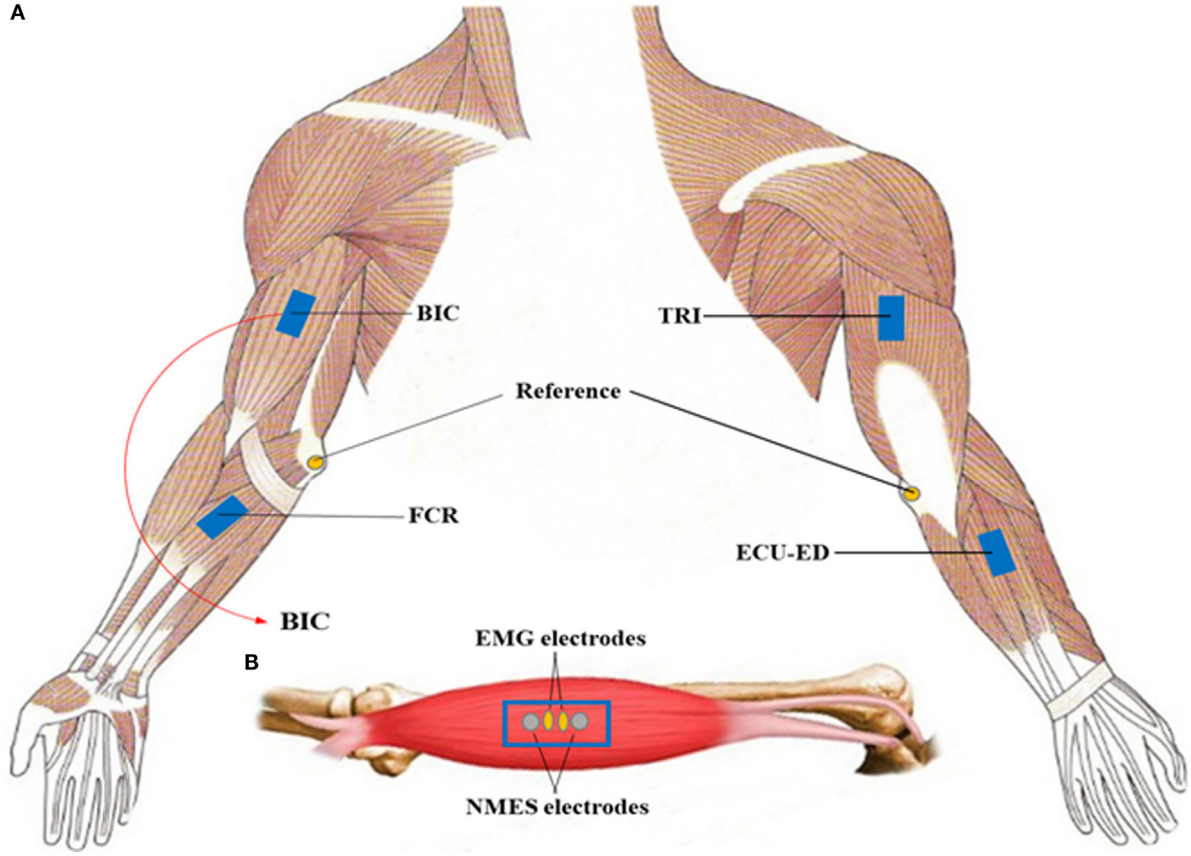

FIGURE 2 | **(A)** The electrode configuration on the target muscles, i.e., the biceps brachii (BIC), the triceps brachii (TRI), flexor carpi radialis (FCR), and the muscle union of the extensor carpi ulnaris and extensor digitorum (ECU-ED). The reference electrode was attached on the olecranon; **(B)** the illustration of the configuration of the electromyography electrodes and neuromuscular electrical stimulation (NMES) electrodes on a target muscle.

(square-wave pulses with a constant amplitude of 80 V, stimulation frequency at 40 Hz, individual pulse width at 100 μs) to the target muscle (i.e., the driving muscle in a motion phase) in the related motion phase. Once the joint motors and the NMES were initiated by the EMG signals from the driving muscle, there was no voluntary effort needed from the participant and the training system would help the limb complete the rest of the motion in the phase. All EMG signals were amplified with a gain of 1,000 (amplifier: INA 333, Texas Instruments Inc.), band-pass filtered from 10 to 500 Hz, and then sampled with 1,000 Hz for digitization. The EMG signals during the triggering period for the initiation of the movements were full-wave rectified and moving-averaged with 100 ms window to obtain the EMG activation levels.

Subject Recruitment and Training Protocol

The study was approved by the Human Subjects Ethics Subcommittee of Hong Kong Polytechnic University and Joint Chinese University of Hong Kong-New Territories East Cluster Clinical Research Ethics Committee. We screened the stroke inpatients in the teaching hospital, and recruited participants with upper limb motor deficits satisfying the following inclusion criteria: (1) had a singular and unilateral brain lesion due to a stroke acquired within 4 months; (2) had standard medical care and sustained in a stable condition; (3) had enough cognition to understand the content or purpose of the study and follow simple instructions as assessed by the Mini-Mental State Examination (MMSE > 21) (38); (4) motor impairments affected in the upper limb ranged from severe to moderate as assessed by Fugl-Meyer Assessment (15 < FMA < 45, with a maximal score of 66 for the upper limb) (39); (5) the spasticity affected at the elbow, the wrist and the fingers below 3 as measured by the Modified Ashworth Scale [MAS, ranged from 0 (no increase in the muscle tone) to 4 (affected part rigid)] (40); (6) the passive ROM of the participants for the wrist was from 45° extension to 60° flexion and the ROM for the elbow was from 30° flexion to 180° extension; (7) aged from 18 to 78 years (41, 42); (8) had detectable voluntary EMG from the target muscles (i.e., three times of the SD above the baseline); (9) had a stable medical condition for physical training with multiple sessions. Subjects were excluded if they did not meet the above inclusion criteria, or had the following conditions: (1) currently pregnant, (2) severe aphasia, and (3) had an implanted pacemaker.

The study was a pilot randomized controlled trial with a 3-month follow-up (3MFU). Inpatients after stroke were screened by a collaborative clinician according to the inclusion criteria 7–10 days before the start of the training, in a project

period of 24 months. The potential participants were told about the training program of the study, and the recruited participants gave the written consent on the participation in the training program which could be either the device-assisted training or the traditional treatment before the randomization. Then, the recruited participants were randomly assigned into two groups, according to a computer-based random number generator, i.e., the computer program generated either "1" (the experimental group) or "2" (the control group) with an equal probability of 0.5 (Matlab 2015, Mathworks, Inc.). The recruitment of the subjects was in a relatively sequential way due to the availability of the training device (only one set for the respective left and right sides) and the hospital stay of the participants in the management. Once both sides of the robotic arms were occupied for the training, the recruitment was suspended. In the subject screening period, the clinician also needed to take into account of the availability of the device for left or right hemiplegia in the coming possible NMES-robot-assisted training. **Figure 3** shows the Consolidated Standards of Reporting Trials flowchart of the training program.

In the experimental group, i.e., the NMES-robot group, each participant received 20-session upper limb training assisted by the NMES-robot system with an intensity of 5 sessions/week, 1 session/day (from Monday to Friday), finished in one month. In each session, a participant was instructed to conduct the device-assisted and repeated limb motions, i.e., (1) elbow extension, (2) wrist extension and hand open, (3) wrist flexion, and (4) elbow flexion for totally 40 min. There was a break of 10 min after a practice of 20 min to avoid the muscle fatigue. In this work, the training loads between the NMES-robot group and the control group were matched by the time and the frequency of the sessions for the upper limb training. The upper limb rehabilitation time of a session for the NMES-robot group was deducted from the routine upper limb training (1 h from Monday to Friday in a common treatment room in the management of the collaborative hospital) by human therapists. The routine upper limb treatment included muscle stretching, passive/assistive ROM and occupational treatments such as feeding/eating, grooming practices. In the practical operation in this work, the participants in the NMES-robot group were transferred to another treatment room to receive the 40-min device-assisted training, and then returned to receive the rest of the routine physical treatments on the upper limb. For most of the participants in the NMES-robot group, they only practiced the muscle stretching and passive ROM after returned from the NMES-robot training for around 10–15 min, due to the fatigue experienced in the upper limb. The participants in the control group only received the routine rehabilitation therapies on the upper limb (i.e., 1 h in the common treatment room).

Training Effects Evaluation

Clinical Assessments

In this study, functional evaluation for each participant on their paretic upper limbs were scored by the following assessments: the FMA (the full score ranging from 0 to 66, the shoulder/elbow part ranging from 0 to 42, and the wrist/hand part ranging from 0 to 24),

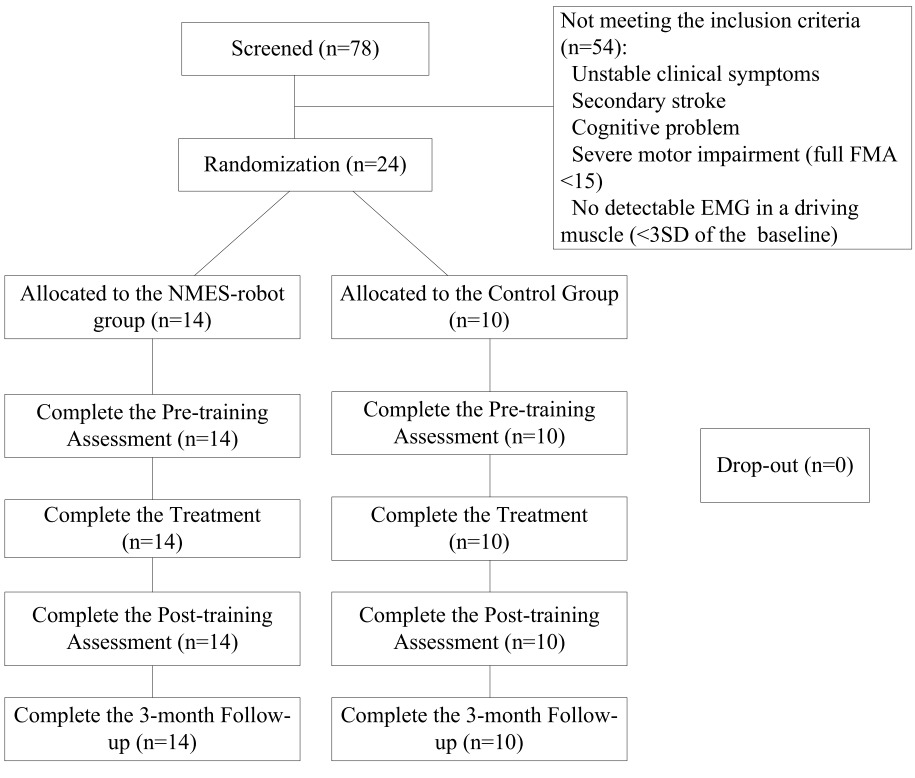

FIGURE 3 | The Consolidated Standards of Reporting Trials flowchart of the experimental design.

applied for performance-based measurement of motosensory functions on the poststroke hemiplegia (39); the Action Research Arm Test (ARAT), mainly used to measure one's hand functions to handle objects in different size, weight and shape (43); the Function Independence Measurement (FIM) for the evaluation of patients' activities of daily living (ADL) (44); and the MAS, applied for the evaluation of poststroke spasticity at the elbow, the wrist and the fingers (40). All the clinical assessments were conducted before the training started and immediately after the 20 training sessions, as well as 3 months later after the training by a training-blinded assessor. The stroke participants in the study and the assessor were told not to communicate on the training details and the assessor was kept blinded to the training protocol.

Session-By-Session Evaluation by EMG

In each training session for the NMES-robot group, a participant was first instructed to perform a bare-arm evaluation task before the device-assisted rehabilitation training, in order to trace the evolution of the muscle coordination during the recovery as we did in the robot-assisted upper limb training on chronic stroke previously (31). The evaluation task had two parts, i.e., horizontal task and vertical task. In the horizontal task, a participant was required to use the affected limb to grasp a sponge and transport it to the lateral side with a distance of 50 cm on a table; then, release the sponge. After that, the participant needed to pick up the sponge again and then transport it back to the original place. In the vertical task, the participant was required to complete the pick-up and release cycle vertically between two layers of a shelf on the table (31, 32). The horizontal and vertical tasks were repeated twice for each with a 5 min break between two consecutive practices to avoid the muscle fatigue. The detailed configuration and description of the two bare-arm evaluation tasks could be found in our previous work (31, 32). The main objective of the bare-arm evaluation in each session is to simulate upper limb motions in daily activities (i.e., hand grasping, arm reaching, and withdrawing) and to reveal the recovery progress across the training sessions of the upper limb motor function without device assistance. In each evaluation task, EMG recording was started when a participant received the command from the trainer, and ended when the testing arm released the sponge at target position. It was understood that subacute patients might not be able to complete the tasks by using their affected limbs independently due to the early muscle weakness in the first several sessions. Therefore, we set a 10-s maximum time limit: if the paretic arm could not grasp the sponge or lift up in 10 s then the participants would be allowed to use the intact hand to help the affected arm grasp or lift up. Only the EMG signals within the 10 s were included for analysis. All participants in the NMES-robot group could grasp the sponge and conduct the horizontal arm transportation with the affected limb in the evaluation from the first session. The major difficulties encountered by the participants were hand open to release the sponge and the lift of the whole arm in the vertical tasks. Therefore, successful hand release of the sponge was not required in this study, although the participants were required to make the voluntary efforts to extend the fingers. The 10-s maximum time limit was mainly applied to the vertical tasks in the early sessions. During the 10-s period, the participants were required to exert voluntary effort to achieve the task by using all possible muscular coordinating strategies in the affected upper limb, with the purpose to record the muscular patterns for an intended target motion. According to our empirical observation, longer attempt periods would cause frustration due to failure and fatigue, i.e., less muscular effects exerted. At the 20th session of the training, all participants recruited in the NMES-robot group could complete the evaluation tasks by the paretic arm without the support from the unaffected limb.

EMG Parameters

Two EMG parameters were used for quantitative cross-session monitoring of the muscle activation and coordination pattern changes during the evaluation in this work: (1) normalized EMG activation level of each muscle; and (2) normalized co-contraction index (CI) between the muscle pairs. The processing methods of the normalized EMG activation level was calculated as follows, i.e.,

$$\overline{\mathrm{EMG}} = \frac{1}{T}\int_0^T \mathrm{EMG}_i(t)\,dt, \tag{1}$$

where $\overline{\mathrm{EMG}}$ was the EMG activation level of muscle i, $\mathrm{EMG}_i(t)$ was the EMG linear envelope with respect to the maximal value recorded during the bare-arm evaluation tasks and maximum voluntary contractions in each session, and T was the length of the signal as we did previously (22, 28). In this work, the EMG activation levels in a session for an individual participant were further normalized with respect to the maximal EMG activation level of the participant recorded across the training sessions. This operation would show the tendency of the EMG activation level of a participant across the training session with the normalized values vary from 0 to 1, in order to minimize the variations among different participants as we encountered previously (22, 28).

The CI between a pair of muscles could be expressed as:

$$\mathrm{CI} = \frac{1}{T}\int_0^T A_{ij}(t)\,dt, \tag{2}$$

where $A_{ij}(t)$ represented the overlapping activity (i.e., $Minimum[\mathrm{EMG}_i(t), \mathrm{EMG}_j(t)]$) of the EMG linear envelopes for muscle i and j, and T was the length of the signal, $\mathrm{EMG}_{i,j}(t)$ are the EMG envelopes as in Eq. 1 (22, 28). An increase of the CI values would represent an enlarged co-contraction phase of a muscle pair; and a decrease would suggest a separation in the co-contraction phase of the two muscles within the same joint or across multi joints. Similar normalization on the CI values in a session with respect to the maximal CI value across the sessions for individual participants was conducted as we did for the EMG activation levels. Monitoring the varying patterns of the EMG parameters across the 20 training sessions would provide a better understanding on the recovery progress of the affected upper limb functions.

Statistical Analysis

The baselines of the two groups were first compared by independent t-test with an insignificant statistical difference ($P > 0.05$) on all clinical assessments (i.e., pre-assessments on FMA, MAS,

ARAT, and FIM scores, **Table 2**) to ensure the likelihood of the baseline equivalence (45). Two-way analysis of covariance (ANCOVA) was then used to evaluate the differences with respect to the independent factors of the group (i.e., the NMES-robot and the control groups) and the time point on the clinical assessments (i.e., the pre-, the post-, and the 3MFU assessments) by taking the pre-assessment as a covariate, with the purpose to further minimize the possible baseline difference between the groups (45). Then, one-way analysis of variance (ANOVA) was conducted to investigate the intragroup difference of either NMES-robot group or control group at different time points with the Bonferroni *post hoc* tests. The *post hoc* between-group comparisons on the clinical scores at the respective post- and 3MFU assessments were evaluated by one-way ANCOVA with the pre-assessment as a covariate. The EMG parameters (i.e., EMG levels and CI values) across the 20 sessions were also analyzed by one-way ANOVA for the investigation of recovery process across the whole training sessions in the NMES-robot group. The primary outcomes of the study were the FMA and MAS clinical scores; and the other clinical scores and EMG parameters were the secondary outcomes. It was because FMA could reflect task-specified voluntary motor functions in the whole upper limb and MAS could reflect the variation of muscle spasticity at different joints in the upper limb compared to other clinical scores. The levels of statistical significance were indicated at 0.05, 0.01, and 0.001 in this study.

TABLE 1 | Demographic data of the participants after the randomization.

Group	No. of participants	Min/Max days after stroke	Stroke types, hemorrhage/ischemic	Lesion site, left/right	Gender, female/male	Age (years)
Neuromuscular Electrical Stimulation (NMES)-robot	14	25/148	9/5	11/3	5/9	54.6 ± 11.3
Control	10	14/142	6/4	9/1	4/6	64.6 ± 3.43

TABLE 2 | The mean and 95% confidence intervals for each measurement of the clinical assessments, and the probabilities with the estimated effect sizes of the statistical analyses.

	Pre	Post	3MFU	1-way ANOVA	2-way analysis of covariance		
					P (Partial η^2)		
Evaluation	**Mean (95% Confidence Interval)**			***P* (Partial η^2)**	**Session**	**Group**	**S*G**
FMA							
Full score, Neuromuscular Electrical Stimulation (NMES)-robot	22.3 (16.5–28.1)	43.6 (37.9–49.4)	42.5 (36.7–48.3)	$0.001^{\#\#\#}$ (0.475)	$0.000^{\Delta\Delta\Delta}$ (0.615)	$0.000^{\Delta\Delta\Delta}$ (0.282)	$0.003^{\Delta\Delta}$ (0.160)
Control	20.3 (14.2–26.4)	30.1 (24.0–36.2)	30.9 (24.8–37.0)	$0.031^{\#}$ (0.227)			
Shoulder/elbow, NMES-robot	13.6 (10.1–17.0)	24.1 (20.6–27.5)	22.3 (18.9–25.7)	$0.000^{\#\#\#}$ (0.360)	$0.000^{\Delta\Delta\Delta}$ (0.401)	$0.000^{\Delta\Delta\Delta}$ (0.112)	0.029^{Δ} (0.047)
Control	11.6 (8.2–15.0)	17.3 (13.9–20.7)	17.4 (14.0–20.8)	$0.030^{\#}$ (0.229)			
Wrist/hand, NMES-robot	8.7 (5.3–12.1)	19.6 (16.2–22.9)	20.2 (16.8–23.6)	$0.000^{\#\#\#}$ (0.435)	$0.000^{\Delta\Delta\Delta}$ (0.551)	$0.000^{\Delta\Delta\Delta}$ (0.311)	$0.001^{\Delta\Delta\Delta}$ (0.184)
Control	8.7 (4.8–12.6)	12.8 (8.9–16.7)	13.5 (9.6–17.4)	0.176 (0.021)			
ARAT							
NMES-robot	15.7 (8.8–22.6)	29.2 (22.3–36.1)	33.2 (26.3–40.1)	$0.002^{\#\#}$ (0.268)	$0.000^{\Delta\Delta\Delta}$ (0.279)	0.284 (0.018)	0.912 (0.003)
Control	12.0 (4.0–20.0)	24.2 (16.2–32.2)	26.6 (18.6–34.6)	$0.030^{\#}$ (0.229)			
FIM							
NMES-robot	44.7 (38.8–50.6)	56.6 (50.7–62.5)	61.6 (55.7–67.5)	$0.001^{\#\#\#}$ (0.311)	$0.000^{\Delta\Delta\Delta}$ (0.542)	0.117 (0.037)	0.418 (0.027)
Control	44.3 (39.3–49.3)	62.1 (57.1–67.1)	64.6 (59.6–69.6)	$0.000^{\#\#\#}$ (0.603)			
MAS							
Elbow, NMES-robot	0.8 (0.3–1.3)	0.3 (−0.2–0.8)	0.6 (0.1–1.0)	0.362 (0.051)	0.051 (0.087)	$0.000^{\Delta\Delta\Delta}$ (0.204)	$0.001^{\Delta\Delta\Delta}$ (0.201)
Control	0.3 (−0.1–0.7)	0.8 (0.5–1.2)	1.2 (0.8–1.5)	$0.005^{\#\#}$ (0.322)			
Wrist, NMES-robot	0.7 (0.3–1.0)	0.1 (−0.2–0.4)	0.3 (0.0–0.7)	$0.048^{\#}$ (0.145)	0.119 (0.064)	$0.000^{\Delta\Delta\Delta}$ (0.232)	$0.000^{\Delta\Delta\Delta}$ (0.241)
Control	0.3 (−0.1–0.6)	0.8 (0.4–1.1)	1.1 (0.7–1.4)	$0.009^{\#\#}$ (0.292)			
Finger, NMES-robot	0.5 (0.2–0.9)	0.3 (−0.1–0.6)	0.2 (−0.1–0.5)	0.354 (0.052)	0.425 (0.026)	$0.000^{\Delta\Delta\Delta}$ (0.176)	$0.005^{\Delta\Delta}$ (0.152)
Control	0.4 (0.1–0.7)	0.7 (0.4–1.1)	1.1 (0.8–1.4)	$0.025^{\#}$ (0.240)			

*Differences with statistical significance are marked with superscripts beside the P values ("#" for 1-way-ANOVA intragroup tests, "Δ" for 2-way ANCOVA tests on the group and session effects with the pre-assessment as the covariate). Significant levels are indicated as, 1 superscript for <0.05, 2 superscripts for ≤0.01, and 3 superscripts for ≤0.001. The degrees of freedom in the 1-way-ANOVA tests are (1) NMES-robot group, the corrected total = 41, between-group = 2, and within-group = 39; (2) the control group, the corrected total = 29, between-group = 2 and within-group = 27. The degrees of freedom in the 2-way ANCOVA tests are (1) the corrected total = 71, (2) pre-test = 1, (3) Session = 2, (4) Group = 1, and (5) S*G = 67.*

*FMA, Fugl-Meyer Assessment; MAS, Modified Ashworth Score; ARAT, Action Research Arm Test; FIM, Functional Independence Measurement; 3MFU, 3-month follow-up; ANOVA, analysis of variance; S*G, the interaction between the session and group.*

RESULTS

We screened 78 stroke inpatients in the wards of the hospital, and 54 of them did not meet the inclusion criteria with single or multiple reasons of (1) unstable clinical symptoms for continuous and long-term physical training, (2) secondary stroke, (3) cognitive impairment, (4) severe motor impairment (full FMA < 15), and (5) no detectable EMG in a driving muscle (<3 SD of the baseline). A total of 24 participants fulfilled the inclusion criteria and were recruited in this study. They were randomly assigned into two groups: the NMES-robot group ($n = 14$) and the control group ($n = 10$). The demographic data of the participants after the randomization are presented in **Table 1**.

Figure 4 presents the clinical scores of participants in both the NMES-robot and control groups, with FMA, ARAT, FIM, and MAS evaluated at three time points: before the first training session (pre-training assessment), immediately after the last (20th) training session (post-training assessment), and 3 months after the last training session (i.e., 3MFU). **Table 2** summarizes the means and 95% confidence intervals of each clinical assessment together with the two-way ANCOVA probabilities and the estimated effect sizes (EFs) with respect to session and group, and the one-way ANOVA probabilities with the EFs for the intragroup evaluation with respect to the assessment sessions. **Table 3** shows the probabilities and EFs of the between-group comparison on the respective post- and

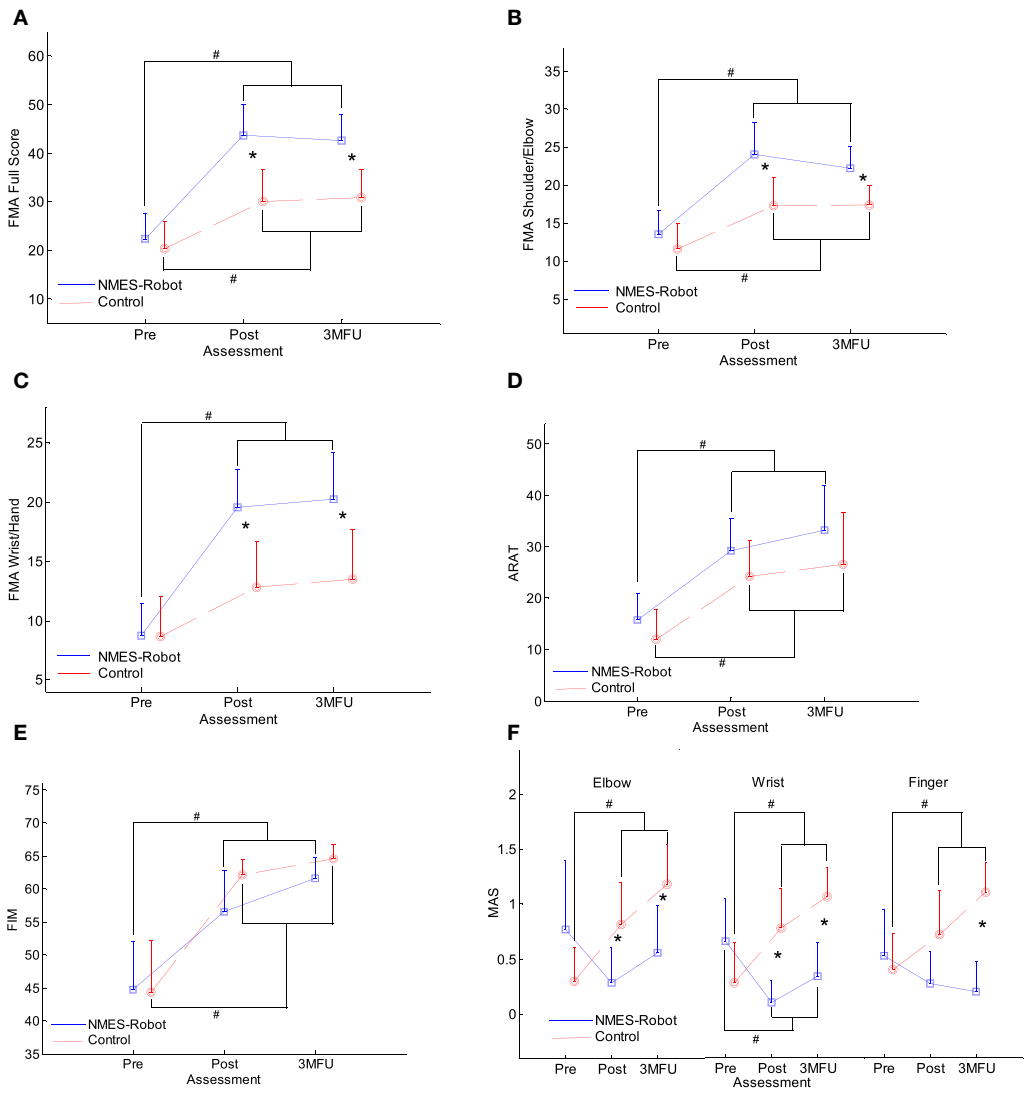

FIGURE 4 | The clinical scores [evaluated before the first and after the 20th training session, as well as the 3-month follow-up (3MFU)] of the participants in both neuromuscular electrical stimulation (NMES)-robot and control groups: **(A)** Fugl-Meyer Assessment (FMA) full scores, **(B)** FMA shoulder/elbow scores, **(C)** FMA wrist/hand scores, **(D)** Action Research Arm Test (ARAT) scores, **(E)** Function Independence Measurement (FIM), and **(F)** Modified Ashworth Score (MAS) scores at the elbow, the wrist, and the fingers, presented as mean value with 2-time SE (error bar) in each evaluation session. The solid lines are for the NMES-robot group, and the dashed lines are for the control group. The significant inter-group difference is indicated by "*" ($P < 0.05$, one-way analysis of covariance), and "#" is used to indicate the significant intragroup difference ($P < 0.05$, one-way analysis of variance with Bonferroni *post hoc* tests).

3MFU assessments by one-way ANCOVA with the adjustment of the baseline effect.

Figures 4A–C show the variation in FMA scores at the three evaluation sessions. Significant differences were observed with respect to the factors of group and session in the FMA full score, the FMA shoulder/elbow and FMA wrist/hand sub-scores (two-way ANCOVA, $P < 0.05$, **Table 2**). The interactions between the group and session factors were also statistically significant for the three FMA scores ($P < 0.05$, **Table 2**), where the FMA wrist/hand achieved the most significant level ($P = 0.001$, EF = 0.184, **Table 2**) and the FMA shoulder/elbow achieved the least significant level ($P = 0.029$, EF = 0.047, **Table 2**). For the FMA full score (**Figure 4A**), both groups demonstrated significant increases immediately after the training (i.e., post-assessment), and these increments with respect to the pre-assessment were maintained 3 months later after the training ($P < 0.05$, one-way ANOVA with *post hoc* tests, **Table 2**). The increments in the FMA full score for the NMES-robot group were significantly higher than the control group at the post- and 3MFU assessments (one-way ANCOVA, $P < 0.01$, **Table 3**). In **Figures 4B,C**, the FMA shoulder/elbow and wrist/hand scores demonstrated the similar behaviors as those observed in the FMA full score. However, the FMA wrist/hand scores indicated more significant levels with larger EFs in the interaction between the group and session (two-way ANCOVA, **Table 2**), and in the between-group one-way ANCOVA comparisons at the post- and 3MFU assessments (**Table 3**). There was no significant improvement in the FMA wrist/hand score for the control group after the training ($P > 0.05$, one-way ANOVA, **Table 2**).

Figure 4D presents the ARAT scores in the pre-training assessment, post-training assessment, and 3MFU for both groups. Significant difference was observed with respect to the evaluation sessions ($P < 0.001$, EF = 0.279, two-way ANCOVA, **Table 2**), whereas no significant difference was observed with respect to the groups. The ARAT scores significantly increased after training in both the NMES-robot and the control groups ($P < 0.05$, one-way ANOVA with Bonferroni *post hoc* tests), and the improvement could be maintained for 3 months ($P < 0.05$, one-way ANOVA with Bonferroni *post hoc* tests).

Function Independence Measurement scores in both the NMES-robot and control groups are shown in **Figure 4E**. Significant difference was observed with respect to the factor of the evaluation time points ($P < 0.001$, EF = 0.542 two-way ANCOVA, **Table 2**), whereas no significant difference was observed with respect to the factor of the groups. The FIM scores were significantly higher in the post-training assessment and 3MFU compared with those in the pre-training assessment for both groups ($P \leq 0.001$, one-way ANOVA with Bonferroni *post hoc* test).

Figure 4F displays the variation in MAS scores at the finger, wrist, and elbow across the evaluation sessions for the two groups. Significant group differences were detected by two-way ANCOVA ($P < 0.001$, EF > 0.176, **Table 2**). Significant interactions between the factors of the group and the evaluation time point were also captured at all three parts (i.e., elbow, wrist, and fingers) ($P < 0.01$, EF > 0.152, **Table 2**). The MAS scores were significantly elevated at the elbow, wrist, and fingers at the post-assessment in the control group and were remained above the elevated levels when assessed 3 months later ($P < 0.05$, one-way ANOVA with Bonferroni *post hoc* tests, **Table 2**). Significant decrease in MAS was observed at the wrist for the NMES-robot group, and this decreased level was maintained as detected by the 3MFU assessment (one-way ANOVA, $P = 0.048$, EF = 0.145, **Table 2**). There was no significant variation in the elbow and finger MAS scores for the NMES-robot group ($P > 0.05$, one-way ANOVA, **Table 2**). In the between-group comparison on the MAS, significant lower MAS scores were observed in the NMES-robot group at the elbow and the wrist during the post-assessment ($P < 0.01$, EF > 0.359, one-way ANCOVA, **Table 3**), and at all joints during the 3MFU assessment ($P < 0.01$, EF > 0.334, one-way ANCOVA, **Table 3**).

Figure 5 shows the variation patterns of EMG parameters (i.e., EMG activation level and CI) across the 20 training sessions in the NMES-robot group. A significant reduction was observed in the EMG activation levels of the FCR (**Figure 5A**; $P < 0.05$, one-way ANOVA with Bonferroni *post hoc* tests). The EMG activation levels increased in the first few training sessions and reached the peak around the third session. Subsequently, the values decreased in the following 17 sessions and finally reached a plateau in the last five training sessions. No significant variation was observed in other target muscles (BIC, TRI, and ECU-ED). **Figure 5B** presents the variation patterns of CI values among different muscle pairs either within a single joint or across multiple joints. The CI values of the FCR&BIC and BIC&TRI muscle pairs were significantly reduced along the 20 training sessions ($P < 0.05$, one-way ANOVA with Bonferroni *post hoc* test). The CI values of both muscle pairs reached the peak within the first eight training sessions and then continually decreased in the following process, then reached a steady level in the last three sessions. No significant change was observed in CI values of other muscle pairs.

TABLE 3 | The statistical probabilities and the estimated effect sizes of the 1-way analysis of covariance (ANCOVA) on the respective post-assessment and 3-month follow-up (3MFU) between the groups, by taking the pre-assessment as the covariate.

Evaluation	1-way ANCOVA on the Post- and 3MFU assessments between the groups	
	Post$_{_Pre}$ *P* (Partial η^2)	**3MFU$_{_Pre}$ *P* (Partial η^2)**
FMA		
Full score	0.000*** (0.478)	0.005** (0.319)
Shoulder/elbow	0.037* (0.190)	0.040* (0.186)
Wrist/hand	0.000*** (0.538)	0.005** (0.322)
Action Research Arm Test (ARAT)	0.417 (0.032)	0.455 (0.027)
Function Independence Measurement (FIM)	0.123 (0.109)	0.169 (0.088)
Modified Ashworth Score (MAS)		
Elbow	0.003** (0.359)	0.004** (0.334)
Wrist	0.001*** (0.430)	0.002** (0.367)
Finger	0.074 (0.144)	0.000*** (0.507)

Differences with statistical significance are marked with '' beside the P values. Significant levels are indicated as, * for <0.05, ** for ≤0.01, *** for ≤0.001. The degrees of freedom are (1) the corrected total = 23, (2) pre-test = 1, (3) between-group = 1, and (4) within-group = 21.*

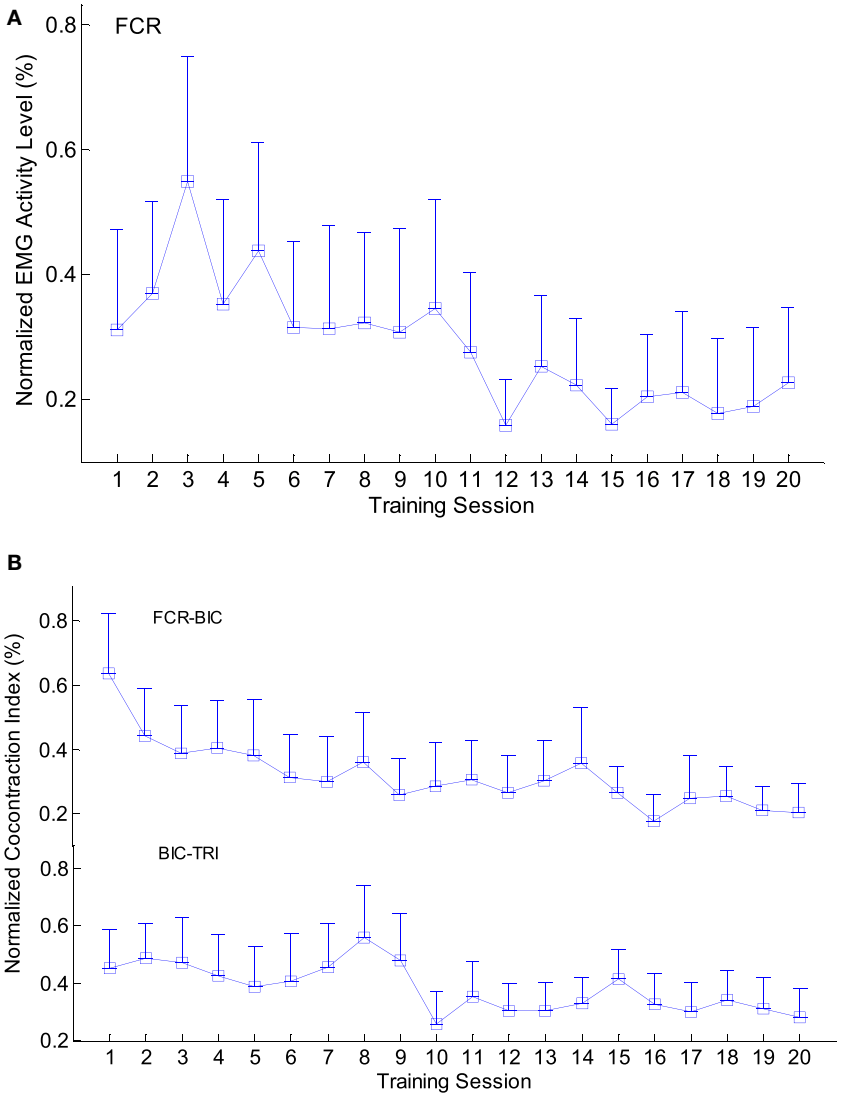

FIGURE 5 | The variation of electromyography (EMG) parameters recorded across the 20 training sessions: **(A)** the changes of the normalized EMG activation levels with significant decline observed in the flexor carpi radialis (FCR) muscle ($P < 0.05$, 1-way analysis of variance (ANOVA) with Bonferroni *post hoc* tests); **(B)** the significant decline of the normalized co-contraction Indexes (CI) values observed in the BIC&TRI and FCR&BIC muscle pairs ($P < 0.05$, 1-way ANOVA with Bonferroni *post hoc* tests). The values are presented as mean value with 2-time SE (error bar) in each session.

DISCUSSION

The results of this study indicated that in the early stage after stroke, motor function in the paretic upper limbs of stroke participants could be significantly improved through both traditional rehabilitation treatment and upper limb training by the EMG-driven NMES-robotic system. The ARAT and FIM scores suggested that the effects of early intervention using EMG-driven NMES-robot training were comparable to the effects of traditional treatments; these findings reflected the improved upper limb function, particularly, in the hand (by ARAT), and improved independence of ADL (by FIM) observed in this study. Although no specific tasks were assigned to the finger joints in this study, the increase in the ARAT scores after NMES-robot training also indicated the voluntary motor improvement in the fingers after the treatments. We noticed that there was no significant improvement in the FIM scores observed after NMES-robot training for chronic stroke patients in our previous study (31). However, in this study, the FIM score results suggested that NMES-robot-assisted intervention was effective in enhancing stroke patients' ADL levels in the early stage after stroke. Moreover, these improvements could last till 3 months later.

As indicated by the FMA scores, the NMES-robotic arm developed in this study could assist stroke patients to improve the motor function of their entire paretic upper limb, with voluntary effort. Both the NMES-robot training and traditional physical therapies improved the participants' motor function at

the shoulder and elbow, and this improvement was maintained even after 3 months. However, the NMES-robot group achieved greater improvement in the FMA shoulder/elbow and wrist/hand scores than did the control group. Two possible reasons for the improvements in the entire upper limb in the NMES-robot group, especially the shoulder (no actuated assistance in the training), motor function are as follows: (1) The participants' shoulder-related muscles for arm lifting were practiced during the training process supported by the hanging system used in this study and (2) when the muscle around a joint was trained, the adjacent proximal joint would be simultaneously improved, as indicated in our previous study (31); accordingly, wrist training led to improved elbow function in our previous study, and elbow training led to shoulder improvement in this study. We also observed that through the EMG-driven NMES-robot-assisted training, participants achieved significant motor improvement in the wrist/hand, as indicated by their FMA scores, whereas no significant improvement was achieved in the participants of the control group, who were given traditional physical treatments. The possible reason could be that compared with the rehabilitation of the proximal joints (e.g., shoulder and elbow), motor recovery in the distal joints is more difficult to manage in the manual rehabilitation. Usually, it is hard for a therapist to manage distal and proximal joint training at the same time in the physical practice; hence, most of the manual-conducted training regimens follow a proximal-to-distal sequence (46, 47). Besides, in the early phase after stroke, manually provided physical trainings are focused on the proximal joints, and little effort is allocated for the distal joints (26, 48). Although the movements provided by the NMES-robot system for a joint were simple flexion and extension, the target joints could be more precisely exercised with the aid of well-positioned motors and NMES, and could be organized into multi-joint coordinated movements with computer programs. In addition, traditional manual therapies alone usually cannot be used to exert voluntary effort in the wrist extensors (i.e., ECU-ED in this study) in the early phase after stroke (48). By contrast, NMES-robot training could be used to apply physical training directly to the wrist joint and to coordinate motor practice across multiple joints synchronously, with mechanical support from the servo motors at the wrist and elbow. The assistance from NMES could produce repetitive motosensory experiences and enable the participants to concentrate more on the target muscles at the distal joints, thus helping to evoke the voluntary effort (49, 50).

After the traditional rehabilitation treatments, the participants' muscle tone (spasticity) increased significantly at all three parts (elbow, wrist, and finger joints). This could be because of the following: (1) the muscle tone was gradually generated through spontaneous recovery process, following the pathological sequence after stroke (51); (2) compensatory muscular activity increased due to the fatigue during the motor practices (31); and (3) motor stimulation in the flexors increased during the traditional physical training process, with a lack of synchronous spasticity control. Although the changes in MAS scores in the NMES-robot group were not significant for the elbow and fingers, the results of interactions (S*G) (**Table 2**) revealed a completely different evolutionary trend in the muscle tone compared with the control group. The muscle tone declined at all three parts (elbow, wrist, and finger joints) in the NMES-robot group, and a significant reduction was observed at the wrist, which suggested that NMES-robot training could effectively release the muscle spasticity at the wrist joint, and this effect could be maintained until 3 months later. One of the possible reasons could be the intensive practice in a short period for the NMES-robot group in this work. The frequency of the EMG-driven NMES-robot arm assisted training (5 sessions/week, finished in one month) was higher than other clinical trials with equivalent total training hours practiced manually, for example, 3 times/week and finished in 16 weeks (52), where between-group differences could be submerged by other baseline effects. A significant release of muscle spasticity at the finger joints was also observed in our previous study on chronic stroke when NMES and robotic assistance were provided to the wrist joint with a high training frequency (31). In this sense, NMES-robot-assisted upper limb rehabilitation could be a relatively affordable complement to the traditional manual rehabilitation, without too much additional manpower due to the automation.

The improvement in upper limb motor function in the NMES-robot group was reflected by the clinical scores, and the session-by-session recovery progress was revealed through the EMG parameters. The reduced EMG activation levels of FCR implied a release of muscle spasticity at the wrist, which was consistent with the variation in the MAS wrist scores. Most of the patients reached a steady state after the 15th training session. The reduction of FCR was also related to the decrease in the CI values of FCR&BIC, indicating a release in the co-contraction patterns between the elbow and wrist joints. These joints could be moved more independently during arm withdrawing/flexing motions. In addition, a significant reduction in CI values between the BIC&TRI muscle pair was observed, suggesting improved coordination between the flexors and extensors at the elbow joint and an improved independence in muscle contraction over the 20 training sessions. The EMG activation levels of the FCR increased in the first 3–4 training sessions, and the CI values of BIC&TRI muscle pairs reached the peak within the first eighth training session. This was reasonable because in subacute stroke, most of the patients experience muscle weakness in the very beginning, and the muscle strength then recovers through both spontaneous processes and physical training. In addition, the participants needed to adapt to the training process in the first several training sessions. The results of the EMG parameters suggested that NMES-robot training could help release the muscle spasticity and promote muscle coordination within and across different joints effectively, particularly at the wrist in this work.

LIMITATION

The main limitation of this study is the small sample size. Despite the relatively small populations recruited, we observed consistent results on the motor improvements achieved in the NMES-robot group by clinical assessments and EMG parameters. The EMG parameters were only recorded for the NMES-robot group to

provide the understanding on the evolutionary process of the muscular activities under the training program. Unbalanced arms were obtained after the randomization in this work, mainly due to the limited project period and the small sample size recruited in a relatively sequential way. Randomized clinical trials with larger scales (e.g., larger sample sizes and multi-centers) will be conducted to consolidate the rehabilitation effectiveness of the EMG-driven NMES-robot-assisted upper limb training in the future.

CONCLUSION

In this work, the EMG-driven NMES-robot arm was applied for multi-joint coordinated upper limb rehabilitation on subacute stroke participants in comparison with the traditional physical therapy. Both of the treatments could significantly promote the independence in daily activities with comparable intensities. The NMES-robot-assisted training could be more effective in releasing muscle tones and in improving the muscle coordination in the whole upper limb, because of the intensive practices on both the proximal and the distal joints delivered in a short period of rehabilitation. All the training effects achieved by the NMES-robot-assisted rehabilitation could be maintained for 3 months after the training. The NMES-robot-assisted upper limb training could be complementary to the traditional manual training to cope with the shortage of the human rehabilitation professionals in the industry.

ETHICS STATEMENT

The study was carried out in accordance with the human ethic guidelines of the Human Subjects Ethics Subcommittee of Hong Kong Polytechnic University and Joint Chinese University of Hong Kong-New Territories East Cluster Clinical Research Ethics Committee. All participants recruited in the study gave written informed consent in accordance with the Declaration of Helsinki before the start of the training. The medical status of the participants was monitored by the routine management in the hospital.

AUTHOR CONTRIBUTIONS

QQ and QL contributed in the NMES-robot arm assisted training experiment, data collection and analysis, and manuscript drafting. SN and WP contributed in the clinical trial design and subject management. YZ contributed in the data analysis. XH conceived of the study and coordinated the whole project, including the clinical trial design, human subject experiments, and manuscript drafting.

FUNDING

The study was supported in part by Innovation Technology Commission of the Hong Kong Government (ITT/039/14GP and ITS/033/12) and The Hong Kong Polytechnic University (1-ZE4R).

REFERENCES

1. Nakayama H, Jørgensen H, Raaschou H, Olsen T. Recovery of upper extremity function in stroke patients: the Copenhagen stroke study. *Arch Phys Med Rehabil* (1994) 75(4):394–8. doi:10.1016/0003-9993(94)90161-9
2. Dobkin B. Rehabilitation after stroke. *N Engl J Med* (2005) 352(16):1677–84. doi:10.1056/NEJMcp043511
3. Kwakkel G, BJ K, van der Grond J, Prevo A. Probability of regaining dexterity in the flaccid upper limb: impact of severity of paresis and time since onset in acute stroke. *Stroke* (2003) 34(9):2181–6. doi:10.1161/01.STR.0000087172.16305.CD
4. Brauer S, Hayward K, Carson R, Cresswell A, Barker R. The efficacy of SMART arm training early after stroke for stroke survivors with severe upper limb disability: a protocol for a randomised controlled trial. *BMC Neurol* (2013) 13(1):71. doi:10.1186/1471-2377-13-71
5. Raghavan P. Upper limb motor impairment after stroke. *Phys Med Rehabil Clin N Am* (2015) 26(4):599–610. doi:10.1016/j.pmr.2015.06.008
6. Good D, Bettermann K, Reichwein R. Stroke rehabilitation. Continuum. *NeuroRehabilitation* (2011) 17(3):545–67. doi:10.1212/01.CON.0000399072.61943.38
7. Zeiler S, Krakauer J. The interaction between training and plasticity in the poststroke brain. *Curr Opin Neurol* (2013) 26(6):609–16. doi:10.1097/WCO.0000000000000025
8. Ng K, Gibson E, Hubbard R, Yang W, Caffo R, Krakauer R, et al. Fluoxetine maintains a state of heightened responsiveness to motor training early after stroke in a mouse model. *Stroke* (2015) 46(10):2951–60. doi:10.1161/STROKEAHA.115.010471
9. Flöel A, Werner C, Grittner U, Hesse S, Jöbges M, Knauss J, et al. Physical fitness training in subacute stroke (PHYS-STROKE) – study protocol for a randomised controlled trial. *Trials* (2014) 15:45. doi:10.1186/1745-6215-15-45
10. Tomori K, Nagayama H, Ohno K, Nagatani R, Saito Y, Takahashi K, et al. Comparison of occupation-based and impairment-based occupational therapy for subacute stroke: a randomized controlled feasibility study. *Clin Rehabil* (2015) 29(8):752–62. doi:10.1177/0269215514555876
11. Brown T, Parmar G, Durant R, Halanych J, Hovater M, Muntner P, et al. Health professional shortage areas, insurance status, and cardiovascular disease prevention in the reasons for geographic and racial differences in stroke (REGARDS) study. *J Health Care Poor Underserved* (2011) 22(4):1179–89. doi:10.1353/hpu.2011.0127
12. Nudo R, Plautz E, Frost S. Role of adaptive plasticity in recovery of function after damage to motor cortex. *Muscle Nerve* (2001) 24(8):1000–19. doi:10.1002/mus.1104
13. Harris J, Eng J. Strength training improves upper-limb function in individuals with stroke: a meta-analysis. *Stroke* (2010) 41(1):136–40. doi:10.1161/STROKEAHA.109.567438
14. Lynch D, Ferraro M, Krol J, Trudell CM, Christos P, Volpe BT. Continuous passive motion improves shoulder joint integrity following stroke. *Clin Rehabil* (2005) 19(6):594–9. doi:10.1191/0269215505cr901oa
15. Ng K, Zhang R, Butler A, Wolf S, Alberts J. Quality-of-life change associated with robotic-assisted therapy to improve hand motor function in patients with subacute stroke: a randomized clinical trial. *Phys Ther* (2010) 90(4):493–504. doi:10.2522/ptj.20090160
16. Grimaldi G, Manto M. Functional impacts of exoskeleton-based rehabilitation in chronic stroke: multi-joint versus single-joint robotic training. *J Neuroeng Rehabil* (2013) 10(1):113. doi:10.1186/1743-0003-10-113
17. Yang C, Lin K, Chen H, Wu C, Chen C. Pilot comparative study of unilateral and bilateral robot-assisted training on upper-extremity performance in patients with stroke. *Am J Occup Ther* (2012) 66(2):198. doi:10.5014/ajot.2012.003103
18. Volpe BT, Ferraro M, Lynch D, Christos P, Krol J, Trudell C, et al. Robotics and other devices in the treatment of patients recovering from stroke. *Curr Atheroscler Rep* (2004) 6(4):314–9. doi:10.1007/s11883-004-0064-z
19. Dipietro L, Ferraro M, Palazzolo J, Krebs H, Volpe B, Hogan N. Customized interactive robotic treatment for stroke: EMG-triggered therapy. *IEEE Trans Neural Syst Rehabil Eng* (2005) 13(3):325–34. doi:10.1109/TNSRE.2005.850423
20. Takahashi C, Der-Yeghiaian L, Le V, Motiwala R, Cramer S. Robot-based hand motor therapy after stroke. *Brain* (2008) 131:425–37. doi:10.1093/brain/awm311

21. Staubli P, Nef T, Klamroth-Marganska V, Riener R. Effects of intensive arm training with the rehabilitation robot ARMin II in chronic stroke patients: four single-cases. *J Neuroeng Rehabil* (2009) 6(1):46. doi:10.1186/1743-0003-6-46
22. Hu X, Tong K, Song R, Zheng X, Leung W. A comparison between electromyography-driven robot and passive motion device on wrist rehabilitation for chronic stroke. *Neurorehabil Neural Repair* (2009) 23(8):837–46. doi:10.1177/1545968309338191
23. Knutson J, Fu M, Sheffler L, Chae J. Neuromuscular electrical stimulation for motor restoration in hemiplegia. *Phys Med Rehabil Clin N Am* (2015) 26(4):729–45. doi:10.1016/j.pmr.2015.06.002
24. Seneviratne C, Then K, Reimer M. Post-stroke shoulder subluxation: a concern for neuroscience nurses. *Axone* (2005) 27(1):26–31.
25. Sujith O. Functional electrical stimulation in neurological disorders. *Eur J Neurol* (2008) 15(5):437–44. doi:10.1111/j.1468-1331.2008.02127.x
26. Chae J, Yu D. Neuromuscular stimulation for motor relearning in hemiplegia. *Crit Rev Phys Rehabil Med* (1999) 11:279–97. doi:10.1615/CritRevPhysRehabilMed.v11.i34.40
27. Hu X, Tong K, Wei X, Rong W, Susanto E, Ho S. The effects of post-stroke upper-limb training with an electromyography (EMG)-driven hand robot. *J Electromyogr Kinesiol* (2013) 23(5):1065–74. doi:10.1016/j.jelekin.2013.07.007
28. Hu X, Tong K, Song R, Tsang V, Leung P, Li L. Variation of muscle coactivation patterns in chronic stroke during robot-assisted elbow training. *Arch Phys Med Rehabil* (2007) 88(8):1022–9. doi:10.1016/j.apmr.2007.05.006
29. Hu X, Tong K, Song R, Zheng X, Lui K, Leung W, et al. Quantitative evaluation of motor functional recovery process in chronic stroke patients during robot-assisted wrist training. *J Electromyogr Kinesiol* (2008) 19(4):639–50. doi:10.1016/j.jelekin.2008.04.002
30. Hu XL, Tong KY, Li R, Chen M, Xue JJ, Ho SK, et al. Post-stroke wrist rehabilitation assisted with an intention-driven functional electrical stimulation (FES)-robot system. *IEEE Int Conf Rehabil Robot* (2011) 2011:5975424. doi:10.1109/ICORR.2011.5975424
31. Hu X, Tong K, Ho S, Xue J, Rong W, Li L. Wrist rehabilitation assisted by an electromyography-driven neuromuscular electrical stimulation (NMES)-robot after stroke. *Neurorehabil Neural Repair* (2015) 29(8):767–76. doi:10.1177/1545968314565510
32. Hu X, Tong K, Li R, Xue J, Ho S, Chen P. The effects of electromechanical wrist robot assistive system with neuromuscular electrical stimulation for stroke rehabilitation. *J Electromyogr Kinesiol* (2012) 22(3):431–9. doi:10.1016/j.jelekin.2011.12.010
33. Lo A, Guarino P, Richards L, Haselkorn J, Wittenberg G, Federman D, et al. Robot-assisted therapy for long-term upper limb impairment after stroke. *N Engl J Med* (2010) 362:1772–83. doi:10.1056/NEJMoa0911341
34. Lee Y, Lin K, Cheng H, Wu C, Hsieh Y, Chen C. Effects of combining robot-assisted therapy with neuromuscular electrical stimulation on motor impairment, motor and daily function, and quality of life in patients with chronic stroke: a double-blinded randomized controlled trial. *J Neuroeng Rehabil* (2015) 12:96. doi:10.1186/s12984-12015-10088-12983
35. Boyaci A, Topuz O, Alkan H, Ozgen M, Sarsan A, Yildiz N, et al. Comparison of the effectiveness of active and passive neuromuscular electrical stimulation of hemiplegic upper extremities: a randomized controlled trial. *Int J Rehabil Res* (2013) 36(4):315–22. doi:10.1097/MRR.0b013e328360e541
36. Langhorne P, Bernhardt J, Kwakkel G. Stroke rehabilitation: stroke care 2. *Lancet* (2011) 377:1693–702. doi:10.1016/S0140-6736(11)60325-5
37. Kamen G, Gabriel D. *Essentials of Electromyography*. Amherst: University of Massachusetts (2010).
38. Folstein M, Folstein S, McHugh P. Mini-mental state: a practical method for grading the cognitive state of patients for the clinician. *J Psychiatr Res* (1975) 12(3):189–98. doi:10.1016/0022-3956(75)90026-6
39. Fugl-Meyer A, Jaasko L, Leyman I, Olsson S, Steglind S. The post-stroke hemiplegic patient.1. A method for evaluation of physical performance. *Scand J Rehabil Med* (1975) 7(1):13–31.
40. Ashworth B. Preliminary trials of carisoprodol in multiple sclerosis. *Practitioner* (1964) 192:540–2.
41. Feigin V, Lawes C, Bennett D, Anderson C. Stroke epidemiology: a review of population-based studies of incidence, prevalence, and case-fatality in the late 20th century. *Lancet Neurol* (2003) 2(1):43–53. doi:10.1016/S1474-4422(03)00266-7
42. Traylor M, Rutten-Jacobs L, Holliday E, Malik R, Sudlow C, Rothwell P, et al. Differences in common genetic predisposition to ischemic stroke by age and sex. *Stroke* (2015) 46(11):3042–7. doi:10.1161/STROKEAHA.115.009816
43. McDonnell M. Action research arm test. *Aust J Physiother* (2008) 54(3):220. doi:10.1016/S0004-9514(08)70034-5
44. Wallace D, Duncan PW, Lai SM. Comparison of the responsiveness of the Barthel Index and the motor component of the Functional Independence Measure in stroke: the impact of using different methods for measuring responsiveness. *J Clin Epidemiol* (2002) 55(9):922–8.
45. Liu S, Lebeau J, Tenenbaum G. Does exercise improve cognitive performance? A conservative message from Lor's Paradox. *Front Psychol* (2016) 7:1092. doi:10.3389/fpsyg.2016.01092
46. Janet H, Roberta B. *Motor Relearning Program for Stroke*. 2nd ed. Aspen Publishers (1987).
47. Kwakkel G, Wagenaar R. Stroke rehabilitation. *Lancet* (1999) 354(9190):1642–3. doi:10.1016/S0140-6736(05)77125-7
48. Gillen G, Ann B. *Stroke Rehabilitation: A Function-Based Approach*. Elsevier (2004). p. 38–9.
49. Chae J, Kilgore K, Triolo R, Yu D. Neuromuscular stimulation for motor neuroprosthesis in hemiplegia. *Crit Rev Phys Rehabil Med* (2000) 12:1–23. doi:10.1615/CritRevPhysRehabilMed.v12.i1.10
50. Doucet B, Lam A, Griffinm L. Neuromuscular electrical stimulation for skeletal muscle function. *Yale J Biol Med* (2012) 85:201–15.
51. Sullivan S. Stroke: motor function. In: Sullivan S, Schmitz T, editors. *Physical Rehabilitation*. Philadelphia: F.A. Davis (2007). 719 p.
52. Winstein C, Wolf S, Dromerick A, Lane C, Nelsen M, Lewthwaite R, et al. Effect of a task-oriented rehabilitation program on upper extremity recovery following motor stroke: the ICARE randomized clinical trial. *JAMA* (2016) 351:571–81. doi:10.1001/jama.2016.0276

Conflict of Interest Statement: The authors declare that the research was conducted in the absence of any commercial or financial relationships that could be construed as a potential conflict of interest.

frontiers in Neurology

ORIGINAL RESEARCH
published: 29 August 2017
doi: 10.3389/fneur.2017.00449

Alterations in Spectral Attributes of Surface Electromyograms after Utilization of a Foot Drop Stimulator during Post-Stroke Gait

Rakesh Pilkar[1,2]*, *Arvind Ramanujam*[1] and *Karen J. Nolan*[1,2]

[1] Human Performance and Engineering Research, Kessler Foundation, West Orange, NJ, United States, [2] New Jersey Medical School, Newark, NJ, United States

Background: A foot drop stimulator (FDS) is a rehabilitation intervention that stimulates the common peroneal nerve to facilitate ankle dorsiflexion at the appropriate time during post-stroke hemiplegic gait. Time–frequency analysis (TFA) of non-stationary surface electromyograms (EMG) and spectral variables such as instantaneous mean frequency (IMNF) can provide valuable information on the long-term effects of FDS intervention in terms of changes in the motor unit (MU) recruitment during gait, secondary to improved dorsiflexion.

Objective: The aim of this study was to apply a wavelet-based TFA approach to assess the changes in neuromuscular activation of the tibialis anterior (TA), soleus (SOL), and gastrocnemius (GA) muscles after utilization of an FDS during gait post-stroke.

Methods: Surface EMG were collected bilaterally from the TA, SOL, and GA muscles from six participants (142.9 ± 103.3 months post-stroke) while walking without the FDS at baseline and 6 months post-FDS utilization. Continuous wavelet transform was performed to get the averaged time–frequency distribution of band pass filtered (20–300 Hz) EMGs during multiple walking trials. IMNFs were computed during normalized gait and were averaged during the stance and swing phases. Percent changes in the energies associated with each frequency band of 25 Hz between 25 and 300 Hz were computed and compared between visits.

Results: Averaged time–frequency representations of the affected TA, SOL, and GA EMG show altered spectral attributes post-FDS utilization during normalized gait. The mean IMNF values for the affected TA were significantly lower than the unaffected TA at baseline ($p = 0.026$) and follow-up ($p = 0.038$) during normalized stance. The mean IMNF values significantly increased ($p = 0.017$) for the affected GA at follow-up during normalized swing. The frequency band of 250–275 Hz significantly increased in the energies post-FDS utilization for all muscles.

Conclusion: The application of wavelet-based TFA of EMG and outcome measures (IMNF, energy) extracted from the time–frequency distributions suggest alterations in MU recruitment strategies after the use of FDS in individuals with chronic stroke. This

OPEN ACCESS

Edited by:
Xiaogang Hu,
University of North Carolina at Chapel Hill, United States

Reviewed by:
Xu Zhang,
University of Science and Technology of China, China
Chenyun Dai,
University of North Carolina at Chapel Hill, United States

***Correspondence:**
Rakesh Pilkar
rpilkar@kesslerfoundation.org

Specialty section:
This article was submitted to Stroke, a section of the journal Frontiers in Neurology

Received: *18 April 2017*
Accepted: *14 August 2017*
Published: *29 August 2017*

Citation:
Pilkar R, Ramanujam A and Nolan KJ (2017) Alterations in Spectral Attributes of Surface Electromyograms after Utilization of a Foot Drop Stimulator during Post-Stroke Gait. Front. Neurol. 8:449. doi: 10.3389/fneur.2017.00449

further establishes the efficacy of FDS as a rehabilitation intervention that may promote motor recovery in addition to treating the secondary complications of foot drop due to post-stroke hemiplegia.

Keywords: time–frequency analysis, functional electrical stimulation, wavelet transform, electromyography, spectral analysis

INTRODUCTION

Stroke is one of the leading causes of serious and long-term disability, and foot drop is one of the most common disabling impairments resulting from hemiplegia due to stroke (1). Foot drop characterized by weakness and/or lack of voluntary control in the ankle and toe dorsiflexor muscles (2) can result in gait related deficiencies (decreased speed, a disruption in weight acceptance and transfer, asymmetry and instability), further limiting the activities of daily living (3, 4). The application of an ankle foot orthosis (AFO) to compensate for foot drop throughout the gait has been the common modality of treatment. Although AFOs have been shown to increase gait speed and functional ambulation (3, 5), as a rehabilitation intervention it is not targeted to restore muscle function (2).

Functional electrical stimulation (FES) has been evident as a targeted rehabilitation intervention that may promote motor recovery, especially when applied in a task-specific environment (6–9). FES applied to the common peroneal nerve through a foot drop stimulator (FDS) provides a focused excitation to the peroneal nerve to promote active ankle dorsiflexion during initial double support at heel strike, at pre-swing lift-off and during the swing phase of gait to sufficiently clear the foot (10–12). Using FDS to drive muscle groups in specific activation patterns during walking has been shown to improve strength, walking speed, spatiotemporal parameters, and retrain ankle dorsiflexor muscle [tibialis anterior (TA)] activation timings (2, 9, 13–16). These demonstrate the efficacy for FDS utilization in post-stroke rehabilitation, but they fail to precisely indicate how FDS technology can restore motor function (2, 12, 14, 16–20).

To understand the role of FDS-based gait rehabilitation in recovering motor function, it is important to understand the intrinsic electrophysiological modifications that may elicit the improvements in the muscle function. Surface electromyography is one of the most effective non-invasive tools, which provide easy access to the underlying physiological processes that cause the muscle to generate force, produce movement, and achieve any functional task (21). Electromyograms (EMG) data collected during gait can provide us with a quantitative measure of muscle activations and activation timings, which could be used to assess the level of improvement post-rehabilitation (10, 15, 22, 23). As a result, the application of various signal processing techniques to extract meaningful information from the EMG data has been an on-going process in stroke rehabilitation. To better understand the electrophysiological processes behind neuromuscular activations, it is essential to study these signals in time as well as frequency domain. Signal processing methods such as empirical mode decomposition (EMD) (24, 25) and wavelet analysis (26–28) have provided researchers tools to interpret non-stationary EMG data in time and frequency domain simultaneously. EMD has gained popularity for analyzing non-stationary signals and has been utilized in filtering EMG signals (25, 29, 30), time–frequency analysis (TFA) (25), fatigue analysis (31) due to its ability to decompose EMG signals into physically meaningful intrinsic mode functions (IMFs). Although EMD-based approach has advantages in analyzing EMG, time–frequency representations obtained using EMD-Hilbert transform could be excessively detailed, making it difficult to interpret, particularly for EMGs collected during dynamic movements such as gait. Although smoothing techniques have been suggested to obtain more continuous Hilbert spectrums, it has been suggested that such techniques may result in degradation of time–frequency resolution as well as physically meaningful content (24). In contrast, wavelet-based TFA provides more continues representation of the data and has been widely utilized to identify motor unit (MU) recruitment patterns (26), motor strategy patterns (28) and perform clinical assessments (27) during gait. In the current literature, these analyses have only been performed in individuals with cerebral palsy, diabetic neuropathy, ankle osteoarthritis, and healthy populations (26–28). The current investigation presents a novel application of wavelet-based TFA of EMG signals in individuals post-stroke during gait. In addition, wavelet-based TFA from lower extremity muscles is further analyzed to assess the neuromuscular changes occurring due to FDS-based gait retraining has not been done yet.

The purpose of this study was to apply a wavelet-based TFA approach to assess the neuromuscular changes in the TA, soleus (SOL), and gastrocnemius (GA) muscles after utilization of an FDS as a gait rehabilitation tool in individuals post-stroke. Changes in the spectral variable—instantaneous mean frequency (IMNF) and energies associated with bands of frequencies (25–300 Hz) extracted from time–frequency distributions of EMGs from TA, SOL, and GA muscles are compared to assess the alterations in MU recruitments post-FDS utilization. We hypothesize that the time–frequency distribution of targeted TA and indirectly stimulated SOL and GA muscles will show changes in time–frequency distribution (TFD) with increased mean IMNF and energy after utilization of an FDS.

MATERIALS AND METHODS

Study Participants

Six individuals (age: 63.7 ± 10.6 years, height: 176.5 ± 6.2 cm, weight: 84.9 ± 8.3 kg, three right side affected, and three left side affected) with drop foot and hemiplegia secondary to stroke (142.9 ± 103.3 months post-stroke) were recruited for participation in this investigation. Hemiplegia was defined as

paralysis affecting only one side of the body diagnosed by the participants' treating physician. All participants (1) were at least 6 months post-stroke, prior to enrollment; (2) uninvolved lower limb had no history of injury or pathology; (3) were able to walk independently for 10 m without any assistive device; and (4) not currently participating in or is a minimum of 30 days post-inpatient or outpatient: stroke, cardiac, pulmonary, or any other physical rehabilitation on the lower extremities at time of enrollment. Individuals with severe cardiac disease, seizure disorders and/or orthopedic, neuromuscular, or neurological pathologies that would interfere with their ability to walk were excluded. All procedures performed in this investigation were approved by the Kessler Foundation Institutional Review Board, and written as well as informed consent was obtained from participants prior to study participation.

Foot Drop Stimulator

All participants received a commercially available FDS (Walkaide®; Innovative Neurotronics, Inc., Austin, TX, USA) at their baseline visit for use during ambulation in the community as part of a larger multi-site clinical trial. The Walkaide® is a battery operated single-channel, asymmetrical biphasic stimulator with programmable pulse width and frequency that was utilized during walking as an FES orthotic device (**Figure 1**). The technology is controlled by a tilt sensor and accelerometer to provide electrically induced muscle activation via two electrodes and electrode leads to dorsiflex the foot on the affected side at the appropriate time during gait. The small device [87.9 g, 8.2 cm (H) × 6.1 cm (W) × 2.1 cm (T)] was attached to a molded cuff located just below the knee, secured with a latch, and properly aligned using anatomical landmarks and visual indicators. The two electrodes were specifically placed near the head of the fibula, directly over the motor nerve and proximal musculature. Each participant used their own FDS device for daily ambulation in the community. Each device was custom programmed (stimulus intensity, timing and duration of muscle activation) during the gait cycle by a licensed clinician at baseline. The pulse width ranged from 25 to 300 μs and stimulation frequency ranged from 17 to 33 Hz.

FIGURE 1 | The Walkaide® used for addressing foot drop.

Testing Procedures

Participants completed 10 walking trials with (five trials) and without (five trials) the FDS at a self-selected pace on level ground (4.5 m) at baseline and following 6 months of FDS use for ambulation in the community. Participants wore shoes during all walking tests, and members of the study team provided non-contact guarding for safety. For consistency, the FDS was worn by the patient during all trials but switched off to prevent stimulation during the trials without the FDS. All walking trials without the FDS were used for subsequent analysis in the current investigation to measure the rehabilitative effect of the device.

Data Acquisition and Processing

Wireless EMG data were collected bilaterally from the TA, SOL, and GA (medial head) muscles at 2,520 Hz using a Noraxon DTS system (Noraxon, Inc., Scottsdale, AZ, USA). All data were imported into Matlab (The Mathworks, Inc., Natick, MA, USA) for custom processing and analysis. EMG data during each walking trial (without FDS) were band pass filtered between 20 and 300 Hz and notch filtered at 60 Hz. The EMG amplitudes were normalized to the maximum voluntary contractions (MVCs). MVCs were collected for all selected muscles at the beginning of each testing session prior to walking trials and were done in accordance with SENIAM (32). Kinematic data were collected at 60 Hz (Motion Analysis Corporation, Santa Rose, CA, USA), and time synchronized with EMG data. During initial post-processing in Cortex software (Motion Analysis Corporation, Santa Rose, CA, USA) heel-strike and toe-off gait cycle events were identified for all trials based on the event of heel contact with the ground (or first foot contact in pathological gait) and the event of toe lift-off of the ground (or the last foot contact with the floor in pathological gait), respectively (**Figure 2A**). All EMG data were divided into gait cycles (GCs) for further analysis. A single GC consisted of consecutive heel-strike events of the same limb (**Figures 2B,C**). Each GC was subdivided into stance and swing based on heel-strike and toe-off events (**Figure 2B**). The total number of GC considered for analysis varied from a minimum of 18 to a maximum of 46 for baseline and a minimum of 11 to a maximum of 36 for follow-up visit across all participants.

Data Analysis and Outcome Measures

Wavelet-Based TFA

One of the challenges of performing frequency or TFA of EMG data is the presence of non-stationarity (33). Non-stationarity in EMG data has been associated with several factors such as metabolic changes that induce fatigue, changes in muscle length as well as muscle force due to dynamic movements or the displacement of electrodes during movements (33). To better understand the underlying electrophysiological modifications that may cause improvements in the muscle function, we used a wavelet-based TFA approach, which has been shown to be suitable for analyzing non-stationary EMG data collected during dynamic muscle contractions (26–28).

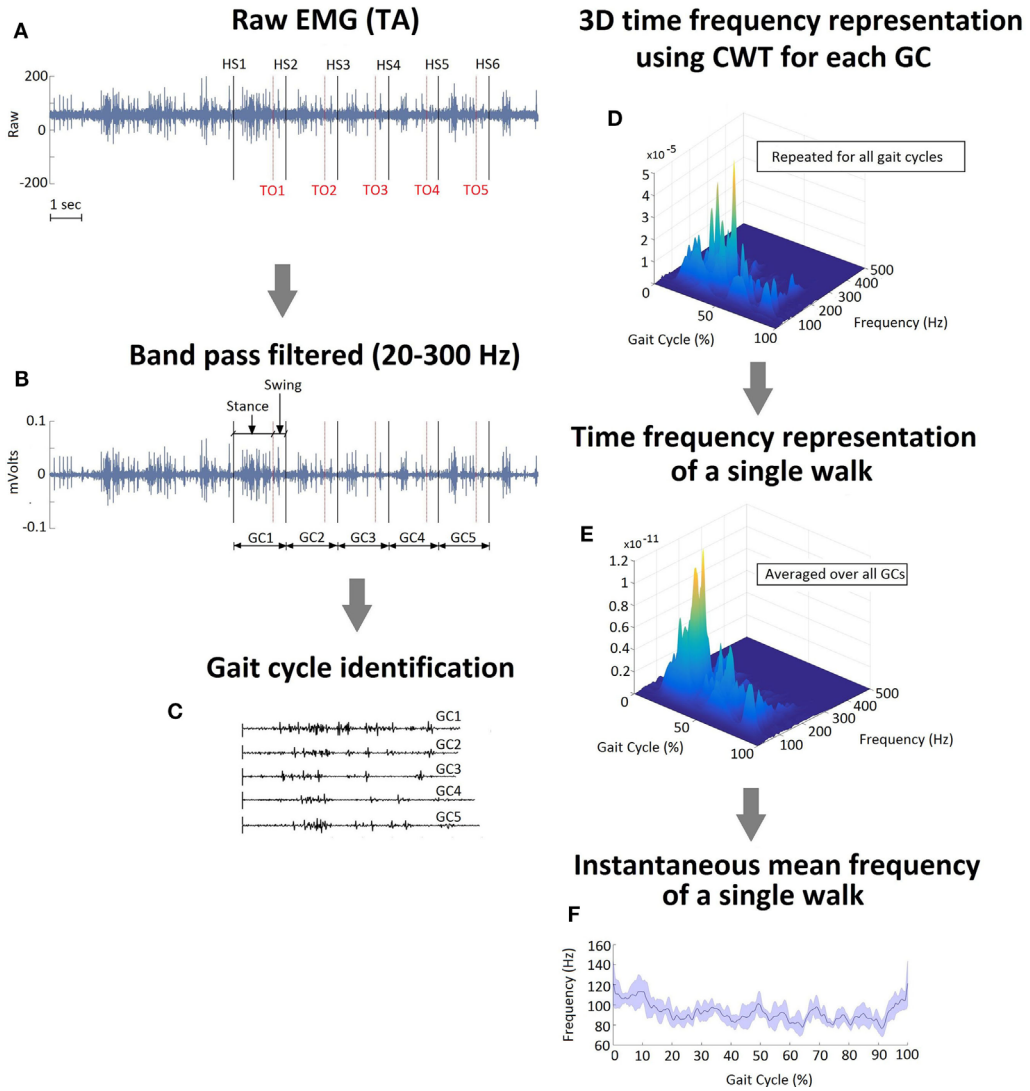

FIGURE 2 | **(A)** Raw EMG signal recorded from tibialis anterior muscle on the affected side of a single representative participant during a single walk. Gait cycle (GC) events, heel strike and toe off, were identified. **(B)** Band pass filtered EMG with stance and swing events identified during a GC. **(C)** Raster plot representation of the individual GCs during a single walk. **(D)** A 3D time–frequency representation of GC1 data using continuous wavelet transform. **(E)** A time frequency representation of a single walk (averaged over five GCs). **(F)** Instantaneous mean frequency profile extracted from time–frequency representation shown in **(E)**. The shaded area in **(F)** represents the SD within the gait cycles during a single walk.

The continuous wavelet transform (CWT) has the following general definition:

$$W(a,b;x,\psi) = |a|^{-\frac{1}{2}} \int_{-\infty}^{\infty} x(t)\psi^{*}\left(\frac{t-b}{a}\right)dt \qquad (1)$$

where $\psi^{*}(\cdot)$ is a complex conjugate of the basic wavelet function, ψ, also called the mother wavelet. The parameter a is the dilation factor the controls the width of the wavelet, and b represents the translation of the origin thus controlling the location of the wavelet on time axis. The variable $1/a$ gives the frequency scale and b gives the temporal location of event for a signal x. In general, $W(a,b;x,\psi)$ represents the energy of signal x of scale a at time, $t = b$. In this investigation, we performed the CWT using the analytic "bump" function as the mother wavelet of center frequency, $f_c = 5/2\pi$ Hz using the command `cwtft` in Matlab. The scales, a, ranged from $f_c/(f_{max} \times dt)$ to $f_c/(f_{min} \times dt)$ where f_{min} and f_{max} were set to 1 and 500 Hz, respectively, as surface EMG signals are band-limited below 500 Hz. Also, dt represents the sampling duration.

For the current analysis, CWT was applied on the EMG data during each GC of varied time length to get the individual time–frequency representation, W. During the stance phase, swing phase and entire GC, W was individually resampled on the time axis to get the normalized representations (**Figure 2D**) for stance (0–100% of stance), swing (0–100% of swing), and entire GC (0–100% of entire GC). As a final step, TFDs were computed for both phases, during all walks (**Figure 2E**), and

all participants were individually averaged to get a combined averaged TFD for each muscle.

Instantaneous Mean Frequency

Mean frequency (MNF) is an average frequency of a power density spectrum of a signal. IMNF can be computed from a TFD, $W(f, t)$ as

$$\mathrm{IMNF}(t) = \frac{\sum_{j=1}^{M} f_j W(f_j, t)}{\sum_{j=1}^{M} W(f_j, t)} \quad (2)$$

Figure 2B shows the IMNF profile for a single normalized walk. IMNF was computed from the TFD of TA, SOL, and GA during stance and swing phases, and each were normalized to 0–100%. The averaged IMNF values were used for comparing the affected and unaffected side at each visit as well as comparing baseline and follow-up for each side.

TFD Energy (E)

The energy values were computed from the TFD, W obtained using CWT for a total of eleven frequency bands, each with a bandwidth of 25 Hz. The first band covered the frequencies from 25 to 50 Hz, the second band ranged from 51 to 75 Hz, and subsequent bands covering up to 300 Hz. Frequencies below 25 Hz and above 300 Hz were not considered for this analysis as the energies associated with these frequencies were negligible due to band pass filtering between 20 and 300 Hz. The TFD energy for each band was computed as a percentage of the total distribution energy as:

$$E(\%) = 100 \times \frac{\sum_{f=f_a}^{f_b} W(f,t)}{\sum W(f,t)} \quad (3)$$

where f_a and f_b are frequency limits for the band. Energy values were computed separately for normalized stance and swing phases, for all the tested muscles at baseline and follow-up. The rationale behind dividing the entire time–frequency spectrum into several frequency bands was to isolate frequencies that showed significant changes in energy which may further help us understand the changes in MU recruitment strategies after the FDS utilization.

Statistical Analysis

Paired sample t-tests were used to compare the differences in IMNF values of TA, SOL, and GA between the affected and unaffected sides. To evaluate the effect of FDS utilization on TA, SOL, and GA, IMNF and energy (E) values at baseline and follow-up visits were also compared using paired sample t-tests. Significance level was set to $p < 0.05$ for all statistical analyses.

RESULTS

Time–frequency plots show distinct patterns of muscle activation and energy association with different phases of the GC for all tested muscles on the affected side (**Figure 3**). During healthy gait, the TA muscle produces two bursts of activation during the normalized gait cycle with initial activation occurring between 0 and 12% GC (during initial double support) and the second burst occurring at 55 and 100% of GC (during swing) (22). **Figures 3A,B** show similar patterns of TA activation at baseline and follow-up; however, the initial burst of activation appears to be prolonged for stroke participants compared to what is observed in healthy gait. At baseline, the highest energy is localized between 20 and 40% of GC and is associated with frequencies between 75 and 100 Hz. Furthermore, the TA inhibitory (inactive) period, which is usually apparent in healthy gait during 13–54% of GC, seems to be indistinct at baseline for stroke participants. At follow-up, time–frequency plot show alterations in TA activation (**Figures 3B,C**). This is characterized by (1) an increase in the energies during 0–10% and 30–40% of GC (**Figure 3C**) and (2) the presence of clear inhibition during approximately 50–70% of GC shown by negligible energy content (**Figure 3B**).

Soleus is active during 6–52% of GC during healthy gait (22). In the case of stroke gait, the energy contained within the SOL muscle is approximately between 5 and 75% of GC (**Figures 3D,E**). At follow-up, TFD of the SOL shows increased energies associated with frequencies ranging from 75 to 200 Hz (**Figure 3F**).

Time–frequency plots of the affected GA show a clear shift in the peak energy localization during normalized gait (**Figures 3G,H**). At baseline, the energies are localized at low frequencies (<50 Hz) between 20% and 30% of GC, suggesting the predominant use of slow-twitch MU (**Figure 3G**). However, after 6 months of FDS utilization, the energy content shows a clear shift toward higher frequencies (50–150 Hz) (**Figures 3H,I**). As seen with TA and SOL, GA time–frequency plots for stroke participants show wide energy spread compared to healthy gait.

To quantify the time–frequency distributions, IMNF was computed during the normalized (0–100%) stance and swing using Eq. 2. **Figure 4** shows difference in the IMNF trajectories between the affected and unaffected side, for all three muscles during baseline and follow-up visits. The unaffected TA has an initial decrease in the averaged IMNF profile approximately during 0–13% of normalized stance followed by a gradual increment and a plateau. During normalized swing, the unaffected TA shows a gradual decrease up to 63% followed by an increase in the averaged IMNF profile. Such a pattern is not apparent for the affected TA during normalized stance as well as swing. The averaged IMNF profiles of the unaffected SOL and GA muscles, being less impaired, show increasing trend in MNF with time during normalized stance (**Figure 4A**, right column) and show decreasing trend with time during normalized swing (**Figure 4B**, right column). Such a characteristic response is not seen on the affected side (**Figures 4A,B**, left columns, respectively). Moreover, it is observed that there is higher variability in IMNF profiles on the affected side across all participants compared to the unaffected side, particularly during normalized stance.

Table 1 presents the mean IMNF values computed during normalized stance and swing for each tested muscle bilaterally during both testing sessions. The mean IMNF values computed from the TA during normalized stance on the affected side were significantly lower than the unaffected side at baseline

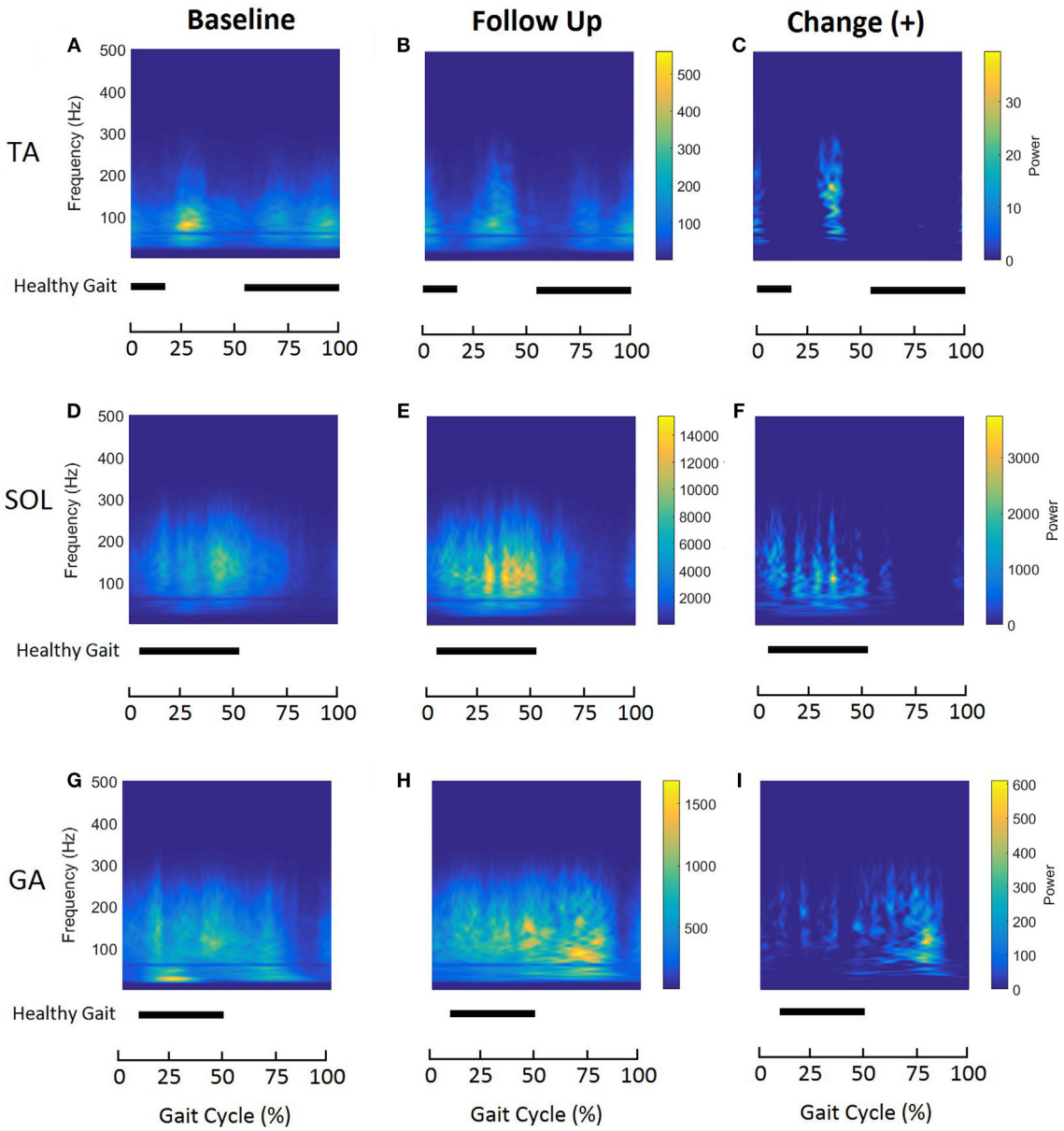

FIGURE 3 | Averaged time–frequency representations of affected tibialis anterior **(A–C)**, soleus **(D–F)**, and gastrocnemius **(G–I)** muscles during normalized gait at baseline (left column) and follow-up (middle column) for all participants ($n = 6$). The right column represents the positive changes in the distributions after follow-up. Energy levels are presented as a color bar for each muscle. Horizontal bars indicate activation (ON–OFF) for the same muscle during normalized healthy gait, reported by Perry and Burnfield (22).

($p = 0.026$) as well as follow-up ($p = 0.038$) (**Table 1**). There were no significant differences in mean IMNF for SOL and GA between affected and unaffected sides during stance (refer to **Table 1**—P_a values). The affected GA muscle showed a significant increment in the mean IMNF values during swing at follow-up ($p = 0.017$). There were no significant differences for the TA and SOL on each side during swing between baseline and follow-up (refer to **Table 1**—P_b values).

To further quantify the time–frequency distribution plots and evaluate the effect of FDS utilization on muscle activation patterns, energies contained within eleven bands, each of 25 Hz bandwidth were computed in terms of percent of total energy and compared between the two visits. In general, the highest percent of energy was contained in low frequency bands and energies decreased as the frequency in the signal increased (**Figure 5**). Of all the energy bands, band 10 (250–275 Hz) was the most consistent in showing significant changes in energies for all three muscles bilaterally during normalized stance and swing, after FDS utilization. On the affected side, the TA showed a significant decrease in energies in band 3 (75–100 Hz) during stance ($p = 0.04$) and band 4 (101–125 Hz) during swing ($p = 0.038$) at follow-up. The unaffected SOL

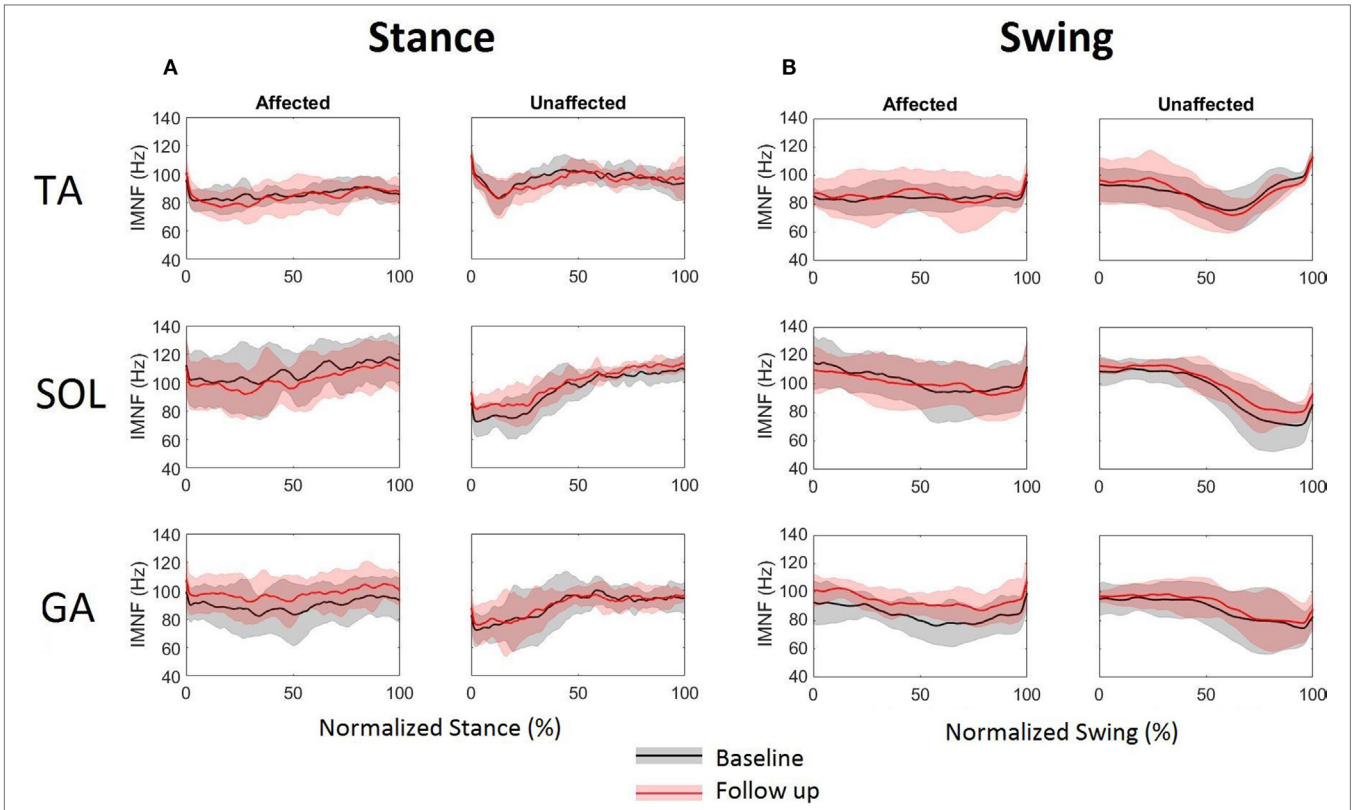

FIGURE 4 | Instantaneous mean frequency profiles extracted from time–frequency distributions of tibialis anterior, soleus, and gastrocnemius EMG for affected (left column) and unaffected (right column) sides during normalized **(A)** stance and **(B)** swing at baseline and follow-up. The solid lines represent the mean and the shaded areas represent the ±SD across six stroke participants.

TABLE 1 | Comparison of mean IMNF of TA, SOL, and GA muscles during normalized stance and swing phases of gait cycle for individuals with stroke ($n = 6$).

		Stance			Swing		
		Baseline	**Follow-up**	**P_b value**	**Baseline**	**Follow-up**	**P_b value**
TA	Affected	83. 8 (6.8)	82.6 (9.3)	0.715	82.9 (7.0)	84.5 (14.1)	0.842
	Unaffected	98.6 (6.7)	95.3 (2.8)	0.518	88.9 (8.1)	87.7 (8.4)	0.926
	P_a value	**0.026***	**0.038***		**0.366**	**0.796**	
SOL	Affected	111.2 (19.2)	102.5 (14.1)	0.451	106.2 (17.6)	100.2 (13.2)	0.867
	Unaffected	95.3 (4.7)	96.7 (8.1)	0.118	96.9 (8.5)	99.7 (3.8)	0.072
	P_a value	**0.201**	**0.713**		**0.366**	**0.847**	
GA	Affected	91.1 (11.5)	97.2 (11.7)	0.116	85.6 (8.6)	92.7 (7.9)	0.017*
	Unaffected	94.6 (18)	88.1 (9.4)	0.944	94.2 (19.8)	90.4 (8.9)	0.646
	P_a value	**0.943**	**0.084**		**0.606**	**0.476**	

P_a: p- values computed using paired t-test for comparing affected and unaffected side for each visit.
P_b: p- values computed using paired t-test for comparing baseline and follow-up visits for each side.
$^*p < 0.05$.

showed a significant increase ($p = 0.025$) in energy in band 4 (101–125 Hz) during swing. The affected GA showed a significant decrease in band 1 (25–50 Hz) during stance and showed a significant increase in energies associated with bands 2 and 3 (51–100 Hz) ($p = 0.007$ and $p = 0.034$, respectively) during swing. On the unaffected side, GA showed significant energy increments in band 2 (50–75 Hz) during stance ($p = 0.008$) as well as swing ($p = 0.03$).

DISCUSSION

Previous assessments to evaluate the efficacy of an FDS in gait retraining have focused on walking speed, spatiotemporal changes and muscle activation timings (2, 11, 12, 15, 16). The purpose of this study was to apply a wavelet-based TFA approach to assess the alterations in neuromuscular activations of TA, SOL, and GA muscles after utilization of an FDS during

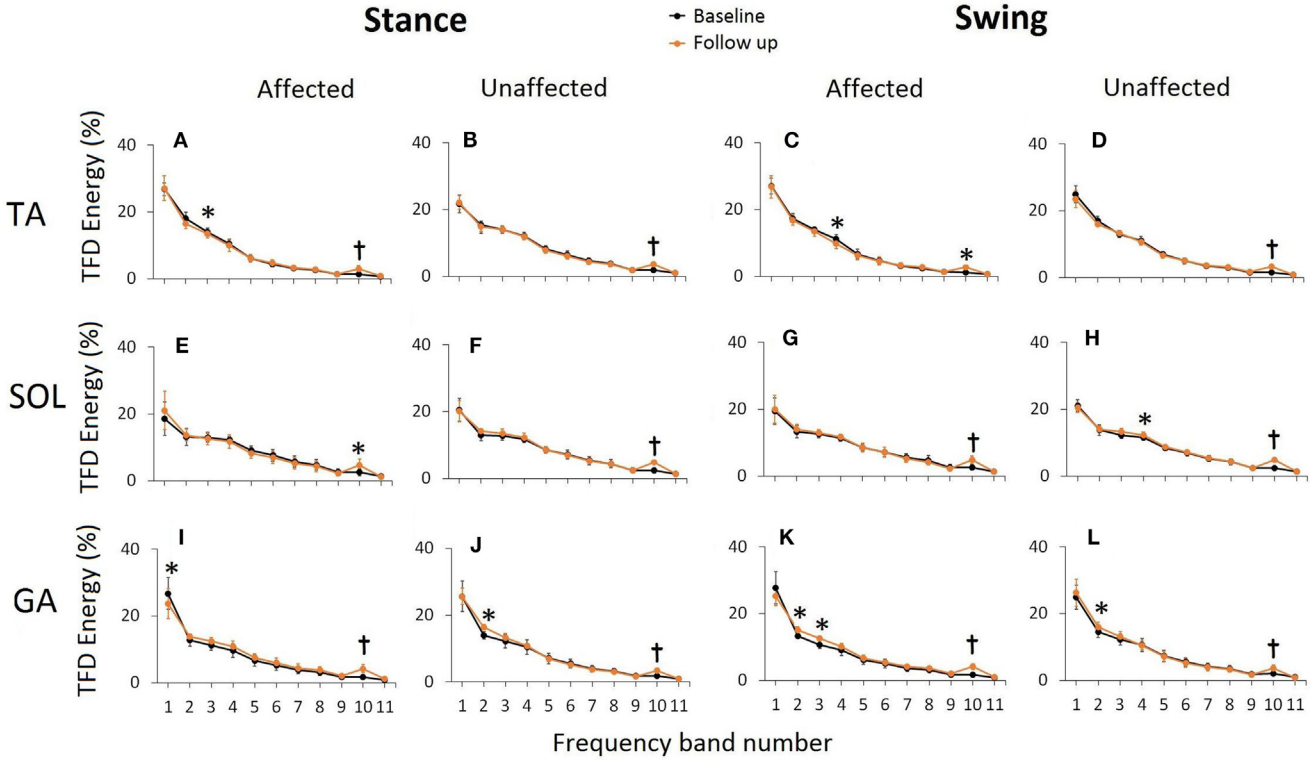

FIGURE 5 | Time frequency distribution (TFD) energies associated with 11 predefined frequency bands during normalized stance and swing at baseline and follow-up for TA **(A–D)**, SOL **(E–H)**, and GA **(I–L)**. TFD energy in each band is presented as a percentage of total TFD energy during a normalized gait averaged across six stroke participants. Error bars represent ±SD. Significant differences are shown as *($p < 0.05$) and †($p < 0.005$). The frequencies associated with the predefined bands are 1: 25–50 Hz, 2: 51–75 Hz, 3: 76–100 Hz, 4: 101–125 Hz, 5: 126–150 Hz, 6: 151–175 Hz, 7: 176–200 Hz, 8: 201–225 Hz, 9: 226–250 Hz, 10: 251–275 Hz, and 11: 276–300 Hz.

gait in individuals with stroke. FDS stimulates the common peroneal nerve which innervates the TA muscle. However, electrical stimulations are not spatially restricted to only stimulated nerves or muscles but also travel and stimulate neighboring muscles due to the electrical conductivity, interconnection within peripheral nervous system and physiological composition of muscles. Hence, although the TA received a targeted stimulation, GA and SOL are also indirectly stimulated during gait. In this study, the walking trials without FDS were used for analysis purposes to potentially examine the training or therapeutic effect of FDS utilization over the 6-month intervention period. Our results begin to demonstrate that utilization of FDS provides FES-based training not only to the TA but also to the GA and SOL muscles. As a result, the changes seen in time–frequency representations, IMNF and energies could be the training effect characterized by alterations in muscle activation patterns.

Application of CWT

Time–frequency representations of TA, SOL, and GA muscles of the affected side showed altered neuromuscular activation during normalized gait post-FDS utilization. These alterations were indicated by increase in the signal energy (for TA and SOL), shifting of localized energy content on the time and frequency axis (for GA) and presence of inhibition (for TA) during normalized gait. The TA on both sides showed energy localization below 100 Hz on the frequency axis. This could suggest that predominantly slow MUs of the TA were recruited during gait due to the neuromuscular impairment as a result of foot drop. A shift in the peak energy localization on the frequency axis (from <50 to >100 Hz) for GA muscle on the affected side could be due to the change in MU recruitment strategies (slow to fast) post-FDS usage. However, there are potentially several reasons that may cause the above changes. The increase in the energy content could be directly related to an increase in the neuromuscular activation, which could be the result of FDS-based retraining. Motor learning using FES is thought to work through the creation of positive feedback of residual myoelectric activity acting to increase long-term potentiation of the corticomuscular connection (6–8, 16). Active repetitive movement training in combination with task-specific FES (such as gait) has shown to be perhaps the most promising use of FES for the facilitation of motor recovery (8). Specifically cyclic or EMG-based FES activation that acts to promote the movement goal in combination with voluntary effort has been found to produce greater physiological and functional gains than FES alone (9). In this study, the participant used the FDS in combination with volitional efforts to perform a cyclic activity—gait that may have promoted the changes in the time–frequency domain for TA, SOL, and GA muscles.

Changes in IMNF

The spectral parameters extracted using wavelet-based analysis have shown to be associated with fatigue, muscle properties (fiber types), and MU recruitment strategies (28, 34, 35). The spectral measures such as IMNF and instantaneous median frequencies (IMDFs) have been extensively used is assessing muscle fatigue during isometric muscle contractions, as IMNF/IMDFs show a clear downward shift in frequency with respect to time as a result of fatigue (36). Furthermore, muscle fatigue may also cause decrease in signal power at high frequencies, a small increase in signal power at low frequency due to alterations in recruitment firing and conduction velocities, and synchronization of the signals (37). During normalized stance as well as swing, TA, SOL, and GA muscles of unaffected side showed distinct patterns of IMNF compared to affected side as shown in **Figure 4**. Mean IMNF values for the TA EMG during normalized stance was significantly lower for the affected side than unaffected side during baseline as well as follow-up visits. With the TA muscle being impaired due to foot drop post-stroke, the decrease in the mean IMNF could be due to impairment in recruitment of fast MU during stance. During swing, this difference was insignificant.

Affected GA muscle showed a significant increase in the mean IMNF values during swing at follow-up. This increment in mean IMNF can be correlated to the shift in peak energy localization to higher frequencies (**Figures 3H,I**) in TFD for affected GA muscle at follow-up. This could be due to either increment in recruitments of number of MUs within band 2 (51–75 Hz), band 3 (76–100 Hz), and band 10 (251–275 Hz), or increment in outputs generated by MUs of firing rates lying among bands 2, 3, and 10 or all. Although our analysis does not identify the exact MUs that underwent such alterations, it definitely identifies the frequency bands within which the alterations in recruitment strategies occurred as a result of FDS-based training in cyclic, task-specific environment such as gait.

The difference between the affected and unaffected sides was demonstrated by IMNF profiles for SOL and GA (**Figure 4**). The IMNF profiles were influenced by the dynamic movement of ankle and knee during gait. During stance, SOL and GA act as plantar flexors to "lock" the ankle so the limb and foot rotate on the forefoot rocker (22). As a result, the increase in IMNF from 0 to 60% during normalized stance for both GA and SOL on the unaffected side could not be associated with the ankle joint positional changes but may suggest the recruitment of MU in the order of slow to fast MUs. Conversely, decrease in IMNF between approximately 50 and 80% of normalized swing on the unaffected side could be related to start of the inhibition/de-recruitment of MU from the order of fast to slow MUs. It has been shown that, at the upper limit of MU recruitment, the mean or median frequencies should reach a plateau (34). This confirms with our IMNF profiles for SOL and GA on the unaffected side during normalized gait where IMNF gradually increases on EMG onset, plateaus during peak activation and subsides prior to the end of the activations.

Changes in the TFD Energies

Previously, foot orthoses have been shown to alter the energies associated with high frequency bands of lower extremity muscle activity in recreational runners (38). We found that the energies associated with the second highest frequency band of 250–270 Hz significantly increased for all tested muscles during normalized gait. There are several physiological factors such as conduction velocity of fibers within MU, shape of intracellular action potentials, number of MU recruited, MU discharge rates, and MU synchronization that may affect the generation of an EMG signal (34). Furthermore, the amplitude of the surface EMG is related to the net MU activity: the recruitment and the discharge rates of active MUs (34). As a result, the energy changes associated with a frequency band in a TFD could be related to either increase or decrease in the amplitudes of MUs with firing rates within that band or the number of MUs recruited, e.g., GA muscle on the affected side showed a significant decrease in the energies associated with low frequencies (25–50 Hz) and significant increase in energies between 50 and 100 Hz. These alterations in the MU recruitment patterns (slower to faster MUs) could be a result of post-stroke spontaneous recovery or long-term recovery due to neuroplasticity or a rehabilitation intervention that promotes motor learning and recovery. In the current investigation, the participants represent a chronic stroke population with duration since last stroke ranging from 33 to 244 months. Hence, the possibility of such alterations in MU recruitment due to spontaneous recovery is unlikely. Therefore, significant energy changes specifically between 250 and 270 Hz could suggest the effect of FDS-based intervention. It should be noted that the purpose of this investigation was not to uniquely identify the activity of individual MUs using the sEMG but to detect the alterations in spectral attributes of EMG which may suggest the changes in recruitment strategies resulting from FDS-based gait retraining.

The SD of IMNF profiles (**Figure 4**) and the TFD energy values (**Figure 5**) at the lower frequency bands (bands 1–4) showed higher variability across the participants. The variability in the EMG data and its spectral correlates across participants can be associated with variability in several factors such as affected areas of the brain, months post-stroke, and compensatory gait strategies. Another factor that may have contributed to variability in the data is FDS parameters (stimulation intensity, pulse width, stimulation frequency, and frequency of FDS use). FDS stimulation frequency ranged from 19 to 33 Hz, and pulse width ranged from 25 to 300 μs. Selection of these parameters was done by a trained clinician based on the gait cycle timing, amount of dorsiflexion needed to lift the foot, gait speed, and patient discomfort threshold. Variability in FDS parameters, FDS dosing, as well as a small sample size may have led to the lack of significant differences for mean IMNF values of affected TA and SOL.

Limitations and Future Work

The changes in EMG and its correlates bilaterally could be further explained by potentially altered spatiotemporal and kinematic parameters after FDS utilization. However, these variables were not analyzed in the current investigation. Future research will explore the relationship between CWT-based time–frequency measures, spatiotemporal parameters, and kinematic variables. The current investigation is also limited by a smaller sample

size. Future research will focus on assessing training effects of FDS-based gait intervention on a larger sample and will also include a control group to isolate the effect of FDS intervention on the spectral properties of EMG data.

CONCLUSION

This investigation demonstrates the applicability of wavelet-based TFA of EMG data to assess the neuromuscular alterations after the use of FDS during gait for individuals with chronic stroke. The changes in time–frequency distributions, IMNF, and energies may suggest the alterations in MU recruitment after FDS utilization during gait, thus further establishing the utility of FDS as a rehabilitative intervention that may promote motor recovery secondary to treating foot drop resulting from hemiplegia post-stroke.

ETHICS STATEMENT

This study was carried out in accordance with the recommendations of Kessler Foundation Institution Review Board (IRB) with written informed consent from all subjects. All subjects gave written informed consent in accordance with the Declaration of Helsinki. The protocol was approved by the Kessler Foundation's IRB Committee.

AUTHOR CONTRIBUTIONS

RP assisted in study design, data collection, performed EMG analysis, and prepared the manuscript. AR assisted with data collection, processed the motion analysis data and assisted with manuscript preparation. KN assisted in study design, data collection, data interpretation, and manuscript preparation.

ACKNOWLEDGMENTS

This work was supported by National Institutes of Health (NIH) grant (R03NS082950-01) and Kessler Foundation. The authors would like to thank Kathleen Chervin at Kessler Foundation for her valuable help in participant recruitment and data collection.

REFERENCES

1. Morone G, Fusco A, Di Capua P, Coiro P, Pratesi L. Walking training with foot drop stimulator controlled by a tilt sensor to improve walking outcomes: a randomized controlled pilot study in patients with stroke in subacute phase. *Stroke Res Treat* (2012) 2012:5. doi:10.1155/2012/523564
2. Stein RB, Everaert DG, Thompson AK, Chong SL, Whittaker M, Robertson J, et al. Long-term therapeutic and orthotic effects of a foot drop stimulator on walking performance in progressive and nonprogressive neurological disorders. *Neurorehabil Neural Repair* (2010) 24(2):152–67. doi:10.1177/1545968309347681
3. Nolan KJ, Savalia KK, Lequerica AH, Elovic EP. Objective assessment of functional ambulation in adults with hemiplegia using ankle foot orthotics after stroke. *PM R* (2009) 1(6):524–9. doi:10.1016/j.pmrj.2009.04.011
4. Nolan KJ, Yarossi M. Weight transfer analysis in adults with hemiplegia using ankle foot orthosis. *Prosthet Orthot Int* (2011) 35(1):45–53. doi:10.1177/0309364610393061
5. Nolan KJ, Yarossi M. Preservation of the first rocker is related to increases in gait speed in individuals with hemiplegia and AFO. *Clin Biomech* (2011) 26(6):655–60. doi:10.1016/j.clinbiomech.2011.03.011
6. Peckham PH, Knutson JS. Functional electrical stimulation for neuromuscular applications. *Annu Rev Biomed Eng* (2005) 7:327–60. doi:10.1146/annurev.bioeng.6.040803.140103
7. Sheffler LR, Chae J. Neuromuscular electrical stimulation in neurorehabilitation. *Muscle Nerve* (2007) 35(5):562–90. doi:10.1002/mus.20758
8. Chae J. Neuromuscular electrical stimulation for motor relearning in hemiparesis. *Phys Med Rehabil Clin N Am* (2003) 14(1 Suppl):S93–109. doi:10.1016/S1047-9651(02)00051-7
9. Daly JJ, Ruff RL. Construction of efficacious gait and upper limb functional interventions based on brain plasticity evidence and model-based measures for stroke patients. *ScientificWorldJournal* (2007) 7:2031–45. doi:10.1100/tsw.2007.299
10. Sabut SK, Lenka PK, Kumar R, Mahadevappa M. Effect of functional electrical stimulation on the effort and walking speed, surface electromyography activity, and metabolic responses in stroke subjects. *J Electromyogr Kinesiol* (2010) 20(6):1170–7. doi:10.1016/j.jelekin.2010.07.003
11. Everaert DG, Thompson AK, Chong SL, Stein RB. Does functional electrical stimulation for foot drop strengthen corticospinal connections? *Neurorehabil Neural Repair* (2010) 24(2):168–77. doi:10.1177/1545968309349939
12. Everaert DG, Stein RB, Abrams GM, Dromerick AW, Francisco GE, Hafner BJ, et al. Effect of a foot-drop stimulator and ankle-foot orthosis on walking performance after stroke: a multicenter randomized controlled trial. *Neurorehabil Neural Repair* (2013) 27:579–91. doi:10.1177/1545968313481278
13. Kottink AI, Hermens HJ, Nene AV, Tenniglo MJ, van der Aa HE, Buschman HP, et al. A randomized controlled trial of an implantable 2-channel peroneal nerve stimulator on walking speed and activity in poststroke hemiplegia. *Arch Phys Med Rehabil* (2007) 88(8):971–8. doi:10.1016/j.apmr.2007.05.002
14. Kottink AI, Oostendorp LJ, Buurke JH, Nene AV, Hermens HJ, IJzerman MJ. The orthotic effect of functional electrical stimulation on the improvement of walking in stroke patients with a dropped foot: a systematic review. *Artif Organs* (2004) 28(6):577–86. doi:10.1111/j.1525-1594.2004.07310.x
15. Pilkar R, Yarossi M, Nolan KJ. EMG of the tibialis anterior demonstrates a training effect after utilization of a foot drop stimulator. *NeuroRehabilitation* (2014) 35:299–305. doi:10.3233/NRE-141126
16. Stein RB, Chong S, Everaert DG, Rolf R, Thompson AK, Whittaker M, et al. A multicenter trial of a foot drop stimulator controlled by a tilt sensor. *Neurorehabil Neural Repair* (2006) 20(3):371–9. doi:10.1177/1545968306289292
17. Taylor PN, Burridge JH, Dunkerley AL, Wood DE, Norton JA, Singleton C, et al. Clinical use of the Odstock dropped foot stimulator: its effect on the speed and effort of walking. *Arch Phys Med Rehabil* (1999) 80(12):1577–83. doi:10.1016/S0003-9993(99)90333-7
18. Kesar TM, Perumal R, Reisman DS, Jancosko A, Rudolph KS, Higginson JS, et al. Functional electrical stimulation of ankle plantarflexor and dorsiflexor muscles: effects on poststroke gait. *Stroke* (2009) 40(12):3821–7. doi:10.1161/STROKEAHA.109.560375
19. Kesar TM, Perumal R, Jancosko A, Reisman DS, Rudolph KS, Higginson JS, et al. Novel patterns of functional electrical stimulation have an immediate effect on dorsiflexor muscle function during gait for people poststroke. *Phys Ther* (2010) 90(1):55–66. doi:10.2522/ptj.20090140
20. Kesar TM, Reisman DS, Perumal R, Jancosko AM, Higginson JS, Rudolph KS, et al. Combined effects of fast treadmill walking and functional electrical stimulation on post-stroke gait. *Gait Posture* (2011) 33(2):309–13. doi:10.1016/j.gaitpost.2010.11.019
21. De Luca CJ. The use of surface electromyography in biomechanics. *J Appl Biomech* (1997) 13:135–63. doi:10.1123/jab.13.2.135
22. Perry J, Burnfield JM. *Gait Analysis: Normal and Pathological Function*. 2nd ed. Thorofare, NJ: Slack Incorporated (2010).

23. Trinh T, Shiner CT, Thompson-Butel AG, McNulty PA. Targeted upper-limb Wii-based movement therapy also improves lower-limb muscle activation and functional movement in chronic stroke. *Disabil Rehabil* (2017) 39: 1939–49. doi:10.1080/09638288.2016.1213892
24. Huang NE, Zheng S, Long SR, Wu MC, Shih HH, Zheng Q, et al. The empirical mode decomposition and the Hilbert spectrum for nonlinear and non-stationary time series analysis. *Proc R Soc Lond* (1998) 454:903–95. doi:10.1098/rspa.1998.0193
25. Pilkar R, Yarossi M, Ramanujam A, Rajagopalan V, Bayram MB, Mitchell M, et al. Application of empirical mode decomposition combined with notch filtering for interpretation of surface electromyograms during functional electrical stimulation. *IEEE Trans Neural Syst Rehabil Eng* (2016) 25:1268–77. doi:10.1109/TNSRE.2016.2624763
26. Ismail AR, Asfour SS. Continuous wavelet transform application to EMG signals during human gait. *Conference Record of Thirty-Second Asilomar Conference on Signals, Systems and Computers*. Pacific Grove, CA. (Vol. 2), (1998).
27. Lauer RT, Stackhouse CA, Shewokis PA, Smith BT, Tucker CA, McCarthy J. A time-frequency based electromyographic analysis technique for use in cerebral palsy. *Gait Posture* (2007) 26:420–7. doi:10.1016/j.gaitpost.2006.10.015
28. Sacco ICN, Hamamoto AN, Onodera AN, Gomes AA, Weiderpass HA, Pachi CG, et al. Motor strategy patterns study of diabetic neuropathic individuals while walking – a wavelet approach. *J Biomech* (2014) 47:2475–82. doi:10.1016/j.jbiomech.2014.04.007
29. Ye Y, Garcia-Casado J, Martinez-de-Juan JL, Ponce JL. Empirical mode decomposition: a method to reduce low frequency interferences from surface electroenterogram. *Med Biol Eng Comput* (2007) 45(6):541–51. doi:10.1007/s11517-007-0189-7
30. Zhang X, Zhou P. Filtering of surface EMG using ensemble empirical mode decomposition. *Med Eng Phys* (2013) 35:537–42. doi:10.1016/j.medengphy.2012.10.009
31. Xie H, Wang Z. Mean frequency derived via Hilbert-Huang transform with application to fatigue EMG analysis. *Comput Methods Programs Biomed* (2006) 82:114–20. doi:10.1016/j.cmpb.2006.02.009
32. Hermens HJ, Freriks B, Merletti R. *European Recommendations for Surface Electromyography: Results of the Seniam Project (SENIAM)*. The Netherlands: Roessingh Research and Development (2000).
33. Bonato P, Roy SH, Knaflitz M, De Luca CJ. Time-frequency parameters of the surface myoelectric signal for assessing muscle fatigue during cyclic dynamic contractions. *IEEE Trans Biomed Eng* (2001) 47(7):745–53. doi:10.1109/10.930899
34. Farina D, Merletti R, Enoka RM. The extraction of neural strategies from the surface EMG. *J Appl Physiol* (2004) 96:1486–95. doi:10.1152/japplphysiol.01070.2003
35. Wakeling JM. Patterns of motor recruitment can be determined using surface EMG. *J Electromyogr Kinesiol* (2009) 19:199–207. doi:10.1016/j.jelekin.2007.09.006
36. Pascal Coorevits P, Danneels L, Cambier D, Ramon H, Druyts H, Karlsson JS, et al. Test-retest reliability of wavelet- and Fourier based EMG (instantaneous) median frequencies in the evaluation of back and hip muscle fatigue during isometric back extensions. *J Electromyogr Kinesiol* (2008) 18:798–806. doi:10.1016/j.jelekin.2007.01.007
37. Phinyomark A, Thongpanja S, Hu H, Phukpattaranont P, Limsakul C. The usefulness of mean and median frequencies in electromyography analysis. In: Naik G, editor. *Computational Intelligence in Electromyography Analysis – A Perspective on Current Applications and Future Challenges*. InTech (2012). doi:10.5772/3315
38. Mündermann A, Wakeling JM, Nigg BM, Humble RN, Stefanyshyn DJ. Foot orthoses affect frequency components of muscle activity in the lower extremity. *Gait Posture* (2006) 23:295–302. doi:10.1016/j.gaitpost.2005.03.004

Conflict of Interest Statement: The authors declare that the research was conducted in the absence of any commercial or financial relationships that could be construed as a potential conflict of interest.

The reviewer, CD, and handling editor declared their shared affiliation.

frontiers in Neurology

ORIGINAL RESEARCH
published: 28 July 2017
doi: 10.3389/fneur.2017.00340

A Longitudinal Electromyography Study of Complex Movements in Poststroke Therapy. 1: Heterogeneous Changes Despite Consistent Improvements in Clinical Assessments

*Negin Hesam-Shariati[1,2], Terry Trinh[1,2], Angelica G. Thompson-Butel[1,2], Christine T. Shiner[1,2] and Penelope A. McNulty[1,2]**

[1] Neuroscience Research Australia, Sydney, NSW, Australia, [2] School of Medical Science, University of New South Wales, Sydney, NSW, Australia

OPEN ACCESS

Edited by:
Cliff Klein, Guangdong Provincial Work Injury Rehabilitation Center, China

Reviewed by:
Valerie Moyra Pomeroy, University of East Anglia, United Kingdom
Carlo Trompetto, Università di Genova, Italy

***Correspondence:**
Penelope A. McNulty
p.mcnulty@neura.edu.au

Specialty section:
This article was submitted to Stroke, a section of the journal Frontiers in Neurology

Received: *20 March 2017*
Accepted: *29 June 2017*
Published: *28 July 2017*

Citation:
Hesam-Shariati N, Trinh T, Thompson-Butel AG, Shiner CT and McNulty PA (2017) A Longitudinal Electromyography Study of Complex Movements in Poststroke Therapy. 1: Heterogeneous Changes Despite Consistent Improvements in Clinical Assessments. Front. Neurol. 8:340. doi: 10.3389/fneur.2017.00340

Poststroke weakness on the more-affected side may arise from reduced corticospinal drive, disuse muscle atrophy, spasticity, and abnormal coordination. This study investigated changes in muscle activation patterns to understand therapy-induced improvements in motor-function in chronic stroke compared to clinical assessments and to identify the effect of motor-function level on muscle activation changes. Electromyography (EMG) was recorded from five upper limb muscles on the more-affected side of 24 patients during early and late therapy sessions of an intensive 14-day program of Wii-based Movement Therapy (WMT) and for a subset of 13 patients at 6-month follow-up. Patients were classified according to residual voluntary motor capacity with low, moderate, or high motor-function levels. The area under the curve was calculated from EMG amplitude and movement duration. Clinical assessments of upper limb motor-function pre- and post-therapy included the Wolf Motor Function Test, Fugl-Meyer Assessment and Motor Activity Log Quality of Movement scale. Clinical assessments improved over time ($p < 0.01$) with an effect of motor-function level ($p < 0.001$). The pattern of EMG change by late therapy was complex and variable, with differences between patients with low compared to moderate or high motor-function levels. The area under the curve ($p = 0.028$) and peak amplitude ($p = 0.043$) during Wii-tennis backhand increased for patients with low motor-function, whereas EMG decreased for patients with moderate and high motor-function levels. The reductions included movement duration during Wii-golf ($p = 0.048$, moderate; $p = 0.026$, high) and Wii-tennis backhand ($p = 0.046$, moderate; $p = 0.023$, high) and forehand ($p = 0.009$, high) and the area under the curve during Wii-golf ($p = 0.018$, moderate) and Wii-baseball ($p = 0.036$, moderate). For the pooled data over time, there was an effect of motor-function ($p = 0.016$) and an interaction between time and motor-function ($p = 0.009$) for Wii-golf movement duration. Wii-baseball movement duration decreased as a function of time ($p = 0.022$). There

was an effect on Wii-tennis forehand duration for time ($p = 0.002$), an interaction of time and motor-function ($p = 0.005$) and an effect of motor-function level on the area under the curve ($p = 0.034$) for Wii-golf. This study demonstrated different patterns of EMG changes according to residual voluntary motor-function levels, despite heterogeneity within each level that was not evident following clinical assessments alone. Thus, rehabilitation efficacy might be underestimated by analyses of pooled data.

Keywords: muscle activation, movement duration, motor-function, upper limb, rehabilitation, chronic stroke

INTRODUCTION

Motor impairment is the most common outcome after stroke (1–4) and is predominately attributed to muscle weakness (5–7) as a consequence of reduced corticospinal drive (8), disuse muscle atrophy (9, 10), impaired voluntary control of muscles (11, 12), spasticity (13–16), and impaired muscle coordination (17–19). These factors, either in isolation or combination, result in abnormal muscle activation during voluntary movements (20–22). Multifactorial contributions to impaired upper limb motor-function are more common than in the lower limb (23, 24) and a more important focus for improving independence in activities of daily living (25, 26). Poststroke upper limb recovery may be slower and more complicated than that of the lower limb, given that upper limb tasks are typically more complex involving more degrees of freedom in multi-joint movements (27, 28).

Recovery after stroke is a complex combination of spontaneous neurological mechanisms and relearning processes (28–30). It is commonly thought that learning-dependant mechanisms are only operative during natural recovery and interact with therapeutic interventions (31, 32). Furthermore, true recovery is thought to be complete between 4 and 10 weeks poststroke (31, 33) or reaches a plateau over 6 months (30–32, 34). It has been speculated that any improvement in the chronic period is not true improvement, but rather a restitution of therapy gains made earlier and lost over time (35). Despite this, significant improvements are possible in chronic stroke, but motor-function in this period needs intensive rehabilitation for continued improvements (1, 22, 36).

Clinical motor assessment both after stroke and with rehabilitation is traditionally based on task completion with limited assessment of movement quality (26, 37–39). Most assessments are qualitative with subjective and categorical scoring and many suffer from ceiling and floor effects (40). To provide more objective and quantitative measures, recent studies have examined muscle activation and joint kinematics to evaluate poststroke motor outcomes; yet, most upper limb studies consist of simple tracking tasks (41–43) or reaching movements (27, 34, 44, 45) constrained in time and space.

In this study, electromyography (EMG) analysis was used in addition to clinical assessments to provide quantitative measures of outcomes with therapy in chronic stroke. The aim of this study was to examine changes in muscle activation (EMG) with an intensive 14-day program of Wii-based Movement Therapy Wii-based Movement Therapy to investigate the mechanisms underlying therapy-induced motor improvements. Wii-based Movement Therapy is the equivalent of current best practice in upper limb stroke rehabilitation, Constraint-induced Movement Therapy (46). The stability of motor-function improvements and changes in EMG during therapy were assessed *via* a longitudinal comparison to 6-month follow-up. We hypothesized that there would be distinct patterns of change in EMG and that these would vary according to the level of residual voluntary motor capacity and correlate with improvements in motor-function quantified using clinical assessments.

MATERIALS AND METHODS

Participants

The data from 30 patients with chronic stroke (i.e., ≥3 months poststroke) were included in this study from those previously recorded from patients consecutively recruited from St. Vincent's and Prince of Wales Hospitals, Sydney, for concurrent studies of Wii-based Movement Therapy (**Figure 1**). The level of residual voluntary motor-function was classified pre-therapy for each patient as low, moderate, or high based on performance of the Box and Block Test of gross manual dexterity and the grooved pegboard test of fine manual dexterity; patients unable

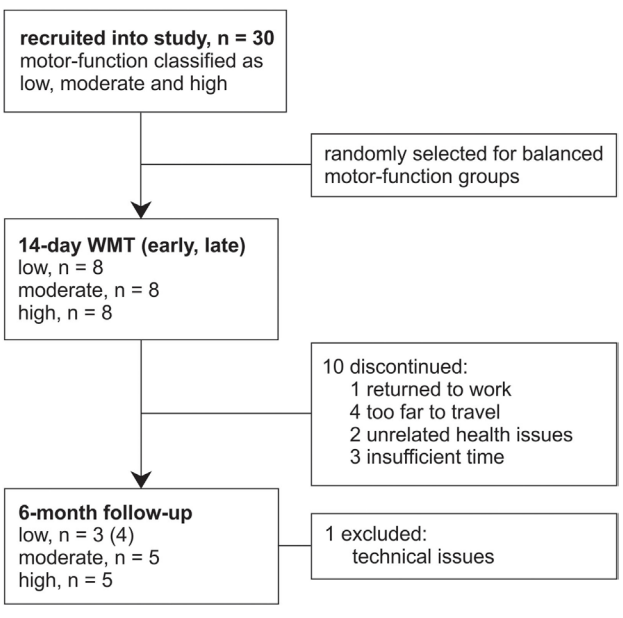

FIGURE 1 | Flow of patients through this study. Patients were recruited from concurrent studies of Wii-based Movement Therapy (WMT) for this data analysis.

to move >1 block in Box and Block Test were classified with low motor-function, those able to move >1 block but unable to complete the pegboard test were classified with moderate motor-function, and those who could complete the pegboard test were classified with high motor-function (47). Thirteen patients were classified with low, nine patients were classified with moderate, and eight patients were classified with high motor-function. To ensure balanced groups, the data for all eight patients with high motor-function were included and the data for eight patients were randomly selected using a computer-generated algorithm from each group of patients with low and moderate motor-function. The data analysis reported here has not been published previously although the clinical assessment data for all patients have been. Twenty patients were included in other Wii-based Movement Therapy trials investigating cardiovascular fitness (48), lower-limb symmetry (25), and motor-function measures (40); 9 patients were included in a randomized-controlled trial comparing Wii-based Movement Therapy and modified Constraint-induced Movement Therapy (46); and 20 patients were also included in a genotype study (49). The inclusion criteria for this study were as follows: unilateral stroke with a contralesional upper limb deficit; ≥3 months poststroke; English communication; ≥10° of voluntary movement in at least one digit of the more-affected hand; age ≥18 years; medically stable; carer available during home practice; and cognitive competency measured as a Mini-Mental State Examination score of ≥24. Exclusion criteria included co-morbidities significantly affecting upper limb sensorimotor function, unstable blood pressure, frail skin that prevented sensor placement and adhesion during recordings, and concurrent formal upper limb therapy. Demographics and baseline characteristics are listed in **Table 1**. All patients gave signed informed consent to the studies, which were approved by St. Vincent's Hospital Human Research Ethics Committee, Sydney, and conducted in accordance with the Declaration of Helsinki. All patients were enrolled in a standardized 14-day program of Wii-based Movement Therapy. No attempt was made to control for activities after this period and prior to the 6-month follow-up, although suggestions were made to each patient on how they might best maintain therapy-induced gains. A follow-up session was conducted for all available patients, i.e., a subset of 13 patients at 6-months post-therapy (3 low, 5 moderate, and 5 high motor-function levels). As shown in **Figure 1**, 10 patients were unavailable, 1 patient returned to work, 4 patients had moved interstate or overseas, 2 patients had unrelated health problems, 3 patients had insufficient time for neurophysiological recordings, and the data for 1 patient was lost due to technical issues.

Therapy

The standardized 14-day Wii-based Movement Therapy program targeted movement quality of the more-affected arm and independence in everyday activities (46, 50). Therapy consists of 1-h formal sessions with an Accredited Exercise Physiologist on 10 consecutive weekdays with increasing prescribed home practice starting on day 2 (see **Figure 2A**). Wii-based Movement Therapy uses the Nintendo Wii and Wii-Sports games (Nintendo, Japan) of golf, baseball, bowling, tennis, and boxing as a rehabilitation tool in a structured protocol that can be individually tailored to the level of motor-function and progress of each patient (46, 51). Patients used only the more-affected upper limb during therapy activities. When unavoidable, assistance was provided either with the less-affected hand or by the therapist. Game performance was recorded during formal sessions, but the scores were used only for motivational purposes and were not the focus of therapy.

EMG Recording

Surface EMG data were recorded during formal Wii-based Movement Therapy sessions at two time-points *during* therapy, i.e., at early (day 2–3) and late (between days 12 and 14) therapy; and for a subset of patients at 6-month follow-up. The EMG was not recorded on day 1 to avoid overwhelming patients as they became familiar with the therapy, the device and the therapist. Recordings were made using wireless telemetry sensors (Trigno, Delsys, USA) placed on the following muscles of the more-affected upper limb: deltoid medius (DM), biceps brachii (BB), flexor carpi radialis (FCR), extensor carpi radialis (ECR), and first dorsal interosseous (FDI). Each sensor employs four silver bar electrodes in two pairs with an interelectrode pair distance of 10 mm. Each sensor is optimized for detecting the maximum EMG signal in an orientation perpendicular to the muscle fibers. The small interelectrode distance helps to minimize crosstalk from adjacent muscles. EMG signals were filtered between 20

TABLE 1 | Baseline patient characteristics.

Motor-function level	Low	Moderate	High	All	
N	8	8	8	24	
Age	59.1 ± 13.9	55.1 ± 11.3	59.4 ± 12.2	57.9 ± 12.1	Range (37–80)
Sex (F/M)	4/4	2/6	2/6	8/16	
More-affected dominant (Y/N)	1/7	3/5	3/5	7/17	
Stroke type (isch/haem)	3/5	7/1	6/2	16/8	
Time poststroke (months)	33.3 ± 9.4	27.3 ± 8.0	19.6 ± 4.5	26.7 ± 4.3	Range (3–88)
Baseline WMFT-tt (s)	81.6 ± 6.9	26.5 ± 10.4	6.3 ± 2.6	38.1 ± 7.8	
Baseline FMA (/66)	25.3 ± 3.4	53.1 ± 3.0	61.6 ± 1.5	46.7 ± 3.6	
Baseline MALQOM (/150)	18.9 ± 11.2	60.0 ± 14.3	101.5 ± 14.7	60.1 ± 8.7	

Age is reported as mean ± SD, remaining data are reported as mean ± SE. More-affected dominant indicates that the more-affected side is the dominant side.
Isch, ischemic; haem, hemorrhage; WMFT-tt, mean time for the Wolf Motor Function-timed tasks where a lower time indicates better motor-function; FMA, upper limb motor Fugl-Meyer Assessment; MALQOM, Motor Activity Log Quality of Movement scale.

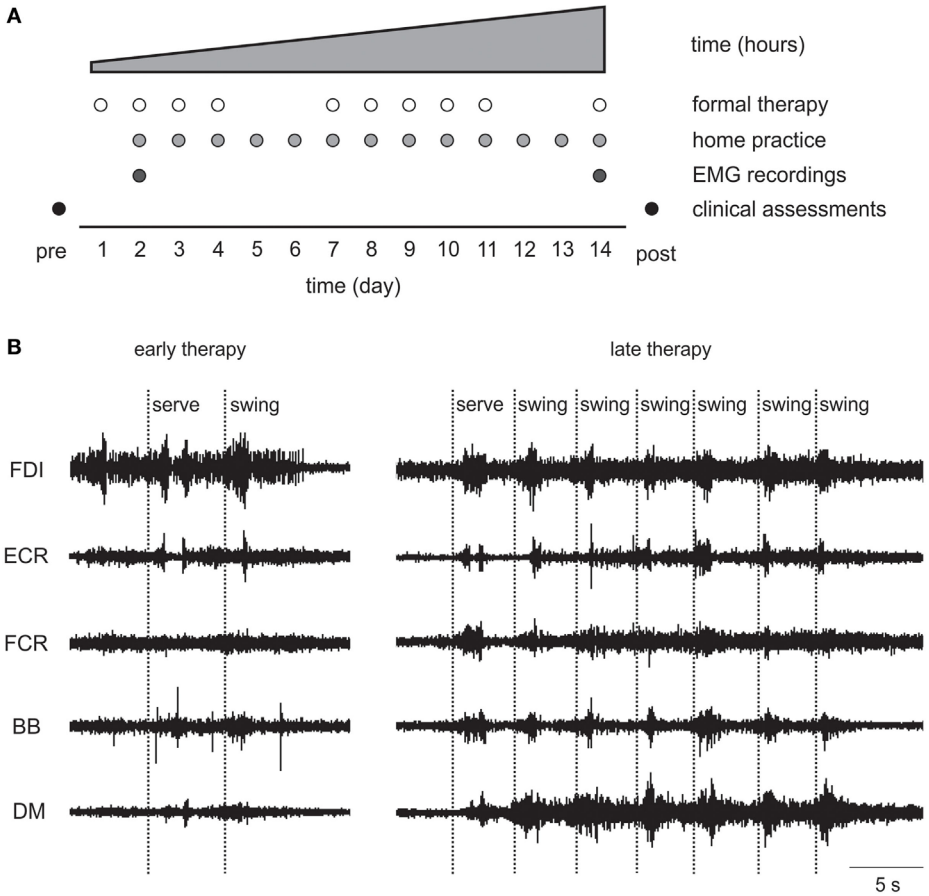

FIGURE 2 | **(A)** Wii-based Movement Therapy (WMT) protocol showing electromyography (EMG) recordings on days 2 and 14. **(B)** Single patient raw EMG at early and late therapy for a 68-year-old female, 46 months poststroke with low motor-function during Wii-tennis. FDI, first dorsal interosseous; ECR, extensor carpi radialis; FCR, flexor carpi radialis; BB, biceps brachii; DM, deltoid medius.

and 450 Hz, amplified 300 times, sampled at 2 kHz at the source in EMGworks (Delsys, USA), and then analyzed using custom scripts in Spike2 software (CED, UK).

To maximize consistency across patients and sessions, the sensors were placed on the most prominent portion of the muscle belly based on manual palpation during a weak voluntary contraction. Each recording session was preceded by a calibration sequence that consisted of three conditions each held for at least 3 s with the limb segment: (1) supported at rest, (2) unsupported against gravity, and (3) unsupported with the addition of a 1 kg weight placed across the distal joint (51).

Primary Outcome Measures

Electromyography data were analyzed for movement duration, averaged peak amplitude, and the area under the curve for stereotypical movements of each activity using custom scripts in Spike2 software (CED, UK). Movement duration, peak amplitude, and area under the curve were averaged for 10 consecutive swings of Wii-golf, -baseball, -tennis forehand, and -tennis backhand of each patient at early and late therapy and for a subset of patients at 6-month follow-up. Wii-tennis forehand and backhand swings were analyzed separately due to the need for distinctly different movement patterns. Wii-bowling data were not analyzed as patients with low motor-function could not coordinate the necessary button press, and the speed of Wii-boxing movements particularly for patients with high motor-function was too fast to enable unambiguous movement identification. Therapy was completed standing for all patients except one (moderate) during Wii-tennis at early therapy due to fatigue.

Secondary Outcome Measures

Upper limb motor-function was assessed using the Wolf Motor Function Test-timed tasks (WMFT-tt) (39) and the upper limb motor Fugl-Meyer Assessment (FMA) (37). The Motor Activity Log Quality of Movement scale (MALQOM) (26) was used to assess independence in activities of daily life. Additionally, the modified Ashworth Scale (52) was used as a clinical measure of muscle resistance at the shoulder, elbow (53), and wrist (54). These clinical tests were measured for all patients immediately pre- (baseline) and post-therapy and for a subset of 13 patients at 6-month follow-up. The clinical assessments were unrelated to the content of therapy.

Although the primary goal of therapy was quality of movement and not game performance, the scores of Wii-golf, -baseball, and -tennis games were recorded during therapy. In Wii-golf, the aim was to successfully land the ball in the hole and each success was noted, while Wii-baseball and -tennis swings were scored when the ball was hit, regardless of whether the hit was successful or not according to the rules of each game.

Data Analysis

Data analysis for this study was conducted by an independent assessor who was not involved in clinical assessments or therapy delivery. We have used the terms early therapy and late therapy to refer to EMG data recorded during formal therapy sessions and pre- and post-therapy to refer to assessments made using clinical tools prior to and following the therapy protocol.

The EMG data were detrended (DC removed), and root mean square (RMS) processed using a sliding 50 ms window. The mean baseline EMG was measured over 2–3 s prior to the commencement of each activity at rest and then subtracted from the EMG signal. High definition video recordings were used to match the EMG signal to therapy movements. Due to the heterogeneous patterns of motor control and impairment between patients and sports, EMG analysis was targeted to the dominant EMG signal for each patient. Proximal muscles (DM/BB) were primarily analyzed. However, if proximal muscles were silent or tonically active with no phasic activity, and clear task-related activity was evident in a distal muscle (FDI, ECR, or FCR), the distal muscle was used. For example, proximal muscle signals were analyzed in Wii-golf and -tennis except for three and two patients, respectively. In Wii-baseball, the distal muscle signals were more distinct compared to proximal muscles in most patients. For consistency, distal muscle signals were analyzed in Wii-baseball where possible. The same muscle was analyzed for each patient at each time-point.

To identify the onset and offset of therapy movements, a threshold level was set at 5 SD above the mean baseline EMG for each activity of each patient. The movement duration was measured as the interval between the onset and offset of movement; the peak amplitude of each movement was averaged over a 50 ms interval around the absolute peak EMG; and the area under the curve was defined as the area above the baseline level between the onset and offset of the RMS-processed EMG. Both peak amplitude and area under the curve were normalized to the *weighted* condition of the calibration sequence to enable comparison between patients.

Statistical Analysis

Data were compared for each motor-function group (low, moderate, and high) from early to late therapy (EMG analysis), or pre- to post-therapy (clinical measures) using paired *t*-tests for normally distributed data and reported as mean and SE; otherwise using Wilcoxon signed-rank tests, reported as median and interquartile range.

Longitudinal data were analyzed using mixed models of repeated measures with factors of motor-function (low, moderate, and high) and time (pre-therapy/early therapy, post-therapy/late therapy, and 6-month follow-up). Linear mixed models provide unbiased estimates for the missing data (55) at 6-month follow-up and are more powerful and flexible (56, 57) than repeated measures ANOVA in the presence of multiple missing data points because of the emphasis on the pattern of change rather than the quantitative difference (57).

The relationship between the change in area under the curve and clinical assessments was investigated using Spearman's rank-order correlation with Bonferroni corrections for multiple comparisons. Statistical analyses were conducted in SPSS 23 software (IBM, USA), and differences were considered significant when $p < 0.05$.

RESULTS

All patients completed all formal therapy sessions, home practice, and clinical assessments; 10 patients were unavailable for 6-month follow-up (**Figure 1**). Data are reported at early and late therapy for Wii-golf putting ($n = 23$), -baseball swing ($n = 24$), and -tennis forehand and backhand ($n = 23$). The same activities at follow-up are reported for 12, 13, and 12 patients, respectively. Data could not be analyzed during therapy for Wii-golf for one patient (with moderate motor-function) due to tonic muscle activity and during Wii-tennis for another patient (low motor-function) with limited shoulder movement that prevented this activity. No adverse events were reported, either minor or major.

Changes in EMG as a Consequence of Therapy (Early to Late Therapy)

Changes in the area under the curve, movement duration, and peak amplitude of muscle activation from early to late therapy for different Wii-activities are listed in **Table 2** and illustrated in **Figure 3**. For Wii-golf putting, the movement duration decreased significantly for patients with moderate ($p = 0.048$) and high motor-function levels ($p = 0.026$); area under the curve was also reduced for patients with moderate motor-function ($p = 0.018$). The movement duration of Wii-baseball swings showed a trend toward decreasing for patients with low motor-function ($p = 0.050$), while there was a reduction in the area under the curve for the patients with moderate motor-function ($p = 0.036$). The movement duration of Wii-tennis forehand ($p = 0.009$) and backhand ($p = 0.023$) decreased for patients with high motor-function by late therapy. Moreover, the movement duration of Wii-tennis backhand decreased ($p = 0.046$) for patients with moderate motor-function. The area under the curve ($p = 0.028$) and peak amplitude ($p = 0.043$) increased for patients with low motor-function during backhand swings, while the area under the curve ($p = 0.050$) showed a reduction trend for patients with high motor-function.

Changes in EMG over Time (Early Therapy, Late Therapy, and Follow-up)

Linear mixed models demonstrated an effect of motor-function during Wii-golf ($p = 0.009$) and an interaction between time and motor-function ($p = 0.016$) for movement duration. Wii-baseball movement duration changed as a function of time ($p = 0.022$). Wii-tennis forehand swing movement duration demonstrated

TABLE 2 | Therapy-induced electromyography changes from early to late therapy for patients with low, moderate, and high motor-function levels.

	Low early	Low late	*p* Value	Mod early	Mod late	*p* Value	High early	High late	*p* Value
Wii-golf putting	***n* = 8**	***n* = 8**		***n* = 7**	***n* = 7**		***n* = 8**	***n* = 8**	
Area under the curve (mV.s/mV; median, IQR)	2.24 (1.76–4.96)	3.26 (2.05–7.27)	0.401	2.36 (1.80–7.00)	1.75 (0.64–2.02)	**0.018**	2.13 (1.35–3.12)	1.48 (1.01–1.86)	0.161
Movement duration (s; mean ± SE)	3.32 ± 0.39	3.83 ± 1.02	0.600	3.08 ± 0.47	2.18 ± 0.47	**0.048**	2.23 ± 0.26	1.89 ± 0.19	**0.026**
Peak amplitude (mV/mV; median, IQR)	1.53 (1.21–3.86)	2.00 (1.21–7.09)	0.674	1.77 (1.31–3.57)	1.98 (1.29–2.23)	0.612	2.28 (1.31–3.08)	1.71 (1.31–2.68)	0.327
Wii-baseball swing	***n* = 8**	***n* = 8**		***n* = 8**	***n* = 8**		***n* = 8**	***n* = 8**	
Area under the curve (mV.s/mV; median, IQR)	1.41 (1.33–1.76)	1.40 (1.30–1.72)	1.000	3.09 (1.30–8.90)	1.85 (0.90–3.26)	**0.036**	1.87 (0.84–4.78)	2.11 (0.49–4.16)	0.123
Movement duration (s; mean ± SE)	0.78 (0.64–1.08)	0.69 (0.57–0.82)	*0.050*	1.31 ± 0.26	1.01 ± 0.17	*0.095*	0.75 ± 0.15	0.73 ± 0.11	0.662
Peak amplitude (mV/mV; median, IQR)	1.49 (1.40–1.55)	1.36 (1.28–1.55)	0.263	6.17 (1.87–12.39)	4.77 (2.17–12.18)	0.575	5.46 (3.58–15.58)	5.72 (2.20–12.44)	0.123
Wii-tennis forehand	***n* = 7**	***n* = 7**		***n* = 8**	***n* = 8**		***n* = 8**	***n* = 8**	
Area under the curve (mV.s/mV; median, IQR)	2.72 (2.20–3.57)	3.95 (2.51–5.02)	*0.091*	2.57 (1.92–4.20)	3.51 (2.11–5.13)	*0.093*	2.10 (1.48–3.82)	1.96 (1.27–3.00)	0.123
Movement duration (s; mean ± SE)	1.81 ± 0.25	1.90 ± 0.34	0.869	1.85 ± 0.18	1.94 ± 0.20	0.682	2.03 ± 0.23	1.55 ± 0.20	**0.009**
Peak amplitude (mV/mV; median, IQR)	3.90 (2.27–5.42)	4.10 (3.04–6.56)	0.128	2.49 (1.69–4.48)	4.16 (2.90–9.24)	*0.093*	2.75 (2.13–5.83)	3.01 (1.74–7.21)	0.401
Wii-tennis backhand	***n* = 7**	***n* = 7**		***n* = 8**	***n* = 8**		***n* = 8**	***n* = 8**	
Area under the curve (mV.s/mV; median, IQR)	1.71 (1.40–3.12)	3.32 (2.30–5.19)	**0.028**	3.33 (1.82–5.39)	3.41 (1.54–5.71)	0.575	3.30 (2.21–6.07)	2.62 (2.06–3.78)	*0.050*
Movement duration (s; mean ± SE)	1.54 ± 0.25	1.65 ± 0.19	0.862	1.87 ± 0.15	1.64 ± 0.09	**0.046**	1.76 ± 0.13	1.48 ± 0.15	**0.023**
Peak amplitude (mV/mV; median, IQR)	2.57 (1.75–5.33)	4.27 (2.75–7.13)	**0.043**	3.75 (3.00–5.38)	5.29 (4.02–10.12)	*0.069*	4.47 (4.00–13.21)	4.92 (3.37–5.67)	0.123

Significant changes are highlighted in bold, and trends in italics.
Mod, moderate; early, early therapy; late, late therapy; IQR, interquartile range.

an effect of time ($p = 0.002$) and an interaction of time and motor-function ($p = 0.005$). In addition, the pattern of change for Wii-tennis backhand movement duration over time showed a non-significant trend ($p = 0.059$). For Wii-golf area under the curve, there was an effect of the level of motor-function ($p = 0.034$), with a non-significant trend for an interaction between time and motor-function ($p = 0.072$). Finally, there was a non-significant trend for the effect of time on Wii-baseball area under the curve ($p = 0.070$).

Changes in Clinical Assessments with Therapy (Pre- to Post-Therapy)

Clinical assessment data showed improvements from pre- to post-therapy for the pooled data ($n = 24$) for WMFT timed tasks ($p = 0.004$), FMA ($p = 0.001$) and MALQOM ($p < 0.001$). There were no changes in Ashworth scores at wrist ($p = 0.355$), elbow ($p = 0.796$), or shoulder ($p = 0.592$) at post-therapy. The detailed results for each level of motor-function are presented in **Figure 4**.

Changes in Clinical Assessments over Time (Pre-Therapy, Post-Therapy, and Follow-up)

Linear mixed models demonstrated improvement over time for WMFT-tt ($p = 0.008$), FMA ($p = 0.001$), and MALQOM ($p < 0.001$). There was an effect of the level of motor-function for the WMFT-tt, FMA, and MALQOM ($p < 0.001$ for all).

Game Performance

Game performance improved from early to late therapy. The successful Wii-golf swings (landing the ball in the hole) increased by 30.7% ($p = 0.004$). The number of Wii-baseball hits increased by 51.5% ($p < 0.001$), while the combined Wii-tennis forehand and backhand hits increased by 91.5% ($p = 0.012$). The increase in game scores was sustained at 6-month follow-up with significant improvements over time for Wii-golf ($p = 0.004$), -baseball ($p < 0.001$), and -tennis ($p = 0.022$).

Qualitative EMG Observations

As detailed earlier, EMG data demonstrated therapy-induced changes particularly for patients with low motor-function. Qualitative observations included that the EMG signal from muscles with prolific single motor unit activity became more compound by late therapy indicating increased motor unit recruitment; tonic activity became more phasic; and there were more distinct and task-related bursts of EMG in more muscles (see **Figure 2B**).

Relationship between Changes in EMG and Clinical Assessments

The correlation between therapy-induced changes in clinical motor assessments (WMFT-tt, FMA, and MALQOM) and the changes in EMG parameters (of Wii-golf, -baseball, -forehand, and -backhand) were examined. For the pooled data, there was no relationship between the change in the clinical assessments

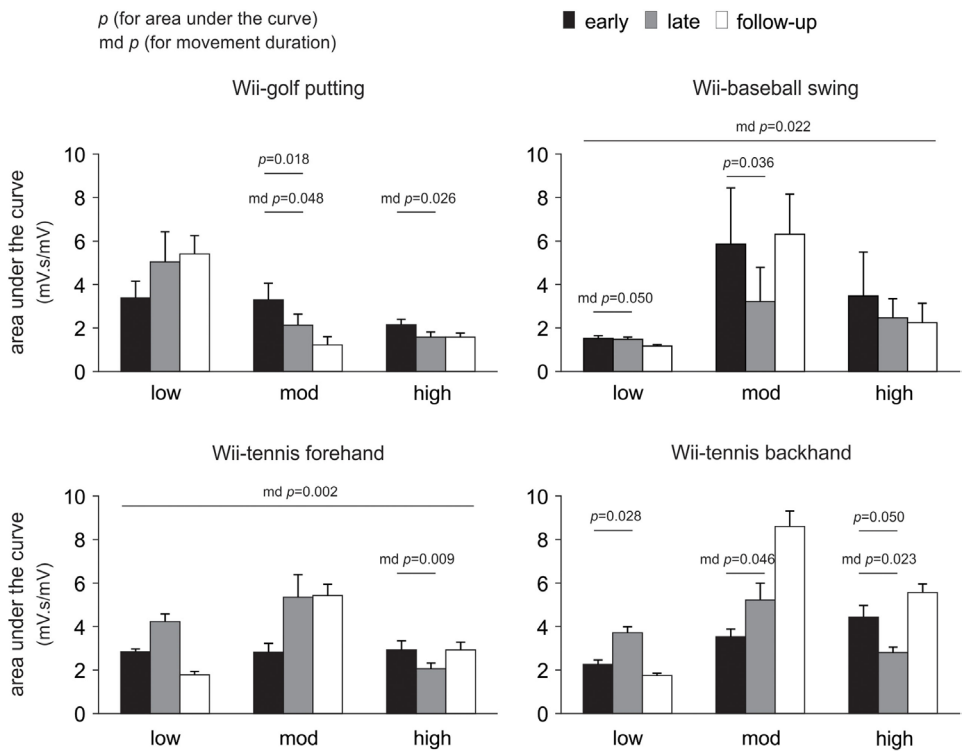

FIGURE 3 | Pooled data showing changes in electromyography over time. Changes are presented as mean ± SE for the area under the curve according to the level of poststroke motor-function. Significant changes in movement duration (md) are also indicated.

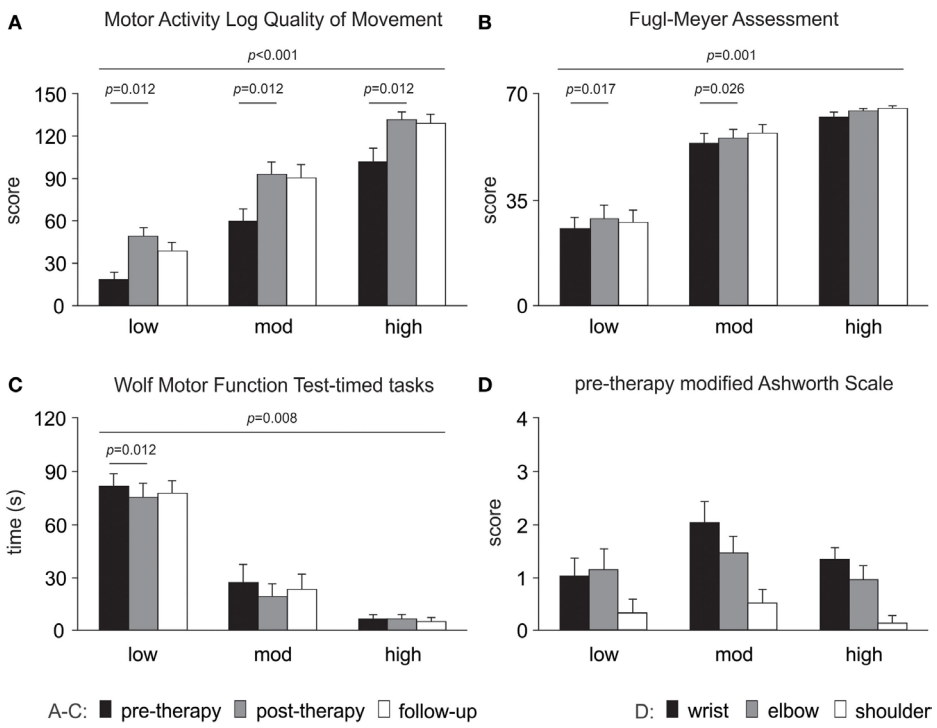

FIGURE 4 | Changes in clinical assessments over time. Significant changes are evident for **(A)** Motor Activity Log Quality of Movement scale, **(B)** upper limb motor Fugl-Meyer Assessment and **(C)** Wolf Motor Function Test-timed tasks (note a decrease in time reflects improved performance). **(D)** Modified Ashworth Scale pre-therapy (baseline) data are presented as there were no changes over time. All data are presented as mean ± SE.

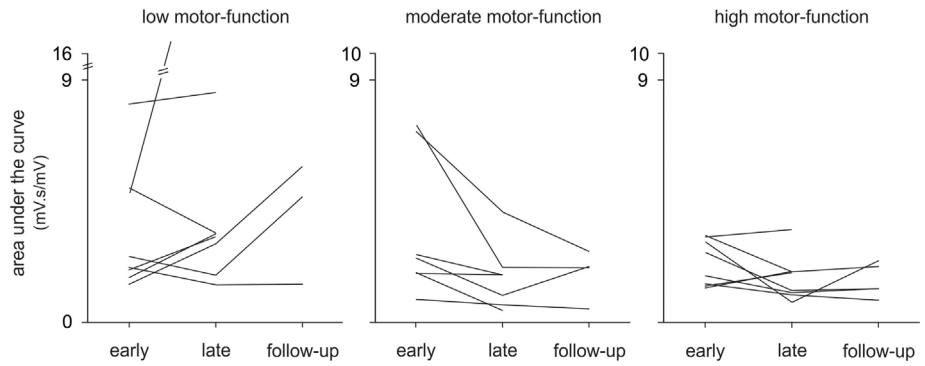

FIGURE 5 | Changes in electromyography over time, individual patient data. The mean area under the curve is shown for each patient (n = 24) with low, moderate, and high motor-function levels at early and late therapy and for a subset of patients (n = 13) at 6-month follow-up during Wii-golf putting.

and the change in area under the curve of each activity ($r < 0.39$, $p > 0.18$ for all comparisons) and the change in movement duration of the same activities ($r < 0.20$, $p > 0.90$ for all comparisons). Furthermore, within each level of motor-function, no relationship was found either for area under the curve (low: $r < 0.45$, $p > 0.78$; moderate: $r < 0.71$, $p > 0.14$; high: $r < 0.54$, $p > 0.50$), or movement duration (low: $r < 0.73$, $p > 0.12$; moderate: $r < 0.62$, $p > 0.30$), with the single exception of a significant correlation that was found between the change in Wii-baseball movement duration and clinical assessments in patients with high motor-function ($r = -0.81$, $p = 0.048$).

DISCUSSION

In this study, we investigated changes in upper limb muscle activation to gain greater insight into the neurophysiological mechanisms of improved motor-function in a heterogeneous stroke cohort from early to late therapy and with a subset of patients at 6-month follow-up. To the best of our knowledge, this study is the first longitudinal analysis of upper limb EMG *during* therapy in chronic stroke. Moreover, the movements we studied were largely unconstrained in time and space with no experimentally pre-defined start- or end-points. Although all patients made significant improvements on clinical assessments, and muscle activation changed with therapy, contrary to our hypothesis, there was no consistent pattern of change in EMG in the pooled data or within any motor-function group (see **Figure 5**). Qualitatively, there were more discrete bursts of EMG, less tonic activity, and less co-contraction (see **Figure 2B**). These findings demonstrate that there is no one pattern of improvement regardless of the level of motor-function, that task-related EMG demands may increase or decrease, and that both are associated with improved therapy (game) performance and independence in everyday tasks.

One of the two primary objectives of Wii-based Movement Therapy is movement quality, rather than EMG activity or game scores. Thus, therapy activities were not modified in any way to enhance the recorded EMG signals (25, 48, 51). Wii-activities provide a wide range of movement demands. For example, the self-paced Wii-golf putting requires movements that are smaller and more-controlled compared to the externally-timed Wii-baseball and -tennis swings that can be used to target movement speed, range, power, and coordination (58).

The pattern of change in the EMG signals by late therapy was complex and variable. There were distinct differences between patients with low motor-function and those with moderate and high motor-function levels (49, 59, 60). The pattern of change in the area under the curve showed an increase for patients with low motor-function from early to late therapy for all activities except Wii-baseball in which there was no change. This pattern was reversed for patients with high motor-function, while those with moderate motor-function had a reduction in Wii-golf putting and -baseball swings and an increase in Wii-tennis forehand and backhand hits. In contrast, clinical motor assessments with the exception of the modified Ashworth Scale improved for the pooled cohort. The differences between the levels of motor-function arise as a consequence of the limitation of each assessment tool, particularly for the modified Ashworth Scale (46, 47, 61). These data emphasize differences in the level of residual voluntary motor capacity in chronic stroke. Although patients with low motor-function retain the capacity to improve, the level of impairment may limit their ability to participate fully in each activity and hence circumscribe the potential for improvement. Those with moderate motor-function have the greatest capacity for improvement, whereas patients with high motor-function are the most likely to show improvements (34). Regardless of changes in EMG and movement ability, the MALQOM data demonstrate that every patient became more independent in activities of daily living (46, 62).

Muscle activation after stroke is typically analyzed during simple single-joint tasks (20, 22, 43), or during experimentally constrained movements (41, 45, 63). Our analysis focused on the area under the curve because it is the product of EMG amplitude and the movement duration and so provides a more holistic view of the movement. While changes in movement duration were larger, there were fewer changes in peak amplitude. In this study, the movements were largely unconstrained, in that patients chose their own starting position within a task-dependent framework and the end position predominantly reflected movement capacity. When essential, positioning assistance was provided either with

the less-affected arm or by the therapist. Wii-golf was self-paced, Wii-baseball was paced by the game but required the development of fine response timing, while the timing of Wii-tennis was variable from swing to swing. Thus, these activities provide a better reflection of upper limb use in everyday life than more constrained experimental tasks and are more likely to reflect the neurophysiology underlying functionally relevant changes in poststroke motor-function.

Despite monotonic improvements in clinical assessments, there were heterogeneous changes in muscle activation patterns during therapy. Patients in each level of motor-function used different strategies to perform a task according to their specific neuromuscular limitations. Wii-activities target various muscles and movements (58), and differences in residual voluntary muscle activation alter the goals of therapy for each patient and result in movement patterns that differ from those of healthy control subjects (46, 50). These differences precluded analysis based on a single pre-determined muscle for all patients. Single muscle analysis provides some information about corticomotor changes in motor control but little about the coordination of muscles in the production of a complex movement. For this reason, these data were further analyzed to investigate the neuromuscular coordination of these complex movements [see (64)].

Clinical Implications

Although all patients completed a standardized protocol of Wii-based Movement Therapy and improved on clinical assessments, the pattern of change in EMG differed. Each motor-function group had a dominant pattern; yet, there was a large amount of variation within each group (see **Figure 5**). Regardless of the pattern of improvement in EMG, therapy-induced changes were reflected in improvements in independence (MALQOM) and quality of movement in activities of daily living that were unrelated to the content of therapy (see **Figure 4**). These data suggest that Wii-based Movement Therapy tasks can target different aspects of motor control. For example, the area under the curve in Wii-golf putting increased over time for patients with low motor-function showing that these patients were able to perform longer and stronger movements after therapy. Therefore, Wii-golf can be used to focus on slower and more-controlled movements with a sustained position at the end of the swing to target positional stability. Patients with moderate and high motor-function levels had a reduction in area under the curve over time indicating more coordinated and smaller movements, confirmed by video recordings. The increased area under the curve during Wii-tennis for patients with low and moderate motor-function levels suggests a greater ability to move from one side of the body to the other so that fuller "strokes" were played for both forehand and backhand as seen in video recordings. In contrast, the reduced area under the curve for patients with high motor-function suggests more efficient movements that can be used to target the difference between making one movement and preparing for the next movement. An ancillary benefit of these changes is that Wii-tennis also promotes greater stepping (25), which we hypothesize will also improve standing balance.

Game scores indicated that patients improved in terms of game performance; however, game scores do not necessarily reflect performance. Task difficulty is increased during therapy based on patient progress (25, 51). The increased difficulty typically lowers game scores resulting in a pattern of oscillating scores with a trend of improvement over time.

Electromyography analysis provides a mean of demonstrating neurophysiological changes in chronic stroke underlying significant improvements in clinical assessments, suggesting that ongoing rehabilitation is effective. Preliminary data from our group (65) emphasize that a continuous trajectory of improvement in clinical measures is possible when additional periods of therapy are provided in the chronic phase of stroke.

Study Limitations

In this study, the sample size within each level of motor-function is small. Yet, the pooled sample size is comparable to published studies of poststroke EMG (66–69). A wide range of poststroke motor impairment is included in this study based on clinical assessment data. Patients with low motor-function are not typically recruited in most neurophysiological studies due to methodological challenges. These patients need special care during assessment and therapy sessions due to pain, limited mobility and fatigue. Significant upper limb motor heterogeneity, together with the largely unconstrained movements during therapy and EMG acquisition from a variety of muscles increase the complexity of EMG analysis and interpretation.

The absence of healthy control subjects is a limitation to this study. Given that therapy focuses on the quality of movements and increasing the use of more-affected upper limb in everyday activities, the instructions given to stroke patients are different from those given to healthy subjects performing the same Wii-activities. The movements used in therapy are designed to replicate movement patterns of real-world sporting activities, despite all activity being targeted as far as possible, to use of the more-affected upper limb alone. Initially movements may be fractionated into their constituent parts for practice using the principles of shaping (70). By the end of therapy, most patients are able to perform the necessary reconstituted whole movements with game performance and scores used only as a motivational tool (46). In contrast, healthy subjects playing the same games used more modified movements than the real-world equivalent, and despite skill acquisition during Wii-Sports, showed no change in clinical assessments of motor-function (50). Thus, these differences in movement patterns may limit the utility of comparisons between healthy subjects and patients.

Although patients were drawn from several concurrent Wii-based Movement Therapy studies, all received the standardized protocol and we have seen very little variation in therapy outcomes across trials (46, 50, 62). The patients were instructed to perform the same task-dependent movements; however, the variability in movement strategies, tonic muscle activity, level of impairment, and the ability to voluntarily relax muscles after each movement prevented the use of single muscle for all analyses. This approach adds complexity to the analysis but was preferable to attempting to ensure all patients activated a given muscle as this was either not possible for some patients or would have produced extraneous or counterproductive movements. To enable comparisons between patients and between multiple time-points, EMG data were

normalized to a standardized condition, even though it has been suggested that EMG normalization in poststroke data might lead to higher variability (45). An unsupported weighted condition was used for normalization as this was considered more reliable for stroke survivors than a maximal voluntary contraction that might be restricted due to pain (71). Such variability is an inherent problem of longitudinal poststroke therapy studies when the aim of therapy is to change the muscles themselves, in addition to changing the neuromuscular control of those muscles.

CONCLUSION

This study demonstrates the magnitude of the variability in poststroke response to therapy and Wii-based Movement Therapy-induced changes in upper limb EMG in chronic stroke. The absence of correlations between EMG activity, game performance, and clinical assessments highlights the complexity and heterogeneity that are characteristic of stroke, even in the chronic period. Despite the absence of readily identifiable patterns across the pooled EMG data, the pattern of changes in EMG was associated with the level of residual voluntary motor capacity. The heterogeneity within each level shown in this EMG study was not evident using clinical assessments of motor-function, although improved independence in everyday activities was evident for all patients. These data emphasize the importance of examining individual patient responses to therapy using multiple tools, as rehabilitation efficacy will be underestimated when data are pooled.

ETHICS STATEMENT

This study was carried out in accordance with the recommendations of St. Vincent Hospital Human Research Ethics Committee, Sydney with written consent from all patients. All patients gave written informed consent in accordance with the Declaration of Helsinki. The protocol was approved by St. Vincent Hospital Human Research Ethics Committee.

AUTHOR CONTRIBUTIONS

PMcN conceived, designed, and supervised the study and manuscript preparation. NH-S assisted with data collection, developed multiple code scripts, analyzed data, and drafted the manuscript. TT implemented data collection. AT-B implemented therapy. CS undertook clinical assessments. All authors contributed to manuscript revision.

ACKNOWLEDGMENTS

The authors gratefully acknowledge Prof. Rob Herbert and Barbara Toson for statistical advice.

FUNDING

This study was funded by National Health and Medical Research Council (NHMRC) and the NSW Office of Science and Medical Research, Australia.

REFERENCES

1. Andrew NE, Kilkenny M, Naylor R, Purvis T, Lalor E, Moloczij N, et al. Understanding long-term unmet needs in Australian survivors of stroke. *Int J Stroke* (2014) 9(A100):106–12. doi:10.1111/ijs.12325
2. Deloitte. *The Economic Impact of Stroke in Australia*. Australia: Deloitte Access Economics (2013).
3. Langhorne P, Coupar F, Pollock A. Motor recovery after stroke: a systematic review. *Lancet Neurol* (2009) 8(8):741–54. doi:10.1016/S1474-4422(09)70150-4
4. Norrving B, Kissela B. The global burden of stroke and need for a continuum of care. *Neurology* (2013) 80(3 Suppl 2):S5–12. doi:10.1212/WNL.0b013e3182762397
5. Ada L, O'Dwyer N, Green J, Yeo W, Neilson P. The nature of the loss of strength and dexterity in the upper limb following stroke. *Hum Mov Sci* (1996) 15(5):671–87. doi:10.1016/0167-9457(96)00015-2
6. Bourbonnais D, Noven SV. Weakness in patients with hemiparesis. *Am J Occup Ther* (1989) 43(5):313–9. doi:10.5014/ajot.43.5.313
7. Canning CG, Ada L, Adams R, O'Dwyer NJ. Loss of strength contributes more to physical disability after stroke than loss of dexterity. *Clin Rehabil* (2004) 18(3):300–8. doi:10.1191/0269215504cr715oa
8. Werring DJ, Toosy AT, Clark CA, Parker GJ, Barker GJ, Miller DH, et al. Diffusion tensor imaging can detect and quantify corticospinal tract degeneration after stroke. *J Neurol Neurosurg Psychiatry* (2000) 69(2):269–72. doi:10.1136/jnnp.69.2.269
9. Hafer-Macko CE, Ryan AS, Ivey FM, Macko RF. Skeletal muscle changes after hemiparetic stroke and potential beneficial effects of exercise intervention strategies. *J Rehabil Res Dev* (2008) 45(2):261. doi:10.1682/JRRD.2007.02.0040
10. Ramsay JW, Barrance PJ, Buchanan TS, Higginson JS. Paretic muscle atrophy and non-contractile tissue content in individual muscles of the post-stroke lower extremity. *J Biomech* (2011) 44(16):2741–6. doi:10.1016/j.jbiomech.2011.09.001
11. Lukács M. Electrophysiological signs of changes in motor units after ischaemic stroke. *Neurophysiol Clin* (2005) 116(7):1566–70. doi:10.1016/j.clinph.2005.04.005
12. Mottram CJ, Suresh NL, Heckman C, Gorassini MA, Rymer WZ. Origins of abnormal excitability in biceps brachii motoneurons of spastic-paretic stroke survivors. *J Neurophysiol* (2009) 102(4):2026–38. doi:10.1152/jn.00151.2009
13. Ada L, O'Dwyer N, O'Neill E. Relation between spasticity, weakness and contracture of the elbow flexors and upper limb activity after stroke: an observational study. *Disabil Rehabil* (2006) 28(13–14):891–7. doi:10.1080/09638280500535165
14. Brainin M. Poststroke spasticity treating to the disability. *Neurology* (2013) 80(3 Suppl 2):S1–4. doi:10.1212/WNL.0b013e3182762379
15. O'dwyer N, Ada L, Neilson P. Spasticity and muscle contracture following stroke. *Brain* (1996) 119(5):1737–49. doi:10.1093/brain/119.5.1737
16. Ryu JS, Lee JW, Lee SI, Chun MH. Factors predictive of spasticity and their effects on motor recovery and functional outcomes in stroke patients. *Top Stroke Rehabil* (2015) 17:380–8. doi:10.1310/tsr1705-380
17. Cheung VC, Turolla A, Agostini M, Silvoni S, Bennis C, Kasi P, et al. Muscle synergy patterns as physiological markers of motor cortical damage. *Proc Natl Acad Sci U S A* (2012) 109(36):14652–6. doi:10.1073/pnas.1212056109
18. Clark DJ, Ting LH, Zajac FE, Neptune RR, Kautz SA. Merging of healthy motor modules predicts reduced locomotor performance and muscle coordination complexity post-stroke. *J Neurophysiol* (2010) 103(2):844–57. doi:10.1152/jn.00825.2009
19. Roh J, Rymer WZ, Beer RF. Evidence for altered upper extremity muscle synergies in chronic stroke survivors with mild and moderate impairment. *Front Hum Neurosci* (2015) 9:6. doi:10.3389/fnhum.2015.00006
20. Canning CG, Ada L, O'Dwyer NJ. Abnormal muscle activation characteristics associated with loss of dexterity after stroke. *J Neurol Sci* (2000) 176(1):45–56. doi:10.1016/S0022-510X(00)00305-1

21. Dewald JP, Pope PS, Given JD, Buchanan TS, Rymer WZ. Abnormal muscle coactivation patterns during isometric torque generation at the elbow and shoulder in hemiparetic subjects. *Brain* (1995) 118(2):495–510. doi:10.1093/brain/118.2.495
22. Ramos-Murguialday A, García-Cossio E, Walter A, Cho W, Broetz D, Bogdan M, et al. Decoding upper limb residual muscle activity in severe chronic stroke. *Ann Clin Transl Neurol* (2015) 2(1):1–11. doi:10.1002/acn3.122
23. Lee SW, Wilson KM, Lock BA, Kamper DG. Subject-specific myoelectric pattern classification of functional hand movements for stroke survivors. *IEEE Trans Neural Syst Rehabil Eng* (2011) 19(5):558–66. doi:10.1109/TNSRE.2010.2079334
24. Song R, Tong K-Y, Hu X, Li L. Assistive control system using continuous myoelectric signal in robot-aided arm training for patients after stroke. *IEEE Trans Neural Syst Rehabil Eng* (2008) 16(4):371–9. doi:10.1109/TNSRE.2008.926707
25. Trinh T, Shiner CT, Thompson-Butel AG, McNulty PA. Targeted upper-limb Wii-based movement therapy also improves lower-limb muscle activation and functional movement in chronic stroke. *Disabil Rehabil* (2017) 39(19):1939–49. doi:10.1080/09638288.2016.1213892
26. Uswatte G, Taub E, Morris D, Vignolo M, McCulloch K. Reliability and validity of the upper-extremity motor activity log-14 for measuring real-world arm use. *Stroke* (2005) 36(11):2493–6. doi:10.1161/01.STR.0000185928.90848.2e
27. Aprile I, Rabuffetti M, Padua L, Di Sipio E, Simbolotti C, Ferrarin M. Kinematic analysis of the upper limb motor strategies in stroke patients as a tool towards advanced neurorehabilitation strategies: a preliminary study. *Biomed Res Int* (2014) 2014:636123. doi:10.1155/2014/636123
28. Levin MF, Kleim JA, Wolf SL. What do motor "recovery" and "compensation" mean in patients following stroke? *Neurorehabil Neural Repair* (2008) 23:313–9. doi:10.1177/1545968308328727
29. Buma F, Kwakkel G, Ramsey N. Understanding upper limb recovery after stroke. *Restor Neurol Neurosci* (2013) 31(6):707–22. doi:10.3233/RNN-130332
30. Langhorne P, Bernhardt J, Kwakkel G. Stroke rehabilitation. *Lancet* (2011) 377(9778):1693–702. doi:10.1016/S0140-6736(11)60325-5
31. Krakauer JW. Motor learning: its relevance to stroke recovery and neurorehabilitation. *Curr Opin Neurol* (2006) 19(1):84–90. doi:10.1097/01.wco.0000200544.29915.cc
32. Kwakkel G, Kollen B. Predicting activities after stroke: what is clinically relevant? *Int J Stroke* (2013) 8(1):25–32. doi:10.1111/j.1747-4949.2012.00967.x
33. Kwakkel G, Kollen B, Twisk J. Impact of time on improvement of outcome after stroke. *Stroke* (2006) 37(9):2348–53. doi:10.1161/01.STR.0000238594.91938.1e
34. van Kordelaar J, van Wegen E, Kwakkel G. Impact of time on quality of motor control of the paretic upper limb after stroke. *Arch Phys Med Rehabil* (2014) 95(2):338–44. doi:10.1016/j.apmr.2013.10.006
35. Stinear CM. Stroke rehabilitation research needs to be different to make a difference. *F1000Res* (2016) 5(F1000 Faculty Rev):1467. doi:10.12688/f1000research.8722.1
36. Teasell RW, Murie Fernandez M, McIntyre A, Mehta S. Rethinking the continuum of stroke rehabilitation. *Arch Phys Med Rehabil* (2014) 95(4):595–6. doi:10.1016/j.apmr.2013.11.014
37. Fugl-Meyer AR, Jääskö L, Leyman I, Olsson S, Steglind S. The post-stroke hemiplegic patient. 1. A method for evaluation of physical performance. *Scand J Rehabil Med* (1974) 7(1):13–31.
38. Mathiowetz V, Volland G, Kashman N, Weber K. Adult norms for the box and block test of manual dexterity. *Am J Occup Ther* (1985) 39(6):386–91. doi:10.5014/ajot.39.6.386
39. Wolf SL, Lecraw DE, Barton LA, Jann BB. Forced use of hemiplegic upper extremities to reverse the effect of learned nonuse among chronic stroke and head-injured patients. *Exp Neurol* (1989) 104(2):125–32. doi:10.1016/S0014-4886(89)80005-6
40. Thompson-Butel AG, Lin G, Shiner CT, McNulty PA. Comparison of three tools to measure improvements in upper-limb function with poststroke therapy. *Neurorehabil Neural Repair* (2015) 29(4):341–8. doi:10.1177/1545968314547766
41. Hughes A, Freeman C, Burridge J, Chappell P, Lewin P, Rogers E. Shoulder and elbow muscle activity during fully supported trajectory tracking in people who have had a stroke. *J Electromyogr Kinesiol* (2010) 20(3):465–76. doi:10.1016/j.jelekin.2009.08.001
42. Sin M, Kim W-S, Park D, Min Y-S, Kim WJ, Cho K, et al. Electromyographic analysis of upper limb muscles during standardized isotonic and isokinetic robotic exercise of spastic elbow in patients with stroke. *J Electromyogr Kinesiol* (2014) 24(1):11–7. doi:10.1016/j.jelekin.2013.10.002
43. Song R, Tong KY. EMG and kinematic analysis of sensorimotor control for patients after stroke using cyclic voluntary movement with visual feedback. *J Neuroeng Rehabil* (2013) 10(1):18. doi:10.1186/1743-0003-10-18
44. Lum PS, Burgar CG, Shor PC. Evidence for improved muscle activation patterns after retraining of reaching movements with the MIME robotic system in subjects with post-stroke hemiparesis. *IEEE Trans Neural Syst Rehabil Eng* (2004) 12(2):186–94. doi:10.1109/TNSRE.2004.827225
45. Silva CC, Silva A, Sousa A, Pinheiro AR, Bourlinova C, Silva A, et al. Co-activation of upper limb muscles during reaching in post-stroke subjects: an analysis of the contralesional and ipsilesional limbs. *J Electromyogr Kinesiol* (2014) 24(5):731–8. doi:10.1016/j.jelekin.2014.04.011
46. McNulty PA, Thompson-Butel AG, Faux SG, Lin G, Katrak PH, Harris LR, et al. The efficacy of Wii-based movement therapy for upper limb rehabilitation in the chronic poststroke period: a randomized controlled trial. *Int J Stroke* (2015) 10:1253–60. doi:10.1111/ijs.12594
47. Thompson-Butel AG, Lin GG, Shiner CT, McNulty PA. Two common tests of dexterity can stratify upper limb motor function after stroke. *Neurorehabil Neural Repair* (2014) 28:788–96. doi:10.1177/1545968314523678
48. Trinh T, Scheuer SE, Thompson-Butel AG, Shiner CT, McNulty PA. Cardiovascular fitness is improved post-stroke with upper-limb Wii-based movement therapy but not dose-matched constraint therapy. *Top Stroke Rehabil* (2016) 23(3):208–16. doi:10.1080/10749357.2016.1138672
49. Shiner CT, Pierce KD, Thompson-Butel AG, Trinh T, Schofield PR, McNulty PA. BDNF genotype interacts with motor function to influence rehabilitation responsiveness poststroke. *Front Neurol* (2016) 7:69. doi:10.3389/fneur.2016.00069
50. Mouawad MR, Doust CG, Max MD, McNulty PA. Wii-based movement therapy to promote improved upper extremity function post-stroke: a pilot study. *J Rehabil Med* (2011) 43(6):527–33. doi:10.2340/16501977-0816
51. Thompson-Butel AG, Scheuer SE, McNulty PA. Improving motor activation patterns after stroke with Wii-based movement therapy. In: Pilowsky PM, Farnham MMJ, Fong AY, editors. *Stimulation and Inhibition of Neurons*, Vol. 78. Totowa, NJ: Humana Press (2013). p. 301–14.
52. Lee K, Carson L, Kinnin E, Patterson V. The Ashworth scale: a reliable and reproducible method of measuring spasticity. *Neurorehabil Neural Repair* (1989) 3(4):205–9. doi:10.1177/136140968900300406
53. Bohannon RW, Smith MB. Interrater reliability of a modified Ashworth scale of muscle spasticity. *Phys Ther* (1987) 67(2):206–7. doi:10.1093/ptj/67.2.206
54. Bodin P, Morris M. Inter-rater reliability of the modified Ashworth scale for wrist flexor spasticity following stroke. *Paper Presented at the Proceedings of the 11th Congress of the World Confederation for Physical Therapy*. London, UK (1991).
55. Ashbeck EL, Bell ML. Single time point comparisons in longitudinal randomized controlled trials: power and bias in the presence of missing data. *BMC Med Res Methodol* (2016) 16(1):43. doi:10.1186/s12874-016-0144-0
56. Bernal-Rusiel JL, Greve DN, Reuter M, Fischl B, Sabuncu MR; Alzheimer's Disease Neuroimaging Initiative. Statistical analysis of longitudinal neuroimage data with linear mixed effects models. *Neuroimage* (2013) 66:249–60. doi:10.1016/j.neuroimage.2012.10.065
57. Krueger C, Tian L. A comparison of the general linear mixed model and repeated measures ANOVA using a dataset with multiple missing data points. *Biol Res Nurs* (2004) 6(2):151–7. doi:10.1177/1099800404267682
58. Deutsch JE, Brettler A, Smith C, Welsh J, John R, Guarrera-Bowlby P, et al. Nintendo wii sports and wii fit game analysis, validation, and application to stroke rehabilitation. *Top Stroke Rehabil* (2011) 18(6):701–19. doi:10.1310/tsr1806-701
59. Cramer SC, Bastings EP. Mapping clinically relevant plasticity after stroke. *Neuropharmacology* (2000) 39(5):842–51. doi:10.1016/S0028-3908(99)00258-0
60. Shiner CT, Tang H, Johnson BW, McNulty PA. Cortical beta oscillations and motor thresholds differ across the spectrum of post-stroke motor impairment, a preliminary MEG and TMS study. *Brain Res* (2015) 1629:26–37. doi:10.1016/j.brainres.2015.09.037
61. Fleuren JF, Voerman GE, Erren-Wolters CV, Snoek GJ, Rietman JS, Hermens HJ, et al. Stop using the Ashworth scale for the assessment of

spasticity. *J Neurol Neurosurg Psychiatry* (2010) 81(1):46–52. doi:10.1136/jnnp.2009.177071
62. McNulty PA, Thompson-Butel AG, Shiner CT, Trinh T. Wii-based movement therapy benefits stroke patients with low and very low movement ability. *Soc Care Neurodisabil* (2013) 4(3/4):5. doi:10.1108/SCN-04-2013-0018
63. Cesqui B, Tropea P, Micera S, Krebs HI. EMG-based pattern recognition approach in post stroke robot-aided rehabilitation: a feasibility study. *J Neuroeng Rehabil* (2013) 10(1):75. doi:10.1186/1743-0003-10-75
64. Hesam-Shariati N, Trinh T, Thompson-Butel AG, Shiner CT, McNulty PA. A longitudinal electromyography study of complex movements in poststroke therapy. 2: Changes in coordinated muscle activation. *Front Neurol Stroke* (2017). doi:10.3389/fneur.2017.00277
65. McNulty PA, Thompson-Butel AG, Shiner CT, Trinh T. Regaining or retraining motor function in chronic stroke: what is the capacity for sustained improvements with additional therapy? *Int J Stroke* (2015) 10:50.
66. Chang SH, Zhou P, Rymer WZ, Li S. Spasticity, weakness, force variability, and sustained spontaneous motor unit discharges of resting spastic–paretic biceps brachii muscles in chronic stroke. *Muscle Nerve* (2013) 48(1):85–92. doi:10.1002/mus.23699
67. Li X, Holobar A, Gazzoni M, Merletti R, Rymer WZ, Zhou P. Examination of poststroke alteration in motor unit firing behavior using high-density surface EMG decomposition. *IEEE Trans Biomed Eng* (2015) 62(5):1242–52. doi:10.1109/TBME.2014.2368514
68. Wagner JM, Dromerick AW, Sahrmann SA, Lang CE. Upper extremity muscle activation during recovery of reaching in subjects with post-stroke hemiparesis. *Neurophysiol Clin* (2007) 118(1):164–76. doi:10.1016/j.clinph.2006.09.022
69. Zhang X, Zhou P. High-density myoelectric pattern recognition toward improved stroke rehabilitation. *IEEE Trans Biomed Eng* (2012) 59(6):1649–57. doi:10.1109/TBME.2012.2191551
70. Taub E, Crago JE, Burgio LD, Groomes TE, Cook EW, DeLuca SC, et al. An operant approach to rehabilitation medicine: overcoming learned nonuse by shaping. *J Exp Anal Behav* (1994) 61(2):281–93. doi:10.1901/jeab.1994.61-281
71. Halaki M, Ginn K. Chapter 7: Normalization of EMG signals: to normalize or not to normalize and what to normalize to? In: Naik GR, editor. *Computational Intelligence in Electromyography Analysis – A Perspective on Current Applications and Future Challenges*. InTech (2012). p. 175–94.

Conflict of Interest Statement: The authors declare that the research was conducted in the absence of any commercial or financial relationships that could be construed as a potential conflict of interest.

frontiers in Neurology

ORIGINAL RESEARCH
published: 20 July 2017
doi: 10.3389/fneur.2017.00277

A Longitudinal Electromyography Study of Complex Movements in Poststroke Therapy. 2: Changes in Coordinated Muscle Activation

*Negin Hesam-Shariati[1,2], Terry Trinh[1,2], Angelica G. Thompson-Butel[1,2], Christine T. Shiner[1,2] and Penelope A. McNulty[1,2]**

[1] Neuroscience Research Australia, Sydney, NSW, Australia, [2] School of Medical Science, University of New South Wales, Sydney, NSW, Australia

Fine motor control is achieved through the coordinated activation of groups of muscles, or "muscle synergies." Muscle synergies change after stroke as a consequence of the motor deficit. We investigated the pattern and longitudinal changes in upper limb muscle synergies *during* therapy in a largely unconstrained movement in patients with a broad spectrum of poststroke residual voluntary motor capacity. Electromyography (EMG) was recorded using wireless telemetry from 6 muscles acting on the more-affected upper body in 24 stroke patients at early and late therapy during formal Wii-based Movement Therapy (WMT) sessions, and in a subset of 13 patients at 6-month follow-up. Patients were classified with low, moderate, or high motor-function. The Wii-baseball swing was analyzed using a non-negative matrix factorization (NMF) algorithm to extract muscle synergies from EMG recordings based on the temporal activation of each synergy and the contribution of each muscle to a synergy. Motor-function was clinically assessed immediately pre- and post-therapy and at 6-month follow-up using the Wolf Motor Function Test, upper limb motor Fugl-Meyer Assessment, and Motor Activity Log Quality of Movement scale. Clinical assessments and game performance demonstrated improved motor-function for all patients at post-therapy ($p < 0.01$), and these improvements were sustained at 6-month follow-up ($p > 0.05$). NMF analysis revealed fewer muscle synergies (mean ± SE) for patients with low motor-function (3.38 ± 0.2) than those with high motor-function (4.00 ± 0.3) at early therapy ($p = 0.036$) with an association trend between the number of synergies and the level of motor-function. By late therapy, there was no significant change between groups, although there was a pattern of increase for those with low motor-function over time. The *variability accounted for* demonstrated differences with motor-function level ($p < 0.05$) but not time. Cluster analysis of the pooled synergies highlighted the therapy-induced change in muscle activation. Muscle synergies could be identified for all patients during therapy activities. These results show less complexity and more co-activation in the muscle activation for patients with low motor-function as a higher number of muscle synergies reflects greater movement complexity and task-related phasic muscle activation. The increased number of synergies and changes within synergies by late-therapy suggests improved motor control and movement quality with more distinct phases of movement.

Keywords: muscle synergy, non-negative matrix factorization, upper limb, rehabilitation, chronic stroke

OPEN ACCESS

Edited by:
Cliff Klein, Guangdong Provincial Work Injury Rehabilitation Center, China

Reviewed by:
Winston D. Byblow, University of Auckland, New Zealand
Sahil Bajaj, University of Arizona, United States

***Correspondence:**
Penelope A. McNulty
p.mcnulty@neura.edu.au

Specialty section:
This article was submitted to Stroke, a section of the journal Frontiers in Neurology

Received: *20 March 2017*
Accepted: *29 May 2017*
Published: *20 July 2017*

Citation:
Hesam-Shariati N, Trinh T, Thompson-Butel AG, Shiner CT and McNulty PA (2017) A Longitudinal Electromyography Study of Complex Movements in Poststroke Therapy. 2: Changes in Coordinated Muscle Activation. Front. Neurol. 8:277. doi: 10.3389/fneur.2017.00277

INTRODUCTION

Fine motor control of the upper limb requires complex movements based on multiple degrees of freedom that permit movement variability and versatility (1, 2). The central nervous system controls such complex motor tasks by coordinated activation of groups of muscles, referred to as "muscle synergies" (3–6). The combination of the brain and spinal circuitry is essential for the simultaneous recruitment of multiple muscle synergies that explain a wide range of movement patterns (7, 8). Muscle synergies have been extracted from electromyography (EMG) recordings to define movements in both animals including frogs (9, 10), rats (11), cats (12–14), and monkeys (15); and humans with reference to gait (16–18), balance and posture (19, 20), hand function and posture (21, 22), arm movements (2, 7, 23), and isometric force (24, 25).

Multiple temporal synergy profiles are weighted and integrated to define coordinated muscle activation during a task (2). Muscle synergies can include any number of muscles and each muscle can contribute to multiple synergies (8). Muscle synergies have been investigated in acute, subacute (26–28), and chronic stroke (17, 23, 29) showing abnormalities compared to healthy people (18, 30, 31). Such changes reflect poststroke motor impairment which can be attributed in large part to disorders in the neural pathway (8), reduced corticospinal drive (32), disuse atrophy (33), and loss of independent joint control and impaired motor coordination (29).

Muscle synergy analysis has detected poststroke abnormalities in the number, structure, and recruitment profile of muscle synergies. For example, the number of muscle synergies recruited in the poststroke gait cycle was reduced in patients with more severe impairment and in comparison to healthy subjects (17, 34). This presumably reflects a change in the number of independent motor subtasks given the standard analysis of the gait cycle in four distinct phases and the use of four synergies for healthy subjects and patients with high motor-function.

Several analysis algorithms have been suggested for the decomposition of muscle activation profiles into muscle synergies. Tresch and colleagues (35) evaluated and compared different matrix factorization methods including factor analysis, independent component analysis alone and applied to principle component analysis, and non-negative matrix factorization (NMF). The authors concluded that these methods identify muscle synergies very similar to one another. In this study, we implemented NMF which has commonly been used to detect muscle synergies from EMG activation (17, 25, 36, 37). NMF quantifies muscle synergies as a linear combination of the timing profile and a weighting assigned to each muscle involved in each synergy.

Few studies have examined the changes in poststroke muscle synergies with rehabilitation, but see Ref. (28). In this study, we extracted muscle synergies during a complex task to investigate the changes in muscle activation profiles (i.e., muscle synergies) in chronic stroke during an intensive 14-day protocol, in this case Wii-based Movement Therapy (WMT) (38, 39). This therapy is as effective as the current best practice in stroke rehabilitation, Constraint-induced Movement Therapy (38, 40). The primary aim of this study was not the therapy itself, but to quantify poststroke muscle synergies during therapy. Muscle synergy analysis cannot be used to investigate recovery mechanisms occurring in the brain but was used here as a neurophysiological indication to distinguish the level of impairment and the effect of therapy on coordinated muscle activation (41). To identify some of the neuromuscular mechanisms underpinning the improvement reported using clinical motor-function assessments (38, 39), NMF was applied to the EMG recorded from six muscles of the more-affected arm and upper body during the Wii-baseball component of WMT. This longitudinal study examined EMG at early and late therapy, and at 6-month follow-up for a subset of patients. We hypothesized that the number of muscle synergies would be correlated with the level of motor-function after stroke and that the number of synergies would change with therapy.

MATERIALS AND METHODS

Participants

Twenty four patients (16 males, 8 females) aged 37–80 years (57.9 ± 12.1, mean $\pm$ SD) and 3–88 months poststroke (26.7 ± 4.3, mean $\pm$ SE) were randomly selected from a larger cohort who were consecutively recruited from St. Vincent's and Prince of Wales' Hospitals, Sydney [the same patients as presented in Hesam-Shariati et al. (42), see Table 1 for a summary of baseline characteristics]. All participants were hemiparetic following either an ischemic or hemorrhagic stroke and were classified into three groups of low, moderate, or high motor-function based on their ability to perform two tests of upper limb manual dexterity (43). The inclusion criteria were as before: $\geq 10°$ of voluntary movement in at least one digit of the more-affected hand; cognitive competency measured as a Mini-Mental State Examination score ≥ 24; suitable skin for sensor placement; and the ability to communicate in English. Exclusion criteria included unstable blood pressure; comorbidities affecting upper limb sensorimotor function; and engagement in any other formal upper limb rehabilitation program. All participants gave signed informed consent to the study that was approved by the St. Vincent's Hospital Human Research Ethics Committee, Sydney, and conducted in accordance with the Declaration of Helsinki. Ten of the 24 patients could not attend the 6-month follow-up session for a range of reasons including: return to work, too far to travel, and unrelated health problems. The data for one patient were excluded for technical issues [see Ref. (42), Figure 1]. As detailed in Hesam-Shariati et al. (42), the clinical assessment results for all patients (but not NMF analyses) have been published previously [see Ref. (44) $n = 20$; (38) $n = 9$; and (40) $n = 8$].

Therapy

WMT is a standardized 14-day program focused on the more-affected upper limb, which consists of 1-h of formal therapy on 10 consecutive weekdays delivered by an Accredited Exercise Physiologist, augmented by prescribed home practice starting on day 2 and increasing throughout the program [see Figure 2A in Ref. (42)]. This therapy uses the Nintendo Wii and Wii-Sports games (Nintendo, Japan) as a rehabilitation tool that targets movement quality and independence in activities of daily living

(38, 39). The movements required in Wii-Sports were modified according to the capacity, range of motion, and strength of each patient. Although WMT games include Wii-golf, -baseball, -tennis, -bowling, and -boxing, the analyses of this study were applied only to Wii-baseball swings. Each patient played two or three games of Wii-baseball during each session of therapy. This Wii-baseball movement was selected for analysis for several reasons. First, all patients were able to complete this game, regardless of the level of residual voluntary motor-function. Second, the game determines the onset of each movement by pitching the ball. This allowed individual movements to be identified more clearly in the EMG signal. Finally, the nature of the game provided the most consistent task demands.

EMG Recording

Surface EMG was recorded from six muscles of the upper body on the more-affected side: trapezius (middle portion), deltoid medius, biceps brachii (BB), extensor carpi radialis, flexor carpi radialis, and first dorsal interosseus (FDI) using Trigno wireless sensors (Delsys, USA). The data were collected continuously during formal WMT sessions at early (day 2–3) and late (between days 12–14) therapy, and in a subset of patients, again during the 6-month follow-up session. Each EMG sensor contains four silver bar electrodes, arranged in two pairs with an interelectrode pair distance of 10 mm. The sensor is designed to maximize the detection of muscle activation in a field perpendicular to the muscle fibers. Data were amplified 300 times, filtered between 20 and 450 Hz, and sampled at 2 kHz using EMGworks (Delsys, USA) as per intrinsic device settings.

Clinical Motor-Function Assessments and Game Performance

The efficacy of WMT was evaluated using clinical motor-function tests as described in Hesam-Shariati et al. (42) including the Wolf Motor Function Test (WMFT) (45), upper limb motor Fugl-Meyer Assessment (FMA) (46), and the Motor Activity Log Quality of Movement scale (MALQOM) (47). The Wii-baseball game performance was assessed as the number of hits, regardless of the outcome according to the rules of baseball, and this was recorded during therapy. However, the primary goal of therapy was movement quality and not game performance. The average duration of each swing for each trial was measured in seconds.

Data Analysis

EMG Preprocessing

Electromyography signals were DC removed, root mean square processed using a sliding 50 ms window and demeaned using Spike2 software (CED, UK). Mean baseline EMG was measured over 1 s prior to the beginning of the Wii-baseball game, while the muscles were at rest. The mean was subtracted from the signal of the same game for each patient. To enable comparison between patients, the EMG of each muscle was normalized to its peak amplitude, then averaged over 10 consecutive Wii-baseball swings for each patient at early and late therapy and at 6-month follow-up.

Non-Negative Matrix Factorization

Muscle synergies were extracted from the EMG signals using the NMF method (4, 35, 48, 49). This optimization method was applied to the EMG recordings of the six muscles using the in-built nnmf function in MATLAB R2014a (MathWorks, USA). Random initial values were generated as the input for the multiplicative algorithm of the function, the output of which provided the initial values of the alternating least squares (ALS) algorithm (50). Then, the ALS algorithm was used to characterize the EMG of the six recorded muscles ($m = 6$) as a lower-rank combination of the relative weighting (W) of each muscle and the timing profile (H) of each synergy (equation below) in a complex movement (see **Figure 1**).

$$\mathrm{EMG} \cong \sum_{k=1}^{m-1} W_k H_k(t)$$

Number of Muscle Synergies

The number of muscle synergies needed to define coordinated muscle activation in a complex movement was determined using the term *variability accounted for* (VAF) (14, 17) and the mean squared error (MSE) term (9, 51) according to the formula below. The VAF is defined as 100 times the squared correlation coefficient between the original EMG ($\mathrm{EMG_o}$) and the reconstructed EMG ($\mathrm{EMG_r}$) from the NMF algorithm (23). The minimum number of synergies was identified when VAF increased by less than 2% when another synergy was added. VAF for the acceptable number of synergies was required to be greater than 97% while the MSE was less than 10×10^{-4}.

$$\mathrm{VAF} = 100 \times \left(1 - \frac{\sum(\mathrm{EMG_o} - \mathrm{EMG_r})^2}{\sum(\mathrm{EMG_o} - \overline{\mathrm{EMG_o}})^2}\right)$$

$$\mathrm{MSE} = \frac{1}{n}\sum_1^n(\mathrm{EMG_o} - \mathrm{EMG_r})^2$$

Similarity of Synergy Timing Profiles

The similarity between individual synergy timing profiles from each subject on a group basis was quantified using the scalar product (1, 31). More than 50% of patients used four distinct synergies to account for the variability of muscle activation at early and late therapy and at 6-month follow-up. The analysis of similarity between timing profiles requires the same number of synergies from each patient to be entered in the analysis to enable the comparison of synergy profiles. Thus, regardless of the actual number of synergies, four synergies were extracted from the muscle activation of all patients. Then, one set of four synergies from one subject was randomly selected in each motor-function group and used as the template. The synergy timing profiles from all other subjects within the same motor-function group at each time point were matched to provide the highest scalar product between two synergies. The scalar product (r-value) is a measure of the similarity in which one numerical vector is projected onto another, so that an r-value of 1 represents complete similarity and a value of 0 represents the absence of any similarity.

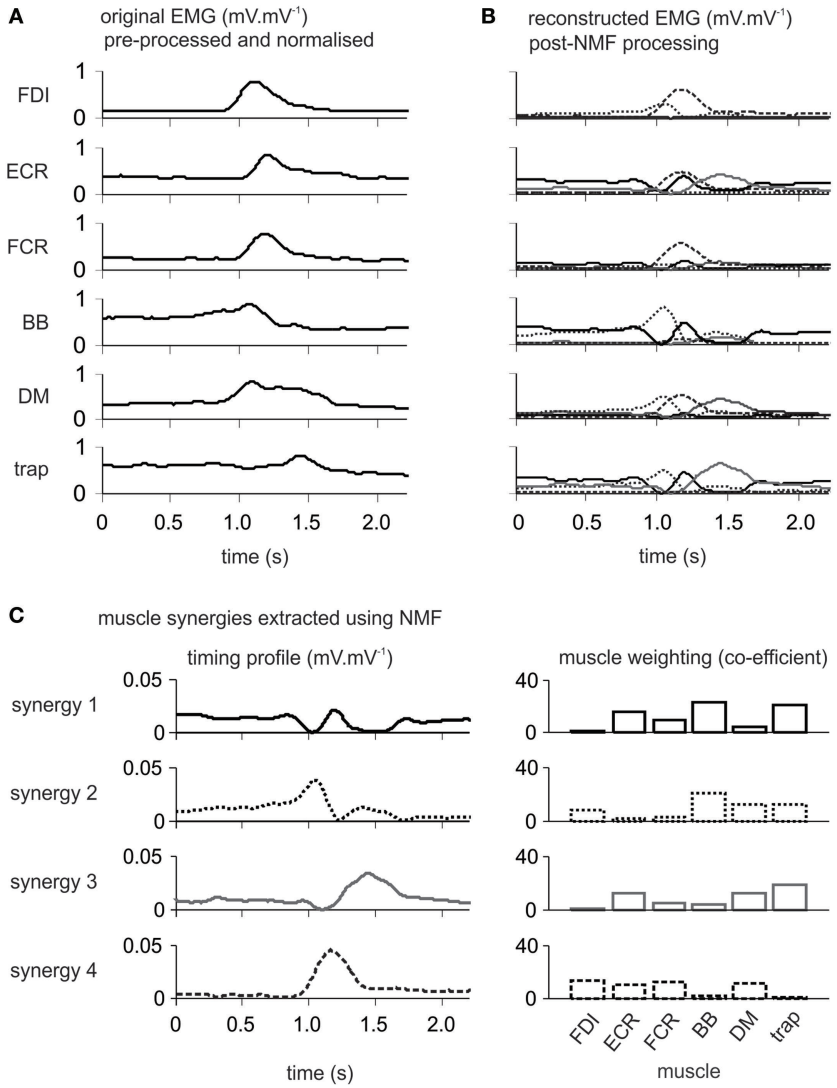

FIGURE 1 | Single patient electromyography (EMG) data showing the progression through analysis using non-negative matrix factorization (NMF). The 61-year-old male patient with moderate motor-function was 5 months poststroke. **(A)** Preprocessed normalized EMG from six upper body muscles on the more-affected side during Wii-baseball swings prior to processing by the NMF algorithm. **(B)** Reconstructed EMG after processing by NMF as the integration of muscle synergies for each muscle. **(C)** Each derived muscle synergy is a combination of the timing profile and muscle weightings. FDI, first dorsal interosseous; ECR, extensor carpi radialis; FCR, flexor carpi radialis; BB, biceps brachii; DM, deltoid medius; trap, trapezius (middle portion).

Clustering Synergy Structures

The muscle weightings of the actual synergies from all subjects were pooled to be categorized using cluster analysis (23, 51) at early and late therapy. This procedure was performed using the in-built functions from the MATLAB statistics toolbox. Euclidean distance was used to measure the similarity between pairs of muscle weightings. The minimum number of clusters was determined based on grouping synergies when there was no more than one synergy from a subject in each cluster. Cluster analysis requires the inclusion of all extracted synergies to avoid overlap and to merge the analysis to a limited and realistic number of clusters. This method avoids the inclusion of more than one synergy from each patient in each cluster.

Statistical Analysis

A potential relationship between the number of muscle synergies and the level of motor-function was investigated using Pearson chi-square test, Fisher's exact test, and linear-by-linear association. If more than 20% of the cells had an expected count <5, the *p*-value of Fisher's exact test was reported instead of Pearson chi-square. In addition, linear-by-linear association was used to reveal trends in larger than 2×2 tables. The same tests were used after the cluster analysis to evaluate the incidence of each cluster in each level of motor-function.

A mixed-effect model was implemented for any given number of synergies (range 1–5) to detect the effect of motor-function level (low, moderate, high) and time (early therapy, late therapy,

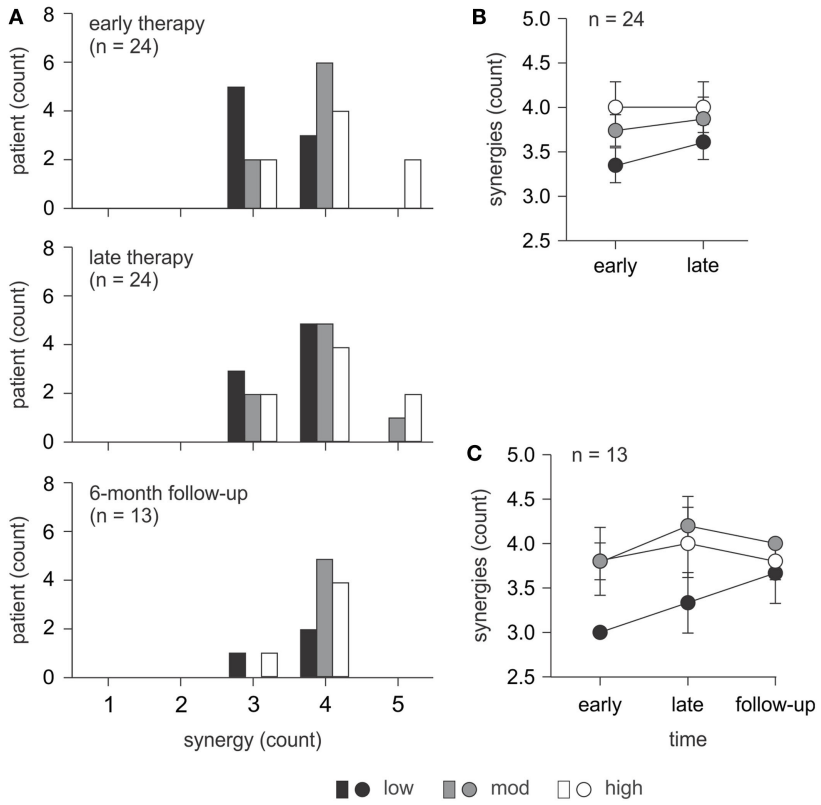

FIGURE 2 | Number of synergies required to define Wii-baseball swing. **(A)** Comparison of the number of synergies used for patients (n = 24) with different levels of motor-function at early and late therapy and for a subset (n = 13) at 6-month follow-up. **(B)** The number of synergies for all patients (n = 24) at early and late therapy (mean ± SE). At early therapy, there was a significant difference between patients with low and high motor-function. There was also a trend toward an increase in the number of synergies from early to late therapy for patients with low and moderate motor-function. **(C)** The number of synergies for the subset of patients (n = 13; 3 low, 5 moderate, and 5 high motor-function) who completed 6-month follow-up assessments (mean ± SE). There was no significant change over time.

follow-up) on VAF. This model is powerful and flexible with missing data (i.e., to account for $n = 13$ at follow-up). Clinical assessments and game performance data were analyzed using paired t-test (for parametric data) and Wilcoxon signed-rank test (for non-parametric data) to compare means between time points. Statistical analyses were conducted in SPSS 23 software (IBM, USA) and the differences were considered significant when $p < 0.05$.

RESULTS

Number of Synergies Extracted from Wii-baseball

Difference in the Number of Synergies across Groups

The number of muscle synergies required to define the Wii-baseball movement is presented in **Figure 2A** for each level of motor-function at each time point. At early therapy, most patients with low motor-function used three synergies, while most patients with moderate and high motor-function used four synergies to define the movement. However, two patients with high motor-function used five synergies. As can be seen in **Figure 2B** at early therapy, the number of synergies (mean ± SE) for patients with low motor-function (3.38 ± 0.18) was significantly less than for patients with high motor-function (4.00 ± 0.27) ($p = 0.036$). At early therapy, Fisher's exact test showed no relationship between the number of muscle synergies and the level of motor-function ($p = 0.217$), although linear-by-linear association indicated a trend ($p = 0.045$).

Changes in the Number of Synergies over Time

At late therapy, an increase in the number of synergies was evident for patients with low and moderate motor-function, albeit not statistically significant (**Figure 2B**). The number of synergies (mean ± SE) increased from 3.38 ± 0.18 to 3.63 ± 0.18 ($p = 0.317$) for patients with low motor-function and from 3.75 ± 0.16 to 3.88 ± 0.23 ($p = 0.564$) for patients with moderate motor-function from early to late therapy. There was no change for patients with high motor-function. For the subset of patients with 6-month follow-up data, the number of synergies over time is illustrated in **Figure 2C**. There were no significant changes over time for this subset of patients.

Consistency of Synergy Timing Profiles within Groups

The synergy timing profiles (**Figure 3**) were similar for patients in each level of motor-function. The timing profile of muscle synergies in each group was matched based on the scalar product

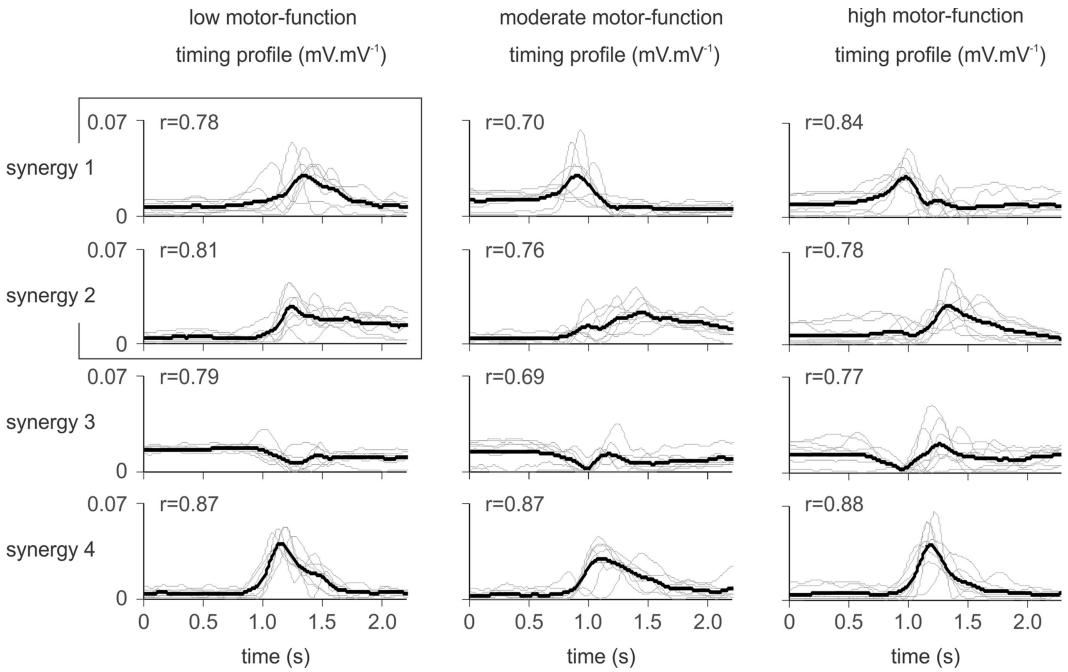

FIGURE 3 | Synergy activation timing for patients according to the level of residual voluntary motor-function. Thin gray lines illustrate the synergy timing profile for each patient (mean of 10 trials), overlaid by the within-group mean (black line). Similar synergies are overlaid based on the scalar product between synergies. The *r*-value shown for each synergy indicates the group-averaged scalar product. For patients with low motor-function, the scalar product between mean synergy 1 and 2 indicated similarity ($r = 0.71$). These two synergies were assumed to be one (as indicated by the overlaid box). Thus, patients with low motor-function used three distinct synergies to define the movement, while patients with moderate and high motor-function required four synergies.

(*r*-value) between pairs of synergies from different patients in each group. The within-group mean *r*-value is shown for each synergy in **Figure 3**. Four distinct synergies demonstrated the profile of muscle synergies for patients with high and moderate motor-function. For patients with low motor-function, the between-synergy scalar product for synergy 1 and 2 ($r = 0.71$) showed high similarity, suggesting a single synergy. Thus, three distinct synergies defined the movement in patients with low motor-function.

Variability (VAF) of Muscle Synergies across Groups

Variability accounted for increased with a higher number of synergies (**Figure 4**). A mixed-effect model revealed changes in VAF according to the level of motor-function over time for any given number of muscle synergies (range 1–5) for each patient. The level of motor-function, but not the time point, had an effect on the VAF (for any given number of synergies $p < 0.05$); although the VAF appears similar between groups in **Figure 4**, the variability within each group was large.

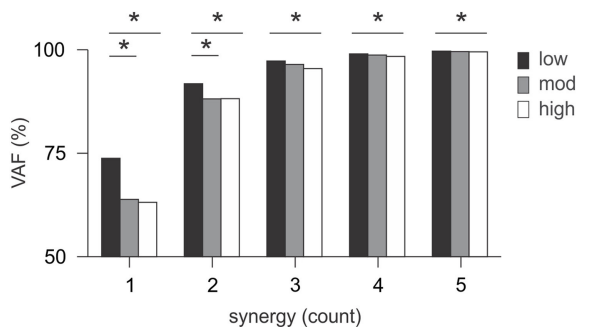

FIGURE 4 | *Variability accounted for* (VAF) in muscle synergies. VAF changed little over time; the mean VAF was measured for any given number of synergies and compared between patients for the three levels of motor-function. For each number of synergies, patients with low motor-function had higher VAF compared to the other two groups ($p < 0.05$). Lower VAF for patients with moderate and high motor-function indicated that the analysis is less able to account for variability of muscle activation because of more movement complexity.

Muscle Synergy Clusters

At early- and late-therapy, the muscle weightings of each synergy from all patients were pooled and then categorized into 10 and 11 clusters, respectively. Thus, all the synergy structures from all patients can be summarized into 10 or 11 distinct synergies (**Figure 5**). At early therapy, there was no significant difference in the incidence of muscle synergies from different levels of patient motor-function in each cluster based on Fisher's exact test, except for cluster 2 (**Figure 6**). However, a trend was observed in the incidence of cluster 3 and 9 using linear-by-linear association (see **Figure 6**).

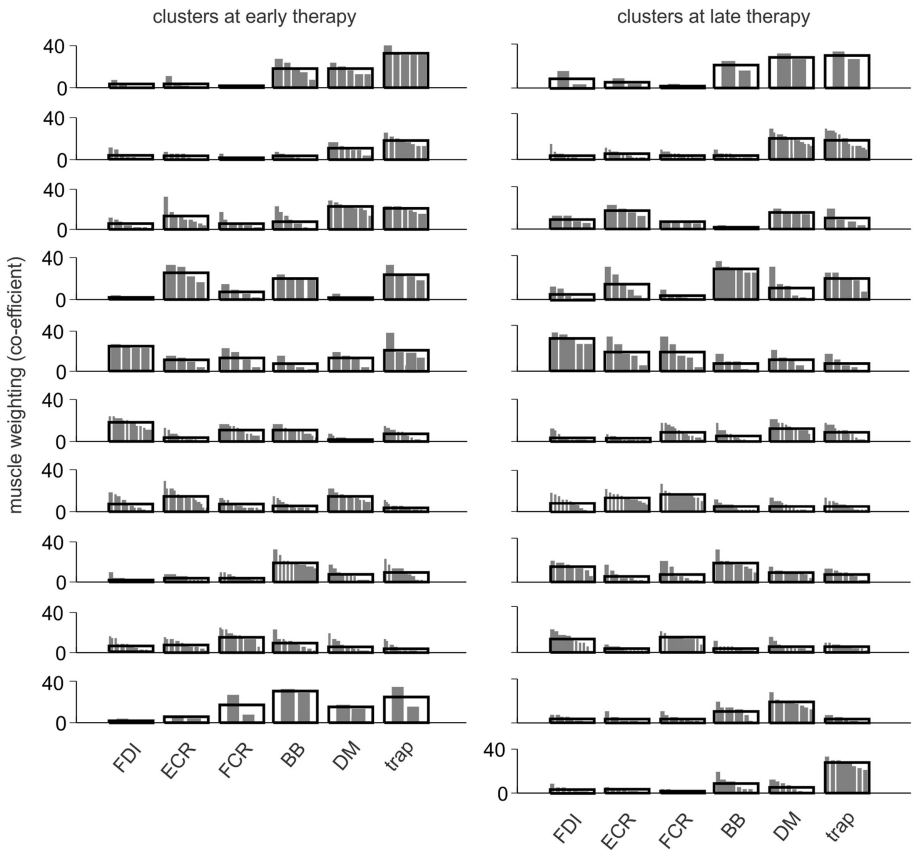

FIGURE 5 | Composition of muscle synergies at early and late therapy. Synergy muscle weightings at early and late therapy were categorized into 10 and 11 clusters, respectively. For each cluster, the distribution of muscle weightings from different synergies is shown, overlaid by the group mean. The synergy clusters changed from early to late therapy except for the first four clusters.

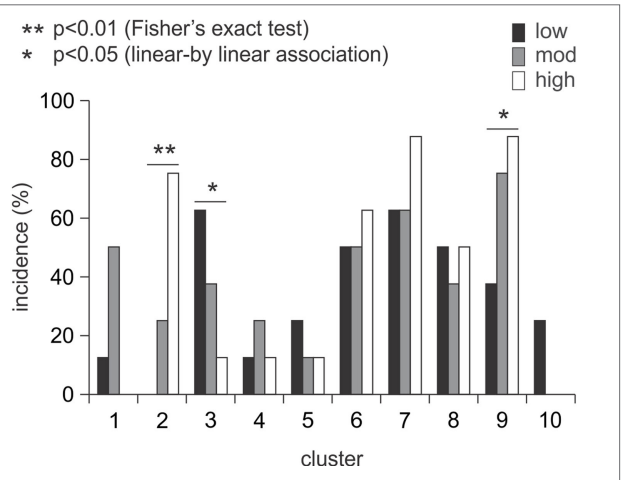

FIGURE 6 | Incidence of muscle synergy clusters across groups at early therapy. The incidence of muscle synergies did not differ with the level of motor-function except for cluster 2 ($p < 0.01$). There was a trend between the incidence of muscle synergies and the level of motor-function in clusters 3 and 9 ($p < 0.05$).

Wii-baseball Game Performance

The number of balls hit by patients was averaged for each recording session. The number of Wii-baseball hits increased ($p < 0.001$) from early therapy (4.42 ± 0.63) to late therapy (7.37 ± 0.40) and was sustained at 6-month follow-up (6.33 ± 0.65, $p = 0.106$). There was no difference in the duration of the Wii-baseball swing between groups (low, 1.30 ± 0.51 s; moderate, 1.37 ± 0.24 s; high, 0.75 ± 0.15 s; $p = 0.379$), i.e., there was no effect of motor-function level.

Clinical Motor-Function Assessments

The clinical motor-function measures showed significant improvements from pre- to post-therapy. WMFT task times for the pooled data reduced (improved) from 38.1 ± 7.8 to 33.6 ± 7.2 s ($p = 0.004$), FMA scores increased from 46.6 ± 3.6 to 48.9 ± 3.6 ($p = 0.001$), and MALQOM scores of 60.1 ± 8.7 increased to 91.3 ± 8.1 ($p < 0.001$). All improvements were sustained at 6-month follow-up so that changes from post-therapy to the follow-up assessments were not significant (WMFT, $p = 0.917$; FMA, $p = 0.107$; MALQOM, $p = 0.454$).

DISCUSSION

In this longitudinal study, we identified and quantified muscle synergies *during* formal therapy sessions for patients with chronic stroke and different levels of motor-function at early and late therapy, and for a subset of patients at 6-month follow-up. As far as we can ascertain, this is the first study to investigate changes in the coordinated activation of muscles in chronic stroke during rehabilitation activities, rather than during unrelated clinical assessment tasks or restricted experimental tasks. The novel aspects of this study include a broad spectrum of poststroke residual voluntary motor-function; and the nature of the complex movement that was largely unconstrained, i.e., the start and end points were not experimentally predetermined. Therapist-guided quality of movement was the primary objective of the task during which EMG was recorded, and not the recording *per se* or game performance. Despite this, we identified differences in the number of muscle synergies used by patients as a function of the level of motor deficit. Thus, the profile of coordinated muscle activation varied by the level of residual motor-function in chronic stroke.

There is abundant evidence in the literature that motor ability is stable in the poststroke chronic period (52–54), even in the presence of some therapy protocols (55). It is also clear that targeted therapy can improve motor ability in contrast to control groups [(56, 57), see Ref. (58)]. The control groups receiving usual care in these studies provide further evidence of the stability of motor performance in chronic stroke for patients not receiving therapy or receiving usual care. In our setting, stable motor performance was established using pre-baseline to baseline testing in a randomized controlled study comparing WMT and modified Constraint-induced Movement Therapy (38).

The statistical outcomes in this study underestimate the level of information provided by this complex series of analyses and reflect the absence of a consistent pattern of change for between-patient EMG as identified in Hasam-Shariati et al. (Paper 1). The number of synergies used during Wii-baseball increased (although not significantly) with therapy for patients with low and moderate motor-function. At early therapy, there was a trend between the number of synergies and the level of motor-function that suggests different patterns of coordinated muscle activation between motor-function groups. The VAF of muscle synergies increased with a higher number of synergies, since the muscle activation can be defined more accurately with more synergies (i.e., smaller error) (17). VAF changed significantly with the level of motor-function but not over time within a level. Clustering the synergies from all patients showed that the incidence of three clusters has an association with the level of motor-function. Cluster analyses provide a means of demonstrating changes in the muscle weighting of some synergies between control and stroke groups (51). This suggests the distribution of muscle weightings within synergies in the present study changed as a consequence of therapy, as most synergy clusters changed from early to late therapy.

The similarity of muscle synergies has been investigated differently across studies. For example, the similarity of muscle weightings was used to demonstrate patients with different levels of motor ability used the same muscles during an isometric force generation task (51); whereas the timing profile was used to reveal different numbers of muscle synergies according to the level of motor ability during gait cycle (17). Our results reflect those of Clark et al. (17), in that the similarity of synergy timing profiles was used to distinguish the difference in the number of muscle synergies between groups: three distinct synergies defined the movement for patients with low motor-function, while four synergies were required for patients with moderate and high motor-function.

The coordination necessary to define a complex movement was associated with the level of residual voluntary motor-function but not the duration of the swing, with differences across time points not as evident as those shown in EMG analysis (42). This was confirmed by video recordings showing less complexity and more muscle co-activation for patients with low motor-function. Yet despite significant improvements in clinical assessments and Wii-baseball game performance, there was no difference in the number of muscle synergies over time. However, the change in the structure of muscle weightings from the cluster analysis at early and late therapy indicates that muscle recruitment changed between time points and that there was more diversity in muscle synergies after therapy.

Typically, muscle synergies for stroke patients are derived from stereotypical (1, 17) or experimentally constrained (30, 51) tasks. However, in this study, the movement was largely unconstrained. Although this may have reduced the sensitivity of the analysis, it is a better reflection of task-related real-world use of the upper limb after stroke. This approach also provides a more direct assessment of the neurophysiological changes induced by therapy (59). Stroke patients with different levels of motor-function use different strategies to resolve the same problem (task) (60). As highlighted by Hesam-Shariati et al. (42), the muscle characteristics for each patient differ depending on various neuromuscular limitations including weakness, hypertonicity, and spasticity. Such differences alter the goals of therapy (38) and result in more deliberate movement patterns than are seen in healthy control subjects (39).

The movement analyzed in this study was performed as part of a structured therapy program (61) with no attempt at standardization as would occur under experimental conditions (7, 51). Due to the range of motor impairment of the patients involved in this study, there were no standardized requirements for specific joint involvement or movement. The aim of this movement during therapy was to increase movement excursion (range of motion), velocity, strength, and control based on the generalized movement parameters of a baseball swing by a healthy subject. Although little attention was paid to the rules of the game, those for Wii-baseball provided some consistency in the patient striking response, in that the ball must be pitched (by the device) within a relatively small area (62). Thus, the onset of movement was determined through the delivery of the ball by the device. When the patient mistimed the movement and did not hit the ball but completed a swing, this movement was included in the analysis. While the start point of the movement was in an unrestricted task-dependant spatiotemporal

framework, the end point, duration, speed, and direction were unconstrained *a priori* (38, 40).

The muscles contributing to a synergy varied from patient to patient and between patients within each level of motor-function. Synergy analysis provides a means of examining changes in motor coordination after stroke independent of the movement strategy of each patient (63). Our previous paper (42) focused on the dominant muscle activated during each activity. Here, synergy analyses provide a means of understanding how the brain coordinates neuromuscular control of movement (64) that can be used to build a dynamic model of the poststroke rehabilitation process.

Clearly, more than six muscles are necessary to produce the movement studied, even poststroke. We were limited in the number of channels available by the recording system and have previously reported EMG of tibialis anterior (59). The upper body muscles in this study were selected for two main reasons. First, they included a distribution along the neuromuscular axis of the more-affected side. Second, this recording montage limits the potential for EMG cross talk (65) while still reflecting the major muscle groups involved in the movement across the patient cohort (62). We incorporated EMG from the trapezius muscle in this analysis as a surrogate marker for trunk rotation where biceps and deltoid activation were insufficient to generate sufficient swing movements in Wii-baseball. EMG data from FDI were included to reflect the use of the hand during therapy because this muscle is readily accessible during therapy and was taken as a surrogate marker of intrinsic hand muscle activity. FDI activation was task dependant during Wii-baseball. EMG from triceps brachii was not recorded due to technical limitations including its very low level of activation compared to BB (66) and problems with loose skin in older patients which when combined with gravity acted to pull the sensor away from the muscle, rendering such recordings unreliable.

Synergy analysis addresses coordinated muscle activation (between muscles) rather than activation within each muscle. It is impossible after stroke to assume any similarity of underlying physiology and anatomy or to individually record the activity of each motor unit contributing to compound muscle activity. Any recording of EMG or method of EMG analysis will provide a biased estimate of activity (67, 68). The number of simultaneous recordings will not reduce the bias; in our experience, it increases the potential for cross talk and phase cancelation. Given the variability of impairment and ability after stroke both in the neuromusculature and factors impinging on the neuromusculature (e.g., somatosensation), in addition to the trial to trial variability for any given patient, it would be extremely difficult to estimate the ideal number of channels necessary for error-free synergy analyses.

Clinical Implications

This study addresses the paucity of neurophysiological studies after stroke and as a consequence of therapy. This longitudinal investigation of changes in muscle synergies with therapy in chronic stroke across patients with different levels of motor-function provides initial insights into some of the neurophysiological mechanisms underpinning a therapy that is the equivalent of current best practice poststroke, namely, Constraint-induced Movement Therapy (38). Although there were few changes in the number of synergies, the altered structure of muscle synergies suggest that the coordination of muscle activation did improve and that this change was reflected in improved clinical assessment data (28) [presented in detail in Hesam-Shariati et al. (42)]. In particular, the significant improvements in MALQOM scores reflect greater independence in activities of everyday living (38).

This study demonstrates that the number of synergies, synergy timing profiles, distribution of muscle weightings, and VAF for muscle synergies differ according to the level of motor-function; particularly for patients with low motor-function at early therapy. These differences provide more detailed information about the neurophysiological functioning after stroke and how this changes with therapy. We hypothesize that altered muscle synergy structure reflects changes in brain connectivity, but this requires specific investigations of brain imaging or brain stimulation (69, 70). Nevertheless, the structure of muscle synergies can be used as an approach to classify stroke patients and to inform rehabilitation methods. However, muscle synergy analyses are insufficient on their own to fully understand neurophysiological changes with therapy after stroke and these analyses further emphasize the absence of any one tool to adequately quantify and explain the changes after stroke or with rehabilitation.

Study Limitations

The primary focus of WMT is on the quality of movement, and increasing independent use of the more-affected upper limb in everyday tasks (38, 39). For this reason, therapy instructions are not those that would be used with healthy control subjects. For example, the different phases of the movement are emphasized differently depending on the level of motor impairment and may be practiced individually before being combined during the game performance using the principles of shaping (71), much like a sporting drill. Although the absence of healthy control subjects is a limitation of this study, the different movement patterns observed during game play (39) may limit the usefulness of such comparisons.

The sample size in this study is small within each level of motor-function. However, the total number of patients compares well with previous stroke studies investigating muscle synergies (18, 23, 30, 51). According to clinical assessment scores, this cohort included a wide range of residual voluntary motor capacity, particularly those with low motor-function who are rarely recruited in poststroke therapy and neurophysiology studies. This approach reduces the potential for statistically significant outcomes when data are pooled (59) but provides data that can be more readily generalized to the stroke population, although this study in chronic stroke cannot be generalized to the acute and subacute phase.

CONCLUSION

Motor control differs for patients with different levels of residual voluntary motor-function when performing the same movement.

Despite this, muscle synergies can be identified and monitored during therapy to understand changes in motor control of a largely unconstrained complex movement. A higher number of muscle synergies reflects greater movement complexity and task-related phasic muscle activation. This result is evidence for less complexity and more co-activation in the patterns of muscle activation for patients with low motor-function. The increased number of synergies by late therapy suggests improved motor control with more distinct phases of movement for patients with low motor-function. The change in the muscle synergy clusters by late therapy and different patterns of recovery indicate that the recruitment and activation of muscles change during therapy.

ETHICS STATEMENT

This study was carried out in accordance with the recommendations of St. Vincent's Hospital Human Research Ethics Committee with written informed consent from all patients. All patients gave written informed consent in accordance with the Declaration of Helsinki. The protocol was approved by the St. Vincent's Hospital Human Research Ethics Committee, Sydney.

AUTHOR CONTRIBUTIONS

PMcN conceived, designed, and supervised the study and manuscript preparation. NH-S assisted with data collection, developed multiple code scripts, analyzed data, and drafted the manuscript, TT implemented data collection, AT-B implemented therapy, and CS undertook clinical assessments. All authors contributed to manuscript revision.

FUNDING

This study was funded by National Health and Medical Research Council and the NSW Office of Science and Medical Research, Australia.

REFERENCES

1. Cheung VC, Piron L, Agostini M, Silvoni S, Turolla A, Bizzi E. Stability of muscle synergies for voluntary actions after cortical stroke in humans. *Proc Natl Acad Sci U S A* (2009) 106(46):19563–8. doi:10.1073/pnas.0910114106
2. d'Avella A, Lacquaniti F. Control of reaching movements by muscle synergy combinations. *Front Comput Neurosci* (2013) 7:42. doi:10.3389/fncom.2013.00042
3. Bizzi E, Cheung V, d'Avella A, Saltiel P, Tresch M. Combining modules for movement. *Brain Res Rev* (2008) 57(1):125–33. doi:10.1016/j.brainresrev.2007.08.004
4. d'Avella A, Saltiel P, Bizzi E. Combinations of muscle synergies in the construction of a natural motor behavior. *Nat Neurosci* (2003) 6(3):300–8. doi:10.1038/nn1010
5. Lee WA. Neuromotor synergies as a basis for coordinated intentional action. *J Mot Behav* (1984) 16(2):135–70. doi:10.1080/00222895.1984.10735316
6. Tresch MC, Saltiel P, d'Avella A, Bizzi E. Coordination and localization in spinal motor systems. *Brain Res Rev* (2002) 40(1):66–79. doi:10.1016/S0165-0173(02)00189-3
7. Coscia M, Cheung VC, Tropea P, Koenig A, Monaco V, Bennis C, et al. The effect of arm weight support on upper limb muscle synergies during reaching movements. *Stroke* (2014) 13(14):32–4. doi:10.1186/1743-0003-11-22
8. Safavynia SA, Torres-Oviedo G, Ting LH. Muscle synergies: implications for clinical evaluation and rehabilitation of movement. *Top Spinal Cord Inj Rehabil* (2011) 17(1):16–24. doi:10.1310/sci1701-16
9. Cheung VC, d'Avella A, Tresch MC, Bizzi E. Central and sensory contributions to the activation and organization of muscle synergies during natural motor behaviors. *J Neurosci* (2005) 25(27):6419–34. doi:10.1523/JNEUROSCI.4904-04.2005
10. Tresch MC, Saltiel P, Bizzi E. The construction of movement by the spinal cord. *Nat Neurosci* (1999) 2(2):162–7. doi:10.1038/5721
11. Kargo WJ, Nitz DA. Early skill learning is expressed through selection and tuning of cortically represented muscle synergies. *J Neurosci* (2003) 23(35):11255–69.
12. Chvatal SA, Macpherson JM, Torres-Oviedo G, Ting LH. Absence of postural muscle synergies for balance after spinal cord transection. *J Neurophysiol* (2013) 110(6):1301–10. doi:10.1152/jn.00038.2013
13. Ting LH, Macpherson JM. A limited set of muscle synergies for force control during a postural task. *J Neurophysiol* (2005) 93(1):609–13. doi:10.1152/jn.00681.2004
14. Torres-Oviedo G, Macpherson JM, Ting LH. Muscle synergy organization is robust across a variety of postural perturbations. *J Neurophysiol* (2006) 96(3):1530–46. doi:10.1152/jn.00810.2005
15. Overduin SA, d'Avella A, Roh J, Bizzi E. Modulation of muscle synergy recruitment in primate grasping. *J Neurosci* (2008) 28(4):880–92. doi:10.1523/JNEUROSCI.2869-07.2008
16. Chvatal SA, Ting LH. Common muscle synergies for balance and walking. *Front Comput Neurosci* (2013) 7:48. doi:10.3389/fncom.2013.00048
17. Clark DJ, Ting LH, Zajac FE, Neptune RR, Kautz SA. Merging of healthy motor modules predicts reduced locomotor performance and muscle coordination complexity post-stroke. *J Neurophysiol* (2010) 103(2):844–57. doi:10.1152/jn.00825.2009
18. Coscia M, Monaco V, Martelloni C, Rossi B, Chisari C, Micera S. Muscle synergies and spinal maps are sensitive to the asymmetry induced by a unilateral stroke. *J Neuroeng Rehabil* (2015) 12(1):39. doi:10.1186/s12984-015-0031-7
19. Chvatal SA, Torres-Oviedo G, Safavynia SA, Ting LH. Common muscle synergies for control of center of mass and force in nonstepping and stepping postural behaviors. *J Neurophysiol* (2011) 106(2):999–1015. doi:10.1152/jn.00549.2010
20. Torres-Oviedo G, Ting LH. Muscle synergies characterizing human postural responses. *J Neurophysiol* (2007) 98(4):2144–56. doi:10.1152/jn.01360.2006
21. Ajiboye AB, Weir R. Muscle synergies as a predictive framework for the EMG patterns of new hand postures. *J Neural Eng* (2009) 6(3):036004. doi:10.1088/1741-2560/6/3/036004
22. Zariffa J, Steeves J, Pai DK. Changes in hand muscle synergies in subjects with spinal cord injury: characterization and functional implications. *J Spinal Cord Med* (2012) 35(5):310–8. doi:10.1179/2045772312Y.0000000037
23. Cheung VC, Turolla A, Agostini M, Silvoni S, Bennis C, Kasi P, et al. Muscle synergy patterns as physiological markers of motor cortical damage. *Proc Natl Acad Sci U S A* (2012) 109(36):14652–6. doi:10.1073/pnas.1212056109
24. Borzelli D, Berger DJ, Pai D, D'avella A. Effort minimization and synergistic muscle recruitment for three-dimensional force generation. *Front Comput Neurosci* (2013) 7:186. doi:10.3389/fncom.2013.00186
25. Roh J, Rymer WZ, Beer RF. Robustness of muscle synergies underlying three-dimensional force generation at the hand in healthy humans. *J Neurophysiol* (2012) 107(8):2123–42. doi:10.1152/jn.00173.2011
26. Gizzi L, Nielsen JF, Felici F, Ivanenko YP, Farina D. Impulses of activation but not motor modules are preserved in the locomotion of subacute stroke patients. *J Neurophysiol* (2011) 106(1):202–10. doi:10.1152/jn.00727.2010
27. Hidler JM, Carroll M, Federovich EH. Strength and coordination in the paretic leg of individuals following acute stroke. *IEEE Trans Neural Syst Rehabil Eng* (2007) 15(4):526–34. doi:10.1109/TNSRE.2007.907689
28. Tropea P, Monaco V, Coscia M, Posteraro F, Micera S. Effects of early and intensive neuro-rehabilitative treatment on muscle synergies in acute post-stroke patients: a pilot study. *J Neuroeng Rehabil* (2013) 10(1):103. doi:10.1186/1743-0003-10-103

29. Dipietro L, Krebs HI, Fasoli SE, Volpe BT, Stein J, Bever C, et al. Changing motor synergies in chronic stroke. *J Neurophysiol* (2007) 98(2):757–68. doi:10.1152/jn.01295.2006
30. Li S, Zhuang C, Zhang X, Niu CM, Xie Q, Lan N. Analysis of muscle synergy for evaluation of task-specific performance in stroke patients. *Paper Presented at the Engineering in Medicine and Biology Society (EMBC), 2016 IEEE 38th Annual International Conference*. Orlando, FL (2016).
31. Roh J, Rymer WZ, Perreault EJ, Yoo SB, Beer RF. Alterations in upper limb muscle synergy structure in chronic stroke survivors. *J Neurophysiol* (2013) 109(3):768–81. doi:10.1152/jn.00670.2012
32. Werring DJ, Toosy AT, Clark CA, Parker GJ, Barker GJ, Miller DH, et al. Diffusion tensor imaging can detect and quantify corticospinal tract degeneration after stroke. *J Neurol Neurosurg Psychiatry* (2000) 69(2):269–72. doi:10.1136/jnnp.69.2.269
33. Ramsay JW, Barrance PJ, Buchanan TS, Higginson JS. Paretic muscle atrophy and non-contractile tissue content in individual muscles of the post-stroke lower extremity. *J Biomech* (2011) 44(16):2741–6. doi:10.1016/j.jbiomech.2011.09.001
34. Kautz S, Brown D. Relationships between timing of muscle excitation and impaired motor performance during cyclical lower extremity movement in post-stroke hemiplegia. *Brain* (1998) 121(3):515–26. doi:10.1093/brain/121.3.515
35. Tresch MC, Cheung VC, d'Avella A. Matrix factorization algorithms for the identification of muscle synergies: evaluation on simulated and experimental data sets. *J Neurophysiol* (2006) 95(4):2199–212. doi:10.1152/jn.00222.2005
36. Chiovetto E, Berret B, Delis I, Panzeri S, Pozzo T. Investigating reduction of dimensionality during single-joint elbow movements: a case study on muscle synergies. *Front Comput Neurosci* (2013) 7:11. doi:10.3389/fncom.2013.00011
37. Frère J, Hug F. Between-subject variability of muscle synergies during a complex motor skill. *Front Comput Neurosci* (2012) 6:99. doi:10.3389/fncom.2012.00099
38. McNulty PA, Thompson-Butel AG, Faux SG, Lin G, Katrak PH, Harris LR, et al. The efficacy of Wii-based Movement Therapy for upper limb rehabilitation in the chronic poststroke period: a randomized controlled trial. *Int J Stroke* (2015) 10(8):1253–60. doi:10.1111/ijs.12594
39. Mouawad MR, Doust CG, Max MD, McNulty PA. Wii-based Movement Therapy to promote improved upper extremity function post-stroke: a pilot study. *J Rehabil Med* (2011) 43(6):527–33. doi:10.2340/16501977-0816
40. Trinh T, Scheuer SE, Thompson-Butel AG, Shiner CT, McNulty PA. Cardiovascular fitness is improved post-stroke with upper-limb Wii-based Movement Therapy but not dose-matched constraint therapy. *Top Stroke Rehabil* (2016) 23(3):208–16. doi:10.1080/10749357.2016.1138672
41. Casadio M, Tamagnone I, Summa S, Sanguineti V. Neuromotor recovery from stroke: computational models at central, functional, and muscle synergy level. *Front Comput Neurosci* (2013) 7:97. doi:10.3389/fncom.2013.00097
42. Hesam-Shariati N, Trinh T, Thompson-Butel AG, Shiner CT, McNulty PA. A longitudinal electromyography study of complex movements in poststroke therapy. 1: heterogenous changes despite consistent improvements in clinical assessments. *Front Neurol* (2017). doi:10.3389/fneur.2017.00340
43. Thompson-Butel AG, Lin GG, Shiner CT, McNulty PA. Two common tests of dexterity can stratify upper limb motor function after stroke. *Neurorehabil Neural Repair* (2014) 28(8):788–96. doi:10.1177/1545968314523678
44. Shiner CT, Pierce KD, Thompson-Butel AG, Trinh T, Schofield PR, McNulty PA. BDNF genotype interacts with motor function to influence rehabilitation responsiveness poststroke. *Front Neurol* (2016) 7:69. doi:10.3389/fneur.2016.00069
45. Wolf SL, Lecraw DE, Barton LA, Jann BB. Forced use of hemiplegic upper extremities to reverse the effect of learned nonuse among chronic stroke and head-injured patients. *Exp Neurol* (1989) 104(2):125–32. doi:10.1016/S0014-4886(89)80005-6
46. Fugl-Meyer AR, Jääskö L, Leyman I, Olsson S, Steglind S. The post-stroke hemiplegic patient. 1. a method for evaluation of physical performance. *Scand J Rehabil Med* (1974) 7(1):13–31.
47. Uswatte G, Taub E, Morris D, Vignolo M, McCulloch K. Reliability and validity of the upper-extremity Motor Activity Log-14 for measuring real-world arm use. *Stroke* (2005) 36(11):2493–6.
48. Lee DD, Seung HS. Learning the parts of objects by non-negative matrix factorization. *Nature* (1999) 401(6755):788–91. doi:10.1038/44565
49. Paatero P, Tapper U. Positive matrix factorization: a non-negative factor model with optimal utilization of error estimates of data values. *Environmetrics* (1994) 5(2):111–26. doi:10.1002/env.3170050203
50. Berry MW, Browne M, Langville AN, Pauca VP, Plemmons RJ. Algorithms and applications for approximate nonnegative matrix factorization. *Comput Stat Data Anal* (2007) 52(1):155–73. doi:10.1016/j.csda.2006.11.006
51. Roh J, Rymer WZ, Beer RF. Evidence for altered upper extremity muscle synergies in chronic stroke survivors with mild and moderate impairment. *Front Hum Neurosci* (2015) 9:6. doi:10.3389/fnhum.2015.00006
52. Krakauer JW. Motor learning: its relevance to stroke recovery and neurorehabilitation. *Curr Opin Neurol* (2006) 19(1):84–90. doi:10.1097/01.wco.0000200544.29915.cc
53. Mirbagheri MM, Rymer WZ. Time-course of changes in arm impairment after stroke: variables predicting motor recovery over 12 months. *Arch Phys Med Rehabil* (2008) 89(8):1507–13. doi:10.1016/j.apmr.2008.02.017
54. Stinear C. Prediction of recovery of motor function after stroke. *Lancet Neurol* (2010) 9(12):1228–32. doi:10.1016/S1474-4422(10)70247-7
55. Mehrholz J, Pohl M, Platz T, Kugler J, Elsner B. Electromechanical and robot-assisted arm training for improving activities of daily living, arm function, and arm muscle strength after stroke. *Cochrane Database Syst Rev* (2015) (11):CD006876. doi:10.1002/14651858.CD006876.pub4
56. Page SJ, Levine P, Leonard A, Szaflarski JP, Kissela BM. Modified constraint-induced therapy in chronic stroke: results of a single-blinded randomized controlled trial. *Phys Ther* (2008) 88(3):333. doi:10.2522/ptj.20060029
57. Wolf SL, Winstein CJ, Miller JP, Taub E, Uswatte G, Morris D, et al. Effect of constraint-induced movement therapy on upper extremity function 3 to 9 months after stroke: the EXCITE randomized clinical trial. *JAMA* (2006) 296(17):2095–104. doi:10.1001/jama.296.17.2095
58. Teasell RW, Murie Fernandez M, McIntyre A, Mehta S. Rethinking the continuum of stroke rehabilitation. *Arch Phys Med Rehabil* (2014) 95(4):595–6. doi:10.1016/j.apmr.2013.11.014
59. Trinh T, Shiner CT, Thompson-Butel AG, McNulty PA. Targeted upper-limb Wii-based Movement Therapy also improves lower-limb muscle activation and functional movement in chronic stroke. *Disabil Rehabil* (2016):1–11. doi:10.1080/09638288.2016.1213892
60. Cirstea M, Levin MF. Compensatory strategies for reaching in stroke. *Brain* (2000) 123(5):940–53. doi:10.1093/brain/123.5.940
61. McNulty PA. Games for rehabilitation: Wii-based Movement Therapy improves poststroke movement ability. *Games Health J* (2012) 1(5):384–7. doi:10.1089/g4h.2012.0055
62. Deutsch JE, Brettler A, Smith C, Welsh J, John R, Guarrera-Bowlby P, et al. Nintendo Wii sports and Wii fit game analysis, validation, and application to stroke rehabilitation. *Top Stroke Rehabil* (2011) 18(6):701–19. doi:10.1310/tsr1806-701
63. McMorland AJ, Runnalls KD, Byblow WD. A neuroanatomical framework for upper limb synergies after stroke. *Front Hum Neurosci* (2015) 9:82. doi:10.3389/fnhum.2015.00082
64. Ting LH, McKay JL. Neuromechanics of muscle synergies for posture and movement. *Curr Opin Neurobiol* (2007) 17(6):622–8. doi:10.1016/j.conb.2008.01.002
65. Hug F. Can muscle coordination be precisely studied by surface electromyography? *J Electromyogr Kinesiol* (2011) 21(1):1–12. doi:10.1016/j.jelekin.2010.08.009
66. Bowden JL, Taylor JL, McNulty PA. Voluntary activation is reduced in both the more-and less-affected upper limbs after unilateral stroke. *Front Neurol* (2014) 5:239. doi:10.3389/fneur.2014.00239
67. De Luca CJ, Gilmore LD, Kuznetsov M, Roy SH. Filtering the surface EMG signal: movement artifact and baseline noise contamination. *J Biomech* (2010) 43(8):1573–9. doi:10.1016/j.jbiomech.2010.01.027
68. Tibold R, Fuglevand AJ. Prediction of muscle activity during loaded movements of the upper limb. *J Neuroeng Rehabil* (2015) 12(1):6. doi:10.1186/1743-0003-12-6
69. Bajaj S, Butler AJ, Drake D, Dhamala M. Brain effective connectivity during motor-imagery and execution following stroke and rehabilitation. *Neuroimage Clin* (2015) 8:572–82. doi:10.1016/j.nicl.2015.06.006
70. Rathee D, Cecotti H, Prasad G. Estimation of effective fronto-parietal connectivity during motor imagery using partial granger causality analysis. *Paper Presented at the Neural Networks (IJCNN), 2016 International Joint Conference*, Vancouver (2016).

71. Taub E, Crago JE, Burgio LD, Groomes TE, Cook EW, DeLuca SC, et al. An operant approach to rehabilitation medicine: overcoming learned nonuse by shaping. *J Exp Anal Behav* (1994) 61(2):281–93. doi:10.1901/jeab.1994.61-281

Conflict of Interest Statement: The authors declare that the research was conducted in the absence of any commercial or financial relationships that could be construed as a potential conflict of interest.

frontiers in Neurology

ORIGINAL RESEARCH
published: 19 July 2017
doi: 10.3389/fneur.2017.00337

Evaluation of Functional Correlation of Task-Specific Muscle Synergies with Motor Performance in Patients Poststroke

Si Li[1], Cheng Zhuang[1], Chuanxin M. Niu[2], Yong Bao[2], Qing Xie[2] and Ning Lan[1,3]**

[1] Institute of Rehabilitation Engineering, Med-X Research Institute, Shanghai Jiao Tong University, Shanghai, China,
[2] Department of Rehabilitation, Ruijin Hospital of School of Medicine, Shanghai Jiao Tong University, Shanghai, China,
[3] Division of Biokinesiology and Physical Therapy, University of Southern California, Los Angeles, CA, United States

The central nervous system produces movements by activating specifically programmed muscle synergies that are also altered with injuries in the brain, such as stroke. In this study, we hypothesize that there exists a positive correlation between task-specific muscle synergy and motor functions at joint and task levels in patients following stroke. The purpose here is to define and evaluate neurophysiological metrics based on task-specific muscle synergy for assessing motor functions in patients. A patient group of 10 subjects suffering from stroke and a control group of nine age-matched healthy subjects were recruited to participate in this study. Electromyography (EMG) signals and movement kinematics were recorded in patients and control subjects while performing arm reaching tasks. Muscle synergies of individual patients were extracted off-line from EMG records of each patient, and a baseline pattern of muscle synergy was obtained from the pooled EMG data of all nine control subjects. Peak velocities and movement durations of each reaching movement were computed from measured kinematics. Similarity indices of matching components to those of the baseline synergy were defined by synergy vectors and time profiles, respectively, as well as by a combined similarity of vector and time profile. Results showed that pathological synergies of patients were altered from the characteristics of baseline synergy with missing components, or varied vector patterns and time profiles. The kinematic performance measured by peak velocities and movement durations was significantly poorer for the patient group than the control group. In patients, all three similarity indices were found to correlate significantly to the kinematics of movements for the reaching tasks. The correlation to the Fugl-Meyer score of arm was the highest with the vector index, the lowest with the time profile index, and in between with the combined index. These findings illustrate that the analysis of task-specific muscle synergy can provide valuable insights into motor deficits for patients following stroke, and the task-specific similarity indices are useful neurophysiological metrics to predict the function of neuromuscular control at the joint and task levels for patients.

Keywords: muscle synergy, stroke, physiological index, reaching movement, motor performance, kinematics

OPEN ACCESS

Edited by:
Sheng Li,
The University of Texas, United States

Reviewed by:
Wei Zhang,
City University of New York, United States
Jinsook Roh,
Rehabilitation Institute of Chicago, United States

****Correspondence:***
Ning Lan
ninglan@sjtu.edu.cn;
Qing Xie
ruijin_xq@sjtu.edu.cn

Specialty section:
This article was submitted to Stroke, a section of the journal Frontiers in Neurology

Received: *04 April 2017*
Accepted: *28 June 2017*
Published: *19 July 2017*

Citation:
Li S, Zhuang C, Niu CM, Bao Y, Xie Q and Lan N (2017) Evaluation of Functional Correlation of Task-Specific Muscle Synergies with Motor Performance in Patients Poststroke. Front. Neurol. 8:337. doi: 10.3389/fneur.2017.00337

INTRODUCTION

Stroke is the top three causes of death in aging population (1), and the followed disability has obliged a compelling medical and social need for rehabilitation (2). Among the impairments, motor dysfunction causes the most widely afflicted medical condition in patients suffering from stroke (3), especially that of the upper extremity due to its high usage in daily activities in life and non-stereotypical motor patterns (4). Even though substantial research efforts have been devoted to improving recovery (2), motor rehabilitation in the upper extremity is still a challenging issue because of limited understanding of the neurophysiological underpinning of recovery and lack of effective interventions (2, 5, 6).

One of the main issues in the rehabilitation of motor function is to assess the residual motor ability of patients quantitatively, so as to determine the amount of intervention necessary and to give precise guide in rehabilitation training. In clinical practice, measurements of kinematics and graded scores have often been used to estimate the overall ability of patients to accomplish daily tasks (4) and are adopted as outcome measures in clinical trials and research (7). The clinical scores commonly used in the evaluation of upper limb functions include Fugl-Meyer (FM) Score, Wolf Motor Function Test, and Motor Assessment Scale (8), which are based on performance outcomes of a set of required motor tasks. These scores lack the detailed information with regard to the ways that muscles and joints are controlled during a motor task (4, 9, 10). Since the motor task may be accomplished by a patient using the normal way (restitution), or using alternative strategies (compensation) (4), it is desirable that the assessment of motor ability can provide additional information that allows clinicians to determine the integrity of neuromuscular control in patients. This is particularly important in clinical intervention using multi-muscle functional electrical stimulation (FES) (11, 12).

To understand the control of the complex, redundant neuromuscular system (13), muscle synergy has been proposed as an optimized strategy by the central nervous system (CNS) (14–17), in which a group of muscles is activated in a specific spatiotemporal pattern (14, 15, 18–28). Muscle synergy allows the description of motor behaviors with a relatively limited set of muscle activation patterns (28). In this study, we adopted the "synchronous synergies" (9, 27, 29, 30), in which motor tasks are controlled by linear combinations of a few stereotyped sets of muscles (synergy vectors) that are activated simultaneously by corresponding temporal sequences (time profiles). Multiple computational approaches using factorization algorithms have demonstrated a robust synergy (31). Studies of upper limb and cyclic movements in healthy human subjects also revealed that muscle synergies are consistent across subjects (32–35).

Muscle synergy changes as new motor skills are acquired in infants with time (36), or with injuries in the CNS (37, 38), such as stroke (33), or in the peripheral neuromuscular system (29). Synergy analysis of a group of motor tasks in upper limb of stroke patients has indicated that nervous injuries might cause direct changes in the spatial connection or temporal activation of synergies (33, 39) and the followed adaptation may lead to merging or fractionation of synergy components in patients (39). A group of isometric force tasks in upper limb showed that muscle synergy differed in patients suffering from mild-to-severe stroke (40). It is also shown that there existed a correlation between clinical scores and performance of individual components of the muscle synergy during cycling in the lower extremity (41). These early studies strongly suggested that synergy analysis may be a potentially promising method for assessing motor functions in patients following stroke. Yet, questions remain as to how well a task-specific muscle synergy, such as reaching by the upper limb (6), could be a good metric for assessing neuromuscular control, task performance, and clinical outcome in hemiparetic patients. This is particularly relevant since task-oriented training (TOT) revealed a better recovery of motor function than non-task specific training (2, 6). Hemiparetic patients often had problems in reaching (42) due to abnormally high spasticity of muscles in the shoulder and elbow joints (42–44), especially in elbow extension (45). The structure of muscle synergy for a specific task may contain useful information on the residual ability, or deficits, of neuromuscular control in patients poststroke.

In this study, we hypothesized that there exists a positive correlation between task-specific muscle synergy and motor functions at joint and task levels in patients following stroke. The objective here was to establish a functional correlation between task-specific muscle synergy and performance at neuromuscular, joint, and task levels. To understand the relationship between normal and pathological synergy patterns, we developed a procedure to analyze synergies of forward and lateral reaching movements in age-matched control subjects and patients with hemiparesis. Both tasks required elbow extension and were highly used in daily activities of life. New similarity indices of synergy vectors, time profiles, and their combination were defined to represent quantitatively the relationship of pathological synergies of patients to the baseline synergy from control group. Analysis was carried out to correlate task-specific similarity indices with kinematics of joint movements, as well as the clinical FM score of patients. The task-specific muscle synergy is relatively simple to obtain clinically, and these quantitative metrics can be used in conjunction with clinical scores for assessing motor abilities and deficits in patients. More importantly, the pathological and baseline patterns of muscle synergies are useful in designing patient specific, assistive FES strategies for stroke rehabilitation (11, 12). Preliminary results of this study were also reported elsewhere in a conference proceeding (46).

MATERIALS AND METHODS

Subjects

Ten hemiparetic patients with poststroke (S04–S13, 60.9 ± 6.6 years, nine males, detailed description in **Table 1**) were recruited from Ruijin Hospital of School of Medicine (Shanghai, China) for this study; they all suffered from moderate-to-severe impairment from ischemic stroke with a Fugl-Meyer score of upper limb (FMul) <50. The clinical scores presented in **Table 1** were measured before the experiment by designated physical therapists. Patients had one of the following conditions were excluded from

TABLE 1 | Description of stroke patients recruited for this study.

Patient ID	Most affected side	Location of lesion	Months poststroke	BS	MMAS	FMul	FMarm
S04	Right	Left thalamus, right temporal lobe	5	IV	1	27	16
S05	Left	Brain stem, bilateral basal ganglia	5	IV	1	28	23
S06	Left	No significant lesions	10	IV	0	18	17
S07	Left	Right lateral ventricle, right frontal lobe	5	III	1	18	16
S08	Left	Right corona radiata	2	III	1	22	16
S09	Left	Right basal ganglia	3	IV	0	31	24
S10	Left	Right basal ganglia, right lateral ventricle, right frontal lobe	2	III	1+	21	20
S11	Left	Right pontine	2	III	0	32	21
S12	Left	Right lateral ventricle	3	IV	0	20	16
S13	Right	Left temporal, parietal and occipital lobe	2	II	1+	20	13

BS, Brunnstrom Scale (I, no movement; IV, appear activities out of cooperative movement); MMAS, Modified Ashworth score for the elbow (0, no increase in muscle tone; 4, marked increase in muscle tone, affected part is rigid); FMul, Fugl-Meyer score of upper limb (full score of 66 for motor function in upper limb); FMarm, Fugl-Meyer score of arm (upper arm and forearm, full score of 44).

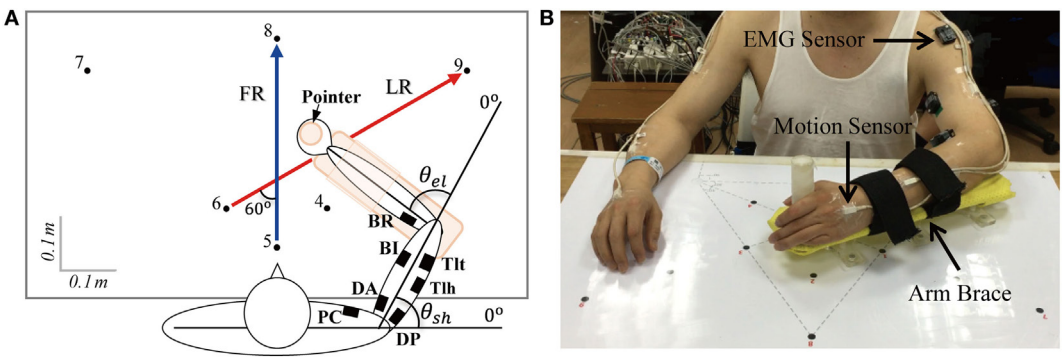

FIGURE 1 | **(A)** Forward reaching (FR) and lateral reaching (LR) tasks and **(B)** experimental set up. Subjects moved the pointer from point 5 to point 8 when performing FR and from point 6 to point 9 for LR when the right arm was evaluated (point 4 to point 7 when the left arm was evaluated). Seven channels of electromyography (EMG) were recorded with wireless EMG sensors indicated by filled squares in **(A)**, the recorded muscles were pectoralis clavicular (PC), anterior deltoid (DA), posterior deltoid (DP), biceps (BI), triceps long head (Tlh), Brachioradialis (BR), and triceps lateral head (Tlt). θ_{el} and θ_{sh} are the angles of elbow and shoulder joints. Signals of position were collected by seven motion sensors (B), and they were put on bilateral upper arms, forearms, palms, and thorax (back of neck).

our study: spasticity higher than 1+ (MMAS); metal implant; cognitive difficulties; any other diseases that cause neurological impairment; and passive attitude with the experiment. Nine age-matched healthy subjects from the institute's campus (H01–H09, 57.8 ± 5.9 years, five males, one left-handed) were recruited randomly as control. This study was approved by the Institutional Review Boards of Ruijin Hospital and the Ethics Committee of Human and Animal Experiments of the Med-X Research Institute of Shanghai Jiao Tong University. All subjects signed the form of informed consent before the experiment.

Experiments

All subjects performed horizontal point-to-point reaching movements by their evaluated upper limb (affected hand of patient and dominant hand of control subject). As shown in **Figure 1**, subjects sat comfortably next to the table, with the trunk restrained with a corrective backrest to reduce its leaning forward and backward. The forearm was configured onto an arm brace on a smoothed motion plane. The hand was holding a vertical handle (pointer) with a diameter of 3 cm. The tasks included forward reaching (FR) and lateral reaching (LR). In FR, subjects moved the pointer from point 5 to 8 (36 cm), and in LR, the reaching was 48 cm from point 6 to 9 (right hand evaluated)/point 4 to 7 (left hand evaluated). The initial and terminal points were indicated by black dots on the horizontal motion plane with a diameter of 1 cm. Before the experiment, the subjects were trained to react to a verbal trigger and perform reaching as fast as possible without displacing their trunk. After practicing about five trials to make smooth reaching tasks, the recording started. During movements, no corrections were allowed and there was no feedback on their performance. Each task was repeated 10 times. A rest of 10 s in between trials and a break of 5 min between tasks were given for the subjects. During the experiment, positions of upper limb were captured at 120 Hz by seven magnetic motion sensors (**Figure 1**) with Motion Monitor II System (Innovative Sports Training, Inc., USA), and joint angles of shoulder and elbow were calculated from sensor signals. Electromyographys (EMGs) of seven muscles, including pectoralis clavicular (PC), anterior deltoid (DA), posterior deltoid (DP), biceps (BI), triceps long head (Tlh), brachioradialis (BR), and triceps lateral head (Tlt), were recorded at 1,925.9 Hz using

the Trigno Wireless EMG System (Delsys Inc., USA), the isolated EMG sensors (37 mm × 26 mm × 15 mm) were placed center of each muscle belly under the guidance of therapists.

Signal Processing

Data of the 10 patients and nine control subjects were pre-processed before synergy analysis. Kinematic data were low-passed filtered with a cutoff frequency of 10 Hz (10th order zero-lag Butterworth) and differentiated to obtain velocity. The time instant where the velocity of hand was 10% of its peak value was defined as the initiation and termination of movement (47). The reaction time was defined as the time period from the instant of verbal trigger to that of movement initiation. A bell-shaped velocity profile (48) was used to fit the hand velocity of subjects (with time length of twice the movement duration, centered on the peak) to a Gaussian distribution curve (Curve Fitting Tool, MATLAB 2012b; MathWorks Inc.), the coefficient of determination (R of bell-shape) was adopted as the goodness of fitting.

Before processing the EMGs, signals from the Motion Monitor system and the Delsys EMG system were synchronized with the trigger signal. The EMG was first notch filtered at 50 and 120 Hz and their higher harmonics (16th order zero-lag Butterworth) to eliminate the interferences of power line and magnetic transmitter of Motion Monitor II System. The EMGs were then demeaned and band-passed filtered between 20 and 400 Hz (48th order zero-lag Butterworth) to remove motion artifacts and high frequency noise. Filtered EMG signals were finally full-wave rectified and low-passed filtered at the cutoff frequency of 20 Hz (19th order zero-lag Butterworth) to obtain the EMG envelope. The signals were filtered with zero phase shift, and all processing were performed off-line by custom developed programs (MATLAB R2012b; MathWorks Inc.).

Muscle Synergy Extraction

We computed task-specific synergy for FR and LR tasks independently. Non-negative matrix factorization (NNMF) algorithm (31, 49) was chosen here to extract synchronized synergy from recorded EMGs of seven muscles (28). The algorithm modeled muscle activities as linear combinations of a sufficient number of synergy vectors (muscle weight) with time profiles of muscle activation. The algorithm was applied to the data set of each subject (including patients and control subjects) to extract individual synergy, as well as a pooled data set from all control subjects to extract a baseline synergy.

For individual synergy extraction, EMG envelopes with a time length of twice movement duration, centered at the peak of hand velocity, were selected to construct EMG matrix. The synergy decomposition was given in the following equation:

$$M_{(t\times 1,000)\times 7} = T_{(t\times 1,000)\times n} V_{n\times 7} + \text{residuals} \quad (1)$$

where M is the original EMG matrix with seven columns of EMG data, t is the number of trials with each trial resampled to 1,000 data points; V is the matrix of n synergy vectors, in which each row contains a combination of the seven muscles with different weights, each vector was normalized to have unit length during factorization, and T is the matrix of time profiles, in which each column contains the activation profiles corresponding to each row of vector in all trials. During the extraction, the number of synergy vector (n) was increased successively from one to seven, and for each iteration of n, the NNMF was repeated 25 times, the repetition with the lowest residuals of reconstruction was selected.

We defined the baseline synergy for each task as that obtained from pooled data of all nine control subjects. For each task, data of all trials from H01 to H09 were cascaded together to construct the pooled EMG matrix, and the baseline synergy was then computed from Eq. 1 using the pooled EMG matrix.

To evaluate the goodness of EMG reconstruction, the criterion of variance account for (VAF) (27, 29, 33, 39, 50) was adopted here in the following equation:

$$\text{VAF} = 1 - (\| M - D \|^2 / \| M - \text{mean}\,(M) \|^2) \quad (2)$$

in which, D is the reconstructed EMG matrix; the operator "mean" constructs a matrix of the same size of M but with the elements of each row replaced by the mean value of corresponding row in M. The number of synergy vectors (k) that sufficiently recaptured the original EMGs was then defined as the minimum number (n) when VAF exceeded 80% (39) in more than half of the subjects in both groups. We checked the goodness of reconstruction of global and individual muscle's EMG at k synergy components with another widely used criterion of variance account for (VAF′) (40, 41, 51) as well, which is sensitive to both shape and amplitude of the signals (50).

$$\text{VAF}' = 1 - (\| M - D \|^2 / \| M \|^2) \quad (3)$$

Similarities of Task-Specific Synergies

To quantify the overall similarity between the synergies of subjects and the baseline synergy for each task, we defined new similarity indices to evaluate the degree of matching (see Appendix in Supplementary Material for computational details). We first calculated a value of closeness of individual synergy vector and time profile in each subject with respect to those of baseline synergy as in previous studies (29, 41, 51). Referring to the maximal scalar product criterion (29), individual synergy vector of a subject was paired to one of the baseline vectors, which had the maximal value of scalar product with it. Closeness of vectors (C_V) was defined as the scalar product of the paired vectors. The two corresponding time profiles were then identified as the same profile, with the closeness (C_T) given by a shape symmetry index (52). In this study, we proposed three similarity indices, such as vector similarity (S_V), time profile similarity (S_T), and combined similarity (S_{COM}), to evaluate the overall similarity of subject's synergy to the baseline synergy. The similarity indices of S_V and S_T were calculated using the closeness of individual vectors (C_V) and time profiles (C_T), respectively, weighted by their contributions (eigenvalues) in the reconstruction of original EMG matrix (see Appendix in Supplementary Material for computational details). The combined similarity (S_{COM}) was the average of S_V and S_T. The three similarity indices of task-specific synergy, such as S_V, S_T, and S_{COM}, were subsequently used to analyze how good was the neuromuscular control in patients than in control subjects.

Statistical and Correlation Analyses

Two-way ANOVA was performed to detect the difference in kinematics, closeness, and similarity indices for group (cross-task, namely the pool of FR and LR) and task (cross-group, namely the pool of patients and control subjects). Independent two-tailed two sample *t*-test was used to detect differences in kinematics, closeness, and similarity indices between tasks within each group and between groups within each task. Linear regression was carried out in each task to assess the correlation of similarity indices to functional performance, such as kinematics and clinical FM scores. Cross-task similarity indices (S_V', S_T', and S_{COM}') were also obtained by averaging the similarity indices of the two tasks, such as FR and LR, which were also correlated to the clinical FM score. Such correlations may allow us to establish the functional relationship of task-specific similarity indices to performance outcomes assessed by kinematic measurements and clinical scores. The significance level in statistical and correlation analyses was set at $p < 0.05$.

RESULTS

Kinematics and EMGs in Control and Stroke Subjects

The kinematics and EMGs of two patients (S04 and S11) and two control subjects (H01 and H09) are presented in **Figure 2**. The synergy patterns of S04 and S11 were analyzed because they showed two extremes of performance in kinematics and clinical score (FMarm), as well as synergy. Comparing the two groups, control subjects showed a short reaction time, a smooth trajectory, and a classic bell-shaped velocity profile. However, the two patients showed a longer reaction time, a stagnated movement trajectory, and a multi-peak velocity profile, especially in FR (see for example in S04). For LR, both groups performed with higher speeds and smoother trajectories than for FR. The envelope of EMGs also exhibited intergroup differences. EMGs of H01 and H09 generally showed high bursting levels during movements and returned to steady state in a short period of time. In contrast, patients tended to activate their Tlt repeatedly in order to extend the elbow to reach to the final position. As shown in **Figure 2C**, both patients had weak firings of their Tlh, but a high background EMG in BR and PC, which impeded elbow and shoulder extensions. Patients also used a prolonged co-contraction of antagonistic muscles to stabilize joints after reaching the destination.

Distribution of cross-task kinematic parameters in the two groups of subjects is plotted in **Figure 3A**. Separated distributions between patients and control subjects in reaction time, duration, R of bell-shape, and peak velocity could be visually recognized. Statistical analysis was performed to detect the differences of kinematics between tasks and groups. When comparing the two groups, significant difference was found in the four kinematics for each individual task (two-tailed, two sample *t*-tests) and the cross-task (two-way ANOVA). More specifically, patients possessed longer reaction time, longer duration of movement, lower R of bell-shape, and smaller velocity ($p = 0.000$ for the four parameters in FR, LR, and cross-task). The larger variability of duration and R of bell-shape ($p = 0.000$ for the two parameters in FR, LR, and cross-task) in patients reflected the varying degree of motor functional deficits. Two-way ANOVA also showed that kinematics except duration were significantly different between the two tasks with the cross-group (**Figure 3B**). LR displayed longer reaction time ($p = 0.028$), larger velocity ($p = 0.000$), and higher R of bell-shape ($p = 0.008$). This is in accordance with better kinematic profiles of LR than FR in **Figures 2A,B**.

Muscle Synergies in Control and Stroke Subjects

In this study, we adopted the 80% VAF criterion (39) in the extraction of task-specific synergy in both control subjects and poststroke patients. For the baseline synergy from nine control subjects, the global VAF was 82.39% for FR with a three-component synergy and 89.95% for LR with a four-component synergy. As for individual subjects, global VAF of all subjects exceeded 80%, except for one case (S06) with a VAF = 74% in LR. When the number of components was increased to four for FR or five for LR, respectively, the improvement of VAF was less than 5%. Thus, we adopted the three-component synergy for FR and the four-component synergy for LR. We calculated the goodness of reconstruction with VAF′ as well (Eq. 3) (40, 41, 51). In both baseline and individual synergies, the global VAF′ for FR at three components and LR at four components were over 94%. In baseline synergy, VAF′ of individual muscle revealed the average of 88 (±13)% for FR at three components (VAF′ of six muscles exceeded 75%, except for muscle BR at 69%), and 90 (±12)% for LR at four components (VAF′ of six muscles exceeded 75%, except for muscle PC at 73%). For synergies of individual subject in the two groups, VAF′ of individual muscle was 93 (±2)% for FR at three components and 94 (±4)% for LR at four components.

Figure 4 depicts the synergies of FR (**Figure 4A**) and LR (**Figure 4B**) for the baseline pattern, a control subject (H09), and two patients (S04 and S11). Matching components and closeness of H09, S04, and S11 were indicated above the vectors and time profiles (also listed in Tables A1 and A2 in Supplementary Material). The matched vectors and time profiles within a task were indicated with the same color. The value of closeness ranged from 0.00 to 1.00, with 1.00 representing the highest degree of resemblance. It was clear that the synergy of H09 (**Figure 4**, b,f) possessed all components of those in the baseline synergy (**Figure 4**, a,e) with a high degree of resemblance in spatial and temporal patterns in both tasks. However, the synergies of patients of S04 (**Figure 4**, c,g) and S11 (**Figure 4**, d,h) deviated significantly from the baseline synergy. In FR task, the Tlt- and Tlh-dominant components of $V_B(1)$ in the baseline synergy were missing in the synergies of both patients. The DP-dominant component of $V_B(2)$ was partially preserved by two subjects, with a low closeness due to the dominating of BI. Only the third component $V_B(3)$ was kept relatively intact. In LR task, the components $V_B(1)$, $V_B(3)$, and $V_B(4)$ were well preserved in the synergies of both patients. Only the second component $V_B(2)$ was missing from the synergies of S04 and S11. The missing component in the two patients could be explained by their weak activations of Tlt and Tlh. Component of $V(3)$ in S04 and $V(4)$ in S11 showed poor closeness to $V_B(4)$, probably due to spastic firing of their PCs. In both tasks, the time

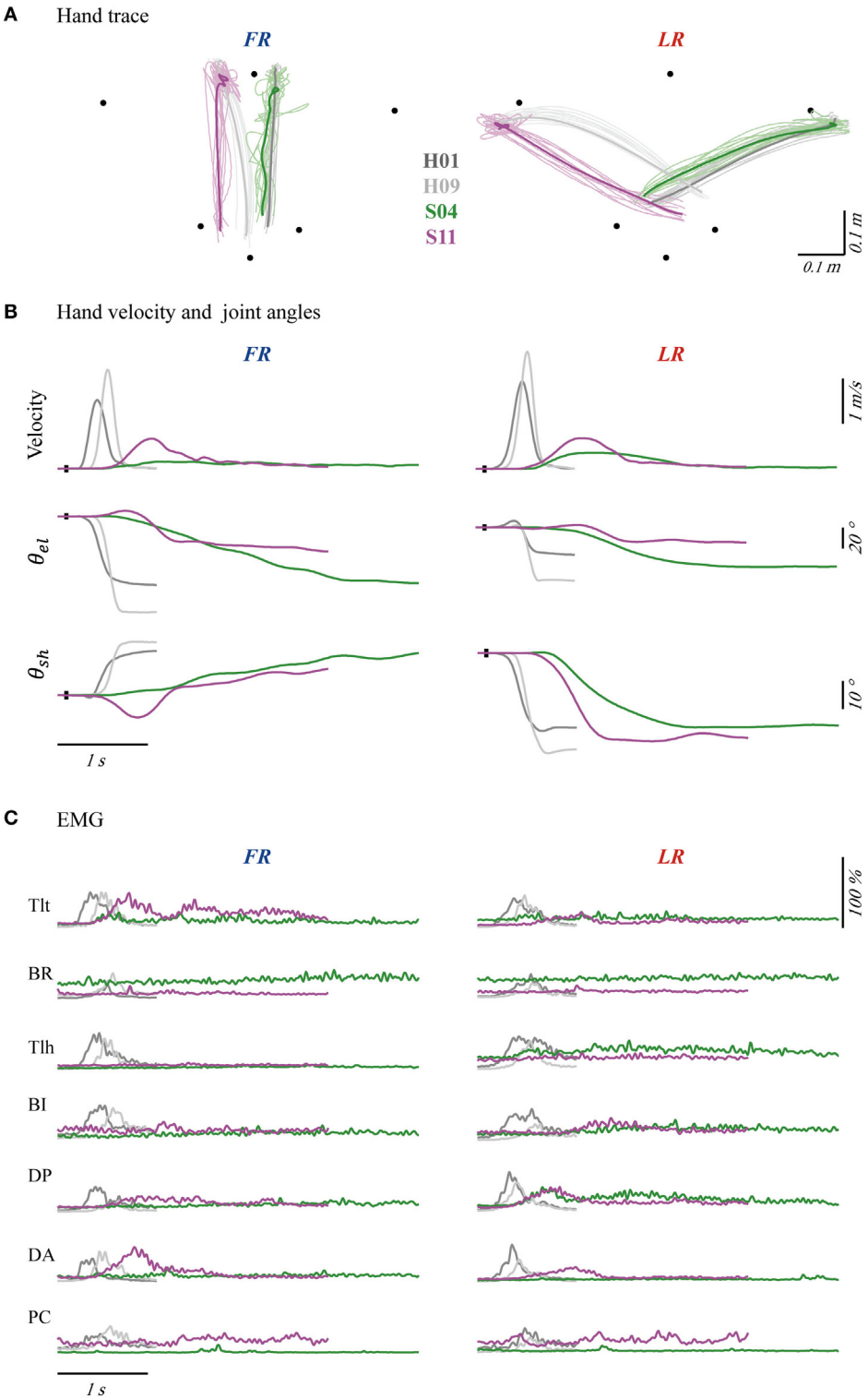

FIGURE 2 | Hand traces **(A)**, hand velocities and joint angles **(B)**, and seven channels of averaged electromyography (EMG) **(C)** of four typical subjects, with forward reaching (FR) in the left column and lateral reaching (LR) in the right column. The bold profiles in **(A)** represent averaged trajectories. The black dots on profiles of velocity and angle indicate trigger tag. θ_{el} and θ_{sh} were angles of elbow and shoulder joint. Initial angles of shoulder and elbow were calibrated to mean of the four subjects' angles. Each channel of EMG was normalized according to its maximal firing level among trials in each task. The EMGs were collected from pectoralis clavicular (PC), anterior deltoid (DA), posterior deltoid (DP), biceps (BI), triceps long head (Tlh), Brachioradialis (BR) and triceps lateral head (Tlt).

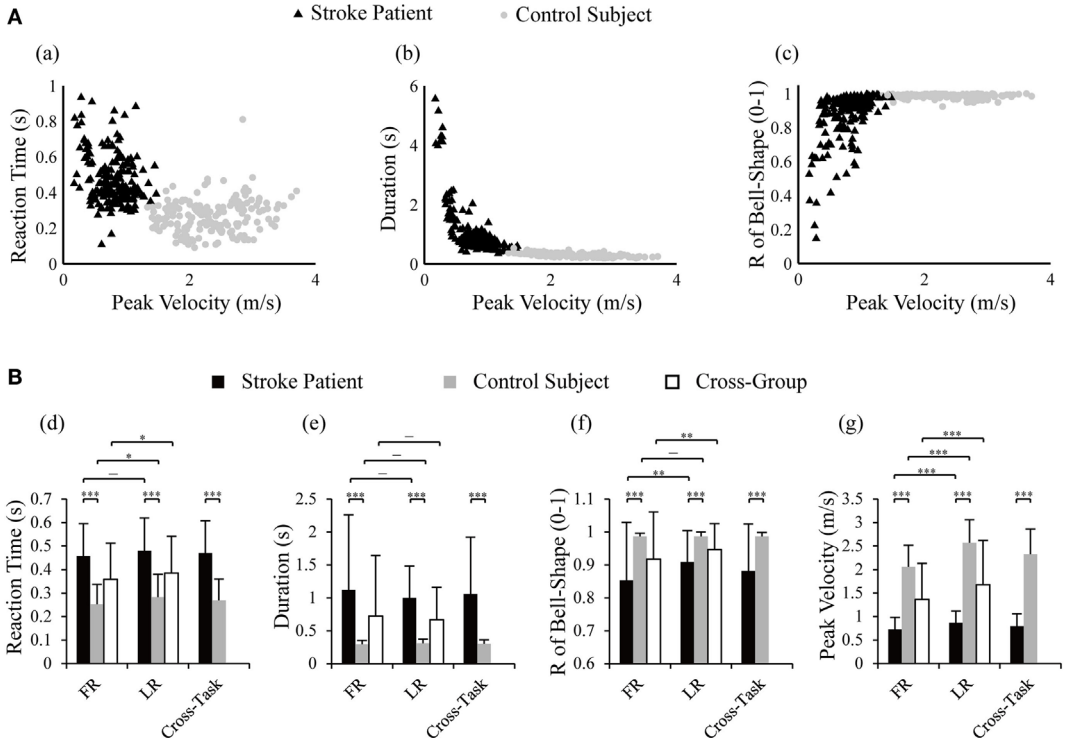

FIGURE 3 | Distribution of reaction time, duration, and R of bell-shape with peak velocity in control subjects and stroke patients **(A)** and statistical comparison between the two groups and tasks **(B)**. Two-way ANOVA was performed with the factor of group (cross-task) and factor of task (cross-group); two-tailed two sample *t*-tests were used to detect differences in kinematics between tasks within one group and between group within one task; $^{*}p < 0.05$, $^{**}p < 0.01$, $^{***}p < 0.001$. R of bell-shape represents the coefficient of determination in fitting the velocity profile to Gaussian distribution curve.

profiles of both patients exhibited lower closeness to those of the baseline synergy than H09.

The matching pairs and closeness values of each vector (C_V) and time profile (C_T) in the two groups of subjects are listed in Tables A1 and A2 in Supplementary Material for FR and LR, respectively (see Appendix in Supplementary Material). As shown in **Figure 4**, the closeness values for FR were ranked generally in the order of the control subject H09 (high), patient S11 (low), and patient S04 (lowest). But for LR, the closeness values in the two patients (S04 and S11) was comparable to those of the control subject (H09), comparing to those of FR.

Inter-task comparison of baseline synergy showed that $V_B(1)$ and $V_B(2)$ in FR had the closeness of 0.97 to $V_B(2)$ and $V_B(1)$ in LR, respectively. $V_B(3)$ in FR and LR had a closeness of 0.84. The high closeness values declared that FR and LR possessed similar pattern of the first three components. This could explain the phenomenon that patients missing $V_B(1)$ of FR often missed $V_B(2)$ of LR simultaneously (**Figure 4**, Tables A1 and A2 in Supplementary Material). $V_B(4)$ was an extra decelerating component required in LR, and it had been well preserved by subjects in both group [closeness of 0.94 averaged from highest closeness to $V_B(4)$ in each subject]. The difference in the first three components between FR and LR lies in contribution of each component and their timing of activation. $V_B(1)$ and $V_B(2)$ acted as accelerating and decelerating units in FR, respectively, while in LR, $V_B(1)$ and $V_B(2)$ were synergistic in extension of the joints. $V_B(3)$ in FR was activated first in FR to flex the shoulder and extend elbow, and in LR, it helped with the extension of elbow after shoulder extension by $V_B(1)$ of LR. The mean closeness in patients to $V_B(1)$, $V_B(2)$, and $V_B(3)$ were 0.70, 0.64, and 0.56 in FR and 0.84, 0.89, and 0.94 in LR, respectively.

Statistical Analysis of Closeness and Similarity

Results of statistical analysis on closeness in all vectors (C_V) and time profiles (C_T) between groups and tasks are plotted in **Figure 5**, a,b. LR showed higher averaged closeness of vectors than FR in patients ($p = 0.001$), control ($p = 0.044$), and cross-group ($p = 0.000$). No difference in C_T was found between FR and LR in patients, control subjects, and cross-group ($p > 0.05$). Between groups, patients presented lower C_V and C_T than those of control subjects in FR, LR, and cross-task, except for C_V in LR (**Figure 5**, a).

To quantify the overall resemblance of muscle synergy of patients to baseline synergy, we defined more comprehensive similarity indices, a vector index (S_V), a time profile index (S_T), and a combined index (S_{COM}) (Eqs A7–A9 in Supplementary Material). Statistical results (**Figure 5B**) indicated significant higher similarity of S_V and S_{COM} in LR than FR in patients, control subjects, and cross-group (p values in legends of **Figure 5**). Between groups, similarity indices of S_V, S_T, and S_{COM} showed significantly higher values for control group than those for

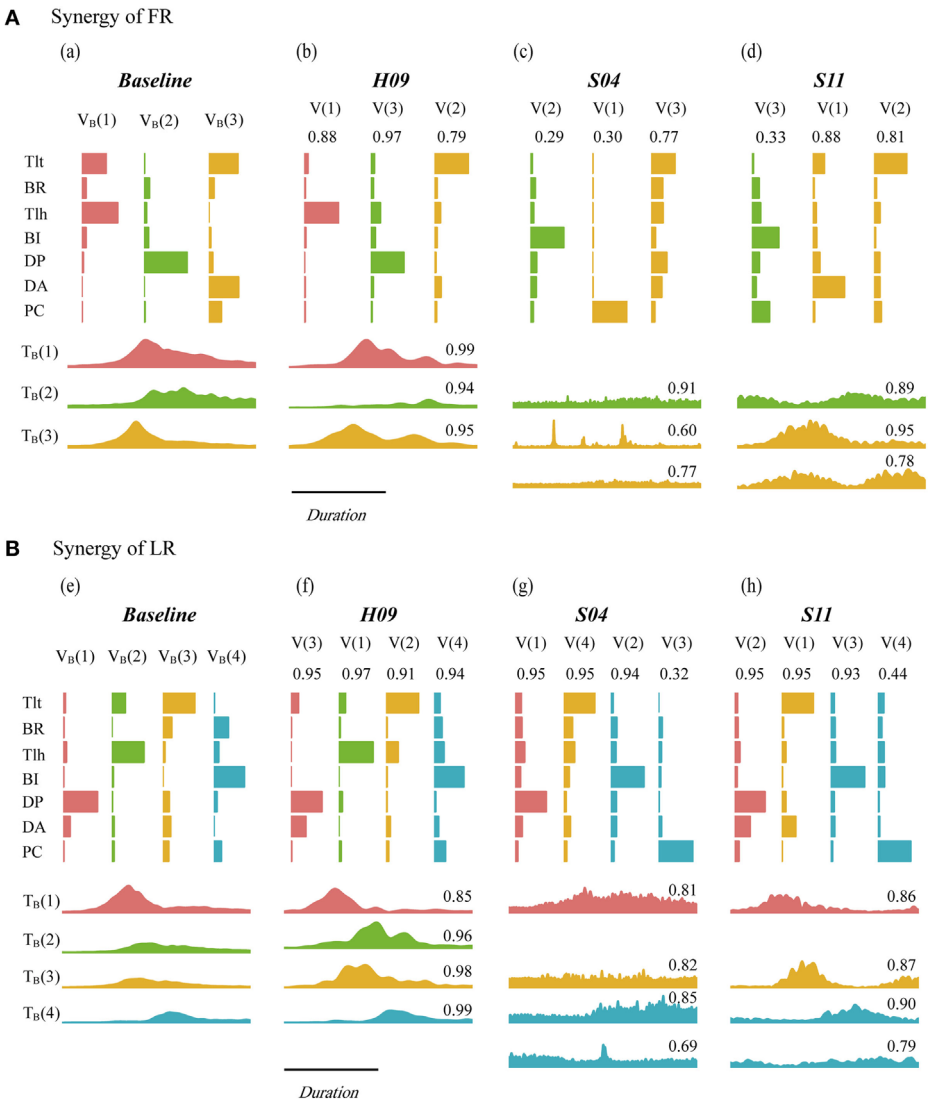

FIGURE 4 | Synergy of baseline pattern, H09, S04, and S11 in forward reaching (FR) **(A)** and lateral reaching (LR) **(B)**. V_B and T_B are the vector component and time profile of the baseline synergy from the nine control subjects of the control group. V and T are the vector component and time profile from individual subject. Paired synergy vectors were plotted with same color for each task, the corresponding time profiles were presented successively under vector plots within each subject. The value on top of each vector and time profile indicates the value of closeness of individual vector and time profile.

the patients in FR, LR, and cross-task (p values in legends of **Figure 5**). This result illustrated that the similarity indices were capable of distinguishing the different abilities of neuromuscular modulation in control subjects from those in patients.

Correlation of Similarity Indices with Kinematics and FM Score

The similarity indices were correlated to kinematics of movements and clinical FM scores of patients, as presented in **Figures 6** and **7**, respectively. In general, significant correlations were found for the three similarity indices with respect to kinematic performance (**Figure 6**, significances were indicated in separated regressions), except for an insignificant correlation between S_T and R of bell-shape in LR (**Figure 6**, e). Patients with a higher value of similarity indices tended to produce a better performance with a higher ratio of peak velocity and duration (P/D) (**Figure 6A**), and a better bell-shape profile (**Figure 6B**). Thus, the three similarity indices represent well the abilities of patients to control FR and LR tasks.

A relationship between patient FM scores and similarity indices is also clearly demonstrated in **Figure 7**. Since the recorded muscles were concerned with functions of the arm, the Fugl-Meyer score of arm (FMarm) was picked out from the Fugl-Meyer score of upper limb (FMul) as a factor for correlation analysis. For FR shown in **Figure 7A**, the FMarm score was found to have a significant positive correlation with S_V ($p = 0.040$) (**Figure 7**, a) and S_{COM} ($p = 0.039$) (**Figure 7**, c). Only a weak correlation between S_T and FMarm ($p = 0.074$) was evident (**Figure 7**, b).

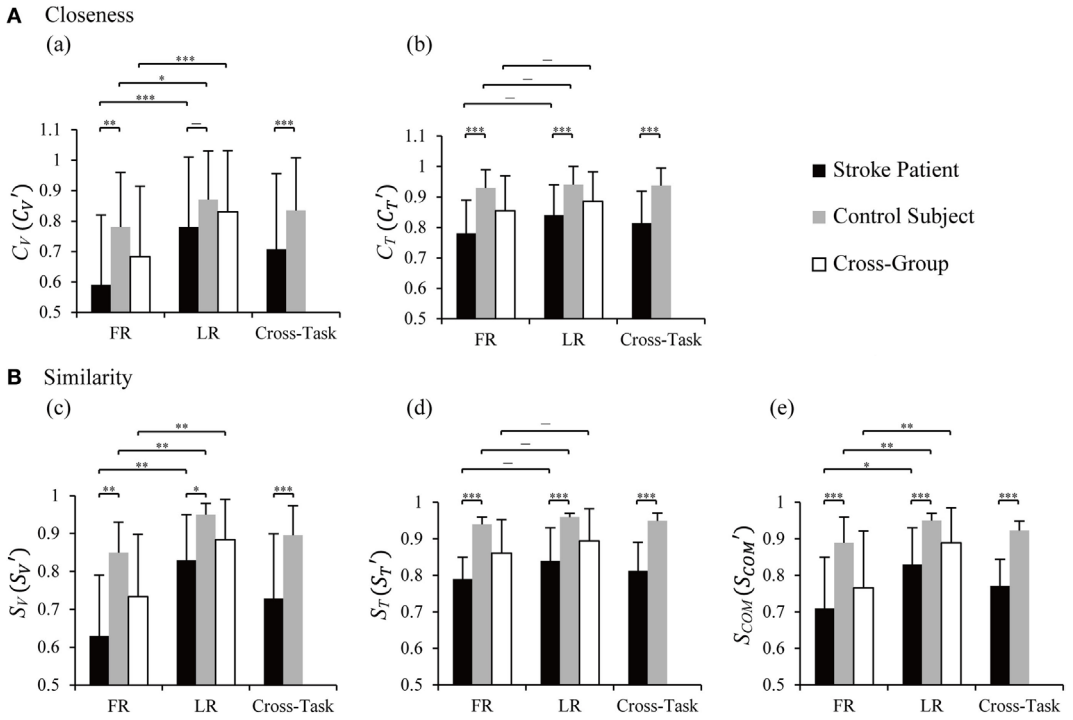

FIGURE 5 | Statistical analysis of closeness **(A)** and similarity indices **(B)** between the two groups and tasks. C_V and C_T are closeness of individual vector and time profile, C_V' and C_T' are closeness in cross-task, and the values were averaged from C_V and C_T of the two tasks, respectively. S_V, S_T, and S_{COM} are similarity indices of vectors, time profiles, and their combination. S_V', S_T', and S_{COM}' were cross-task similarity indices averaged from those of forward reaching (FR) and lateral reaching (LR). Two-way ANOVA was performed with the factor of group (cross-task) and factor of task (cross-group); two-tailed two sample *t*-tests was used to detect differences between tasks within one group and between group within one task; $^*p < 0.05$, $^{**}p < 0.01$, $^{***}p < 0.001$. Significant difference in similarity between FR and LR was found in S_V and S_{COM} in patients [$p(S_V) = 0.007$ and $p(S_{COM}) = 0.018$], control subjects [$p(S_V) = 0.004$ and $p(S_{COM}) = 0.003$], and cross-group [$p(S_V) = 0.002$ and $p(S_{COM}) = 0.006$]. Significantly lower similarities in patients were found in FR [$p(S_V) = 0.002$, $p(S_T) = 0.000$, and $p(S_{COM}) = 0.000$], LR [$p(S_V) = 0.020$, $p(S_T) = 0.000$, and $p(S_{COM}) = 0.001$], and cross-task [$p(S_V) = 0.000$, $p(S_T) = 0.000$, and $p(S_{COM}) = 0.000$].

For LR, however, the correlation of the FMarm was not significant for all three similarity indices (**Figure 7B**). This may be due to the fact that FMarm data points in LR were more scatted around the regression line (**Figure 7B**). Using the cross-task similarity indices (**Figure 7C**), a strong correlation of FMarm was evident, especially for the vector similarity S_V' ($p = 0.007$) (**Figure 7**, g) and the S_{COM}' ($p = 0.018$) (**Figure 7**, i). Nevertheless, a trend was clearly displayed in that patients with a higher FMarm score generally demonstrated a higher value of similarity indices. We also checked that no significant correlation existed between all similarity indices and the Fugl-Meyer score of upper limb (FMul).

DISCUSSION

In this study, we developed a computational procedure to evaluate task-specific synergies of reaching movements in stroke patients and age-matched control subjects. We found that three and four components were required to account for forward and lateral reaching movements, respectively. New quantitative indices of similarity of synergy in patients with respect to the baseline synergy were developed and employed to establish positive correlations to kinematic performance and clinical scores, such as FMarm. The results supported our hypothesis that there is a positive correlation between task-specific similarity indices and motor performance in joint and task levels in patients following stroke. This indicated that the new similarity indices based on task-specific synergy could be useful neurophysiological metrics in clinical evaluation to estimate motor dysfunction, or the ability of motor control in conjunction with clinical scores. The main contribution of this study is that we extended the analyses of muscle synergy (33, 40, 41) into quantitative metrics that may facilitate the clinical evaluation of patient's motor functions with insights into neuromuscular control.

Task-Specific Muscle Synergy

We focused on task-specific synergy in patients and demonstrated that the synergy analysis of a specific task could provide valuable insights into deficits in motor functions. TOT has been widely encouraged in stroke rehabilitation (2). Under certain requirements, patients with motor dysfunction are activated to search for better solutions to motor problems (6), and TOT has revealed better recovery of motor function than unspecific task training (2). We chose reaching tasks because discoordination of joints and abnormal co-activations of muscles in upper limb (43, 44) often resulted in difficulty in performing reaching movements in most stroke patients (42). In particular, elbow extension

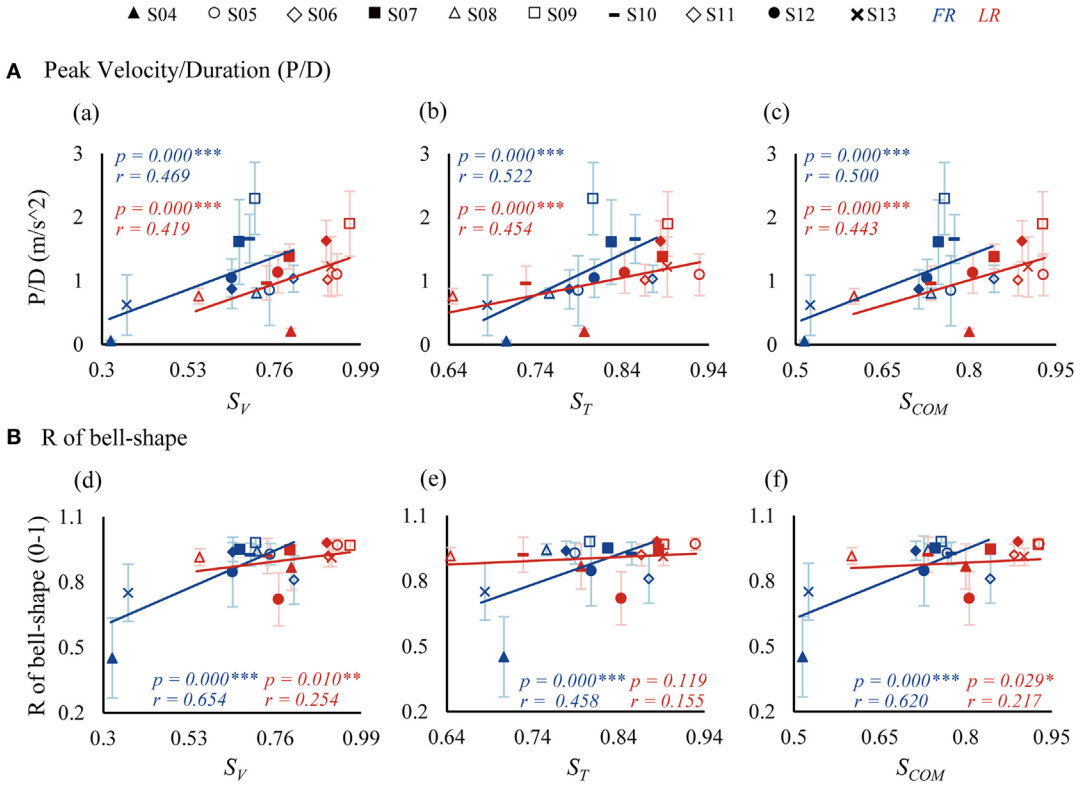

FIGURE 6 | Correlations between similarity indices and kinematics [P/D in **(A)** and R of bell-shape in **(B)**]. P/D is the ratio of peak velocity and duration. R of bell-shape represents the coefficient of determination in fitting the velocity profile to Gaussian distribution curve. S_V, S_T, and S_{COM} are similarity indices of vectors, time profiles, and their combination.

was found to be an important predictor for motor function in patients (45). Thus, instead of pooling a set of arm movements together (33, 35, 39, 40, 53), we chose to examine the forward and lateral reaching movements for task-specific synergy evaluation. This approach could also be applied to other motor tasks that are relevant to clinical task-oriented interventions (2).

We obtained the task-specific baseline synergy as a target of comparison from pooled data of nine control subjects performing FR and LR tasks. Studies have shown that muscle synergies were robust across healthy subjects (32–34). Thus, we adopted the synergy extracted from dominant arms of the control group as an efficient baseline of synergy (54, 55) and compared synergy of the affected arm in patients to the baseline synergy. In our study, synergy baseline extracted from healthy control group presented similar muscle activations with previous studies (28, 32). To evaluate the degree of alteration in individual synergy component in subjects, we adopted scalar product (33, 41) to compute closeness between synergy vectors; a component of synergy of an individual subject was then matched with that of the baseline synergy giving the maximal value of closeness between vectors (29). Closeness of time profiles of paired synergy components was evaluated by a shape symmetry index using cross-correlation (51, 52). Thus, changes of synergy pattern in patients with respect to the baseline synergy could be quantitatively reflected by the values of closeness (Tables A1 and A2 in Supplementary Material). Statistical results showed significant higher closeness in control subjects than those in patients (**Figure 5A**). This confirmed altered muscle synergy in patients after cortical injury (39, 40).

Patients following stroke often had missing components of the baseline synergy (**Figure 4**; Tables A1 and A2 in Supplementary Material). Yet, pathological synergies might still preserve some components of the baseline synergy. Merging in synergy vectors has been observed in patients following stroke (39, 56). This was evident in the task of FR in both patients. $V(3)$ of S04 was the merging of the three components in baseline synergy (reconstruction closeness at 0.98), $V(2)$ of S11 was the combination of $V_B(1)$ and $V_B(3)$ (reconstruction closeness at 0.90). This was in accordance with the finding by Cheung et al. (39), patients had more baseline components that were merged in residual components (S04, comparing with S11) usually showed poorer performance of kinematics and FMarm. This neural compensation may be due to plasticity taking place in the brain (57–59). In addition, identification found fractionation in LR in both patients (39), that $V(3)$ of S04 and $V(4)$ of S11 were differentiated from $V_B(4)$ of baseline synergy. These alterations of synergy vectors in muscle weights in patients shed light not only to the impairment in individual muscle control but also to the regroup of muscles by neural compensation in the brain, which are important indicators of recovery of motor functions after stroke (56).

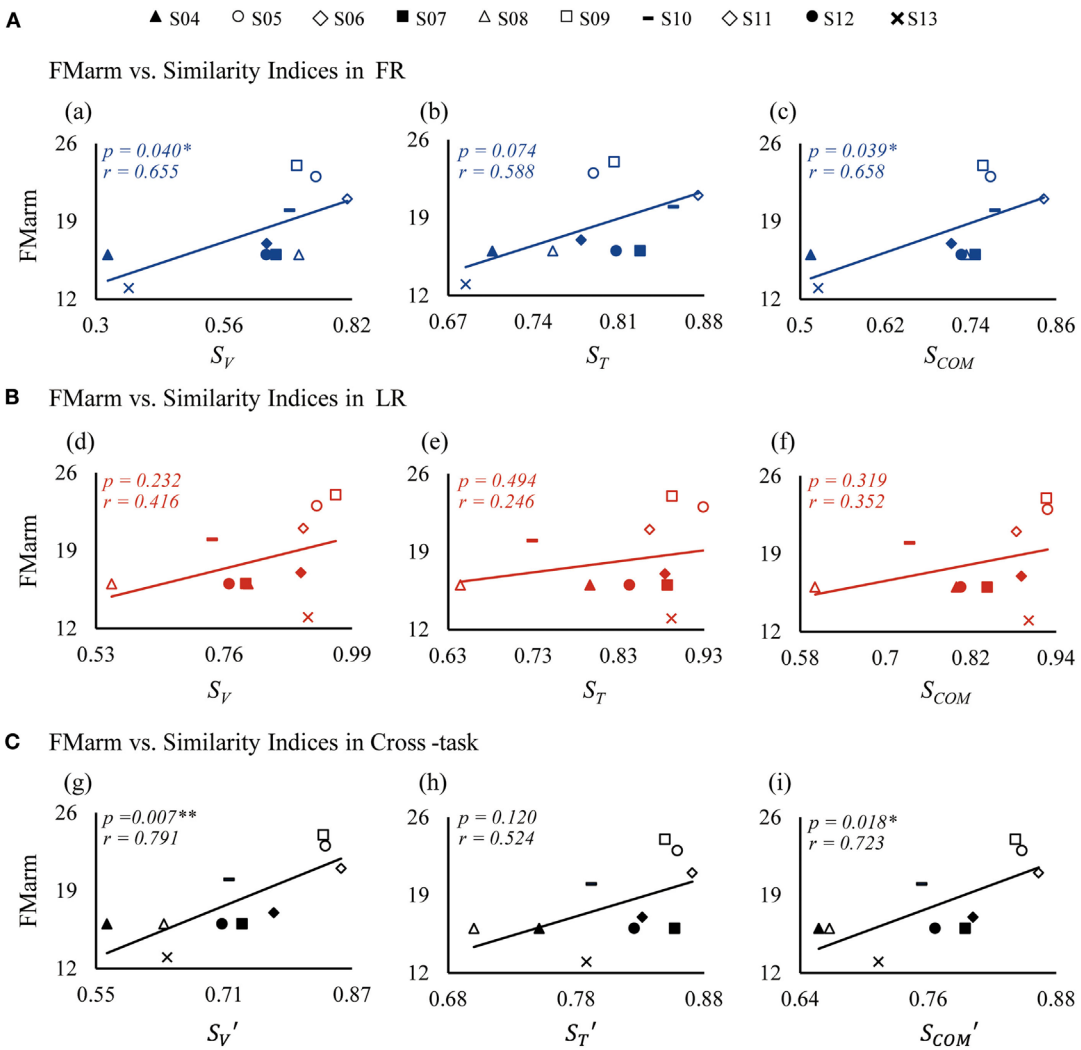

FIGURE 7 | Correlations between similarity indices and FMarm score in forward reaching (FR) **(A)**, lateral reaching (LR) **(B)**, and the cross-task **(C)**. FMarm is Fugl-Meyer score of arm. S_V, S_T, and S_{COM} are similarity indices of vectors, time profiles, and their combination, respectively; while the indices of S_V', S_T', and S_{COM}' are cross-task similarity indices averaged from those of FR and LR.

Similarity Indices and Correlation with Kinematic and Clinical Performance

We extended previous analyses of muscle synergy (33, 40, 41) into quantitative neurophysiological metrics by defining three new similarity indices with values ranging from 0 to 1 to evaluate the integrity of motor functions in patients. An index value of 1 might indicate a nearly normal motor functions, and an index value of 0 might imply a severe loss of motor functions. It is shown that the similarity scores of patients were significantly lower than those of control subjects in both tasks (**Figure 5B**). Significant correlations were found between similarity and kinematics, so as with the Fugl-Meyer score of arm (FMarm). In particular, the similarity indices of synergy vector S_V, and time profile S_T, showed good correlations with movement kinematics (**Figure 6**), indicating a strong causal relation of neural organization of muscle activation with motor performance (9). For FMarm score, its correlation was task sensitive. In FR, the similarity index of vector S_V was well correlated to clinical score of FMarm (**Figure 7A**). This suggested that S_V could be a good estimate of the residual ability of muscle coordination in the execution of motor tasks by patients (40, 41). Cross-task indices that combined the similarity indices of the two tasks, time profile ranked the worst amongst all three indices in the correlation with FMarm (**Figure 7C**). The weak correlation between S_T and FMarm may result from the fact that the clinical score of FMarm is often assessed by the final outcome of task performance, while S_T may be a good indicator of soundness of dynamic planning and execution of motor tasks in patients (9, 41).

It is interesting to note that in LR, there was not a significant correlation between FMarm score and all similarity indices (**Figure 7B**). In fact, baseline vectors of the two tasks were quite similar except for a forth component in LR, while patients showed higher closeness and similarity indices in LR than those of FR (**Figure 5**, a,c,e). This might arise from synergetic role of muscles

in the extension of elbow and shoulder during LR, and in FR, it required the flexion of shoulder and extension of elbow at the same time. Previous study has indicated that the ability to cooperate elbow extension during reach was a significant predictor of motor performance (45). These implied that FR in which a larger range of elbow extension was required might be a task more challenging. In other words, similarity indices are task sensitive, and synergy performance of FR may better distinguish different levels of motor ability in patients with varying degrees of impairment.

Methodological Consideration

In our study, the synergies were extracted from non-normalized EMG, for there is not a method of EMG normalization (60) that may best serve our purpose here. The method of maximal isometric voluntary contraction (MVC) is undermined by the question whether the measured MVC represents the real maximal activating level (60), and measurements in patients are probably affected by their varying degrees of motor deficits. This might bring a larger inter-subject variability (61). Also, EMG is often normalized to the peak or the mean value for a specific task (PEAK/MEAN) (62). Nevertheless, EMG variations between different tasks, and the same task collected at different recovery stages in the same patients could not be intuitively compared by the method of PEAK/MEAN (60). Considering our interest to analyze the difference of synergy between tasks in this study, we did not try to normalize the EMG. In future studies, a proper method of EMG normalization applicable for both healthy and stroke patients may be considered.

Further Implications for Neurorehabilitation

Muscle synergy could also provide guidance to intervention strategy using multi-muscle FES. FES has been widely used in the rehabilitation training in patients poststroke (2), and benefits are obtained both in improvements of movement control and brain cortical perfusion (63, 64). Multichannel stimulation showed an appreciable enhancement of motor ability in affected arm of patients poststroke (11, 64). A spatiotemporal neuromodulation of electrical stimulation series derived from synergy patterns from healthy rats demonstrated a significant recovery of motor function of spinal cord injured rats (65), supporting the use of synergy-based electrical stimulation for rehabilitation of motor control (59, 66). Our earlier study also explored the feasibility of applying synergy-guided electrical stimulation to the rehabilitation of motor control in patients poststroke (67). A synergy-based FES strategy was adopted in a TOT training procedure for patients following stroke using previously developed multichannel FES system (11, 12). Personalized intervention could be designed for each patient (12). It is promising to apply synergy-based approach in the assessment of motor functions and in the intervention of motor rehabilitation for patients poststroke.

CONCLUSION

In this study, a computational approach to evaluate task-specific synergies of reaching movements was established that may be applied to clinical evaluation of motor functions of patients following stroke. New quantitative indices of similarity of synergy of patients were evaluated to establish positive correlations to kinematic performance and clinical scores. Our results illustrated that muscle synergy patterns contain rich information in their spatial components and temporal profiles. Comparing pathological synergies of patients to the baseline synergy can reveal deficits in the underlying neuromuscular coordination and control in patients suffering from stroke. The similarity indices based on such comparisons were found to relate well the individual ability of patients in task control to their kinematic performance and clinical scores of assessments. The analysis of task-specific muscle synergies should offer both researchers and clinicians new insights into the impairments in the neural organization of motor control in patients following stroke. The similarity indices may be useful neurophysiological metrics to evaluate deficits in motor functions and outcome of rehabilitation in conjunction to clinical scores.

ETHICS STATEMENT

This study was approved by the Institutional Review Boards of Ruijin Hospital and the Ethics Committee of Human and Animal Experiments of the Med-X Research Institute of Shanghai Jiao Tong University.

AUTHOR CONTRIBUTIONS

SL designed and performed the human experiments, analyzed the experimental data, and prepared the figures and tables and the manuscript. CZ contributed to human experiments and data analyse. CN contributed to giving intellectual suggestions on experimental design, recruiting patient, and performing experiments. YB contributed to clinical measurement and caring of patients during experiments. QX contributed to assigning clinicians and configurations of patients' experiments and giving constructive suggestions to the study from clinical point of view. NL conceived the human experiments, proposed the analytical and displaying methods, and edited the final version of manuscript.

ACKNOWLEDGMENTS

We would like to thank Drs. Haifang Lai and Yanyan Li for their help in human experiments and assistance from Drs. Xin He and Juan C. Marquez with computation of muscle synergy. This work is supported in part by grants from the Natural Science Foundation of China (No. 81271684 and No. 61361160415), a National Basic Research Program of Project 973 by the Ministry of Science and Technology of China (No. 2011CB013304), and an Interdisciplinary Research Grant for Medicine and Engineering (No. YG2014ZD09) from Shanghai Jiao Tong University.

SUPPLEMENTARY MATERIAL

The Supplementary Material for this article can be found online at http://journal.frontiersin.org/article/10.3389/fneur.2017.00337/full#supplementary-material.

REFERENCES

1. Naghavi M, Wang H, Lozano R, Davis A, Liang X, Zhou M, et al. Global, regional, and national age-sex specific all-cause and cause-specific mortality for 240 causes of death, 1990–2013: a systematic analysis for the Global Burden of Disease Study 2013. *Lancet* (2015) 385:117–71. doi:10.1016/S0140-6736(14)61682-2
2. Langhorne P, Bernhardt J, Kwakkel G. Stroke rehabilitation. *Lancet* (2011) 377:1693–702. doi:10.1016/S0140-6736(11)60325-5
3. Langhorne P, Coupar F, Pollock A. Motor recovery after stroke: a systematic review. *Lancet Neurol* (2009) 8:741–54. doi:10.1016/S1474-4422(09)70150-4
4. Levin MF, Kleim JA, Wolf SL. What do motor "recovery" and "compensation" mean in patients following stroke? *Neurorehabil Neural Repair* (2009) 23:313–9. doi:10.1177/1545968308328727
5. Stein J, Harvey RL, Winstein CJ, Zorowitz RD, Wittenberg G, editors. *Stroke Recovery and Rehabilitation*. 2nd ed. New York, NY: Demos Medical (2014).
6. Ada L, Canning CG, Carr JH, Kilbreath SL, Shepherd RB. Chapter 12 task-specific training of reaching and manipulation. *Advances in Psychology*. Elsevier (2016). p. 239–65. Available from: http://linkinghub.elsevier.com/retrieve/pii/S0166411508612819
7. Gor-García-Fogeda MD, Molina-Rueda F, Cuesta-Gómez A, Carratalá-Tejada M, Alguacil-Diego IM, Miangolarra-Page JC. Scales to assess gross motor function in stroke patients: a systematic review. *Arch Phys Med Rehabil* (2014) 95:1174–83. doi:10.1016/j.apmr.2014.02.013
8. Thompson-Butel AG, Lin G, Shiner CT, McNulty PA. Comparison of three tools to measure improvements in upper-limb function with post-stroke therapy. *Neurorehabil Neural Repair* (2015) 29:341–8. doi:10.1177/1545968314547766
9. Ting LH, Chiel HJ, Trumbower RD, Allen JL, McKay JL, Hackney ME, et al. Neuromechanical principles underlying movement modularity and their implications for rehabilitation. *Neuron* (2015) 86:38–54. doi:10.1016/j.neuron.2015.02.042
10. Safavynia SA, Torres-Oviedo G, Ting LH. Muscle synergies: implications for clinical evaluation and rehabilitation of movement. *Top Spinal Cord Inj Rehabil* (2011) 17:16–24. doi:10.1310/sci1701-16
11. Qu H, Xie Y, Liu X, He X, Hao M, Bao Y, et al. Development of network-based multichannel neuromuscular electrical stimulation system for stroke rehabilitation. *J Rehabil Res Dev* (2016) 52:263–78. doi:10.1682/JRRD.2014.10.0227
12. Niu CM, Zhuang C, Bao Y, Li S, Lan N, Xie Q. Synergy-based NMES intervention accelerated rehabilitation of post-stroke hemiparesis. *Annual Meeting of the Association of Academic Physiatrists*. Las Vegas, Nevada, USA (2017).
13. Bernstein NA. *The Co-ordination and Regulation of Movements*. New York: Oxf Pergamon Press (1967).
14. Bizzi E, Mussa-Ivaldi FA, Giszter S. Computations underlying the execution of movement: a biological perspective. *Science* (1991) 253:287–91. doi:10.1126/science.1857964
15. Tresch MC, Saltiel P, Bizzi E. The construction of movement by the spinal cord. *Nat Neurosci* (1999) 2:162–7. doi:10.1038/5721
16. Bizzi E, Cheung VCK, d'Avella A, Saltiel P, Tresch M. Combining modules for movement. *Brain Res Rev* (2008) 57:125–33. doi:10.1016/j.brainresrev.2007.08.004
17. Giszter SF. Motor primitives – new data and future questions. *Curr Opin Neurobiol* (2015) 33:156–65. doi:10.1016/j.conb.2015.04.004
18. Giszter SF, Mussa-Ivaldi FA, Bizzi E. Convergent force fields organized in the frog's spinal cord. *J Neurosci* (1993) 13:467–91.
19. Saltiel P, Wyler-Duda K, D'Avella A, Tresch MC, Bizzi E. Muscle synergies encoded within the spinal cord: evidence from focal intraspinal NMDA iontophoresis in the frog. *J Neurophysiol* (2001) 85:605–19.
20. Saltiel P, Wyler-Duda K, d'Avella A, Ajemian RJ, Bizzi E. Localization and connectivity in spinal interneuronal networks: the adduction-caudal extension-flexion rhythm in the frog. *J Neurophysiol* (2005) 94:2120–38. doi:10.1152/jn.00117.2005
21. Gentner R, Classen J. Modular organization of finger movements by the human central nervous system. *Neuron* (2006) 52:731–42. doi:10.1016/j.neuron.2006.09.038
22. Rathelot J-A, Strick PL. Muscle representation in the macaque motor cortex: an anatomical perspective. *Proc Natl Acad Sci U S A* (2006) 103:8257–62. doi:10.1073/pnas.0602933103
23. Bizzi E, Cheung VCK. The neural origin of muscle synergies. *Front Comput Neurosci* (2013) 7:51. doi:10.3389/fncom.2013.00051
24. Overduin SA, d'Avella A, Carmena JM, Bizzi E. Microstimulation activates a handful of muscle synergies. *Neuron* (2012) 76:1071–7. doi:10.1016/j.neuron.2012.10.018
25. Overduin SA, d'Avella A, Carmena JM, Bizzi E. Muscle synergies evoked by microstimulation are preferentially encoded during behavior. *Front Comput Neurosci* (2014) 8:20. doi:10.3389/fncom.2014.00020
26. Rana M, Yani MS, Asavasopon S, Fisher BE, Kutch JJ. Brain connectivity associated with muscle synergies in humans. *J Neurosci* (2015) 35:14708–16. doi:10.1523/JNEUROSCI.1971-15.2015
27. Chiovetto E, Berret B, Delis I, Panzeri S, Pozzo T. Investigating reduction of dimensionality during single-joint elbow movements: a case study on muscle synergies. *Front Comput Neurosci* (2013) 7:11. doi:10.3389/fncom.2013.00011
28. d'Avella A, Lacquaniti F. Control of reaching movements by muscle synergy combinations. *Front Comput Neurosci* (2013) 7:42. doi:10.3389/fncom.2013.00042
29. Cheung VCK, d'Avella A, Tresch MC, Bizzi E. Central and sensory contributions to the activation and organization of muscle synergies during natural motor behaviors. *J Neurosci* (2005) 25:6419–34. doi:10.1523/JNEUROSCI.4904-04.2005
30. Tresch MC, Jarc A. The case for and against muscle synergies. *Curr Opin Neurobiol* (2009) 19:601–7. doi:10.1016/j.conb.2009.09.002
31. Tresch MC. Matrix factorization algorithms for the identification of muscle synergies: evaluation on simulated and experimental data sets. *J Neurophysiol* (2005) 95:2199–212. doi:10.1152/jn.00222.2005
32. d'Avella A, Portone A, Fernandez L, Lacquaniti F. Control of fast-reaching movements by muscle synergy combinations. *J Neurosci* (2006) 26:7791–810. doi:10.1523/JNEUROSCI.0830-06.2006
33. Cheung VCK, Piron L, Agostini M, Silvoni S, Turolla A, Bizzi E. Stability of muscle synergies for voluntary actions after cortical stroke in humans. *Proc Natl Acad Sci U S A* (2009) 106:19563–8. doi:10.1073/pnas.0910114106
34. Frère J, Hug F. Between-subject variability of muscle synergies during a complex motor skill. *Front Comput Neurosci* (2012) 6:99. doi:10.3389/fncom.2012.00099
35. Roh J, Rymer WZ, Beer RF. Robustness of muscle synergies underlying three-dimensional force generation at the hand in healthy humans. *J Neurophysiol* (2012) 107:2123–42. doi:10.1152/jn.00173.2011
36. Dominici N, Ivanenko YP, Cappellini G, d'Avella A, Mondi V, Cicchese M, et al. Locomotor primitives in newborn babies and their development. *Science* (2011) 334:997–9. doi:10.1126/science.1210617
37. Hayes HB, Chvatal SA, French MA, Ting LH, Trumbower RD. Neuromuscular constraints on muscle coordination during overground walking in persons with chronic incomplete spinal cord injury. *Clin Neurophysiol* (2014) 125:2024–35. doi:10.1016/j.clinph.2014.02.001
38. Rodriguez KL, Roemmich RT, Cam B, Fregly BJ, Hass CJ. Persons with Parkinson's disease exhibit decreased neuromuscular complexity during gait. *Clin Neurophysiol* (2013) 124:1390–7. doi:10.1016/j.clinph.2013.02.006
39. Cheung VCK, Turolla A, Agostini M, Silvoni S, Bennis C, Kasi P, et al. Muscle synergy patterns as physiological markers of motor cortical damage. *Proc Natl Acad Sci U S A* (2012) 109:14652–6. doi:10.1073/pnas.1212056109
40. Roh J, Rymer WZ, Beer RF. Evidence for altered upper extremity muscle synergies in chronic stroke survivors with mild and moderate impairment. *Front Hum Neurosci* (2015) 9:6. doi:10.3389/fnhum.2015.00006
41. Barroso FO, Torricelli D, Bravo-Esteban E, Taylor J, Gómez-Soriano J, Santos C, et al. Muscle synergies in cycling after incomplete spinal cord injury: correlation with clinical measures of motor function and spasticity. *Front Hum Neurosci* (2015) 9:706. doi:10.3389/fnhum.2015.00706
42. Kamper DG, McKenna-Cole AN, Kahn LE, Reinkensmeyer DJ. Alterations in reaching after stroke and their relation to movement direction and impairment severity. *Arch Phys Med Rehabil* (2002) 83:702–7. doi:10.1053/apmr.2002.32446

43. Ellis MD, Holubar BG, Acosta AM, Beer RF, Dewald JPA. Modifiability of abnormal isometric elbow and shoulder joint torque coupling after stroke. *Muscle Nerve* (2005) 32:170–8. doi:10.1002/mus.20343
44. Dewald JPA, Pope PS, Given JD, Buchanan TS, Rymer WZ. Abnormal muscle coactivation patterns during isometric torque generation at the elbow and shoulder in hemiparetic subjects. *Brain* (1995) 118:495–510. doi:10.1093/brain/118.2.495
45. Massie CL, Fritz S, Malcolm MP. Elbow extension predicts motor impairment and performance after stroke. *Rehabil Res Pract* (2011) 2011:1–7. doi:10.1155/2011/381978
46. Li S, Zhuang C, Zhang X, Niu CM, Xie Q, Lan N. Analysis of muscle synergy for evaluation of task-specific performance in stroke patients. *2016 38th Annual International Conference of the IEEE Engineering in Medicine and Biology Society*. Orlando, FL, Piscataway, NJ, USA: IEEE (2016).
47. Atkeson CG, Hollerbach JM. Kinematic features of unrestrained vertical arm movements. *J Neurosci* (1985) 5:2318–30.
48. Flash T, Hogan N. The coordination of arm movements: an experimentally confirmed mathematical model. *J Neurosci* (1985) 5:1688–703.
49. Lee DD, Seung HS. Learning the parts of objects by non-negative matrix factorization. *Nature* (1999) 401:788–91. doi:10.1038/44565
50. Torres-Oviedo G, Macpherson JM, Ting LH. Muscle synergy organization is robust across a variety of postural perturbations. *J Neurophysiol* (2006) 96:1530–46. doi:10.1152/jn.00810.2005
51. Ambrosini E, De Marchis C, Pedrocchi A, Ferrigno G, Monticone M, Schmid M, et al. Neuro-mechanics of recumbent leg cycling in post-acute stroke patients. *Ann Biomed Eng* (2016) 44(11):3238–51. doi:10.1007/s10439-016-1660-0
52. Chen H-Y, Chen S-C, Chen J-JJ, Fu L-L, Wang YL. Kinesiological and kinematical analysis for stroke subjects with asymmetrical cycling movement patterns. *J Electromyogr Kinesiol* (2005) 15:587–95. doi:10.1016/j.jelekin.2005.06.001
53. Roh J, Rymer WZ, Perreault EJ, Yoo SB, Beer RF. Alterations in upper limb muscle synergy structure in chronic stroke survivors. *J Neurophysiol* (2013) 109:768–81. doi:10.1152/jn.00670.2012
54. Sainburg R. Evidence for a dynamic-dominance hypothesis of handedness. *Exp Brain Res* (2002) 142:241–58. doi:10.1007/s00221-001-0913-8
55. Urra O, Casals A, Jané R. Synergy analysis as a tool to design and assess an effective stroke rehabilitation. *Conf Proc IEEE Eng Med Biol Soc* (2014) 2014:3550–3. doi:10.1109/EMBC.2014.6944389
56. Hashiguchi Y, Ohata K, Kitatani R, Yamakami N, Sakuma K, Osako S, et al. Merging and fractionation of muscle synergy indicate the recovery process in patients with hemiplegia: the first study of patients after subacute stroke. *Neural Plast* (2016) 2016:1–7. doi:10.1155/2016/5282957
57. Johansson BB. Brain plasticity and stroke rehabilitation: the Willis lecture. *Stroke* (2000) 31:223–30. doi:10.1161/01.STR.31.1.223
58. Nudo RJ, Plautz EJ, Frost SB. Role of adaptive plasticity in recovery of function after damage to motor cortex. *Muscle Nerve* (2001) 24:1000–19. doi:10.1002/mus.1104
59. Nudo RJ. Plasticity. *NeuroRx* (2006) 3:420–7. doi:10.1016/j.nurx.2006.07.006
60. Burden A. How should we normalize electromyograms obtained from healthy participants? What we have learned from over 25 years of research. *J Electromyogr Kinesiol* (2010) 20:1023–35. doi:10.1016/j.jelekin.2010.07.004
61. Allison GT, Marshall RN, Singer KP. EMG signal amplitude normalization technique in stretch-shortening cycle movements. *J Electromyogr Kinesiol* (1993) 3:236–44. doi:10.1016/1050-6411(93)90013-M
62. Knutson LM, Soderberg GL, Ballantyne BT, Clarke WR. A study of various normalization procedures for within day electromyographic data. *J Electromyogr Kinesiol* (1994) 4:47–59. doi:10.1016/1050-6411(94)90026-4
63. Cecatto RB. The effects of functional electrical stimulation on upper-extremity function and cortical plasticity in chronic stroke patients. *Clin Neurophysiol* (2014) 125:1709. doi:10.1016/j.clinph.2013.11.025
64. Hara Y, Obayashi S, Tsujiuchi K, Muraoka Y. The effects of electromyography-controlled functional electrical stimulation on upper extremity function and cortical perfusion in stroke patients. *Clin Neurophysiol* (2013) 124:2008–15. doi:10.1016/j.clinph.2013.03.030
65. Wenger N, Moraud EM, Gandar J, Musienko P, Capogrosso M, Baud L, et al. Spatiotemporal neuromodulation therapies engaging muscle synergies improve motor control after spinal cord injury. *Nat Med* (2016) 22:138–45. doi:10.1038/nm.4025
66. Levy RM, Harvey RL, Kissela BM, Winstein CJ, Lutsep HL, Parrish TB, et al. Epidural electrical stimulation for stroke rehabilitation: results of the prospective, multicenter, randomized, single-blinded everest trial. *Neurorehabil Neural Repair* (2016) 30:107–19. doi:10.1177/1545968315575613
67. Zhuang C, Marquez JC, Qu HE, He X, Lan N. A neuromuscular electrical stimulation strategy based on muscle synergy for stroke rehabilitation. *2015 7th International IEEE/EMBS Conference on Neural Engineering (NER)*. Montpellier, France: IEEE (2015). p. 816–9.

Conflict of Interest Statement: The authors declare that the research was conducted in the absence of any commercial or financial relationships that could be construed as a potential conflict of interest.

frontiers in Neurology

ORIGINAL RESEARCH
published: 14 June 2017
doi: 10.3389/fneur.2017.00284

Neural Plasticity in Moderate to Severe Chronic Stroke Following a Device-Assisted Task-Specific Arm/Hand Intervention

Kevin B. Wilkins[1,2], *Meriel Owen*[1,2], *Carson Ingo*[1], *Carolina Carmona*[1], *Julius P. A. Dewald*[1,2,3,4] *and Jun Yao*[1,2]*

[1] Department of Physical Therapy and Human Movement Sciences, Northwestern University, Chicago, IL, United States, [2] Northwestern University Interdepartmental Neuroscience, Northwestern University, Chicago, IL, United States, [3] Department of Biomedical Engineering, Northwestern University, Chicago, IL, United States, [4] Department of Physical Medicine and Rehabilitation, Northwestern University, Chicago, IL, United States

Currently, hand rehabilitation following stroke tends to focus on mildly impaired individuals, partially due to the inability for severely impaired subjects to sufficiently use the paretic hand. Device-assisted interventions offer a means to include this more severe population and show promising behavioral results. However, the ability for this population to demonstrate neural plasticity, a crucial factor in functional recovery following effective post-stroke interventions, remains unclear. This study aimed to investigate neural changes related to hand function induced by a device-assisted task-specific intervention in individuals with moderate to severe chronic stroke (upper extremity Fugl-Meyer < 30). We examined functional cortical reorganization related to paretic hand opening and gray matter (GM) structural changes using a multimodal imaging approach. Individuals demonstrated a shift in cortical activity related to hand opening from the contralesional to the ipsilesional hemisphere following the intervention. This was driven by decreased activity in contralesional primary sensorimotor cortex and increased activity in ipsilesional secondary motor cortex. Additionally, subjects displayed increased GM density in ipsilesional primary sensorimotor cortex and decreased GM density in contralesional primary sensorimotor cortex. These findings suggest that despite moderate to severe chronic impairments, post-stroke participants maintain ability to show cortical reorganization and GM structural changes following a device-assisted task-specific arm/hand intervention. These changes are similar as those reported in post-stroke individuals with mild impairment, suggesting that residual neural plasticity in more severely impaired individuals may have the potential to support improved hand function.

Keywords: stroke, hand rehabilitation, EEG, cortical reorganization, voxel-based morphometry, functional electrical stimulation, gray matter, neuroplasticity

OPEN ACCESS

Edited by:
Xiaogang Hu,
University of North Carolina at Chapel Hill, United States

Reviewed by:
Ping Zhou,
University of Texas Health Science Center at Houston, United States
Guang H. Yue,
Kessler Foundation, United States

***Correspondence:**
Jun Yao
j-yao4@northwestern.edu

Specialty section:
This article was submitted to Stroke, a section of the journal Frontiers in Neurology

Received: *25 April 2017*
Accepted: *01 June 2017*
Published: *14 June 2017*

Citation:
Wilkins KB, Owen M, Ingo C, Carmona C, Dewald JPA and Yao J (2017) Neural Plasticity in Moderate to Severe Chronic Stroke Following a Device-Assisted Task-Specific Arm/Hand Intervention. Front. Neurol. 8:284. doi: 10.3389/fneur.2017.00284

INTRODUCTION

Nearly 800,000 people experience a new or recurrent stroke each year in the US (1). Popular therapies, such as constraint-induced movement therapy (CIMT), utilize intense task-specific practice of the affected limb to improve arm/hand function in acute and chronic stroke with mild impairments (2, 3). Neuroimaging results partially attribute the effectiveness of these arm/hand interventions to

cortical reorganization in the ipsilesional hemisphere following training in acute and mild chronic stroke (4). Unfortunately, CIMT requires certain remaining functionality in the paretic hand to execute the tasks, and only about 10% of screened patients are eligible (5), thus disqualifying a large population of individuals with moderate to severe impairments. Recently, studies using device-assisted task-specific interventions specifically targeted toward moderate to severe chronic stroke reported positive clinical results (6–8). However, these studies primarily focus on clinical measures, but it is widely accepted that neural plasticity is a key factor for determining outcome (9–11). Consequently, it remains unclear whether moderate to severe chronic stroke [upper extremity Fugl-Meyer Assessment (UEFMA) < 30] maintains the ability to demonstrate neural changes following an arm/hand intervention.

Neural changes induced by task-specific training have been investigated widely using animal models (12). For instance, monkeys or rodents trained on a skilled reach-to-grasp task express enlarged representation of the digits of the hand or forelimb in primary motor cortex (M1) following training as measured by intracortical microstimulation (13, 14). Additionally, rapid local structural changes in the form of dendritic growth, axonal sprouting, myelination, and synaptogenesis occur (15–18). Importantly, both cortical and structural reorganization corresponds to motor recovery following rehabilitative training in these animals (19, 20).

The functional neural mechanisms underlying effective task-specific arm/hand interventions in acute and chronic stroke subjects with mild impairments support those seen in the animal literature described above. Several variations of task-specific combined arm/hand interventions, including CIMT, bilateral task-specific training, and hand-specific robot-assisted practice, have shown cortical reorganization such as increased sensorimotor activity and enlarged motor maps in the ipsilesional hemisphere related to the paretic arm/hand (21–24). These results suggest increased recruitment of residual resources from the ipsilesional hemisphere and/or decreased recruitment of contralesional resources following training. Although the evidence for a pattern of intervention-driven structural changes remains unclear in humans, several groups have shown increases in gray matter (GM) density in sensorimotor cortices (25), along with increases in fractional anisotropy in ipsilesional corticospinal tract (CST) (26) following task-specific training in acute and chronic stroke individuals with mild impairments.

The extensive nature of neural damage in moderate to severe chronic stroke may result in compensatory mechanisms, such as contralesional or secondary motor area recruitment (27). These individuals show increased contralesional activity when moving their paretic arm, which correlates with impairment (28, 29) and may be related to the extent of damage to the ipsilesional CST (30). This suggests that more impaired individuals may increasingly rely on contralesional corticobulbar tracts such as the corticoreticulospinal tract to activate the paretic limb (29). These tracts lack comparable resolution and innervation to the distal parts of the limb, thus sacrificing functionality at the paretic arm/hand (31). Since this population is largely ignored in current arm/hand interventions, it is unknown whether an arm/hand intervention for these more severely impaired post-stroke individuals will increase recruitment of residual ipsilesional corticospinal resources. These ipsilesional CSTs maintain the primary control of hand and finger extensor muscles (32) and are thus crucial for improved hand function. Task-specific training assisted by a device may reengage and strengthen residual ipsilesional corticospinal resources by training distal hand opening together with overall arm use.

The current study seeks to determine whether individuals with moderate to severe chronic stroke maintain the ability to show cortical reorganization and/or structural changes alongside behavioral improvement following a task-specific intervention. We hypothesize that following a device-assisted task-specific intervention, moderate to severe chronic stroke individuals will show similar functional and structural changes as observed in mildly impaired individuals, demonstrated by (i) a shift in cortical activity related to paretic hand opening from the contralesional hemisphere toward the ipsilesional hemisphere and (ii) an increase in GM density in sensorimotor cortices in the ipsilesional hemisphere.

MATERIALS AND METHODS

Subjects

Eight individuals with chronic hemiparetic stroke (age: 63.5 ± 4) and moderate to severe impairment (UEFMA: 11–24) participated in this study. Clinical information for each subject is provided in **Table 1** and lesion locations in **Figure 1**. All individuals were screened for inclusion by a licensed physical therapist. Inclusion criteria include a UEFMA between 10 and 30 out of 66, no cognitive

TABLE 1 | Subject demographics and clinical characteristics.

Subject	Age range	Time since stroke (years)	Lesioned hemi	Lesion location	UE FMA	Pre BBT	Post BBT	Pre AROM (°)	Post AROM (°)
S01	60–65	9	L	IC	23	0	6	−20	11
S02	60–65	8	R	IC, BG	12	1	3	0	5
S03	65–70	3	R	Par, Occ, IC	17	0	1	0	0
S04	60–65	22	R	IC, BG, Thal	11	0	1	0	17.5
S05	60–65	13	R	Occ, IC	24	0	0	0	2.5
S06	70–75	20	L	IC, BG, Thal	13	0	0	0	1.5
S07	55–60	6	L	IC, BG	24	0	3	0	5
S08	60–65	9	L	IC, Thal	22	11	13	38.5	55

AROM, active range of motion; BBT, Box and Blocks Test; BG, basal ganglia; FMA, Fugl-Meyer Assessment; IC, internal capsule; Occ, occipital lobe; Par, parietal lobe; Thal, thalamus; UE, upper extremity.

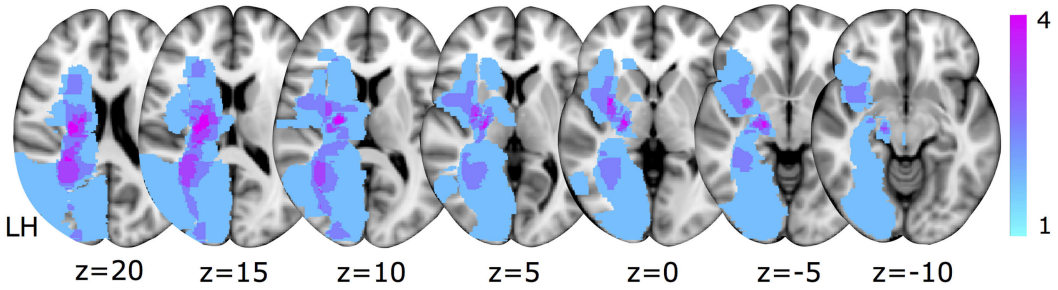

FIGURE 1 | Lesion locations for the eight subjects overlaid on axial Montreal Neurological Institute T1 slices. The color bar indicates the number of subjects with lesioned tissue in a particular voxel. LH indicates the lesioned hemisphere.

or perceptual impairment, no botulinum toxin within the last 6 months, MRI compatibility, no lesion including sensorimotor cortices, the ability to elicit enough EMG activity at wrist/finger extensors, and the ability for the FES to generate a hand opening of at least 4 cm between the thumb and the index finger. This study was approved by the Northwestern University institutional review board, and all subjects gave informed consent.

Experimental Protocols

Intervention

Subjects participated in a 7-week intervention consisting of three 2-h visits per week. During the visit, subjects completed 20–30 trials of the following sequence of movements: (1) reaching out toward a jar, (2) driving the wrist/finger extensors to open the paretic hand, (3) grabbing the jar, (4) bringing the jar back toward themselves, and (5) releasing the jar. The weight, distance/height, and orientation of the jar relative to the subject were progressively altered to increase the challenge to each subject, as determined by the physical therapist. All subjects started the motor task with the arm supported by the table. Depending on ability, subjects were encouraged to progressively lift the paretic limb actively. During the task, a novel EMG-FES device, called ReIn-Hand, was used to assist paretic hand opening (see Figure S1 in Supplementary Material). This device recorded EMG activities from eight muscles (deltoid, biceps brachii, triceps, extensor communis digitorum, extensor carpi radialis (ECR), flexor digitorum profundus, flexor carpi radialis (FCR), and abductor pollicis). While the user performed the functional reaching and opening, the ReIn-Hand detected hand opening by extracting EMG features to trigger an Empi transcutaneous electrical neuro-stimulation device (Vista, CA, USA). The stimulation electrodes were applied to the wrist/finger extensors with the following settings: biphasic waveform, frequency = 50 Hz ± 20%, pulse width = 300 μs, amplitude = sufficient for maximal hand opening without discomfort, and duration = 3 s. The novelty of this device is that even with the increased expression of the flexion synergy at the elbow (33), wrist, and fingers (34, 35) during reaching that is prevalent in this population, the device can still detect the hand opening and drive the paretic hand open, thus allowing for a user-driven stimulation to support functional usage of the paretic hand and arm. All participants could successfully use the device to complete the described task (including opening, grasping, and releasing), although some subjects experienced difficulty in sufficiently supinating the hand when releasing the jar to keep it upright on the table. Additionally, the physical therapist stretched the hand and arm at the beginning of the experiment and between trials to effectively elicit hand openings with the EMG-FES device.

Pre- and Post-Intervention Tests

Clinical Assessments

For each subject, within 1 week prior to and following the intervention, a licensed physical therapist completed a set of clinical assessments, with the motor-related parts including UEFMA, Box and Blocks Test (BBT), and active range of motion (AROM) averaged over the II and V digit.

Structural Imaging of the Brain

Within 2 weeks prior to and following the intervention, subjects participated in MRI scans at Northwestern University's Center for Translation Imaging on a 3 TS Prisma scanner with a 64-channel head coil. Structural T1-weighted scans were acquired using an MP-RAGE sequence (TR = 2.3 s, TE = 2.94 ms, FOV 256 mm × 256 mm) producing an isotropic voxel resolution of 1 mm × 1 mm × 1 mm. Visual inspection of acquired images was performed immediately following the data acquisition to guarantee no artifacts and stable head position.

Functional Imaging Related to Hand Opening

Within 1 week prior to and following the intervention, subjects also participated in an EEG experiment. During the EEG experiment, participants sat in a Biodex chair (Biodex Medical Systems, Shirley, NY, USA), which restrained the trunk with straps crossing the chest and abdomen. The subject's paretic arm was placed in a forearm-hand orthosis attached to the end effector of an admittance controlled robotic device (ACT^{3D}) instrumented with a six degree of freedom load cell (JR3, Inc., Woodland, CA, USA). At the beginning of each trial, subjects moved their hand to a home position, with the shoulder at 85° abduction, 40° flexion, and the elbow at 90° flexion angle. The subject then received an auditory cue. Following the cue, subjects relaxed at the home position for 5–7 s and then self-initiated a maximum attempted paretic hand opening with the arm resting on a haptic table.

Subjects were instructed to avoid eye movements by focusing on a point and avoid movements of other body parts during the performance of each trial, which was visually confirmed by the experimenter. Subjects performed 60–70 trials of attempted paretic hand opening, broken into blocks (one block consisted of 20–30 trials). Rest periods varied between 15 and 60 s between trials and 10 min between blocks. The typical duration of the experiment was around 5–6 h, including ~2 h of setup, ~1 h for lunch, and ~2 h of data collection.

Scalp recordings were made with a 160-channel high-density EEG system using active electrodes (Biosemi, Inc., Active II, Amsterdam, The Netherlands) mounted on a stretchable fabric cap based on a 10/20 system. Simultaneously, EMGs were recorded from the ECR, FCR, and intermediate deltoid of the paretic arm. All data were sampled at 2,048 Hz. The impedance was kept below 5 kΩ for the duration of the experiment. Additionally, the positions of EEG electrodes on the subject's scalp were recorded with respect to a coordinate system defined by the nasion and preauricular notches using a Polaris Krios handheld scanner and reflective markers (NDI, ON, Canada). This allowed for coregistration of EEG electrodes with each subject's anatomical MRI data. Due to post-stroke abnormal synergy, finger/wrist extensors and flexors, and often the shoulder abductors, usually co-activate together when performing maximal hand opening (34). Therefore, in order to provide a reliable indicator of movement onset, EMGs were simultaneously recorded from the ECR, FCR, and anterior deltoid (IDL) of the paretic arm.

Data Analysis

Reorganization of Cortical Activity Related to Hand Opening

EEG data were aligned to the earliest EMG onset of the three muscles and segmented from −2,200 to +200 ms (with EMG onset at 0 ms) using Brain Vision Analyzer 2 software (Brain Products, Gilching, Germany). Data were then visually inspected for the presence of artifacts. Trials exhibiting artifacts (e.g., eye blinks) were eliminated from further analysis. The remaining EEG trials were baseline-corrected (from −2,180 to −2,050 ms), low-pass-filtered at 70 Hz, and ensemble-averaged. The averaged EEG signals were down-sampled to 256 Hz and imported into CURRY 6 (Compumedics Neuroscan Ltd., El Paso, TX, USA). The cortical current density strength ($\mu A/mm^2$) in the time between 150 and 100 ms prior to EMG onset was computed using the standardized low-resolution electromagnetic brain tomography (sLORETA) method (Lp = 1) based on a subject-specific boundary element method model with the regulation parameter automatically adjusted to achieve more than 99% variance counted (36, 37). Possible sources were located on a cortical layer with 3 mm distance between each node. Although the inverse calculation was performed over the whole cortex, only the activity in bilateral sensorimotor cortices was further analyzed. Specific regions of interest (ROI) included bilateral primary sensorimotor cortices [primary motor cortex (M1) + primary sensory cortex (S1)] and secondary motor cortices [supplementary motor area (SMA) + premotor area (PM)].

To investigate the shift of cortical activity related to hand opening, we used the estimated current density strengths to calculate a laterality index [LI = (I − C)/(I + C)], where I and C are the current density strengths from the ipsilesional and contralesional sensorimotor cortices, respectively (i.e., combined primary sensorimotor and secondary motor cortices). LI reflects the relative contributions of each cerebral hemisphere to the source activity, with a value close to +1 for an ipsilesional source distribution and −1 for a contralesional source distribution.

Additionally, we quantified a cortical activity ratio $\mathrm{CAR} = \frac{\sum_1^n S_n}{\sum_1^m S_m}$ for each of the four ROIs, where S represents the current density strength of one of the nodes, and n and m represent the number of nodes in the ROI and whole sensorimotor cortices, respectively. The cortical activity ratio reflects the relative strength from one ROI as normalized by the total combined strength of the four ROIs.

Structural Changes in GM Density

Anatomical T1 data were analyzed with FSL-voxel-based morphometry (VBM) 1.1 (https://fsl.fmrib.ox.ac.uk/fsl/fslwiki/FSLVBM; Oxford University, Oxford, United Kingdom) (38) using FSL tools (39). First, T1 images for participants who have left hemisphere lesions were flipped to ensure that the lesions of all subjects were in the right hemisphere. The T1 images were then brain-extracted using the Brain Extraction Tool and segmented into GM using FAST4. The resulted GM partial volume images were aligned to Montreal Neurological Institute (MNI) 152 standard space using the affine registration tool FLIRT and averaged to create a study-specific GM template. Subsequently, individual GM partial volume images in native space were non-linearly registered to this template using FNIRT, modulated to correct for local expansion or contraction due to the non-linear component of the spatial transformation, and then smoothed with an isotropic Gaussian kernel with a sigma of 3 mm. Finally, a voxel-wise General Linear Model was applied with Threshold-Free Cluster Enhancement (40) to detect changes in GM density following the intervention. Voxel-based threshold of changes in GM density was set at $p < 0.001$ uncorrected.

Statistical Analysis

Statistics were performed using SPSS (IBM, V23). Clinical and neural measures were examined for normality using a Shapiro–Wilk test. A Wilcoxon signed rank test was used if assumptions of normality were not met. A paired *t*-test was performed on LI. A 2 (time) × 4 (region) repeated measures ANOVA was performed on the cortical activity ratio. We performed *post hoc* paired *t*-tests when a main ANOVA effect was found. Significance was set at $p < 0.05$. Individual data are depicted for all significant findings.

RESULTS

Changes in Arm/Hand Function following EMG-FES Task-Specific Training

Table 1 shows pre and post BBT and AROM scores. Notably, most subjects initially scored a 0 on the pre-assessment BBT and

showed 0° of AROM due to the severity of their motor impairments at the arm/hand. The clinical data violated the assumptions of normality based on the Shapiro–Wilk test. Therefore, a Wilcoxon signed rank test was used and reported a significant increase in BBT following the intervention (average increase of 1.9 blocks per minute, $p = 0.03$; **Table 1**) and AROM (average increase of 9.9°, $p = 0.03$; **Table 1**), indicating improvement of paretic arm/hand control, although FMA did not change.

Cortical Reorganization Related to the Hand

Figure 2A shows an example of ensemble-averaged EEG for the 160 channels for Subject 1. There is a clear baseline from roughly −2 to −1.5 s prior to EMG onset and then a slow increase in electrical potential when approaching EMG onset, consistent with the Bereitschaftspotential. The reconstructed cortical activity for Subject 1 while performing hand opening on the table is depicted in **Figure 2B** pre-intervention and in **Figure 2C** post-intervention. This subject showed bilateral activity in sensorimotor cortex prior to the intervention as seen in **Figure 2B** and dominant ipsilesional activity following the intervention as seen in **Figure 2C**. We quantified the pre- and post-intervention LI in each of the participants (see results in **Figure 3**). A paired *t*-test found a significant increase in LI following the intervention [$t(7) = 3.09$, $p = 0.02$], signifying a post-intervention shift toward the ipsilesional hemisphere.

To further investigate regions responsible for the post-intervention LI changes, we quantified the pre- and post-intervention cortical activity ratios for primary sensorimotor (M1/S1) and secondary motor (SMA/PM) cortices (see results in **Figure 4**). A 2 (time) × 4 (region) repeated measures ANOVA found a significant time × region interaction [$F(1,7) = 3.47$, $p = 0.03$]. *Post hoc* paired *t*-tests found that following the

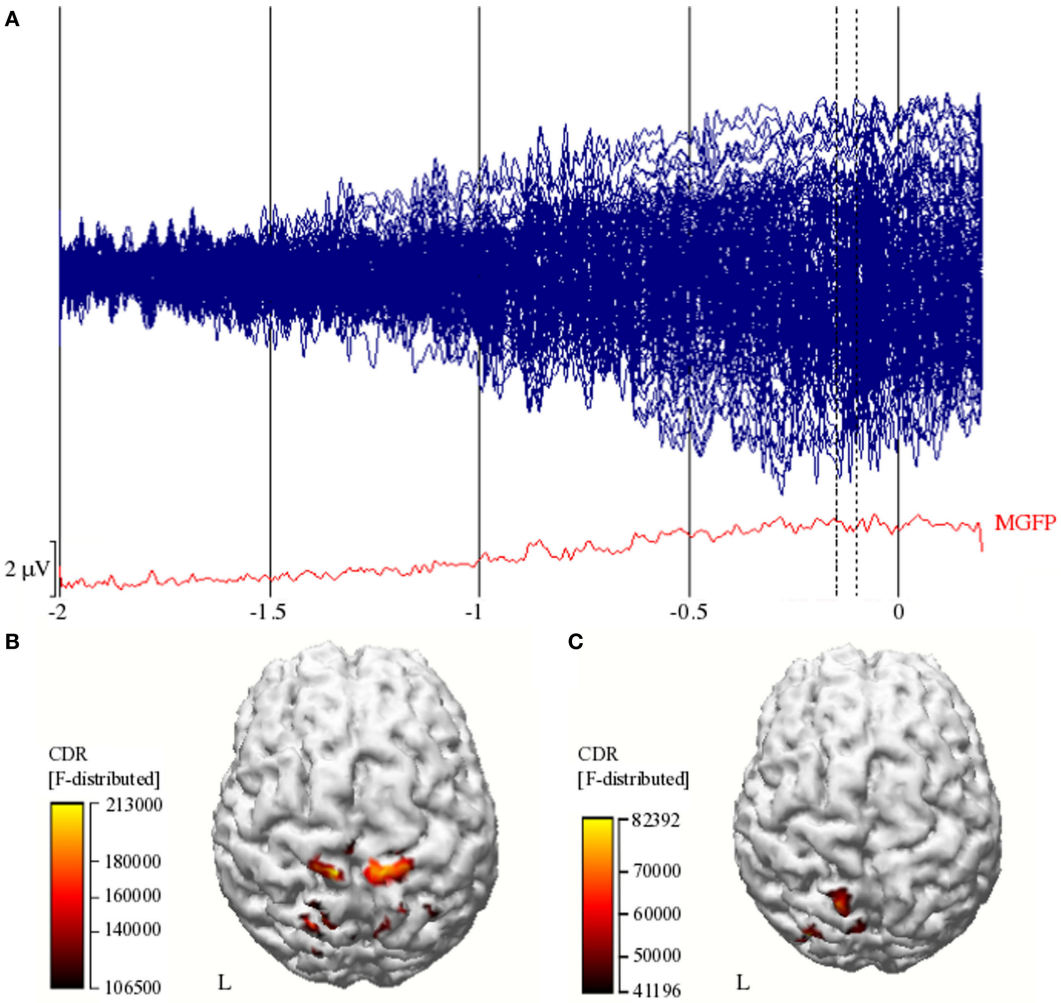

FIGURE 2 | **(A)** Ensemble-averaged EEG of the 160 channels (blue butterfly plot) and Mean Global Field Power (MGFP; red line) from −2 s to +0.2 s (0 = EMG onset). Vertical dashed lines represent the start and end of the window of interest (−150 to −100 ms). A scale bar is included in the lower left; **(B)** reconstructed cortical activity between −150 and −100 ms prior to movement onset for Subject 1 during hand opening pre-intervention, and **(C)** post-intervention. Color bars indicate the current density reconstruction (CDR) statistic from sLORETA. Left hemisphere is the lesioned hemisphere.

intervention, there was a decrease in the cortical activation ratio in contralesional M1/S1 ($p = 0.04$) and a trending increase in ipsilesional SMA/PM ($p = 0.06$) related to paretic hand opening.

GM Density

Following the intervention, subjects displayed significantly greater GM density in M1 and S1 in the lesioned hemisphere ($x = 52$, $y = -16$, $z = 30$, t-value = 2.55, $p < 0.001$) and a decrease in GM density in M1 and S1 in the non-lesioned hemisphere ($x = -46$, $y = -20$, $z = 60$, t-value = 2.41, $p < 0.001$; $x = -44$, $y = -18$, $z = 36$, t-value = 2.79, $p < 0.001$) as depicted in **Figures 5A,B**.

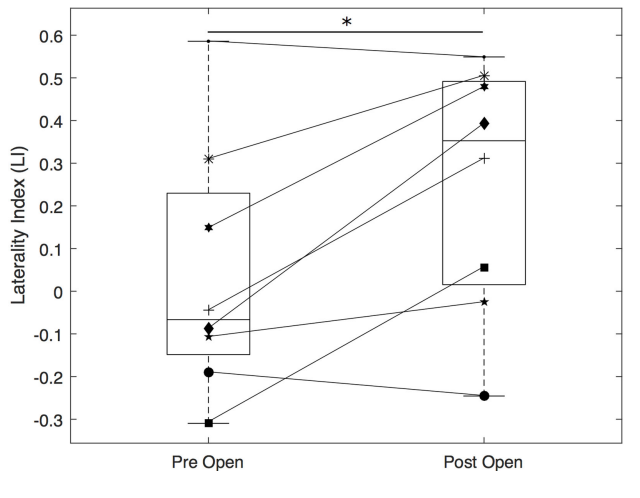

FIGURE 3 | Box plots of laterality index (LI) prior to and following the intervention for paretic hand opening. Positive LI indicates predominantly ipsilesional activity. *indicates $p < 0.05$.

Additionally, subjects displayed greater GM density in the thalamus in the lesioned hemisphere ($x = 2$, $y = -20$, $z = 10$, t-value = 3.13, $p < 0.001$) as shown in **Figure 5C**. A complete list of significant regions is provided in Table S1 in Supplementary Material.

DISCUSSION

The present study investigated neural changes in individuals with moderate to severe stroke following an EMG-FES-assisted task-specific arm/hand intervention. Specifically, we found a shift of sensorimotor cortical activity related to hand opening from contralesional to ipsilesional cortex, along with structural changes in the form of increased ipsilesional M1/S1 and decreased contralesional M1/S1 GM density. Although similar device-assisted hand/arm training in this population has been investigated before to examine behavioral improvements (7, 41, 42), this study provides evidence for corresponding neural changes even in this more severe chronic population.

Shift toward Ipsilesional Hemisphere

As expected, before the intervention, subjects showed cortical activity predominantly from the contralesional hemisphere related to open the paretic hand, as reflected by the overall negative LI. This contralesional activity may suggest an increased reliance on low-resolution contralesional corticobulbar pathways such as the corticoreticulospinal tract (31, 43) for general paretic arm function. In fact, more severely impaired subjects actually tend to involuntarily close the hand and activate shoulder muscles when asked to open (35), which may reflect this increased reliance on ipsilateral corticobulbar pathways that innervate primarily flexor hand and proximal muscles compared to extensors (44). These

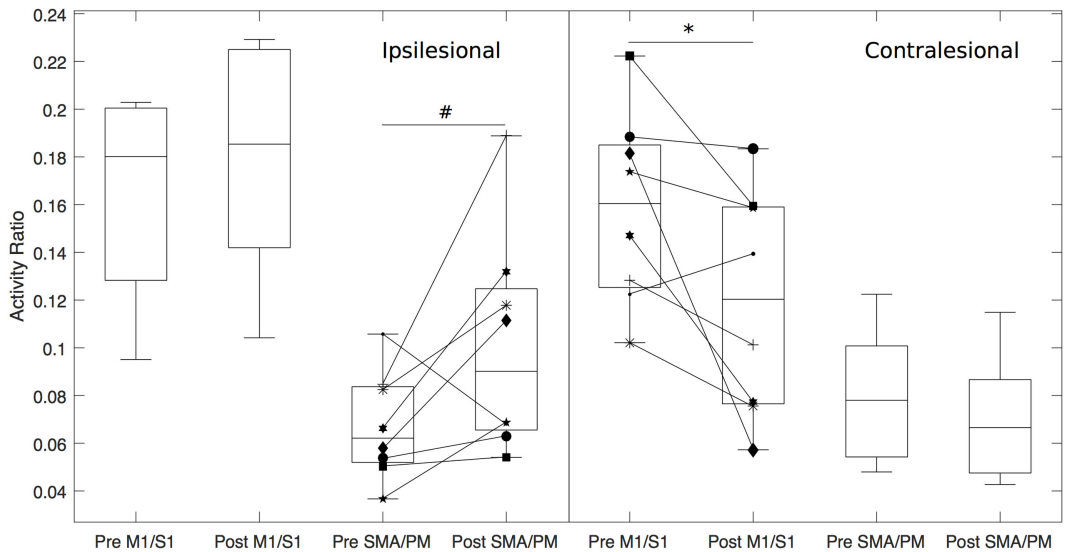

FIGURE 4 | Box plots depicting cortical activity ratio prior to and following the intervention for hand opening on the table. Regions of interests include M1/S1 and supplementary motor area/premotor area (SMA/PM) for both ipsilesional (left side of figure) and contralesional (right side of figure) hemispheres. *indicates $p < 0.05$, #indicates $p = 0.06$.

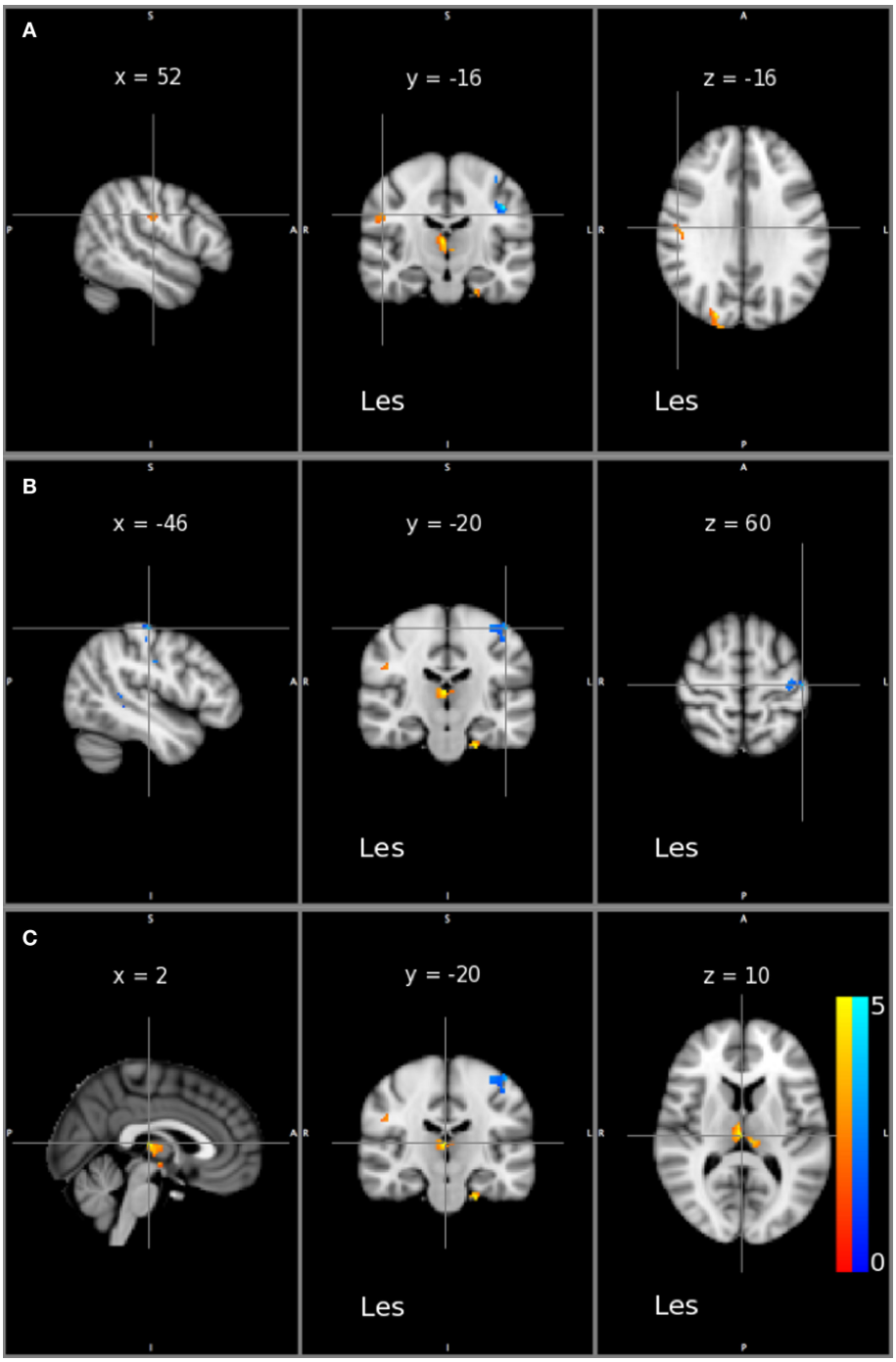

FIGURE 5 | Statistical maps of gray matter (GM) density changes across all patients. Significant increases (red/yellow) and decreases (Blue) in GM density are depicted on sagittal, coronal, and axial sections (left to right) on Montreal Neurological Institute T1 slices. Sections show the maximum effect on **(A)** ipsilesioned M1/S1, **(B)** contralesional M1/S1, and **(C)** ipsilesional thalamus. Les indicates the side of the lesioned hemisphere. Color maps indicate the t values at every voxel. A statistical threshold was set at $p < 0.001$ uncorrected.

pathways lack sufficient innervation to extensor muscles of the hand to produce appropriate hand opening (45) and are often associated with greater motor impairment (29, 31).

Effective hand/arm interventions in mildly impaired post-stroke individuals have reported a post-intervention shift toward ipsilesional sensorimotor areas (46, 47). This shift is thought to be a beneficial since it may indicate increased use of ipsilesional CSTs, which maintain the primary innervations to the extensor muscles of the hand (32). Intervention-induced shifts toward the ipsilesional hemisphere have rarely been investigated in more

severely impaired post-stroke individuals, especially not for arm/hand training partially due to the lack of inclusion of these subjects in arm/hand interventions. In this study, we found that a ReIn-Hand-assisted arm/hand intervention induced a positive change in LI. Our results suggest that even moderate to severe chronic stroke subjects maintain the ability to show similar cortical reorganization back toward the ipsilesional hemisphere following task-specific training as seen in more mild subjects. This ipsilesional shift may suggest decreased recruitment of contralesional corticobulbar pathways and increased reliance on ipsilesional CSTs during paretic hand opening, which may allow for greater functionality at the hand as seen by the increase in BBT and AROM. Additionally, it could reflect increased ability to actually drive hand opening when instructed rather than involuntary closing and activating proximal muscles (35). It is worth noting that only six out eight participants exhibited this intervention-induced shift despite all showing improvements on either BBT or AROM, possibly reflecting compensatory behavioral strategies following the intervention rather than recovery in these two participants.

Changes in Cortical Activity Driving LI Shift

We calculated the cortical activity ratio in each sensorimotor region to further elucidate which regions were contributing to the LI shift. Following the intervention, subjects showed decreased activity in contralesional primary sensorimotor cortex (M1/S1) and a trending increase in ipsilesional secondary motor cortex (SMA/PM).

Increased contralesional primary sensorimotor cortex activity is associated with greater impairment following stroke (48, 49) and greater damage to CST (50, 51). Therefore, this decreased activity could reflect either decreased recruitment of contralesional descending motor pathways or changes in interhemispheric balance between primary sensorimotor cortices (52) and thus allow for increased functional usage of the affected hand.

Stroke patients tend to activate secondary motor areas more following greater CST damage (51) and show positive correlations between ipsilesional secondary motor area activation and recovery (53, 54). The increased recruitment of ipsilesional SMA/PM may be due to increased recruitment of direct projections to the spinal cord (55), although these connections are not as efficacious as connections from M1 to the spinal cord (56). Alternatively, plasticity within intrinsic cortico-cortico neuronal connections in M1 (57) may allow increased communication between SMA/PM and M1 following injury. Thus, ipsilesional secondary motor areas may serve as a potential avenue for functionally relevant cortical reorganization *via* either descending or intrinsic connections in addition to removal of contralesional cortical activity.

Increased GM Density in Ipsilesional Sensorimotor Cortex

Previous work demonstrated significant decreases in GM volume in ipsilesional precentral gyrus following a subcortical stroke, which was associated with greater impairment (58). However, following task-specific training, mild chronic stroke subjects showed increases in GM density in ipsilesional sensorimotor cortex (25), and increases in perilesional GM density were associated with better recovery in acute stroke (59). Similarly, we found increased ipsilesional M1/S1 GM density following the intervention in our moderate to severe stroke population. Additionally, a significant positive correlation was found between changes in LI and changes in GM density in ipsilesional M1/S1 following the intervention ($R^2 = 0.70$, $p < 0.05$; Figure S2 in Supplementary Material), showing that activity shifting to the ipsilesional hemisphere was associated with increased ipsilesional M1/S1 GM density.

Increases in GM density may suggest potential synaptogenesis, dendritic growth, or gliogenesis at the cortex (60). Thus, these changes may be due to new synapse formation and dendritic growth commonly seen in animal training models (61). Additionally, these subjects likely experienced cortical atrophy prior to the intervention due to disuse of the paretic limb, which may have been partially remedied following the intervention due to increased use of the paretic arm/hand. Despite greater damage to ipsilesional descending motor tracts, these severely impaired individuals demonstrate the ability to reorganize ipsilesional primary sensorimotor cortices.

In these more severely impaired post-stroke individuals, we also found intervention-induced decreases in contralesional M1/S1 GM density, which were not reported before in mildly impaired individuals. This decrease may be specific to more severe patients since post-stroke, increased use of the contralesional hemisphere occurs to a greater degree in severely impaired individuals compared with milder individuals (29). The decrease in GM density in contralesional M1/S1 may indicate a decrease in dendritic complexity or synapses in these areas (62). These structural changes may be a result of decreased activation in these areas due to decreased recruitment during movement or overall decreased use (63, 64). Alternatively, they may be due to decreased tonic activity in these contralesional sensorimotor areas, which is thought to be a contributor to hyperexcitability in the brainstem and subsequent increased tone in this population (65, 66).

The increases in GM density seen in the thalamus in our results may be due to the repeated use of electrical stimulation throughout the intervention. Although we focused on the motor changes in this study, it is likely that these subjects show sensory neural changes as well due to the augmented afferent feedback generated by the EMG-FES device. Therefore, it is not surprising to see changes in the thalamus due to its central role as a sensory relay station for both the cutaneous and proprioceptive sensory modalities (67).

Limitations

The main limitation of the current study is the small sample size. Despite the relatively small n, we observed consistent patterns of functional and structural changes. These changes signify the importance of examining the potential neural mechanisms found here in a larger population of moderate to severe chronic stroke subjects. Additionally, there was no control group in the present study. However, this study was aimed at investigating whether this population maintained the ability to show neural changes following an intervention, rather than answering the question

of what is the optimal intervention for this population. Another potential confounding factor from the task-specific intervention is the amount of stretching. However, stretching on its own is unlikely to drive the functional and structural changes found in this study (68), even though it may temporarily reduce the stretch reflex activation of wrist and finger flexors (69). Additionally, reduced flexion synergy and subsequent decreased involuntary shoulder abduction/adduction force generation during hand opening (34) could contribute to intervention-induced changes in LI.

One of the primary long-term goals of the current study is to substantially increase the population included in task-specific therapy. Although the current ReIn-Hand device allowed our cohort of moderate to severe chronic stroke individuals to participate in task-specific training, it does require both detectable extensor EMGs to drive the device and responsiveness to FES to create sufficient hand opening. In our experience, limiting our inclusion criteria to an FMA ≥10 satisfied these requirements in most of initially screened participants (18 out of 20). However, due to the current sample size, it is difficult to accurately specify the portion of individuals who could utilize the ReIn-Hand device. However, considering that only ~5% of nearly 800 post-stroke individuals in the Clinical Neuroscience Research Registry hosted by the Rehabilitation Institute of Chicago and Northwestern University exhibit FMA scores less than 10, it clearly substantially increases coverage compared with conventional task-specific training.

CONCLUSION

The present study shows the ability of even moderate to severe chronic stroke subjects to show cortical reorganization at both the functional and structural levels following a device-assisted task-specific intervention in a manner resembling that seen in mild chronic stroke subjects. Despite the tendency to focus on acute or mild chronic stroke patients in hand function rehabilitation, the current study encourages the continued push to use devices to involve moderate to severe chronic stroke subjects in task-specific arm/hand rehabilitation.

ETHICS STATEMENT

This study was carried out in accordance with the recommendations of Northwestern University Institutional Review Board with written informed consent from all subjects. All subjects gave written informed consent in accordance with the Declaration of Helsinki. The protocol was approved by Northwestern University Institutional Review Board.

AUTHOR CONTRIBUTIONS

KW helped with design of the intervention and neuroimaging pre-/posttests, acquired the EEG data, ran intervention sessions, conducted EEG and VBM data analysis, contributed to interpretation, and was primary author of the manuscript. MO acquired MRI data, aided in the VBM data analysis, and contributed to interpretation and manuscript writing. CI aided in MRI data acquisition, VBM data analysis, and contributed to interpretation and manuscript writing. CC helped with the design of the intervention, ran intervention sessions, acquired the EEG data, conducted pre/post clinical assessments, conducted clinical measure data analysis, and contributed to interpretation. JD helped with the design of the intervention and neuroimaging pre-/posttests and provided interpretation to the data as well as contributions to manuscript writing. JY was the primary designer of the intervention and neuroimaging pre-/posttests, ran the intervention sessions, aided in the acquisition of the EEG data, aided in EEG analysis, provided interpretation to the data, and contributed to manuscript writing.

ACKNOWLEDGMENTS

The authors want to acknowledge Dr. Justin Drogos for assistance with the intervention and Dr. Daniel Corcos for manuscript feedback.

FUNDING

This work was supported by an HHS grant 90IF0090-01-00 (formerly DOE NIDRR H133G120287) and NICHD 2RO1H-D039343 grants.

SUPPLEMENTARY MATERIAL

The Supplementary Material for this article can be found online at http://journal.frontiersin.org/article/10.3389/fneur.2017.00284/full/#supplementary-material.

REFERENCES

1. Mozaffarian D, Benjamin EJ, Go AS, Arnett DK, Blaha MJ, Cushman M, et al. Heart disease and stroke statistics – 2015 update: a report from the American Heart Association. *Circulation* (2015) 131(4):e29–322. doi:10.1161/CIR.0000000000000157
2. Wolf SL, Winstein CJ, Miller JP, Taub E, Uswatte G, Morris D, et al. Effect of constraint-induced movement therapy on upper extremity function 3 to 9 months after stroke: the EXCITE randomized clinical trial. *JAMA* (2006) 296(17):2095–104. doi:10.1001/jama.296.17.2095
3. Taub E, Uswatte G, Elbert T. New treatments in neurorehabilitation founded on basic research. *Nat Rev Neurosci* (2002) 3(3):228–36. doi:10.1038/nrn754
4. Favre I, Zeffiro TA, Detante O, Krainik A, Hommel M, Jaillard A. Upper limb recovery after stroke is associated with ipsilesional primary motor cortical activity: a meta-analysis. *Stroke* (2014) 45(4):1077–83. doi:10.1161/STROKEAHA.113.003168
5. Kwakkel G, Veerbeek JM, van Wegen EE, Wolf SL. Constraint-induced movement therapy after stroke. *Lancet Neurol* (2015) 14(2):224–34. doi:10.1016/S1474-4422(14)70160-7
6. Page SJ, Levine PG, Basobas BA. "Reps" aren't enough: augmenting functional electrical stimulation with behavioral supports significantly reduces impairment in moderately impaired stroke. *Arch Phys Med Rehabil* (2016) 97(5):747–52. doi:10.1016/j.apmr.2016.01.004
7. Klamroth-Marganska V, Blanco J, Campen K, Curt A, Dietz V, Ettlin T, et al. Three-dimensional, task-specific robot therapy of the arm after

stroke: a multicentre, parallel-group randomised trial. *Lancet Neurol* (2014) 13(2):159–66. doi:10.1016/S1474-4422(13)70305-3
8. Singer BJ, Vallence AM, Cleary S, Cooper I, Loftus AM. The effect of EMG triggered electrical stimulation plus task practice on arm function in chronic stroke patients with moderate-severe arm deficits. *Restor Neurol Neurosci* (2013) 31(6):681–91. doi:10.3233/RNN-130319
9. Krakauer JW, Carmichael ST, Corbett D, Wittenberg GF. Getting neurorehabilitation right: what can be learned from animal models? *Neurorehabil Neural Repair* (2012) 26(8):923–31. doi:10.1177/1545968312440745
10. Pekna M, Pekny M, Nilsson M. Modulation of neural plasticity as a basis for stroke rehabilitation. *Stroke* (2012) 43(10):2819–28. doi:10.1161/STROKEAHA.112.654228
11. Starkey ML, Schwab ME. How plastic is the brain after a stroke? *Neuroscientist* (2014) 20(4):359–71. doi:10.1177/1073858413514636
12. Nudo RJ. Recovery after brain injury: mechanisms and principles. *Front Hum Neurosci* (2013) 7:887. doi:10.3389/fnhum.2013.00887
13. Nudo RJ, Milliken GW, Jenkins WM, Merzenich MM. Use-dependent alterations of movement representations in primary motor cortex of adult squirrel monkeys. *J Neurosci* (1996) 16(2):785–807.
14. Kleim JA, Barbay S, Nudo RJ. Functional reorganization of the rat motor cortex following motor skill learning. *J Neurophysiol* (1998) 80(6):3321–5.
15. Gibson EM, Purger D, Mount CW, Goldstein AK, Lin GL, Wood LS, et al. Neuronal activity promotes oligodendrogenesis and adaptive myelination in the mammalian brain. *Science* (2014) 344(6183):1252304. doi:10.1126/science.1252304
16. Kleim JA, Barbay S, Cooper NR, Hogg TM, Reidel CN, Remple MS, et al. Motor learning-dependent synaptogenesis is localized to functionally reorganized motor cortex. *Neurobiol Learn Mem* (2002) 77(1):63–77. doi:10.1006/nlme.2000.4004
17. Maier IC, Baumann K, Thallmair M, Weinmann O, Scholl J, Schwab ME. Constraint-induced movement therapy in the adult rat after unilateral corticospinal tract injury. *J Neurosci* (2008) 28(38):9386–403. doi:10.1523/JNEUROSCI.1697-08.2008
18. Biernaskie J, Corbett D. Enriched rehabilitative training promotes improved forelimb motor function and enhanced dendritic growth after focal ischemic injury. *J Neurosci* (2001) 21(14):5272–80.
19. Nudo RJ, Wise BM, SiFuentes F, Milliken GW. Neural substrates for the effects of rehabilitative training on motor recovery after ischemic infarct. *Science* (1996) 272(5269):1791–4. doi:10.1126/science.272.5269.1791
20. Tamakoshi K, Ishida A, Takamatsu Y, Hamakawa M, Nakashima H, Shimada H, et al. Motor skills training promotes motor functional recovery and induces synaptogenesis in the motor cortex and striatum after intracerebral hemorrhage in rats. *Behav Brain Res* (2014) 260:34–43. doi:10.1016/j.bbr.2013.11.034
21. Sawaki L, Butler AJ, Leng X, Wassenaar PA, Mohammad YM, Blanton S, et al. Constraint-induced movement therapy results in increased motor map area in subjects 3 to 9 months after stroke. *Neurorehabil Neural Repair* (2008) 22(5):505–13. doi:10.1177/1545968308317531
22. Takahashi CD, Der-Yeghiaian L, Le V, Motiwala RR, Cramer SC. Robot-based hand motor therapy after stroke. *Brain* (2008) 131(Pt 2):425–37. doi:10.1093/brain/awm311
23. Boake C, Noser EA, Ro T, Baraniuk S, Gaber M, Johnson R, et al. Constraint-induced movement therapy during early stroke rehabilitation. *Neurorehabil Neural Repair* (2007) 21(1):14–24. doi:10.1177/1545968306291858
24. McCombe Waller S, Whitall J, Jenkins T, Magder LS, Hanley DF, Goldberg A, et al. Sequencing bilateral and unilateral task-oriented training versus task oriented training alone to improve arm function in individuals with chronic stroke. *BMC Neurol* (2014) 14:236. doi:10.1186/s12883-014-0236-6
25. Gauthier LV, Taub E, Perkins C, Ortmann M, Mark VW, Uswatte G. Remodeling the brain: plastic structural brain changes produced by different motor therapies after stroke. *Stroke* (2008) 39(5):1520–5. doi:10.1161/STROKEAHA.107.502229
26. Fan YT, Lin KC, Liu HL, Chen YL, Wu CY. Changes in structural integrity are correlated with motor and functional recovery after post-stroke rehabilitation. *Restor Neurol Neurosci* (2015) 33(6):835–44. doi:10.3233/RNN-150523
27. Hamzei F, Dettmers C, Rijntjes M, Weiller C. The effect of cortico-spinal tract damage on primary sensorimotor cortex activation after rehabilitation therapy. *Exp Brain Res* (2008) 190(3):329–36. doi:10.1007/s00221-008-1474-x
28. Ward N. Assessment of cortical reorganisation for hand function after stroke. *J Physiol* (2011) 589(Pt 23):5625–32. doi:10.1113/jphysiol.2011.220939
29. Chen A, Yao J, Dewald JPA. Increased ipsilateral cortical activity as a function of shoulder abduction loading: evidence for increased reliance on reticulospinal pathways. *Conference Proceedings: 36th Annual International Conference of the IEEE Engineering in Medicine and Biology Society*. Chicago, IL (2014).
30. Stinear CM, Barber PA, Smale PR, Coxon JP, Fleming MK, Byblow WD. Functional potential in chronic stroke patients depends on corticospinal tract integrity. *Brain* (2007) 130(Pt 1):170–80. doi:10.1093/brain/awl333
31. Baker SN, Zaaimi B, Fisher KM, Edgley SA, Soteropoulos DS. Pathways mediating functional recovery. *Prog Brain Res* (2015) 218:389–412. doi:10.1016/bs.pbr.2014.12.010
32. Lawrence DG, Kuypers HG. The functional organization of the motor system in the monkey. I. The effects of bilateral pyramidal lesions. *Brain* (1968) 91(1):1–14. doi:10.1093/brain/91.1.1
33. Sukal TM, Ellis MD, Dewald JP. Shoulder abduction-induced reductions in reaching work area following hemiparetic stroke: neuroscientific implications. *Exp Brain Res* (2007) 183(2):215–23. doi:10.1007/s00221-007-1029-6
34. Miller LC, Dewald JP. Involuntary paretic wrist/finger flexion forces and EMG increase with shoulder abduction load in individuals with chronic stroke. *Clin Neurophysiol* (2012) 123(6):1216–25. doi:10.1016/j.clinph.2012.01.009
35. Lan Y, Yao J, Dewald JPA. The impact of shoulder abduction loading on volitional hand opening and grasping in chronic hemiparetic stroke. *Neurorehabil Neural Repair* (2017) 31(6):521–9. doi:10.1177/1545968317697033
36. Bradley A, Yao J, Dewald J, Richter CP. Evaluation of electroencephalography source localization algorithms with multiple cortical sources. *PLoS One* (2016) 11(1):e0147266. doi:10.1371/journal.pone.0147266
37. Yao J, Dewald JP. Evaluation of different cortical source localization methods using simulated and experimental EEG data. *Neuroimage* (2005) 25(2):369–82. doi:10.1016/j.neuroimage.2004.11.036
38. Douaud G, Smith S, Jenkinson M, Behrens T, Johansen-Berg H, Vickers J, et al. Anatomically related grey and white matter abnormalities in adolescent-onset schizophrenia. *Brain* (2007) 130(Pt 9):2375–86. doi:10.1093/brain/awm184
39. Smith SM, Jenkinson M, Woolrich MW, Beckmann CF, Behrens TE, Johansen-Berg H, et al. Advances in functional and structural MR image analysis and implementation as FSL. *Neuroimage* (2004) 23(Suppl 1):S208–19. doi:10.1016/j.neuroimage.2004.07.051
40. Winkler AM, Ridgway GR, Webster MA, Smith SM, Nichols TE. Permutation inference for the general linear model. *Neuroimage* (2014) 92:381–97. doi:10.1016/j.neuroimage.2014.01.060
41. Lo AC, Guarino PD, Richards LG, Haselkorn JK, Wittenberg GF, Federman DG, et al. Robot-assisted therapy for long-term upper-limb impairment after stroke. *N Engl J Med* (2010) 362(19):1772–83. doi:10.1056/NEJMoa0911341
42. Platz T, van Kaick S, Mehrholz J, Leidner O, Eickhof C, Pohl M. Best conventional therapy versus modular impairment-oriented training for arm paresis after stroke: a single-blind, multicenter randomized controlled trial. *Neurorehabil Neural Repair* (2009) 23(7):706–16. doi:10.1177/1545968309335974
43. Yao J, Chen A, Carmona C, Dewald JP. Cortical overlap of joint representations contributes to the loss of independent joint control following stroke. *Neuroimage* (2009) 45(2):490–9. doi:10.1016/j.neuroimage.2008.12.002
44. Zaaimi B, Edgley SA, Soteropoulos DS, Baker SN. Changes in descending motor pathway connectivity after corticospinal tract lesion in macaque monkey. *Brain* (2012) 135(Pt 7):2277–89. doi:10.1093/brain/aws115
45. Baker SN. The primate reticulospinal tract, hand function and functional recovery. *J Physiol* (2011) 589(Pt 23):5603–12. doi:10.1113/jphysiol.2011.215160
46. Askim T, Indredavik B, Vangberg T, Haberg A. Motor network changes associated with successful motor skill relearning after acute ischemic stroke: a longitudinal functional magnetic resonance imaging study. *Neurorehabil Neural Repair* (2009) 23(3):295–304. doi:10.1177/1545968308322840
47. Michielsen ME, Selles RW, van der Geest JN, Eckhardt M, Yavuzer G, Stam HJ, et al. Motor recovery and cortical reorganization after mirror therapy in chronic stroke patients: a phase II randomized controlled trial. *Neurorehabil Neural Repair* (2011) 25(3):223–33. doi:10.1177/1545968310385127
48. Ward NS, Brown MM, Thompson AJ, Frackowiak RS. Neural correlates of motor recovery after stroke: a longitudinal fMRI study. *Brain* (2003) 126(Pt 11):2476–96. doi:10.1093/brain/awg145

49. Calautti C, Naccarato M, Jones PS, Sharma N, Day DD, Carpenter AT, et al. The relationship between motor deficit and hemisphere activation balance after stroke: a 3T fMRI study. *Neuroimage* (2007) 34(1):322–31. doi:10.1016/j.neuroimage.2006.08.026
50. Schaechter JD, Perdue KL, Wang R. Structural damage to the corticospinal tract correlates with bilateral sensorimotor cortex reorganization in stroke patients. *Neuroimage* (2008) 39(3):1370–82. doi:10.1016/j.neuroimage.2007.09.071
51. Ward NS, Newton JM, Swayne OB, Lee L, Thompson AJ, Greenwood RJ, et al. Motor system activation after subcortical stroke depends on corticospinal system integrity. *Brain* (2006) 129(Pt 3):809–19. doi:10.1093/brain/awl002
52. Grefkes C, Fink GR. Reorganization of cerebral networks after stroke: new insights from neuroimaging with connectivity approaches. *Brain* (2011) 134(Pt 5):1264–76. doi:10.1093/brain/awr033
53. Hubbard IJ, Carey LM, Budd TW, Levi C, McElduff P, Hudson S, et al. A randomized controlled trial of the effect of early upper-limb training on stroke recovery and brain activation. *Neurorehabil Neural Repair* (2015) 29(8):703–13. doi:10.1177/1545968314562647
54. Johansen-Berg H, Dawes H, Guy C, Smith SM, Wade DT, Matthews PM. Correlation between motor improvements and altered fMRI activity after rehabilitative therapy. *Brain* (2002) 125(Pt 12):2731–42. doi:10.1093/brain/awf282
55. Macpherson J, Wiesendanger M, Marangoz C, Miles TS. Corticospinal neurones of the supplementary motor area of monkeys. A single unit study. *Exp Brain Res* (1982) 48(1):81–8. doi:10.1007/BF00239574
56. Maier MA, Armand J, Kirkwood PA, Yang HW, Davis JN, Lemon RN. Differences in the corticospinal projection from primary motor cortex and supplementary motor area to macaque upper limb motoneurons: an anatomical and electrophysiological study. *Cereb Cortex* (2002) 12(3):281–96. doi:10.1093/cercor/12.3.281
57. Sanes JN, Donoghue JP. Plasticity and primary motor cortex. *Annu Rev Neurosci* (2000) 23:393–415. doi:10.1146/annurev.neuro.23.1.393
58. Cai J, Ji Q, Xin R, Zhang D, Na X, Peng R, et al. Contralesional cortical structural reorganization contributes to motor recovery after sub-cortical stroke: a longitudinal voxel-based morphometry study. *Front Hum Neurosci* (2016) 10:393. doi:10.3389/fnhum.2016.00393
59. Abela E, Seiler A, Missimer JH, Federspiel A, Hess CW, Sturzenegger M, et al. Grey matter volumetric changes related to recovery from hand paresis after cortical sensorimotor stroke. *Brain Struct Funct* (2015) 220(5):2533–50. doi:10.1007/s00429-014-0804-y
60. Zatorre RJ, Fields RD, Johansen-Berg H. Plasticity in gray and white: neuroimaging changes in brain structure during learning. *Nat Neurosci* (2012) 15(4):528–36. doi:10.1038/nn.3045
61. Murphy TH, Corbett D. Plasticity during stroke recovery: from synapse to behaviour. *Nat Rev Neurosci* (2009) 10(12):861–72. doi:10.1038/nrn2735
62. Sowell ER, Thompson PM, Tessner KD, Toga AW. Mapping continued brain growth and gray matter density reduction in dorsal frontal cortex: inverse relationships during postadolescent brain maturation. *J Neurosci* (2001) 21(22):8819–29.
63. Zito K, Svoboda K. Activity-dependent synaptogenesis in the adult mammalian cortex. *Neuron* (2002) 35(6):1015–7. doi:10.1016/S0896-6273(02)00903-0
64. Langer N, Hanggi J, Muller NA, Simmen HP, Jancke L. Effects of limb immobilization on brain plasticity. *Neurology* (2012) 78(3):182–8. doi:10.1212/WNL.0b013e31823fcd9c
65. Brown P. Pathophysiology of spasticity. *J Neurol Neurosurg Psychiatry* (1994) 57(7):773–7. doi:10.1136/jnnp.57.7.773
66. Li S, Francisco GE. New insights into the pathophysiology of post-stroke spasticity. *Front Hum Neurosci* (2015) 9:192. doi:10.3389/fnhum.2015.00192
67. Kandel ER, Schwartz JH, Jessell TM, Siegelbaum SA, Hudspeth AJ. *Principles of Neural Science*. 5th ed. New York: McGraw-Hill Companies, Inc. (2013).
68. Teasell R, Foley N, Salter K, Bhogal S, Jutai J, Speechley M. Evidence-based review of stroke rehabilitation: executive summary, 12th edition. *Top Stroke Rehabil* (2009) 16(6):463–88. doi:10.1310/tsr1606-463
69. Schmit BD, Dewald JP, Rymer WZ. Stretch reflex adaptation in elbow flexors during repeated passive movements in unilateral brain-injured patients. *Arch Phys Med Rehabil* (2000) 81(3):269–78. doi:10.1016/S0003-9993(00)90070-4

Conflict of Interest Statement: The authors declare that the research was conducted in the absence of any commercial or financial relationships that could be construed as a potential conflict of interest.

frontiers in Neurology

ORIGINAL RESEARCH
published: 29 May 2017
doi: 10.3389/fneur.2017.00221

Multiparameter Electromyography Analysis of the Masticatory Muscle Activities in Patients with Brainstem Stroke at Different Head Positions

Chuyao Jian[1†], Miaoluan Wei[1†], Jie Luo[1], Jiayin Lin[1], Wen Zeng[1], Weitian Huang[2] and Rong Song[1]*

[1]*Key Laboratory of Sensing Technology and Biomedical Instrument of Guang Dong Province, Guangdong Provincial Engineering and Technology Center of Advanced and Portable Medical Devices, Sun Yat-sen University, Guangzhou, China,* [2]*Department of Stroke Rehabilitation, Guangdong Work Injury Rehabilitation Center, Guangzhou, China*

The performance of the masticatory muscle is frequently affected and presents high heterogeneity poststroke. Surface electromyography (EMG) is widely used to quantify muscle movement patterns. However, only a few studies applied EMG analysis on the research of masticatory muscle activities poststroke, and most of which used single parameter—root mean squares (RMS). The aim of this study was to fully investigate the performance of masticatory muscle at different head positions in healthy subjects and brainstem stroke patients with multiparameter EMG analysis. In this study, 15 healthy subjects and six brainstem stroke patients were recruited to conduct maximum voluntary clenching at five different head positions: upright position, left rotation, right rotation, dorsal flexion, and ventral flexion. The EMG signals of bilateral temporalis anterior and masseter muscles were recorded, and parameters including RMS, median frequency, and fuzzy approximate entropy of the EMG signals were calculated. Two-way analysis of variance (ANOVA) with repeated measures and Bonferroni *post hoc* test were used to evaluate the effects of muscle and head position on EMG parameters in the healthy group, and the non-parametric Wilcoxon signed rank test was conducted in the patient group. The Welch–Satterthwaite *t*-test was used to compare the between-subject difference. We found a significant effect of subject and muscles but no significant effect of head positions, and the masticatory muscles of patients after brainstem stroke performed significantly different from healthy subjects. Multiparameter EMG analysis might be an informative tool to investigate the neural activity related movement patterns of the deficient masticatory muscles poststroke.

Keywords: stroke, entropy, vestibular stimulation, masticatory muscles, median frequency

OPEN ACCESS

Edited by:
Xiaoyan Li,
University of Texas, United States

Reviewed by:
Xu Zhang,
University of Science and Technology of China, China
Jinsook Roh,
Rehabilitation Institute of Chicago, United States

***Correspondence:**
Jie Luo
jluo_bme@foxmail.com

†These authors have contributed equally to this work.

Specialty section:
This article was submitted to Stroke, a section of the journal Frontiers in Neurology

Received: *03 March 2017*
Accepted: *08 May 2017*
Published: *29 May 2017*

Citation:
Jian C, Wei M, Luo J, Lin J, Zeng W, Huang W and Song R (2017) Multiparameter Electromyography Analysis of the Masticatory Muscle Activities in Patients with Brainstem Stroke at Different Head Positions. Front. Neurol. 8:221. doi: 10.3389/fneur.2017.00221

INTRODUCTION

Stroke, a cerebrovascular disease with a high incidence and a high mortality rate, is divided into hemorrhagic and ischemic types (1). The cerebral damage in survived patients was often left with sequela of motor dysfunction and abnormal muscle activation. Patients frequently have disorders of masticatory system, with masticatory muscle activity, bite force, flexibility of tongue, lip force and

chewing performance affected, especially after brainstem stroke (2). It is important for stroke patients to go through a rehabilitation training and recover the masticatory function. However, the impairments of the masticatory system are usually of a high heterogeneity, and the effect of the masticatory rehabilitation training should be enhanced. To improve the effect of training, the overall characteristics of the impaired masticatory system and their responses to neural stimuli in patients after stroke should be studied.

The motor nucleus of the trigeminal in the brainstem is responsible for providing motor innervation to the masticatory muscles (3). The vestibular stimuli caused by changing head positions can affect the performance of the masticatory muscles. Evidences shown in the studies of Funakoshi et al. (4) and Deriu et al. (5) proved that the activation of masticatory muscles was different at different head positions. On the other hand, Kushiro et al. (6) showed a reverse effect that chewing gums increased postural stability when people stood uprightly. Besides, animal experiments suggested that there could be an anatomical connection between the vestibular nuclei and trigeminal motoneurons in the brainstem (7–9). We hypothesized that the impairment of the brainstem might interrupt the responses of the masticatory system to the changes in head position. However, former studies were performed in healthy people. Therefore, the effect of changes in head position on the performance of the masticatory muscles needs further studies.

Surface electromyography (EMG) is a useful tool for quantifying the activation patterns of muscles. However, there were only a few studies evaluating the impairment of masticatory system based on an EMG signal analysis. Cruccu et al. (10) and Wang et al. (11) used a linear EMG parameter, root mean squares (RMS), to evaluate the excitability of muscles (12) and found that the activation of the masticatory muscles was lower in the affected side of patients poststroke during clenching. Another linear parameter, median frequency (MDF), is also widely used to describe spectral characteristics of EMG signals with a good specificity and sensitivity in reflecting the muscle electrophysiology (13, 14). Due to the non-linearity and complexity of EMG signals, it has been reported that non-linear EMG parameters should be included (15, 16). Entropy, as a non-linear parameter, is introduced to assess the complexity of the EMG signal. Approximate entropy (ApEn) and sample entropy were two of the most used entropy estimations. Giannasi et al. (17) evaluated the reliability of several EMG parameters in the masticatory muscles of cerebral palsy patients and demonstrated that RMS, MDF, and ApEn were most reliable. Fuzzy approximate entropy (fApEn) uses an exponential fuzzy function to enhance the consistency and monotonicity, and it is considered as an improved version of ApEn (18). Previous studies reported that fApEn was related to motor unit recruiting and firing (19). A combination of above linear and non-linear EMG analysis would help to obtain more information, from different perspectives, about the performance of the masticatory muscles.

This study aimed to investigate whether there existed a certain activation pattern of the masticatory muscles in patients after brainstem stroke. Fifteen healthy subjects and six brainstem stroke patients were recruited and requested to occlude as hard as possible at five different head positions: (1) upright position; (2) turning left by 30° (left rotation); (3) turning right by 30° (right rotation); (4) turning up by 30° (dorsal flexion); (5) turning down by 30° (ventral flexion). In the meanwhile, surface EMG signals of bilateral temporal anterior and masseter muscles were recorded and analyzed with RMS, MDF, and fApEn.

MATERIALS AND METHODS

Subject Recruitment

Six brainstem stroke patients (five males, one female, mean age was 59.33 ± 13.79 years) were recruited from Stroke Rehabilitation Department at Guangdong Work Injury Rehabilitation Center. This study received permission from local ethics committee and volunteered to take part in this study. They all signed the written informed consent about the purpose and procedures of the study prior to the experiment. The neurologist accompanied beside the patients during the experiment to avoid accidents. The clinical diagnosis of the patients was evaluated by neurologist based on MRI or CT scanning images. No patient had a history of neurological disorders or symptoms prior to stroke. The Function Oral Intake Scale (FOIS) was used to evaluate the masticatory function of patients. Low scores indicated weak masticatory function. The exclusion criteria were: associated diseases such as dental problems, missing teeth (between the premolar and molar in the left and right side), temporomandibular disorder, feeling painful during clenching and changing head positions, and under an orthodontic treatment. The demographic and clinical characteristics of all the patients were listed in **Table 1**. Specially, one of the patients had no FOIS score, but he did not have any facial asymmetry and did a good job in the experiment.

Fifteen healthy subjects (8 males, 7 females, age: 22 ± 2 years) were recruited from Sun Yat-sen University. All subjects were in general good health and had a normal occlusion without any pathologic changes in the orofacial myofunction, masticatory system, or cervical spine. The inclusion criteria were completeness of natural permanent teeth, i.e., at least 28 teeth, including complete bilateral molar and premolar. Thirteen healthy subjects habitually chewed with their right sides. One of the remaining two subjects usually used the left side to chew, and the other had no habitually chewing side.

TABLE 1 | Demographic and clinical information of patients.

No.	Age (years)	Sex	Duration (months)	Type	FOIS	Facial sagging side
1	58	M	32	H	1	R
2	44	M	28	H	5	R
3	64	F	5	I	5	W
4	43	M	28	H	–	W
5	77	M	16	I	3	W
6	70	M	35	H	1	R

M, male; F, female; H, hemorrhage; I, ischemia; FOIS, Function Oral Intake Scale; –, without the diagnosis of clinical doctor; L, left; R, right; W, without facial asymmetry.

Recording System

Surface EMG signals were recorded with disposable Ag–AgCl bipolar electrodes. Before the placement of the electrodes, the skin beneath the electrodes was cleaned with 70% alcohol. Surface electrodes were positioned on the muscular bellies of bilateral temporal anterior and masseter muscles of subjects, paralleled to muscular fibers with an inter-electrode distance of 20 mm. For the temporal anterior muscle, the electrodes were placed vertically along the anterior margin of the muscle, while for the masseter muscle, at the lower third of the line between the lateral angle of eye and the gonial angle. Subjects were requested to clench to adjust the location of electrodes. The reference electrodes were positioned at the corresponding ipsilateral elbow joint.

The activation of muscles was recorded by a four-channel EMG amplifier, sampled at 1,000 Hz by a 16-bit data acquisition card (DAQ USB-6341, National Instrument Corporation, Austin, TX, USA). The bandwidth of the on-board analog band-pass filter was 10–500 Hz. A program was designed in LabVIEW™ (LabVIEW 2012, National Instruments Corporation, Austin, TX, USA) to store the data.

Experimental Protocol

Figure 1 described the schematic diagram of the experimental setup. During the experiment, subjects seated straightly on a fixed chair with their hands put on the knees. The knee joints were kept at 90°. A smooth wall, with five markers indicating the five head positions, was in front of the subjects with a distance X_1. Point O on the smooth wall represented the upright position. When the subjects turned their heads to straightly face the other four points, they actually turn their head 30° in the four directions: left, right, up, and down. The height of point O was determined by the height of the participant's eyes. X_1 was measured before the experiment. The positions of the other four points on the wall representing head positions of left rotation, right rotation, dorsal flexion, and ventral flexion were determined by $D = X_1 \times \tan 30^{\circ}$.

A short training was conducted before the experiment. Then the subjects were requested to turn their head to straightly face the five different markers on the wall in turn to induce static vestibular stimuli. After each change in head position, the subjects followed the verbal instruction of beginning the clench at 7 s (**Figure 2**, command), such as "clench," and they occluded as hard as possible [to generate maximum voluntary clenching: maximal voluntary clenching (MVC)]. The occlusion phase of a trial lasted for 10 s. At each head position, the trial was repeated four times, so the task consisted of five 4-trial blocks. To avoid fatigue, there was a 30-s rest after each trial, and a 2-min rest between each two blocks.

Data Analysis

A representative example of raw EMG signals of the left masseter muscle of three subjects during MVC in the upright position was displayed in **Figure 2**. Patient 1 could not eat with mouth and was tube dependent, and his FOIS score was 1. Patient 2 had a FOIS score of 5. Although the two patients had different FOIS scores, their raw EMG signals were similar. The delay between the clenching command and the actual EMG clenching onset was due to the response time of the research assistant and the subject. The duration of the MVC phase was 10 s in each trial, and a 5-s analysis window was added from 3 to 8 s of the clench phase (**Figure 2**). The raw data were preprocessed with a fourth-order 10–300 Hz band-pass digital Butterworth filter. RMS, MDF and fApEn were calculated using the filtered EMG signals.

Root mean squares represented the amplitude of the signals, and it was calculated using the following formula:

$$\mathrm{RMS} = \sqrt{\frac{1}{N}\sum_{i} u_i^2}$$

where u_i was the filtered EMG signals ($i = 0, 1, \ldots, N-1$), and N was the length of the EMG signals. MDF was defined as the

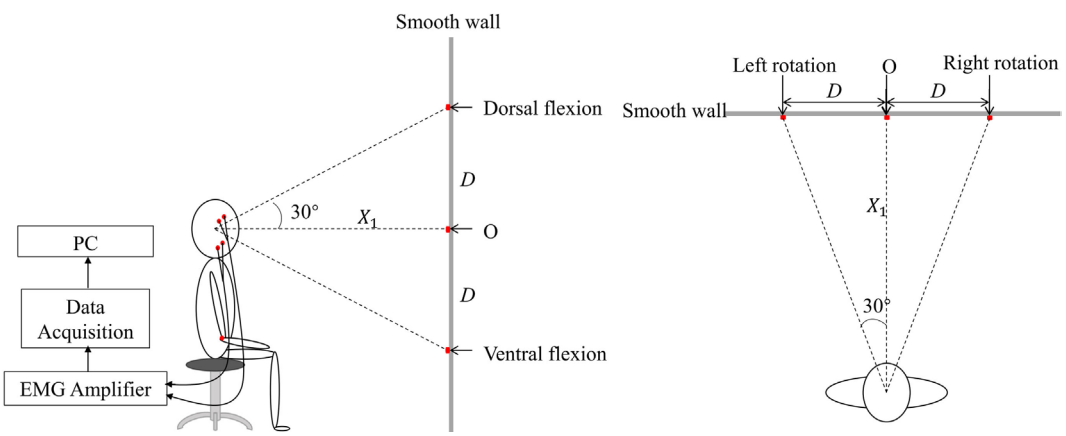

FIGURE 1 | The lateral and vertical view of the schematic diagram of experiment in the experiment. There were five markers on the smooth wall. Point O was of the same height as those of the subject's eyes. The others were, respectively, located on the wall to the left, right, upside, and downside of the point O with a distance *D*, represented various head positions, i.e., left rotation, right rotation, dorsal flexion, and ventral flexion.

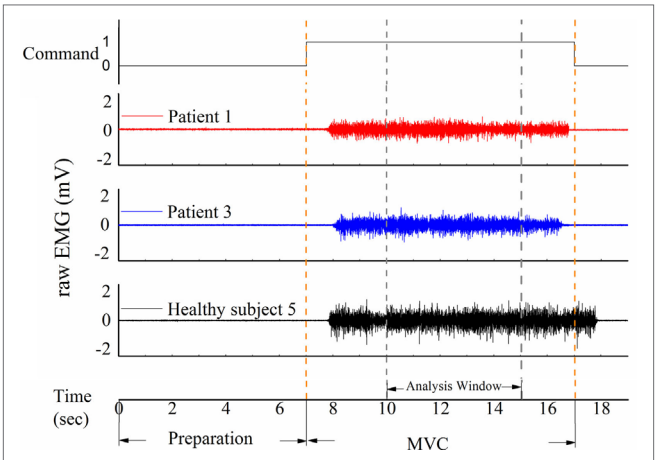

FIGURE 2 | Three samples of raw electromyography (EMG) signal of the masticatory muscle in response to the command in patients and healthy subjects. The task was divided into a 7-s preparation phase and a 10-s maximal voluntary clenching (MVC) phase. An analysis window was added from 10 to 15 s.

frequency point that divided the spectrum into two equal parts. To calculate MDF, the following equation should be satisfied.

$$\sum_{j=1}^{\mathrm{MDF}} P_j = \sum_{j=\mathrm{MDF}}^{M} P_j = \frac{1}{2}\sum_{j=1}^{M} P_j$$

where P_j represents the power spectrum of the filtered EMG, j represents the j-th discrete frequency, and M represents the bandwidth of the power spectrum analysis.

The calculation steps of fApEn were as follows:

$$X_i^m = \{u(i), u(i+1), \ldots, u(i+m-1)\} - u0(i), i = 1,2,\ldots, N-m+1, n = N-m+1$$

where X_i^m represented an m dimensional vector reconstructed with the filtered EMG signals $u(i)$. $u0$ (i) was the average value of the m discrete filtered EMG data, and was defined as $u0(i) = \frac{1}{m}\sum_{j=0}^{m-1} u(i+j)$. The distance between two different m dimensional vectors was calculated as

$$d_{ij}^m = \max_{i \neq j} \left| X_i^m - X_j^m \right|$$

where X_i^m and X_j^m were the two reconstructed m dimensional vectors, and d_{ij}^m was the distance between X_i^m and X_j^m. According to the concept of fuzzy entropy (18), the smaller the distance, the higher the similarity. The similarity degree of X_i^m and X_j^m was determined by a fuzzy function of d_{ij}^m, n and r:

$$D_{ij}^m(n,r) = \exp\left(-\left(\frac{d_{ij}^m}{n}\right)^r\right)$$

where D_{ij}^m denoted the similarity degree, r was the similarity tolerance should be predefined, the parameter n reweighted the contribution of distance d_{ij}^m, e.g., a larger n indicating more contribution of smaller distances of d_{ij}^m.

$$\varnothing^m(n,r) = \frac{1}{n-m}\sum_{i=1}^{N-m}\left(\frac{1}{N-m}\sum_{j=1, j\neq i}^{N-m} D_{ij}^m\right)$$

where $\varnothing^m(n,r)$ was averaged similarity. According to above equations, $\{X_i^{m+1}\}$ and $\varnothing^{m+1}$ could be calculated in the same manner, and

$$\mathrm{fApEn}(m,n,r,N) = \ln\varnothing^m(n,r) - \ln\varnothing^{m+1}(n,r)$$

where fApEn was the fuzzy approximate entropy of an N sample time series.

It was important to set proper values of m, r, and n before calculating the fApEn. Previous studies recommended m to use 2 or 3 because the length of the physiological signal was often not long enough to satisfy the need of the lager value of m (18), and $m = 2$ was the choice in this study. The similarity boundary was determined by the value of r and n. A too narrow boundary increased the sensitivity to noise, while a too wide one resulted in information loss. Besides, Sun et al. used the EMG data of a stroke patient to test how the fApEn changed with the values of N and r, and they found that when $N > 300$ and r ranged from 0.02 to 1, there was no crossover effect in the performance of the fApEn (19). Consequently, N, r, and n were respectively set to 1,000, 0.15, and 2 in this study (18–20).

All above calculations were processed in Matlab (Matlab R2014a, MathWorks Inc., Natick, MA, USA).

Statistical Analysis

All the parameters were described as mean ± SD in the paper. The level of significance was set at 0.05 ($P < 0.05$). Levene test was used to test for normal distribution of the data. If the Levene test result showed no significant deviations from variance homogeneity, the data were analyzed by three-way analysis of variance (ANOVA) with repeated measures. The three factors were: subject (healthy and patient), muscle (left temporal, right temporal, left masseter, right masseter) and head position (upright position, left rotation, right rotation, ventral flexion, dorsal flexion). If a large variance with non-normal distribution in the data of a subject group, a non-parametric test should be selected to analyze the data (21). Song et al. (22) suggested that the Wilcoxon signed rank test should be applied to analyze the statistical significance in a small sample size of subjects with high heterogeneity. In the current study, the sample size of the patient group was small. It is complex to perform a non-parametric test of multi-factors and their interactions (23, 24). If the patients' data did not pass the Levene test and did not display normality, we would use the Wilcoxon signed rank test to analyze the within-subject effects of muscle, head position and their interaction in the patient group based on manually paired data. In addition, if one of the effect was non-significant, we merged the data in the corresponding groups and performed the Wilcoxon signed rank test again to perform multiple comparison. If the healthy group passed the Levene test, a two-way analysis of variance (ANOVA) with repeated measures was used to evaluate the influences of the

two within-subject factors. Bonferroni *post hoc* test was used to detect the subgroup differences after the ANOVA comparison. To compare the between-subject differences with unequal-variance data, the Welch–Satterthwaite *t*-test was applied and the significant within-subject effect was controlled. All the statistical procedures were computed using the Statistical for Social Science (SPSS) version 22.0.

RESULTS

Figure 3 shows performance of the four masticatory muscles, in terms of RMS, MDF and fApEn, at different head positions. Some trends in the activities of masticatory muscles could be observed in the healthy subjects. For example, when they turned their head to the left, the muscles in the left was activated more than the contralateral ones', while the muscles in the right had higher RMS means when turning to the right. However, no such trend was observed in the patients. Besides, fApEn means in the patient group had a much larger SD, which surpassed the effect of head position.

The healthy subject's data passed the Levene test (RMS: $P = 0.367$; MDF: $P = 0.563$; fApEn: $P = 0.667$), but the patients' data did not pass the Levene test (RMS: $P = 0.001$; MDF: $P = 0.013$; fApEn: $P < 0.001$).

The two-way repeated measure ANOVA results showed that muscle had significant effect (RMS: $P = 0.001$; MDF: $P = 0.416$; fApEn: $P = 0.179$), but head position and muscle × head position interaction had no significant effect (head position: $P = 0.905$; interaction: $P = 0.818$). Bonferroni *post hoc* test showed that the RMS mean of the left masseter muscle was significantly lower than all the other muscles.

The Wilcoxon signed rank test conducted in the patient group showed a significant effect of Muscle but no significant effect of Head position (data not shown) and muscle × head position interaction (**Table 2**). Besides, the Wilcoxon signed rank test (**Figure 4**) indicated that the *RMS* means of any paired muscles were significantly different ($P < 0.007$) except that of the right masseter and temporal muscles, the scores of bilateral masseter muscles were significantly higher than those of bilateral temporal muscles in MDF ($P < 0.005$), and the masseter muscles had significantly higher fApEn means than the ipsilateral temporal muscles ($P < 0.005$).

We observed significant between-subject *RMS* differences in all muscles except the left masseter muscle ($P < 0.001$). The patient group showed significantly higher *MDF* means in the bilateral masseter muscles ($P < 0.001$). Besides, significant lower *fApEn* means were detected in all the muscles except the left masseter muscle ($P < 0.005$) (**Figure 4**).

For each parameter, we plotted a case-by-case plot to compare each patient's mean value with the subject mean in the healthy group (**Figure 5**). We found that the *RMS* means of Patients 1–4 and Patients 5 and 6 clustered into two patterns: Type I and Type II. Type I was characterized by significantly less activation in the right masticatory muscles, while Type II was characterized by equal weakness of all the four muscles. For the MDF, we found that all the patients' data varied in the same way, and the mean values of the bilateral masseter muscles laid above the healthy subjects' corresponding means. The fApEn case-by-case plot showed a large heterogeneity of patients.

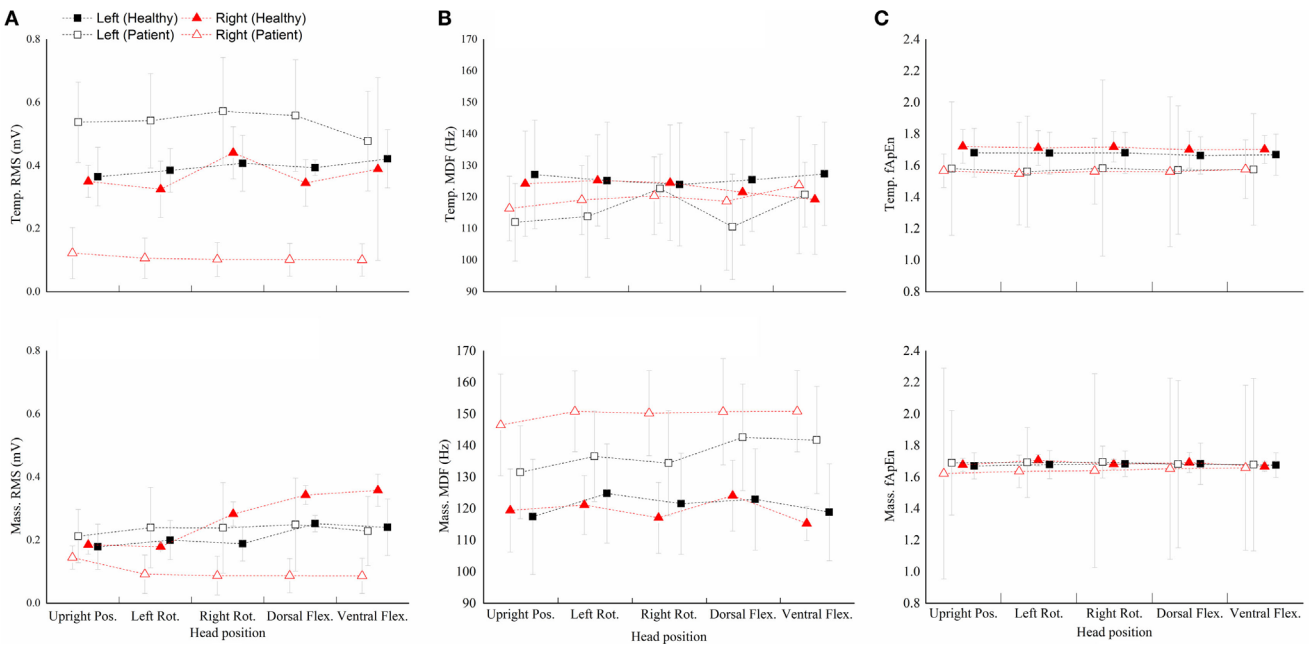

FIGURE 3 | The root mean squares (RMS) (A), median frequency (MDF) (B), fuzzy approximate entropy (C) means and SDs of the four masticatory muscles at different head positions in healthy subjects and patients. Temp., temporal anterior muscle; Mass., masseter muscle; Pos., position; Rot., rotation; Flex., flexion.

TABLE 2 | The result of the Wilcoxon signed rank test for statistical significance of muscle × head position interaction on the three electromyography parameters.

Muscles	Head positions[i]	Head positions[j]	Root mean squares		Median frequency		Fuzzy approximate entropy	
			Z	*P*	*Z*	*P*	*Z*	*P*
Left Temp.	Upright Pos.	Left Rot.	−0.447	0.655	−0.447	0.655	−1.342	0.180
		Right Rot.	−0.447	0.655	−1.342	0.180	−0.447	0.655
		Dorsal Flex.	−0.447	0.655	−0.447	0.655	−1.342	0.180
		Ventral Flex.	−1.342	0.180	−1.342	0.180	−1.342	0.180
	Left Rot.	Right Rot.	−0.447	0.655	−1.342	0.180	−1.342	0.180
		Dorsal Flex.	−0.447	0.655	−0.447	0.655	−1.342	0.180
		Ventral Flex.	−1.342	0.180	−1.342	0.180	−1.342	0.180
	Right Rot.	Dorsal Flex.	−0.447	0.655	−1.342	0.180	−1.342	0.180
		Ventral Flex.	−0.447	0.655	−1.342	0.180	−0.447	0.655
	Dorsal Flex.	Ventral Flex.	−0.447	0.655	−1.342	0.180	−1.342	0.180
Right Temp.	Upright Pos.	Left Rot.	−1.342	0.180	−0.447	0.655	−1.342	0.180
		Right Rot.	−1.342	0.180	−0.447	0.655	−0.447	0.655
		Dorsal Flex.	−1.342	0.180	−0.447	0.655	−0.447	0.655
		Ventral Flex.	−1.342	0.180	−0.447	0.655	−1.342	0.180
	Left Rot.	Right Rot.	−0.447	0.655	−0.447	0.655	−0.447	0.655
		Dorsal Flex.	−0.447	0.655	−0.447	0.655	−0.447	0.655
		Ventral Flex.	−0.447	0.655	−0.447	0.655	−1.342	0.180
	Right Rot.	Dorsal Flex.	−0.447	0.655	−0.447	0.655	−0.447	0.655
		Ventral Flex.	−0.447	0.655	−0.447	0.655	−0.447	0.655
	Dorsal Flex.	Ventral Flex.	−1.342	0.180	−1.342	0.180	−0.447	0.655
Left Mass.	Upright Pos.	Left Rot.	−0.447	0.655	−1.000	0.317	−1.342	0.180
		Right Rot.	−0.447	0.655	−0.447	0.655	−0.447	0.655
		Dorsal Flex.	−1.342	0.180	−0.447	0.655	−0.447	0.655
		Ventral Flex.	−1.342	0.180	−1.342	0.180	−1.342	0.180
	Left Rot.	Right Rot.	−0.447	0.655	−1.342	0.180	−0.447	0.655
		Dorsal Flex.	−1.342	0.180	−1.000	0.317	−0.447	0.655
		Ventral Flex.	−1.342	0.180	−0.447	0.655	−1.342	0.180
	Right Rot.	Dorsal Flex.	−1.342	0.180	−1.342	0.180	−0.447	0.655
		Ventral Flex.	−1.342	0.180	−1.342	0.180	−0.447	0.655
	Dorsal Flex.	Ventral Flex.	−0.447	0.655	−0.447	0.655	−0.447	0.655
Right Mass.	Upright Pos.	Left Rot.	−1.342	0.180	−1.000	0.317	−1.342	0.180
		Right Rot.	−1.342	0.180	−0.447	0.655	−1.342	0.180
		Dorsal Flex.	−1.342	0.180	−0.447	0.655	−1.342	0.180
		Ventral Flex.	−1.342	0.180	−1.342	0.180	−1.342	0.180
	Left Rot.	Right Rot.	−1.342	0.180	−1.342	0.180	−0.447	0.655
		Dorsal Flex.	−1.342	0.180	−1.000	0.317	−0.447	0.655
		Ventral Flex.	−1.342	0.180	−0.447	0.655	−0.447	0.655
	Right Rot.	Dorsal Flex.	−0.447	0.655	−1.342	0.180	−1.342	0.180
		Ventral Flex.	−0.447	0.655	−1.342	0.180	−1.342	0.180
	Dorsal Flex.	Ventral Flex.	−0.447	0.655	−0.447	0.655	−1.342	0.180

Head positions[i]: one of the head positions in the task; Head positions[j]: a different head position which was used to pair with Head positions[i]; Temp., temporal anterior muscle; Mass., masseter muscle; Pos., position; Rot., rotation; Flex., flexion.

DISCUSSION

This study was designed to investigate the activation pattern of masticatory muscle at different head positions in the healthy subjects and brainstem stroke patients when performing the maximal voluntary clenching (MVC). RMS, MDF and fApEn were used to analyze the EMG data. Significant differences between the healthy subjects and the patients were found in certain muscles.

Comparison between the Healthy Subjects and Stroke Patients

The lower RMS means of the stroke patients' right masticatory muscles compared with those of the healthy subjects' implied that the muscle excitation of their right muscles was quite low. Wang et al. (11) and Cruccu et al. (10) found that the affected side activated lower during clenching. The reduction of the muscle activation in patients was consistent with previous studies.

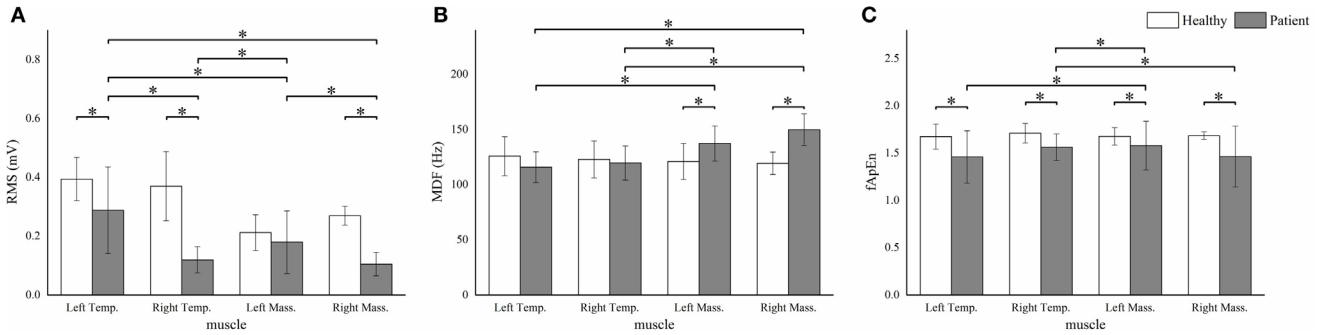

FIGURE 4 | The root mean squares (RMS) (A), median frequency (MDF) (B), fuzzy approximate entropy (fApEn) (C) means and SDs of the four masticatory muscles in healthy subjects and patients. *$P < 0.05$; Temp., temporal anterior muscle; Mass., masseter muscle.

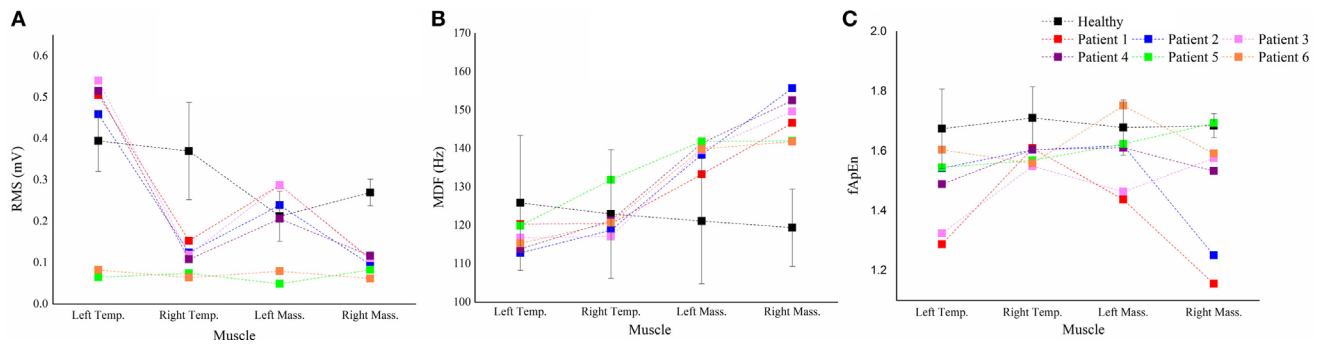

FIGURE 5 | The case-by-case plot. Comparison of the root mean squares (RMS) **(A)**, median frequency (MDF) **(B)**, fuzzy approximate entropy (fApEn) **(C)** means of each muscle in each patient with the subject means of the corresponding muscle in all healthy subjects. Temp., temporal anterior muscle; Mass., masseter muscle.

Compared to healthy subjects, the MDF means of the bilateral masseter muscles in patients was higher. Since MDF was associated with the conduction velocity in the muscle fiber and the action duration of motor unit (25), a higher MDF mean might suggest a higher conduction velocity and a smaller action duration. The shift of the spectrum toward higher frequencies might implied that, after brainstem stroke, the proportion of fast-twitch motor units that were enrolled in masticatory movement was lower (26). Another possible interpretation of the spectrum shift might be the deficiency of the monoaminergic neurons in the brainstem poststroke. The monoaminergic input amplifies the small motor neurons' current non-linearly and causes the slow-twitch motor units to sustain the contraction even after the action potential is over (27). After brainstem stroke, the monoaminergic regulation of the input–output properties might be affected (28, 29), and the contribution of the slow-twitch motor units in the masseter muscles was then lowered.

The fApEn means of all the muscles in the stroke patients were smaller than those in healthy subjects. Previous studies reported that fApEn might be related to the amount of recruited motor units and the firing rate (30). Therefore, the decrease of fApEn in the three muscles might be due to the changes in the neurological control after stroke, such as reduction of the number of recruited motor unit or lowering of the firing rate. The decreased firing rate in stroke patients was recently proven by a high-density EMG study (31). The large variability of fApEn in stroke patients suggested that large arithmetic cancels should happen when calculating means, hence some real situation might be hidden behind the fApEn means. In the case-by-case plot (**Figure 5C**), Patient 3 and 6 showed marked lower fApEn values of the left masseter muscle, while the other patients' data lied around the healthy subject's fApEn mean.

Influences of Muscles

For healthy subjects, the right masseter muscle yielded a higher RMS compared to the left one, which could be interpreted by different activations of the working-side and the balancing-side of the masseter muscles (32). It might reflect the truth that most (13/15) of the healthy subjects in this study habitually chewed with their right side. However, we observed no significantly different MDF and fApEn among different muscles. It might suggest that the neurological control of the jaw muscles in healthy subjects may be homologous.

For patients, mean values of the RMS and MDF between bilateral masseter muscles were statistically different, and the bilateral temporal muscles exhibited significantly different RMS but non-significantly different MDF. The lower RMS means of the right masticatory muscles might be due to the weakness of the

right masticatory muscles. According to the case-by-case RMS plot, four patients exhibited right-side weakness, but only two of them had right face sagging (**Table 1**). EMG analysis might reveal the unseen weakness of the patients. MDF is a parameter often used to characterize fatigue (33), and both masseter and temporal muscles yield lower MDFs in a sustain clench fatigue experiment (34). Previous studies have reported that successive recruitment of new motor units might be the reason of spectrum shift during muscular fatigue (35). The task in our study was fatigue-free, and the higher MDF in the right masseter muscle might due to the smaller action duration of the motor units (36).

The large variability of the fApEn implied that it might be more sensitive to the pathological status of the patients. From the case-by-case fApEn plot, we observed that most of the data points of patients were lower than the corresponding healthy subjects' means, which was in agreement with previous study showing smaller fApEn in the patient group (37). Combined fApEn with RMS, we might obtain more information about the masticatory function of the patient. For example, although Patient 5 and 6 had Type II RMS muscle pattern, the right masseter muscle's data of Patient 5 lied within the mean ± SD interval of healthy subjects, while Patient 6's data lied markedly beneath that interval. It suggested a larger deficiency of the neuromuscular control of the right side in Patient 6, and this patient had a form of right face sagging (**Table 1**).

Influences of Head Positions

Changing head position is a kind of static vestibular stimulation (5), which interferences balance control. In the other hand, occlusion is widely interrelated to gaze stabilization (38) and balance control (39) through activating complex nervous reflexes (40). A previous study (4) observed two types of EMG responses of the masticatory muscles to changes in head position. In the balanced type, the corresponding bilateral muscles (e.g., left and right temporal muscles) were activated equally when subjects performing ventral and dorsal flexion, while ipsilateral activation was observed in the rotation or tilting of the head. The unbalanced type exhibited asymmetrical and irregular activations. Although our results showed no statistical significance of head position, there exhibited similar trends to Ref. (4), i.e., the right muscles of the healthy subjects were much more activated when rotating to the right. The neuromuscular mechanism of changes in head position influencing muscle activation might be due to the tonic neck reflex, which was demonstrated with rats (41). The reasons why head position was a non-significant effect in our study might be due to the interindividual variation, also pointed out in the previous study (4), and the different experimental protocol we used, i.e., we instructed the subjects to clench as hard as possible instead of recording their rest EMG signals. Biting hard activated the whole muscle synchronously (42), and the weak tonic-neck-reflex origin EMG signal would be buried in the large firing signal. However, the sternocleidomastoid muscles would be co-activated (43) during maximum voluntary clenching. Therefore, the tonic neck reflex might be actually enhanced (44) although we could not see it. From the case-by-case EMG parameter values to head position curve of patients (data not show), we found again the high heterogeneity of patients' performance, but the clinical relevance was not clear.

Limitation of the Study

In the current study, we have investigated the muscle activities in response to variations in head position using three EMG parameters in both the healthy subjects and brainstem stroke patients. However, several limitations still should be addressed. First, we recruited the healthy youths rather than age-matched healthy adults. It should be noted that age might be one of the factors that influenced the EMG parameters, but age effect was not included in this study. In this preliminary study, we mainly focused on whether the three EMG parameters were discriminating and suited for assessing the masticatory function poststroke. The age effect should be further studied in the future. Second, more patients should be recruited in the future study to improve the statistical power of the study.

CONCLUSION

In this study, three EMG parameters, RMS, MDF and fApEn, were used to evaluate the activities of bilateral masseter and temporal muscles at different head positions in healthy subjects and brainstem stoke patients. We found that subject and muscle effected significantly on these parameters, but head position was a non-significant effect. The stroke patient group performed differently during MVC compared with healthy subjects and exhibited a large heterogeneity. Several patterns and trends were detected using multiparameter EMG analysis. Multiparameter EMG analysis might provide rich information and should be a potential useful tool of quantifying the neural activity related movement patterns of the deficient masticatory muscles poststroke.

ETHICS STATEMENT

This study received permission from local ethics committee. All the participants were volunteered to take part in this study and signed the written informed consent about the purpose and procedures of the study prior to the experiment.

AUTHOR CONTRIBUTIONS

Both CJ and MW conducted most of the experiments, collected and analyzed the data, interpreted the results, and finished the draft manuscript. JL designed the study, helped to analyze the data, and interpreted the results and revised the manuscript. JL and WZ participated in the data collection and analysis. WH conducted part of the experiments, recruited the subjects, collected data, and interpreted the results. RS designed the study and helped to interpret part of the results.

ACKNOWLEDGMENTS

The authors would like to thank Yunchu Hou, Jiaru Cheng, and Yingjian Wu for doing the experiments and collecting the data. The authors also would like to thank Jiangtao Sun for revising the manuscript.

FUNDING

This research was supported by the grant from National Nature Science Foundation of China (No. 61403430).

REFERENCES

1. Corsalini M, Rapone B, Grassi FR, Di VD. A study on oral rehabilitation in stroke patients: analysis of a group of 33 patients. *Gerodontology* (2010) 27(3):178–82. doi:10.1111/j.1741-2358.2009.00322.x
2. Schimmel M, Leemann B, Herrmann FR, Kiliaridis S, Schnider A, Müller F. Masticatory function and bite force in stroke patients. *J Dent Res* (2011) 90(2):230–4. doi:10.1177/0022034510383860
3. Lund JP. Mastication and its control by the brain stem. *Crit Rev Oral Biol Med* (1991) 2(1):33–64. doi:10.1177/10454411910020010401
4. Funakoshi M, Fujita N, Takehana S. Relations between occlusal interference and jaw muscle activities in response to changes in head position. *J Dent Res* (1976) 55(55):684–90. doi:10.1177/00220345760550042401
5. Deriu F, Podda MV, Milia M, Chessa G, Sau G, Pastorino M, et al. Masseter muscle activity during vestibular stimulation in man. *Arch Ital Biol* (2000) 138(3):205–15.
6. Kushiro K, Goto F. Effect of masticating chewing gum on postural stability during upright standing. *Neurosci Lett* (2011) 487(2):196–8. doi:10.1016/j.neulet.2010.10.021
7. Delmas CB, Compoint C, Delfini C, Buisseret P. Organisation of reciprocal connections between trigeminal and vestibular nuclei in the rat. *J Comp Neurol* (1999) 409(1):153–68. doi:10.1002/(SICI)1096-9861(19990621)409:1<153::AID-CNE11>3.0.CO;2-#
8. Pinganaud G, Bourcier F, Delmas CB, Buisseret P. Primary trigeminal afferents to the vestibular nuclei in the rat: existence of a collateral projection to the vestibulo-cerebellum. *Neurosci Lett* (1999) 264(1–3):133–6. doi:10.1016/S0304-3940(99)00179-2
9. Deriu F, Podda MV, Chessa G, Tolu E. Trigeminal integration of vestibular and forelimb nerve inputs. *Arch Ital Biol* (1999) 137(1):63–73.
10. Cruccu G, Fornarelli M, Manfredi M. Impairment of masticatory function in hemiplegia. *Neurology* (1988) 38(2):301–6. doi:10.1212/WNL.38.2.301
11. Wang JS, Lee JH, Kim NJ. Effects of neuromuscular electrical stimulation on masticatory muscles inelderly stroke patients. *J Phys Ther Sci* (2015) 27(9):2767–70. doi:10.1589/jpts.27.2767
12. Rokicki LA, Houle TT, Dhingra LK, Weinland SR, Urban AM, Bhalla RK. A preliminary analysis of EMG variance as an index of change in EMG biofeedback treatment of tension-type headache. *Appl Psychophysiol Biofeedback* (2003) 28(3):205–15. doi:10.1023/A:1024633230584
13. Graham RB, Wachowiak MP, Gurd BJ. The assessment of muscular effort, fatigue, and physiological adaptation using EMG and wavelet analysis. *PLoS One* (2015) 10(8):e0135069. doi:10.1371/journal.pone.0135069
14. Huber C, Göpfert B, Kugler PF, Von TV. The effect of sprint and endurance training on electromyogram signal analysis by wavelets. *J Strength Cond Res* (2010) 24(6):1527–36. doi:10.1519/JSC.0b013e3181dc42f6
15. Nieminen H, Takala EP. Evidence of deterministic chaos in the myoelectric signal. *Electromyogr Clin Neurophysiol* (1996) 36(1):49–52.
16. Gitter JA, Czerniecki MJ. Fractal analysis of the electromyographic interference pattern. *J Neurosci Methods* (1995) 58(58):103–8. doi:10.1016/0165-0270(94)00164-C
17. Giannasi LC, Matsui MY, Politti F, F Batista SR, Caldas BF, Amorim JB, et al. Test-retest reliability of electromyographic variables of masseter and temporal muscles in patients with cerebral palsy. *Arch Oral Biol* (2014) 59(12):1352–8. doi:10.1016/j.archoralbio.2014.08.011
18. Chen W, Wang Z, Xie H, Yu W. Characterization of surface EMG signal based on fuzzy entropy. *IEEE Trans Neural Syst Rehabil Eng* (2007) 15(2):266–72. doi:10.1109/TNSRE.2007.897025
19. Sun R, Ao D, Song R. Comparison of complexity of EMG signals between a normal subject and a patient after stroke – a case study. *Conf Proc IEEE Eng Med Biol Soc* (2013) 2013:4965–8. doi:10.1109/EMBC.2013.6610662
20. Xie HB, Guo JY, Zheng YP. Fuzzy approximate entropy analysis of chaotic and natural complex systems: detecting muscle fatigue using electromyography signals. *Ann Biomed Eng* (2010) 38(4):1483–96. doi:10.1007/s10439-010-9933-5
21. Daniel WW, Cross CL. *Biostatistics: A Foundation for Analysis in the Health Sciences*. 10th ed. Hoboken, NJ:John Wiley & Sons (2013). p. 671–2.
22. Song R, Tong KT, Hu X, Li L. Assistive control system using continuous myoelectric signal in robot-aided arm training for patients after stroke. *IEEE Trans Neural Syst Rehabil Eng* (2008) 16(4):371–9. doi:10.1109/TNSRE.2008.926707
23. Kubinger KD. A note on non-parametric tests for the interaction in two-way layouts. *Biom J* (1986) 28(1):67–72. doi:10.1002/bimj.4710280113
24. Lemmer HH, Stoker DJ. A distribution-free analysis of variance for the two-way classification. *South Afr Stat J* (1967) 1:67–74.
25. Compston J. Reliability: what is it, and how is it measured? *Physiotherapy* (2000) 86:94–9. doi:10.1016/S0031-9406(05)61211-4
26. Chinn S. The assessment of methods of measurement. *Stat Med* (1990) 9(4):351–62. doi:10.1002/sim.4780090402
27. Luschei ES, Goldberg LJ. Neural mechanisms of mandibular control: mastication and voluntary biting. *Compr Physiol* (2011) (Suppl 2):237–1274. doi:10.1002/cphy.cp010227
28. Murphy SA, Berrios R, Nelson PA, Negro F, Farina D, Schmit B, et al. Impaired regulation post-stroke of motor unit firing behavior during volitional relaxation of knee extensor torque assessed using high density surface EMG decomposition. *Conf Proc IEEE Eng Med Biol Soc* (2015) 2015:4606–9. doi:10.1109/EMBC.2015.7319420
29. Mcpherson JG, Ellis MD, Heckman CJ, Dewald JP. Evidence for increased activation of persistent inward currents in individuals with chronic hemiparetic stroke. *J Neurophysiol* (2008) 100(6):3236–43. doi:10.1152/jn.90563.2008
30. Biglandritchie B, Donovan EF, Roussos CS. Conduction velocity and EMG power spectrum changes in fatigue of sustained maximal efforts. *J Appl Physiol* (1981) 51(5):1300–5.
31. Li X, Holobar A, Gazzoni M, Merletti R. Examination of poststroke alteration in motor unit firing behavior using high-density surface EMG decomposition. *IEEE Trans Biomed Eng* (2014) 62(5):1242–52. doi:10.1109/TBME.2014.2368514
32. Hylander WL, Ravosa MJ, Ross CF, Wall CE, Johnson KR. Symphyseal fusion and jaw-adductor muscle force: an EMG study. *Am J Phys Anthropol* (2000) 112(4):469–92. doi:10.1002/1096-8644(200008)112:4<469::AID-AJPA5>3.0.CO;2-V
33. Gonzálezizal M, Malanda A, Gorostiaga E, Izquierdo M. Electromyographic models to assess muscle fatigue. *J Electromyogr Kinesiol* (2012) 22(4):501–12. doi:10.1016/j.jelekin.2012.02.019
34. Chung JW, Kim C, McCall WD. Effect of sustained contraction on motor unit action potentials and EMG power spectrum of human masticatory muscles. *J Dent Res* (2002) 81(9):646–9. doi:10.1177/154405910208100914
35. Hägg GM. Comparison of different estimators of electromyographic spectral shifts during work when applied on short test contractions. *Med Biol Eng Comput* (1991) 29(5):511–6. doi:10.1007/BF02442323
36. Hermens HJ, Bruggen TA, Baten CT, Rutten WL, Boom HB. The median frequency of the surface EMG power spectrum in relation to motor unit firing and action potential properties. *J Electromyogr Kinesiol* (1992) 2(1):15–25. doi:10.1016/1050-6411(92)90004-3
37. Ao D, Sun R, Tong KY, Song R. Characterization of stroke- and aging-related changes in the complexity of EMG signals during tracking tasks. *Ann Biomed Eng* (2015) 43(4):990–1002. doi:10.1007/s10439-014-1150-1
38. Yurchenko M, Hubálková H, Klepáček I, Machoň V, Mazánek J. The neuromuscular approach towards interdisciplinary cooperation in medicine. *Int Dent J* (2014) 64(1):12–9. doi:10.1111/idj.12057
39. Boyd CH, Slagle WF, Boyd CM, Bryant RW, Wiygul JP. The effect of head position on electromyographic evaluations of representative mandibular positioning muscle groups. *Cranio* (1987) 5(1):50–4.
40. Valentin B, Melito F. Functional relationships between the muscles of mastication and the muscles of the leg. *Surg Radiol Anat* (1991) 13(1):33–7. doi:10.1007/BF01623138
41. Funakosh M, Amano N. Effects of the tonic neck reflex on the jaw muscles of the rat. *J Dent Res* (1973) 52(4):668–73. doi:10.1177/00220345730520040501
42. Kawamura Y, Kato I, Takata M. Jaw-closing muscle activities with the mandible in rest position. *J Dent Res* (1967) 46(6):1356–62. doi:10.1177/00220345670460063601
43. Clark GT, Browne PA, Nakano M, Yang Q. Co-activation of sternocleidomastoid muscles during maximum clenching. *J Dent Res* (1993) 72(11):1499–502. doi:10.1177/00220345930720110701
44. Venegas M, Valdivia J, Fresno MJ, Miralles R, Gutiérrez MF, Valenzuela S, et al. Clenching and grinding: effect on masseter and sternocleidomastoid

electromyographic activity in healthy subjects. *Cranio* (2009) 27(3): 159–66. doi:10.1179/crn.2009.024

Conflict of Interest Statement: The authors declare that the research was conducted in the absence of any commercial or financial relationships that could be construed as a potential conflict of interest.

frontiers in Neurology

ORIGINAL RESEARCH
published: 15 May 2017
doi: 10.3389/fneur.2017.00202

Altered Motor Unit Discharge Coherence in Paretic Muscles of Stroke Survivors

*Chenyun Dai[1], Nina L. Suresh[2,3], Aneesha K. Suresh[4], William Zev Rymer[2,3] and Xiaogang Hu[1]**

[1] *Joint Department of Biomedical Engineering, University of North Carolina at Chapel Hill and North Carolina State University, Raleigh, NC, USA,* [2] *Sensory Motor Performance Program, Rehabilitation Institute of Chicago, Chicago, IL, USA,* [3] *Department of Physical Medicine and Rehabilitation, Feinberg School of Medicine, Northwestern University, Chicago, IL, USA,* [4] *Committee on Computational Neuroscience, University of Chicago, Chicago, IL, USA*

After a cerebral stroke, a series of changes at the supraspinal and spinal nervous system can alter the control of muscle activation, leading to persistent motor impairment. However, the relative contribution of these different levels of the nervous system to impaired muscle activation is not well understood. The coherence of motor unit (MU) spike trains is considered to partly reflect activities of higher level control, with different frequency band representing different levels of control. Accordingly, the objective of this study was to quantify the different sources of contribution to altered muscle activation. We examined the coherence of MU spike trains decomposed from surface electromyogram (sEMG) of the first dorsal interosseous muscle on both paretic and contralateral sides of 14 hemispheric stroke survivors. sEMG was obtained over a range of force contraction levels at 40, 50, and 60% of maximum voluntary contraction. Our results showed that MU coherence increased significantly in delta (1–4 Hz), alpha (8–12 Hz), and beta (15–30 Hz) bands on the affected side compared with the contralateral side, but was maintained at the same level in the gamma (30–60 Hz) band. In addition, no significant alteration was observed across medium–high force levels (40–60%). These results indicated that the common synaptic input to motor neurons increased on the paretic side, and the increased common input can originate from changes at multiple levels, including spinal and supraspinal levels following a stroke. All these changes can contribute to impaired activation of affected muscles in stroke survivors. Our findings also provide evidence regarding the different origins of impaired muscle activation poststroke.

Keywords: motor unit, coherence, stroke, synchronization, surface electromyogram

OPEN ACCESS

Edited by:
Ayrton R. Massaro, Hospital Sirio-Libanes, Brazil

Reviewed by:
Rakesh Pilkar, Kessler Foundation, USA
Dong Feng Huang, Sun Yat-sen University, China

****Correspondence:***
Xiaogang Hu
xiaogang@unc.edu

Specialty section:
This article was submitted to Stroke, a section of the journal Frontiers in Neurology

Received: *18 November 2016*
Accepted: *25 April 2017*
Published: *15 May 2017*

Citation:
Dai C, Suresh NL, Suresh AK, Rymer WZ and Hu X (2017) Altered Motor Unit Discharge Coherence in Paretic Muscles of Stroke Survivors. Front. Neurol. 8:202. doi: 10.3389/fneur.2017.00202

INTRODUCTION

After a cerebral stroke, a series of changes at the spinal and supraspinal levels of the nervous system can influence the control of muscle activation, leading to different motor impairment. One convenient way of identifying the different levels of contributions to altered muscle activation is to characterize the discharge patterns of motor unit (MU), given that MU discharge activities at the populational level can now be readily obtained from the skin surface (1, 2). Since different alpha motor neurons receive common synaptic excitations from spinal and supraspinal pathways during sustained contraction (3–6), the discharging times of MU should exhibit some degree of correlation.

The cross-correlation analysis of MU spike trains in the time domain has been widely used to study the connectivity between the motor neuron pool and the spinal or cortical inputs (7–11). However, the relative strength of correlation across different levels cannot be systematically quantified using this approach.

In contrast, the coherence analysis, which reflects the cross-correlation of MU spike trains in the frequency domain, provides complementary and important information from another perspective that can reveal these activities of higher level control (12–14). Previous studies have established the findings that the coherence of MU spike trains under 60 Hz is critically important and can be separated into four different frequency bands, including delta band (1–4 Hz), alpha band (8–12 Hz), beta band (15–30 Hz), and gamma band (30–60 Hz) (5, 15–17). Moreover, physiological origins for the synchronization of each band have been widely accepted. Specifically, the delta band is thought to reflect the common modulation of firing rates (18, 19); the alpha band highly depends on the feedback from muscle spindles and possibly results from rhythmical activities of the spinal reflex loop (20, 21); the beta band may reflect cortical and subcortical activities (15, 19); and the gamma band also represents cortical activities (19).

Previous studies have found that the MU synchronization of certain frequency bandwidths change under atypical conditions. A recent study reported an increase of MU coherence in delta, alpha, and beta bands after muscle fatigue (17). Another recent study (22) examined the variation of coherence with muscle pain. Their results indicated that muscle pain led to an increase in the coherence of MU spike trains in the delta band, but a decrease in the alpha band. Given the direct and indirect cortical and subcortical projections to the motor neuron pool, it can be conjectured that the alteration of synaptic inputs to motor neurons may influence the MU coherence at different frequency bandwidths. To date, few studies have examined the possible changes of MU synchronization in stroke survivors (23, 24). These studies were mostly based on electroencephalogram—electromyogram (EMG) synchronization rather than the coherence of MU spike train itself—and did not specifically quantify the variation of coherence in each frequency corresponding to specific physiological implications.

Accordingly, the objective of our current study was to systematically investigate the potentially altered control at different levels in contribution to impaired finger muscle activation in stroke survivors. In our study, MU spike trains were acquired from the decomposition of surface electromyogram (sEMG) of the first dorsal interosseous (FDI) muscle at a wide range of index finger abduction forces on both paretic and contralateral sides of hemispheric stroke survivors. The discharge coherence of concurrently active MUs was calculated across four frequency bandwidths at different force levels and was compared between the affected and contralateral muscles. The finger muscle was examined because stroke survivors tend to show persistent impairment in finger muscle activation. Particularly, the FDI muscle was tested because FDI is the only muscle involved in index finger abduction force, which can avoid force contribution of other muscles, and because the FDI is superficial and is accessible from the skin surface during EMG recordings. Our findings provide evidence that there are substantial changes in the common input, arising from the spinal and supraspinal circuitry, to the motor neuron pool innervating affected muscles, which can modify the control of muscle activation of stroke survivors.

MATERIALS AND METHODS

Experimental Apparatus and Procedures

Participants

Experimental data from 14 chronic hemiparetic stroke participants (detailed demographic information is shown in **Table 1**) were acquired at the Rehabilitation Institute of Chicago. All participants provided written informed consent. The experimental protocols were approved by the Institutional Review Board (#STU00084379) at Northwestern University.

The major inclusion criteria for stroke participants included (1) ability to provide written informed consent; (2) ability to communicate with and understand the instructions of the experimenter; (3) the duration since stroke >6 months; (4) impairment level of hand function measured with the Chedoke-McMaster score ranged from 2 to 6; (5) no medication; (6) no upper extremity inflammation, recent injury, pain, or other concurrent severe medical illness; (7) no history of vascular impairment.

Experimental Setup

The detailed information about the experimental setup has been reported in a previous study (25, 26). Briefly, participants sat in the experimental apparatus with their upper arm comfortably placed on a support, their forearm oriented at a full pronation position, secured with a cast and located in a ring mount interface attached to a forearm rest, and their wrist held neutral with respect to flexion/extension (**Figure 1A**). Their middle, ring, and little fingers were abducted away from the index finger resting on a supporting frame. The index finger casted and fixed to another ring mount interface was placed at approximately 60° apart from the thumb and directly attached to a 6 degree-of-freedom load cell (ATI, Inc., Apex, NC, USA). The recorded isometric

TABLE 1 | Participant demographic information.

Participant ID	Gender	Age	Years	Side	Chedoke	Fugl-Meyer
1	M	61	4	R	6	63
2	F	62	15	L	2	17
3	F	59	23	R	2	22
4	M	66	9	L	4	16
5	F	53	3	R	6	63
6	F	58	5	R	4	38
7	F	71	7	R	6	66
8	M	60	11	R	5	52
9	M	61	7	R	4	3
10	F	69	15	L	4	30
11	M	58	4	R	5	45
12	F	59	1	L	3	20
13	F	62	9	R	6	53
14	M	48	7	L	5	60

Age, year of age; Years, years since stoke; Side, paretic side; Chedoke, Chedoke-McMaster stroke assessment ranging from 1 to 7, with 1 being the most severe impairment; Fugl-Meyer, Fugl-Meyer assessment ranging from 1 to 66, with 1 being the most severe impairment; M, male; F, female; R, right; L, left.

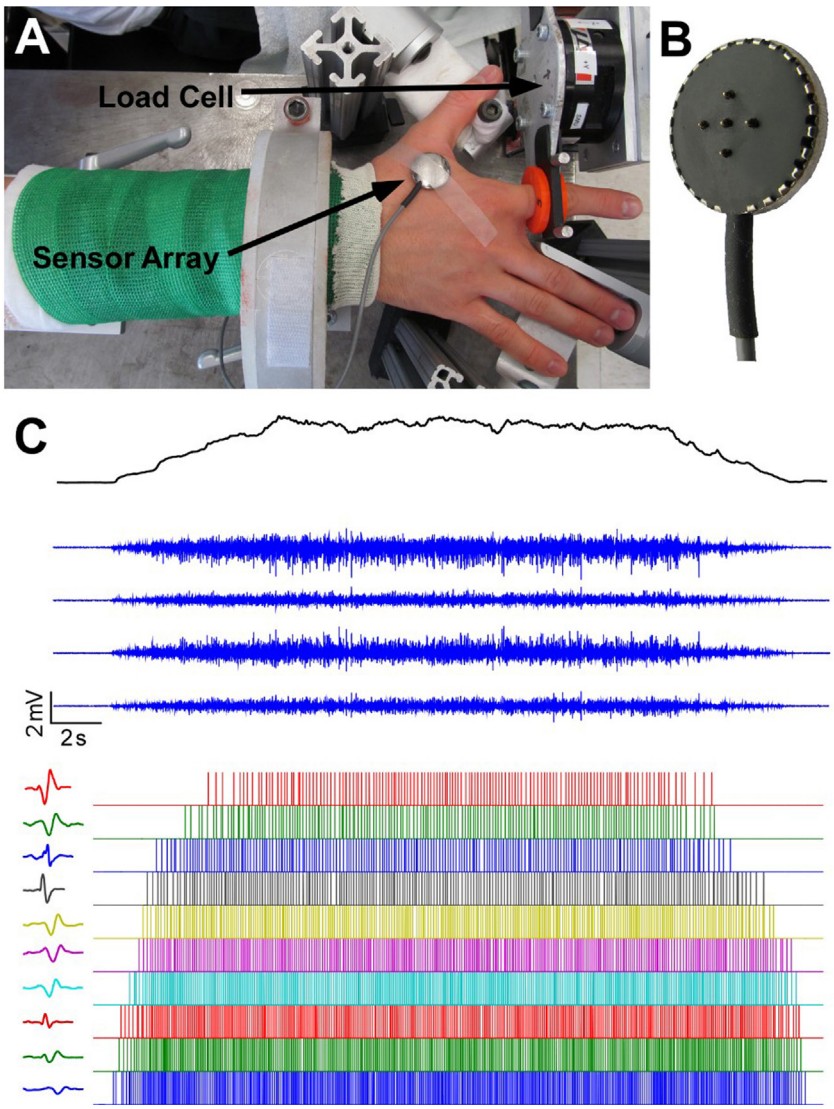

FIGURE 1 | **Experimental apparatus, electromyogram recordings and motor unit decomposition**. **(A)** Experimental setup. **(B)** The five-probe sensor array. **(C)** The four-channel surface electromyogram (sEMG) signals during a trapezoidal force production. In addition, motor unit spike trains and corresponding templates after sEMG decomposition are also displayed.

index finger abduction forces were low-pass filtered at 200 Hz cutoff frequency and sampled at 2 kHz, and a high sampling rate is required to avoid aliasing effect from channel cross-talk. The participant's skin above the FDI muscle was scrubbed with alcohol pads to reduce background noise. A five-pin sensor array (Delsys, Inc., Natick, MA, USA) was placed on the skin surface. Five 0.5-mm diameter cylindrical probes are located at the center of sensor array within a 5 mm × 5 mm square (**Figure 1B**). The sensor array and a reference electrode were connected to a Delsys Bagnoli sEMG system to record sEMG signals generated by the pairwise differentiation of these five electrodes. The sEMG recordings were amplified by a 1,000 gain and filtered with a bandwidth of 20–2 kHz with a sampling frequency at 20 kHz (**Figure 1C**).

Procedures

The data collection included two main sessions (one for each side) with same experimental protocols. Before the two main sessions, participants were required to perform maximum voluntary contractions (MVCs) for 3 s. Three repeated trials with 60 s rest between trials were tested to obtain the largest force value, which was designated as the MVC. To ensure a fair comparison between two sides, the MVC of paretic side was used during the force tasks on the contralateral side, such that the two sides produced the same absolute forces. Then, participants performed five repeated trials for five isometric contraction levels at 20, 30, 40, 50, and 60% MVC. The force trajectory contained a 5-s quiescent period for baseline noise calculation, an up-ramp increasing at 10% MVC/s, a constant force at prescribed MVC for 12 s, a down-ramp

decreasing at 10% MVC/s, and a final 3-second quiescent period. The order of the force levels was randomly selected for each participant. One minute of rest period was provided between trials to avoid cumulative fatigue.

Data Analysis

Preprocessing

The sEMG and force recordings selected for further data analysis must satisfy the following requirements: (1) no sudden change in the up-ramp force; (2) the variability of force during steady state within ±2 SDs of background force level; (3) the sEMG signal with the baseline noise level within ±10 μV, and signal-to-noise ratio greater than 5 (signal-to-noise ratio was defined as peak–peak amplitude of the EMG signal at steady state contractions divided by peak–peak amplitude of the baseline noise). Based on the criteria above, three trials for each MVC level per participant were finally selected for the coherence analysis. During the analysis, the accepted number of MU must be over eight to be included in the analysis because the large number of MUs resulted in an accurate coherence estimate.

MU Acceptance

All raw sEMG recordings were automatically decomposed using Nawab's algorithm (1). The autodecomposition algorithm extracted the firing times, and four different MU action potential waveforms (from the four-channel EMG recordings) of each identified MU spike train. Then, a robust postexamination method, spike trigger average (STA) algorithm (27), was used to determine which MUs were retained for further analysis. The STA method reestimated MU action potential templates based on the firing times, MU action potential templates, and raw EMG signals obtained from Delsys. A high agreement of two different algorithms for each MU provided confidence regarding the reliability of decomposition results. The STA method calculated the coefficient of variation (CV) for peak–peak amplitude of MU action potential templates and the maximum correlation coefficient between STA MU action potential estimation and Delsys MU action potential templates. Only MUs with a mean correlation >0.7 and CV <0.3 across four channels were selected for data analysis based on our previous studies (17, 27, 28).

Coherence Calculation

The magnitude of coherence increased substantially with the number of MU spike trains selected. Therefore, using more MUs for coherence calculation was recommended (29, 30), providing a better estimation than a small number of MUs. Moreover, the coherence values can only be compared across different trials when the same amount of MU spike trains was analyzed. Since some trials only had a small number of accepted MU spike trains, eight MUs were selected for coherence calculation. For those trials with more than eight accepted MUs, the same amount of MU spike trains was randomly chosen from accepted MUs pool. A total of eight spike trains were randomly separated into two groups and then summed up into two composite spike trains (CSTs). The Welch's averaged, modified periodogram method (31), adopted by multiple previous MU coherence studies (16, 17, 22), was performed to calculate the magnitude of squared coherence $C_{xy}(f)$ between the two CSTs:

$$C_{xy}(f) = \frac{\left|P_{xy}(f)\right|^2}{P_{xx}(f)P_{yy}(f)}, \quad (1)$$

where $P_{xy}(f)$ is the cross-spectrum mean of two CSTs, and $P_{xx}(f)$ and $P_{yy}(f)$ are, respectively, their autospectrum densities. The calculation of the coherence-square used the MATLAB function "mscohere" with a length of 1,024 sample segments tapered by a Hann window and overlapped by 75% to estimate the entire frequency spectrum. The data processing steps are summarized in **Figure 2**. To obtain a better coherence estimate, the parameter selection for the coherence calculation was based on a previous study (32). In addition, to reduce the effect caused by random selection, 100 repeated tests were operated and averaged to acquire final coherence estimation for each trial. [An exemplar coherence estimation of the affected and contralateral sides of a stroke survivor is shown in **Figure 3** (top)].

The confidence limit for coherence estimate was

$$\gamma^2_{1-\alpha} = 1 - \alpha^{\left[1/(\mathrm{EDOF}-1)\right]}, \quad (2)$$

where α is (1 − α)% confidence level, and EDOF is the equivalent degree of freedom for Hann window (33).

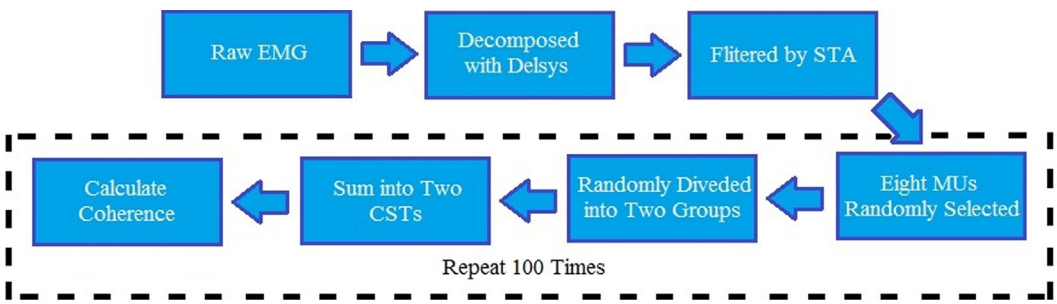

FIGURE 2 | Block diagram for the entire data analysis. EMG, electromyography; STA, spike trigger average algorithm; CST, composite spike train; MU, motor unit.

Four different bands—delta band (1–4 Hz), alpha band (8–12 Hz), beta band (15–30 Hz), and gamma band (30–60 Hz)—were analyzed separately due to their different physiological meanings. We began by exploring the potential influence of three factors (two sides, four bands, and three MVC levels) on coherence. The magnitude of coherence for each band was quantized by its mean band coherence:

$$\mathrm{MBC} = \frac{\int_{f_1}^{f_2} C_{xy}(f)\,df}{B}, \tag{3}$$

where $C_{xy}(f)$ is the magnitude of squared coherence, B is the width of one frequency band, and f_1 and f_2 are the lower and upper bounds of the corresponding band, respectively.

Correlation Analysis

A linear regression was performed to investigate the relationship between the possible factors (age, years poststroke, and the severity of impairment measured with Fugl-Meyer assessment) and the increased percentage of coherence on the paretic side compared with the contralateral side. We chose Fugl-Meyer assessment instead of Chedoke because the values of Fugl-Meyer assessment spread across a wider range from 1 to 66, which can give a better resolution for linear regression, and the correlation coefficient between Fugl-Meyer and Chedoke was 0.82. Therefore, only Fugl-Meyer was included in the regression.

Statistics

The coherence estimate was examined mainly on three aspects: comparisons of coherence amplitude across different MVC levels, comparisons between the affected and contralateral side, and comparisons of coherence amplitude across different frequency bands. The differences were tested statistically using a three-way repeated measures ANOVA, with *post hoc* pairwise comparisons conducted using Bonferroni correction method. A significance level of $p = 0.05$ was used. To satisfy the ANOVA test assumption, all coherence values (C) were transformed to Fisher's values (FZ), which has been used in previous MU coherence studies (16, 34, 35). The fisher's z-transformation equation is

$$\mathrm{FZ} = \arctan h\sqrt{C}. \tag{4}$$

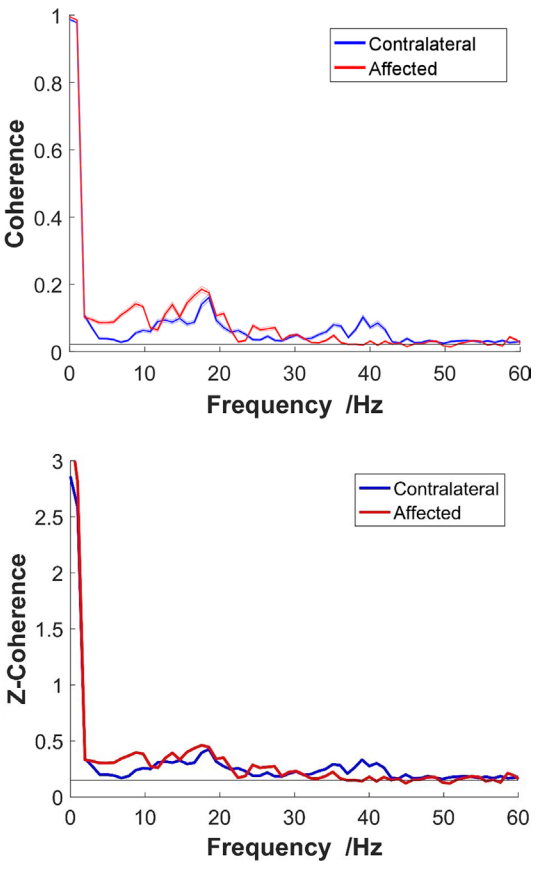

FIGURE 3 | Top: non-standardized coherence; bottom: z-coherence. An exemplar frequency-coherence plots from a representative stroke participant at 40% maximum voluntary contraction. The solid thick red line represents the coherence of the affected side, and the blue line represents the contralateral side. Thin lines present SE.

RESULTS

After decomposition and cross validation between STA and Delsys, the overall number of accepted MU spike trains is shown in **Table 2**. Low contraction levels that yielded a small number of MUs caused two main issues: (1) the number of accepted MUs cannot satisfy the requirement of coherence calculation (≥8). The "<8" column in **Table 2** presents the number of trials with number of MUs < 8; (2) the random grouping algorithm for coherence calculation may be biased due to a small MU pool. Therefore, 40, 50, and 60% MVC were used for the final data analysis, while 20 and 30% MVC were excluded. (See Section "Discussion" for further details regarding the choice of MU numbers.) For these participants, under 40, 50, and 50% contraction levels, the average number of accepted MU spike trains was 17.73 ± 5.57 per single trial for the affected side and 20.27 ± 6.38 for the contralateral side; while the corresponding mean firing rates were 13.55 ± 4.04 pulse per second (pps) and 12.90 ± 3.31 pps, respectively.

A three-way repeated measures ANOVA was tested across three isometric contraction levels (40, 50, and 60%) on two sides and four different frequency bands. The ANOVA results showed that there is an interaction [$F(3,39) = 9.708$, $p < 10^{-4}$] between the side and frequency band. However, the third factor MVC showed no

TABLE 2 | The number of accepted motor units across different maximum voluntary contraction levels on two sides.

	Affected side	Contralateral side	<8
20%	15.24 ± 4.51	18.71 ± 6.32	4
30%	16.76 ± 3.33	19.24 ± 6.10	3
40%	17.40 ± 4.94	20.10 ± 5.80	0
50%	17.76 ± 5.45	20.22 ± 6.33	0
60%	18.02 ± 6.26	20.50 ± 7.07	0

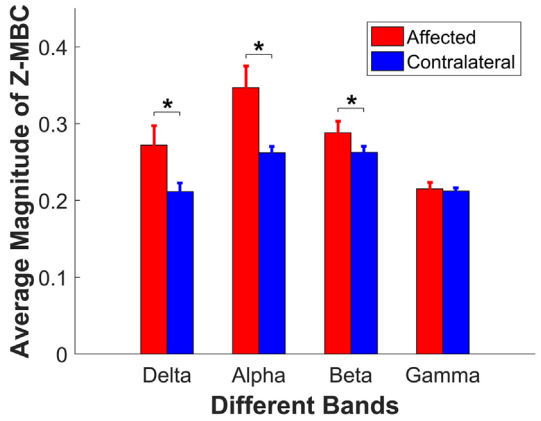

FIGURE 4 | Comparison of the z-coherence of different frequency bands between affected side and contralateral sides. Each bar presents its corresponding average magnitude of mean band z-coherence (z-MBC), and the error bar presents its SE across 14 participants. Asterisks indicate the significant difference.

significant difference [$F(2,26) = 1.666, p = 0.209$], and also showed no interaction with other factors {[$F(2,26) = 0.030$, $p = 0.971$] between MVC and side; [$F(6,78) = 0.982$, $p = 0.443$] between MVC and frequency band; and [$F(6,78) = 0.086$, $p = 0.997$] for all three}.

The interaction (side × frequency band) led us to conduct further *post hoc* pairwise comparisons separately. First, we compared the difference between paretic side and contralateral side for each individual band. The pairwise comparisons showed that the coherences were significantly different for delta band ($p = 0.013$), alpha band ($p = 0.005$), and beta band ($p = 0.022$), between the affected and contralateral sides, but not different for gamma band ($p = 0.717$). The average z-transformed mean coherence across all participants for delta band, alpha band, and beta band on affected side were 0.2720 ± 0.0254, 0.3468 ± 0.0282, and 0.2881 ± 0.0150, which were higher than those on the contralateral side (0.2116 ± 0.0112, 0.2620 ± 0.0082, and 0.2625 ± 0.0078, respectively, as shown in **Figure 4**). The baseline coherence was 0.2123 ± 0.004 and is comparable to the gamma band coherence.

Second, *post hoc* pairwise comparisons were tested across four bands on two sides separately, and both showed a significant difference. For the paretic side, **Figure 5** (top) shows *post hoc* evaluation, which revealed that (1) the alpha band had the highest mean coherence ($p < 0.05$); (2) the gamma band had the lowest mean value ($p < 0.05$); (3) the magnitude of delta band and beta hand had no statistical difference ($p = 0.284$). For the contralateral side, the *post hoc* comparison (**Figure 5**, bottom) showed that (1) the alpha and beta bands had significantly high coherence compared with the delta band and gamma band ($p < 0.001$); (2) the magnitude of the alpha and beta bands, or the delta and gamma bands had no statistical difference ($p > 0.9$).

Third, a linear regression was performed between three possible factors (age, years of poststroke, and the severity of stroke

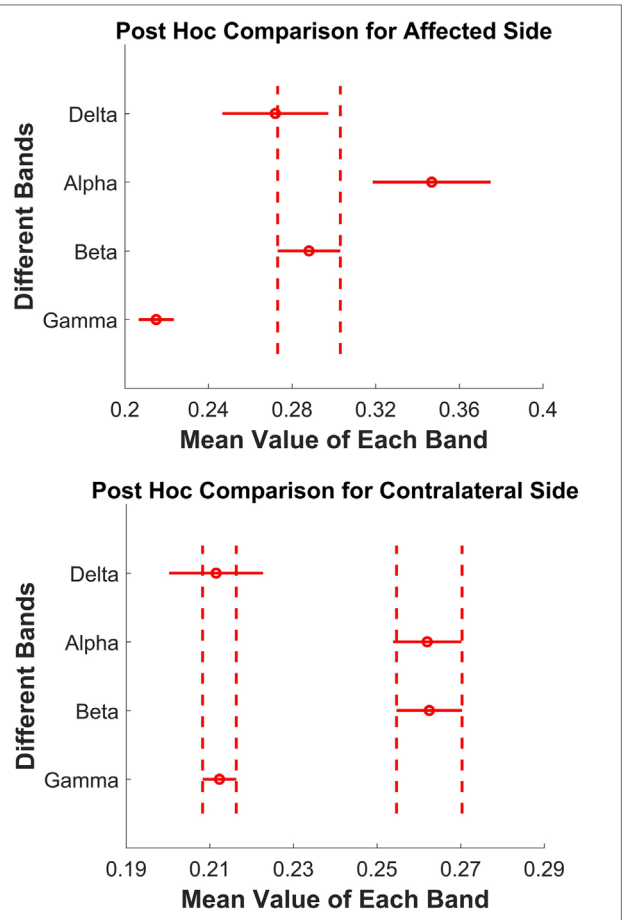

FIGURE 5 | Top: paretic side; bottom: contralateral side. *Post hoc* pairwise comparison across four bands. Each red circle presents the mean value of one frequency band, and the red horizontal line is its corresponding 95% confidence interval. The vertical dashed lines show the overlap of two bands, which means no significant difference.

TABLE 3 | The fitting coefficients with corresponding *p* values, the r^2 value of the linear regression on four bands.

	Age	Years since stroke	Fugl-Meyer	r^2
Delta	−0.0035 (0.0755)	0.0175 (0.3632)	0.0057 (0.2854)	0.372
Alpha	−0.0202 (0.2460)	0.0064 (0.7150)	0.0083 (0.1064)	0.364
Beta	−0.0133 (0.1278)	0.0074 (0.3969)	0.0014 (0.5470)	0.264
Gamma	−0.0120 (0.0314)*	0.0081 (0.1407)	0.0022 (0.1507)	0.505

Individual p-values are shown in parentheses.
**Significance at 95% level.*

measured using Fugl-Meyer) and the increased percentage of coherence on paretic side compared with contralateral side. Separate regression was performed on the four different bands. **Table 3** shows the fitting coefficients with the r^2 value of each frequency band. The r^2 values of the linear regression for the delta, alpha, beta, and gamma bands were 0.372, 0.364, 0.264, and 0.505, respectively. The results showed that the three factors

tended to have a linear relation with the increased coherence value.

DISCUSSION

The coherence of MU spike trains is considered to partly reveal the relations between the motor neuron pool and spinal/superaspinal network, and the coherence of each frequency bandwidth can reflect the relative connectivity between the motor neuron pool and the upstream circuitry. Our current study quantified the changes of the coherence of each frequency band on the affected side, compared with the contralateral side of hemiparetic stroke survivors. Our results provided strong evidence that the coherences of three frequency bands (delta, alpha, and beta) showed a significant increase compared with the contralateral side. The coherence of the delta band and the alpha band increased substantially on the affected side (increased by 28.5 and 32.4%, respectively), compared with the contralateral side. The coherence in the beta band on the affected side also revealed moderate increase (by 9.6%), compared with the contralateral side. However, the magnitude of the gamma band coherence remained unchanged. Our general findings indicate that there are substantial changes in the common input to the motor neuron pool, arising from the spinal and supraspinal circuitry, which can modify the control of muscle activations after a stroke.

Influence of Muscle Activation Level on Coherence

We found that the coherence estimates are consistent across a range of medium–high force levels (40–60%), indicating that the relative contribution of common synaptic input to the motor neuron pool is not sensitive to the levels of muscle contraction. The findings suggest that we can use a single prespecified muscle activation level (40–60% MVC) to estimate the coherence at different frequency ranges. It should be emphasized that the MVC levels affect the number of recruited MUs. During the coherence analysis, only a fixed number of MUs are randomly selected to the pool. Therefore, if the number of MUs used for the coherence analysis was identical, the MVC level within 40–60% MVC did not influence the estimate of coherence. However, the coherence estimate at force levels outside of the range was not examined, because lower force levels tend to yield a smaller number of MUs (see **Table 2**, some 20 and 30% trials cannot meet the minimum requirement), which may bias the coherence calculation. In contrast, higher forces tend to induce early muscle fatigue, which has been shown as a factor that can affect MU coherence (17). These factors can potentially bias our current coherent estimation, due to the sampling requirement of the coherence analysis and a relative steady MU discharge rate based on the assumption of the discharge spectrum analysis.

Physiological Implications for the Variation of Each Band

Although the partition of frequency band range from different studies was not identical, the four specific ranges were divided similarly, and the corresponding physiological concepts have been widely accepted (17, 19, 22). In our present study, the gamma band always maintained at a stable and low power level on both paretic and contralateral sides. A substantial increase of the delta and alpha bands coherence was observed in the affected muscle in our stroke cohort. It is believed that the delta coherence is associated with the modulation of mean firing rate of the MUs. The increased delta coherence may reflect a compensatory change in response to the reduced firing rate and the reduced modulation of firing rate of MUs observed in stroke survivors (36). The large SE (see **Figure 4**) on the affected side also illustrated that the increased rate of these common inputs was different across participants, possibly due to the different severity of stroke. The alpha band coherence is associated with afferent feedback/spinal reflex contributions. In addition, previous studies indicated that the coherence between MUs increased with increasing muscle spindle activities (20, 22, 37). A flexed finger posture, potentially due to hyperreflexia, is a common feature in spastic stroke survivors. In addition, hyperreflexia is one common pathology in stroke survivors (38, 39), and it is conceivable that there is an increased spinal reflex contribution to the MU activation. However, we do not have direct evidence that the FDI muscle is hyperreflexia in our stroke cohort, since spasticity is not routinely assessed in the finger muscles.

The increase of common synaptic inputs affected beta band that revealed cortical and subcortical activities and short-term MU synchronization. The increased coherence in beta band results provided a consistent evidence with previous studies, which reported that the coherence of MU firing times had significant linear relationship with shared motor neuron inputs (6, 40). The stronger correlated higher level input to the FDI motor neuron pool may reflect more centralized control with a few cortical neurons directly projecting to the whole motor neuron pool, rather than having a complex network directly and indirectly modulating the activation of the motor neuron pool. In addition, a reduction of inhibitory high level input, due to stroke, could also contribute to more synchronized input. Clearly, additional studies are necessary to verify these potential changes.

Correlations with Subject Demographic Information

To identify potential associations between the change of coherence in the affected FDI and the participant clinical information, separate multiple linear regression was performed for each coherence bandwidth. A moderate overall correlation was found as indicated by the r^2 values. However, the individual demographic factors were not significant predictors on the change of coherence. A lack of strong correlations may arise from multiple aspects. First, the heterogeneous features of our stroke cohort of 14 participants may limit our correlation estimates, and a larger sample size may yield a better fit. Second, the change of coherence at different bandwidth may have stronger associations with other clinical features such as the lesion location or the integrity of the cortical spinal track, and the Fugl-Meyer

or time poststroke may not be specific enough to show a strong correlation.

CONCLUSION

In conclusion, we observed a significant increase of MU spike train coherence on the affected side of stroke survivors in the delta band, the alpha band, and the beta band, compared with the contralateral side. Our findings indicate that changes at multiple levels, including spinal and supraspinal levels, can all contribute to altered activation of affected muscles in stroke survivors. Further studies may be necessary to investigate possible relations between common drive and other frequency bands for stroke survivors and to explore if the increase in common drive on paretic side can lead to MU synchronization across different muscles.

AUTHOR CONTRIBUTIONS

CD analyzed the data and drafted the manuscript; NS, AS, and XH acquired the data; CD, NS, AS, WR, and XH discussed the study and revised the manuscript.

FUNDING

This work was supported by National Institutes of Health Award Number: R03 NS085492-01A1.

REFERENCES

1. Nawab SH, Chang SS, De Luca CJ. High-yield decomposition of surface EMG signals. *Clin Neurophysiol* (2010) 121:1602–15. doi:10.1016/j.clinph.2009.11.092
2. Holobar A, Zazula D. Multichannel blind source separation using convolution kernel compensation. *IEEE Trans Signal Process* (2007) 55:4487–96. doi:10.1109/TSP.2007.896108
3. Keen DA, Fuglevand AJ. Common input to motor neurons innervating the same and different compartments of the human extensor digitorum muscle. *J Neurophysiol* (2004) 91:57–62. doi:10.1152/jn.00650.2003
4. Farina D, Negro F, Jiang N. Identification of common synaptic inputs to motor neurons from the rectified electromyogram. *J Physiol* (2013) 591(10):2403–18. doi:10.1113/jphysiol.2012.246082
5. Farmer SF, Bremner FD, Halliday DM, Rosenberg JR, Stephens JA. The frequency content of common synaptic inputs to motoneurones studied during voluntary sometric contraction in man. *J Physiol* (1993) 470:127–55. doi:10.1113/jphysiol.1993.sp019851
6. Conway BA, Halliday DM, Farmer DM, Shahani U, Maas P, Weir AI, et al. Synchronization between motor cortex and spinal motoneuronal pool during the performance of a maintained motor task in man. *J Physiol* (1995) 489(Pt 3):917–24. doi:10.1113/jphysiol.1995.sp021104
7. Kirkwood PA. On the use and interpretation of cross-correlation measurements in the mammalian central nervous system. *J Neurosci Methods* (1979) 1:107–32. doi:10.1016/0165-0270(79)90009-8
8. Farmer SF, Halliday DM, Conway BA, Stephens JA, Rosenberg JR. A review of recent applications of cross-correlation methodologies to human motor unit recording. *J Neurosci Methods* (1997) 74:175–87. doi:10.1016/S0165-0270(97)02248-6
9. Semmler JG, Nordstrom MA. A comparison of cross-correlation and surface EMG techniques used to quantify motor unit synchronization in humans. *J Neurosci Methods* (1999) 90:47–55. doi:10.1016/S0165-0270(99)00069-2
10. Bedenbaugh P, Gerstein GL. Multiunit normalized cross correlation differs from the average single-unit normalized correlation. *Neural Comput* (1997) 9:1265–75. doi:10.1162/neco.1997.9.6.1265
11. Rosenbaum R, Trousdale J, Josić K. The effects of pooling on spike train correlations. *Front Neurosci* (2011) 5:58. doi:10.3389/fnins.2011.00058
12. Rosenberg JR, Amjad AM, Brillinger DR, Halliday DM. The Fourier approach to the identification of functional coupling between neuronal spike trains. *Prog Biophys Mol Biol* (1989) 53:1–31. doi:10.1016/0079-6107(89)90004-7
13. Negro F, Farina D. Factors influencing the estimates of correlation between motor unit activities in humans. *PLoS One* (2012) 7(9):e44894. doi:10.1371/journal.pone.0044894
14. Semmler JG. Motor unit synchronization and neuromuscular performance. *Exerc Sport Sci Rev* (2002) 30(1):8–14. doi:10.1097/00003677-200201000-00003
15. Halliday DM, Conway BA, Farmer SF, Rosenberg JR. Load-independent contributions from motor-unit synchronization to human physiological tremor. *J Neurophysiol* (1999) 82(2):664–75.
16. Castronovo AM, Negro F, Conforto S, Farina D. The proportion of common synaptic input to motor neurons increases with an increase in net excitatory input. *J Appl Physiol* (2015) 119:1337–46. doi:10.1152/japplphysiol.00255.2015
17. McManus L, Hu X, Rymer WZ, Suresh NL, Lowery MM. Muscle fatigue increases beta-band coherence between the firing times of simultaneously active motor units in the first dorsal interosseous muscle. *J Neurophysiol* (2016) 115(6):2830–9. doi:10.1152/jn.00097.2016
18. De Luca CJ, Erim Z. Common drive of motor units in regulation of muscle force. *Trends Neurosci* (1994) 17:299–305. doi:10.1016/0166-2236(94)90064-7
19. Lowery MM, Myers LJ, Erim Z. Coherence between motor unit discharges in response to shared neural inputs. *J Neurosci Methods* (2007) 163:384–91. doi:10.1016/j.jneumeth.2007.03.011
20. Erimaki S, Christakos CN. Coherent motor unit rhythms in the 6–10 Hz range during time-varying voluntary muscle contractions: neural mechanism and relation to rhythmical motor control. *J Neurophysiol* (2008) 99:473–83. doi:10.1152/jn.00341.2007
21. Christakos CN, Papadimitriou NA, Erimaki S. Parallel neuronal mechanisms underlying physiological force tremor in steady muscle contractions of humans. *J Neurophysiol* (2006) 95:53–66. doi:10.1152/jn.00051.2005
22. Yavuz US, Negro F, Falla D, Farina D. Experimental muscle pain increases variability of neural drive to muscle and decreases motor unit coherence in tremor frequency band. *J Neurophysiol* (2015) 114(2):1041–7. doi:10.1152/jn.00391.2015
23. Mima T, Toma K, Koshy B, Hallett M. Coherence between cortical and muscular activities after subcortical stroke. *Stroke* (2001) 32:2597–601. doi:10.1161/hs1101.098764
24. Datta AK, Farmer SF, Stephens JA. Central nervous pathways underlying synchronization of human motor unit firing studied during voluntary contractions. *J Physiol* (1991) 432:401–25. doi:10.1113/jphysiol.1991.sp018391
25. Hu X, Suresh AK, Rymer WZ, Suresh NL. Altered motor unit discharge patterns in paretic muscles of stroke survivors assessed using surface electromyography. *J Neural Eng* (2016) 13:046025. doi:10.1088/1741-2560/13/4/046025
26. Hu X, Suresh AK, Rymer WZ, Suresh NL. Assessing altered motor unit recruitment patterns in paretic muscles of stroke survivors using surface electromyography. *J Neural Eng* (2016) 12:066001. doi:10.1088/1741-2560/12/6/066001
27. Hu X, Suresh AK, Rymer WZ, Suresh NL. Motor unit pool organization examined via spike triggered averaging of the surface electromyogram. *J Neurophysiol* (2013) 110:1205–20. doi:10.1152/jn.00301.2012
28. Hu X, Rymer WZ, Suresh NL. Reliability of spike triggered averaging of the surface electromyogram for motor unit action potential estimation. *Muscle Nerve* (2013) 48:557–70. doi:10.1002/mus.23819
29. Farina D, Merletti R, Enoka RM. The extraction of neural strategies from the surface EMG: an update. *J Appl Physiol* (2014) 117:1215–30. doi:10.1152/japplphysiol.00162.2014
30. Negro F, Farina D. Linear transmission of cortical oscillations to the neural drive to muscles is mediated by common projections to populations of motoneurons in humans. *J Physiol* (2011) 589:629–37. doi:10.1113/jphysiol.2010.202473
31. Welch PD. The use of fast Fourier transform for the estimation of power spectra: a method based on time averaging over short, modified periodograms. *IEEE Trans Audio Electroacoust* (1967) 15:70–3. doi:10.1109/TAU.1967.1161901
32. Terry K, Griffin L. How computational technique and spike train properties affect coherence detection. *J Neurosci Methods* (2008) 168(1):212–23. doi:10.1016/j.jneumeth.2007.09.014

33. Thomson RE, Emery WJ. *Data Analysis Methods in Physical Oceanography*. Waltham: Elsevier (2014).
34. Maris E, Oostenveld R. Nonparametric statistical testing of EEG- and MEG-data. *J Neurosci Methods* (2007) 164:177–90. doi:10.1016/j.jneumeth.2007.03.024
35. Poston B, Danna-Dos Santos A, Jesunathadas M, Hamm TM, Santello M. Force-independent distribution of correlated neural inputs to hand muscles during three-digit grasping. *J Neurophysiol* (2010) 104:1141–54. doi:10.1152/jn.00185.2010
36. Mottram CJ, Heckman CJ, Powers RK, Rymer WZ, Suresh NL. Disturbances of motor unit rate modulation are prevalent in muscles of spastic-paretic stroke survivors. *J Neurophysiol* (2014) 111:2017–28. doi:10.1152/jn.00389.2013
37. Semmler JG, Kornatz KW, Dinenno DV, Zhou S, Enoka RM. Motor unit synchronization is enhanced during slow lengthening contractions of a hand muscle. *J Physiol* (2002) 545:681–95. doi:10.1113/jphysiol.2002.026948
38. Katz RT, Rymer WZ. Spastic hypertonia: mechanisms and measurement. *Arch Phys Med Rehabil* (1989) 70:144–55.
39. Sommerfeld DK, Eek EU, Svensson AK, Holmqvist LW, Arbin MH. Spasticity after stroke its occurrence and association with motor impairments and activity limitations. *Stroke* (2004) 35:134–9. doi:10.1161/01.STR.0000105386.05173.5E
40. Brown P. Cortical drives to human muscle: the Piper and related rhythms. *Prog Neurobiol* (2000) 60:97–108. doi:10.1016/S0301-0082(99)00029-5

Conflict of Interest Statement: The authors declare that the research was conducted in the absence of any commercial or financial relationships that could be construed as a potential conflict of interest.

frontiers in Neurology

CASE REPORT
published: 20 March 2017
doi: 10.3389/fneur.2017.00107

Advanced Myoelectric Control for Robotic Hand-Assisted Training: Outcome from a Stroke Patient

*Zhiyuan Lu[1], Kai-yu Tong[2], Henry Shin[1], Sheng Li[1] and Ping Zhou[1,3]**

[1] Department of Physical Medicine and Rehabilitation, University of Texas Health Science Center at Houston, TIRR Memorial Hermann Research Center, Houston, TX, USA, [2] Division of Biomedical Engineering, Department of Electronic Engineering, The Chinese University of Hong Kong, Hong Kong, Hong Kong, [3] Guangdong Work Injury Rehabilitation Center, Guangzhou, China

A hand exoskeleton driven by myoelectric pattern recognition was designed for stroke rehabilitation. It detects and recognizes the user's motion intent based on electromyography (EMG) signals, and then helps the user to accomplish hand motions in real time. The hand exoskeleton can perform six kinds of motions, including the whole hand closing/opening, tripod pinch/opening, and the "gun" sign/opening. A 52-year-old woman, 8 months after stroke, made 20× 2-h visits over 10 weeks to participate in robot-assisted hand training. Though she was unable to move her fingers on her right hand before the training, EMG activities could be detected on her right forearm. In each visit, she took 4× 10-min robot-assisted training sessions, in which she repeated the aforementioned six motion patterns assisted by our intent-driven hand exoskeleton. After the training, her grip force increased from 1.5 to 2.7 kg, her pinch force increased from 1.5 to 2.5 kg, her score of Box and Block test increased from 3 to 7, her score of Fugl–Meyer (Part C) increased from 0 to 7, and her hand function increased from Stage 1 to Stage 2 in Chedoke–McMaster assessment. The results demonstrate the feasibility of robot-assisted training driven by myoelectric pattern recognition after stroke.

Keywords: electromyography, myoelectric pattern recognition, hand exoskeleton, rehabilitation, case report

OPEN ACCESS

Edited by:
Ayrton R. Massaro, Hospital Sirio-Libanes, Brazil

Reviewed by:
Jun Yao, Northwestern University, USA
Michele Linda Callisaya, University of Tasmania, Australia

****Correspondence:***
Ping Zhou
ping.zhou.1@uth.tmc.edu

Specialty section:
This article was submitted to Stroke, a section of the journal Frontiers in Neurology

Received: *07 October 2016*
Accepted: *03 March 2017*
Published: *20 March 2017*

Citation:
Lu Z, Tong KY, Shin H, Li S and Zhou P (2017) Advanced Myoelectric Control for Robotic Hand-Assisted Training: Outcome from a Stroke Patient. Front. Neurol. 8:107. doi: 10.3389/fneur.2017.00107

INTRODUCTION

Robot-assisted upper limb training is considered to be more efficient (1) and economic (2) than conventional therapy in neurorehabilitation. Controlling the robot with the user's own electromyography (EMG) signals connects the user's intended motion and his actual movements. It can therefore enhance therapeutic effects and promote motor learning (3–5). Various EMG-driven robots and exoskeletons have been developed for neurorehabilitation (6–8), primarily based on one-to-one mapping, which typically maps one channel of EMG signal to a corresponding single degree-of-freedom (DOF) or variable such as speed and torque using a conventional "on-off" or proportional strategy. Robots based on such control strategy work well on training joints with only a few DOFs such as elbow and wrist. However, a human hand has up to 27 DOFs (9) and is controlled by complex temporal and spatial coordination of multiple muscles. It is therefore not feasible to regain hand dexterity through conventional control strategies. Myoelectric pattern-recognition techniques have been developed to extract motion intentions from EMG signals (10, 11). The extracted intentions can then be used to control a multiple-DOF robot such as a prosthesis (12). Previous studies have also shown that motion intentions can still be extracted after neurological impairment (13–15).

We therefore developed an intent-driven hand training system. The system employs an exoskeleton hand, which is controlled by myoelectric pattern recognition. As soon as the user's intention is detected (usually within 250 ms), the system is able to assist to accomplish the intended motions (16).

CASE REPORT

Subject

A 52-year-old woman participated in this robotic hand-assisted training 8 months after stroke. She was right-handed before stroke and had hemiplegia on her right side after her stroke. She was able to walk independently with an ankle foot orthosis but had difficulties in moving her right arm. Her fingers were flexed naturally. She was unable to move any of the fingers on her right hand, but EMG signals were able to be recorded from her forearm. Her Fugl–Meyer score (Part A–D, max 66) was 16, with a 0 in Part C (Hand, max 14). She had no pain when her whole hand was passively opened or closed. She did not receive any other hand or upper limb therapies while participating in this study. During her visits, she was able to understand and follow all the instructions.

Exoskeleton Hand

The exoskeleton hand, Hand of Hope (Rehab-Robotics, Hong Kong), was used in this study to help the subject move her hand (**Figure 1**). The exoskeleton hand has five individual fingers. Each finger is actuated by a linear actuator that can pull and push linearly. The mechanical design of the fingers converts these linear movements into the rotations of a virtual metacarpophalangeal (MCP) joint and a virtual proximal interphalangeal (PIP) joint. Both joints rotate together to help the hand perform closing and opening movements (7). The motion range is 55° and 65° for MCP and PIP joints, respectively. The subject's palm and five fingers are fixed to the exoskeleton hand with Velcro belts. Each finger can be bent or straightened individually by the exoskeleton hand. The exoskeleton hand stands on a brace, which also supports the subject's forearm, so that the subject can be totally relaxed when attached to the exoskeleton. The exoskeleton hand used in this study can perform six different motion patterns, including hand closing (HC); hand opening (HO); thumb, index, and middle fingers closing (TIMC or tripod pinch); thumb, index, and middle fingers opening; middle, ring, and little fingers closing (MRLC or the "gun" sign); and middle, ring, and little fingers opening. The exoskeleton hand can perform HC, TIMC, or MRLC when it is open. However, after performing any one from these three patterns, it can only return to the original open status (e.g., there is no direct way from the "tripod pinch" to the "gun" sign).

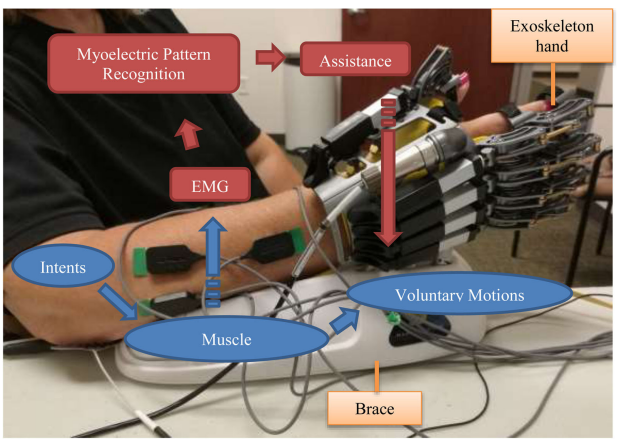

FIGURE 1 | Training with the exoskeleton hand driven by myoelectric pattern recognition.

Conventional EMG control of the device was applied in previous studies for training hand opening/closing function for stroke survivors (17, 18). In order to make all these six motion patterns available for the subject, a myoelectric pattern-recognition system was developed for this study to control the exoskeleton hand. This system is able to detect and recognize the subject's muscle activity patterns, indicate his/her intended hand motions, and then assist the patient in accomplishing these motions in real time. When the subject tries to perform a hand motion, EMG signals can be detected from those activated muscles. The myoelectric pattern-recognition system then extracts the motion intent from these EMG signals and maps the intent into control commands. The exoskeleton hand therefore performs the same motion as the subject's intent, so that the subject can accomplish the motion with both robotic assistance and his/her own participation.

Protocol

The subject made 20 visits (experiments) for the robot-assisted training, 2 visits per week. During the experiment, the subject was seated comfortably in a chair, next to a small height-adjustable side table. The exoskeleton hand was placed beside her on the table on her right side. Her right hand was fixed in the exoskeleton, and her forearm was placed on the brace (**Figure 1**). The exoskeleton was placed and locked on the brace. Therefore, the subject's right arm and hand could be totally relaxed instead of resisting gravity. The height of the table was adjusted to make the angle between her upper arm and her trunk about 45°, and the angle between her upper arm and her forearm about 90°. The subject was free to move her left hand. She was also allowed to move her right arm by moving the brace when she took breaks between two training sessions. Considering that the virtual palm was locked, the subject's right hand was always in a neutral position, and her forearm was never rotated even when she moved the brace. The brace would be moved to its initial position before another training session began.

Seven bipolar surface electrodes (Delsys 2.1) were attached on the subject's forearm using double-sided tapes, covering the first dorsal interossei, flexor digitorum superficialis, flexor digitorum profundus, extensor digitorum, abductor pollicis longus, extensor digiti minimi, and extensor pollicis longus muscles. The reference electrode was placed on the olecranon. The skin was cleaned using sterile alcohol wipes before electrodes were placed. EMG signals were acquired using a Bagnoli-8 EMG System (Delsys Inc., Boston, MA, USA), which amplified raw EMG signals 10,000 times and filtered the signals using a 20–450 Hz band pass filter. The acquired EMG signals were then input into a desktop

running Windows 7 through a data acquisition device, USB-6221 (National Instruments Inc., Austin, TX, USA), which digitized the signals at 1,000 Hz with a 16-bit resolution.

The digitized EMG signals were then analyzed by a myoelectric pattern-recognition program developed for this study, which aimed to extract motion intentions from multi-channel EMG signals. The analysis was based on the EMG signals recorded in the most recent 200 ms (named a processing window) and was performed every 100 ms, so that the recognition result could be updated at 10 Hz (19), which is acceptable for real-time control. A motion detection algorithm was first performed to tell whether this window contained EMG signals that corresponded to the user's voluntary motions. It calculated the mean absolute value (MAV) (20) of the processing window. If the MAV was smaller than a given threshold (it was 80% of the average MAV of EMG signals recorded from this subject at her median force level), no further processing would be performed, and the recognition result was "no motion." Otherwise, a motion was considered to be detected because one or more muscles were active. Then, a pattern-recognition algorithm was performed, in which a support vector machine classifier (21) was applied to recognize motions based on a set of features including root mean square amplitude (20), fourth order auto regressive coefficients (22), and waveform length (20). The output of the classifier was then mapped onto control commands and sent to the hand exoskeleton.

Each visit included five sessions. In the first session, the subject repeated each motion pattern 15 times. Although she was unable to move her fingers, she was encouraged to try controlling the fingers. For each motion pattern, the subject was asked to imagine moving her fingers in the desired motion. The first 2 s of above-threshold EMG signals were recorded before the exoskeleton subsequently provided assistance corresponding to the motion pattern. These EMG signals recorded in these 2-s periods were used to train the classifier. The next four sessions were all training sessions. In each session, the subject controlled the exoskeleton using her own motion intent. She was asked to try performing all of the six motion patterns and then to follow through with the exoskeleton hand while it moved through its full motion range. When the exoskeleton reached the final range, it stopped, and began waiting for another motion intent from the subject. The subject was therefore encouraged to perform the next motion right after the exoskeleton stopped. The subject was always free to choose any of the executable patterns, but sometimes the experimenter gave suggestions in order to balance the training amount of each motion pattern. Considering the subject's EMG signals were very weak, it was necessary for her to perform motions using about 70% of her maximal force in all these sessions. Consequently, she got fatigued quickly after 8–10 min training. In order to avoid fatigue, each training session was set to 10 min and could be terminated at any time after 8 min. Moreover, she was given as much time as needed to rest between sessions. Therefore, each visit took about 2 h, including approximately 40 min training.

RESULTS

Assessments, including grip force (using Jamar Plus + Digital Hand Dynamometer, Patterson Medical, Warrenville, IL, USA), pinch force (using PG-60 Pinch Gauges, B&L Engineering, Santa Ana, CA, USA), Box and Block test (23), Fugl–Meyer (Part C only, ranging from 0 to 14), and Chedoke–McMaster (the Hand Stage only, ranging from 1 to 7) (24), were performed before and after the 20-visit training. Results are shown in **Table 1**. The results of both the grip force and the pinch force were the maximal readings from three measurements. The result of Box and Block test was the highest score of three trials. As to the Fugl–Meyer and Chedoke–McMaster assessment, only the hand-related score were reported because only hand function was trained. The average control accuracy of the 1st and the 20th visit was also calculated. The subject was requested to report every time when the exoskeleton hand performed a motion that was different from her intent. The control accuracy was calculated based on the number of wrong motions and the total number of motions.

After the training, the results of all the assessments were improved dramatically. The grip force and pinch force were almost doubled. She also regained some voluntary finger movements. These improvements were quantified by three functional assessments from different aspects. Before the training, she was not able to perform observable finger movements. Her Fugl–Meyer score (Part C) was 0 and Chedoke–McMaster stage was 1 because she failed to do all the tasks in these assessments. After the training, she could flex all her fingers in a small range, so that she was able to partially perform many of the tasks. For example, she was able to hold a pencil, though loosely. As a result, she obtained 1 point in each grip task in the part C of the Fugl–Meyer assessment except the task "flexion in interphalangeal joints and extension in MCP." Also because of these active motions, she met the criteria of Hand Stage 2 in the Chedoke–McMaster assessment. However, she did not get to Stage 3 because her range of motion was not greater than 50% plus that she did not have opposition to bring the thumb to the index finger. The same functional improvement increased her score in the Box and Block test. Because she was not able to open/close her hand before the training, she developed an alternative way to accomplish this task, which was to push a block into the space between her thumb and other fingers using arm movements. When she managed to push two corners of a block into her hand, she could pick up the block. Holding the block in hand was difficult given that her grip was weak and she was not holding the whole block. As a result, preventing dropping the block half way was more challenging for her, compared with releasing the block. After the training, she used the same way to move the blocks. Although the range of motion for HO was still not large enough to pick up or hold one block, it was easier for her to push the block in. And she could hold the block for a longer

TABLE 1 | Assessment results before and after the training.

Tests	Pretreatment	Posttreatment
Grip force (kg)	1.5	2.7
Pinch force (kg)	1.5	2.5
Box and Block	3	7
Fugl–Meyer (part C)	0	7
Chedoke–McMaster (hand)	1	2
Control accuracy (%)	75.0	76.9

time because of her increased grip force, so that she had more time to move the block over the barrier. The scores of her three trials after training were 4, 7, and 4, respectively, while her highest score before training was 3.

DISCUSSION

In the previous studies applying conventional control (17, 18), the exoskeleton was triggered when the EMG amplitude of the monitored muscle(s) exceeded a given threshold, while other muscles' activities were ignored. However, finger motions are generated by coordinating a series of muscles. Pattern-recognition algorithms were therefore introduced in this study in order to analyze the motion patterns of up to seven muscles. These algorithms also made it possible to control the hand exoskeleton in multiple DOFs and provided an approach to training fine motions and improving hand dexterity. Both the myoelectric pattern-recognition techniques and the robot-assisted training are safe. No adverse event was observed, and no discomfort was reported. Although fatigue was reported sometimes, it usually went away after a few minutes break.

This intent-driven control required the subject to be active during the training. This subject was able to activate her muscles though she could not perform finger motions. The real-time assistance from the exoskeleton gave her the feedback of muscle activities and helped her strengthen her motion patterns. Although the subject had severely impaired hand functions before the training (Hand Stage 1 according to the Chedoke–McMaster assessment), she still achieved 75% control accuracy. Our algorithms recognized most of the subject's motion intents correctly, which assisted her in accomplishing these motions. Her hand function improved after the training, and all the assessments showed consistent improvements.

Although the training program for this subject demonstrates promising outcomes, a comprehensive evaluation of the effectiveness of the robotic hand-assisted training driven by myoelectric pattern recognition requires testing with a larger number of stroke subjects. We are aware that for a wide range of stroke patients with mild to severe impairment, some patients may not be suitable for such training due to lack of muscle activity or impaired muscle activity patterns (25, 26), while those stroke subjects who are able to generate muscle activity patterns and achieve reasonable accuracies can participate in the training program. In this regard, a pre-examination or assessment might be necessary to determine the stroke subjects who are able to control the exoskeleton hand with myoelectric pattern recognition, and who can benefit most from the robotic hand aided training.

ETHICS STATEMENT

This study was approved by the Committee for the Protection of Human Subjects (CPHS) of The University of Texas Health Science Center at Houston and TIRR Memorial Hermann (Houston, TX, USA). All procedures of the study were performed in accordance with the Declaration of Helsinki. The subject gave written and informed consent before the experimental procedures.

AUTHOR CONTRIBUTIONS

ZL performed experiment, analyzed data, and wrote the manuscript. KT developed the robotic exoskeleton hand and helped with data analysis. HS helped with experiment and data analysis. SL helped with data analysis and interpretation. PZ oversaw the study and helped with experiment, data analysis, and interpretation. All the authors read, revised, and approved the manuscript.

ACKNOWLEDGMENTS

The authors would like to thank Kathryn Nedley, OTR, OTD, for performing functional assessments and useful discussions.

FUNDING

This study was supported by American Heart Association (grant number 16GRNT29100012).

REFERENCES

1. Lum PS, Burgar CG, Shor PC, Majmundar M, Van der Loos M. Robot-assisted movement training compared with conventional therapy techniques for the rehabilitation of upper-limb motor function after stroke. *Arch Phys Med Rehabil* (2002) 83(7):952–9. doi:10.1053/apmr.2001.33101
2. Wagner TH, Lo AC, Peduzzi P, Bravata DM, Huang GD, Krebs HI, et al. An economic analysis of robot-assisted therapy for long-term upper-limb impairment after stroke. *Stroke* (2011) 42(9):2630–2. doi:10.1161/STROKEAHA.110.606442
3. Song R, Tong KY, Hu XL, Li L. Assistive control system using continuous myoelectric signal in robot-aided arm training for patients after stroke. *IEEE Trans Neural Syst Rehabil Eng* (2008) 16:371–9. doi:10.1109/TNSRE.2008.926707
4. Lum PS, Burgar CG, Kenney DE, Vander Loos HF. Quantification of force abnormalities during passive and active-assisted upper-limb reaching movements in post-stroke hemiparesis. *IEEE Trans Biomed Eng* (1999) 46:652–62. doi:10.1109/10.764942
5. Hu XL, Tong KY, Song R, Zheng XJ, Leung WW. A comparison between electromyography-driven robot and passive motion device on wrist rehabilitation for chronic stroke. *Neurorehabil Neural Repair* (2009) 23:837–46. doi:10.1177/1545968309338191
6. Schabowsky CN, Godfrey SB, Holley RJ, Lum PS. Development and pilot testing of HEXORR: hand exoskeleton rehabilitation robot. *J Neuroeng Rehabil* (2010) 7:36. doi:10.1186/1743-0003-7-36
7. Ho NSK, Tong KY, Hu XL, Fung KL, Wei XJ, Rong W, et al. An EMG-driven exoskeleton hand robotic training device on chronic stroke subjects: task training system for stroke rehabilitation. *IEEE Int Conf Rehabil Robot* (2011) 2011:5975340. doi:10.1109/ICORR.2011.5975340
8. Heo P, Gu GM, Lee SJ, Rhee K, Kim J. Current hand exoskeleton technologies for rehabilitation and assistive engineering. *Int J Precis Eng Manuf* (2012) 13:807–24. doi:10.1007/s12541-012-0107-2
9. Lin J, Wu Y, Huang TS. Modeling the constraints of human hand motion. *Proceedings Workshop on Human Motion*. Washington, DC: IEEE (2000). p. 121–6.
10. Lu Z, Chen X, Li Q, Zhang X, Zhou P. A hand gesture recognition framework and wearable gesture-based interaction prototype for mobile devices. *IEEE Trans Hum Mach Syst* (2014) 44:293–9. doi:10.1109/THMS.2014.2302794
11. Oskoei MA, Hu H. Myoelectric control systems – a survey. *Biomed Signal Process Control* (2007) 2(4):275–94. doi:10.1016/j.bspc.2007.07.009

12. Parker P, Englehart K, Hudgins B. Myoelectric signal processing for control of powered limb prostheses. *J Electromyogr Kinesiol* (2006) 16:541–8. doi:10.1016/j.jelekin.2006.08.006
13. Liu J, Zhou P. A novel myoelectric pattern recognition strategy for hand function restoration after incomplete cervical spinal cord injury. *IEEE Trans Neural Syst Rehabil Eng* (2013) 21:96–103. doi:10.1109/TNSRE.2012.2218832
14. Zhang X, Zhou P. High-density myoelectric pattern recognition toward improved stroke rehabilitation. *IEEE Trans Biomed Eng* (2012) 59(6):1649–57. doi:10.1109/TBME.2012.2191551
15. Liu J, Li X, Marciniak C, Rymer WZ, Zhou P. Extraction of neural control commands using myoelectric pattern recognition: a novel application in adults with cerebral palsy. *Int J Neural Syst* (2014) 24(7):1450022. doi:10.1142/S0129065714500221
16. Lu Z, Chen X, Zhang X, Tong K, Zhou P. Real-time control of an exoskeleton hand robot with myoelectric pattern recognition. *Int J Neural Syst* (2016) 27:1750009. doi:10.1142/S0129065717500095
17. Hu XL, Tong KY, Wei XJ, Rong W, Susanto EA, Ho SK. The effects of post-stroke upper-limb training with an electromyography (EMG)-driven hand robot. *J Electromyogr Kinesiol* (2013) 23:1065–74. doi:10.1016/j.jelekin.2013.07.007
18. Rong W, Tong KT, Hu XL, Ho SK. Effects of electromyography-driven robot-aided hand training with neuromuscular electrical stimulation on hand control performance after chronic stroke. *Disabil Rehabil Assist Technol* (2015) 10:149–59. doi:10.3109/17483107.2013.873491
19. Li Z, Wang B, Sun F, Yang C, Xie Q, Zhang W. sEMG-based joint force control for an upper-limb power-assist exoskeleton robot. *IEEE J Biomed Health Inform* (2014) 18:1043–50. doi:10.1109/JBHI.2013.2286455
20. Chowdhury RH, Reaz MB, Ali MA, Bakar AA, Chellappan K, Chang TG. Surface electromyography signal processing and classification techniques. *Sensors (Basel)* (2013) 13(9):12431–66. doi:10.3390/s130912431
21. Chang C, Lin C. LIBSVM: a library for support vector machines. *ACM Trans Intell Syst Technol* (2011) 27:1–27. doi:10.1145/1961189.1961199
22. Khokhar ZO, Xiao ZG, Menon C. Surface EMG pattern recognition for real-time control of a wrist exoskeleton. *Biomed Eng Online* (2010) 9:41. doi:10.1186/1475-925X-9-41
23. Mathiowetz V, Volland G, Kashman N, Weber K. Adult norms for the Box and Block test of manual dexterity. *Am J Occup Ther* (1985) 39(6):386–91. doi:10.5014/ajot.39.6.386
24. Gowland CA. Staging motor impairment after stroke. *Stroke* (1990) 21:19–21.
25. Cesqui B, Tropea P, Micera S, Krebs HI. EMG-based pattern recognition approach in post stroke robot-aided rehabilitation: a feasibility study. *J Neuroeng Rehabil* (2013) 10(1):75. doi:10.1186/1743-0003-10-75
26. Lee SW, Wilson KM, Lock BA, Kamper DG. Subject-specific myoelectric pattern classification of functional hand movements for stroke survivors. *IEEE Trans Neural Syst Rehabil Eng* (2011) 19(5):558–66. doi:10.1109/TNSRE.2010.2079334

Conflict of Interest Statement: The authors declare that the research was conducted in the absence of any commercial or financial relationships that could be construed as a potential conflict of interest.

frontiers in Neurology

ORIGINAL RESEARCH
published: 03 March 2017
doi: 10.3389/fneur.2017.00070

Alterations of Muscle Activation Pattern in Stroke Survivors during Obstacle Crossing

Chenming Ma[1,2†], Na Chen[1†], Yurong Mao[1], Dongfeng Huang[1], Rong Song[2] and Le Li[1*]*

[1] Department of Rehabilitation Medicine, Guangdong Engineering Technology Research Center for Rehabilitation Medicine and Clinical Translation, The First Affiliated Hospital, Sun Yat-sen University, Guangzhou, China,
[2] Key Laboratory of Sensing Technology and Biomedical Instrument of Guang Dong Province, School of Engineering, Sun Yat-sen University, Guangzhou, China

Objective: This study investigates changes in the neuromuscular activation pattern of the lower limb muscles in stroke survivors when crossing obstacles of three different heights.

Methods: Eight stroke survivors and eight age-, height-, and gender-matched healthy controls were recruited and instructed to cross over obstacles with heights of 10, 20, and 30% leg length. Surface electromyography (EMG) signals were recorded from the rectus femoris (RF), biceps femoris (BF), tibialis anterior (TA), and medial gastrocnemius (MG) of both limbs. Muscle activation signals were normalized to maximum voluntary contraction. Differences between groups and heights were compared using the root mean square of EMG, the cocontraction index of agonist and antagonist muscles, and power spectral analysis based on the mean power frequency (MPF). The correlations between the calculated variables and clinical scales such as Berg Balance Scale and Fugl-Meyer assessment (FMA) were also examined.

Results: During the leading limb swing phase, the activation levels of all four muscles were greater in the stroke group than the healthy controls ($p < 0.05$), and the TA showed increased activation level with increasing obstacle height in both groups ($p < 0.05$). Cocontraction between the TA and MG was higher in the stroke group during the swing phase of the leading limb and between the RF and BF during the stance phase ($p < 0.05$). Similarly, for the trailing limb, increased cocontractions between the two pairs of agonist and antagonist muscles were found during the stance phase in the stroke group ($p < 0.05$). During the crossing stride, the frequency analysis showed significantly smaller MPF values in all four lower limb muscles in the leading limb of stroke survivors compared with healthy controls ($p < 0.05$). Moreover, significant correlations were found between the FMA scores and the BF and TA activations in the leading limb during the swing phase ($p < 0.05$).

Conclusion: Greater activation levels of the lower limb muscles resulted in higher muscular demands for stroke survivors, which might lead to greater difficulty in maintaining balance. The increased cocontraction during obstacle crossing might be compensation

OPEN ACCESS

Edited by:
Xiaogang Hu,
University of North Carolina at Chapel Hill, USA

Reviewed by:
Cliff Klein,
Guangdong Provincial Work Injury Rehabilitation Center, China
Xu Zhang,
University of Science and Technology of China, China

***Correspondence:**
Rong Song
songrong@mail.sysu.edu.cn;
Le Li
lile5@mail.sysu.edu.cn

[†]These authors have contributed equally to this work.

Specialty section:
This article was submitted to Stroke, a section of the journal Frontiers in Neurology

Received: *21 December 2016*
Accepted: *16 February 2017*
Published: *03 March 2017*

Citation:
Ma C, Chen N, Mao Y, Huang D, Song R and Li L (2017) Alterations of Muscle Activation Pattern in Stroke Survivors during Obstacle Crossing. Front. Neurol. 8:70. doi: 10.3389/fneur.2017.00070

for the affected stability and enable safe crossing for stroke survivors. The reduced MPF in the affected limb of the stroke group might be due to impairments in motor units or other complex neuromuscular alterations.

Keywords: stroke, obstacle crossing, electromyography, gait analysis, activation pattern

INTRODUCTION

Stroke is a leading cause of disability associated with a loss of ability to generate force, which results in activity limitations and has a negative impact on motor function (1). Following a stroke, motor control impairments such as weakness, slow movements, spasticity, fatigue, and incoordination often occur in the lower limbs, which lead to gait abnormalities (2).

Daily walking commonly involves avoiding obstacles, such as doorsteps, stones, and stairs, and stepping across obstacles has been demonstrated to require greater muscle force, increased balance control, and enhanced muscle coordination than level walking (3, 4). One study showed that almost half of the tested stroke survivors failed to step across an obstacle, and their ability to maintain balance was compromised (5). The loss of balance in stroke survivors during obstacle crossing may lead to a high risk of falls and cause soft tissue injuries or fractures. Therefore, it is important to analyze the characteristics of the motion during obstacle crossing in stroke survivors. In spite of compromised balance, it is possible that stroke survivors may use compensatory strategies to avoid falls. It would therefore be helpful to understand the mechanism of preventing falls and ensuring safe crossing.

The balance and postural stability of stroke survivors have been quantified using kinematic and kinetic parameters, such as joint angles, joint moment, end-point distance, the distance between the center of mass and the center of pressure, and the ground reaction force (6–8). The balance was compromised in stroke survivors, and they might take a strategy involving greater pelvic posterior tilt and greater joint angles to ensure enough toe-obstacle clearance compared with healthy controls during obstacle crossing. However, little has been investigated about the neuromuscular changes during obstacle crossing. Electromyography (EMG) signals recorded from the surface of the muscles show the activity of motor neurons, which can reflect the relative level of muscle activation and provide valuable information about muscle function (9). Hahn et al. compared the EMG signals of the lower limb muscles between the elderly and the young (10). They found that elderly adults were able to negotiate different heights during walking and that the higher muscular demands could lead to a high risk of falls. The level of activity was reduced in the hemiparetic muscles in stroke survivors compared with the normal subjects, while the muscle's activity of the non-paretic side was increased compared with the normal subjects, which helped maintain standing balance in response to sideways pushes (11). However, the neuromuscular mechanism of maintaining balance when crossing obstacles of different heights remains to be investigated in stroke survivors. Stepping over obstacles of different heights requires varying the activation levels of the agonist and antagonist muscles. Muscle cocontraction is the simultaneous activity of agonist and antagonist muscles (12, 13). Kitatani et al. demonstrated increased muscle coactivation in the trailing limb of stroke survivors with increasing obstacle heights, which could increase postural stability and decrease the rate of trips (14). However, they did not compare the coactivation patterns between healthy subjects and stroke survivors during obstacle crossing to understand more about the coordination mechanism following stroke.

Electromyography signals can also be analyzed in the frequency domain based on the power spectrum to reflect the neuromuscular function. The mean power frequency (MPF) and median frequency (MF) mainly reflect changes in the conduction velocity of the active motor units which could be damaged after stroke (15). It has been speculated that alternations of the EMG spectrum are related to loss of muscle fibers, changes in the composition of motor unit type (peripheral), synchronization of multiple motor units, and disorder control of motor unit (central factors). Many studies have investigated the relationship between muscle activation level and MPF and MF values for both healthy people and stroke survivors. Decreased MPF values are usually found in the muscles of the paretic side compared with the non-paretic side (16, 17). The amplitude of the EMG signals increases with the level of muscle force, but studies on the relationship between the EMG spectrum and contraction force remain uncertain. Hu et al. found slightly decreased MF values in the paretic biceps brachii with increased muscle contraction in stroke survivors (18), while Kaplanis et al. reported increased MF in the EMG of the biceps brachii with increased isometric torque in healthy subjects (19). EMG spectral analysis could help better understand the cause of neuromuscular changes in the stroke survivors during obstacle crossing, which has not been investigated in previous studies.

This study investigates neuromuscular changes in stroke survivors to maintain balance when crossing obstacles of different heights in comparison with healthy controls. We examined the relative muscle activation levels, the cocontraction of the agonist and antagonist muscles of the knee joint and ankle joint, and the power spectrum of the muscles, also their relationship with the clinical scales. The results may provide knowledge of the mechanism of motor control during obstacle crossing and information for designing fall prevention programs for rehabilitation following stroke.

MATERIALS AND METHODS

Participants

Eight stroke survivors and eight healthy subjects matched by age, height, and gender were recruited in this study (**Table 1**). The inclusion criteria for the stroke survivors included (i) the occurrence

TABLE 1 | Basic characteristics of study subjects.

Characteristic	Stroke group ($n = 8$)	Control group ($n = 8$)	p-Value
Age, years (mean ± SD)	58.88 ± 10.61	60.62 ± 8.33	0.445
Height, cm	167.33 ± 7.35	165.51 ± 5.92	0.296
Mass, kg	63.57 ± 7.68	61.67 ± 8.94	0.392
Gender	Male = 6, female = 2	Male = 6, female = 2	
Brain lesion side	4 Right and 4 left		
Duration post-stroke, months (range)	12.51 ± 11.22 (3–29)		
Berg test scores (range)	40.38 ± 6.94 (27–47)	56 ± 0 (56)	<0.001[a]
FMA scores (range)	23.12 ± 3.48 (18–28)	34 ± 0 (34)	<0.001[a]

[a]*Significant effect using an independent t-test.*
FMA, Fugl-Meyer assessment scale of the motor function in paretic low-extremity (total score: 34).

of a first stroke with unilateral hemiparesis lesions confirmed by magnetic resonance imaging or computed tomography; (ii) an interval of at least 3 months post-stroke; (iii) the ability to step across an obstacle height of 30% leg length; and (iv) the ability to sign an informed consent form. This study was approved by the Ethics Committee of the First Affiliated Hospital of Sun Yat-sen University. All procedures were conducted according to the Declaration of Helsinki and all subjects provided written consent before the experiments. The motor function of stroke survivors was evaluated by an experienced physiotherapist based on the Berg Balance Scale (BBS) and Fugl-Meyer assessment (FMA) for lower extremities.

Apparatus

Circular silver–silver chloride (Ag–AgCl) electrodes with a diameter of 5 mm and inter-electrode distance of 20 mm were bilaterally attached to the bellies of the rectus femoris (RF), biceps femoris (BF), tibialis anterior (TA), and medial gastrocnemius (MG) of the lower limbs of the subjects. The muscle groups showed obvious changes when stepping over obstacles (20). Eight pre-amplified wireless transmission modules (DTS Noraxon, Scottsdale, AZ, USA) at a gain of 4,000 were linked with the electrodes to record EMG signals at a sample frequency of 1 kHz.

A total of 35 spherical 15-mm infrared-reflective markers were fastened to the subject's whole body according to the Vicon Plug-In Gait marker placement. A 6-camera 3D motion analysis system (Vicon Motion Systems, Oxford, UK) recorded the marker positions at a sample frequency of 100 Hz. Two force plates (464 mm × 508 mm × 83 mm, AMTI, Watertown, MA, USA) at a sample frequency of 1 kHz were placed in the middle of the path with the obstacle between them. All the EMG, kinematic, and kinetic signals were recorded simultaneously and processed by the Vicon Nexus operating system.

Procedure

Anthropometric characteristics were measured before the gait analysis (height, leg length, and bodyweight). Leg length was measured with scaled tape from the anterior superior iliac spine to the lateral malleolus and used to calculate the obstacle height of each individual. The electrodes and spherical markers were then attached to the corresponding locations on the subject. Before the electrode placement, the area around the muscles were shaved and cleaned with alcohol, and surgical tape was used as appropriate around the electrode and amplifier to obtain better EMG signals.

When the preparation was finished and the subjects had enough rest, the subjects were instructed to walk at a self-selected speed with bare feet along an 8-m walkway with a height-adjustable obstacle placed midway. The leading limb was defined as the first limb to cross the obstacle. The stroke subjects were instructed to use their affected leg as the leading limb of the obstacle crossing, and the healthy controls were instructed to use their dominant leg. The obstacle was set to three height conditions (10, 20, and 30% leg length). The three height conditions were performed in random order, and three trials of each height condition were recorded. Trials in which the subjects touched the obstacle were ignored and excluded from analysis. Prior to the trials, subjects visually and manually inspected the obstacle, and then practiced two to three trials according to the therapist's instructions. Subjects were reminded to perform the task within their limits of safety and stop if they felt at risk. A therapist accompanied the subject and walked to the side to provide protection and assistance if required.

After all the trials were finished, the subject was asked to rest for a few minutes and then instructed to lay supine with the tested limb placed at 90° hip and knee flexion, and the other limb resting in neutral to perform maximum voluntary contraction (MVC) tests (21). Another experienced therapist held a hand-held dynamometer (MicroFET3, Hoggan Inc., UT, USA; with the precision of 0.4 N and range from 13 to 1,330 N) stably as a resistance at the corresponding position of the measured joint (22), and the subject used tested muscle group to push maximally against the hand-held dynamometer for about 5 s. To measure the MVC of the TA and MG, the hand-held dynamometer was placed proximally to metatarsophalangeal joints on dorsal and plantar surface of foot. To measure the MVC of the RF and BF, the hand-held dynamometer was placed proximally to ankle on anterior and posterior surface of leg (23). The subject performed 2–3 submaximum voluntary contractions before the MVC test began to become familiar with the test procedure. MVC test included knee flexion and extension, dorsiflexion, and plantar flexion, and the MVC was recorded three times for each muscle. During the MVC procedure, subjects were verbally encouraged to ensure maximal recruitment.

Data Processing

For all MVC and gait trials, raw EMG signals were collected at 1 kHz, band-pass filtered through a fourth-order Butterworth filter with a bandwidth of 10–350 Hz, full-wave rectified, and low-pass filtered through a second-order Butterworth filter with a cut off frequency of 6 Hz. The root mean square was calculated during a particular phase of the gait. The filtered signals from the gait trials were then normalized to the MVC for each muscle to determine the relative activation levels. The calculation of the cocontraction index (CI) required two more steps with a linear envelope: (1) subtraction of the average resting EMG activity and

(2) normalization to the maximum value of EMG activation in each muscle during the MVC tests (24). The CI value is given by

$$\mathrm{CI}=\frac{1}{T}\int_{T} A_{ij}(t)\,dt$$

where $A_{ij}(t)$ is the overlapping activity of EMG linear envelopes after subtraction and normalization for the agonist and antagonist muscles i and j, T is the length of the signal period. The CI value varies from 0 to 1. Zero means there is no overlapping of the two EMG envelopes, and 1 means the two muscles are fully activated to 100% MVC during the trial.

The MPF was calculated using the band-pass filtered signals (through a fourth-order Butterworth filter with a bandwidth of 10–350 Hz) for each time window (the stance, swing, or entire gait cycle). The MPF value is given by

$$\mathrm{MPF}=\frac{\int_{0}^{\infty} fP(f)\,df}{\int_{0}^{\infty} P(f)\,df}$$

where $P(f)$ indicates the power intensity curve and f indicates the frequency. The kinematic data were filtered by a 20-Hz low-pass Butterworth filter. We considered the toe-off time to be when the toe marker was 2 mm off the ground and the heel-strike time as when the force platform received enough signals to make the measurement reliable (25). The gait cycle was then divided into a swing phase and stance phase for a single lower limb.

Statistical Analysis

Descriptive statistics (mean values and SD) were calculated for all dependent variables. The normalized EMG activation, CI, and MPF values were subjected to a repeated-measures two-way (group: stroke and control × obstacle height: 10, 20, and 30% of leg length) analysis of variance (ANOVA). The ANOVA results were adjusted using a Bonferroni *post hoc* test. If there was an interaction between the two effects, then one-way ANOVA was separately performed for the group effect and height effect. Pearson product–moment correlations were used to examine the relationships between the calculated variables and clinical scales. The level of significance was set at an alpha level of 0.05. All statistical analyses were done using SPSS 19 statistical software.

RESULTS

All subjects were able to complete the tasks with three different obstacle heights and the MVC tasks. No incidents of falling were observed, and we discarded the trials in which the subjects touched the obstacle or received help from the therapist. Subjects did not indicate discomfort during the tasks, nor did they show any feelings of fatigue.

The rectified and normalized EMG signals showed that the muscles were activated at a corresponding phase during the gait in a typical trial of a stroke subject and control subject (**Figure 1**). The muscle activation level and activation duration were greater among the stroke survivors than the healthy controls in the four muscles of the leading limb respectively. Also, there were some abnormal cocontractions among stroke survivors. For example, the TA and MG (a pair of agonist and antagonist muscles) had greater coactivation level in the stroke survivor (CI = 12.15%) compared to the healthy control (CI = 4.31%) during the swing phase of the obstacle crossing, as indicated by a circle in **Figure 1**.

The stroke survivors showed greater relative activation levels in the leading and trailing limbs compared to healthy controls (**Table 2**). For all height conditions during the swing phase, the TA activation of the stroke survivors reached an average of 41% of their maximum capacity, in contrast to 29% in the healthy controls. Interactions were found between the groups and heights in the TA muscle of the leading limb during both swing and stance phases. The activation of the TA of the leading limb significantly increased with the obstacle height during both swing and stance phases (one-way ANOVA with *post hoc* tests, $p < 0.05$). The TA activation was significantly greater in the stroke survivors compared to the healthy controls at the 20 and 30% heights during the swing phase and at 30% height during the stance phase (one-way ANOVA, $p < 0.05$). For the trailing limb, the activation of the BF and TA also significantly increased with the obstacle height during the swing phase ($p < 0.05$).

During the stance phase in the leading limb, the average CI for all height conditions of the RF and BF of the stroke survivors was 17.95 ± 7.90%, which was significantly greater than the average of 13.81 ± 4.89% ($p < 0.05$) for the healthy controls. Also, the average CI of the TA and MG was also significantly higher for the stroke survivors (10.53 ± 5.54%) than the healthy controls (7.60 ± 2.98%) during the swing phase ($p < 0.05$). Similarly, in the trailing limb, the average CI of the RF and BF (15.51 ± 5.18%) and the TA and MG (14.33 ± 8.52%) were significantly larger among stroke survivors than the healthy controls (RF and BF: 7.48 ± 2.39%, TA and MG: 7.85 ± 2.54%, $p < 0.05$), but only during the stance phase. The average CI showed no significant difference between stroke survivors and healthy controls in other conditions ($p > 0.05$).

Figure 2 shows the details of the CI at each obstacle height for both the leading and trailing limbs during the swing and stance phases. For the CI of the two muscle pairs of the leading limb, a between-group difference was found at the 30% height in the RF and BF and the 20 and 30% heights for the TA and MG ($p < 0.05$). There was a significant difference between the 10 and 30% and the 20 and 30% heights for the RF and BF during the stance phase, as well as between the 10 and 30% and the 20 and 30% heights for the TA and MG ($p < 0.05$). For the trailing limb, between-group differences in CI were found during the stance phase except for the TA and MG at the 10% height ($p < 0.05$). There was also a significant difference between the 10 and 30% heights and the 20 and 30% heights for the TA and MG during the swing phase ($p < 0.05$, **Figure 2**).

The stroke survivors had significantly smaller global MPF values of the leading limb during the entire crossing gait cycle (RF: 130.18 ± 13.33 Hz, BF: 134.67 ± 18.69 Hz, TA: 145.35 ± 12.52 Hz, MG: 130.18 ± 13.51 Hz) than the healthy controls (RF: 139.26 ± 10.21 Hz, BF: 148.40 ± 9.57 Hz, TA: 151.89 ± 6.96 Hz, MG: 140.18 ± 17.49 Hz), respectively ($p < 0.05$). However, no significant difference was found in the MPF values of the trailing limb during the entire crossing gait cycle between groups ($p > 0.05$). **Figure 3** shows a more detailed comparison of MPF

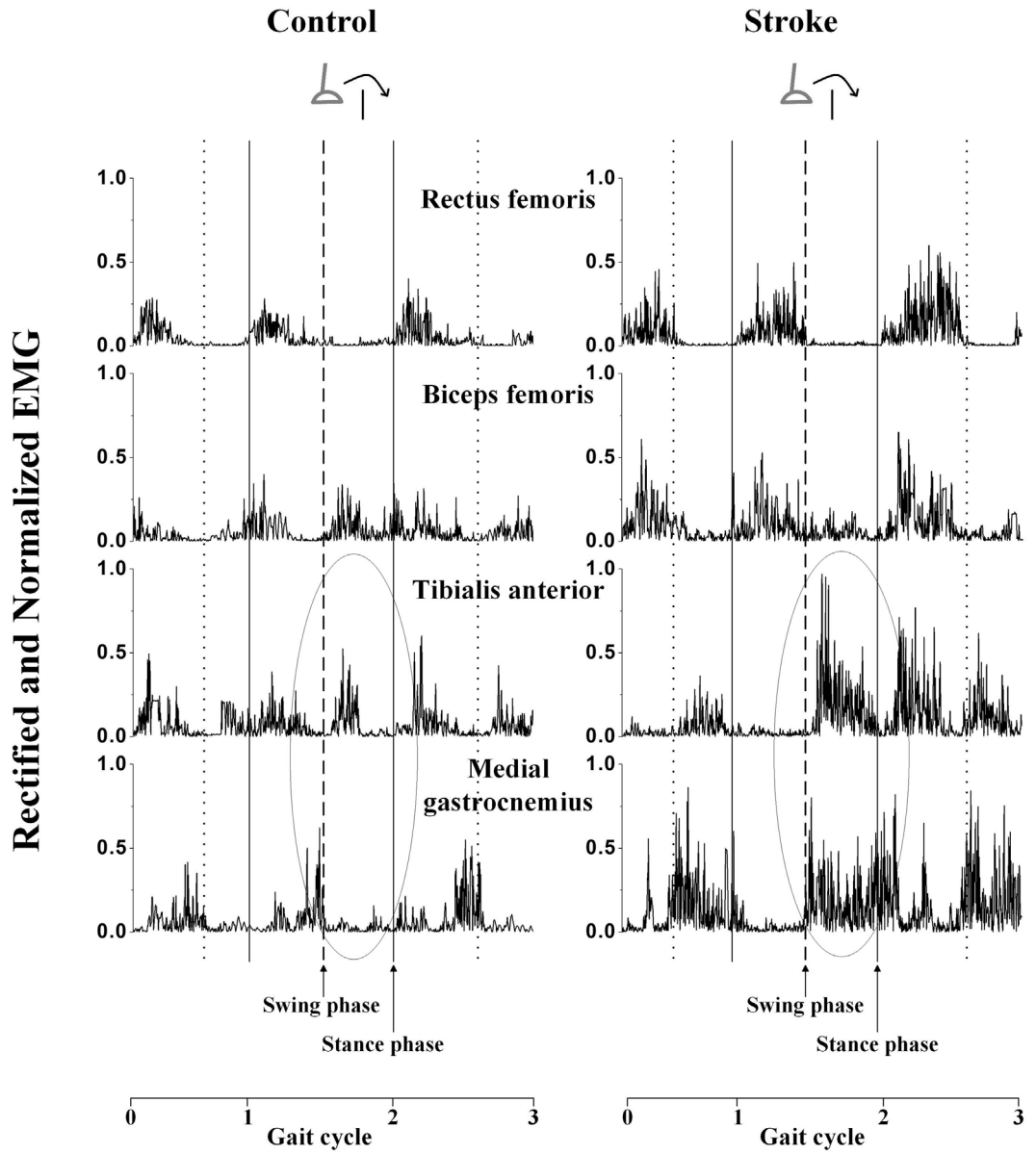

FIGURE 1 | The rectified and normalized electromyography (EMG) signals of the four muscles of the leading limb of a stroke survivor and a healthy control during 10% obstacle height. The solid vertical lines indicate the time of foot contact, the dot vertical lines indicate the time of toe-off, and the dashed vertical lines indicate the time of toe-off when crossing the obstacle. Gait cycle 0–1 indicates the cycle before the obstacle, gait cycle 1–2 indicates the crossing cycle, and gait cycle 2–3 indicates the cycle after the obstacle. The circle labeled zone is used to demonstrate the phenomenon of cocontraction.

values in the leading limb at each obstacle height during different phases. The MPF of the four muscles of the leading limb was significantly smaller in the stroke survivors than the healthy controls ($p < 0.05$). There was also a decreasing trend (no significant difference) for the MPF value of the muscles as the obstacle height increased in most conditions. However, the MPF value of the TA in the leading limb showed an increasing trend (no significant difference) with increasing obstacle height.

We also examined the correlation between the calculated variables including activation levels, CI, and MPF values and the clinical scales (FMA and BBS). We only found a significant positive correlation between the activation of BF and FMA ($r = 0.802$, $p = 0.017$) and a significant negative correlation between the activation of TA and FMA ($r = -0.817$, $p = 0.013$) during the swing phase at the 10% obstacle height (**Figure 4**). No significant difference was found in other situations or between other variables and clinical scales.

DISCUSSION

In this study, we recorded the EMG signals of the four main lower limb muscles of stroke survivors and healthy controls

TABLE 2 | Normalized electromyography activation percentages during swing and stance phases for rectus femoris (RF), biceps femoris (BF), tibialis anterior (TA), medial gastrocnemius (MG) of both leading and trailing limbs: mean (SD).

Limb/time	Muscle	Group	Obstacle height (% leg length)			
			10	20	30	Effect
Leading limb, swing phase	RF	Healthy	6.54 (4.06)	6.76 (4.02)	9.49 (8.02)	[a]
		Stroke	19.02 (18.44)	17.51 (16.30)	21.71 (19.68)	
	BF	Healthy	11.93 (5.96)	12.70 (4.51)	13.62 (5.48)	[a]
		Stroke	16.21 (9.67)	17.74 (7.92)	20.53 (11.25)	
	TA	Healthy	29.14□ (6.23)	30.14[d] (6.82)	32.66□,[d] (8.09)	[a,b,c]
		Stroke	34.03Δ,□ (10.49)	44.23Δ,○,[d] (13.89)	56.38□,○,[d] (16.78)	
	MG	Healthy	19.27 (4.99)	22.91 (7.13)	25.5 (10.47)	[a]
		Stroke	34.21 (11.00)	35.98 (17.42)	36.48 (22.5)	
Leading limb, stance phase	RF	Healthy	15.76 (10.52)	18.28 (11.23)	16.63 (12.10)	[a]
		Stroke	27.25 (14.68)	31.16 (16.53)	33.20 (14.24)	
	BF	Healthy	21.26 (7.06)	20.33 (5.55)	21.23 (3.89)	[a]
		Stroke	23.00 (11.49)	38.55 (12.71)	36.92 (12.47)	
	TA	Healthy	27.13 (12.80)	27.05 (16.72)	27.63[d] (12.09)	[c]
		Stroke	27.24 (7.43)	28.88○ (11.41)	42.08○,[d] (16.27)	
	MG	Healthy	27.21 (6.66)	29.77 (10.30)	34.05 (11.21)	[a,b]
		Stroke	27.75 (11.47)	44.05 (20.79)	42.11 (13.32)	
Trailing limb, stance phase	RF	Healthy	13.61 (8.39)	12.41 (6.91)	12.67 (8.45)	[a]
		Stroke	20.03 (12.42)	19.93 (11.8)	31.13 (26.62)	
	BF	Healthy	8.08 (4.49)	8.66 (3.40)	9.42 (4.03)	[a]
		Stroke	24.42 (11.26)	28.71 (17.22)	30.38 (14.39)	
	TA	Healthy	21.04 (10.31)	19.34 (7.02)	22.54 (12.12)	[a]
		Stroke	36.22 (15.25)	40.38 (11.29)	41.64 (18.34)	
	MG	Healthy	18.05 (5.94)	18.09 (7.58)	21.07 (8.71)	
		Stroke	28.16 (18.73)	27.94 (17.22)	28.84 (17.82)	
Trailing limb, swing phase	RF	Healthy	8.62 (2.53)	8.39 (2.78)	7.97 (2.77)	[a]
		Stroke	14.81 (5.92)	14.04 (4.87)	14.29 (5.44)	
	BF	Healthy	21.97 (8.98)	24.41 (9.57)	29.91 (13.69)	[b]
		Stroke	23.18 (11.51)	26.94 (15.68)	29.66 (14.08)	
	TA	Healthy	21.31 (6.74)	29.89 (7.17)	32.04 (5.54)	[a,b]
		Stroke	32.46 (12.23)	35.99 (12.05)	44.62 (16.74)	
	MG	Healthy	20.25 (8.44)	22.06 (6.78)	25.32 (9.61)	[a]
		Stroke	39.24 (7.73)	33.39 (10.31)	37.71 (12.61)	

[a]*Significant group effect.*
[b]*Significant height effect.*
[c]*Significant interaction effect.*
[d]*Significant group effect by post hoc test.*
Δ,□,○*Significant height effect by post hoc test. "Δ" means significant height effect between 10 and 20% leg length height. "□" means significant height effect between 10 and 30% leg length height. "○" means significant height effect between 20 and 30% leg length height.*

during obstacle crossing. Our study demonstrated the activation levels of the muscles and the coactivation of agonist and antagonist muscles were greater, and the MPF values of the muscles were lower in the stroke survivors than the healthy controls, which indicated abnormal patterns of the gait and obstacle crossing following stroke. In addition, the significant correlations between the muscle activation of BF, TA, and FMA provided a reliable method to analyze the muscles of stroke survivors.

Muscle Activation Level

When crossing the obstacles, the two groups encountered the same mechanical challenge (obstacle heights equal to the same percentage of leg length), but the stroke survivors showed greater overall muscle activation levels than the healthy controls in both the leading limb and the trailing limb (**Table 2**). Postural stability and the ability to maintain balance were impaired after stroke. Kirker et al. demonstrated that while a normal pattern of hemiparetic muscle activation was found in stepping, these muscles remained badly impaired in response to a perturbation and compensated by increased activity of the non-paretic muscles (11). Obstacle crossing challenges the stroke survivors to the limits of their capacity, and they are required to activate a greater level of their neuromuscular capacity to walk and safely step across obstacles. This may cause more serious postural instability (6). Similar results were also found in children with cerebral palsy. The RF and MG activation have been reported to increase in the swing phase of gait, which is considered an abnormal activation pattern that results from muscle weakness caused by cerebral palsy (26). According to Hahn et al., the relatively higher activation level might lead to muscular fatigue and place stroke survivors at higher risk of falls (10).

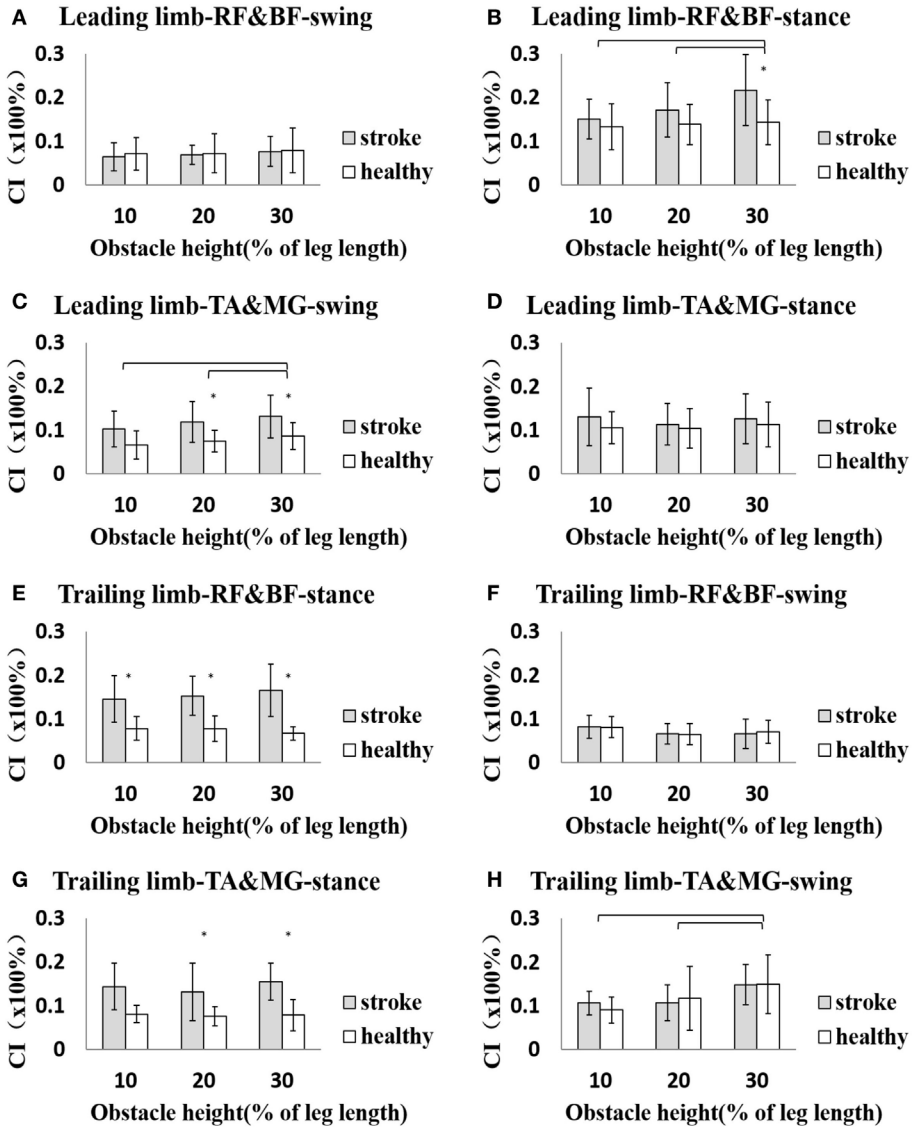

FIGURE 2 | The details of cocontraction index (CI) of each height for both leading and trailing limbs during swing and stance phases. **(A)** The CI of rectus femoris (RF) and biceps femoris (BF) of leading limb during swing phase. **(B)** The CI of RF and BF of leading limb during stance phase. **(C)** The CI of tibialis anterior (TA) and medial gastrocnemius (MG) of leading limb during swing phase. **(D)** The CI of TA and MG of leading limb during stance phase. **(E)** The CI of RF and BF of trailing limb during stance phase. **(F)** The CI of RF and BF of trailing limb during swing phase. **(G)** The CI of TA and MG of trailing limb during stance phase. **(H)** The CI of TA and MG of trailing limb during swing phase. The asterisk (*) indicates significant effect between groups. The bar (-) indicates significant effect between heights.

We found that the activation level of TA increased with increasing obstacle height in the swing phase of both leading and trailing limbs in stroke survivors. The TA muscle is the primary ankle dorsiflexor and is activated from the initial swing to let the ankle joint turn into a neutral position. However, Antonopoulos et al. found no significant height effect of the activation of the TA muscle for young adults during obstacle crossing (27). The increased activation level of TA in stroke may related to spasticity. Because of the excessive coactivation of the antagonist (MG), the increased activation level of TA was necessary to ensure a safe clearance during obstacle crossing.

Muscle Cocontraction

Although cocontraction is inefficient for joint movement, it might be important for providing joint stability, especially in tasks like obstacle crossing (14). When the leading limb steps over an obstacle, the cocontraction of the TA and MG is greater in the stroke survivors compared with the healthy controls and also increased with increasing obstacle height (**Figure 2C**). The dorsiflexor (TA) strength is weakened after stroke, and the cocontraction of the antagonist (MG) might reduce the dorsiflexion range but increase the stability during the swing phase to ensure safe crossing (28). Also, the cocontraction

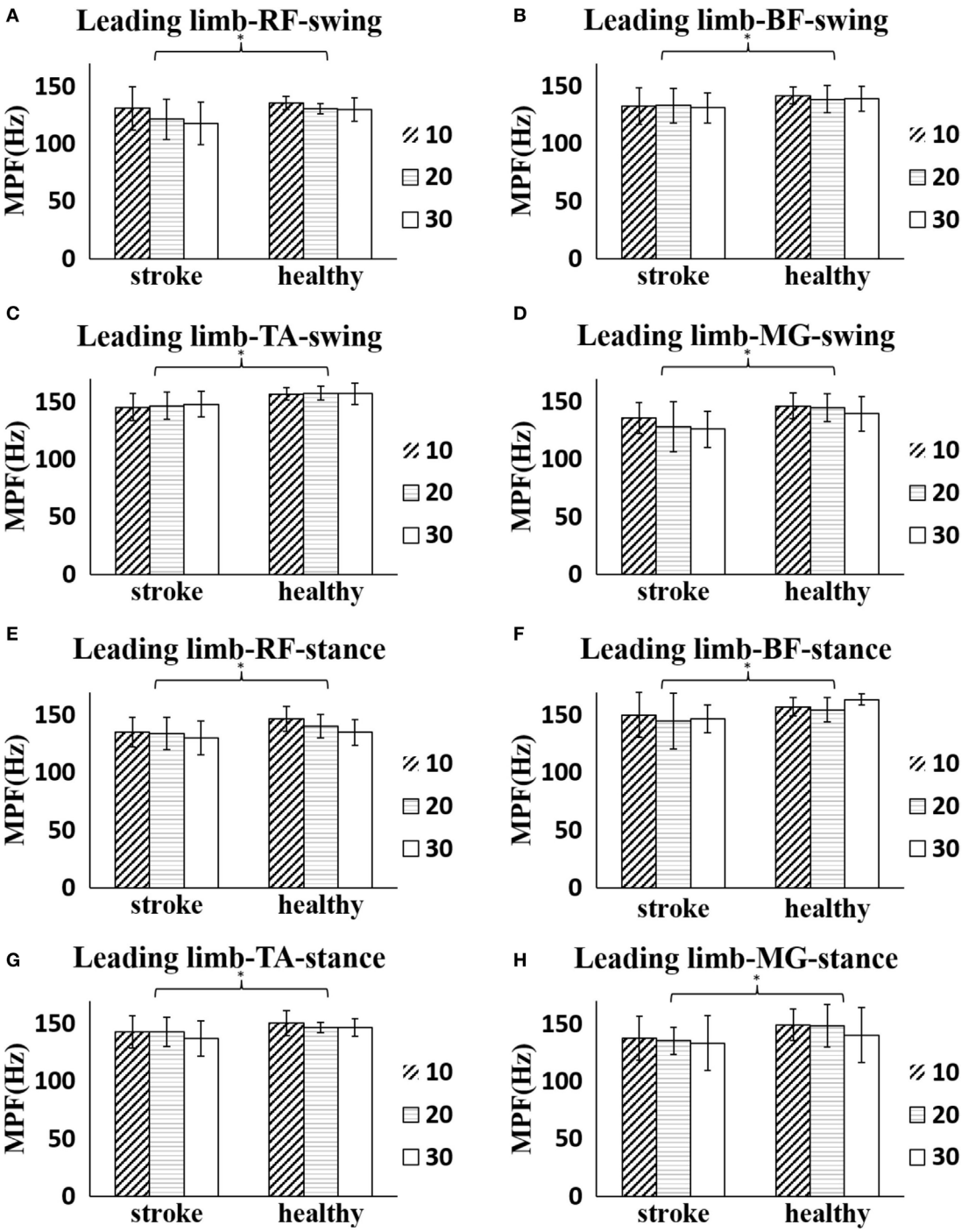

FIGURE 3 | The details of mean power frequency (MPF) value of four muscles of the leading limb of each height for both stroke survivors and healthy controls during obstacle crossing. **(A)** The MPF of rectus femoris (RF) during swing phase. **(B)** The MPF of biceps femoris (BF) during swing phase. **(C)** The MPF of tibialis anterior (TA) during swing phase. **(D)** The MPF of medial gastrocnemius (MG) during swing phase. **(E)** The MPF of RF during stance phase. **(F)** The MPF of BF during stance phase. **(G)** The MPF of TA during stance phase. **(H)** The MPF of MG during stance phase. The asterisk (*) indicates significant effect between groups.

of thigh muscles (BF and RF) is greater in the post-obstacle stance phase of the leading limb of the stroke survivors compared with the healthy controls, which is helpful to maintain balance by controlling the knee position during loading (29) (**Figure 2B**).

The greater cocontraction of the two pairs of lower limb muscles with increasing height also indicated muscle weakness on the paretic side of stroke survivors, who needed greater cocontraction to maintain balance when crossing obstacles of higher heights. Muscle cocontraction is also related to postural stability

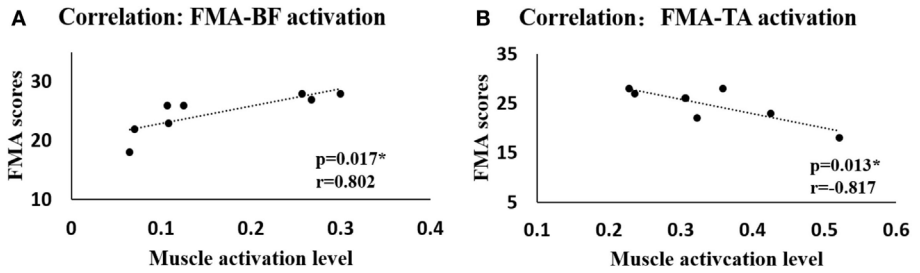

FIGURE 4 | The correlation between the Fugl-Meyer assessment (FMA) scores and the muscle activation levels when crossing the 10% leg length height obstacle. **(A)** Correlation between FMA scores and muscle activation level of biceps femoris (BF). **(B)** Correlation between FMA scores and muscle activation level of tibialis anterior (TA).

and dynamic strength in osteoarthritis (30), cerebral palsy (31), and Parkinson's disease (32). The increased muscle cocontraction is a metabolically costly process (33), but it may help preserve some mobility in those with weakness (34).

When the trailing limb steps over the obstacle, the cocontraction of the TA and MG also showed a height effect, but there was no significant difference between groups during the swing phase (**Figure 2H**). This indicates that the cocontraction might be an adaptation strategy for both stroke survivors and healthy controls to increase postural stability. Both of the two pairs of lower limb muscles showed greater cocontraction in stroke survivors during the trailing limb stance phase (**Figures 2E,G**), which could be attributed to the need for greater stability and motor adaptation to the weakness of the affected leading limb to support body weight (35, 36). With motor recovery, the muscle strength could be increased and enable a more efficient strategy with decreased muscle cocontraction. Hu et al. investigated the motor function recovery process in cases of chronic stroke and found that CI values decreased during the recovery process as motor function improved (24). Assessing muscle cocontraction helps us to understand the coordination mechanism in stroke survivors and the adaptation strategy they use to ensure safe crossing.

Analysis of Power Spectrum

The overall power spectrum analysis of all subjects indicated that stroke survivors had reduced MPF of the surface EMG in the leading limb compared with healthy controls (**Figure 3**). The reduction in MPF or MF on the paretic side has been report previously (16, 17). The decrease in MPF values of the paretic muscles could be due to the loss of muscle fibers and impairments in the motor unit following stroke. The firing rate has been demonstrated to be lower on the paretic side of stroke survivors compared both with the non-paretic side of stroke survivors and with the healthy controls during contraction (37, 38), which might also cause the reduced MPF values.

Alternations in the EMG spectrum have also been reported in children with cerebral palsy. Wakeling et al. and Gestel et al. found increased MPF value in such children compared with asymptomatic controls during gait and related it to the muscle dysfunction (26, 39). The assessment of the EMG spectrum could be used as an evaluation tool for functional muscle strength. No significant difference of MPF was found in the trailing limb between stroke survivors and healthy controls. This might be due to our instruction to the stroke survivors to use their affected side to cross the obstacle first and to use the unaffected limb as the trailing limb. This might have taken less effort to cross the obstacle and resulted in the lack of a significant between-group difference.

Obstacle crossing is a complex task, and the different heights place different demands on the subjects. Both groups showed a decreasing trend in MPF value with increasing obstacle height in the leading limb except for the MPF of the TA (**Figure 3**). Gabriel and Kamen also reported a significant decrease in the spectra with the force in the biceps brachii (40). With increased muscle activation level, there might be an increased degree of motor unit synchronization for the stroke survivors with the increasing obstacle height, which was likely to lead to reduction in the MPF values and fatigue (41, 42).

Correlation

One interesting finding in our study is that there were significant correlations between calculated muscle activation levels of BF and TA in the leading limb and FMA scores measured by the therapists during swing phase at 10% leg length height (**Figure 4**) in stroke survivors. No significant correlation was found between muscle activation levels and FMA scores during 20 or 30% leg length height obstacle crossing in stroke survivors. Performance of stroke survivors was more disturbed during challenging task such as for obstacle crossing of higher height (43), and they couldn't take good control of themselves which led to abnormal patterns and large variations within group when step across the obstacle. The activation level of the BF increased while that of the TA decreased with increasing obstacle height. Proximal control is more efficient than distal control in the lower limbs for stroke survivors to ensure safe obstacle crossing according to kinematic analysis (7). Our research showed through EMG analysis that stroke survivors with high FMA scores had greater BF activation, which controlled the hip joint and knee joint to elevate the toe. At the same time, the TA (which is related to ankle dorsiflexion) was abnormally activated to a larger degree in the face of fall risk among stroke survivors with lower FMA scores. Similar to Li et al., we found no significant correlation between the MPF values and clinical scales or between CI and clinical scales (16). Nevertheless, the significant correlation between the muscle activation levels and FMA scores means that it is reliable to use EMG signals to analyze the muscles of stroke survivors.

Limitations

This study has several limitations. The recruited stroke survivors in this study had good function, so the results might not be useful for moderate or severe stroke survivors. We instructed the stroke survivors to use their hemiparetic side to take the first step over the obstacle and to use the unaffected side as the supporting limb, which is safer for them. We neglected situations using the other limb as the leading limb, which might lead to a minor difference in the results. Moreover, significant differences between stroke survivors and healthy controls should also be interpreted with caution considering the relatively small sample size. We plan to recruit more stroke survivors of different functional levels and to instruct them to use both limbs as the leading limb in future work to obtain a more comprehensive understanding of the neuromuscular changes.

Conclusion

In this study, stroke survivors were recruited to step across obstacles of three different heights and compared with healthy controls to investigate motor control mechanisms that could not be reflected during level walking. Although the stroke survivors could safely step across the obstacles, they demonstrated abnormal motor control patterns, such as greater overall muscle activation level and larger cocontraction of the agonist and antagonist muscles. These might result in muscle fatigue, which would lead to a high risk of tripping and higher energy cost. The reduction in the MPF values of the paretic side of stroke survivors could be related to impairments of the motor unit or other complex neuromuscular alterations. The decreasing trend of the MPF values when crossing higher heights might due to greater motor unit synchronization, which could also lead to fatigue. The significant correlations between muscle activation levels and clinical scales provided a reliable method of analyzing the muscle functions of stroke survivors. These findings could help therapists to understand the neuromuscular changes following stroke and work out specific methods for rehabilitation of the lower limb muscles.

AUTHOR CONTRIBUTIONS

CM analyzed the data, interpreted the results, and wrote the draft of the manuscript. NC conducted the experiment and collected the data. YM and DH participated in the experiment and interpreted the results. RS participated in data analysis and interpretation and revised the manuscript. LL designed the study and performed all stages of the study including data collection, analysis, interpretation, and substantial revision of the manuscript. All the authors approved the final version of the manuscript.

FUNDING

This work was supported in part by the National Natural Science Foundation of China under Grant 31100669 and Guangdong Science and Technology Department (No. 2015B020214003, 2015A050502022, 2014B090901056, 2013b090500099) and partly supported by Natural Science Foundation of Guangdong Province, China (No. 2015A030313139) and Guangzhou Research Collaborative Innovation Projects (No. 2014Y2-00507).

REFERENCES

1. Mozaffarian D, Benjamin EJ, Go AS, Arnett DK, Blaha MJ, Cushman M, et al. Executive summary: heart disease and stroke statistics—2015 update: a report from the American Heart Association. *Circulation* (2015) 131(4):434–41. doi:10.1161/CIR.0000000000000157
2. Andrews AW, Bohannon RW. Distribution of muscle strength impairments following stroke. *Clin Rehabil* (2000) 14(1):79–87. doi:10.1191/026921500673950113
3. Chou LS, Draganich LF. Stepping over an obstacle increases the motions and moments of the joints of the trailing limb in young adults. *J Biomech* (1997) 30(30):331–7. doi:10.1016/S0021-9290(96)00161-3
4. Haefeli J, Vögeli S, Michel J, Dietz V. Preparation and performance of obstacle steps: interaction between brain and spinal neuronal activity. *Eur J Neurosci* (2011) 33(2):338–48. doi:10.1111/j.1460-9568.2010.07494.x
5. Said CM, Goldie PA, Patla AE, Sparrow WA, Martin KE. Obstacle crossing in subjects with stroke. *Arch Phys Med Rehabil* (1999) 80(80):1054–9. doi:10.1016/S0003-9993(99)90060-6
6. Said CM, Goldie PA, Patla AE, Culham E, Sparrow WA, Morris ME. Balance during obstacle crossing following stroke. *Gait Posture* (2008) 27(1):23–30. doi:10.1016/j.gaitpost.2006.12.009
7. Lu TW, Yen HC, Chen HL, Hsu WC, Chen SC, Hong SW, et al. Symmetrical kinematic changes in highly functioning older patients post-stroke during obstacle-crossing. *Gait Posture* (2010) 31(4):511–6. doi:10.1016/j.gaitpost.2010.02.012
8. Bowden MG, Balasubramanian CK, Neptune RR, Kautz SA. Anterior-posterior ground reaction forces as a measure of paretic leg contribution in hemiparetic walking. *Stroke* (2006) 37(37):872–6. doi:10.1161/01.STR.0000204063.75779.8d
9. Kleissen RF, Buurke JH, Harlaar J, Zilvold G. Electromyography in the biomechanical analysis of human movement and its clinical application. *Gait Posture* (1998) 8(2):143–58. doi:10.1016/S0966-6362(98)00025-3
10. Hahn ME, Lee HJ, Chou LS. Increased muscular challenge in older adults during obstructed gait. *Gait Posture* (2006) 22(4):356–61. doi:10.1016/j.gaitpost.2004.11.012
11. Kirker SG, Simpson DS, Jenner JR, Wing AM. Stepping before standing: hip muscle function in stepping and standing balance after stroke. *J Neurol Neurosurg Psychiatry* (2000) 68(4):458–64. doi:10.1136/jnnp.68.4.458
12. Milner TE. Adaptation to destabilizing dynamics by means of muscle cocontraction. *Exp Brain Res* (2002) 143(4):406–16. doi:10.1007/s00221-002-1001-4
13. Arias P, Espinosa N, Robles-García V, Cao R, Cudeiro J. Antagonist muscle co-activation during straight walking and its relation to kinematics: insight from young, elderly and Parkinson's disease. *Brain Res* (2012) 1455(1455):124–31. doi:10.1016/j.brainres.2012.03.033
14. Kitatani R, Ohata K, Watanabe A, Yu H, Yamakami N, Sakuma K, et al. Muscle coactivation during obstacle crossing corresponding to increasing obstacle height in patients with hemiplegia after stroke. *Gait Posture* (2014) 39(11):S104. doi:10.1016/j.gaitpost.2014.04.143
15. Arendt-Nielsen L, Mills KR. The relationship between mean power frequency of the EMG spectrum and muscle fibre conduction velocity. *Electroencephalogr Clin Neurophysiol* (1985) 60(2):130–4. doi:10.1016/0013-4694(85)90019-7
16. Li X, Shin H, Zhou P, Niu X, Liu J, Rymer WZ. Power spectral analysis of surface electromyography (EMG) at matched contraction levels of the first dorsal interosseous muscle in stroke survivors. *Clin Neurophysiol* (2014) 125(5):988–94. doi:10.1016/j.clinph.2013.09.044
17. Yao B, Zhang X, Li S, Li X, Chen X, Klein CS, et al. Analysis of linear electrode array EMG for assessment of hemiparetic biceps brachii muscles. *Front Hum Neurosci* (2015) 9:569. doi:10.3389/fnhum.2015.00569
18. Hu XL, Tong KY, Li L. The mechanomyography of persons after stroke during isometric voluntary contractions. *J Electromyogr Kinesiol* (2007) 17(4):473–83. doi:10.1016/j.jelekin.2006.01.015
19. Kaplanis PA, Pattichis CS, Hadjileontiadis LJ, Roberts VC. Surface EMG analysis on normal subjects based on isometric voluntary contraction.

J Electromyogr Kinesiol (2009) 19(1):157–71. doi:10.1016/j.jelekin.2007.03.010
20. Wang Y, Watanabe K, Asaka T, Wan F. Muscle synergies in preparation to a step made with and without obstacle. *Eur J Appl Physiol* (2014) 114(12):2561–9. doi:10.1007/s00421-014-2978-7
21. Dorsch S, Ada L, Canning CG, Al M. The strength of the ankle dorsiflexors has a significant contribution to walking speed in people who can walk independently after stroke: an observational study. *Arch Phys Med Rehabil* (2012) 93(6):1072–6. doi:10.1016/j.apmr.2012.01.005
22. Liu P, Wang Y, Hu H, Mao Y, Huang D, Li L. Change of muscle architecture following body weight support treadmill training for persons after subacute stroke: evidence from ultrasonography. *Biomed Res Int* (2014) 2014(350):270676. doi:10.1155/2014/270676
23. Bohannon RW. Test-retest reliability of hand-held dynamometry during a single session of strength assessment. *Phys Ther* (1986) 66(2):206–9.
24. Hu XL, Tong KY, Song R, Zheng XJ, Lui KH, Leung WW, et al. Quantitative evaluation of motor functional recovery process in chronic stroke patients during robot-assisted wrist training. *J Electromyogr Kinesiol* (2008) 19(4):639–50. doi:10.1016/j.jelekin.2008.04.002
25. Stanhope SJ, Kepple TM, McGuire DA, Roman NL. Kinematic-based technique for event time determination during gait. *Med Biol Eng Comput* (1990) 28(4):355–60. doi:10.1007/BF02446154
26. Wakeling J, Delaney R, Dudkiewicz I. A method for quantifying dynamic muscle dysfunction in children and young adults with cerebral palsy. *Gait Posture* (2007) 25(4):580–9. doi:10.1016/j.gaitpost.2006.06.009
27. Antonopoulos C, Patikas D, Koutlianos N, Papadopoulou SD, Chatzopoulos D, Hatzikotoulas K, et al. The effect of fatigue on electromyographic characteristics during obstacle crossing of different heights in young adults. *J Sports Sci Med* (2014) 13(4):724–30.
28. Mari S, Serrao M, Casali C, Conte C, Martino G, Ranavolo A, et al. Lower limb antagonist muscle co-activation and its relationship with gait parameters in cerebellar ataxia. *Cerebellum* (2013) 13(2):226–36. doi:10.1007/s12311-013-0533-4
29. Werner C, Von FS, Treig T, Konrad M, Hesse S. Treadmill training with partial body weight support and an electromechanical gait trainer for restoration of gait in subacute stroke patients: a randomized crossover study. *Stroke* (2002) 33(12):2895–901. doi:10.1161/01.STR.0000035734.61539.F6
30. Heiden TL, Lloyd DG, Ackland TR. Knee joint kinematics, kinetics and muscle co-contraction in knee osteoarthritis patient gait. *Clin Biomech* (2009) 24(10):833–41. doi:10.1016/j.clinbiomech.2009.08.005
31. Poon DM, Huichan CW. Hyperactive stretch reflexes, co-contraction, and muscle weakness in children with cerebral palsy. *Dev Med Child Neurol* (2009) 51(2):128–35. doi:10.1111/j.1469-8749.2008.03122.x
32. Ramsey VK, Miszko TA, Horvat M. Muscle activation and force production in Parkinson's patients during sit to stand transfers. *Clin Biomech* (2004) 19(4):377–84. doi:10.1016/j.clinbiomech.2003.08.004
33. Missenard O, Mottet D, Perrey S. The role of cocontraction in the impairment of movement accuracy with fatigue. *Exp Brain Res* (2008) 185(1):151–6. doi:10.1007/s00221-007-1264-x
34. Detrembleur C, Dierick F, Stoquart G, Chantraine F, Lejeune T. Energy cost, mechanical work, and efficiency of hemiparetic walking. *Gait Posture* (2003) 18(2):47–55. doi:10.1016/S0966-6362(02)00193-5
35. Raja B, Neptune RR, Kautz SA. Quantifiable patterns of limb loading and unloading during hemiparetic gait: relation to kinetic and kinematic parameters. *J Rehabil Res Dev* (2012) 49(49):1293–304. doi:10.1682/JRRD.2011.02.0018
36. Olney SJ, Richards C. Hemiparetic gait following stroke. Part I: characteristics. *Gait Posture* (1996) 4(2):136–48.
37. Hu XL, Tong KY, Hung LK. Firing properties of motor units during fatigue in subjects after stroke. *J Electromyogr Kinesiol* (2006) 16(5):469–76. doi:10.1016/j.jelekin.2005.09.005
38. McNulty PA, Lin G, Doust CG. Single motor unit firing rate after stroke is higher on the less-affected side during stable low-level voluntary contractions. *Front Hum Neurosci* (2014) 8(8):518. doi:10.3389/fnhum.2014.00518
39. Gestel LV, Wambacq H, Aertbeliën E, Meyns P, Bruyninckx H, Bar-On L, et al. To what extent is mean EMG frequency during gait a reflection of functional muscle strength in children with cerebral palsy? *Res Dev Disabil* (2012) 33(3):916–23. doi:10.1016/j.ridd.2011.12.010
40. Gabriel DA, Kamen G. Experimental and modeling investigation of spectral compression of biceps brachii SEMG activity with increasing force levels. *J Electromyogr Kinesiol* (2009) 19(3):437–48. doi:10.1016/j.jelekin.2007.10.009
41. Yao W, Fuglevand RJ, Enoka RM. Motor-unit synchronization increases EMG amplitude and decreases force steadiness of simulated contractions. *J Neurophysiol* (2000) 83(1):441–52.
42. Naik GR, Kumar DK, Yadav V, Wheeler K, Arjunan S, editors. Testing of motor unit synchronization model for localized muscle fatigue. *31st Annual International Conference of the IEEE Engineering in Medicine and Biology Society*. Minneapolis (2009).
43. Vitório R, Pieruccinifaria F, Stella F, Gobbi S, Gobbi LT. Effects of obstacle height on obstacle crossing in mild Parkinson's disease. *Gait Posture* (2010) 31(1):143–6. doi:10.1016/j.gaitpost.2009.09.011

Conflict of Interest Statement: The authors declare that the research was conducted in the absence of any commercial or financial relationships that could be construed as a potential conflict of interest.

frontiers in Neurology

TECHNOLOGY REPORT
published: 21 November 2016
doi: 10.3389/fneur.2016.00197

Wavelet Packet Feature Assessment for High-Density Myoelectric Pattern Recognition and Channel Selection toward Stroke Rehabilitation

Dongqing Wang[1], Xu Zhang[1], Xiaoping Gao[2], Xiang Chen[1] and Ping Zhou[3,4,5]*

[1]Department of Electronic Science and Technology, University of Science and Technology of China, Hefei, China, [2]Department of Rehabilitation Medicine, First Affiliated Hospital of Anhui Medical University, Hefei, China, [3]Department of Physical Medicine and Rehabilitation, University of Texas Health Science Center at Houston, Houston, TX, USA, [4]TIRR Memorial Hermann Research Center, Houston, TX, USA, [5]Guangdong Work Injury Rehabilitation Center, Guangzhou, China

This study presents wavelet packet feature assessment of neural control information in paretic upper limb muscles of stroke survivors for myoelectric pattern recognition, taking advantage of high-resolution time–frequency representations of surface electromyogram (EMG) signals. On this basis, a novel channel selection method was developed by combining the Fisher's class separability index and the sequential feedforward selection analyses, in order to determine a small number of appropriate EMG channels from original high-density EMG electrode array. The advantages of the wavelet packet features and the channel selection analyses were further illustrated by comparing with previous conventional approaches, in terms of classification performance when identifying 20 functional arm/hand movements implemented by 12 stroke survivors. This study offers a practical approach including paretic EMG feature extraction and channel selection that enables active myoelectric control of multiple degrees of freedom with paretic muscles. All these efforts will facilitate upper limb dexterity restoration and improved stroke rehabilitation.

Keywords: myoelectric control, pattern recognition, wavelet packet transform, channel selection, stroke rehabilitation

OPEN ACCESS

Edited by:
Xiaogang Hu,
University of North Carolina at Chapel Hill, USA

Reviewed by:
Muhib Khan,
Michigan State University, USA
Francesco Negro,
University of Göttingen, Germany

****Correspondence:***
Xu Zhang
xuzhang90@ustc.edu.cn

Specialty section:
This article was submitted to Stroke, a section of the journal Frontiers in Neurology

Received: *08 August 2016*
Accepted: *25 October 2016*
Published: *21 November 2016*

Citation:
Wang D, Zhang X, Gao X, Chen X and Zhou P (2016) Wavelet Packet Feature Assessment for High-Density Myoelectric Pattern Recognition and Channel Selection toward Stroke Rehabilitation. Front. Neurol. 7:197. doi: 10.3389/fneur.2016.00197

INTRODUCTION

Restoration of upper limb function is an important but challenging task in stroke rehabilitation due to arm/hand dexterity (which is critical for daily activities). A number of upper limb robotic devices have been designed to assist rehabilitation training for promoting upper limb motor recovery (1, 2) among which some recently emerging ones involve different human–machine interfaces enabling active response to user's intention. Compared with passive training, such an active control approach has proven to be more effective for motor function improvement (3, 4).

Electromyogram (EMG) is one of the most commonly used control signals for artificial limbs, rehabilitation robots, and other assistive devices (5–7). Most development in myoelectric control is primarily based on a simple control strategy that the EMG of a single muscle is mapped to a single degree of freedom (DOF). Considering the complexity of upper limb functional movements performed by multiple muscles, it is unfeasible to control multiple DOFs through such a straightforward mapping (8). Because of this, myoelectric pattern recognition has been developed for controlling of

multiple DOFs (8–10). So far, the myoelectric pattern recognition control strategy has been primarily focused on improving dexterity of prosthesis control for amputee users, whereas its application for neurological injury patients has not been fully explored (5). Only very recently, myoelectric pattern recognition was first reported to detect movement intention of affected limb after stroke (8). A more comprehensive assessment of neural control information from paretic muscles of stroke subjects was further performed using high-density surface EMG recording and pattern recognition techniques (4).

While high-density surface EMG pattern recognition has revealed substantial neural control information that can be extracted from neurologically impaired muscles, there are a number of issues to be considered for developing a myoelectric control system. These include assessment of different EMG features, selection of a practical number of appropriate EMG channels (myoelectric control sites), and user-specific design according to individual need and performance. A variety of features describing surface EMG signals in different (time, frequency, time–frequency, etc.) domains have been used for myoelectric pattern recognition analysis, but primarily aimed at prosthetic control (9–12). So far for patients with neurological injuries, the myoelectric pattern recognition analysis has been limited to using conventional time-domain (TD) feature set [four time domain statistics proposed by Hudgins et al. (9) and auto-regressive (AR) + root mean square (RMS) feature set (a combination of AR coefficients and RMS amplitude) (5)]. Assessment of EMG features for neurological injury patients might be promising to improve myoelectric pattern recognition performance, particularly given the neurologic injury induced muscle impairments (such as weakness, spasticity, and abnormal coactivation) (13).

Time–frequency analysis has been developed as a useful tool for processing non-stationary biosignals (such as EMG). Time–frequency representations of surface EMG such as using wavelet packet transform (WPT) can also be applied in myoelectric pattern recognition, as demonstrated in amputees or able-bodied subjects (10, 14, 15). In the current study, the utility of applying WPT to stroke subjects was examined. The WPT is able to generate a redundant set of subspaces arranged in a binary tree structure with any designed depth/resolution, where the input signal can be accordingly decomposed. Performing wavelet packet analysis of surface EMG recordings from paretic muscles has several advantages. For example, its high resolution in both time and frequency domains makes it feasible to produce a sufficient number of features, from which those highly associated with different movement intentions of the affected limb (i.e., discriminable features) can be easily selected *via* a best basis selection approach to maximize the pattern separability (15, 16). Moreover, such a feature selection approach can be expanded for selecting surface EMG channels (myoelectric control sites) from the high-density surface EMG recordings (by adopting the same discriminant measure). The advantages of the WPT analysis for myoelectric pattern recognition and channel selection were demonstrated for stroke patients. These findings provide useful information for developing a pattern recognition-based myoelectric control system for stroke rehabilitation.

METHODS

Dataset Description

The dataset used in this study was selected from a database previously reported in Zhang and Zhou (4), which was approved by the Institute Review Board of Northwestern University (Chicago, IL, USA). This database included high-density surface EMG recordings from 12 chronic stroke subjects with hemiparesis during their performance of different functional movements involving the affected upper limb, notably the affected hand. The detailed demographic information and clinical assessment for the stroke subjects can be found in Ref. (4). All subjects gave their informed consent before the experiment. **Table 1** displays demographics and clinical information of all stroke subjects in detail.

During the experiment, each subject was instructed to perform 20 functional movements using the affected upper limb, namely, wrist flexion/extension, wrist supination/pronation, elbow flexion/extension, hand open/close, thumb flexion/extension, index finger flexion/extension, finger 3–5 flexion/extension, fine pinch, lateral pinch, tip pinch, gun posture, and ulnar wrist down/up. A video demonstration of each movement was used as a guide for subjects to follow and perform the movement. The experiment protocol comprised of 20 trials, each trial consisting of 5 repetitions of the same movement. For each repetition, the subject was asked to hold the muscle contraction for roughly 3 s and then relaxed for a rest period of 5–20 s.

The high-density surface EMG signals in the original database were recorded *via* 89 monopolar surface electrodes placed on the affected upper arm, forearm, and hand muscles. A Refa EMG recording system (TMS International BV, Netherlands) with a band-pass filter between 20 and 500 Hz was used for multi-channel EMG recording at a sampling rate of 2 kHz per channel. Due to improved myoelectric classification performance and more clinical relevance compared with monopolar configuration, 46-channel bipolar surface EMG data were produced from the original 89-channel EMG recordings. The detailed information about the electrode formation and single spatial differential filter is shown in **Figure 1**. Besides, 10 bipolar channels, namely, the channel 9, 13, 17, 19–21, 23, and 41–43 were selected from

TABLE 1 | Subject demographics and clinical information.

Subject #	Age	Sex	Duration	Paretic	FMUE	C–M hand
1	59	F	13	L	28	2
2	56	M	23	L	15	2
3	67	M	8	L	20	4
4	63	F	7	R	19	2
5	45	M	6	L	58	5
6	58	F	2	R	23	2
7	64	M	8	L	38	2
8	61	M	7	R	56	4
9	65	M	15	L	20	2
10	46	M	13	L	52	3
11	81	M	17	L	28	2
12	71	F	22	R	22	3

Duration, years post stroke; paretic, the side of hemiparesis; FMUE, the Fugl-Meyer assessment scale of the paretic upper-extremity (total score: 66); C–M hand, the hand impairment part of the Chedoke–McMaster stroke assessment scale (from 1 to 7).

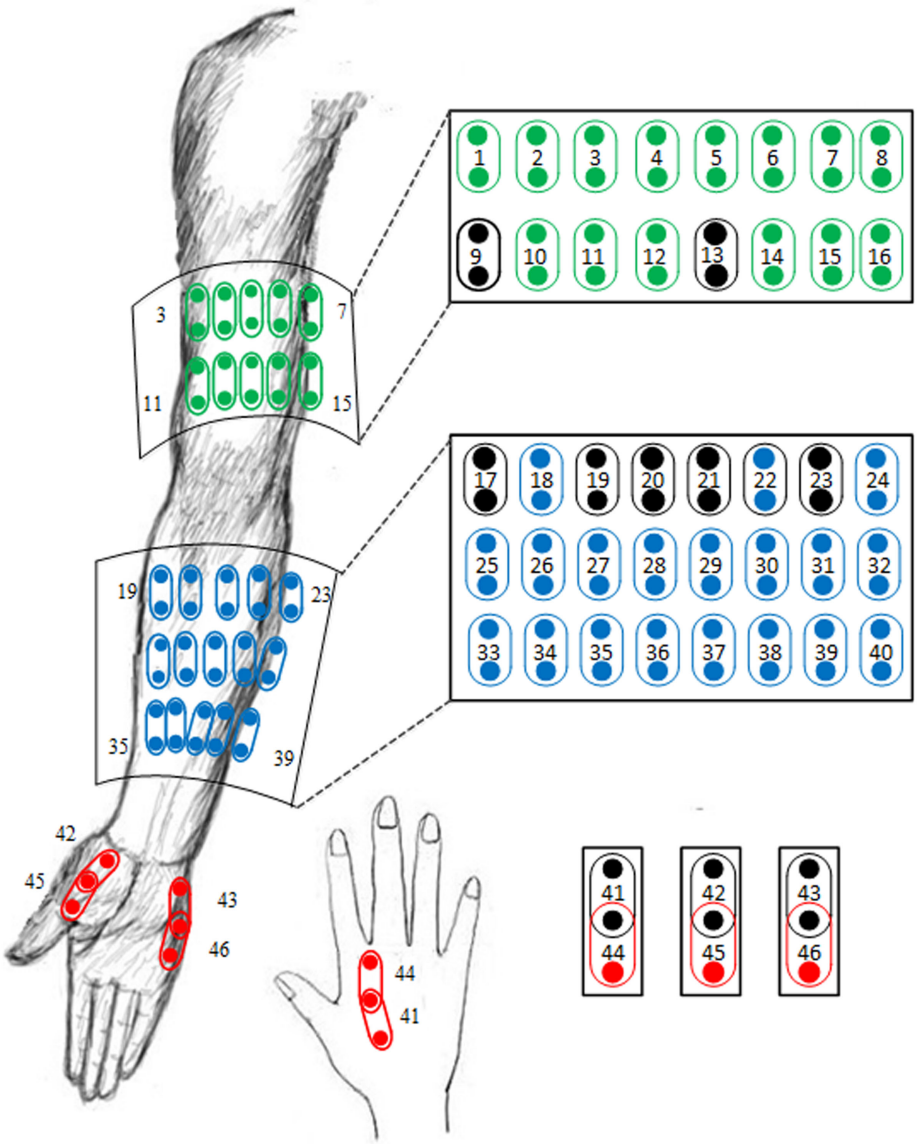

FIGURE 1 | Illustration of the electrode placement for 46-channel bipolar sEMG signal recordings derived from 89-channel monopolar sEMG database. The 10 electrode channels marked in a black/darker color are included in an empirically defined channel set.

the 46 channels to form a channel set. The selection of such a channel set was in accordance with electrode sites frequently used in many previously reported myoelectric control systems (8). These channels were regarded to target at primary muscles with high relevance to functional movements of the upper limb, as marked in a black/darker color in **Figure 1**. In this study, such an empirically defined channel set was compared with all 46 high-density channels or a number of optimally selected channels in terms of myoelectric control performance.

For the recorded signals, the onset and offset of a voluntary EMG activity segment corresponding to each repetition of muscle contraction were determined first as described in Ref. (4). For each repetition of muscle contraction, the EMG activity segment in a form of multiple channels was further segmented into a series of overlapping analysis windows with a window length of 256 ms and an overlapping rate of 75% for two consecutive windows. Consequently, the following feature extraction and classification procedures were performed on these analysis windows.

Feature Extraction Using WPT

The WPT was a generalized version of classical wavelet decomposition method that offers a multi-resolution and time–frequency analysis of non-stationary, such as biomedical signals (17, 18). Define the original signal space as $\Omega_{0,0}$. The WPT is able to split the signal into an approximation (in subspace $\Omega_{1,0}$) and a detail (in subspace $\Omega_{1,1}$). Each approximation or detail obtained from the top-level, supposed in the subspace $\Omega_{j,k}$, can be further split into a new approximation and a new detail, located in two orthogonal subspaces $\Omega_{j+1,2k}$ and $\Omega_{j+1,2k+1}$, respectively. This process can be iteratively performed to a targeted depth J. Here, j is a scale index

ranging from 0 to J, and k represents subband index within the scale, ranging from 0 to $2^j - 1$. Consequently, the WPT generates a binary tree structure of subspaces spanned by a set of bases, to which a signal can be mapped for multi-resolution analysis. Such a characteristic allows WPT to be successfully applied to feature extraction in the fields of pattern recognition (14, 15, 18).

In this study, the WPT with the five-order symmlet wavelet was first applied to each channel of an analysis window for feature extraction. The five-order symmlet wavelet was selected from many mother wavelet functions frequently used in previous reports (10, 14, 15) and was further determined by some pretests in terms of classification performance. The WPT depth is also an important factor for WPT analysis. It is acknowledged that a small depth cannot yield sufficient resolution for extracting effective features, whereas a large depth leads to much more computational complexity. By considering this trade-off, the WPT depth of 3 or 4 has been recommended by previous studies (15, 19). The WPT depth of 4 was chosen in this study after some pretests, thus producing 30 subspaces in total. After the WPT, the energy values of all 30 subspaces were calculated as potential features (refer to feature selection approach in the following section), where the energy of each subspace was defined as a logarithmic value of the summation of the squares of all wavelet packet coefficients in the subspace. The logarithmic transform was chosen for showing better performance of classification after some tests.

Feature Selection Using Best Basis Selection

The WPT binary tree yielded a redundant set of subspaces due to the subspace overlap in frequency axis. Afterward, the features extracted from all subspaces were regarded to carry redundant information. A great number of redundant features were likely to impose high computational cost and compromise classification performance. For application of the WPT analysis to feature extraction or pattern recognition, a best basis is usually chosen to maximize the class separability in terms of a proper discriminant measure. To achieve this goal, a feature selection procedure relying on a best basis selection algorithm is necessary. In this study, the algorithm was designed to choose the best set of subspaces from the WPT binary tree, since each subspace produced a potential feature. To determine the best subspace, Fisher's class separability index (FCSI) described in Ref. (20) was employed as the discriminant measure, which is introduced below.

Suppose that $\left\{x_{i,(j,k)}^{(c)}\right\}_{i=1}^{N_c}$ represents a set of energy features extracted from the subspace $\Omega_{j,k}$ of the training signals belonging to class c ($1 \le c \le C$, here $C = 20$), where N_c is the number of samples (i.e., analysis windows) in class c.

For each subspace, the mean and variance of these features grouped by class can be calculated as

$$\overline{m}_{j,k}^{(c)} = \frac{1}{N_c}\sum_{i=1}^{N_c}\left\{x_{i,(j,k)}^{(c)}\right\}_{i=1}^{N_c}, \tag{1}$$

$$\underset{1\le i\le N_c}{\mathrm{var}}\left(x_{i,(j,k)}^{(c)}\right) = \frac{1}{N_c}\sum_{i=1}^{N_c}\left(x_{i,(j,k)}^{(c)} - \overline{m}_{j,k}^{(c)}\right)^2. \tag{2}$$

Here, the operator $\mathrm{var}_i(\cdot)$ is defined to calculate the variance of a set of constant variables indexed by i. Thus, the FCSI, for the subspace $\Omega_{j,k}$, is finally defined as

$$\mathrm{FCSI} = \sum_{p=1}^{K-1}\sum_{q=p+1}^{K}\frac{\left|\overline{m}_{j,k}^{(p)} - \overline{m}_{j,k}^{(q)}\right|^2}{\underset{1\le i\le N_p}{\mathrm{var}}\left(x_{i,(j,k)}^{(p)}\right) + \underset{1\le i\le N_q}{\mathrm{var}}\left(x_{i,(j,k)}^{(q)}\right)}. \tag{3}$$

where p and q represent the indices of two different classes. Generally, a higher value of FCSI indicates higher degree of class separability. The best basis selection algorithm using FCSI is able to rank the features and make it practical to choose a subset of these regarded as being most discriminant.

In this study, feature selection approach was independently performed on each channel. Many previous studies regarding wavelet packet features also took the same procedure (10, 21, 22). For each channel, the number of selected subspaces/features needed to be carefully determined. It should be acknowledged that inadequate number of features may not guarantee the classification performance, whereas too many features lead to much computational cost. Considering such a trade-off, we set the number of subspaces/features per channel to 12 after performing sensitivity analysis (in terms of classification accuracy) by varying the feature number per channel from 1 to 25. Finally, the features from all channels were further concatenated as a high-dimensional feature vector for each analysis window.

Feature Dimensionality Reduction and Classification

Even with the above feature selection procedure, the high-density surface EMG recordings still resulted in very high-dimensional feature vectors (i.e., 552-dimensional feature vectors with 12 best bases for each of 46 channels). In this case, feature dimensionality reduction is required to ensure the generalization capability of a classifier (23). In this study, uncorrelated linear discriminant analysis (ULDA) was used to reduce the feature dimension, which minimizes within-class distance and maximize between-class distance by an optimal transformation (24).

After the feature dimensionality reduction, linear discriminant classifier (LDC) was employed in this study. The LDC is able to model the within-class density of each class as a multi-variant Gaussian distribution and gives decisions of unknown samples by using the maximum a posteriori probability (MAP) rule and Bayesian principles (9, 25). The LDC was used due to its ease of implementation and efficient classification performance (4, 8).

In this study, the pattern classification was conducted in a user-specific manner, where both training dataset and testing dataset were derived from the same stroke subject. A fivefold cross-validation was conducted to evaluate the classification performance. This indicated that the EMG data from any four repetitions of muscle contraction were selected and assigned as training dataset, while the EMG data from the remaining repetition were used to form the testing dataset. The classification performance for each subject was evaluated as classification accuracy, which was calculated as the percentage of correctly classified windows over all the testing windows including all movement patterns over testing dataset. These window numbers were summed up over all fivefold tests for each subject.

For the performance comparison, the routine TD feature set including four statistics of the surface EMG signals, namely, mean absolute value (MAV), the number of zero crossing (ZC), the slope sign change (SSC), and the waveform length (WL), was also employed during the tests. The TD feature set was used in a similar way as previous studies that all TD features from all the considered channels were concatenated to form a feature vector for each analysis window. The same feature dimension reduction approach using ULDA was applied as well before LDC classifier implementation.

Channel Selection

The use of FCSI for quantifying the discriminating power of features was further extended to channel selection from high-density surface EMG recordings. After the feature extraction and selection methods introduced above, a subset of features was determined for each channel and used to form a vector representing the most discriminable information from that channel. In order to perform channel selection, it was necessary to assess the discriminating power of feature vectors rather than scalars. Thus, the FCSI was accordingly modified as follows.

Here, let $\left\{\mathbf{x}_{i,l}^{(c)}\right\}_{i=1}^{N_c}$ be a set of feature vectors extracted from the l-th channel of the training data belonging to class c. The mean of these feature vectors, originally defined in Eq. 1, needs to be modified, and their variance, namely $\underset{1\le i\le N_c}{\text{var}}\left(\mathbf{x}_{i,l}^{(c)}\right)$, is further defined to be the summation of all variances calculated along any single dimension of the vector, as depicted in Eqs 4 and 5.

$$\overline{\mathbf{m}}_l^{(c)} = \frac{1}{N_c}\sum\nolimits_{i=1}^{N_c}\mathbf{x}_{i,l}^{(c)}, \tag{4}$$

$$\underset{1\le i\le N_c}{\text{var}}\left(\mathbf{x}_{i,l}^{(c)}\right) = \underset{1\le i\le N_c}{\text{var}}\left(x1_{i,l}^{(c)}\right) + \underset{1\le i\le N_c}{\text{var}}\left(x2_{i,l}^{(c)}\right) + \cdots + \underset{1\le i\le N_c}{\text{var}}\left(xd_{i,l}^{(c)}\right), \tag{5}$$

where $\mathbf{x} = [x1, x2, \ldots, xd]^T$ denotes a d-dimensional vector. Thus, the FCSI, for the l-th channel, can be finally computed *via*

$$\text{FCSI} = \sum\nolimits_{p=1}^{K-1}\sum\nolimits_{q=p+1}^{K}\frac{\left|\overline{\mathbf{m}}_l^{(p)} - \overline{\mathbf{m}}_l^{(q)}\right|^2}{\underset{1\le i\le N_p}{\text{var}}\left(\mathbf{x}_{i,l}^{(p)}\right) + \underset{1\le i\le N_q}{\text{var}}\left(\mathbf{x}_{i,l}^{(q)}\right)}, \tag{6}$$

where p and q represent the indices of two different classes again. Similarly, a higher FCSI value indicates a higher degree of class separability for a certain channel. Following the strategy of feature selection using FCSI, a subset of optimal channels can be selected by ranking the channels using FCSI. This channel selection approach was termed as FCSI method in this study.

Channel selection has also been conducted in previous studies (25, 26) to assess the myoelectric pattern recognition performance using a reduced number of EMG channels selected from high-density signal recordings. A straightforward algorithm, termed as sequential feedforward selection (SFS), was often used, which iteratively adds the most informative channels in terms of classification accuracy. In the first iteration of this algorithm, each of all candidate channels is independently used and the channel producing the highest classification accuracy was selected to be the first optimal channel. During the next iteration, the previously selected channels were combined with each of the other channels to form a new subset sequentially, and the subset producing the highest classification accuracy was determined. This procedure can be iteratively performed when meeting a desired number of selected EMG channels. Note that the SFS directly uses the classification accuracy as the criterion, which conventionally requires classifier training and testing procedures in each iteration. Thus, the channels selected by the SFS algorithm are more likely to be overfitted to the testing data with limited generalization ability. In order to avoid such overestimated performance in some degree, the SFS algorithm used in this study was performed only on the training dataset. This required the original training dataset consisting of four repetitions of muscle contraction to be further divided into two parts, one consisting of three repetitions for SFS training and the other consisting of the remaining repetition for SFS testing. To evaluate the classification performance with the channels selected by the SFS algorithm, a classifier was implemented with all the four repetitions (used for SFS) as training dataset and the remaining fifth repetition (which was not used for SFS) as testing dataset.

The channel selection using FCSI is able to independently choose a subset of best channels in any size m. It should be acknowledged that the m best channels may not be the best m channels. By contrast, the standard SFS algorithm offers a practical way of selecting a subset of appropriate channels by taking the effect of channel combination into account, but it conventionally suffers from the overfitting problem. By taking advantage of both methods to overcome its own drawbacks, a novel channel selection method named FCSI + SFS was proposed in this study. For clarity, the FCSI + SFS algorithm can be briefly described as follows:

(a) Initialize a candidate channel set $\Phi = \{l | l = 1, 2, \ldots, L\}$ and a selected channel set $\psi =$ empty, where L denotes the total channel number.
(b) For any channel l in Φ, calculate its FCSI value *via* Eqs 4–6.
(c) Choose the channel l_m that yields the highest FCSI value among channels in Φ and then move the channel l_m from Φ to ψ.
(d) For any remaining channel l in Φ, combine the channel l with all channels in ψ and calculate the FSCI value of their combination *via* Eqs 4–6. Note that in this case, the feature vector $\mathbf{x}$ is formed by concatenating features from all combined channels. If applicable, the high dimensionality of these feature vectors was reduced by ULDA prior to the FSCI evaluation.
(e) Choose the channel l_m that yields the highest FCSI value, when it is combined with all channels in ψ, and then move the channel l_m from Φ to ψ.
(f) Repeat the steps (d) and (e), until the size of the selected channel set ψ reaches into a preset number.

Consequently, the performance of the proposed FCSI and FCSI + SFS algorithms was examined and compared with solely using the SFS algorithm for channel selection. To ensure a fair comparison, all the three algorithms selected their respective desired channels using the training dataset (i.e., four repetitions), while the classification performance of the selected channels was

evaluated using the fifth one (not involved in channel selection process) as testing dataset for the classifier.

RESULTS

Feature Selection and Classification

An example of the effectiveness of FCSI for quantifying the discriminating power of features is shown in **Figure 2**, where the distribution of features for three representative classes were demonstrated in three scatter plots: (a) with the lowest FCSI values, (b) with the highest FCSI values, and (c) from three TD parameters (WL, ZC, and SSC). From the visual inspection, it can be found that the features determined by three highest FCSI values reflect good class separability in the figure, whereas such separability was not observed for features with lowest FCSI values or three TD features.

Following the wavelet packet feature extraction and selection using FCSI, along with LDC classification, pattern recognition analysis was implemented in a user-specific manner for all 12 stroke subjects. **Table 2** summarizes the classification performance in terms of overall accuracy for identifying 20 intended upper limb movement, when both the WPT-based method and TD feature extraction method were applied to the EMG data consisting of 46 high-density channels or 10 predefined channels, respectively. A two-way repeated-measure ANOVA was applied on the classification accuracies, with the channel number (high-density 46 and 10) and feature set (WPT and TD) both considered as within-subject factors, in order to examine their effect. It can be unsurprisingly observed that high classification accuracies above 95% were achieved for almost all subjects when the 46 high-density channels were totally used, regardless of the feature extraction methods. By contrast, the use of predefined 10 channels led to a performance compromise with an averaged accuracy of 91.15% for the TD features and 92.91% for the WPT features, respectively. An overall significant effect of both channel number ($F = 14.597$, $p = 0.003$) and feature set ($F = 10.031$, $p = 0.009$) on classification accuracy was revealed by the ANOVA. In this case, the WPT-based feature extraction approach showed superior performance to the routine TD feature extraction method by about 2% accuracy improvement with statistical significance.

Channel Selection

The performance of the proposed method for selecting an appropriate subset of channels was further examined. Admittedly, the performance of myoelectric pattern recognition is sensitive to both the channel number and the number of extracted features per channel. By changing both factors, their effect on the classification performance was simultaneously examined using the FCSI algorithm. **Figure 3** shows a representative example from Subject 2 illustrating how the classification performance (as described by error rate) changes in the extracted/selected feature number per channel varying from 1 to 25 and the channel number varying from 1 to 20. It can be observed that very low (approximately 1 or 2) feature number per channel or channel number

TABLE 2 | Classification accuracy (unit: %) in stroke subjects when both TD and WPT features were extracted from the EMG data of 46 high-density channels and 10 predefined channels, respectively.

Subject #	46 high-density channels		10 predefined channels	
	TD	WPT	TD	WPT
1	94.36	98.74	82.89	86.57
2	91.15	95.75	80.61	82.46
3	94.07	98.56	93.47	89.34
4	87.36	98.00	82.93	87.69
5	96.81	94.22	96.73	98.49
6	95.02	98.61	86.56	86.65
7	99.65	100.0	94.67	96.56
8	99.58	100.0	96.39	99.47
9	93.63	98.96	95.94	94.90
10	97.84	99.78	86.80	96.26
11	99.32	99.78	98.60	97.95
12	100.0	100.0	98.20	98.60
Average	95.73 ± 3.90	98.53 ± 1.82	91.15 ± 6.68	92.92 ± 5.95

TD, the time domain feature set; WPT, the proposed feature set using wavelet packet transform.

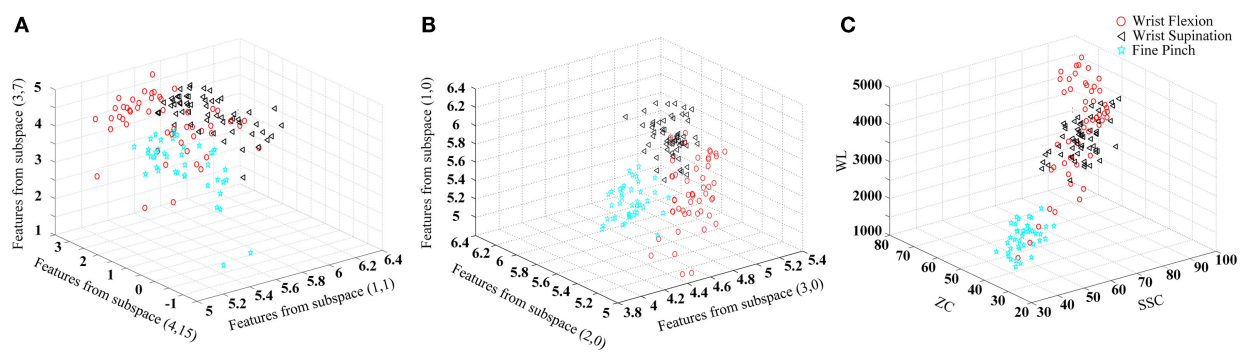

FIGURE 2 | Illustration of the effect of FCSI values on feature separability. Three upper limb movements (wrist flexion, wrist supination, and fine pinch) in the 18-th channel from Subject 3 are used as an example to produce the scatter plots. The three-dimensional coordinate axes stand for feature values. **(A)** Three features with the lowest FCSI values; **(B)** three features with the highest FCSI values; and **(C)** three TD features (WL, ZC, and SSC) used for comparison.

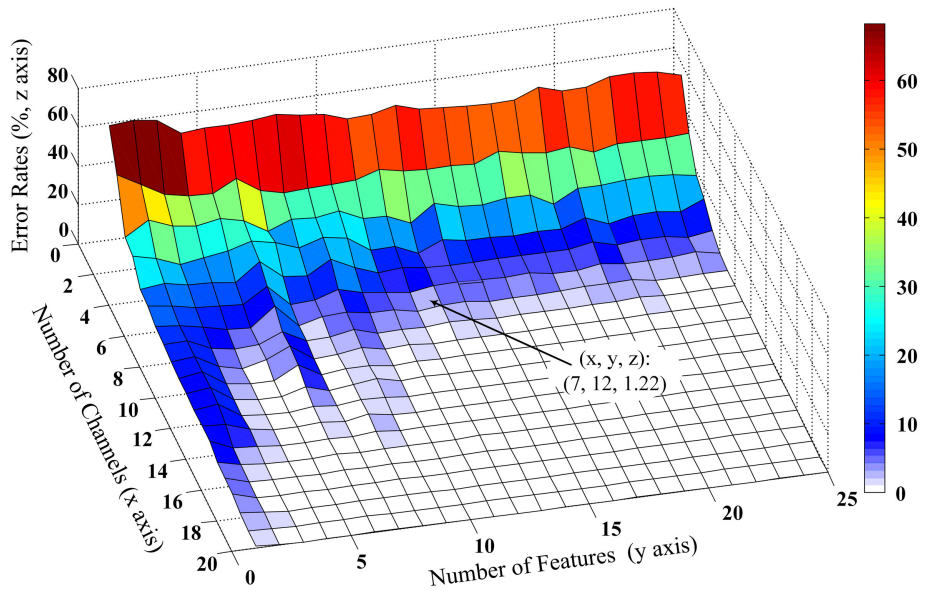

FIGURE 3 | Effect of number of optimal wavelet basis on the channel selection performance from Subject 2. The three-dimensional *x*, *y*, and *z* coordinate axes stand for number of channels, number of features, and error classification rates evaluated by LDC classifier. The number of optimal wavelet basis can be determined based on features first reaching the minimum error rate and the trade-off of computational cost and classification performance.

could not produce high classification performance (low error rate) and the increase of channel number played a critical role in performance improvement. Similar findings were observed for the other subjects. Considering the trade-off between classification performance and practicability (i.e., low computational cost and reduced number of channels), the feature number was set to be 12, producing an error rate of 1.22% for Subject 2 when the channel number was reduced to 7. This confirmed our setting of feature number per channel to 12 in both previous and following data analyses.

After the feature number per channel was appropriately determined, the performance of three channel selection algorithms was evaluated. **Figure 4** reports the classification accuracies averaged across 12 stroke subjects, when the EMG channels were progressively selected using FCSI, SFS, and FCSI + SFS, respectively. When applying WPT and TD feature extraction methods on 10 predefined channels, in addition, the achieved classification accuracies are indicated as two horizontal dashed lines in **Figure 4** for comparison purpose. It can be found that each of the three algorithms yielded a similar increasing trend of classification accuracy when the channel number increased. The classification accuracy increased rapidly to approximately or over 90% at channel number ranging from 1 to 10 and then remained almost steady or slightly increased with further channel number increasing. The proposed FCSI + SFS method demonstrated its superior performance to the other two with highest average accuracies. Specifically, by using 10 optimally selected channels as compared with the 10 predefined channels, improved classification performance was obtained. Meanwhile, the use of only 5 channels optimally selected by either FCSI + SFS or SFS algorithm was found to produce classification performance comparable to that of using 10 predefined channels. Furthermore, a series of bivariate Pearson's correlation analyses were conducted to further examine the effect of subjects' clinical information (including years post stroke, FMUE, and C–M hand scores) on the classification accuracies derived from the use of any channel number (high-density 46, predefined 10, or optimally selected 10 channels by FCSI_SFS or SFS) along with any feature set (WPT or TD), respectively. No significant correlation was found between any clinical information and the classification accuracy ($p > 0.058$) except the correlation between the FMUE score and the classification performance with WPT feature extracted from 10 predefined channels (correlation coefficient $R = 0.651$, $p = 0.022$).

Table 3 shows the first 10 selected channels for each subject using the 3 methods. It was found, as would be expected, that the selected channels were different across subjects even using the same method. For each subject, the selected channels also varied when three methods were performed, respectively. However, for each subject, several channels (marked in bold numbers, though, with varying order of selection) were commonly selected using any of the three algorithms.

DISCUSSION

Myoelectric pattern recognition has great potential for implementing interactive control of assistive robotic devices, which is of particular importance for restoration of dexterous arm/hand functions. Previous high-density surface EMG pattern recognition analysis using conventional TD or AR + RMS features has revealed that substantial neural control information can be readily extracted from paretic muscles of stroke patients. In the current study, a feature extraction method based on WPT was re-examined and applied to high-density surface EMG signals from stroke subjects for improved myoelectric pattern-recognition performance. Taking advantage of the classic wavelet packet feature extraction and selection approach, a novel channel selection

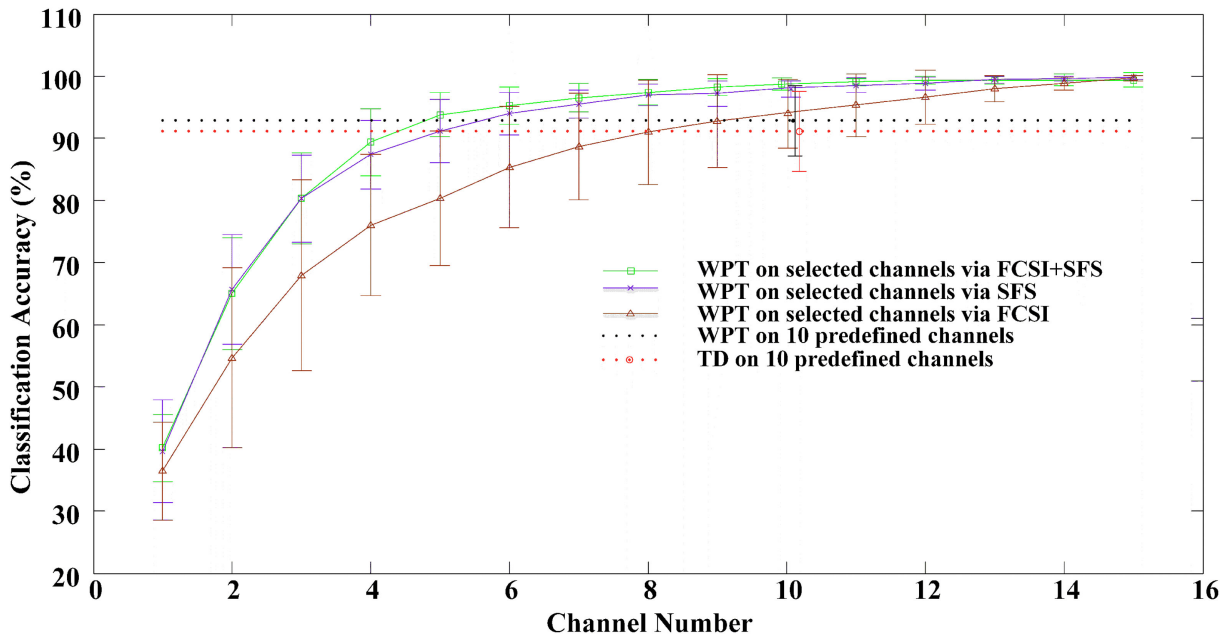

FIGURE 4 | The classification performance as a function of number of channels selected *via* the FCSI, SFS, and FCSI + SFS methods, respectively. For each subject, the classification accuracies were derived from the testing dataset. The classification accuracies from all 12 subjects were averaged and plotted with SD error bars. The classification accuracies derived from applying both WPT and TD features to 10 predefined channels are indicated as two horizontal dashed lines.

TABLE 3 | List of the first 10 selected channels for all 12 stroke subjects using 3 channel selection methods, respectively.

Subject #	FCSI + SFS	SFS	FCSI
	Channel combination	Channel combination	Channel combination
1	(**46**, 6, **7**, 29, 40, 5, 26, 27, 20, 44)	(6, **46**, 2, 27, 3, 17, 36, 29, 26, **7**)	(19, 11, 3, **46**, 43, 20, 2, 12, **7**, 21)
2	(**10**, **17**, **44**, 1, 6, 13, 34, 36, 24, 8)	(4, 25, **44**, 5, 6, **10**, 31, **17**, 7, 27)	(2, **44**, 13, **17**, 25, **10**, 1, 5, 38, 16)
3	(22, 38, **45**, 12, 18, 43, 44, 31, 2, 25)	(18, 30, **45**, 5, 43, 25, 26, 29, 27, 1)	(**45**, 30, 42, 31, 41, 1, 38, 8, 23, 22)
4	(30, 42, 46, 22, 12, 32, **4**, 25, 35, 21)	(**4**, 45, 5, 35, 39, 22, 19, 6, 26, 20)	(33, 32, 28, 25, 20, 17, 19, 12, **4**, 40)
5	(**37**, 42, 17, 21, 44, 24, 34, **27**, 46, 9)	(24, **37**, 43, **27**, 31, 35, 18, 10, 32, 4)	(42, 45, **37**, 3, 38, 4, 9, 44, 41, **27**)
6	(**46**, 24, 37, 40, 5, 34, 30, 6, 42, 43)	(**46**, 30, 18, 40, 32, 20, 24, 17, 34, 16)	(41, 44, 43, **46**, 27, 5, 28, 13, 38, 18)
7	(37, 43, 46, 31, 41, 17, 22, 24, 13, 19)	(37, 23, 17, 34, 27, 30, 35, 39, 15, 26)	(1, 13, 16, 9, 10, 5, 8, 14, 6, 27)
8	(4, 43, 41, 38, 17, **11**, 5, 32, 23, 3)	(17, 19, 23, 29, 26, 13, 39, 8, **11**, 6)	(5, 4, 13, 22, 12, 3, 2, **11**, 8, 25)
9	(21, 38, **22**, **44**, 24, 37, 9, 29, 42, 17)	(37, **22**, 20, 41, 10, **44**, 35, 21, 12, 23)	(**44**, **22**, 17, 4, 2, 26, 10, 40, 32, 7)
10	(10, 31, **33**, 45, 16, 30, 26, 44, 11, 38)	(30, 18, 15, 28, 25, 23, **33**, 34, 26, 38)	(10, 16, 8, 9, 1, **33**, 7, 15, 32, 2)
11	(**31**, **17**, 40, 30, 28, 45, 42, 43, 24, 23)	(31, 25, 13, 36, 4, 16, 18, 5, 21, **17**)	(42, 45, 46, 43, 25, 37, 23, 39, **31**, **17**)
12	(**24**, 21, 5, 16, 43, 44, 12, 17, 32, 38)	(**24**, 5, 37, 27, 9, 1, 35, 3, 7, 6)	(32, 43, 44, 25, 41, 37, **24**, 4, 2, 12)

The bold numbers represent commonly selected channels using any of the three methods for each subject.

method was furthermore developed to determine a practical number of appropriate EMG channels for maintaining high classification accuracies, an issue particularly important for implementing a practical myoelectric control system.

The FCSI was used in this study to quantify the discriminating power of each feature or wavelet packet basis/subspace where the feature was derived. There have been different algorithms or criteria for determining the best basis or subspace in WPT analysis (15, 20). For pattern recognition analysis, the adopted criterion is preferably associated with class separability. The FCSI is such a criterion that is able to measure the class separability of a feature or feature vector, more specifically, in almost the same way as the LDC classifier does. The FCSI was used to determine the most discriminating features from those produced by WPT analysis in various time–frequency scales. Due to the advantages of time–frequency resolution provided by the WPT as well as the FCSI analysis, the wavelet packet feature extraction and selection approaches demonstrated improved performance, as compared with the previously used conventional time domain or frequency domain feature sets, especially for subjects with relatively high levels of impairments. For example, 5 of 12 stroke subjects (i.e., Subjects 1, 2, 3, 4, and 9) produced relatively low classification accuracies below 95.0%, respectively, when the TD feature set was applied, whereas improved accuracies above 95% (**Table 2**) were achieved for these subjects using the wavelet packet features. It is worth noting that the TD and AR features were often employed

for myoelectric pattern recognition for amputee subjects toward prosthesis control, which can achieve comparable performance to more complicated features including wavelet packet features (8, 9, 25). In contrast, the advantages of wavelet packet feature extraction and selection appeared more evident in processing stroke data, presumably due to the fact that the residual muscles of an amputee subject are neurologically intact, whereas the paretic muscles of stroke subjects usually suffer from different symptoms such as weakness, spasticity, etc. Due to the fact that neural control information delivery is hampered by injuries to neuromuscular pathways after stroke, more complicated features (e.g., WPT features) are likely to emerge their advantage in characterizing such paretic EMG signals, which was demonstrated in this study.

The FCSI used for WPT feature selection was further extended for channel selection, in combination with the SFS method. The combined FCSI + SFS method demonstrated superior performance for channel selection in terms of classification performance than solely using the SFS or the FCSI method. Using the FCSI rather than the direct classification accuracy in combination with the SFS algorithm avoids repeated training and testing of a classifier (required for each iteration). Furthermore, in this study, the channel selection procedure and the performance testing procedure were not based on the same datasets in order to overcome the overfitting problem. Besides, when the same number (e.g., 10) of channels were employed, the channels selected *via* an optimal algorithm (e.g., FCSI + SFS) yielded higher classification accuracies across all 12 stroke subjects than those predefined electrode sites. In addition, with the WPT feature set, the correlation analyses revealed dependence of the classification performance on the FMUE score with statistical significance ($p = 0.021$) when a set of predefined 10 channels were used. Such dependence disappeared when high-density 46 channels or optimally selected 10 channels were adopted ($p > 0.021$), indicating that those subjects with relatively high levels of impairments (i.e., low clinical assessment scores) had substantial improvement of classification performance. The channel selection analysis not only confirms previous findings in Ref. (4, 27) that it is feasible to use a small number of EMG channels (rather than a high-density electrode array) for decoding sufficient neural control information from paretic muscles but also indicates the necessity of determining appropriate control site locations (rather than predefined channels) for improved classification performance. Therefore, effective algorithms, such as the FCSI + SFS, reported in this study are of critical demand for developing a practical myoelectric control system, particularly for stroke users.

When examining the selected channel index, it was found that the selected channels were different among 12 stroke subjects even using the same channel selection method, primarily due to individual subject difference following stroke (such as impairment nature and level, recovery status, daily activity, etc.). It confirms our previous suggestion (4) that the myoelectric pattern recognition should be designed or conducted in a user-specific manner. The designed system may include appropriate EMG features and channels (e.g., electrode number, location, configuration, etc.) that maximize the classification accuracy to enhance its usability for stroke subjects with any impairment level, while its suitability for real time application (such as computational cost, adaptability to slight electrode movement, etc.) should also be considered. We acknowledge that the examined WPT-based feature extraction and selection approach may induce relatively higher computational complexity than using conventional TD feature set. Even so, the WPT method is still very practical for real-time implementation demonstrated by an enormous number of previous studies (10, 14, 28). Also, the choice of the target movements or controlled function should consider subject need and classification performance. Although high-density surface EMG recording contains much redundant information for myoelectric pattern recognition analysis, it provides a very useful and essential way to optimize the myoelectic control system designed for individual stroke patients. In this regard, the high-density sEMG recording, along with effective channel selection, can be designed as a necessary calibration procedure. Such a procedure is recommended to be conducted just once, rather than regularly, during the prescription of the myoelectrically controlled robotic training for stroke patients with different impairment levels.

CONCLUSION

In this study, a feature extraction method based on WPT was applied to myoelectric pattern recognition analysis in stroke survivors. By processing high-density surface EMG recordings from paretic muscles of 12 stroke subjects, the WPT features achieved an improved performance for classification of 20 different arm/hand movements compared with the conventional TD EMG features. Furthermore, a novel channel selection method was developed by combining the FCSI and the SFS analyses, which can effectively determine a small number of appropriate EMG channels without significantly compromising the classification performance achieved from high-density surface EMG. These novel feature extraction and channel selection analyses confirm substantial neural control information available in paretic muscles of stroke survivors, and moreover, demonstrate the feasibility of extracting such information with a practical number of EMG channels. The findings are helpful for development of myoelectric control systems for stroke rehabilitation.

AUTHOR CONTRIBUTIONS

DW analyzed the data, interpreted the results, and wrote the first draft of the manuscript. XZ designed the study and performed all stages of the study including data collection, analysis, interpretation, and substantial revision of the manuscript. XG, XC, and PZ participated in data analysis and interpretation and revised the manuscript. All the authors approved the final version of the manuscript.

FUNDING

This work was supported in part by the National Natural Science Foundation of China under Grant 61401421 and the Fundamental Research Funds for the Central Universities under Grant WK2100230014.

REFERENCES

1. Krebs HI, Volpe BT, Williams D, Celestino J, Charles SK, Lynch D, et al. Robot-aided neurorehabilitation: a robot for wrist rehabilitation. *IEEE Trans Neural Syst Rehabil Eng* (2007) 15(3):327. doi:10.1109/TNSRE.2007.903899
2. Dipietro L, Krebs HI, Fasoli SE, Volpe BT, Stein J, Bever C, et al. Changing motor synergies in chronic stroke. *J Neurophysiol* (2007) 98(2):757–68. doi:10.1152/jn.01295.2006
3. Van Peppen RP, Kwakkel G, Wood-Dauphinee S, Hendriks HJ, Van der Wees PJ, Dekker J. The impact of physical therapy on functional outcomes after stroke: what's the evidence? *Clin Rehabil* (2004) 18(8):833–62. doi:10.1191/0269215504cr843oa
4. Zhang X, Zhou P. High-density myoelectric pattern recognition toward improved stroke rehabilitation. *IEEE Trans Biomed Eng* (2012) 59(6):1649–57. doi:10.1109/TBME.2012.2191551
5. Oskoei MA, Hu H. Myoelectric control systems – a survey. *Biomed Signal Process Control* (2007) 2(4):275–94. doi:10.1016/j.bspc.2007.07.009
6. Bottomley AH. Myo-electric control of powered prostheses. *J Bone Joint Surg Br* (1965) 47(3):411–5.
7. Battye CK, Nightingale A, Whillis J. The use of myo-electric currents in the operation of prostheses. *J Bone Joint Surg Br* (1955) 37(3):506–10.
8. Lee SW, Wilson KM, Lock BA, Kamper DG. Subject-specific myoelectric pattern classification of functional hand movements for stroke survivors. *IEEE Trans Neural Syst Rehabil Eng* (2011) 19(5):558–66. doi:10.1109/TNSRE.2010.2079334
9. Hudgins B, Parker P, Scott RN. A new strategy for multifunction myoelectric control. *IEEE Trans Biomed Eng* (1993) 40(1):82–94. doi:10.1109/10.204774
10. Englehart K, Hudgins B, Parker PA, Stevenson M. Classification of the myoelectric signal using time-frequency based representations. *Med Eng Phys* (1999) 21(6):431–8. doi:10.1016/S1350-4533(99)00066-1
11. Zardoshti-Kermani M, Wheeler BC, Badie K, Hashemi RM. EMG feature evaluation for movement control of upper extremity prostheses. *IEEE Trans Rehabil Eng* (1995) 3(4):324–33. doi:10.1109/86.481972
12. Boostani R, Moradi MH. Evaluation of the forearm EMG signal features for the control of a prosthetic hand. *Physiol Meas* (2003) 24(2):309. doi:10.1088/0967-3334/24/2/307
13. Dewald JP, Pope PS, Given JD, Buchanan TS, Rymer WZ. Abnormal muscle coactivation patterns during isometric torque generation at the elbow and shoulder in hemiparetic subjects. *Brain* (1995) 118(2):495–510. doi:10.1093/brain/118.2.495
14. Chu JU, Moon I, Mun MS. A real-time EMG pattern recognition system based on linear-nonlinear feature projection for a multifunction myoelectric hand. *IEEE Trans Biomed Eng* (2006) 53(11):2232–9. doi:10.1109/TBME.2006.883695
15. Wang G, Wang Z, Chen W, Zhuang J. Classification of surface EMG signals using optimal wavelet packet method based on Davies-Bouldin criterion. *Med Biol Eng Comput* (2006) 44(10):865–72. doi:10.1007/s11517-006-0100-y
16. Zhang S, Mathew J, Ma L, Sun Y. Best basis-based intelligent machine fault diagnosis. *Mech Syst Signal Process* (2005) 19(2):357–70. doi:10.1016/j.ymssp.2004.06.001
17. Unser M, Aldroubi A. A review of wavelets in biomedical applications. *Proc IEEE* (1996) 84(4):626–38. doi:10.1109/5.488704
18. Rafiee J, Rafiee MA, Yavari F, Schoen MP. Feature extraction of forearm EMG signals for prosthetics. *Expert Syst Appl* (2011) 38(4):4058–67. doi:10.1016/j.eswa.2010.09.068
19. Hariharan M, Fook CY, Sindhu R, Ilias B, Yaacob S. A comparative study of wavelet families for classification of wrist motions. *Comput Electr Eng* (2012) 38(6):1798–807. doi:10.1016/j.compeleceng.2012.08.009
20. Englehart K. *Signal Representation for Classification of the Transient Myoelectric Signal*. Fredericton, NB: University of New Brunswick, Department of Electrical & Computer Engineering (1998).
21. Kiatpanichagij K, Afzulpurkar N. Use of supervised discretization with PCA in wavelet packet transformation-based surface electromyogram classification. *Biomed Signal Process Control* (2009) 4(2):127–38. doi:10.1016/j.bspc.2009.02.004
22. Lucas M-F, Gaufriau A, Pascual S, Doncarli C, Farina D. Multi-channel surface EMG classification using support vector machines and signal-based wavelet optimization. *Biomed Signal Process Control* (2008) 3(2):169–74. doi:10.1016/j.bspc.2007.09.002
23. Yen GG, Lin K-C. Wavelet packet feature extraction for vibration monitoring. *IEEE Trans Ind Electron* (2000) 47(3):650–67. doi:10.1109/41.847906
24. Ye J, Li T, Xiong T, Janardan R. Using uncorrelated discriminant analysis for tissue classification with gene expression data. *IEEE/ACM Trans Comput Biol Bioinform* (2004) 1(4):181–90. doi:10.1109/TCBB.2004.45
25. Huang H, Zhou P, Li G, Kuiken TA. An analysis of EMG electrode configuration for targeted muscle reinnervation based neural machine interface. *IEEE Trans Neural Syst Rehabil Eng* (2008) 16(1):37–45. doi:10.1109/TNSRE.2007.910282
26. Lal TN, Schröder M, Hinterberger T, Weston J, Bogdan M, Birbaumer N, et al. Support vector channel selection in BCI. *IEEE Trans Biomed Eng* (2004) 51(6):1003–10. doi:10.1109/TBME.2004.827827
27. Li Y, Chen X, Zhang X, Zhou P. Several practical issues toward implementing myoelectric pattern recognition for stroke rehabilitation. *Med Eng Phys* (2014) 36(6):754–60. doi:10.1016/j.medengphy.2014.01.005
28. Fontana JM, Chiu AW. Analysis of electrode shift effects on wavelet features embedded in a myoelectric pattern recognition system. *Assist Technol* (2014) 26(2):71–80. doi:10.1080/10400435.2013.827138

Conflict of Interest Statement: The authors declare that the research was conducted in the absence of any commercial or financial relationships that could be construed as a potential conflict of interest.

Advantages of publishing in Frontiers

OPEN ACCESS
Articles are free to read for greatest visibility and readership

FAST PUBLICATION
Around 90 days from submission to decision

HIGH QUALITY PEER-REVIEW
Rigorous, collaborative, and constructive peer-review

TRANSPARENT PEER-REVIEW
Editors and reviewers acknowledged by name on published articles

Frontiers
Avenue du Tribunal-Fédéral 34
1005 Lausanne | Switzerland

Visit us: www.frontiersin.org
Contact us: info@frontiersin.org | +41 21 510 17 00

REPRODUCIBILITY OF RESEARCH
Support open data and methods to enhance research reproducibility

DIGITAL PUBLISHING
Articles designed for optimal readership across devices

FOLLOW US
@frontiersin

IMPACT METRICS
Advanced article metrics track visibility across digital media

EXTENSIVE PROMOTION
Marketing and promotion of impactful research

LOOP RESEARCH NETWORK
Our network increases your article's readership